The Origin and Evolution of Hercynian Crustal Fluids, South Cornwall, England

Jamie John Wilkinson

Ph.D. Thesis

DECEMBER 1989

THE UNIVERSITY OF SOUTHAMPTON

To
Mum, Dad and Roo

without whom this would not exist

CONTENTS

UNIVERSITY OF SOUTHAMPTON

ABSTRACT

FACULTY OF SCIENCE

GEOLOGY

Doctor of Philosophy

THE ORIGIN AND EVOLUTION OF HERCYNIAN CRUSTAL FLUIDS, SOUTH CORNWALL, ENGLAND

by Jamie John Wilkinson

Crustal fluids, mobilised in Devonian metasediments during and subsequent to the Hercynian orogeny in south Cornwall, have been investigated by a detailed study of fluid inclusions present in vein material. Four stages of vein formation are distinguished, related to the three main deformation events which affected the area. Within each stage, up to four different vein types are recognised, occurring in distinct structural and/or lithological settings.

Fluid inclusion data, in combination with pumpellyite-actinolite mineral assemblages and vitrinite reflectance data indicate that low grade regional metamorphism in south Cornwall occurred at 330 ± 30°C and 3.4 ± 0.5 kbar. Dense (0.95 ± 0.3 g cm^{-3}), low salinity (1-4.5 wt% NaCl equivalent), H_2O-rich (X_{H2O}>0.986), peak metamorphic fluids were evolved via prograde devolatilisation reactions, contemporaneous with the first compressional deformation event (D1). The major element compositions of these fluids were buffered by quartz + albite + K-mica + chlorite ± paragonite assemblages in greywacke and slate host rocks. Thermodynamic calculations suggest that the peak metamorphic fluids could have transported significant (ppm) quantities of base metals and silver as chloro-complexes, and tin as hydroxy-complexes.

High temperature metamorphic fluids migrated up imbricate thrusts to shallower crustal levels during the second deformation event (D2). These fluids caused limited sericitic and chloritic alteration of wallrocks, and became increasingly saline (up to 8 wt% NaCl equivalent) as a result of hydration reactions. CO_2 and N_2 contents increased, possibly as a result of oxidation of organic carbon and ammonium in the wallrocks due to cooling and decreasing oxygen fugacity. Lower ore mineral solubilities in these fluids may have resulted in precipitation, producing low-grade metal enrichment in the upper crust. Fluid inclusion data indicate that fluid temperatures and pressures did not fall below 200°C and 500 bars respectively, during D2.

$CO_2(+N_2+CH_4)$-bearing fluids, possibly generated by mixing of approximately equal proportions of magmatic and contact metamorphic fluids, were mobilised up to 5 km laterally from the roof zone of the Cornubian granite batholith during emplacement. These fluids unmixed at 400-200°C and 1000-500 bars to produce low density CO_2-rich vapour and high density, moderately to highly saline, aqueous fluids (8-42 wt% NaCl equivalent). Up to 28 ppm tin could have been transported in the hypersaline fluids, primarily as chloro-complexes. High density, CO_2-rich fluids (up to 85 mol% CO_2) were produced in distal parts of the contact aureole, probably as a result of condensation of low density vapours.

Low salinity (1-5 wt% NaCl equivalent), H_2O-rich fluids separated from the Megilliggar pegmatites during crystallisation. These fluids unmixed at ≈400°C to produce a low density, $CO_2(\pm CH_4 \pm N_2)$-bearing vapour and moderately saline (8-10 wt% NaCl equivalent) aqueous liquid. Magmatic fluids of this type, possibly in combination with contact metamorphic fluids, were responsible for high temperature mineralisation phenomena. The initiation of convective fluid circulation, and dilution of magmatic ± metamorphic fluids with meteoric water at or below ≈300°C, resulted in the formation of the bulk of the Sn-W-polymetallic sulphide deposits observed in the province.

Basinal brines migrated along wrench faults into the Cornubian peninsula and mixed with convecting meteoric fluids at structural intersections on the southern flank of the granite batholith at 140-200°C and <500 bars. Mixing caused base metal deposition by increasing pH and decreasing salinity.

ACKNOWLEDGEMENTS

All research projects have to start somewhere, and credit for getting things going, and for their input over the last three years must go to my supervisors Dr Bob Foster and Dr Jim Andrews.

On the practical side, thanks go to Dr Ian Croudace for his help with all things geochemical, and to Robin (Henry VIII) Saunders for XRD and SEM info, for keeping the Bubble Lab in order, and for having an endless supply of everything one could ever need. Thanks also to the Basement Boys, Bob Jones and Clive Balcombe (RIP), for all their cutting, grinding and polishing, and Barry Marsh for his photographic expertise. I am grateful to Lola and Frances for allowing me a brief fling with their laser printers.

In the field, the local knowledge of Jim Andrews proved essential for the location of the best ~~Public Houses~~ exposures. Thanks also to Robin Shail and the rest of the Variscan Workshop for some excellent events, both social and geological. Chris Farmer gets a mention for organising an experience down South Crofty and thanks to Stan of Gunwalloe for the use of his quarry. Especial thanks go to Carol and Bob Cookson who made me feel so welcome at *Pentre* and didn't complain once about the rocks in the sink or the boots in the hall.

A number of people have made invaluable contributions on the scientific side during my time at Southampton. From the outside, thanks to Andy Rankin for the discussions, advice and access to the ICP at Imperial College. Many thanks also to Tom Shepherd for many useful chats and for providing volatile analysis facilities and training at the (ex) BGS Isotope Laboratory, Grays' Inn Road. I am indebted to Tony Fallick and Gawen Jenkin at SUURC, East Kilbride for performing fluid inclusion stable isotope analyses. On the inside, thanks to Bob Foster for always being accessible and for almost always being available(!). Without the rest of the Bubble Boys, homogenising would have been much less entertaining, so thanks to Dave Bennett, Alan Carter, Steve Roberts, Roberto (Bobo) Xavier and Steve Dee. Thanks also to the Gold Boys: Jon G., Rudi J., Tony S., and Alan C., for making me an honorary member of the club. *Richard Knight, Retusotriletes Philipsii* and *Grandispora Echinata* made possible my brief foray into the mysterious world of palynology, and Steve Hillier taught me something about clay mineralogy (I think) - cheers lads!

Southampton wouldn't have been the same without the Escape Committee and its whacky antics. So for all their help in tunnelling I'd like to send a big "hurrah!" to Dr Chairman - Slap(aser) Hillier, Dr J. Stone, Dr R. ("Craig") Taylor, Dr 40P. O'Brien, Dr T. Moat (well escaped boys!), Al, Rich, Jon, Tony, Phil, Chris P., Mark & Mrs A., Dave, Martin (the mouth), Andrea, Rahim, Chris E., and not forgetting Chern and Shell who managed to bribe their way out so quickly. Special thanks to Alan Carter for sharing an office and for sharing the trials and tribulations of writing-up in a confined space, and to 40p for keeping the house in order while we did it. Financial support was courtesy of NERC.

As C.J. once said: "I didn't get where I am today" without the support and encouragement of my parents. Finally, I'd like to thank Roo for the many hours sacrificed over the last five years in leading me along the rocky road to Doctorhood, and for the great hatchet job on the first draft. Thanks everyone!

CHAPTER 1: INTRODUCTION

1.1 RATIONALE

There is abundant evidence that fluids are involved in many geological phenomena. From the time that new crust is produced at a constructive plate margin to its uplift and exposure at the surface of the earth, fluids play an important role in mass transport, modifying rock composition and catalysing deformation processes.

During the last ten years, there has been a rapid increase in the number of researchers studying the role of fluids in a variety of fundamental geological problems. Much of the work has centred on specific processes such as metamorphism (*e.g.* Walther & Wood 1986), fluid flow and deformation (Fyfe *et al.* 1978), faulting (Sibson *et al.* 1975), vein formation (Cox & Etheridge 1983, Beach 1977) and mineralisation (Barnes 1979). Relatively few studies have been concerned with the controls and effects of progressive fluid evolution in an evolving orogenic belt.

The aim of the present study has been primarily to determine the temperature, pressure and chemical composition of fluids passing through a slab of continental crust during a collision orogeny. These data have been used to gain an insight into the nature and importance of the fluid phase involved in processes intimately related to the development of a metallogenic province. The main areas addressed are listed below:

1. Fluid sources
2. Fluid mobilisation
3. Fluid migration
4. Controls of fluid composition
5. P-T evolution
6. Fluid-fluid interactions
7. Fluid-rock interactions
8. Fluid volumes
9. Fluid/rock ratios
10. Metal transport
11. Ore deposition

1.2 STUDY AREA

The area chosen for the study is situated on the west coast of the Lizard Peninsula in southwest Cornwall (Fig. 1.1). The coast provides a superbly exposed section through upper Palaeozoic marine sediments, metamorphosed and complexly deformed during the Hercynian orogeny. The rocks display multiple phases of vein generation representing successive stages of fluid mobilisation, during both Hercynian tectonism and intrusion of the late orogenic Cornubian granite batholith (see section 1.3.2) and subsequent hydrothermal mineralisation (see 1.3.5).

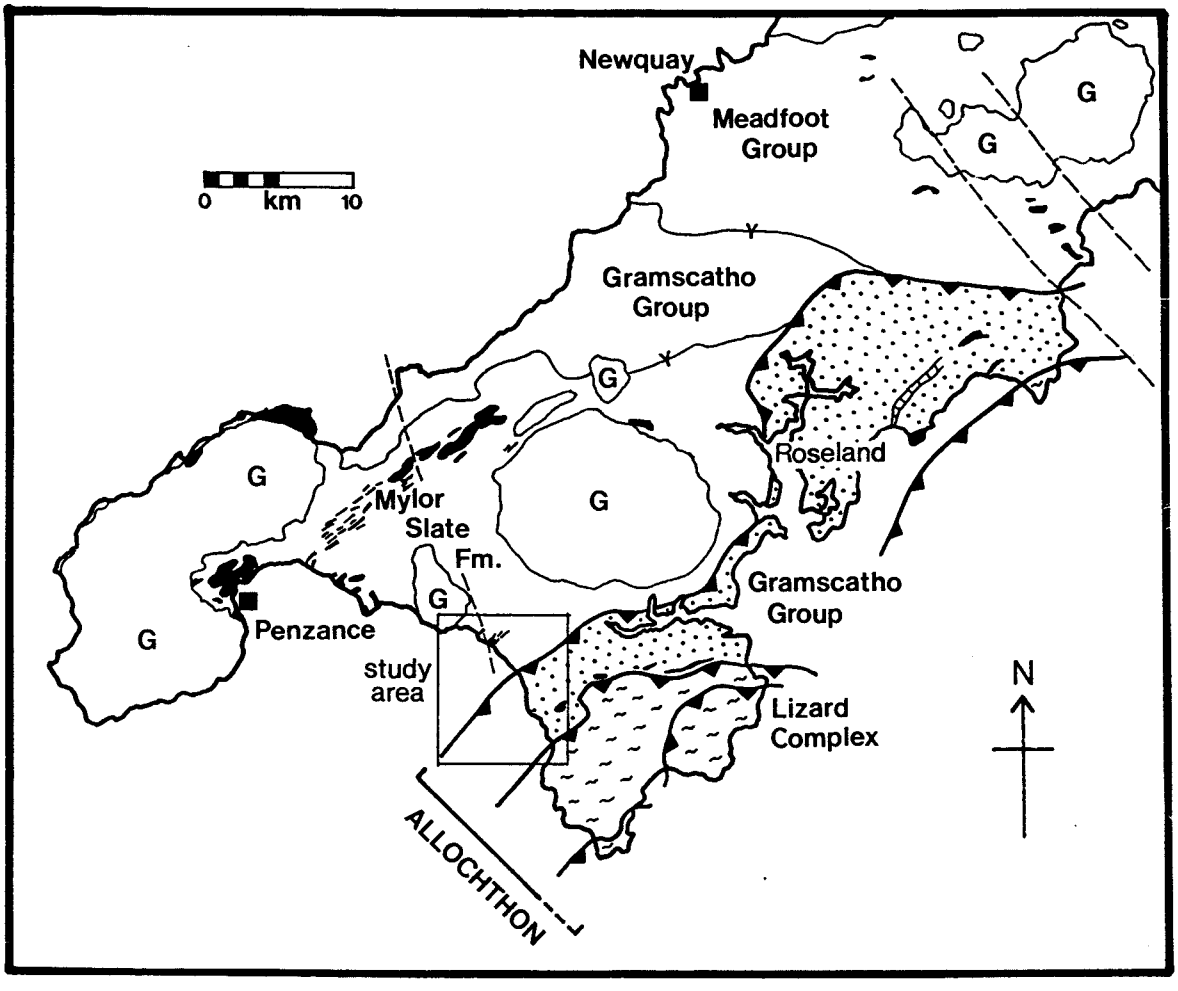

Figure 1.1 Simplified geological map of south Cornwall showing major lithostratigraphic units (labelled) and granite plutons (G). Regional younging directions are shown. The parautochthonous region is un-ornamented; the allochthonous region is stippled. Dashed lines represent post-Hercynian wrench faults.

The Lizard Peninsula area was chosen for a number of reasons. Firstly, it provides a section through part of the crust which was subject to more than 80 My of deformation, metamorphism, magmatism and associated fluid activity during the Hercynian orogeny. Secondly, the area is situated within the Cornubian orefield, a classic area of dominantly Sn-W-Cu mineralisation with a long history of exploitation (Willis-Richards & Jackson, in press). The coastline provides a cross-section through Hercynian structures, giving good structural control, as well as a transect into the contact aureole of

the Tregonning granite (Fig. 1.1), a late magmatic feature (see 1.3.2). Thus, the section allows easy sampling of material unaffected by granite-related thermal, deformational and fluid overprinting, in addition to sampling throughout the contact metamorphosed zone.

Access to most of the section is good, although strongly tide-dependent. Cliff sections provide excellent 2D exposures with many small, and several large, wave-cut platforms supplying additional 3D control. Inland outcrops are scarce and of limited extent. Sampling was therefore concentrated on the coastal exposures.

1.3 GEOLOGY

1.3.1 Lithostratigraphy

The rocks exposed in the area are a series of Middle to Upper Devonian marine sediments which were deposited to the south of the Old Red Sandstone continent (House 1968). The lithostratigraphic terminology adopted in this study is that defined by Holder & Leveridge (1986). They divided south Cornwall into two parts: a parautochthon which forms the northern and central portions of the peninsula, and an allochthon, the "Carrick Nappe" (Leveridge *et al.* 1984), which is exposed on the south coast (Fig. 1.1).

The parautochthon comprises four lithostratigraphic units: Lower Devonian Dartmouth Beds and Meadfoot Group, broadly Middle Devonian Gramscatho Group (Porthtowan Formation) and Upper Devonian Mylor Slate Formation (Fig. 1.2). Only the Mylor Slate Formation is represented in the study area (Fig. 1.1). The allochthon is subdivided into four formations: the Portscatho Formation, considered by Holder & Leveridge (1986) to be of Lower Devonian-Eifelian age; the Pendower and Carne Formations of Middle Devonian age; and the Roseland Breccia Formation of Frasnian age (Fig. 1.2). Together, these Formations comprise the allochthonous Gramscatho Group. Only the Portscatho and Carne Formations outcrop in the allochthonous part of the study section (Fig. 1.1).

Carne Formation

The Carne Formation consists of channel slumped and turbiditic sandstones and laminated siltstones, interpreted as deep water slope and inner fan deposits (Holder & Leveridge 1986). The deposits north of the Lizard in the field area were correlated with the Carne Formation by Holder & Leveridge (1986), although slumped and lenticular bedded greywacke turbidite sandstones in a slaty matrix are dominant.

The suggestion of a sedimentary origin for the sequence was first made by Simpson (1951) and this is now universally accepted over previous tectonic breccia interpretations (*e.g.* Hill & MacAllister 1906). Barnes (1982) interpreted the Carne Formation in the area (his Poldhu (melange) Member of the Meneage Formation) as mainly olistostrome because of the presence of locally derived, often internally bedded, phacoids and intercalations of bedded sequences.

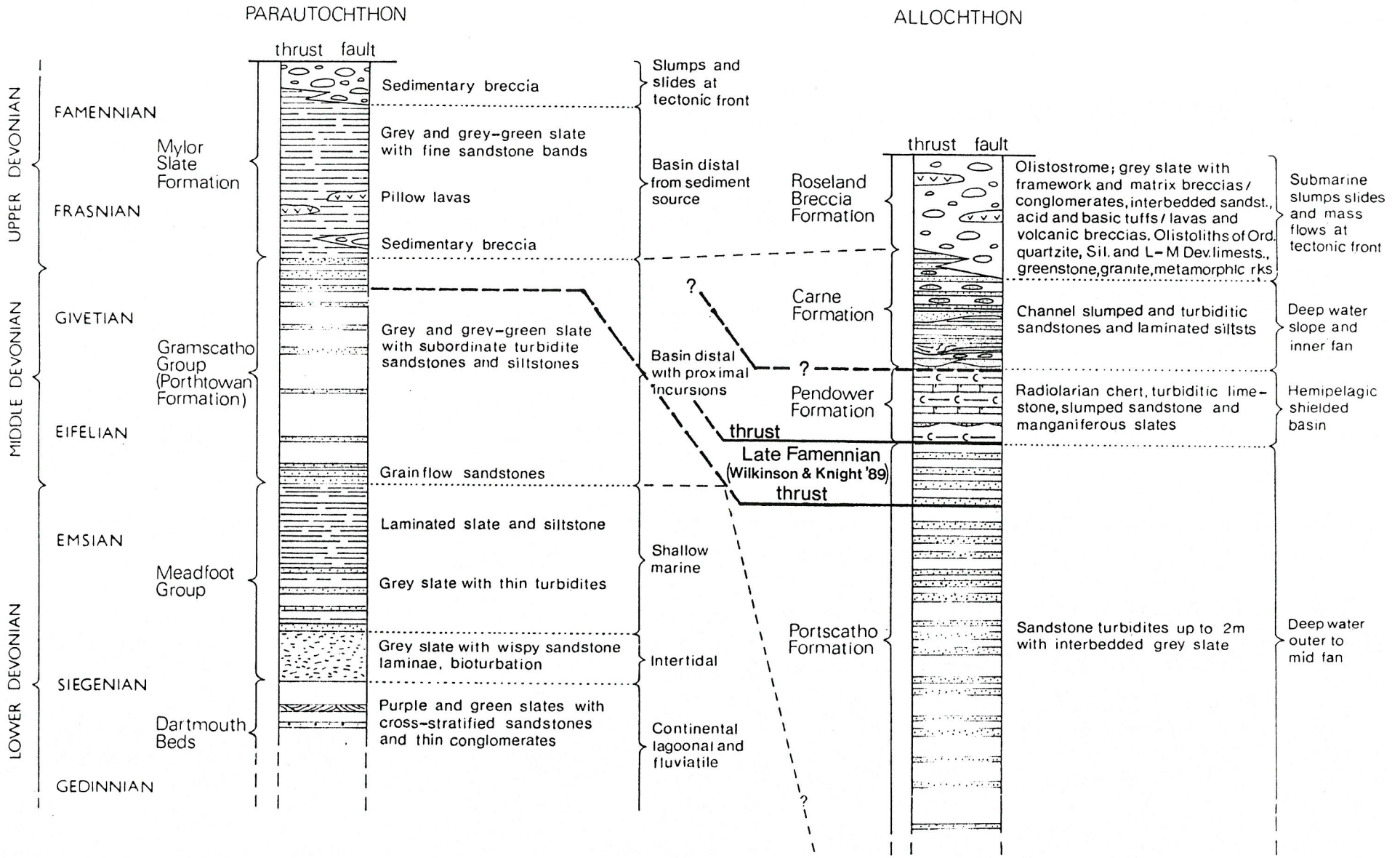

Figure 1.2 Lithostratigraphic sequences of south Cornwall (modified after Holder & Leveridge 1986).

The age of the Carne Formation in the field area is controversial. Holder and Leveridge (1986) place it in the Givetian because the top of the underlying Pendower Formation in Roseland (Fig. 1.2) has been dated as uppermost Eifelian (Sadler 1973). However, the occurrence of Frasnian palynomorphs from the top of the underlying Portscatho Formation in the study section (Le Gall *et al.* 1985) suggests that the Carne Formation is probably Frasnian or Famennian in age (Fig. 1.2), perhaps representing a southerly equivalent of the Mylor Slate Formation.

Portscatho Formation

The Portscatho Formation is typified by fine to medium grained sandstones with interbedded dark grey mudstone (Fig. 1.3). Component sandstones vary in thickness from 0.1-2.0m and are largely turbidites (Walker 1978) often displaying partial Bouma sequences. A deep water outer- to mid-fan depositional environment is generally assumed (*e.g.* Holder & Leveridge 1986). Most of the sandstones are lithic greywackes, although some plot in the feldspathic greywacke field (Holder & Leveridge 1986). Quartz-feldspar-lithics plots of sandstone framework grains suggest a dissected magmatic arc provenance (Floyd & Leveridge 1987).

The Portscatho Formation extends from Jangye-ryn Cove in the south of the area, where it is structurally overlain by the Carne Formation, to north of Loe Bar where a complex downward transition into the Mylor Slate Formation is observed (Fig. 1.4). Early workers interpreted the sequence as a conformable southerly younging succession, with the Portscatho Formation stratigraphically overlying the Mylor Slate Formation (Hill & MacAllister 1906; Hendriks 1937). More recent interpretations of this zone have been presented (*e.g.* Stone 1966; Wilson & Taylor 1976; Rattey & Sanderson 1984; Leveridge & Holder 1985), with a difference of opinion on the order of succession.

Evidence suggesting a Late Devonian age for the Mylor Slate Formation (Turner *et al.* 1979) and a Frasnian or older age for the Portscatho Formation, which structurally overlies it, (Le Gall *et al.* 1985; Holder & Leveridge 1986) supports the concept of an allochthonous Portscatho Formation (see Fig. 1.7). Leveridge *et al.* (1984) proposed that the southern boundary between the Mylor Slate Formation and the Gramscatho Group in south Cornwall is a thrust, the "Carrick Thrust". Leveridge & Holder (1985) interpreted the transition zone between the two llthofacies, exposed between Loe Bar and Caca-stull Zawn (Fig. 1.4), as a major olistostrome at the top of the Mylor Slates, containing coarse extrabasinal detritus derived from the Portscatho Formation as a result of emergent thrusting. However, Wilkinson & Knight (1989) concur with previous explanations of the zone as a transition between the two main lithofacies (*e.g.* Stone 1966). They emphasise the importance of D2 imbricate thrusting in producing the complex lithological intercalations and place the major thrust (their Blue Rock Thrust) to the south of Loe Bar (Figs 1.4, 1.7) on palynological, lithological and structural grounds.

The evidence is ambiguous, despite the excellent cliff exposures. The concept of an allochthonous "Carrick Nappe", comprising the Portscatho Formation and Carne Formation in the study section, has been widely accepted. However, resolution of the remaining stratigraphic and structural problems will only come with further palynological finds.

Figure 1.3

Figure 1.3: Captions

A. Typical Mylor slate from Porthleven Sands. Pale, silty layers, showing F1, F2 and F3 fold interference structures, are rhythmically interbedded with dark grey mudstone. Viewing direction: ENE; Scale bar = 5cm.

B. Typical greywacke turbidites of the Portscatho Formation from Baulk Head. Refraction of S1 cleavage through sandy units shows that beds are inverted. Viewing direction: NE; Scale bar = 30cm.

C. Slightly overturned, NNW-facing, F1 chevron folds in turbidites of the Portscatho Formation, Jangye-ryn Cove. Viewing direction: E; Scale bar = 1m.

D. F1 fold with axial planar slaty cleavage (S1) in sandstone-dominated Portscatho Formation rocks, Gunwalloe Fishing Cove Beach. Viewing direction: E; Scale bar = 40cm.

E. North facing F2 folds and axial planar pressure-solution cleavage (S2), south Loe Bar. Note folding of S1 pressure solution cleavage around F2 hinge in thick, sandstone unit. Sub-axial planar quartz veins are well-developed. Viewing direction: ENE; Scale bar = 20cm.

F. Small-scale illustration of large-scale D2 structure. Planar D2 thrust with imbrication and quartz veining in hanging wall sandstone units, south Loe Bar. Viewing direction: ENE;Scale bar = 20cm.

G. S3 crenulation cleavage axial planar to F3 ptygmatic folds in pre-D3 quartz veins, Mylor Slate Formation, just south of Porthleven Harbour. Viewing direction: E; Scale bar = 2cm.

H. Boudinaged quartz vein, wrapped by S3 crenulation cleavage, Mylor Slates, Porthleven Sands. Note north vergent F2 fold, defined by pale, silty bedding horizons. Viewing direction: ENE; Scale bar = 5cm.

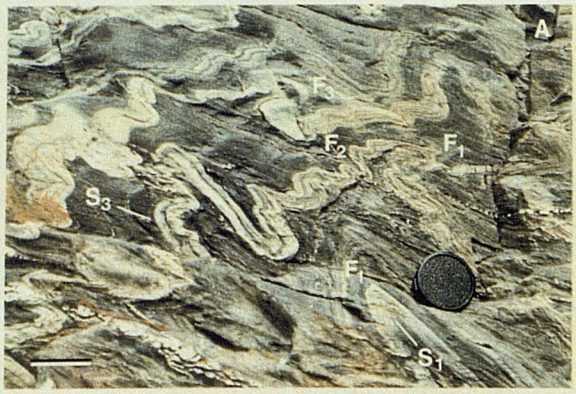
A
F
F2
F1
S3
F1
S1


B


C
F1


D
S0
F1
S1


E
S1
S2
F2
S3

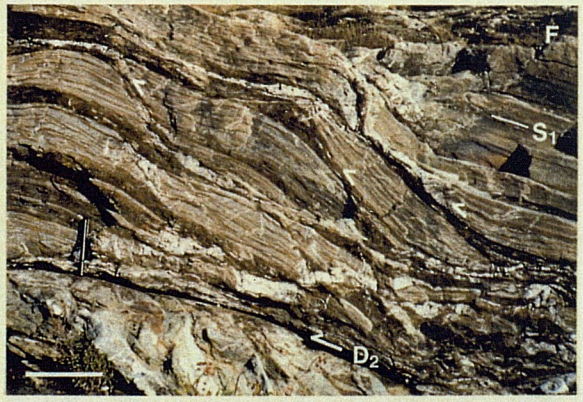
F
S1
D2

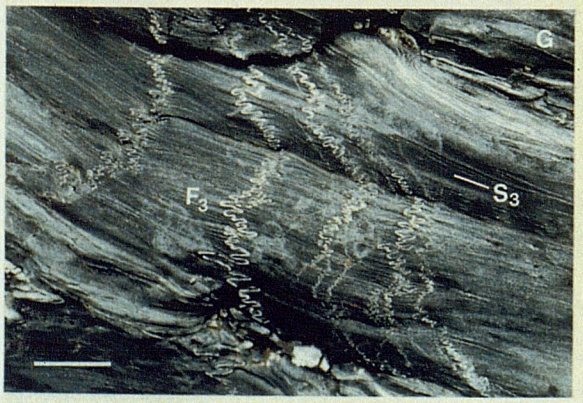
G
F3
S3

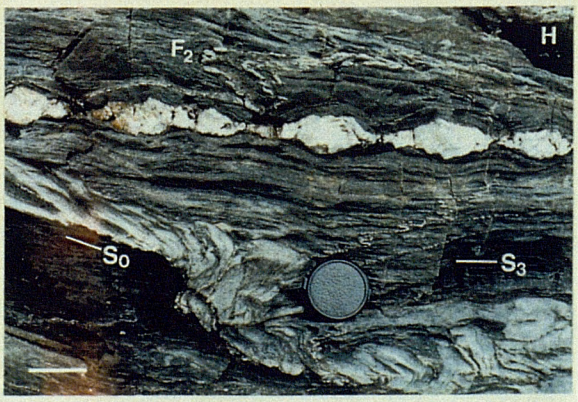
H
F2
S0
S3

Figure 1.4

Figure 1.4: Geological Maps

The following three pages are reproductions of field maps produced during the period October 1986 to October 1988. The three maps cover the coastal section from Tremearne to Church Cove, and are included sequentially from north to south. For the location of the area covered by the maps, see Fig. 1.1.

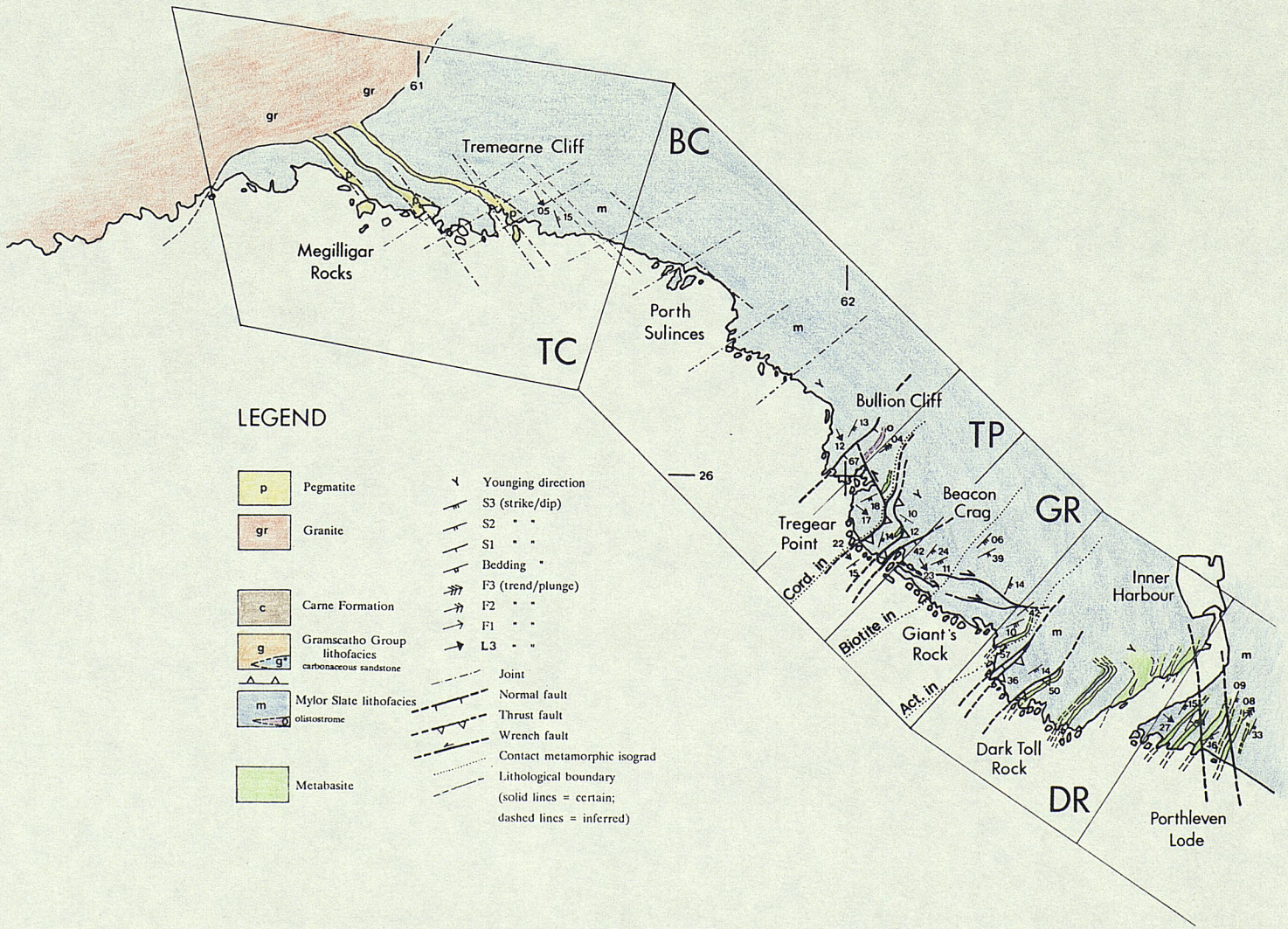
Tremearne Cliff
Megilligar Rocks
Porth Sulinces
Bullion Cliff
Tregear Point
Beacon Crag
Giant's Rock
Dark Toll Rock
Inner Harbour
Porthleven Lode
Cord. in
Biotite in
Act. in
BC
TC
TP
GR
DR
61
62
26
gr
p
m
LEGEND
Pegmatite
Granite
Carne Formation
Gramscatho Group lithofacies
carbonaceous sandstone
Mylor Slate lithofacies
olistostrome
Metabasite
Younging direction
S3 (strike/dip)
S2 " "
S1 " "
Bedding "
F3 (trend/plunge)
F2 " "
F1 " "
L3 " "
Joint
Normal fault
Thrust fault
Wrench fault
Contact metamorphic isograd
Lithological boundary
(solid lines = certain;
dashed lines = inferred)

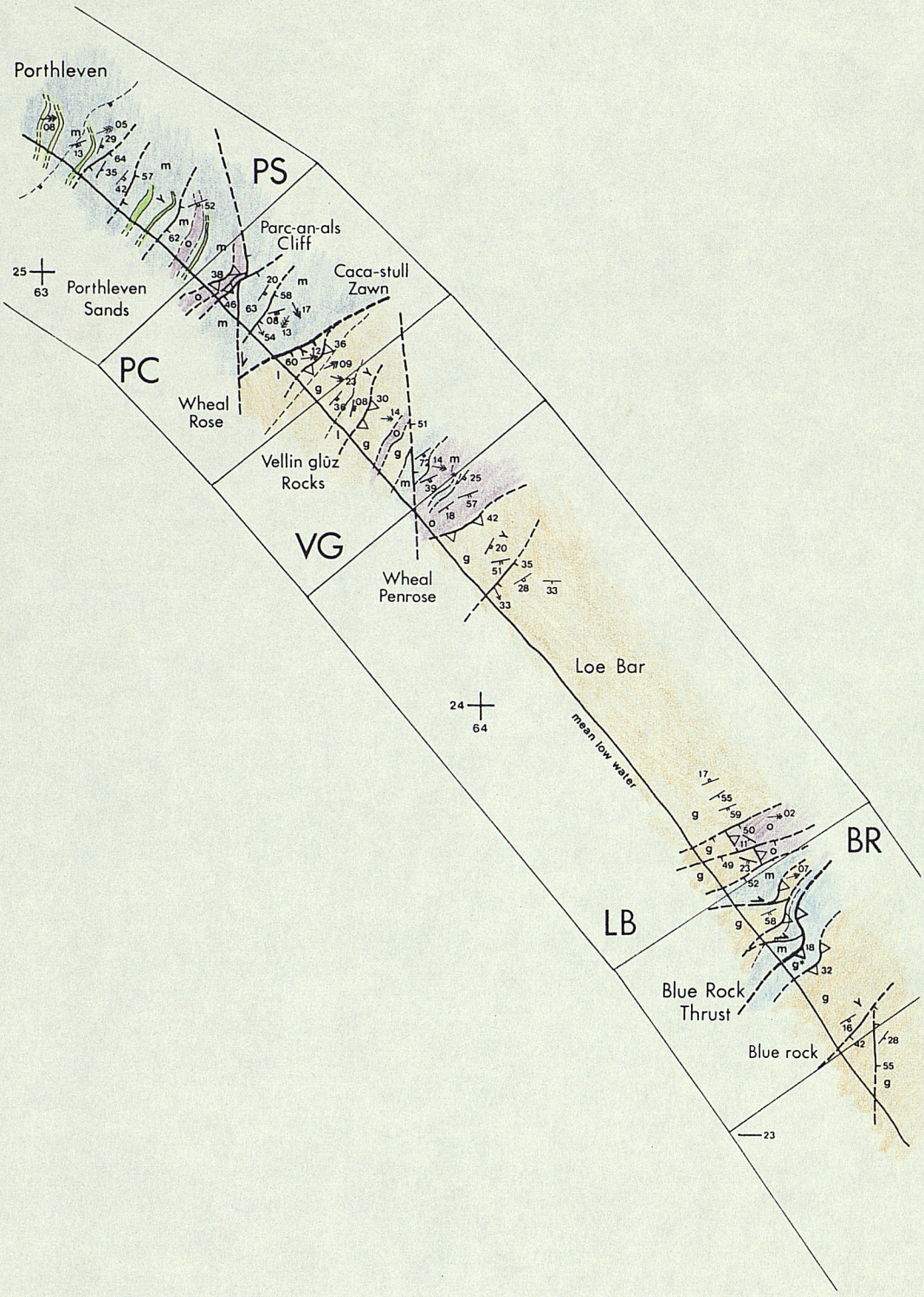
Porthleven
PS
Parc-an-als Cliff
Caca-stull Zawn
25
63
Porthleven Sands
PC
Wheal Rose
Vellin glüz Rocks
VG
Wheal Penrose
Loe Bar
24
64
mean low water
BR
LB
Blue Rock Thrust
Blue rock
23

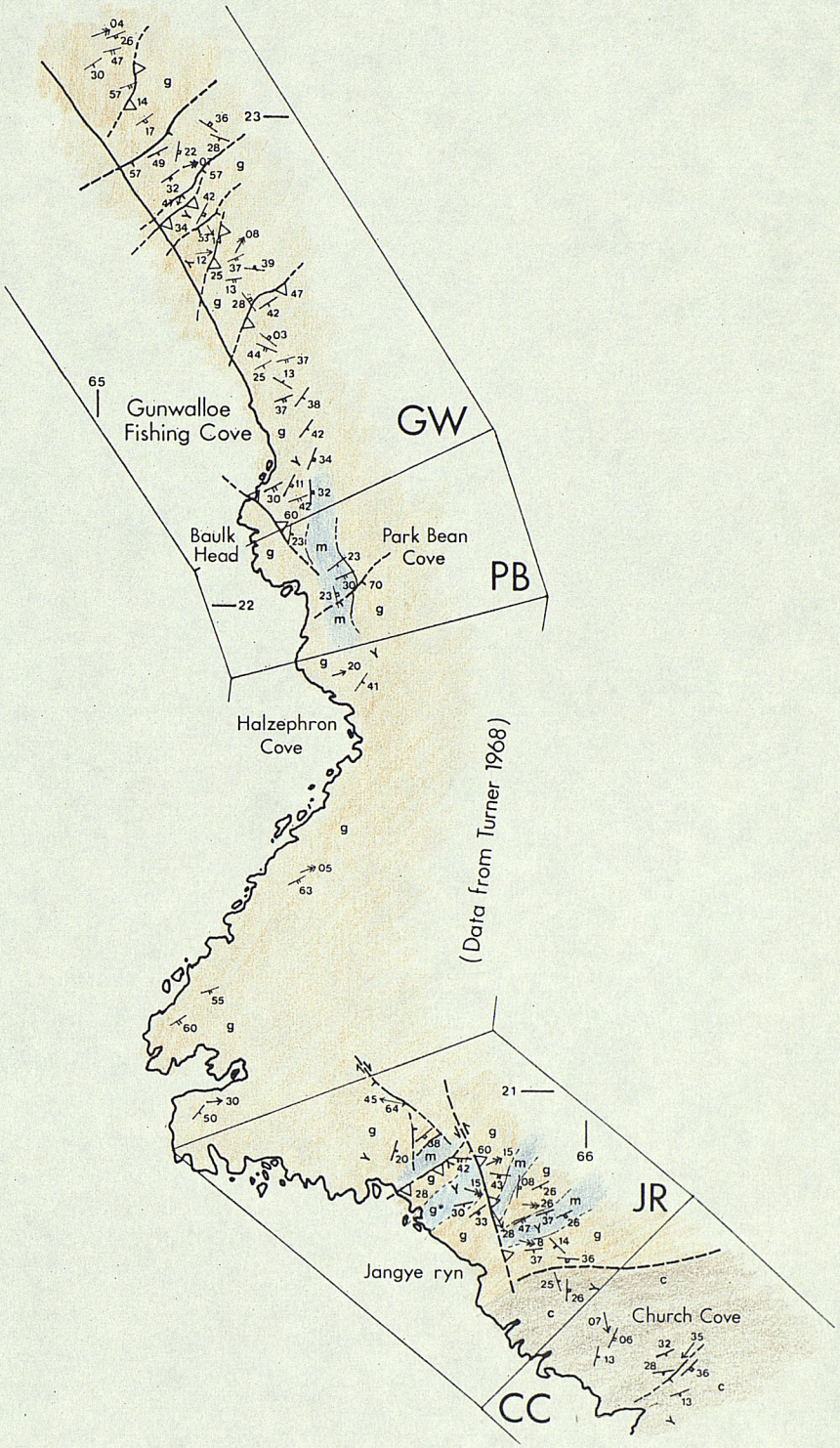
Gunwalloe
Fishing Cove
GW
Baulk
Head
Park Bean
Cove
PB
Halzephron
Cove
(Data from Turner 1968)
Jangye ryn
JR
Church Cove
CC
65
66
23
22
21

Mylor Slate Formation

The Mylor Slate Formation comprises dark grey or grey-green slates with thin, fine sandstone or siltstone bands. The common rhythmic alternation of these two lithotypes produces a distinctive striped appearance in outcrop (Fig. 1.3). Olistostromes up to 100m thick are common, particularly towards the top of the Formation, occurring as discrete units within bedded sequences. They comprise small, locally derived, matrix-supported phacoids generally less than 10cm long, set in a fine grained, slaty matrix and strongly flattened in the S1 cleavage.

These rocks are usually interpreted as basinal sediments distal from the terrigenous source (Wilson & Taylor 1976) with occasional turbidite incursions and slumping. They are believed to have been deposited in a deepening continental margin environment (Leveridge & Holder 1985). Oceanic turbidites of the Gramscatho Group were deposited to the south and were subsequently juxtaposed with the Mylor Slate Formation by movement on the Carrick Thrust (Figs. 1.1, 1.4).

The Formation is almost entirely devoid of recognisable microfossils. This is probably due to the distal environment, far from a diverse shelf-type planktonic fauna and palynomorph supply, and also to granite related thermal degradation. Poorly preserved acritarchs and spores have been recorded (Turner *et al.* 1979) suggesting a Famennian age for at least part of the Formation. Recent work by Wilkinson & Knight (1989) indicates a possible Late Famennian or younger age for the top of the Portscatho Formation, implying that the overlying Mylor Slate Formation extends into the Carboniferous.

1.3.2 Intrusive rocks

Mafic Sills

A series of metadiorite sills, known locally as greenstones, outcrop in the southern part of the Mylor Slate Formation near Porthleven (Fig. 1.4). They are up to 10m thick with contacts sub-parallel to bedding. Surrounding individual bodies are narrow contact metamorphic zones defined by the development of fine prismatic crystals, now pseudomorphs of chlorite and sericite probably after andalusite.

The sills display few relict igneous textures and are highly altered to chlorite, sericitised feldspars, epidote, pumpellyite, sphene, siderite and opaques. The significance of this predominantly regional metamorphic mineral assemblage is discussed in section 1.3.4. Closer to the granite (Giant's Rock, Tregear Point, Bullion Cliff) the greenstones show the development of biotite, fibrous actinolite and brown amphibole with increasing grade of contact metamorphism (see 1.3.4). The sills outcropping to the north of Tregear Point are variously mineralised with the development of pyrite, arsenopyrite, chalcopyrite, galena, sphalerite and ilmenite (see 1.3.5). Fine, prismatic arsenopyrite is the most abundant opaque phase.

Immobile element plots, based on bulk rock geochemistry carried out on the least altered sills, indicate that the rocks have alkalic chemical affinities, suggestive of intrusion in a continental back-arc extensional basin (Floyd 1972).

Granites

The Tregonning Granite, exposed in the north of the area (Fig. 1.4), is a late intrusion in the composite Tregonning-Godolphin stock (Stone 1975). The cupola was emplaced at a late magmatic stage, rising from the southern flank of the main Cornubian batholith.

The Godolphin Granite, which forms the northern and earliest part of the composite stock, is a fine porphyritic biotite granite (Stone 1975). The Tregonning granite, a non-porphyritic, Li/F-rich, topaz bearing variety, intruded the earlier Godolphin granite mass as well as extending further south into the Mylor Slates. It represents a late stage, highly evolved differentiate of the Cornubian magma and is extremely rich in alkalis (Li, K, Rb, Cs) and volatiles such as boron and fluorine.

Granite intrusion was accompanied by deformation and metamorphism of the metasedimentary country rocks. These phenomena are discussed in sections 1.3.3 and 1.3.4 respectively.

Pegmatites

A distinctive feature of the Tregonning granite, and observed elsewhere in the province (Badham 1980), is the presence of a well developed pegmatite-aplite complex in the roof zone of the stock. Lenticular, banded pegmatite-aplite bodies are developed along many subhorizontal or shallowly dipping granite contacts, indicating the importance of volatile "ponding" in their genesis. Extending out of the roof zone of the granite body, and traversing the hornfelsed slates of the contact aureole for 400m (Fig. 1.4), are a series of complex pegmatite-aplite sills (Stone 1969) which contain metasomatic K-feldspar megacrysts produced by the separation of a K-H_2O fluid from a pegmatite silicate melt (Badham 1980). Distal quartz veins occur at the terminations of the pegmatite-aplite sills, interpreted as being formed by crystallisation of a "spent" pegmatite aqueous fluid (see 2.2.11, 4.5.1).

1.3.3 Structural evolution

The importance of thrust tectonics in the geological evolution of south Cornwall has long been recognised. Flett (1933) and Hendriks (1937) were early proponents of thrusting as a significant deformation process in the area. Hendriks' concept of a major nappe structure produced by the emplacement of the Lizard Complex revolutionised structural interpretations of the region. More recently, Leveridge *et al.* (1984), Rattey & Sanderson (1984) and Holder & Leveridge (1986) produced models of the tectonic evolution of the province, with a variety of emphases. It is now generally accepted that major thrust nappe development had an important control on the distribution of the main lithostratigraphic units (*e.g.* Holder & Leveridge 1986).

Detailed structural work in the study area (Stone 1966; Turner 1969; Rattey 1980*a*) led to the recognition of three major phases of deformation. Both D1 and D2 relate to Hercynian compression and thrust tectonics, whereas D3 is believed to accompany intrusion of the Cornubian batholith (Turner 1969; Rattey 1979). A number of late, relatively minor phases of deformation have also been recognised (*e.g.* Smith 1965; Rattey 1980b).

D1 Deformation

The first phase of deformation identified in south Cornwall is characterised by tight to isoclinal, NNW-verging folds (F1) with subhorizontal or gently ENE- or WSW-dipping axes. The folds predominantly face upwards to the NNW, except in zones of intense D2 refolding. Fold style is strongly lithology dependent, with tight chevron folds developed in the Gramscatho Group (Fig. 1.3) and tight to isoclinal, often disharmonic folds with rounded hinges in the Mylor Slates (Fig. 1.3). Associated with the folds and subparallel to their long (right-way-up) limbs is a regionally developed, gently SSE-dipping cleavage (S1). Previously unrecorded, low angle D1 thrusts are present throughout the sequence. Slickenside striae developed in quartz on these fault planes are sub-parallel to the weak stretching lineation observed on S1 surfaces (L1) and indicate reverse dip-slip movement. The relationships between D1 structures and fabric elements are shown in Figure 1.5.

In hand specimen, the S1 fabric is manifest as a penetrative slaty cleavage in pelitic lithologies, and as a spaced, pressure solution fabric in psammites. In thin section, the slaty cleavage is generally domainal on a mm-scale (Rattey & Sanderson 1984; Hobbs *et al.* 1976) with dark seams of mica, chlorite and opaques alternating with quartz-rich bands. The pressure solution cleavage is typified by anastomosing seams of opaques and phyllosilicates with a spacing of 1-10mm. This spacing decreases with decreasing sandstone grain size and increasing deformation intensity. The phyllosilicate-rich seams separate zones dominated by detrital quartz, feldspar and lithic grains. Quartz grains in these regions display shape modification as a result of pressure solution. The common occurrence of pressure shadows around framework grains also testifies to the importance of pressure solution as a deformation mechanism (*e.g.* Beach 1979).

Several zones of oblique F1 folds have been recorded, with N-S trending axes and moderately inclined axial planes (Fig. 1.5). First described by Dearman (1969), they have been interpreted as initiating in zones related to differential movement of Lizard Complex thrust sheets during D1 (Rattey & Sanderson 1984). The oblique D1 folds observed in the field area are spatially and geometrically related to lateral ramp structures. Similar relationships, although on a smaller scale, are displayed by D2 structures (see below). In an extension of the ideas of Rattey & Sanderson (1982, 1984), it is here suggested that the folds were rotated from the regional trend as a result of lateral shear, locally developed in proximity to sidewall ramp structures in the deforming flysch sequence.

This interpretation holds on all scales, from metre-scale zones of oblique folding in the hangingwall of minor lateral ramps in the field area, to a kilometre-wide zone of oblique folds associated with a major sidewall ramp in the "Carrick Thrust" near Truro, mapped by Holder & Leveridge (1986). The sequential stepping and apparent sinistral movement across the major structures may be interpreted as antithetic faulting in response to a small component of dextral shear across the belt during continental collision.

K-Ar dating of micas from the Portscatho Formation at Gunwalloe, as well as elsewhere in south Cornwall, suggests an early Viséan age (*c.* 350 Ma) for closure through the K-Ar blocking temperature (Dodson & Rex 1971). This cooling age, combined with the Late Famennian age recorded for sediments affected by D1 in the section (Wilkinson & Knight 1989), constrain D1 to the Lower Carboniferous.

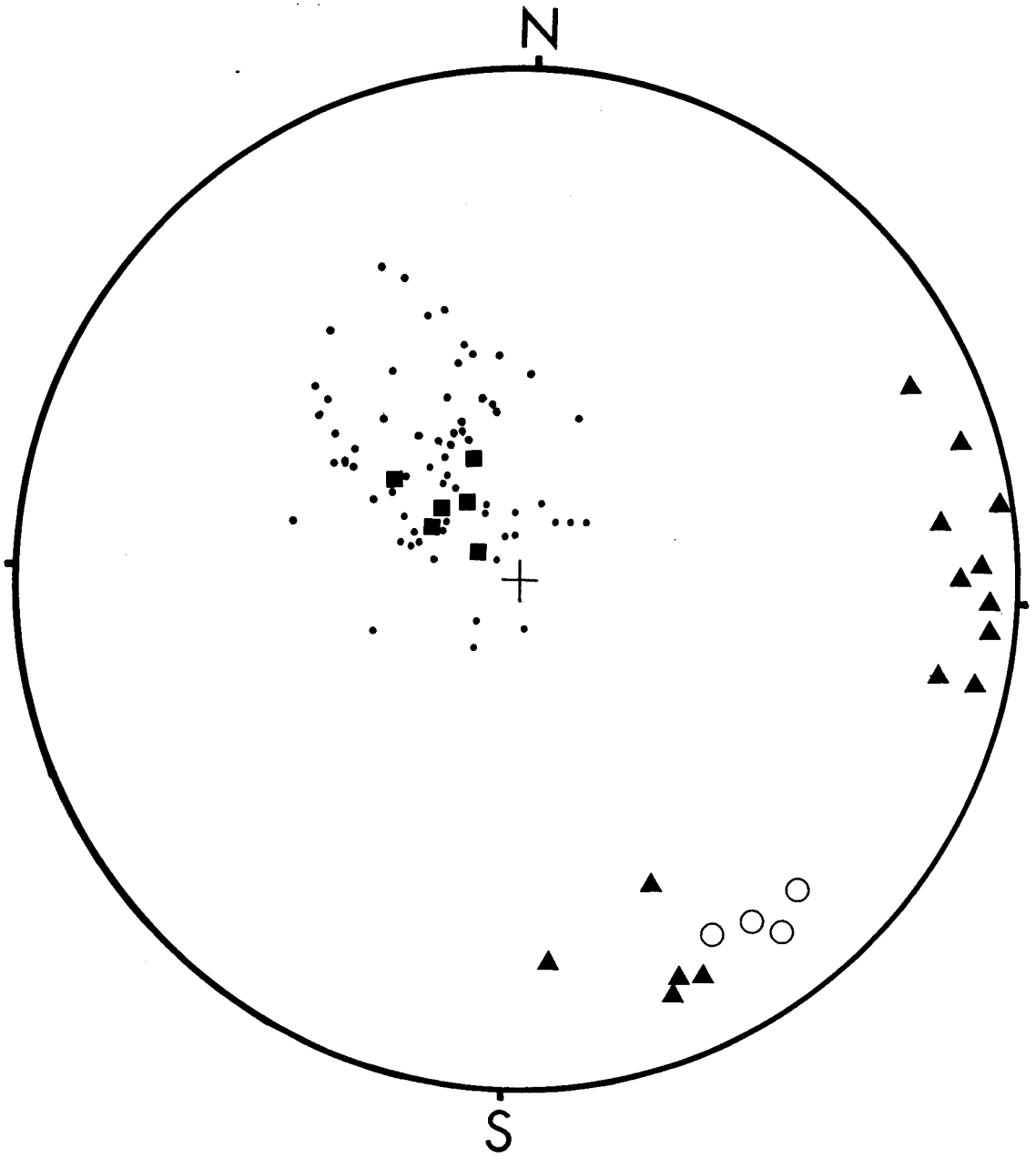

Figure 1.5 Equal area stereographic projection showing D1 structural elements. Dots = poles to S1, squares = poles to D1 thrust planes, triangles = F1 fold axes, open circles = slickenside striae on D1 thrust planes.

D2 Deformation

Throughout southwest Cornwall, a second phase of deformation was superposed coaxially with F1 structures. It was first recognised by Smith (1965) between Hayle and Portreath on the north Cornish coast, and subsequently established as a regional deformation phase (Sanderson 1973; Rattey 1980*b*).

F2 folds in the field area are moderately inclined, NNW-vergent, open to close structures with ENE-WSW trending subhorizontal axes. Fold axial planes dip shallowly to steeply SSE and are sub-parallel to an S2 crenulation cleavage. This fabric finely crenulates S1 in pelitic horizons, but

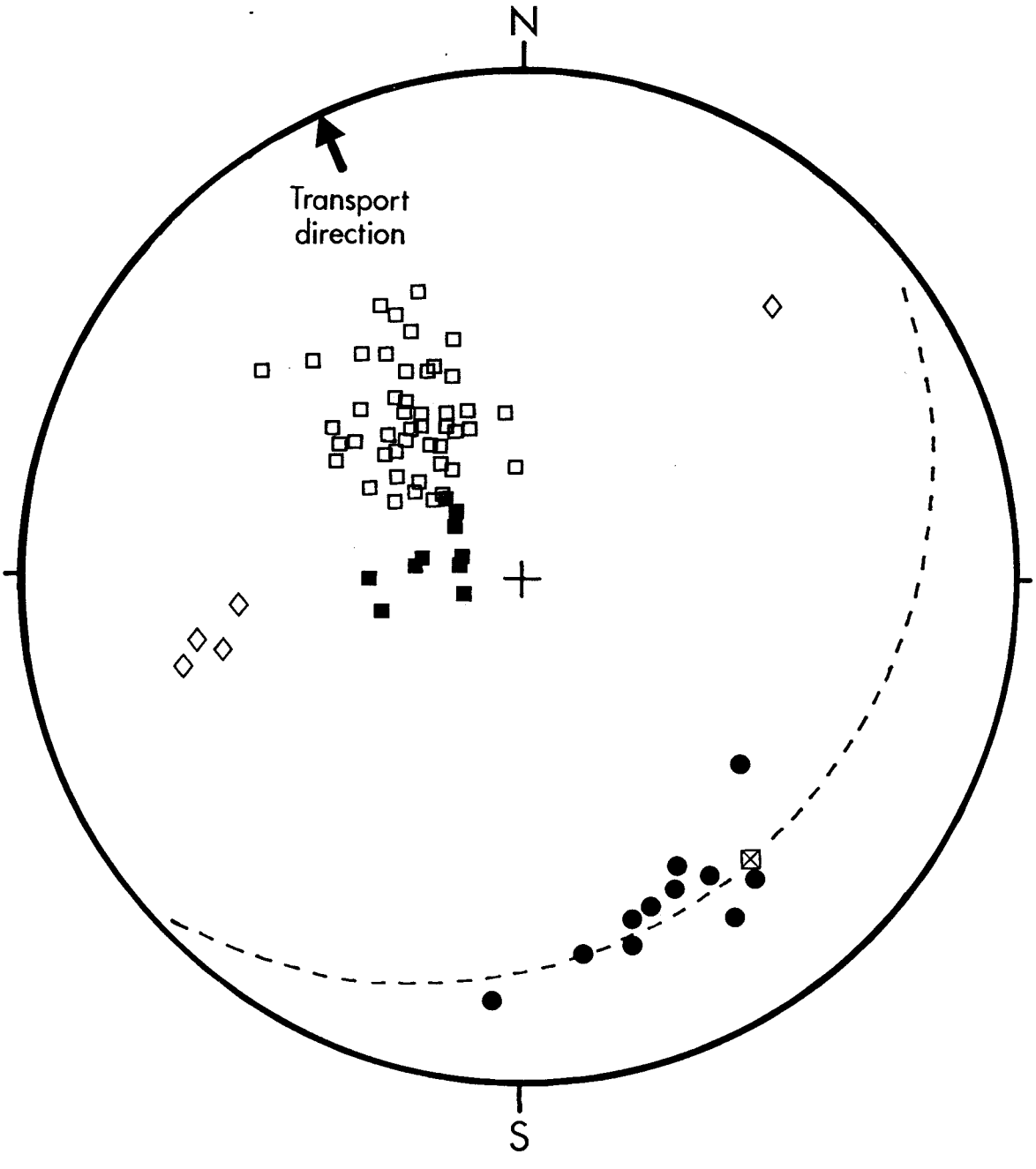

Figure 1.6 Equal area stereographic projection showing D2 structural elements. Open and filled squares=poles to D2 thrust ramps and flats respectively, diamonds=poles to lateral ramps, circles=slickenside striae on D2 thrust planes, square box with cross=average down-dip direction.

in sandstones is very similar to S1, comprising spaced, anastomosing pressure solution seams.

D2 thrust ramps are commonly observed in the field because of the locally intense associated deformation. Low angle "flats" have also been recorded but are less common (Fig. 1.6). The field observations suggest that the development of a leading imbricate fan system (Butler 1982) was responsible for producing D2 structures. The apparent absence of D2 duplexes may merely be a result of the limited vertical exposure, in which case a hinterland dipping duplex model (Butler 1982)

would be more appropriate. Such a duplex would probably be soled by the "Carrick Thrust" and roofed by the Lizard Boundary Thrust (Fig. 1.7).

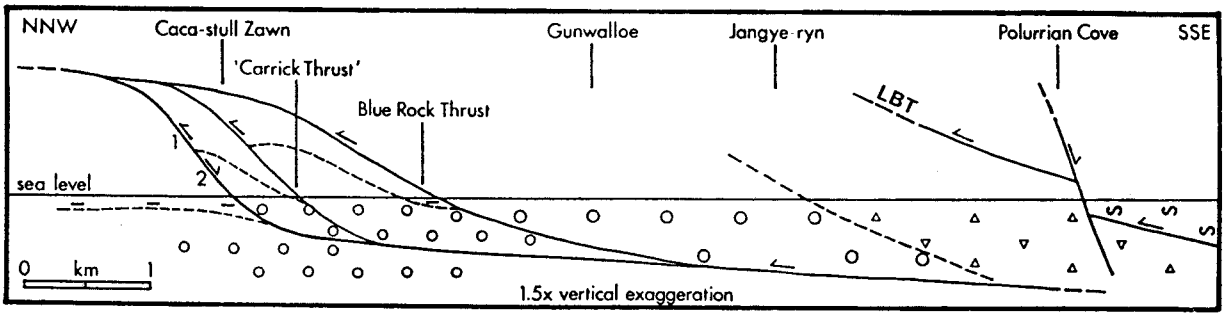

Figure 1.7 Simplified interpretative cross-section, constructed perpendicular to regional strike (from Wilkinson & Knight 1989). Dashes=Mylor Slate Fm., small circles=Portscatho Fm. (transitional), large circles=Portscatho Fm., triangles=Carne Fm., squiggles=Lizard Complex, LBT=Lizard Boundary Thrust.

Where S2 is well developed, a weak stretching lineation (L2) may be observed. L2 is generally subparallel to slickenside striae on D2 thrust planes (Fig. 1.6) and has a similar trend to L1, but a steeper SSE plunge. The lineations are consistent with NNW-directed reverse, dominantly dip-slip motion on D2 thrust ramps. A slight sinistral component of movement is suggested by the slickenside striae data (Fig. 1.6).

The intensity and attitude of D2 structures varies locally and is clearly related to proximity to D2 thrusts. Several broad zones of high D2 strain have been delineated. Rattey (1980*b*) and Rattey & Sanderson (1982) identified two main D2 "shear zones" in the field area, where S2 shallows and crenulates S1 more intensely. A zone of low angle D2 shear immediately north of the Lizard Complex resulted in extension of bedding and little refolding (Rattey & Sanderson 1982). Higher angle D2 thrusting further north (Wilkinson & Knight 1989) resulted in shortening of bedding (except on steep inverted limbs of F1 folds), and abundant F2 folding. The area most affected by D2 deformation in the section is between Caca-stull Zawn and Loe Bar (Fig. 1.4), at the allochthon thrust front (Wilkinson & Knight 1989). Much of the stratigraphic complexity in this zone results from extensive D2 imbrication.

D3 Deformation

An intense, flat-lying crenulation cleavage (S3), axial planar to minor recumbent folds (F3), is well developed in the north of the area (Fig. 1.3). North of Porthleven, this cleavage becomes dominant, transposing earlier fabrics. These D3 structures, first described by Stone (1966, his F2, S2) from Porthleven and Smith (1965) from the north coast, have been shown by subsequent work (Turner 1969; Rattey 1980*a*) to be confined to the roof zone and flanks of the Cornubian batholith. The spatial and geometric relationships between D3 structures and the batholith suggest that D3 was the result of granite emplacement. A summary of D3 structural data is presented in Figure 1.8.

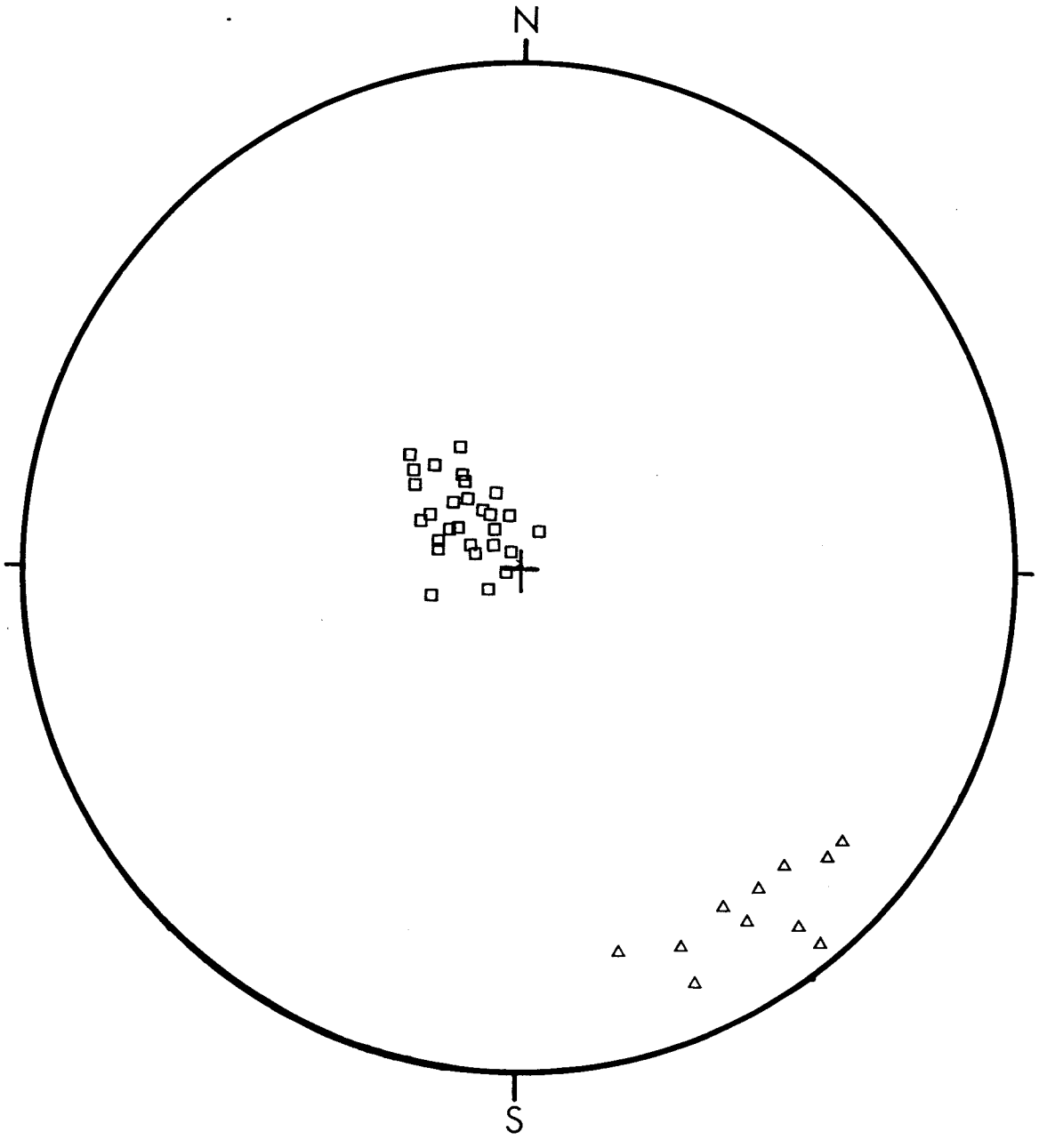

Figure 1.8 Equal area stereographic projection showing D3 structural elements. Squares=poles to S3 cleavage, triangles=L3 mineral lineation on S3 surfaces.

F3 folds are only developed on steeply inclined limbs of earlier structures, giving rise to distinctive interference patterns (Figs. 1.3, 1.10). In the field area, they invariably verge to the southeast, directly away from the granite. Rattey (1980*a*) showed that F3 vergence is always directed away from granite apophyses, indicating a component of concentric simple shear contemporaneous with the radial compression responsible for S3 formation (Fig. 1.9). It may be concluded that irregularities were developed in the roof of the batholith during D3. Some of these "highs" acted as sites for subsequent intrusion of highly differentiated magmas (*e.g.* the Tregonning Granite).

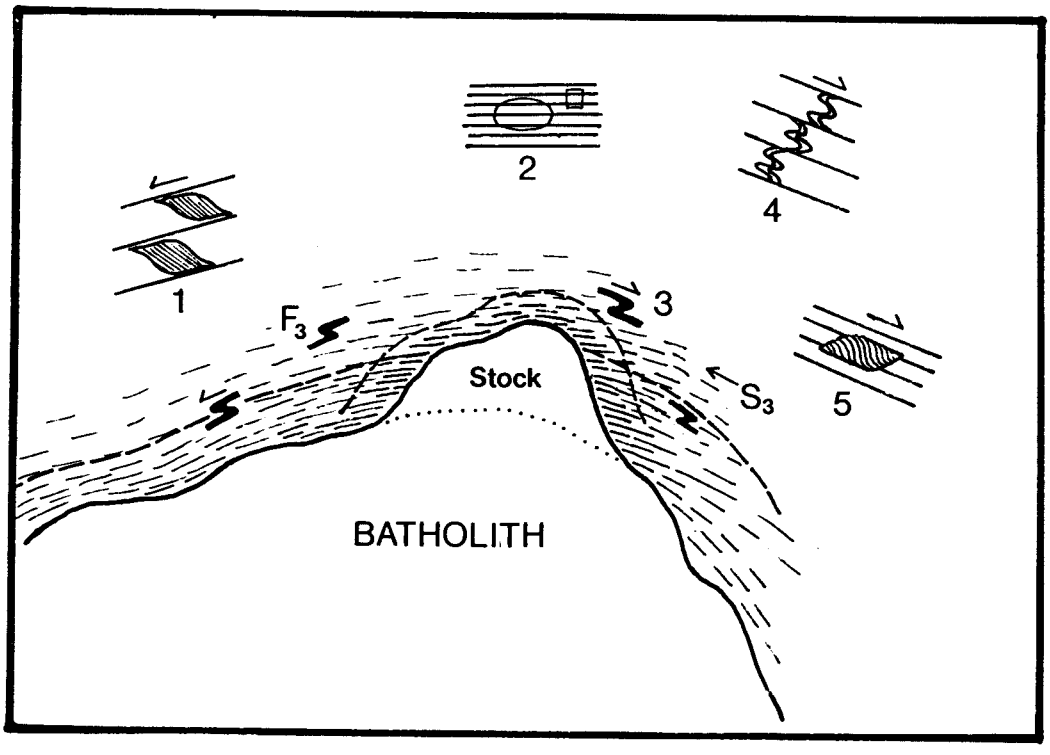

Figure 1.9 Summary diagram illustrating relationships between D3 microstructures and the Tregonning stock. 1. Asymmetric mica fish, 2. Post-tectonic cordierite and andalusite porphyroblasts, 3. Vergence of F3 folds, 4. Offsets across S3 pressure solution seams, 5. Asymmetric included fabrics.

Evidence supporting syn-D3, S3-parallel shear comes from offsets of early veins and bedding across cleavage surfaces (Fig. 1.3) and a variety of microstructures (Fig. 1.9). In the section, these offsets always show a top-to-the-south sense consistent with concentric stretching over the batholith during emplacement. These features are consistent with an in situ ballooning mechanism for granite intrusion (Bateman 1985), which has been closely approximated by experimental modelling (Dixon 1975). Late D3 vein and fault arrays in the contact aureole (see 2.2.9-10) suggest that magma was intruded by faulting and shearing of the host rocks towards the end of D3. A similar process has been proposed for intrusion of a late lobe of the Arran Granite, Scotland (Woodcock & Underhill 1987)

A weak to strongly developed stretching lineation (L3) is present on S3 surfaces. Cordierite porphyroblasts, which grew syntectonically, are elongated parallel to L3 (Fig. 1.10). The lineation trends SSE (Fig. 1.8) and is at its most intense on the flanks of the batholith. Both these features are accurately predicted by the experimental modelling of Dixon (1975). A strain estimate made using the Fry method (Fry 1979), on a sample containing syntectonic cordierite porphyroblasts, gave a D3 finite strain ellipsoid with axial ratios 2.4:1.4:1. This falls just in the constriction field (Flinn 1962) and represents 61% extension in X, 6% constriction in Y and 33% constriction in Z (assuming no volume change). If no mimetic growth occurred, this would represent a minimum estimate of the total D3 strain since it does not include any strain suffered prior to nucleation of cordierite crystals.

Figure 1.10

Figure 1.10: Captions

A. Normal fault showing ≈50cm displacement of sandstone units, Portscatho Formation, Jangye-ryn Cove. Viewing direction: E; Scale bar = 50cm.

B. Coaxial refolding of F1 isoclinal fold during D2. Minor F3 folds are developed on steep limbs of earlier folds, Mylor Slate Formation, Caca-stull Zawn. Viewing direction: ENE; Scale bar = 10cm.

C. Cordierite porphyroblasts, elongated parallel to the L3 stretching lineation, on an S3 cleavage surface, Mylor Slate Formation, Giant's Rock. Viewing direction: ENE; Scale bar = 2cm.

D. D3 detachment, parallel to S3 crenulation cleavage. Note minor F3 folds, picked out by bedding and thin, pre-D3 quartz veins, Mylor Slate Formation, Giant's Rock. Viewing direction: E; Scale bar = 4cm

E. Photomicrograph of post-tectonic elongate andalusite and rounded cordierite porphyroblasts, Mylor Slate Formation, Tremearne Cliff. Section parallel to S3 fabric; Scale bar = 1mm.

F. Photomicrograph of syn-tectonic cordierite porphyroblasts, developed in ?olistostrome, Mylor Slate Formation, Tregear Point. XZ-section; Scale bar = 1mm.

G. Photomicrograph of S3 pressure solution seams displacing detrital quartz grains and cross-cutting S1 fabric, silty layer, Mylor Slate Formation, Tregear Point. XZ-section, viewed from the WSW; Scale bar = 100μm.

H. Photomicrograph of S3 crenulation cleavage, axial planar to folded mafic layer and penetrative S1 fabric in siltstone, Mylor Slate Formation, Tregear Point. Note development of contact metamorphic actinolite and biotite. XZ-section, viewed from the ENE; Scale bar = 1mm.

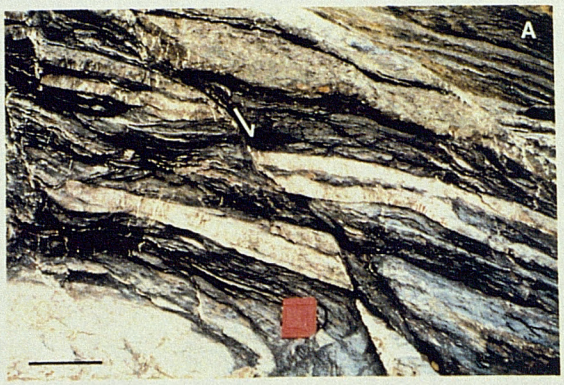
A


B
F_2
$S_{0/1}$
F_1
S_3
S_2

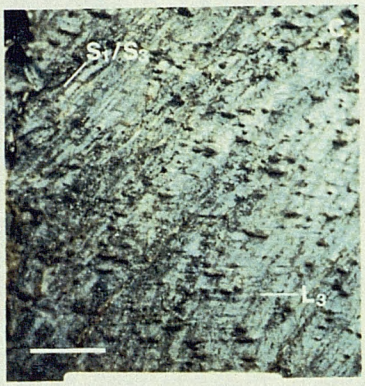
S_1/S_2
L_3

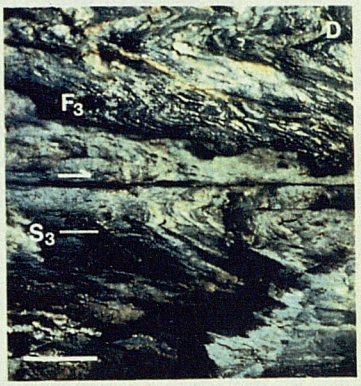
D
F_3
S_3

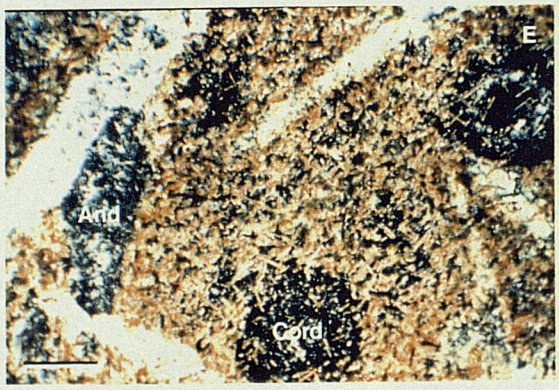
E
Arid
Cord

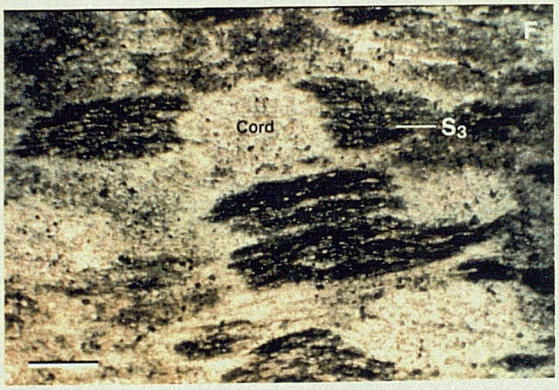
F
Cord
S_3

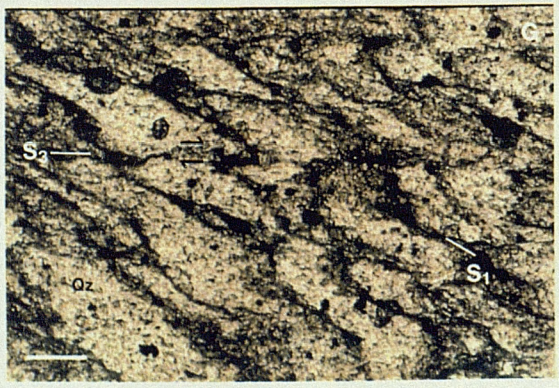
G
S_2
Qz
S_1


H
Bi
S_3
Act
$S_{1/2}$

Exposed contacts between the Tregonning granite stock and the slates are steep and crosscut the S3 fabric (Fig. 1.9). However, the cleavage dips radially away from the stock (Fig. 1.9) suggesting that either there was a pre-existing granite apophysis or stock emplacement was accompanied by slight doming of an earlier S3 fabric. There is a lack of deformation at the contacts which suggests that the final stages of emplacement were via passive stoping.

The late stocks exposed in Cornwall, including the Tregonning-Godolphin cupola, crosscut S3 and thus postdate D3. Rb-Sr dating of the Tregonning granite at 280±2 Ma (Darbyshire & Shepherd 1987) provides a minimum age for D3 in the area. A K-Ar age of 295 Ma for dolerite dykes at Meldon, Devon, contact metamorphosed by the Dartmoor granite (Hawkes & Dangerfield 1978) and a similar K-Ar age of 292 Ma for contact metamorphosed slates at Porthleven (Miller & Mohr 1964) suggest a Stephanian age (Harland *et al.* 1981) for the deformation (*c.* 300-290 Ma).

Normal Faults

Normal faults are common throughout the section. Abundant crosscutting relationships indicate that they post-date D3. The brittle deformation and open cavity vein fillings associated with the faults (see 2.2.14) suggest that, at the current level of exposure, they formed at low temperatures (*c.* 200°C) and at a high level in the crust (<3km).

The faults invariably dip SSE, generally at 30-60° (Fig. 1.11), with steeper structures usually post-dating shallower ones. This is consistent with observations made in active extensional areas, where extension is known to result in rotation of faults to shallower angles (Jackson & McKenzie 1983). When first phase faults are rotated to *c.* 30°, the contribution of gravity is insufficient to allow further slip on the fault plane. New, steep faults then propagate (Morton & Black 1975; Jackson & McKenzie 1983) and the first generation faults become inactive.

Reactivation of thrusts is also a common phenomenon in such terrains (*e.g.* McKenzie 1978). Brittle, normal reactivation of thrusts is sometimes observed in the study area, particularly in the case of steeper D1 or D2 thrust ramps. The relative scarcity of late normal faults in the southern part of the study section (Fig. 1.4) suggests that much of the early post-orogenic extension was taken up by slip along pre-existing structures. This interpretation is supported by seismic studies by Day (1985) who recognised back-slip on Hercynian thrusts during development of Permo-Triassic basins to the south of the Cornubian Peninsula.

Wrench Faults

A series of NNW-SSE trending wrench faults cut through the area, some of which contain base metal mineralisation (see 1.3.5). The age of these structures is uncertain, although at least some movement occurred post-D3. Their orientations, parallel to Tertiary dextral wrench faults developed throughout southwest England (Dearman 1963) suggest that at least some movement may have occurred during the Tertiary. There is much evidence of reactivation, both in the study area and elsewhere in southwest England. Some of the structures may have initiated as transfer faults during Hercynian compression (*e.g.* Holloway & Chadwick 1986; see 2.2.14).

Fluid inclusion data suggest that the wrench faults were active during mainstage sulphide mineralisation (Shepherd & Scrivener 1987; see section 4.6). This would equate with their initiation or reactivation as dextral transfer faults during the early development of Permian basins to the south

of the Cornubian Peninsula (see 6.1.5).

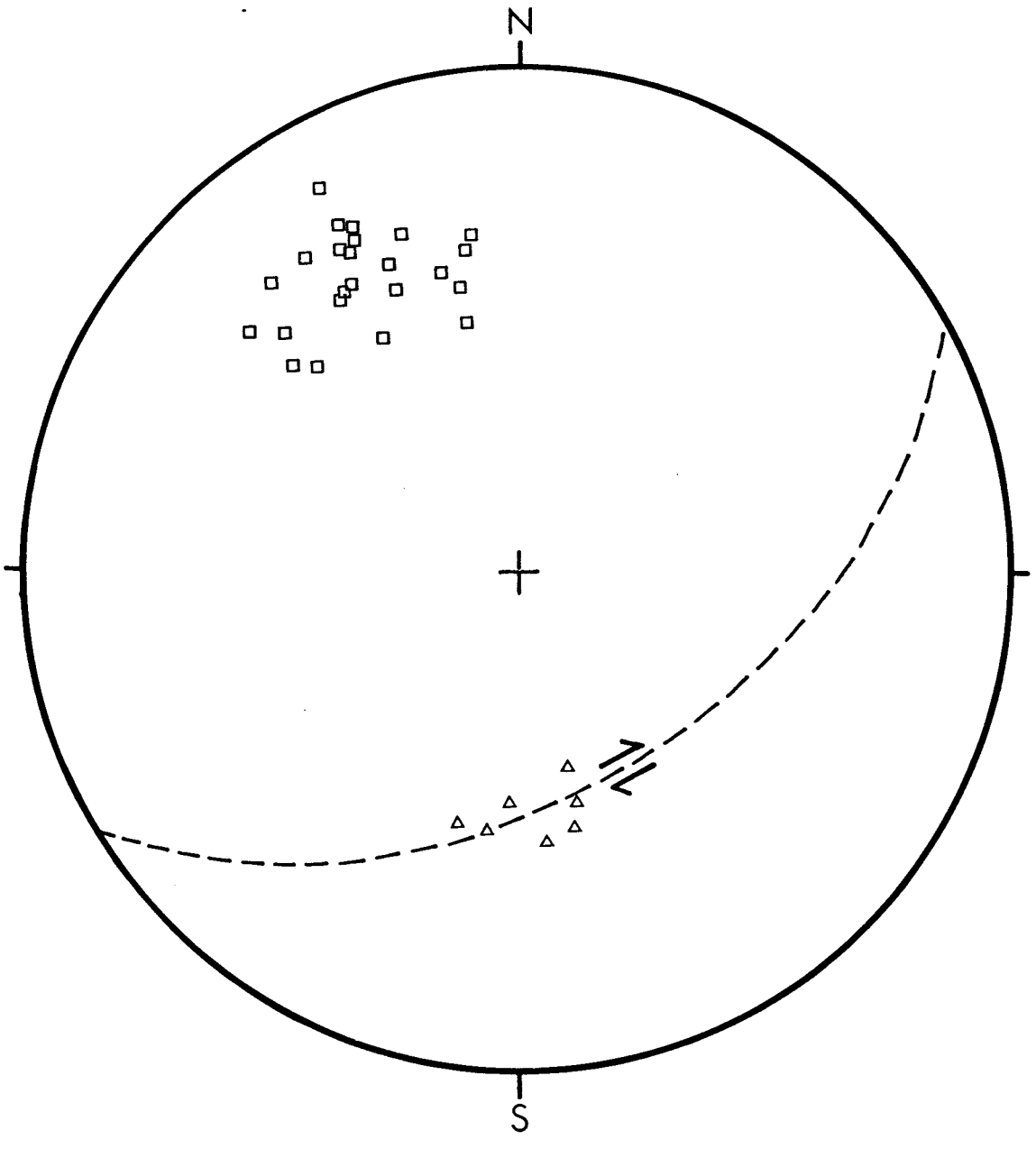

Figure 1.11 Equal area stereographic projection showing normal fault structural data. Squares=poles to fault planes, triangles=slickenside striae, dashed line=average fault plane and sense of oblique slip.

Also observed in the area, and sporadically developed throughout south Cornwall, are a series of open, upright folds which clearly postdate D3. Axial planar to these folds is a steep NNW-SSE trending crenulation cleavage. Another E-W trending crenulation cleavage has also been described by Smith (1965, her D5) from the north coast. The spatial and geometric relationships between these structures and the wrench fault zones described above has been noted by previous workers (*e.g.* Rattey & Sanderson 1984). However, Rattey & Sanderson (1984) considered that there was no genetic relationship, suggesting the wrench faults required N-S compression whereas the NNW-SSE

crenulations were formed under ENE-WSW compression. They concluded that the wrench faults reactivated earlier NNW-SSE trending crenulation/fold zones. The E-W trending crenulation cleavage was considered to be unrelated to both of the other deformation events.

Fluid inclusion data reported in section 3.2.8 and discussed in 4.6 suggests that contemporaneous movement occurred on the dextral wrench faults and on the normal faults described in the previous section. It is possible that E-W trending structures, formed during granite emplacement, were reactivated as sinistral antithetic faults during the wrench faulting episode. Evidence of sinistral shear across mineralised E-W lodes has been recorded (*e.g.* Farmer 1988), as well as oblique sinistral movement on normal faults in the study area (Fig. 1.11). These observations lend support to the regional interpretation. The above discussion implies a close temporal relationship between movement on the NNW-SSE trending mineralised wrench faults ("cross-courses") and mainstage lode formation. Fluid inclusion data also suggest that such a relationship may exist (Shepherd & Scrivener 1987; section 4.6).

1.3.4 Metamorphism

Regional metamorphism

It has long been recognised that low grade regional metamorphism affected south Cornwall during the Hercynian orogeny (*e.g.* Reid 1907). Since only low temperatures were reached in dominantly pelitic or psammitic rocks, metamorphic studies have been rather difficult. It is only relatively recently that advances in our understanding of low grade mineral assemblages and the thermodynamic and kinetic controls of their formation have been made. These studies have made possible the estimation of low grade metamorphic conditions, in terms of the peak temperatures and pressures reached.

Metabasic lithologies are the most sensitive to low temperature metamorphism, and hence show the best developed and most diagnostic mineral assemblages. Consequently, much of the information regarding regional metamorphic conditions in south Cornwall comes from these rocks. Reid (1907) and Flett (1946) were the first to recognise the chlorite + sericite + albite ± actinolite ± carbonate assemblages as resulting from low grade metamorphism, although the alteration was originally thought to be due to sub-aqueous spilitisation of extruded magmas.

More recently, Barnes and Andrews (1981) identified pumpellyite and prehnite as well as actinolite, albite, clinozoisite, carbonate, chlorite and sericite in metabasic lithologies. The occurrence of these minerals in D1 veins, pressure shadows and growing sub-parallel to S1 led them to conclude that the peak of metamorphism was contemporaneous with D1.

The greenstones in the field area (see 1.3.2) were studied under transmitted light, and are composed predominantly of chlorite, sericite, albite, epidote, carbonate and opaques. Fine grained pumpellyite has been tentatively identified. Such an assemblage is comparable with those described from mafic phacoids in the Roseland Breccia Formation and Carne Formation (Barnes & Andrews 1981; Barnes 1982).

Barnes & Andrews (1981) described similar assemblages from the arenites in south Cornwall. Electron microprobe analyses showed that detrital plagioclase has been albitised (anorthite<0.6%)

and commonly contains flecks of pumpellyite, sericite and chlorite. Phyllosilicate-rich seams defining the S1 fabric (see 1.3.3) contain chlorite and sericite. In a number of areas (Jangye-ryn, Blue Rock) carbonate is abundant, cementing detrital grains, and has been shown by staining and X.R.D. in this study (see 3.6) to be siderite or ankerite.

Pumpellyite from the metabasites is typically aluminium-rich (Barnes & Andrews 1981), signifying a relatively high temperature of formation. The association with actinolite suggests regional metamorphism in the pumpellyite-actinolite facies, at temperatures between 250 and 350°C (Coombs *et al.* 1976). Supporting evidence from conodont colour (>300°C) and a meta-anthracite coal described from Pendower Beach (Cook *et al.* 1972), interpreted as forming at *c.* 350°C, indicate that peak metamorphic temperatures were in the range 300-350°C. Recent vitrinite reflectance work from the Loe Bar-Porthleven section (Fig. 1.4) indicates peak temperatures of 320-344°C (R.R.W. Knight, pers. comm. 1989).

The coexistence of pumpellyite and actinolite suggests pressures in excess of 3 kbar during peak metamorphism. This is consistent with fluid inclusion data (see 4.2.1) which indicate that D1 fluid pressures were of the order of 3-4 kbar. Since it is common for $P_F = P_L$ under such conditions, this pressure range is considered to be a good estimate of P_L during metamorphism, indicating an overburden of *c.* 13 km (see 6.1.1).

Contact Metamorphism

A large proportion of the rocks forming the peninsula of southwest England have been affected by the high heat flow accompanying emplacement of the Cornubian batholith. This is particularly true in south Cornwall, where only the most southern coastal exposures have been unaffected. The metamorphic aureole mapped by the British Geological Survey (Sheets 351, 352) in the field area extends as far south as Loe Bar, approximately 4km from exposed granite (Fig. 1.4). The thermal anomaly is very similar in extent to the contemporaneous D3 deformation envelope which was also produced during granite intrusion (see 1.3.3).

Two phases of contact metamorphism have been recognised (Rattey 1980*a*) and their distinction is important in understanding the mineral-fabric relationships in the affected rocks. The two stages are also significant in the early stages of granite-related fluid evolution (see 4.4).

A broad thermal anomaly, characterised by moderate thermal gradients, accompanied intrusion of the main batholith. This resulted in widespread devolatilisation of the host pelites and metabasites, recrystallisation, and new mineral growth (syn-D3). Spotted pelites, produced by cordierite and/or andalusite growth, are observed in the study area (Fig. 1.10). Most spots have an ellipsoidal form and are now chlorite, pinnite and quartz pseudomorphs, probably after cordierite (Fig. 1.10). Some have a rhombic cross-section and are pseudomorphed by sericite and quartz; these were probably originally andalusite. Both porphyroblast types overgrow a pre-existing fabric (Fig. 1.10), either S1 or early S3 (Fig. 1.10). This fabric is misoriented with repect to the foliated matrix and suggests that rotation has occurred. The presence of pressure shadows around the porphyroblasts and microfolds nucleating against them indicate that D3 continued after crystal growth. Asymmetry in these microstructures, in addition to asymmetric mica fish and vein or bedding offsets across S3 cleavages (Fig. 1.10), consistently indicate a top-to-the-SSE shear sense (Fig. 1.9), in agreement with macrofold vergence and S3-parallel displacements (see 1.3.3).

Nearer to the Tregonning Granite, porphyroblasts overgrow S3 and show no evidence of D3 deformation (Fig. 1.10). Apparent flattening within the S3 plane is the result of preferential growth, rather than deformation. The spots are not elongated parallel to L1, unlike the syntectonic porphyroblasts. At Tremearne (Fig. 1.4) square-section andalusite needles are observed in conjunction with cordierite (Fig. 1.10). The occurrence of andalusite is strongly lithology dependent; it only occurs in discrete horizons where cordierite is noticeably subordinate. This may be the result of variations in the primary iron content of the sediments, with Fe-rich horizons favouring cordierite growth and inhibiting andalusite.

Post-tectonic porphyroblast growth is the result of higher temperatures, higher thermal gradients and more localised metamorphism associated with the emplacement of the Tregonning stock (see 1.3.2). Figure 1.5 illustrates the spatial distribution of the two metamorphic domains and shows the development of an outer contact zone, characterised by syntectonic spotting; an intermediate zone of mixed syntectonic and post-tectonic spotting; and an inner zone where only post-tectonic spotting is observed.

Other minerals developed during contact metamorphism include new white mica, chlorite, biotite, ilmenite, tourmaline, albite, epidote, actinolite and a brown amphibole. At higher grades, K-feldspar is also observed. Chlorite is well developed at lower grades, particularly in mafic lithologies. It also occurs as a late retrogression product of amphiboles and biotite. Actinolite, epidote and albite are mainly restricted to the basic sills, although actinolite is sometimes observed in thin, mafic, bedding-parallel horizons, tentatively identified as tuff layers (Fig. 1.10). Biotite is common in the metabasites, but also occurs as small porphyroblasts in the pelites. A rare, brown amphibole, overgrown by acicular actinolite, has been observed in one sill at Tregear Point (Fig. 1.4). Fine-grained tourmaline and ilmenite are abundant, being concentrated in the phyllosilicate-rich bands defining S3. Approximate isograds marking the introduction of some of these phases are shown in Figure 1.4.

The occurrence of pervasive fluid flow along S3 during contact metamophism is suggested by the presence of disseminated mineral phases such as arsenopyrite, tourmaline and ilmenite, distributed along the S3 cleavages and apparently unrelated to quartz veins. This interpretation has important implications for fluid flow during contact metamorphism. It implies that both pervasive and fracture-controlled fluid movement occurred in the inner 2km of the contact aureole during granite emplacement (see 6.1.4).

1.3.5 Mineralisation

Exploitation of the Cornish ores has been more or less continuous since the Bronze Age, with an estimated total production of $2.5x10^6$ tonnes of tin, $2x10^6$ tonnes of copper, $2x10^6$ tonnes of iron ore and lesser amounts of Pb, As, Mn, Zn, W, U, Sb and Ag (Dunham *et al.* 1978). Recent (1988) estimates of annual production from the three operating mines are 5000 tonnes of tin concentrates and 6000 tonnes of zinc concentrates (Willis-Richards & Jackson, in press). At present, however, the principal mineral commodity is kaolinite, with an annual production of $3x10^6$ tonnes, worth approximately £200M.

The Cornubian metallogenic province is a classic area for studying granite-related hydrothermal ore deposits. The literature describing mineralisation phenomena is extremely extensive and printed accounts date back to the seventeenth century (Richard Carew 1602). The first major work discussing mineralisation processes was the *Mineralogica Cornubiensis* (William Pryce 1778). Slightly more recent summaries include Dines (1956), Hosking (1964), Hawkes (1974) and Dunham *et al.* (1978). An extensive bibliography of the subject (Halls *et al.* 1985) provides further valuable references.

Three metallogenic stages may be recognised in the province. Minor pre-granite mineralisation included stratabound Fe-Mn oxy-hydroxide and Fe-Cu sulphide syn-sedimentary deposits (Jackson *et al.*, in press). The so-called "mainstage event" was related to the intrusion and protracted crystallisation history of the Cornubian batholith, when hydrothermal vein hosted and disseminated Sn-W-Cu-As-Fe-Zn-Pb deposits were formed. Post-granite epithermal veins containing Pb, Ag, Sb, Ba, Zn, Fe, U, Co, Ni and Au were formed from the Mesozoic onwards as a result of the continuing thermal anomaly induced by the high heat producing granite (Jackson *et al.*, in press).

Early mineralisation

Pre-granite deposits in the study area are restricted to minor syn-sedimentary pyrite, which is particularly common in green siltstones and mudstones (*e.g.* Vellin-Glûz Rocks, see Fig. 1.4) and limited pyrite-chalcopyrite mineralisation related to major thrusts (*e.g.* Blue Rock Thrust, see 1.3.3). Early pyrites have been highly oxidised by syn-orogenic fluid activity and later weathering phenomena, resulting in haematitic alteration.

Fresh, euhedral pyrites have been observed in major, brittle thrust zones, in association with extensive quartz veining. Cubes up to 3mm are present in both black slate and sandstone lithologies. In reflected light, these are seen to be brittly deformed with fractures infilled with chalcopyrite. Minor alteration of chalcopyrite to covellite is also observed.

Mainstage mineralisation

The complex nature of the mainstage phenomena preclude a detailed discussion. However, a number of generalisations may be made which hold for the bulk of the deposits.

Pegmatite-hosted ores, which both pre- and post-date joint formation, are relatively uncommon. Early pegmatites, such as the Tregonning example, often contain aggregates of löllingite, arsenopyrite and molybdenite with minor wolframite, cassiterite and native bismuth (Bromley & Holl 1987). More abundant, late pegmatitic pods and veins are particularly well developed in the Land's End and

Carnmenellis plutons. Wolframite is common and may be accompanied by bertrandite, stilbite, stokesite, cassiterite, sphalerite, pyrite and galena (Jackson 1977). Metal-enriched volatiles are clearly important in the genesis of these late magmatic mineral deposits (see 6.2.2).

Much of the mineralisation in the province occurs in *lodes and replacement deposits* in the roof and margins of the major plutons and satellite stocks. Massive and disseminated cassiterite and Cu-Fe-As sulphides occur in both granite and hornfelsed envelope, usually within 1km of the granite contact (Jackson *et al.*, in press). In the field area, disseminated arsenopyrite, chalcopyrite, pyrite, sphalerite and galena are observed up to 1.5 km from the Tregonning Granite (see 1.3.4). Hydrothermal alteration associated with these deposits is often intense and may be phyllic, tourmalinitic, chloritic or feldspathic (Jackson *et al.*, in press).

Sheeted vein swarms, usually hosted by granite or granite porphyry, are also important sites of mineralisation. They comprise subparallel sets of steeply dipping quartz veins with greisen borders (quartz+muscovite/Li-mica+topaz). In the study area, veins of this type are metasediment-hosted and have quartz/tourmaline/?Li-mica alteration haloes (see 2.2.12). Bunches of bladed wolframite crystals and equigranular cassiterite, often nucleating on the vein wall, are common ore minerals. Polymetallic sulphides, including pyrite, arsenopyrite, chalcopyrite, stannite and bismuthinite usually occur interstitial to polygranular quartz in the central parts of the vein. Gangue minerals include tourmaline, feldspar, mica and haematite.

Most of the worked deposits in the orefield are hosted by swarms of large (0.5-2.0m) *fissure veins (lodes)*, occupying steeply dipping faults or fractures. These structures display many features indicative of a prolonged history of evolution. Textures typical of cavity filling and replacement are common and active tectonism is evidenced by brecciation and shear fabrics. Although assemblages in these veins are complex, four main types have been distinguished (Garnett 1961; Bromley & Holl 1987; Jackson *et al.*, in press).

Tungsteniferous greisen bordered lodes are comparable with the sheeted vein swarms and probably formed in a similar manner. Wolframite is dominant with accessory löllingite, arsenopyrite, cassiterite and native bismuth. This assemblage suggests a possible genetic link with the early pegmatite-hosted mineralisation.

The most important tin-bearing structures in the province are *tourmalinite breccia lodes* (Bromley & Holl 1987). These lodes comprise sheared and crushed clasts of wallrock, quartz and tourmaline cemented by fine grained quartz, tourmaline and cassiterite. Haematite-cassiterite mineralisation often postdates quartz-tourmaline-cassiterite in these veins.

Stanniferous feldspathic lodes usually occur at deeper levels in the mineralised zone and contain intergrown quartz, K-feldspar, arsenopyrite, cassiterite and sometimes fluorite. Wallrock alteration is dominantly K-feldspathic, although often overprinted by a variety of other assemblages.

The fourth group of mineralised veins are known as *stanniferous and sulphide bearing chloritic lodes*. These are the most complex structurally and paragenetically, being composed of chloritised wallrock and vein breccia and a variety of ore minerals. Cassiterite accompanies polymetallic sulphides in the early stages, whereas it is absent from later mineralisation. Alteration around these veins is dominantly of chlorite-sericite type.

There are two dominant mainstage vein types known as "main" and "caunter" lodes which display slightly different orientations. They are E-W to NE-SW trending structures which intersect at a small angle. Both types host similar polymetallic mineral assemblages, with oxide parageneses generally pre-dating sulphides. Moore (1975) interpreted the lodes as forming in a conjugate system of normal faults and extension fractures. The orientations are consistent with their formation as oblique slip extensional faults, with antithetic sinistral displacements, under a regional dextral transtensional regime (see 1.3.3).

Base metal mineralisation

A distinct mineral paragenesis is present in N-S to NW-SE trending lodes, known locally as "cross-courses" or "guides". These lodes invariably crosscut the main and caunter lodes, which generally show dextral oblique-slip offsets, and are thus interpreted as postdating the mainstage event. However, recent fluid inclusion studies (Shepherd & Scrivener 1987; this work) suggest that fluids responsible for the cross-course mineralisation were invading the main and caunter lode structures during the mainstage event (see 4.6.4, 6.2.3).

The cross-course lodes commonly carry galena, sphalerite, chalcopyrite, pyrite and some silver, in addition to Fe- and Sb-bearing minerals such as tetrahedrite, bournonite, siderite, haematite, marcasite, jamesonite and stibnite (Exley *et al.* 1983). Wallrock alteration is limited and is dominated by silicification. In the study area, a number of parageneses are observed, depending primarily on host rock composition and structural setting. These features are summarised in Figure 2.26.

It is likely that many cross-courses reactivated earlier NW-SE to N-S trending structures (see 1.3.3, 2.2.15). However, dextral movement on these faults, as well as an element of down-dip extension, is consistent with regional NW-SE extension from the Permian onwards (see 1.3.3). Such faulting would be contemporaneous with dominantly normal movement on the main and caunter lodes.

The geology of the south Cornish region, summarised in this chapter, provides an important foundation upon which much of the remainder of the thesis is built. In the following chapters, various aspects of crustal fluid evolution are addressed. Initially, the fluids mobilised at different stages of Hercynian tectonism are characterised in terms of their composition, temperature, pressure and density. The relationships between the fluids generated at each stage are then examined in order to constrain possible evolutionary trends. The potential of the different fluids for transporting metals is then assessed using a thermodynamic approach. Finally, the ideas generated in the main body of the thesis are brought together into a model describing the processes which played important roles in the metallogenic evolution of the Cornubian province.

CHAPTER 2: VEIN GENESIS

Although there is, perhaps, in no part of the world, a district of equal size, which can compare with Cornwall in the number and variety of its mineral veins, and the geological phenomena which attend them; most of the writers on this part of geology have, 'till lately, drawn their facts and illustrations from foreign countries. This is not at all surprising; for it is but a few years since Britain has been roused to the pursuit of this science; and still fewer since Cornwall has attracted that degree of attention, either from strangers or from its own inhabitants, which is now so generally paid to it. Perhaps, however, few circumstances have occurred in relation to mineral veins, either in Hungary, Saxony or Bohemia, which may not be observed in the veins of our own country.

Joseph Carne, Esq., 1822.

The development of syntectonic vein systems is ubiquitous in deformed low grade metamorphic terrains. These veins usually contain samples of the fluid which was flowing through the rock at the time of formation of the fracture, trapped in the form of fluid inclusions. They may also contain samples of fluid representative of the subsequent uplift history of the rock in sealed secondary microfractures. A study of such veins can provide a wealth of information, not only regarding the mechanisms and conditions of vein growth but also on the progressive evolution of fluids mobilised during tectonism.

2.1 VEIN CHRONOLOGY

In order to study the temporal as well as spatial variations in fluids mobilised in the south Cornish crustal segment during the Hercynian orogeny, it was necessary to categorise veins within a chronological framework. Fluid inclusions present in the vein material provide direct data on palaeofluid evolution (section 3.1). Indirect evidence of fluid temperature and composition was provided by a study of alteration in the wallrocks adjacent to the veins (see section 3.6).

The vein chronology provides the foundation for all subsequent fluid evolution modelling. Uncertainties in the classification could cause serious problems in interpretation of fluid data, and result in erroneous conclusions being drawn. Consequently, this part of the study is presented in some detail.

2.1.1 Vein classification

A number of detailed structural analyses of the section have been carried out (see section 1.3.3). Both Turner (1969) and Rattey (1980a) completed structurally-based Ph.D. theses on the area and a number of papers have been published, notably Stone (1966) and Rattey & Sanderson (1982, 1984). As a result, the structural evolution of the area is well-constrained in terms of the main phases of deformation and their relationships with metamorphic and magmatic events. Notwithstanding these constraints, the large scale structure, stratigraphy and tectonic evolution of the area are relatively poorly understood (Wilkinson & Knight 1989).

With the exception of general descriptions of veins found in the province (*e.g.* Carne 1822) and studies relating to mineral lodes in and around the granites, no detailed work has been published on veins formed during the Hercynian orogeny in Cornwall.

During the course of the study, veins were examined from a 10 km coastal section extending from Church Cove to Tremearne (Fig. 1.4). Using a variety of structural criteria (see 2.1.2), veins were classified according to their relative ages of formation, lithological and structural setting. This classification system is presented in Table 2.1.

Those veins considered to form during D1 are defined as V1 veins. Similarly, those veins formed during the D2 and D3 deformation events (see section 1.3) are classed as V2 and V3 veins respectively. Veins formed after D3 (post-orogenic veins) are classed as V4. This scheme provides a simple framework for grouping veins formed during the same time period. The four categories are subdivided with a single letter subscript denoting the particular structural setting of the veins within each group (see Table 2.1).

The simplifications inherent in such a classification scheme do not, in general, cause problems in the interpretation of the fluid data (Chapter 4). The fluid studies have shown that there are rarely significant variations between fluids mobilised in different structural settings at different stages of the same deformation event (sections 4.2.3, 4.3.3). The changes in fluid P-T-X appear on the whole to be relatively gradual and cannot be resolved within the timescale of the deformation phase.

Table 2.1 Descriptive chronological/lithological/structural vein classification scheme

DEFORMATION PHASE	VEIN TYPE	STRUCTURAL SETTING
D1	$V1_G$	Greywacke-hosted vein
	$V1_T$	Thrust plane or related veining
	$V1_F$	Intimately related to F1 Fold
	$V1_B$	Boudin-neck extension fracture
D2	$V2_T$	Thrust plane or related veining
	$V2_F$	Intimately related to F2 Fold
	$V2_E$	Extension fracture
D3	$V3_C$	Sub-parallel to S3 Cleavage
	$V3_G$	Greenstone-hosted, sub-vertical vein
	$V3_S$	Slate-hosted, steeply inclined vein
Post-D3	$V4_P$	Pegmatite-related quartz
	$V4_J$	Joint-hosted vein
	$V4_N$	Normal fault plane or related veining
	$V4_W$	Wrench fault plane or related veining

2.1.2 Structural criteria

The various structural criteria used to ascertain the "absolute" or relative age of a vein observed in the field are summarised in Table 2.2 below. The term "absolute age" is used here where a vein may be assigned to a particular phase of deformation; it does not imply a vein age in terms of "millions of years before present". A relative age may be assigned where a vein crosscuts or is deformed by a structure which is known to have formed during a particular deformation phase. This provides a lower or upper limit for the age of the vein. In favourable circumstances, a number of criteria may be combined to further constrain the vein age relative to the main phases of deformation. Occasionally, this allows an "absolute" vein age to be determined.

Table 2.2 Structural criteria used for constraining relative or absolute vein age

CONSTRAINT	DESCRIPTION	AGE
Absolute	Vein orientation related to principal stress trajectory during D_n	D_n
	Vein formed during F_n folding	D_n
	Vein formed during S_n fabric development	D_n
Relative	Vein cross-cutting V_n vein	post-D_n
	Vein cross-cutting F_n fold	post-D_n
	Vein cross-cutting S_n fabric	post-D_n
	Vein cross-cut by V_n vein	pre-D_n
	Vein folded around F_n fold	pre-D_n
	Folded vein with axial-planar S_n	pre-D_n

2.2 VEIN STRUCTURES

The complete spectrum of veins developed in the area were studied macroscopically in the field and microscopically in thin section under transmitted light. A variety of macro- and microstructural features were observed which provide evidence for the mechanism and conditions of vein growth, as well as subsequent deformation. The relationships between fluid inclusions and the microstructures allow additional constraints to be placed on the age of entrapment of the fluids (see section 3.2). Due to the complexity and wide range of vein types observed in the area, the discussion of microstructures will be mainly restricted to those veins selected for microthermometry (section 3.2). Other veins providing additional information with regard to growth mechanisms will also be included.

2.2.1 $V1_G$ veins

Field relations

There are commonly four vein sets developed which pre-date or formed early in the history of F1 folding. They are all restricted to competent sandstone horizons in alternating sandstone-shale sequences and, as a result, are best developed in the Portscatho Formation (see section 1.3.1).

The veins are predominantly less than 1.5cm thick and are closely related to F1 folds, being most abundant near the hinge regions (Fig. 2.1). Set 1 veins form sub-perpendicular to the fold axis and are interpreted as extension fractures, forming perpendicular to the least principal stress direction. Vein sets 2 and 3 are bisected by set 1 and are interpreted as conjugate shear fractures (Hobbs *et al.* 1976). The fourth set are sub-parallel to F1 axes but consistently dip steeply to the NNW (Fig. 2.1). An equal area stereographic projection illustrating these relationships is presented in Figure 2.3. A field photograph showing crosscutting veins from sets 2, 3 and 4 is shown in Figure 2.4.

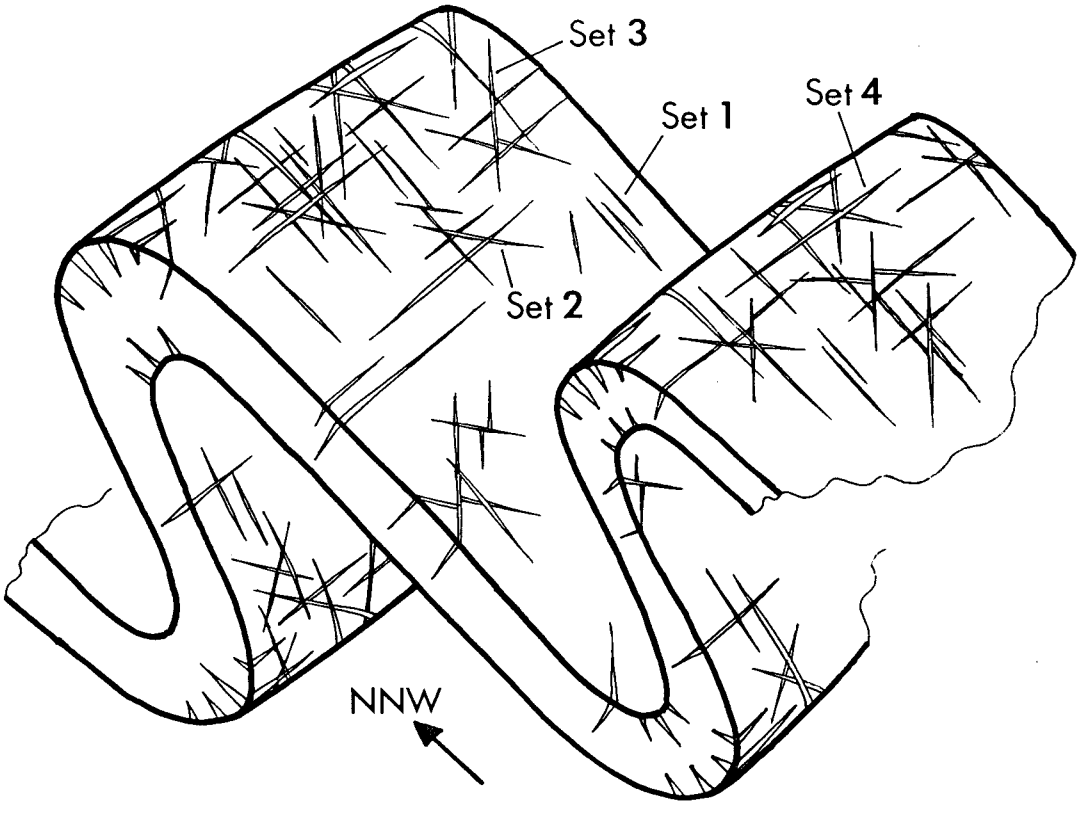

Figure 2.1 Diagram illustrating relationships between F1 folds in competent unit and $V1_G$ vein sets.

All four vein sets exhibit inconsistent cross-cutting relationships and it is concluded that they formed essentially contemporaneously. The close spatial and geometric associations of these veins with F1 folds suggest that they formed during fold development. However, the vein sets have been rotated during folding, displaying different orientations on the normal and inverted fold limbs (Fig. 2.2). These features indicate that the veins formed immediately prior to and/or contemporaneously with fold initiation. Local stresses developed in the sandstones as a result of the onset of flexural slip folding, possibly combined with high pore pressures in the same units, may have been the cause of preferential hydraulic failure in competent horizons in the hinge regions (*cf.* Beach 1977).

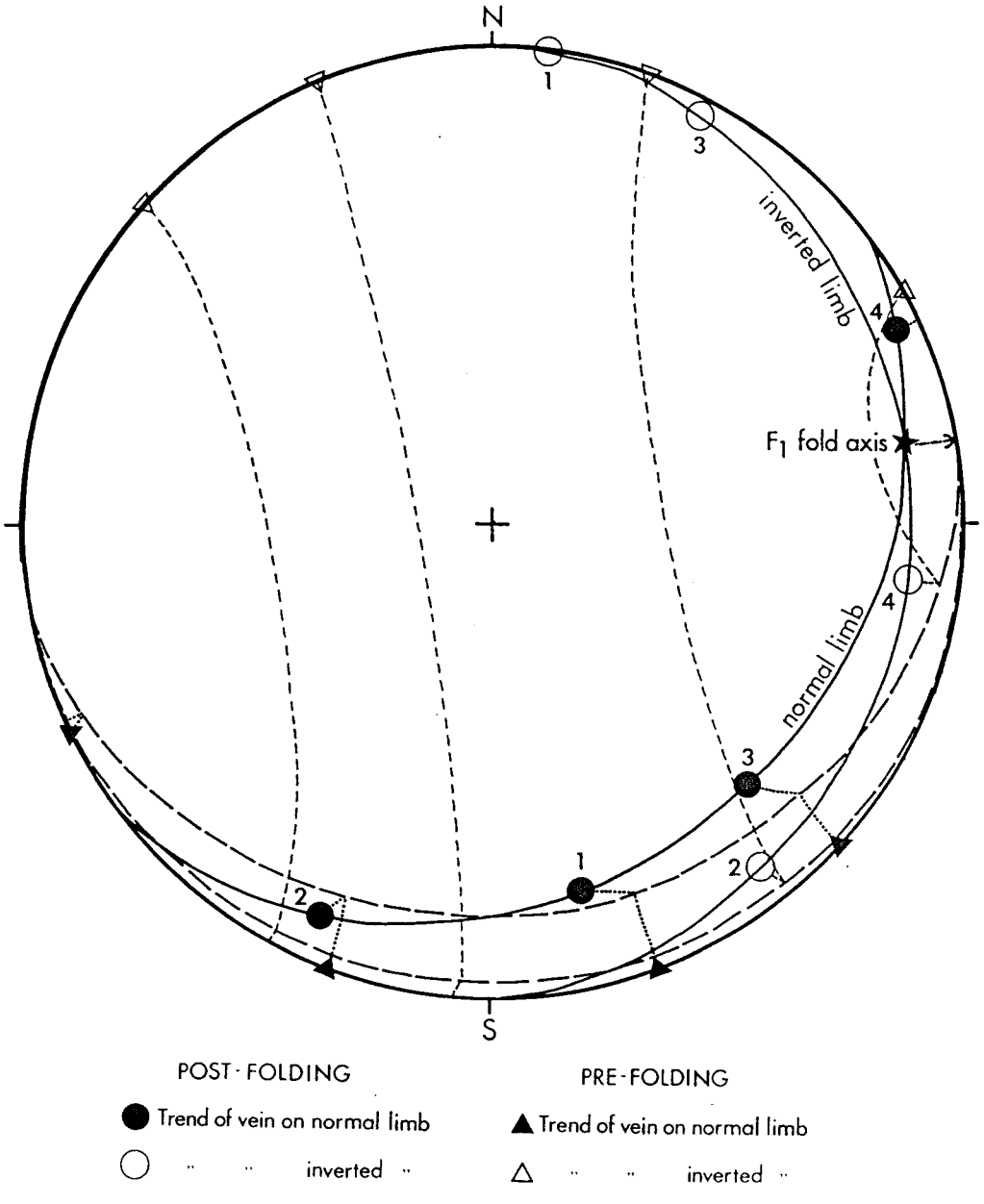

Figure 2.2 Equal area stereographic projection illustrating $V1_G$ veins folded around F1 fold hinge. Solid lines represent bedding plane orientations. Their intersection defines the fold axis. The measured trends of $V1_G$ veins on the bedding surfaces are indicated by circular symbols on these great circles. The fold was unfolded by rotating the fold axis through a vertical plane to the horizontal (dot-dash line) and then rotating the normal and inverted limbs around the axis, back to their pre-folding orientation. The loci followed by the $V1_G$ veins during this procedure are indicated by dotted lines (veins on normal limb) and dashed lines (veins on inverted limb). After unfolding, the trends for veins on both normal and inverted limbs coincide, indicating a common orientation prior to folding.

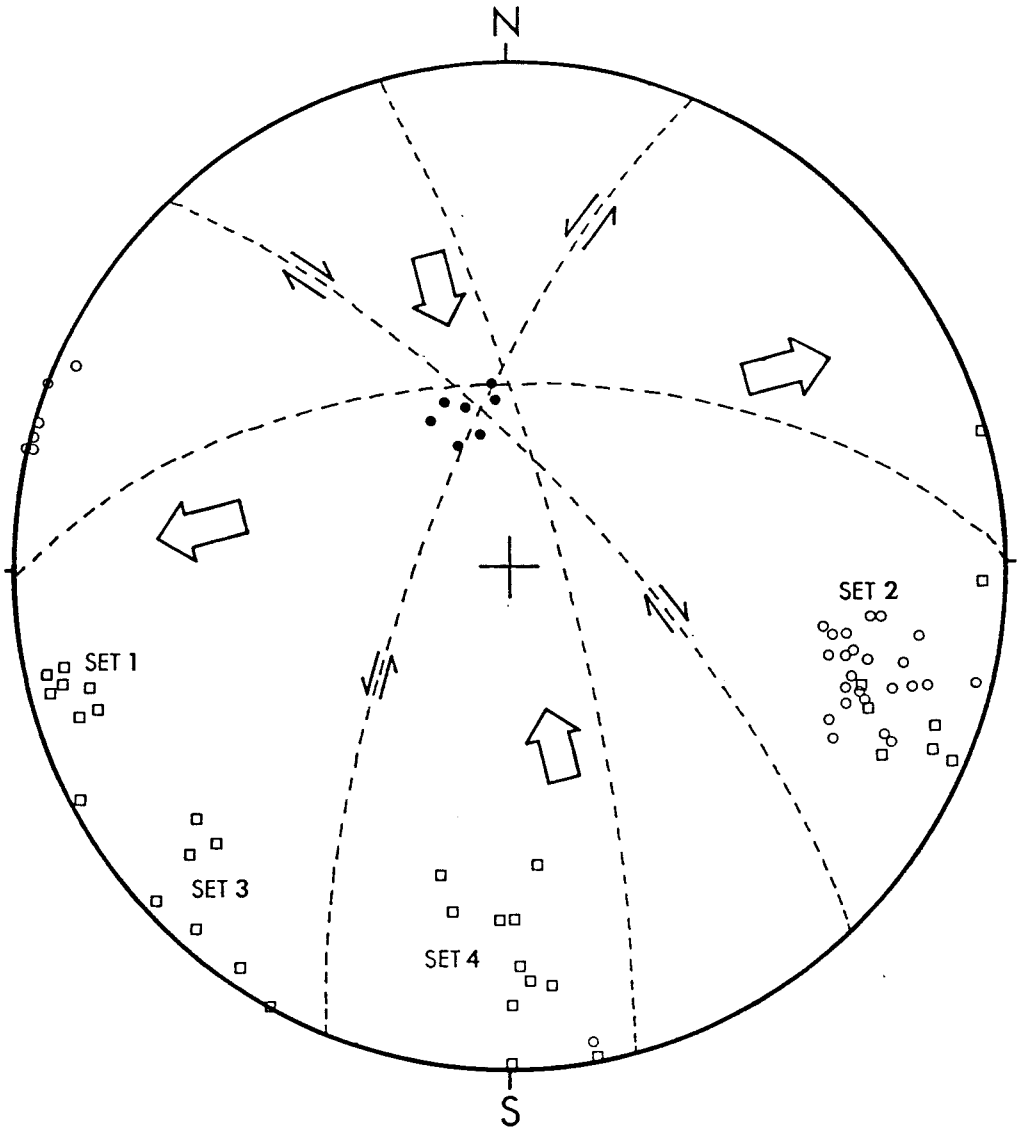

Figure 2.3 Equal area stereographic projection showing orientations of $V1_G$ veins from two localities. Squares = poles to $V1_G$ veins from Jangye-ryn Cove (*JR*), open circles = poles to $V1_G$ veins from Baulk Head (*GW*). Solid circles = poles to bedding, Jangye-ryn. Dashed lines represent average $V1_G$ orientations, showing sense of shear across set 2 and set 3 veins. Large arrows denote principal stresses within bedding plane. Note coincidence of bedding poles and intersection of vein orientations.

Microstructure

$V1_G$ veins have been subject to post-D1 deformation, resulting in recrystallisation and sometimes obliteration of the primary textures. This can make identification of features produced during vein growth rather difficult. However, it is generally possible to select for study veins which have not suffered significant deformation and which do preserve primary fabrics. This is also advantageous for a fluid inclusion study, since undeformed veins are less likely to have suffered a significant fluid

overprint and thus contain fewer secondary fluid inclusions.

The ubiquitous vein-filling material is quartz, with the relatively rare development of carbonate (siderite or ankerite), chlorite and white mica. These less abundant vein minerals occur with quartz in composite veins (Ramsay & Huber 1983) or, more commonly, as irregular aggregates within a quartz-dominated vein. Quartz usually exhibits a "stretched crystal" structure (Durney & Ramsay 1973) with linear fibres extending in optical continuity across the vein (Fig. 2.4). In vein sets 1 and 4 the fibres are oriented perpendicular to the vein walls indicating pure dilation. Vein sets 2 and 3 display oblique fibre growth, consistent with an origin as shear fractures (see above). Sigmoidal fibres are not observed indicating that incremental strains were coaxial (Ramsay & Huber 1983).

Stretched crystal vein fillings are believed to form by repeated microfracturing parallel to the vein wall and sealing by precipitation of quartz in optical continuity with the pre-existing fibres (Durney & Ramsay 1973). The occurrence of planes of tiny (<5um) fluid inclusions parallel to the vein walls throughout the length of the fibres supports this theory. In most cases the initial fracture passed through detrital quartz grains in the sandstone host. The fluid introduced into the fracture then precipitated quartz in optical continuity with the broken wallrock grains. Crystals with their c-axes oriented perpendicular to the vein walls grew more rapidly and quickly obliterated less favourably oriented grains (Spry 1969). In the thicker veins this resulted in large fibres (relative to the detrital grain size) of similar optical orientation dominating the vein structure.

Occasionally, drusy fabrics are observed as described by Beach (1977) from similar veins developed in the Carboniferous flysch of North Cornwall. However, such textures are limited to the centres of the thicker veins. This evidence suggests that in these sites the rate of vein dilation exceeded the rate of quartz precipitation, particularly towards the latter stages of vein growth. This resulted in crystal growth into a fluid-filled cavity and development of typical wedge-shaped drusy crystals (see 2.2.7). The preservation of drusy and fibrous fabrics indicates that temperatures did not exceed c.350°C; above this temperature, spontaneous recrystallisation would have occurred as a result of the thermodynamically unstable nature of such crystal habits (Ramsay & Huber 1983).

Subsequent deformation of $V1_G$ veins led to the modification and, in some cases, obliteration of the microstructures described above. The two main causes of later deformation are progressive shear and vein rotation during the later stages of D1 and the superposition of D2 strain, producing buckle folds, recrystallisation and/or pressure solution effects. Crystal plastic deformation mechanisms were dominant, giving rise to widespread undulose extinction and subgrain development. Fibre boundaries have been modified by grain boundary migration, resulting in suturing and eventually the formation of new small grains. In more deformed examples, patches and bands of small, equidimensional quartz crystals indicate that dynamic recrystallisation occurred. An example of a set 2 vein affected by D2 deformation is shown in Fig. 2.4).

Figure 2.4

Figure 2.4: Captions

A. $V1_G$ Set 2, 3 and 4 veins exposed on bedding surface of sandstone unit, Jangye-ryn Cove. Viewing direction: NNW; Scale bar = 2cm.

B. Photomicrograph (crossed polars) of $V1_G$ Set 4 vein (*JW001*) showing "stretched crystal" vein fabric with optically continuous fibres extending across vein. Scale bar = 2mm.

C. Photomicrograph (plane polarised light) of $V1_G$ Set 2 vein deformed by development of S2 pressure solution seams (*J05GW*). Scale bar = 2mm.

D. Photomicrograph (crossed polars) of previous vein showing recrystallisation, undulose extinction and subgrain development resulting from vein deformation. Scale bar = 2mm.

E. $V2_E$ veins sub-parallel to S2 in hinge region of F2 fold, south Loe Bar. Note sigmoidal form of early veins (inked) which indicate NNW-directed shear parallel to S2. Viewing direction ENE; Scale bar = 5cm.

F. Photomicrograph (crossed polars) of $V2_F$ veins which show extensive pressure solution and sericitisation along their margins (*J38LB*). Note complete recrystallisation of internal vein fabric. Scale bar = 2mm.

G. Bedding and S1 pressure solution cleavage folded by F2, from between Caca-stull Zawn and Vellin-glûz Rocks. Note $V2_F$ veins in hinge region, formed by outer arc extension. Viewing direction ENE; Scale bar = 10cm.

H. Photomicrograph (plane polarised light) of $V2_F$ vein showing heterogeneous pressure solution along vein margin (*J23GW*). Note spaced S2 seams, sub-parallel to vein cross-cutting penetrative S1 fabric. Scale bar = 2mm.

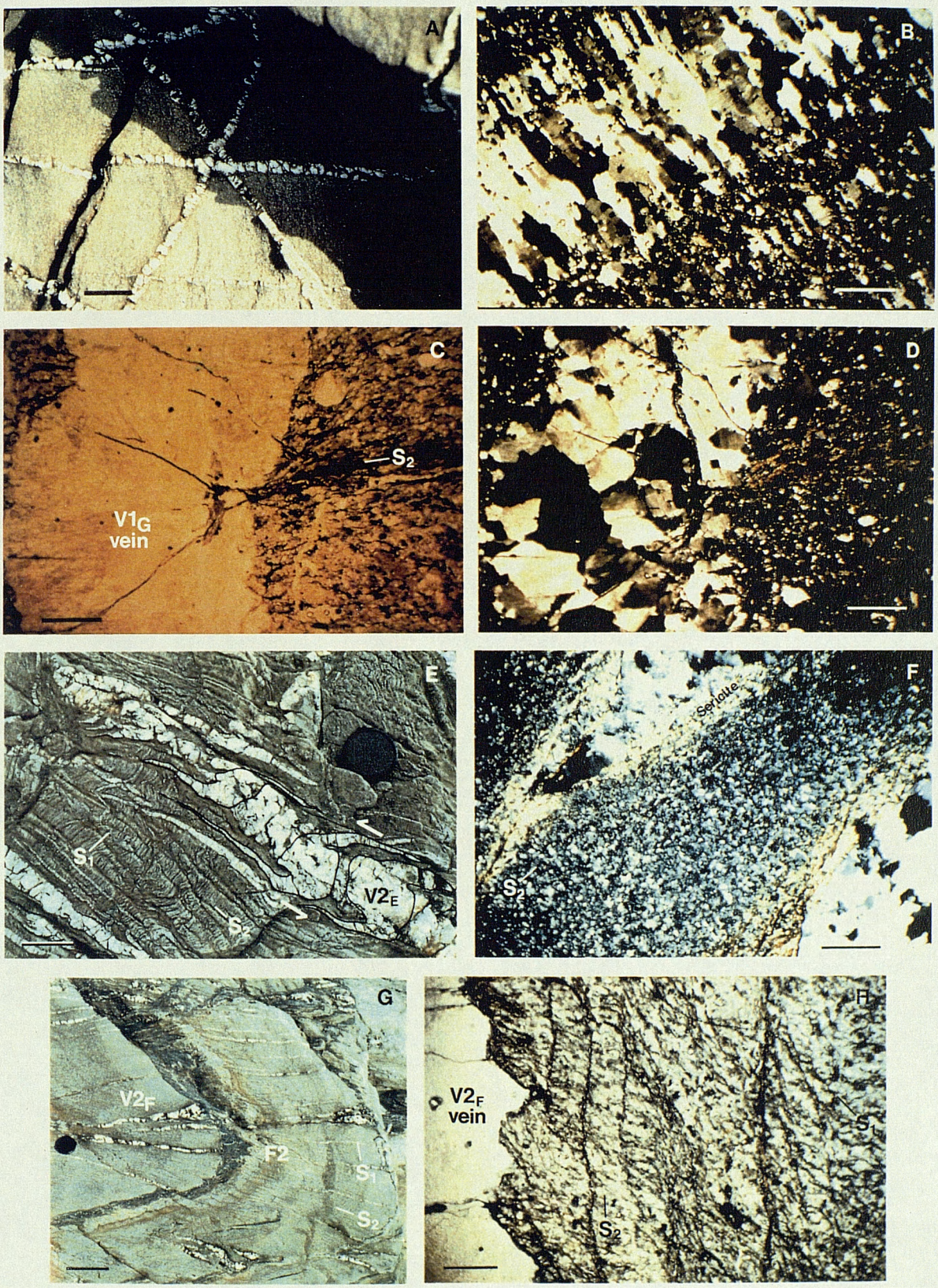
A
B
C
S_2
$V1_G$ vein
D
E
S_1
$V2_E$
S_2
F
Sericite
S_2
G
$V2_F$
F2
S_1
S_2
$V2_F$ vein
F2
S_1
S_2

2.2.2 $V1_T$ veins

Field relations

This group includes all veins formed on demonstrable D1 thrust planes and related fractures. Such veins are of variable thickness and length, ranging from millimetres to centimetres across and extending for up to tens of metres. It is common for a set of sub-parallel veins to develop in the vicinity of a thrust by propagation of fractures outward from the fault plane, often into the hanging wall. Such fracture sets are comparable with en echelon vein arrays which may be used as indicators of the shear sense (Fig. 2.5).

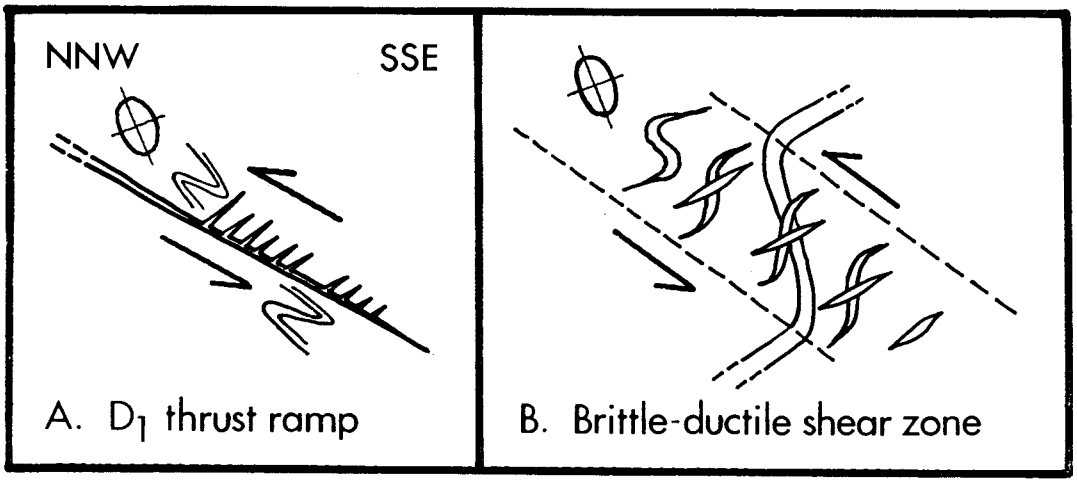

Figure 2.5 Comparison between $V1_T$ veins and extension veins formed in a brittle-ductile shear-zone (after Ramsay & Huber 1983). Commonly $V1_T$ veins are sheared subsequent to formation, rotating into the stretching direction. If such rotation is not identified, an incorrect shear-sense will be assigned.

The major problem with classifying veins in this group is the positive identification of D1 thrusts in the field. Also, since many of the early thrusts show evidence of reactivation during the D2 event, the veins associated with these structures cannot be confidently assigned to either D1 or D2. As a result, only veins related to thrusts which show no evidence of reactivation were sampled.

Microstructure

Quartz is by far the most abundant vein-filling material. Chlorite is relatively common, occurring as amorphous patches, and often shows evidence of more than one generation of growth. Altered wallrock screens are also observed which are invariably phyllosilicate-rich, predominantly chlorite and/or sericite. Ankerite is relatively rare and, where present, occurs as small isolated aggregates.

No well-developed primary fabrics are observed in these veins. The high strains and continuous nature of deformation and vein formation in the thrust zones mean that fibrous vein fillings were obliterated as soon as they formed. Crystal plastic deformation mechanisms were dominant as a result of the relatively high temperatures at this stage (*c.* 300°C).

Intense undulose extinction in larger quartz grains is common. In zones of higher strain, migration of dislocations within the crystal resulted in the formation of tilt boundaries defining new subgrains (White 1977). These subgrains often display a grain shape fabric, being elongated sub-parallel to the principal extension direction. Further grain-size reduction occurred in the most highly strained zones where dynamic recrystallisation produced bands of tiny (10-100μm), equant quartz crystals.

2.2.3 $V1_F$ veins

Field relations

These veins are only developed in the outer or inner hinge regions of folded competent horizons, sub-parallel to the fold axial plane and fanning slightly. They are usually thicker than $V1_G$ veins (up to 3cm) and consistently crosscut them where the two generations intersect. Ramsay (1974) describes such veins as "outer" or "inner arc extension fissures" which form when excess differential stress in the hinge zone of a competent unit is relieved by brittle failure. The model for chevron fold formation proposed by Ramsay (1974) suggests that outer arc fissures should form in the hinge region at an early stage, when the interlimb angle is relatively large. Inner arc fissures form at a late stage when the folds become tight. The relationships between these veins and associated fabrics are shown in Fig. 2.6. It should be noted that outer arc veins may be subject to pressure solution during the later stages of folding as the region of cleavage formation migrates outwards. Conversely, inner arc fissures may open up along previously formed pressure solution seams.

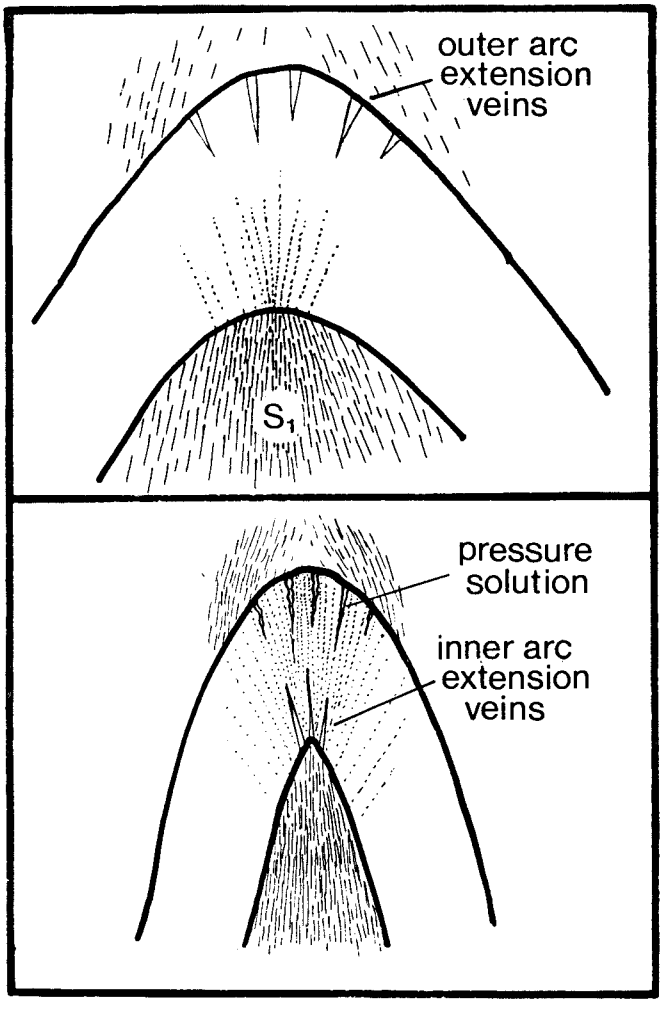

Figure 2.6 Diagram illustrating formation of $V1_F$ veins in a competent unit as a result of outer or inner arc extension. Early outer arc veins are modified by pressure solution at a later stage.

These veins, unlike $V1_G$ veins, contain fluid inclusions large enough for microthermometry, primarily as a result of the larger size of quartz crystal developed. They have also escaped much of the deformation and resultant recrystallisation suffered by other V1 veins because of their orientation sub-parallel to the D2 XY-plane, perpendicular to the principal D2 compressive strain.

Microstructure

Quartz is the dominant vein-filling mineral in these structures, commonly accompanied by variable amounts of chlorite and carbonate (siderite or ankerite) and minor sericite. The accessory minerals are generally present as small discrete crystals or fine grained aggregates distributed throughout the quartz.

Similar microstructures to those observed in $V1_G$ veins are present (see above). One significant difference is that fibrous quartz is less well developed and a more prismatic habit is in evidence. The generation of such textures is discussed in more detail in section 2.2.7.

2.2.4 $V1_B$ veins

Field relations

Local extensional strains developed during D1 resulted in boudinage of competent bedding horizons. Boudins are usually observed in the steeper, inverted limbs of F1 folds where the XY-plane of the incremental strain ellipsoid is at a low angle to bedding, resulting in the formation of extensional structures (Fig. 2.7). The intimate association of these boudins with F1 folds (their axes are sub-parallel to F1 axes), and the wrapping of the S1 fabric around them (Fig. 2.7) indicate that they formed during D1. Extensional structures are also observed in the inverted limbs of F2 folds, probably produced by a similar mechanism. However, the more brittle deformation characteristic of D2 is reflected in the development of transtensional shears and microfaults rather than boudins.

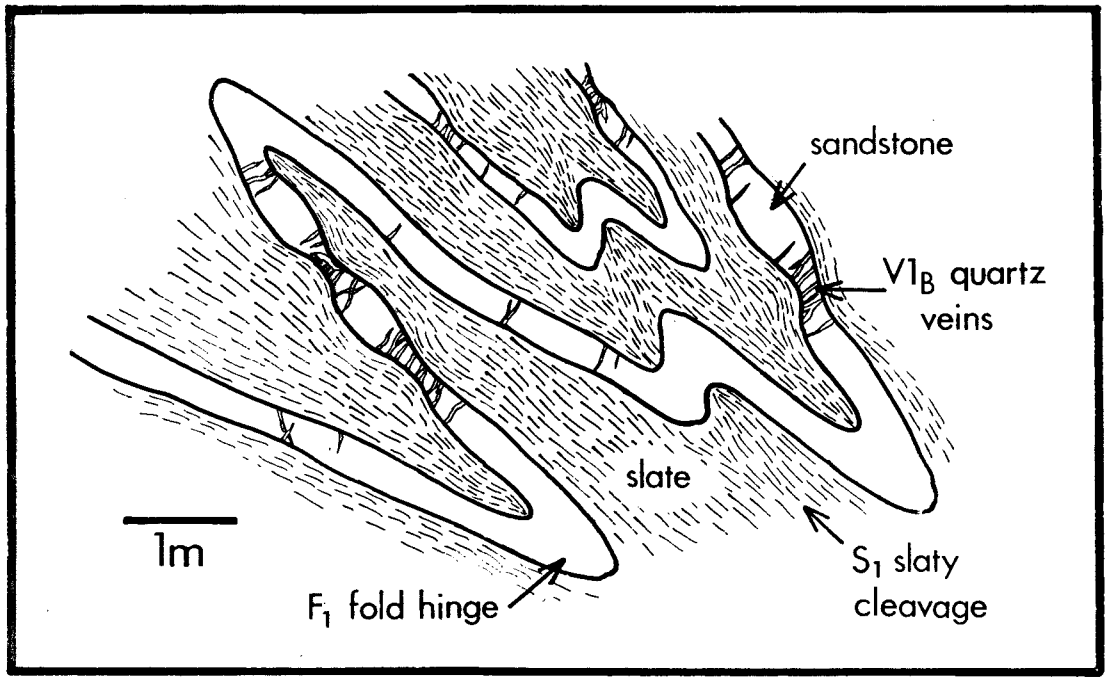

Figure 2.7 Diagram illustrating development of D1 boudins and associated $V1_B$ veins in competent units on inverted limbs of F1 folds. Sketch is drawn perpendicular to strike, representing a NNW-SSE section.

Microstructure

Quartz-filled tension gashes are often developed in the necks of the boudins described above. It is these veins which have been classified as type $V1_B$. Although quartz is dominant, albite, chlorite and sericite are also present as vein fillings. Clear evidence of vein formation occurring by repeated fracturing is indicated by the presence of composite fillings. Growth substages, characterised by the successive precipitation of chlorite, sericite and quartz, have been observed.

Quartz microstructures are dominated by the effects of plastic deformation subsequent to crystal growth. However, there is some evidence, in the form of relict elongate grains sub-parallel to S1, that fibrous crystals grew by a crack-seal mechanism in the boudin necks during extension. Subsequent grain size reduction and recovery has all but obliterated these primary structures.

The larger quartz grains (up to 5mm) have very irregular boundaries and show evidence of grain boundary migration, with the obliteration of early fluid inclusions around grain margins (Fig. 2.14). They also display strong undulose extinction and extensive subgrain development. The new subgrains are generally elongated parallel to the principal extension direction (parallel to L1). Bands of small, dynamically recrystallised quartz grains are often observed and these acted as a favourable growth site for late vermicular chlorite. This is probably due to the high solubility of such quartz (having a high defect density and high surface energy (Wintsch 1985)) decreasing the activation energy and increasing the rate of the reaction: quartz(deformed) + Fe,Mg,Al(fluid) -> chlorite.

2.2.5 $V2_T$ veins

Field relations

As is the case with D1 thrusts, the identification of D2 thrusts in the field can be difficult. Sometimes D2 thrusts may be positively identified on the basis of an intimate spatial and geometric relationship with proven F2 folds or S2 fabric (Fig. 2.8). A general pattern has been noted, with proven D2 thrusts usually displaying greater dips (see 1.3.3) and more intense associated veining than their D1 counterparts. These differences were used to infer the probable age of faults where other structural criteria were lacking.

Quartz is invariably developed on D2 thrust planes and both hangingwall and footwall usually contain thrust-related veins. It is common for such veins to be relatively undeformed in the hangingwall, defining en echelon arrays with a NNW-directed sense of shear, consistent with the D2 transport direction. The footwall veining, in contrast, is highly irregular and generally more intense.

Microstructure

Quartz is the dominant vein-filling mineral. Chlorite is common and occurs primarily as finely crystalline clots, although a vermicular habit is observed where chlorite is forming at the expense of highly deformed quartz (*cf.* $V1_T$ veins). Ankerite or siderite is only present as small, randomly distributed grains in veins that are developed in carbonate-rich parts of the sequence (Jangye-Ryn, Blue Rock). This suggests local derivation of at least some of the components of the fluid possibly including silica derived by pressure solution as well as carbonate.

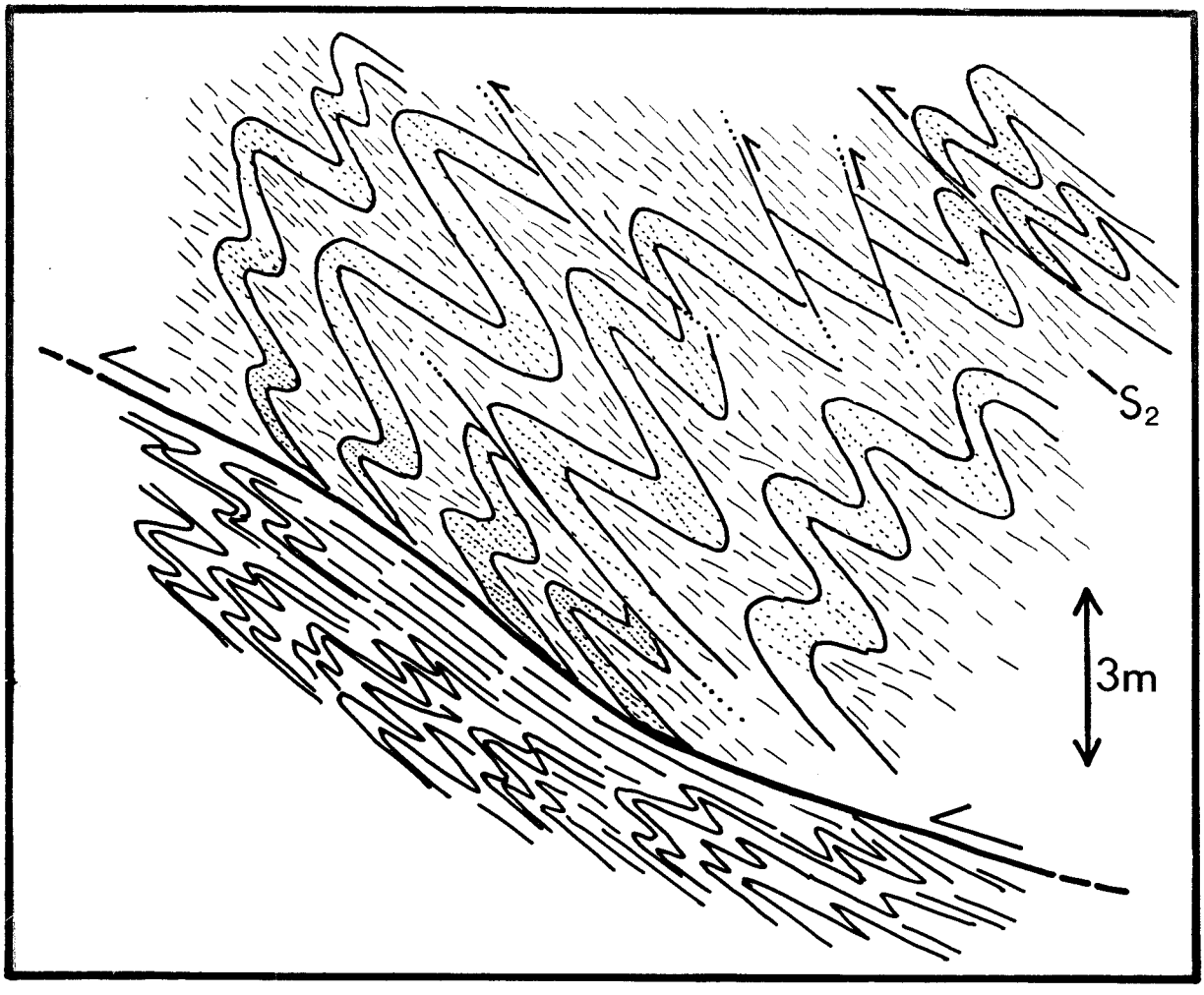

Figure 2.8 Field sketch from south Caca-stull Zawn, illustrating relationships between F2 folds and D2 thrusts. Dotted lines represent S2 in sandstone units; dashed lines represent S1/S2 in mudstone units.

The microstructures developed in these veins depend largely on the P, T conditions, strain rate and degree of deformation. Quartz from fault planes is invariably highly deformed and examples of both plastic- and cataclastic-dominated deformation have been observed. Plastic deformation mechanisms, operating at higher temperatures and lower strain rates, result in gradual grain size reduction through subgrain development. Subgrains are usually elongated in the principal extension direction, as are larger, less deformed crystals. Undulose extinction is ubiquitous and dynamic recrystallisation is common, particularly in narrow shear bands. Such zones often show the development of vermicular chlorite.

Where faulting has occurred under more brittle conditions, either at a lower temperature or at a higher strain rate, cataclastic textures are observed. Grains are physically broken and rounded by "milling" to produce fine crystals (0.1-1mm) set in a microcrystalline matrix. Opaques commonly form a component of the matrix medium.

2.2.6 $V2_F$ veins

Field relations

These veins and those of the following group ($V2_E$) often both occur in the vicinity of F2 fold hinges, and have similar orientations in these regions. In these cases, they are difficult to distinguish. In some cases "composite" veins form which seem to have initiated as $V2_F$ veins and then developed in a similar manner to $V2_E$ veins. This point is discussed further in the following subsection.

$V2_F$ veins are developed solely in competent units in the hinge region of F2 folds. As with the $V1_F$ veins, they are sub-parallel to the fold axial plane and fan slightly around the hinge (Fig 2.4). They have been observed both on the outer and inner arcs of competent horizons and they always have a wedge-shaped form with maximum dilation at the margin of the host unit. They are believed to form in a similar manner to $V1_F$ veins, as a result of stress heterogeneity in the hinge region during folding. Outer arc extension fissures sometimes show evidence of marginal pressure solution due to changes in the principal strain orientations as folding progressed. Conversely, inner arc fissures do not show these features, indicating their formation at a relatively late stage, probably utilising the locally pre-existing S2 fabric.

Microstructure

Quartz is dominant in $V2_F$ veins, with minor chlorite in the form of small "fans" or with a vermicular habit. Carbonate (ankerite or siderite) is only observed where the host rock is rich in carbonate cement. Sericite is not observed in the vein, only at the margins where significant pressure solution has occurred (Fig. 2.4).

Most $V2_F$ veins have similar microstructures to their $V1_F$ counterparts. The least deformed examples show relict primary structures indicating that they formed as extensional fractures with quartz fibres growing perpendicular to the vein walls (see 2.2.1). Generally, they display "stretched crystal" forms, this being primarily controlled by the abundance of the vein-filling mineral in the host rock (Cox & Etheridge 1983). Well-preserved primary structures are rare; most microstructures have been considerably modified by later D2 (and in some cases D3) shearing and pressure solution.

Outer arc veins which formed relatively early during D2 are always modified to a greater or lesser extent by the development of S2 pressure solution seams. Their formation in a similar orientation to the S2 fabric and subsequent rotation into sub-parallelism with it, means that dissolution of vein quartz occurs along the vein edges. Carious margins are common where preferential dissolution in spaced zones occurred (Fig. 2.4). This may reflect anisotropic dissolution kinetics of the vein crystals, and hence the preferential removal of favourably oriented grains. However, the primary control appears to be the angle of intersection of S1 pressure solution seams with the vein wall. Where this angle is high (Fig. 2.4), as in the hinge regions of F2 folds, the most extreme heterogeneous solution is observed.

Extension in the D2 XY-plane (parallel to L2) sometimes resulted in boudinage of $V2_F$ veins, which may have been enhanced by pressure solution. Crystal plastic processes were the dominant deformation mechanisms and were most active in locally highly-strained quartz, such as in boudin necks. Early suturing of primary fibre boundaries was followed by considerable grain boundary migration to produce distinctive zones of small new subgrains. Undulose extinction is observed

throughout, as is the development of subgrains in a "chicken-wire" texture, resulting from the migration of both screw and edge dislocations (White 1988). New quartz grains are generally elongated sub-parallel to the vein walls, mirroring the orientation of the D2 finite strain ellipsoid.

2.2.7 $V2_E$ veins

Field relations

A set of veins which proved difficult to classify are particularly well-developed in zones of high D2 strain. The veins may be conspicuously short and thick, forming lenses up to 25cm across and 2m long, although thinner, more extensive veins are also observed. They always strike ENE and display variable dips, from 25° to the north to 30° to the south. A plot of vein orientations on a stereographic projection (Fig. 2.9) shows that poles to veins fall on a great circle which represents a plane almost perpendicular to the average F2 fold axis. Where the differently oriented veins intersect, the north-dipping veins are always younger, as well as being shorter and thicker than the south-dipping examples. This evidence strongly suggests that the veins formed as north-dipping extension fractures and were subsequently rotated, to a greater or lesser degree, by NNW-directed D2 shear (Fig. 2.9). Occasionally, folded examples of sub-vertical veins are observed, indicating initial rotation into the compressional field prior to late stage extension.

A distinctive characteristic of these veins is that, unlike the majority of the vein types previously discussed, they are not limited to the more competent units and are commonly observed extending for several metres through both sandstone and slate horizons. They are particularly well-developed in the thicker, finer grained units in the transitional sequence (see 1.3.3), such as the laminated green siltstones outcropping at Caca-stull Zawn and Vellin-glûz Rocks (Fig. 1.4). Examples of early veins of this type, which have experienced higher shear strains in the fine grained lithologies, and late veins which show no evidence of shearing or rotation are common (Fig. 2.9).

In the hinge regions of F1 and F2 folds, $V2_E$ veins are often difficult to distinguish from $V1_F$ and $V2_F$ veins. Also, on the long limbs of F1 folds where no F2 structures are evident, some $V2_E$ veins have similar orientations to $V1_G$ fractures (compare north-dipping $V2_E$ veins with $V1_G$ Set 4 veins in Figures 2.9 and 2.3). Where these ambiguities could not be resolved by detailed examination of the fabric relationships, sampling for further analysis was avoided.

Microstructure

Thin section examination reveals that these veins are composed of relatively large, subhedral to euhedral quartz crystals (up to 10mm) showing variable amounts of plastic deformation. Chlorite is common, occurring as masses of small vermicular grains located along sutured grain boundaries and other zones of high defect density in quartz. Platy or lath-like chlorite crystals are sometimes developed along stylolitic sutures, probably representing altered wallrock screens.

The presence of large, sub- to euhedral quartz grains in these veins is difficult to account for in terms of a classic "crack-seal" mechanism. In the literature, explanations of such phenomena are conspicuous by their absence. "Drusy" fabrics of this type in syntectonic veins have been described by many authors, including Durney & Ramsay (1973) and Phillips (1974). Cox (1987) also describes

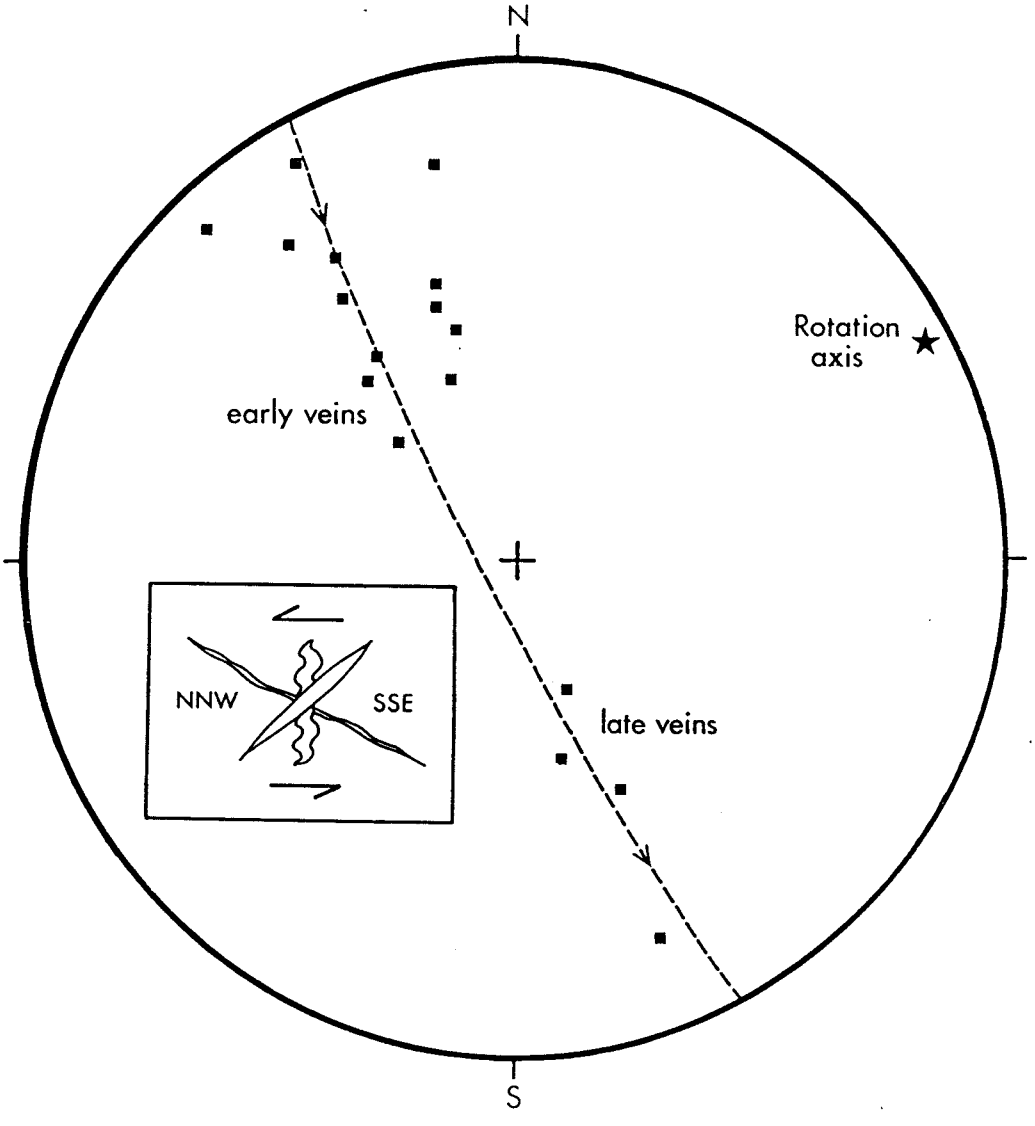

Figure 2.9 Equal area stereographic projection showing poles to $V3_E$ veins. Dashed line is a great circle fit to the data, illustrating rotation about an ENE-trending axis (star). Inset: model for vein formation, with extensional veins rotating through the compressional field into the extensional field.

similar vein fabrics from a comparable low-grade greywacke terrain, suggesting the vein formed by an antitaxial crack-seal mechanism with the texture of the main "zone of irregular grain fabrics" resulting from heterogeneous growth kinetics. However, this does not account for the presence of subhedral or euhedral grains. Some may be due to high temperature annealing of primary fibrous crystals. However, in many cases, this is not a viable mechanism and the fabric must be produced by a primary crystallisation process.

A general observation is that such fabrics are commonly developed in thicker veins and dominate the vein structure. Fibrous margins are sometimes observed but these often show evidence of having formed at an early stage as small, discrete veins and are unrelated to the growth of the main vein. Much more frequently, "drusy" type fabrics are observed throughout the vein (as in type $V1_F$, $V2_F$ veins), with numerous small crystals at the margins rapidly giving way to relatively few, large, euhedral grains in the centre.

The paradoxical occurrence of fabrics normally produced by crystallisation into an open cavity in veins formed at depth where it is impossible for open fractures to be sustained (*e.g.* Fyfe *et al.* 1978) is a problem. It is suggested that extension fractures, under conditions of high fluid pressure, may be transiently opened allowing crystals to grow into a fluid-filled void. This implies that high fluid pressures must be maintained during opening of a macroscopic fracture and are only relieved once relatively large subhedral quartz crytals have formed. This may be analogous to the "seismic-pumping" mechanism described by Sibson *et al.* (1975). Thus, the development of such textures may be indicative of the operation of such a process.

2.2.8 $V3_C$ veins

Field relations

A distinctive, although relatively poorly developed, vein set is observed locally in the Mylor Slate Formation, between Caca-stull Zawn and Tremearne (Fig. 1.4). The veins are sub-parallel to the local S3 fabric, dipping shallowly southeast (Fig. 2.12), with the steepest dips observed furthest away from the granite. Sometimes they are boudinaged, with the S3 fabric wrapping around the lenses (Fig. 2.14).

$V3_C$ veins are interpreted as forming as a result of hydraulic failure during peak contact metamorphism and are synchronous with S3 fabric development. This may be explained if fluid pressures sufficient for hydrofracturing are only attained at the peak of metamorphism when the rate of fluid release by devolatilisation reactions is at a maximum (Yardley 1985).

The formation of veins sub-parallel to a fabric forming contemporaneously with peak metamorphism is a common phenomenon. The mechanical weakness introduced as a result of cleavage development controls the fracture orientation, rather than the principal strain axes.

Microstructure

$V3_C$ veins are composed almost entirely of quartz with minor chlorite, the latter occurring in fans of acicular crystals in crosscutting fractures or as platy crystals replacing stylolitised slivers of wallrock. Primary vein fabrics have been largely obliterated by progressive D3 shear which resulted in considerable grain size reduction. Zones of small subgrains are common. Larger subgrains, generated by tilt boundary formation, dominate the vein structure. These grains are generally elongated at a low angle to the vein walls in an orientation indicative of vein-parallel, SE-directed shear, consistent with D3 tectonism (see 1.3.3).

The common occurrence of stylolitised wallrock slivers within the vein provides evidence concerning the growth mechanism. The vein margins are irregular, with the development of wall-parallel veinlets indicative of fluid penetration along the cleavage planes. This process results in the separation of cleavage-bound fragments of wallrock which are rapidly chloritised as they become incorporated in the vein. The vein thus grows by an antitaxial crack-seal mechanism, typical of quartz veins forming in a quartz-poor medium (Durney & Ramsay 1973). The fact that the dominant external fabric (composite S2/S3 or S3 slaty cleavage) is parallel to the vein walls clearly has an important control on the type of vein fabric developed.

In antitaxial veins forming at an angle to the penetrative fabric in the host rock, solid inclusion bands (Ramsay 1980) usually form during the crack-seal process as an overgrowth of host rock phyllosilicates (Cox & Etheridge 1983; Cox 1987). However, where the vein is cleavage-parallel, these textures do not form because the phyllosilicate preferred growth direction is at a high angle to the dilation direction. Instead, erratic incorporation of wallrock slivers occurs as described above from $V3_C$ veins. Growth of quartz fibres is inhibited as the presence of a sliver prevents successive syntaxial overgrowths on pre-existing grains; as a result, fibrous vein fillings are not observed.

2.2.9 $V3_G$ veins

Field relations

Two very distinctive vein sets are developed crosscutting the metabasite sills exposed near Porthleven (Fig. 1.4). They clearly postdate a number of variably oriented, planar and folded thin veins, including some presumed to have originally been carbonate-filled and now empty as a result of recent weathering. These early veins are believed to represent fracturing and fluid movement through the sills during D1; veins characteristic of D2 appear to be absent within the sills themselves, although they are abundant in the slates in the vicinity.

The late veins, classified as type $V3_G$, have a fresh appearance, are relatively thick (1-15cm), and are composed of splintery, greyish, translucent quartz. Only the widest veins extend into the surrounding, locally hornfelsed, slates and then only for a few metres. As a result, it proved difficult to ascertain their age as the sills only poorly preserve deformation fabrics.

The veins clearly crosscut the weak S1 fabric developed in the sills, as well as F1/F2 fold structures present in some of the thinner units. The few veins that penetrate the slates, where fabrics are much better developed, show evidence of some D3 deformation in the form of buckle folds with axial planes sub-parallel to S3. Although limited, this evidence all points to a D3 origin for the veins.

The two dominant vein orientations only show slight variations from sill to sill (Fig. 2.10). The dominant set (Set 1) invariably contains the thicker veins which are subvertical or dip steeply NE and trend NNW-SSE. They often show evidence of shearing along their margins, a point which has a bearing on their mode of formation (see below). Set 2 veins trend NNE-SSW to NE-SW and dip at 40-90° to the NW. Poles to Set 2 veins (Fig. 2.10) fall on a great circle suggesting that rotation may have occurred; this also has implications for the mechanism of vein growth and subsequent deformation.

Crosscutting relationships between the two vein sets are inconsistent. This observation, combined with fluid inclusion evidence (see 3.2.3) points to their contemporaneous formation. The conjugate nature of the vein arrays suggests that they formed in a shear zone, the orientations being consistent with a Riedel shear model (Riedel 1929).

Set 1 veins are interpreted as initiating as R1 Riedel shears which formed at a low angle to the shear zone and show the same sense of shear as the zone itself. Set 2 veins may have initiated as extension fractures which suffered significant subsequent rotation, possibly being reactivated as R2

anti-Riedel shears. Alternatively, they may have initiated as R2 anti-Riedel shears. Either way, the fact that they sometimes display shear displacements with an opposite sense to those developed across the Set 1 veins (Fig. 2.11) suggests that at least some anti-Riedel shearing occurred.

Offsets of one vein set across the other provide conflicting evidence regarding the sense of shear. The apparent anti-clockwise component of rotation displayed by Set 2 veins suggests a horizontal component of sinistral shear across the zone. Where Set 2 veins are displaced across Set 1, both sinistral and dextral offsets are observed, where only one sense would be expected. Rare Set 1 vein offsets across Set 2 veins indicate dextral movement, although small, late faults in a similar orientation displace Set 1 veins sinistrally (Fig. 2.11). Offsets of sill margins where Set 1 veins extend into the slates are predominantly in a dextral sense.

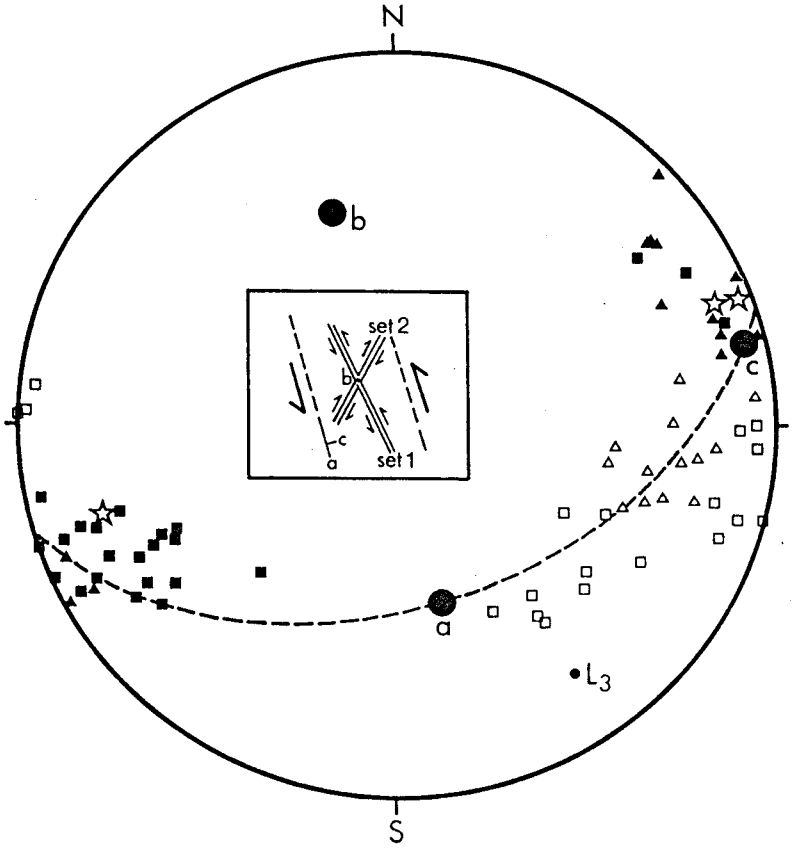

Figure 2.10 Equal area stereographic projection showing orientations of $V3_G$ veins. Solid symbols = Set 1 veins, open symbols = Set 2 veins; squares = Porthleven Harbour, triangles = Western Tye, stars = veins reactivated during dextral wrench faulting. Inset: horizontal section through postulated shear zone. Reference axes a, b and c are shown.

The key to resolving these problems is the recognition of reactivation of the steep,NNW-trending (Set 1) structures during the late wrench faulting and base metal mineralisation episode (see 1.3.5). Clear evidence of reactivation is provided by the brittle deformation evident along the margins of some of the Set 1 veins and the introduction of siderite, sphalerite and galena, typical components of $V4_W$ veins (see 2.2.15). The late wrenching is known to be in a dextral sense (see 1.3.3) and late

dextral reactivation of the Set 1 structures, and possibly sinistral reactivation of some of the Set 2 fractures can neatly account for the observed contradictory evidence.

The interpreted shear orientation and sense, with the shear plane (ab) defined as being at a low angle (20°) to the Set 1 (Riedel) fractures, are illustrated in Figure 2.10. The b-direction is constrained by the vein intersections. The kinematic axes a, b and c are orthogonally related to the shear zone orientation (see inset, Fig. 2.10).

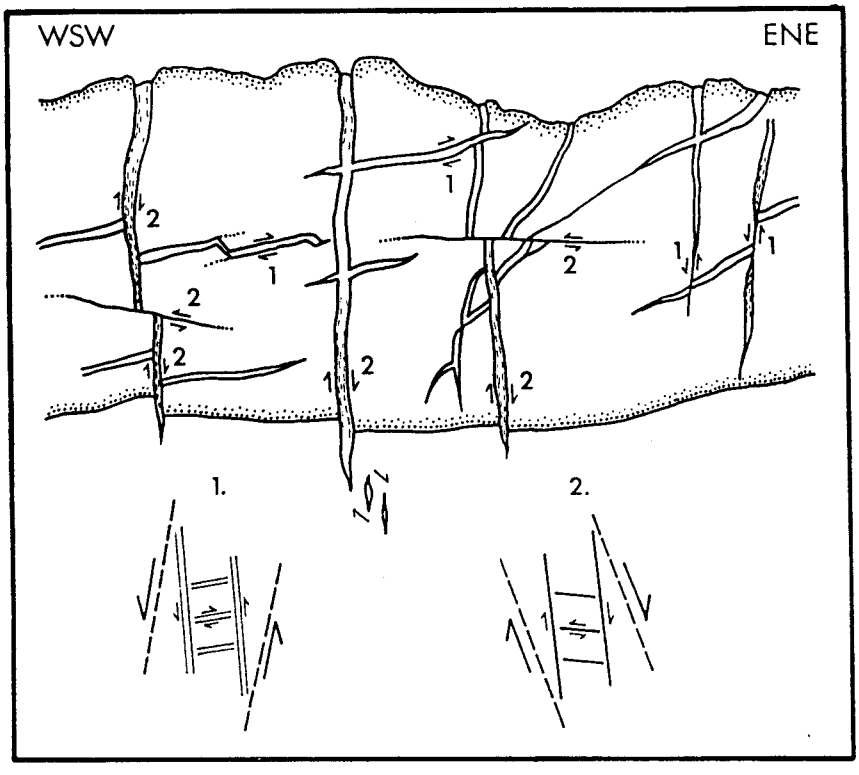

Figure 2.11 Sketch of metabasic sill exposed just south of Porthleven Harbour showing $V3_G$ veins. Numbers refer to initial shear sense across fractures (1) and late reactivation (2).

Microstructure

Apart from quartz, minor amounts of white mica, pale green mica, chlorite and carbonate are present. Several examples of fibrous actinolite (formed during contact metamorphism) growing into $V3_G$ veins at Tregear Point (Fig. 1.4) have been observed. The micas usually occur as a replacement of altered and stylolitised wallrock fragments, although scattered crystals within the vein suggest that some direct precipitation from the fluid occurred. A pale greenish-blue colour is taken to indicate a high ferrous iron and/or chromium content, suggesting a local (greenstone) source for at least some of the components of the fluid. Chlorite, often oxidised to a brown colour, is present only in stylolitic seams where it commonly replaces white mica and appears to be related to a late fluid event. Siderite occurs as irregularly distributed small crystals or aggregates of crystals and only forms a very minor component of the veins.

Opaque phases have been observed, particularly in veins and their wallrocks nearer the granite. Galena has been identified from a $V3_G$ vein from Porthleven Sands, whereas in the Giant's Rock/Tregear Point region, arsenopyrite is common. Sulphide mineralisation in the greenstones of the latter area is abundant in the wallrocks and is relatively rare within the vein itself (see 1.3.5).

Quartz crystals are usually large (up to 20mm long) and have a subhedral bladed or prismatic form. Occasionally, drusy terminations and cavities are observed in vein centres. Deformation of the veins is generally moderate or weak and is reflected by weak to strong undulose extinction and moderate subgrain development, commonly in a "chicken-wire" texture. Some (reactivated) vein margins show evidence of brittle shearing with the development of cataclastic textures typified by grain size reduction. The most highly deformed veins are invariably those trending NNW-SSE, subparallel to the D3/post-D3 shearing direction.

The growth mechanism for $V3_G$ veins is uncertain. There is no evidence to support a crack-seal process, although syntectonic recrystallisation at elevated temperatures would obliterate characteristic crack-seal features such as fibrous textures or solid inclusion bands. Recrystallisation is likely to be important in $V3_G$ veins developed to the north of Porthleven, which formed at temperatures in excess of 350°C (see section 4.4.2).

2.2.10 $V3_S$ veins

Field relations

Syn-D3 veins observed in the slates of the contact aureole, are particularly well-developed to the north of Porthleven (Fig. 1.4). As with the $V3_G$ veins, two dominant vein sets are observed (Fig. 2.12). The first group (Set 1) are the most abundant and display very similar orientations to $V3_G$ Set 1 veins. The other group (Set 2) consistently dip moderately ENE and appear to be related to the same shearing event. Both vein sets sometimes form en-echelon arrays, particularly at the termination of small, non-dilatant wrench faults (Fig. 2.13).

Detailed mapping in the Giant's Rock section (Fig 2.13) combined with the orientation data (Fig. 2.12), have assisted the production of a model for vein formation. As described above for $V3_G$ veins, the geometry of $V3_S$ vein arrays may be explained by formation in a shear zone.

Set 1 veins are interpreted as initiating as R1 Riedel shears. The occurrence of some Set 1 veins in arrays parallelling the orientation of Set 2 veins suggests that they may also form as extension fractures during anti-Riedel shearing (inset, Fig. 2.13). The dispersion of Set 1 poles around a great circle may be due to rotation during progressive shear. Set 2 veins display orientations consistent with their formation as extension fractures (inset, Fig. 2.12). Detailed mapping indicates that they usually define arrays parallel to Set 1 veins and thus probably initiate as extension fractures during Riedel shearing (*cf.* $V3_G$ Set 2 veins). Estimates of the shear zone orientation, shear direction and sense, consistent with the Riedel model are shown in Figure 2.12.

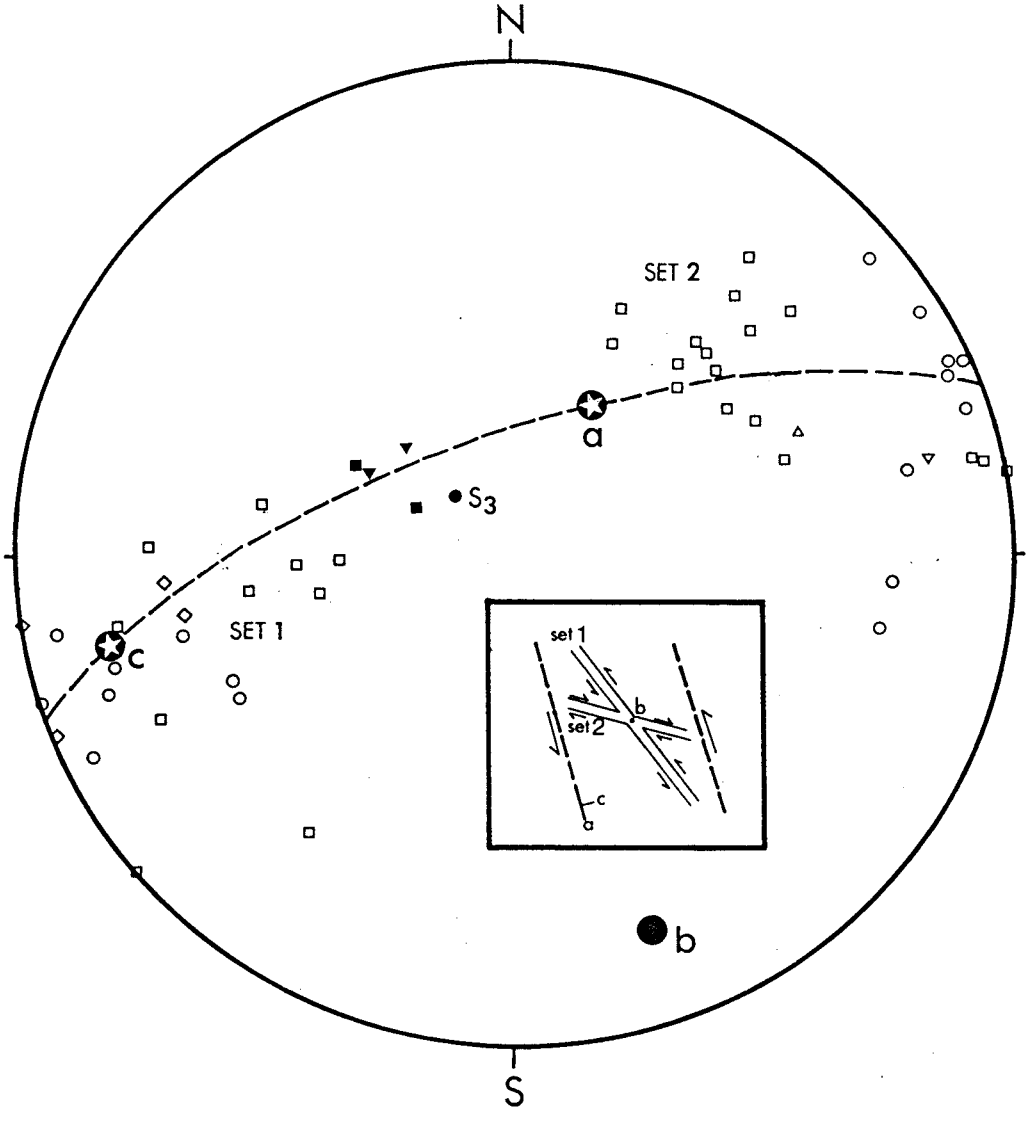

Figure 2.12 Equal area stereographic projection showing $V3_S$ and $V3_C$ vein orientations. Solid symbols = $V3_C$ veins, open symbols = $V3_S$ veins; triangles = Loe Bar, inverted triangles = Parc-an-als Cliff, circles = Vellin glûz Rocks, squares = Giant's Rock, diamonds = Tregear Point. Inset: horizontal section through postulated shear zone. Reference axes a, b and c are shown.

The shear plane (ab) is in a similar orientation to that estimated for the $V3_G$ veins. However, the movement direction (a) is upward to the SSE, rather than downward to the SSE. Further work will be required, both to test the proposed models of $V3_G$ and $V3_S$ vein formation, and to assess the role of the proposed shear zones in deformation of the contact aureole during granite emplacement.

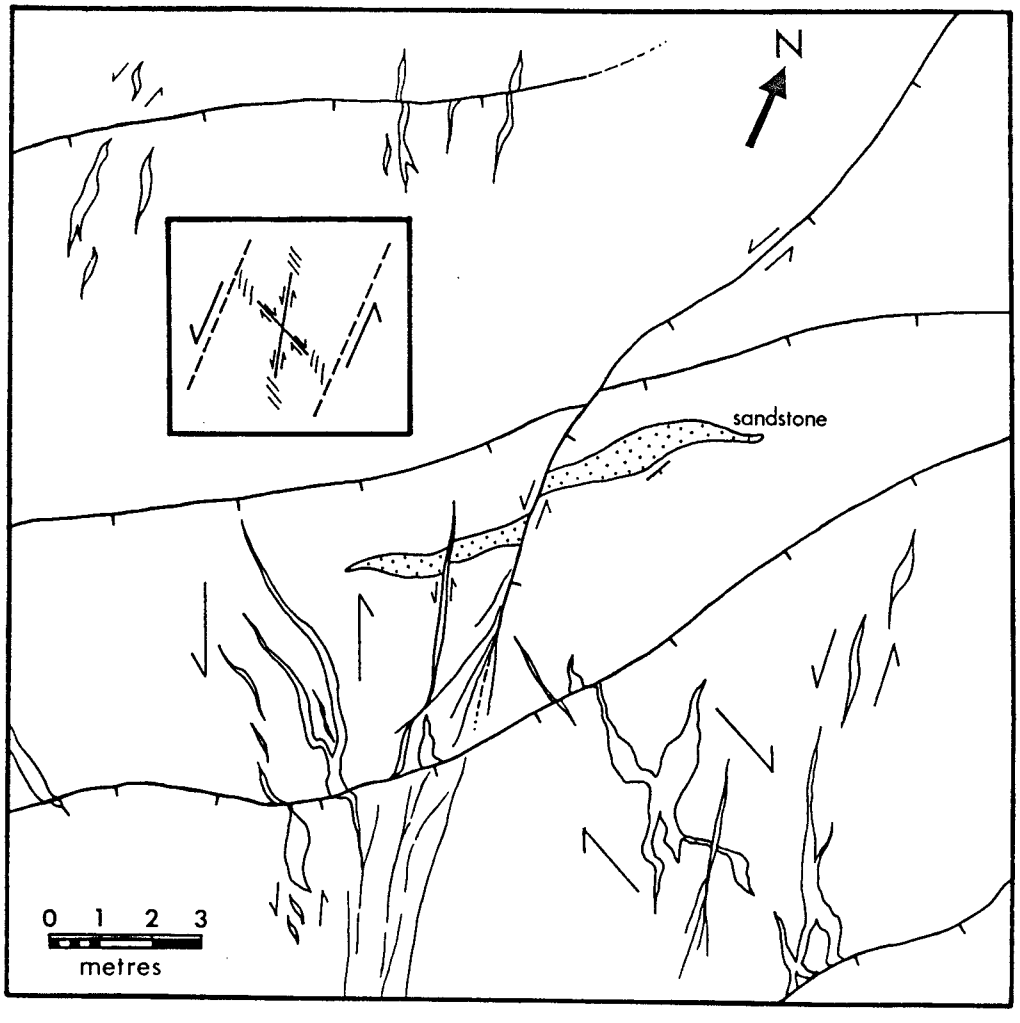

Figure 2.13 Map showing distribution of veins and faults in the Giant's Rock area (bottom left corner is SW 6230 2575). Inset: Sinistral shear zone interpretation of vein and fault arrays. Note extensional pinnate fractures associated with Riedel ant anti-Riedel shears.

Microstructure

Almost identical microstructures are developed in $V3_S$ veins to those described from $V3_G$ veins (see above). A general observation is that deformation textures are better developed in the $V3_S$ veins. This is presumably because the $V3_G$ veins are protected from deformation by the relatively rigid greenstone host rock whereas the slate-hosted veins are subject to significant shearing during the D3 event.

Ore minerals in these veins are more abundant than their $V3_G$ counterparts. Reflected light microscopy has revealed that arsenopyrite is the most common phase with minor chalcopyrite, pyrite, galena and sphalerite. The phases are best developed in the wallrocks but arsenopyrite is also common within the vein, nucleating on altered wallrock slivers.

2.2.11 $V4_P$ veins

Field relations

Vein and pegmatite quartz in intimate association with the granite pegmatite-aplite sheets exposed at Megiliggar Rocks in the north of the section (see 1.3.2) are classified in this group.

The lithium- and fluorine-rich pegmatite sills have their origin in the volatile-rich roof zone of the Tregonning granite stock. They were intruded 400m into hornfelsed slates, sub-parallel to the S3 fabric. The contacts of the stock crosscut, and do not deform, S3 indicating that it was emplaced by relatively passive stoping, after the cessation of S3 cleavage development (*e.g.* Stone 1975). The intimate association of the pegmatites with the granite indicates that they were also emplaced post-D3 and exploited the country rock anisotropy by preferential intrusion along the S3 cleavage.

The uppermost sill terminates at Tremearne (Fig. 1.4) in an irregular mass of quartz veins which are sub-parallel to S3. These veins are closely associated with the pegmatites and probably represent the crystallisation of quartz from a distal, silica-rich, aqueous fluid, which separated from the pegmatite melt (Badham 1980). As such, they are included in the $V4_P$ classification. This group represents fluid activity at a very early post-D3 stage and is particularly important as it reflects a continuum from late stage magmatic to early hydrothermal events in the fluid evolution history. This point is considered in more detail in section 4.5.

Microstructure

Quartz crystals are generally large (up to several cm), sub- to euhedral and equigranular. The pegmatites are composed of quartz, K-feldspar, plagioclase, lepidolite, topaz and other accessories (see Stone 1975 for details). In the quartz veins, albite is sometimes observed and is intimately intergrown with quartz. Arsenopyrite and löllingite are relatively common (Badham 1980) and actinolite is also observed, usually occurring in cavities and in crosscutting fractures.

Deformation is slight as evidenced by weak undulose extinction in quartz, developed throughout. More significant deformation is represented by late, crosscutting fractures which formed during later stages of vein growth ($V4_J$ veins). Associated with these fractures are minerals and fluid inclusions representative of the subsequent events. These are difficult to resolve where no obvious (macroscopic) fractures are present. Detailed examination of the relationships between fluid inclusion trails and grain boundaries are vital in identifying such late fluid overprints (section 3.2.4).

2.2.12 $V4_{J1}$ veins

Field relations

Veins in two subvertical orientations are particularly well-developed in the vicinity of the granite. Both $V4_{J1}$ veins and the following group ($V4_{J2}$) trend WSW-ENE and NNW-SSE, the directions being controlled by the regional post-D3 stress field (Moore 1975). The two vein types may be distinguished in the field by the macroscopic vein fabric, and wallrock alteration which reflect the mechanism and temperature of formation.

$V4_{J1}$ veins strike dominantly WSW-ENE and dip steeply to the north or south, parallel to the trend of the batholith and the majority of the mineralised lodes (*e.g.* Hosking 1964). They are typically up to 10mm across and are composed of translucent, equigranular quartz. Intense wallrock alteration, extending for distances up to 30cm from the veins, is clearly apparent in the field. This alteration, which is characterised by a tourmaline-quartz assemblage, is a relatively high temperature phenomenon (*c.* 400°C), often described as an early greisening event (Exley *et al.* 1983).

Veins of this type are usually interpreted as forming by hydraulic fracturing of the carapace (in this case metasedimentary rather than granitic) above a high temperature, high fluid pressure reservoir (*e.g.* Halls 1987). Although the development of "locked-in" tensile stresses occurs during cooling, calculations indicate that these stresses are insufficient in themselves to cause fracturing (Jackson *et al.*, in press), and that an additional factor (hydraulic pressure or tectonism) is required.

Microstructure

Thin section examination reveals that the veins are composed of quartz with abundant brown tourmaline needles (up to 4mm long) and fine mica flakes distributed throughout (Fig. 2.14). The micas have a very pale brown colour and are likely to be Li- and/or Fe-rich (lepidolite or zinnwaldite respectively). Lepidolites are common in the lithium-rich Tregonning granite (Stone 1975) and zinnwaldite has often been recorded from early greisen veins (*e.g.* Charoy 1979). No opaque minerals have been observed in the samples, although the veins are interpreted as being contemporaneous with mainstage cassiterite, wolframite and polymetallic sulphide mineralisation (see 1.3.5).

Quartz crystals are generally equidimensional with slightly irregular boundaries. 120° triple junctions are common indicating thermodynamically stable grain boundaries. There is no evidence to suggest multi-stage vein growth, although any primary fabrics may have been obliterated by high temperature annealing.

The veins are essentially undeformed, with only very weak undulose extinction observed in quartz. They also display little evidence of a late fluid overprint (see 3.2.6), which may be explained by their orientation, subparallel to the major post-D3 fractures.

2.2.13 $V4_{J2}$ veins

Field relations

These veins, which are usually 5-20mm thick, display identical orientations to the last group and relate to the same regional stress field. They may be distinguished from $V4_{J1}$ veins in the field by the lack of high temperature wallrock alteration (although distinct alteration is still observed - see section 3.6) and the presence of drusy quartz. They represent a later, lower temperature stage in the history of granite-driven hydrothermal circulation.

Although commonly regarded as being the result of fluid flow through pre-existing contractional cooling joints, stress modelling by Jackson *et al.*, in press) suggests that such veins require a hydraulic pressure to form. Thus, in a similar manner to the $V4_{J1}$ veins discussed previously, the combination of a "locked-in" tensile stress due to cooling with a high fluid pressure

Figure 2.14

Figure 2.14: Captions

A. $V3_C$ vein, showing slight boudinage and wrapping by S3 fabric, Mylor Slate Formation, Giant's Rock (*J91GR*). Viewing direction: E; Scale bar = 5cm.

B. Photomicrograph (crossed polars) of sub-vertical $V4_{J1}$ vein from Tremearne Cliff (*JW005*) showing complete replacement of slate wallrock by tourmaline, quartz and K/Li mica. Tourm = tourmaline, Lep = lepidolite. Note preservation of sub-horizontal S3 fabric and irregular vein fabric. Scale bar = 2mm.

C. Photomicrograph (plane polarised light) of sub-vertical $V4_{J2}$ vein from Tremearne Cliff (*JW007*) showing drusy quartz vein fabric and incorporation of chloritised fragments of wallrock. Qz = quartz, Chl = chlorite. Scale bar = 1mm.

D. Hanging-wall of $V4_N$ structure, Parc-an-als Cliff, showing brittle deformation, development of drusy quartz and pyrite (Py) mineralisation. Viewing direction: NE; Scale bar = 2cm.

E. Margin of Wheal Rose ($V4_W$), Parc-an-als Cliff, showing banded drusy quartz and siderite, coarse galena (Gn) and incorporation of wallrock fragments. Viewing direction: SE; Scale bar = 5cm.

F. Photomicrograph (plane polarised light) showing growth zone in drusy quartz (Qz) and galena (Gn) in $V4_W$ vein (*J98PC2D*). Scale bar = 2mm.

G. Photomicrograph (plane polarised light) of deformed V1 vein (*J18GW*), with quartz showing dusting of tiny ($<5\mu$m) fluid inclusions. Note obliteration of inclusions along recrystallised grain boundaries. Scale bar = 200μm.

H. Photomicrograph (crossed polars) of previous field of view showing sutured grain boundaries and deformed wallrock stringer (upper left corner).

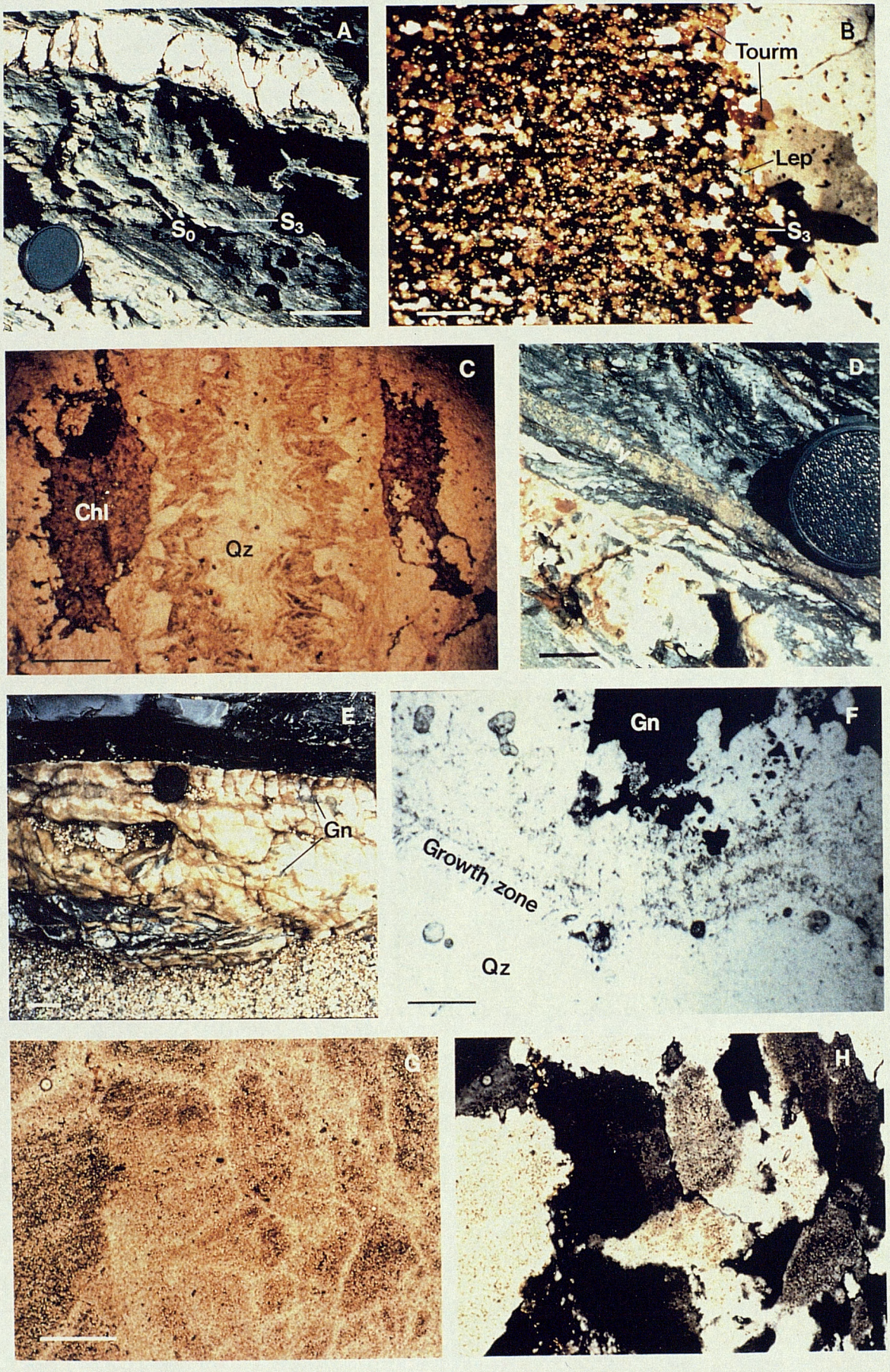
A
S_0
S_3
B
Tourm
Lep
S_3
C
Chl
Qz
D
E
Gn
F
Gn
Growth zone
Qz
G
H

resulted in failure. Since these veins formed at a lower temperature, the tensile stresses developed during thermal retrogression would have been greater. Consequently, the pore fluid pressures required to overcome the combined lithostatic pressure and rock strength would have been less. The development of drusy fabrics indicates that, once formed, the fractures were able to remain open, allowing free crystallisation of quartz into a fluid-filled cavity.

Microstructure

The most distinctive feature of $V4_{J2}$ veins is the presence of euhedral, drusy quartz crystals (Fig. 2.14). Generally less than 10mm long, the crystals are usually slightly wedge-shaped, hexagonal prisms with pyramidal terminations formed of a combination of rhombohedral and trigonal pyramid faces. Often cavities remain in vein centres where quartz infilling was incomplete. Growth zones, defined by bands of primary fluid inclusions and fine mica flakes, are extremely well developed (Fig. 2.14), particularly parallel to the rhombohedral crystal faces on which most of the quartz precipitation occurred during crystal growth. Fine white mica flakes are distributed throughout the growth zones, indicating that a change in physicochemical conditions accompanied zone development. Small carbonate grains are also occasionally observed, usually near the vein centres. Altered wallrock stringers, now composed of chlorite/sericite intergrowths and opaques are sometimes present (Fig. 2.14).

Numerous small new quartz grains nucleated along vein margins during the early stages of growth, rather than precipitation of quartz as overgrowths on wallrock crystals (*cf.* $V1_G$ veins). Favourably oriented grains rapidly occluded other crystals as described earlier for the margins of $V1_G$ veins. As a result, the vein centres tend to be dominated by relatively few, large crystals in a common crystallographic orientation.

Deformation of the veins is slight, with only weak undulose extinction indicating minor lattice disturbances. Later fracturing is more common and many structures have been the site of more than one stage of vein formation, now characterised by zones of multiple anastomosing veinlets.

2.2.14 $V4_N$ veins

Field relations

Close to the granite, joints were the most important fluid pathways during the later stages of convective hydrothermal circulation (see 6.1.5). Further away, as well as originally at higher levels in the crust, fluid flow was concentrated along fewer, more widely spaced structures. These structures are a series of normal faults which developed primarily in the country rock above the flanks of the batholith, during and after its emplacement. Late stages of movement on these faults probably relates to the formation of Permo-Triassic and later basins to the north and south of the Cornubian Peninsula (see 6.1.5).

The faults dip consistently southeast at 40-70° (Fig. 1.11). The earliest structures usually display the lowest angles of dip, possibly as a result of progressive rotation during extension (see 1.3.3). Quartz is invariably developed on the fault plane and there is commonly extensive associated veining (Fig. 2.14). Dilation across faults is often significant with quartz-filled zones up to tens of

centimetres across. Such regions show the development of large (up to 5cm) drusy crystals typical of open cavity growth. Although comparable with some of the important ore-bearing lodes in the province, these veins are only weakly mineralised in the field area, with the development of pyrite (Fig. 2.14), chalcopyrite and sometimes galena and sphalerite (see 1.3.5).

Microstructure

As with type $V4_{J2}$ veins, $V4_N$ veins are dominated by large, growth zoned, drusy quartz crystals. The growth zones are primarily defined by highly irregular, primary fluid inclusions elongated in the growth direction. Outside the growth zones, quartz crystals are remarkably devoid of inclusions, perhaps as a result of very slow, stable growth conditions.

Microstructural evidence of vein deformation varies considerably, depending on the sample position. Quartz from fault-related veining is often relatively undeformed with the development of weak and only occasionally strong undulose extinction. Brittle deformation is more common and is well developed in zones that have suffered later movement. Cataclastic deformation was the dominant process, with brecciation of pre-formed crystals or wallrock and incorporation of the fragments into later veins.

2.2.15 $V4_W$ veins

Field relations

There are three examples of late, mineralised wrench faults exposed in the area. The major zone, composed of anastomosing faults and fractures, trends NNW-SSE and is exposed immediately south of Porthleven Harbour (Fig. 1.4). This fault system is likely to be the southern extension of the "Great Flukan" (Dearman 1963), a mineralised cross-course (see 1.3.5) which traverses the peninsula starting at Hayle on the north Cornish coast. The two other lodes, which trend N-S, are exposed further south. Wheal Rose outcrops on the foreshore below Parc-an-als Cliff (Fig. 2.14) and the other worked vein is exposed to the south of Vellin-glûz Rocks (Fig. 1.4).

Minor veins associated with all of the lodes trend N-S as well as NNW-SSE. This evidence, combined with the similar parageneses developed, suggests that the veins and faults all formed under the same stress conditions. Abundant mine data (Henwood 1843) and structural studies (*e.g.* Dearman 1963) indicate that the cross-courses always trend between N-S and NW-SE and usually display dextral wrench offsets, although variable dip-slip displacements are also observed. Details of the tectonic regime under which these structures formed are discussed in section 1.3.5.

The history of these fractures is complex and reactivation is common (*e.g.* Holloway & Chadwick 1986). The Porthleven Lode shows evidence of initiation as a sinistral structure during D1/2 compression or D3 sinistral shear, prior to minor dextral reactivation during base metal mineralisation (Fig. 2.15). Wheal Rose shows clear reactivation of a $V3_S$ structure, with milky quartz (containing V3 fluid inclusions typical of $V3_S$ veins) forming the margins of the later, $V4_W$ vein. The early quartz is brecciated and incorporated in the later vein material. The $V4_W$ structure also has a complex relationship with a pre-existing normal fault at this locality, further complicating interpretations of the structural and fluid evolution history of this stage (see 4.6.4, 6.1.5).

Figure 2.15

Figure 2.15: 1:30 Scale maps of the Porthleven Lode

The following three pages are reproductions of 1:20 scale field maps of the Zn-Pb mineralised $V4_w$ vein exposed on Porthleven Sands (Porthleven Lode, Fig. 1.4). The maps run sequentially from NNW to SSE, starting at SW 6282 2545, approximately 80 metres southeast of Porthleven Pier. There is slight overlap between the three maps presented.

1

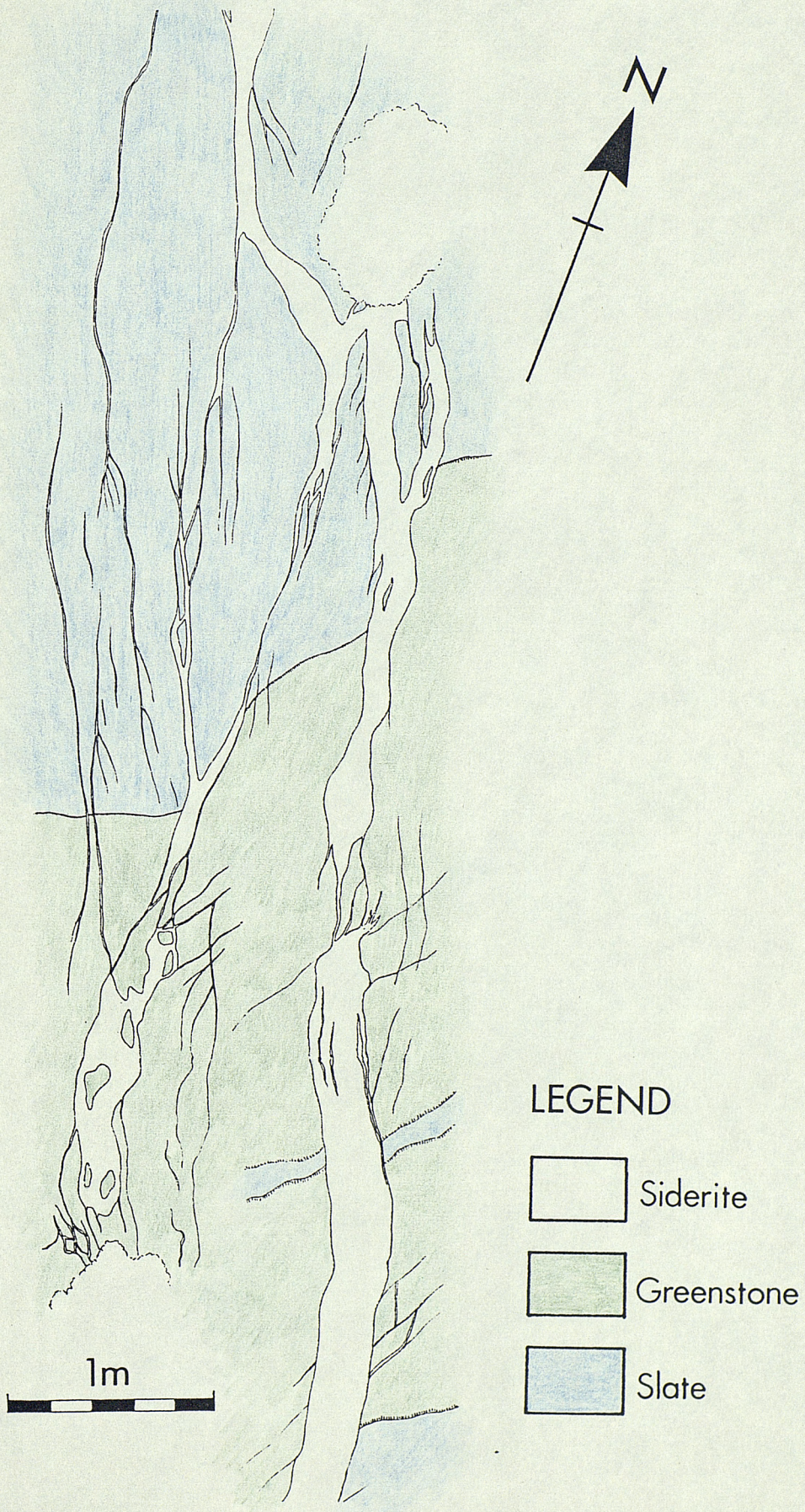

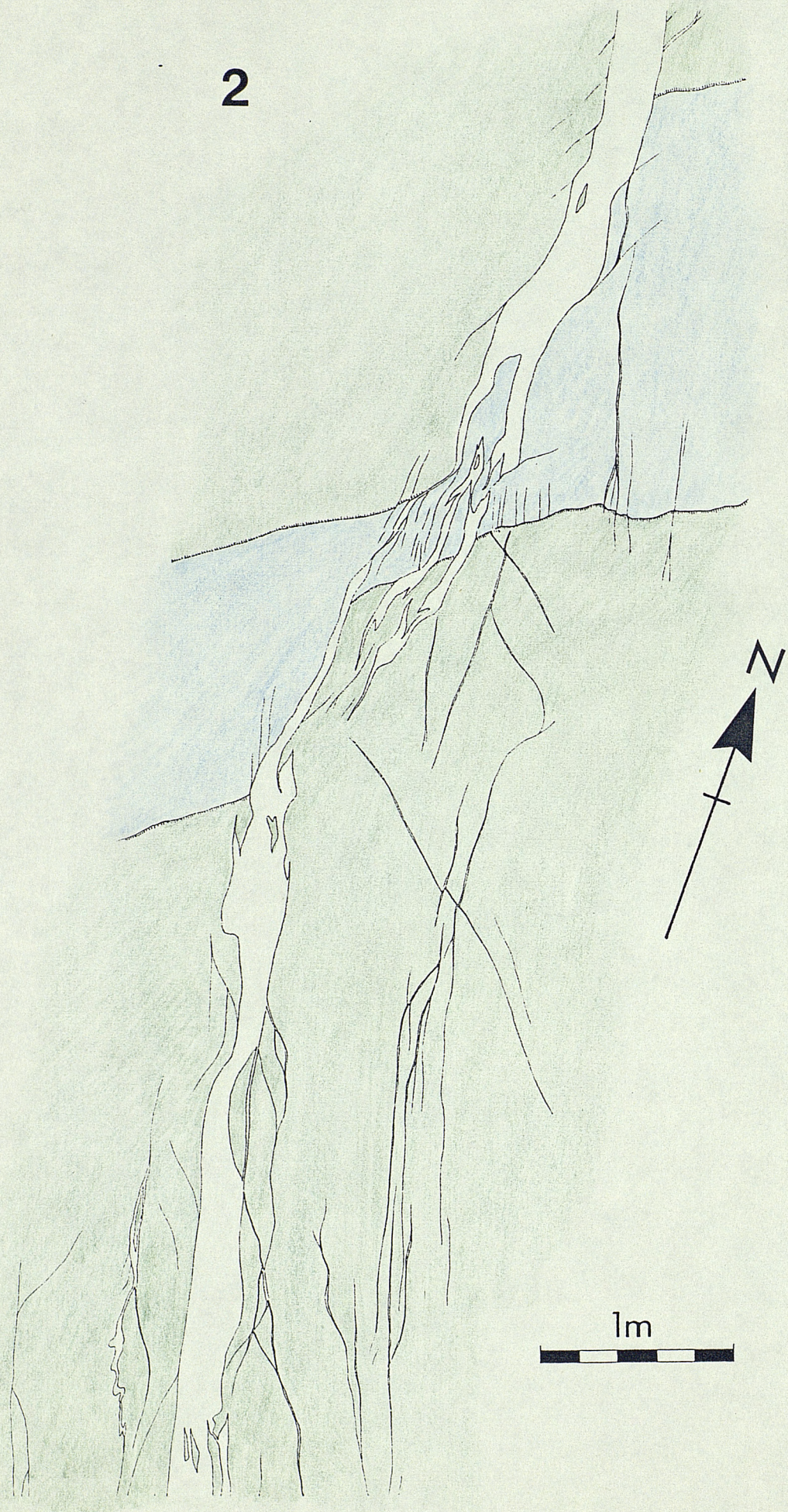
2
N
1m

3

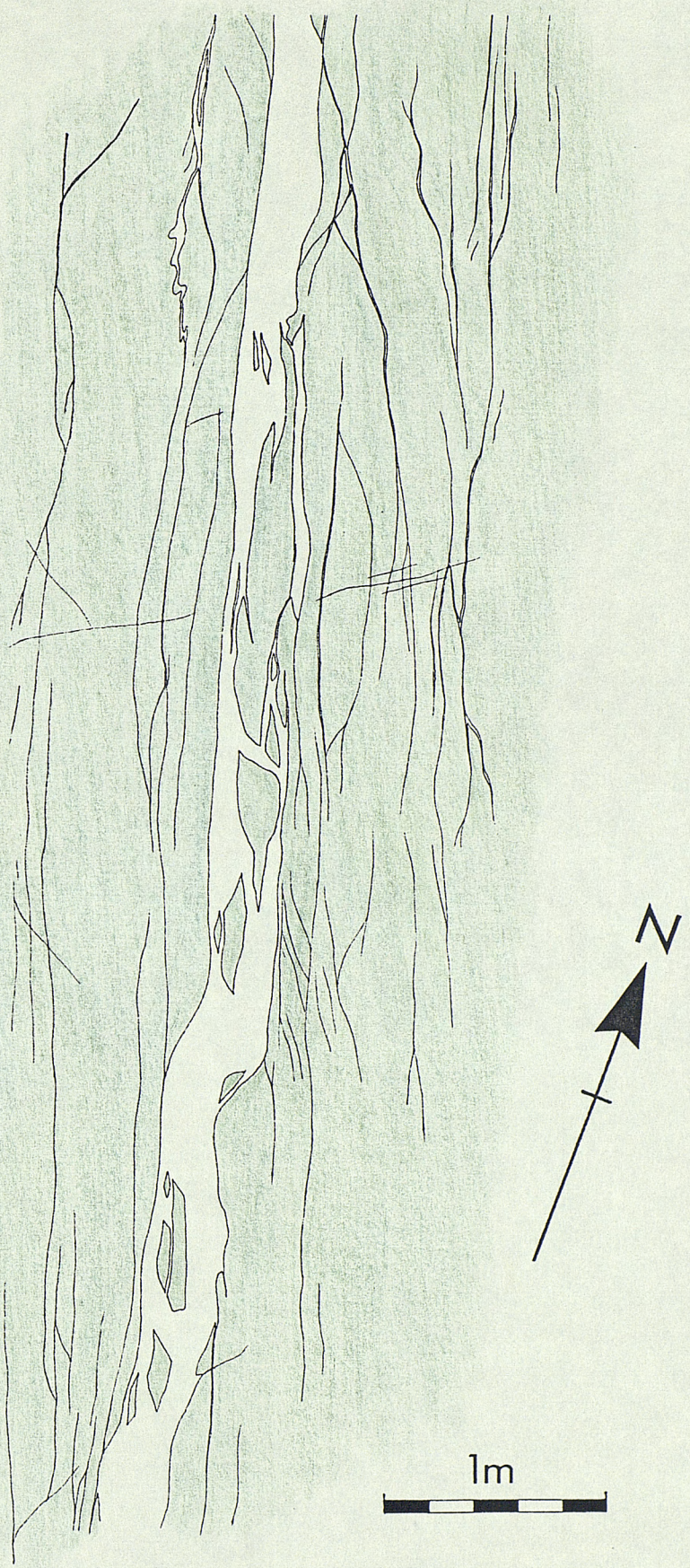

Microstructure

The fabrics developed in $V4_W$ veins are very similar to those described from $V4_N$ structures, suggesting a comparable mode of formation. However, the vein mineralogy and the fluids responsible are very different (see 3.2.8, 4.6).

The four main parageneses observed in these veins are summarised in Figure 2.16. All are characterised by the alternate precipitation of siderite and quartz, although the order may vary and the veins are commonly composite. Chalcopyrite is usually the earliest ore mineral, followed by sphalerite (contemporaneous with siderite) and galena (usually associated with quartz). Galena is often the first phase to precipitate after the formation of a growth zone; this problem is considered in more detail in section 5.5.3.

Quartz and siderite are the dominant vein-filling minerals and occur mainly in drusy habits, although fine grained, granular varieties are also observed. These features are consistent with crystal growth into an open, fluid-filled fissure.

Vein deformation is, as with $V4_N$ veins, localised, with many quartz crystals showing only very weak undulose extinction. Some zones, particularly along the margins of the fault-hosted quartz veins, display intense brittle deformation with wallrock and vein fragments cemented by later generations of vein infill. The occurrence of angular, matrix-supported fragments suggests that catastrophic implosion of the wallrocks as a result of a sudden drop in fluid pressure was a common phenomenon.

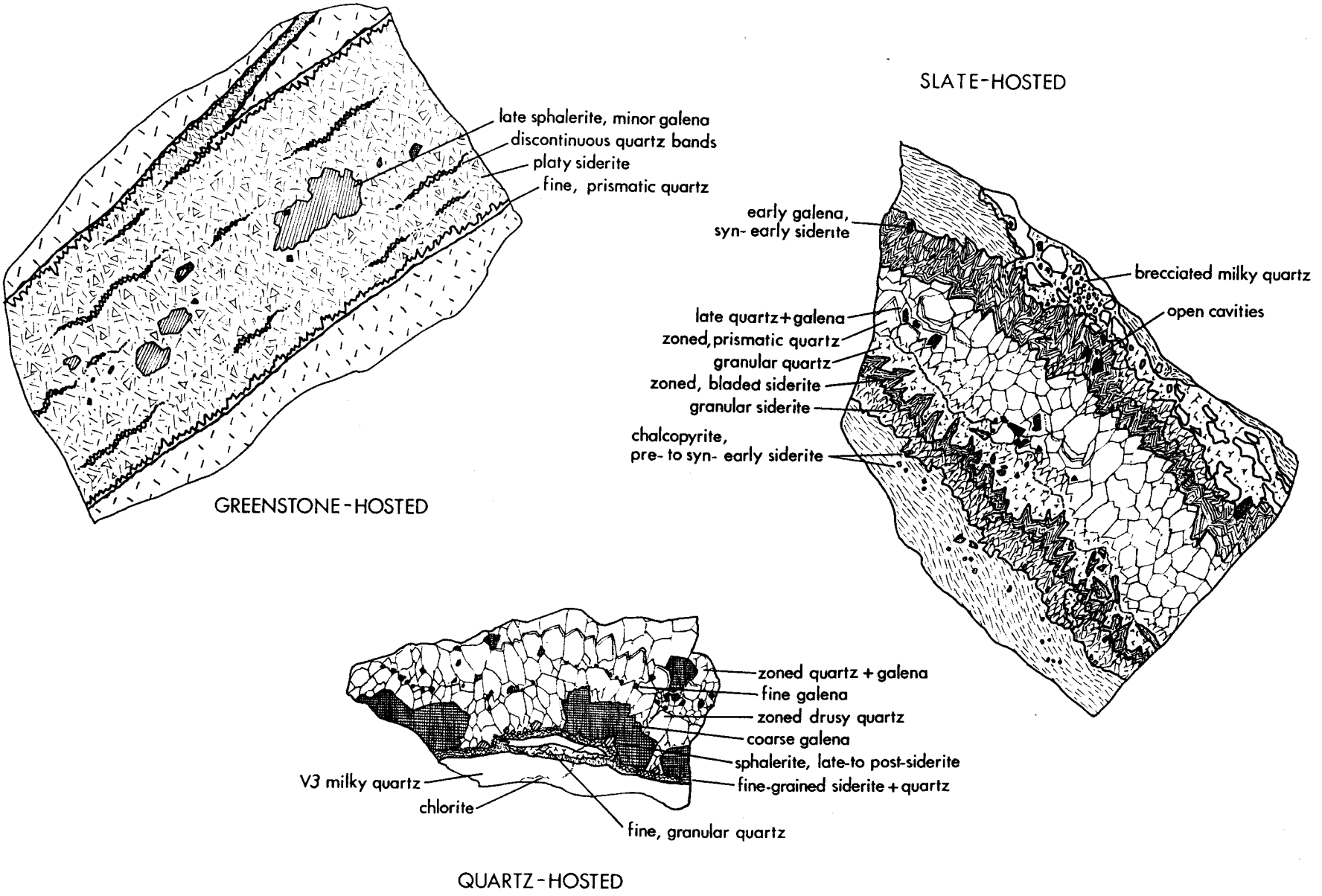

Figure 2.16 Parageneses of $V4_W$ veins observed in the study area.

2.3 SUMMARY

This chapter summarises the methods and field and petrographic data used to classify veins formed throughout the orogenic development of the crustal segment being studied. The descriptive vein classification system presented, although of necessity a simplification, provides adequate resolution of the major fluid events.

Four tectonic stages are distinguished, related to the three main deformation events which affected the area. Within each stage, up to four different vein types have been recognised, occurring in distinct structural and/or lithological settings.

V1 group veins are particularly well-developed in the south of the area, where they are also less affected by subsequent deformation events. V2 veins are best developed in the central part of the field area, at the allochthon thrust front (see 1.3.3). V3 veins are developed throughout the zone affected by D3, being observed up to 5km from the Tregonning granite. Granite-related veins ($V4_P$, $V4_J$) are observed proximal to the Tregonning granite, not occurring further than 2km laterally from the granite contact. Late veining related to normal and wrench faults ($V4_N$, $V4_W$) is sporadically developed throughout the area.

Fluid inclusions in samples of all of these vein types have been analysed by a variety of techniques. In the following chapters, these data are presented and discussed with the aim of characterising and modelling the fluids mobilised during each tectonic stage.

The sample numbering scheme and its use in identifying the zone from which a sample came is detailed in Appendix A1. A table of samples examined, identifying those which proved suitable for further analytical studies, is presented in Appendix A2.

CHAPTER 3: FLUID CHARACTERISATION

Fluid inclusions present in Hercynian quartz veins developed in south Cornwall (see Chapter 2) have been investigated using a variety of techniques in order to characterise the fluids mobilised at each stage of the tectonothermal evolution of the area. These techniques are briefly outlined and the limitations discussed. Detailed descriptions of equipment calibration procedures are included in Appendix C. The fluid data obtained are summarised in this chapter and are presented in full in Appendix D. Models for fluid evolution, metal tansport and ore deposition, based on the data reported in this chapter, are presented in Chapters 4, 5 and 6.

3.1 EXPERIMENTAL APPROACH

The primary aim of the study was to characterise the fluids flowing through the crustal segment of south Cornwall during the Hercynian orogeny. The variables of interest were the fluid composition (X), fluid temperature (T) and fluid pressure (P). Not only are these parameters important in modelling fluid evolution and metal transport, but they also allow constraints to be placed on the tectonothermal evolution of the Hercynian thrust belt.

Two main approaches were used to determine fluid P-T-X. The direct approach involved the analysis of fluid inclusions, which represent actual samples of the fluids that flowed through the rock, trapped during, or subsequent to, crystal growth. The indirect approach, which comprised an X-ray diffraction (XRD) study of wallrock alteration, allowed fluid P-T-X to be inferred from theoretical and empirical data.

The direct analytical methods include techniques which provide information on individual pulses of fluid flow as well as those which reflect the net (bulk) effect of the passage of several generations of fluid. Obviously, the former methods are the most valuable for defining trends in fluid evolution. However, they are limited by the availability of experimental data which are vital in interpreting the results, and by the general lack of appropriate microanalytical hardware. The bulk techniques are statistically superior and more rapid, but are subject to interpretative problems which may only be overcome by careful sample selection (see 3.3.1). Figure 3.1 summarises the above discussion and relates each technique to the information which may be obtained (P, T or X).

The techniques used provide quantitative, semi-quantitative and qualitative data. In combination, they provide a much greater degree of confidence in the P-T-X data than any one alone. Such a combined approach is believed to be essential in any study of fluid evolution and fluid-rock interaction.

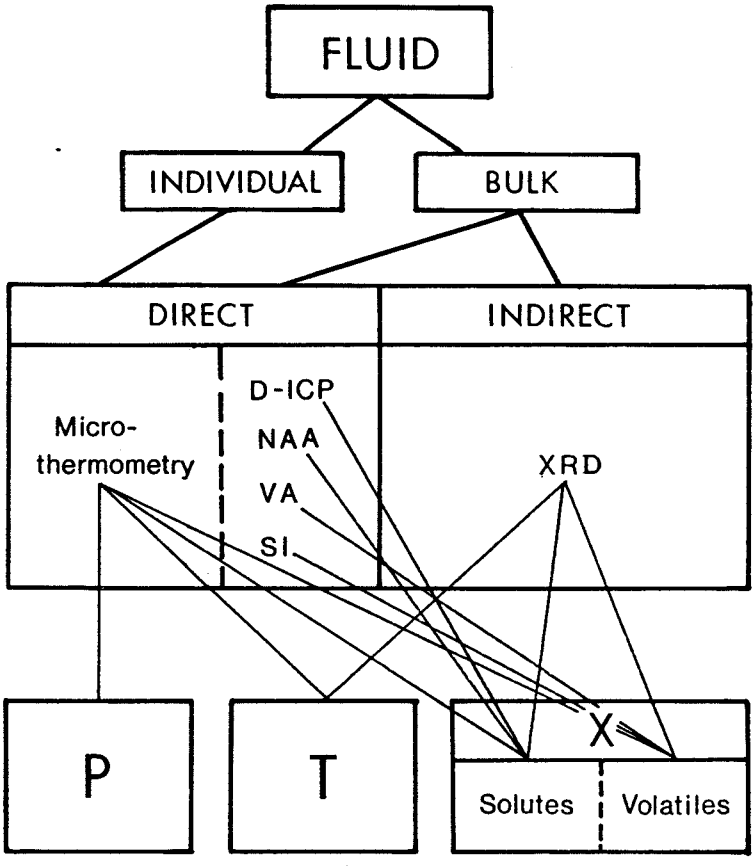

Figure 3.1 Relationships between analytical techniques and the type of data obtained.

3.2 MICROTHERMOMETRY

3.2.1 Introduction

The significance of fluid inclusions in natural and laboratory grown minerals was first recognised by Henry Sorby in 1858. In his classic paper of that year, he argued that fluid inclusions in minerals represent trapped portions of the liquids, gases and melts from which the crystal had grown and could be used to establish the environment in which a rock or mineral might have formed. Despite Sorby's work, few advances in fluid inclusion research occurred until the 1950's when their potential use in a wide variety of geological studies became more apparent. The work of Roedder (1958, 1962) was the spur for many subsequent studies. Within the last ten years, the growth in interest has been rapid, with applications being found in extremely diverse branches of the subject. The fluid inclusion literature is vast; particularly useful texts and reference sources include Roedder (1984), Hollister & Crawford (1981) and Shepherd *et al.* (1985).

Thermometric analysis

Thermometric analysis is the most popular technique for the analysis of fluid inclusions. Not only is it non-destructive, but it is based on simple principles and requires relatively inexpensive equipment.

The method involves the recognition and measurement of the phase changes which take place in inclusions during heating or cooling. Reference to simple (usually 1, 2 or 3 component) fluid systems allows the derivation of the P-V-T-X state of the fluids at the time of trapping. The main limitation of the technique is the fact that most natural systems are multi-component so that P-V-T-X estimates are strictly only semi-quantitative. In such cases, the interpretation of thermometric data is difficult. There is at present a great deal of experimental and theoretical work being carried out in order to increase our knowledge of multi-component fluid systems. A detailed account of the theoretical arguments used in the interpretation of thermometric data is beyond the scope of this work. For more information the reader is referred to Hollister & Crawford (1981), Roedder (1984) and Shepherd *et al.* (1985).

An optical and thermometric fluid inclusion study formed a major part of the research project and provided an essential foundation for subsequent analytical work. A thorough knowledge of the fluid inclusion assemblage in a sample and the microthermometric characteristics are vital for the interpretation of bulk analytical data.

During the course of the investigation, fluid inclusions in 116 samples of vein quartz were studied in thin section under transmitted light, with 42 proving suitable (in terms of inclusion size and optical clarity) for thermometric analysis. Fluid inclusions were analysed thermometrically using 100-200μm thick, doubly-polished wafers (see Appendix B2) in conjunction with Linkam TH600 and THM600 heating-freezing stages. In all, some 1500 inclusions were analysed with up to 8 measurements made on each. For details of the operating procedures see Shepherd *et al.* 1985. The calibration method for both types of heating-freezing stage is outlined in Appendix C1.

In the following sections, descriptions of the optical and thermometric characteristics of the different sample groups are presented. For the sake of simplicity, samples from the same tectonic stage (*i.e.* D1, D2, D3, post D3) but from different structural settings (see 2.1.1) that contain essentially the same fluid inclusion assemblages are generally grouped together. For pre-granite samples this means that there are effectively two fluid types: a syn-D1 fluid and a syn-D2 fluid. Although there is some overlap, as a result of the progressive nature of deformation and associated fluid mobilisation, the two fluids are surprisingly well defined. For syn- and post-D3 samples, the picture is more complex, with much greater variability in terms of fluid P-T-X and in the structural controls of fluid flow (see sections 2.2.8 to 2.2.14). These samples will therefore be discussed in more detail.

Fluid inclusion age

The relative age of fluid inclusion populations within a sample is often a difficult problem to resolve, since the simplest criteria for recognising "primary" inclusions, those which formed contemporaneously with vein growth (Roedder 1984), are commonly ambiguous, if not completely lacking. For example, in V1 samples, standard criteria would indicate that some of the inclusions may be primary, but that the majority are of pseudosecondary or secondary origin. However, the thermometric data indicate that essentially one fluid is present, represented by a complex fluid inclusion assemblage. In addition, the P-V-T properties of this fluid are consistent with trapping under peak metamorphic conditions (see 4.2.1). This evidence suggests that most of the inclusions in V1 samples were formed during or soon after peak metamorphism.

Many recent studies of fluid flow during regional and contact metamorphism (*e.g.* Walther & Orville 1982) have shown that transient microfracture permeability is likely to be significant during deformation (see 6.1.2). A consequence of this is that fluid inclusions in annealed fractures in vein material, which represent fluids flowing through the pervasive microfracture permeability, may be at least as significant as primary fluid inclusions present in macroscopic veins. On this basis, it would be logical to expect fluid inclusions formed by both these mechanisms to represent the same fluid. This is strongly supported by the thermometric data for V1 fluid inclusions which indicate the presence of one fluid type in inclusions of various origins. On the basis of these arguments, it is considered that the commonly used approach of classifying inclusions with regard to their mode of formation is unsatisfactory for syn-orogenic vein material. The preferred method (*e.g.* Crawford & Hollister 1986), is to identify relative inclusion ages where possible, such as by the relationships between inclusion trails and quartz microstructures. This allows constraints to be placed on variations in the P-V-T-X properties of fluids flowing through microfractures during orogenic evolution.

Evidence regarding the absolute age of these fluids comes from the P-V-T properties of the inclusions and the probable age of formation of quartz deformation structures. In the case of V1 samples, most inclusions occur in trails that pre-date grain boundary migration (see Figs. 2.14, 3.2). This implies that the majority of inclusions formed prior to significant quartz deformation and are therefore likely to represent fluids mobilised at an early stage of orogenic evolution. This is in agreement with the P-V-T-X properties, as mentioned above.

3.2.2 V1 fluid inclusions

Optical characteristics

Type V1 veins are composed of milky, fibrous or granular quartz (see 2.2.1-3). The opacity results from the presence of myriads of tiny fluid inclusions. Two main inclusion types may be distinguished both optically and thermometrically. A synoptic sketch of the nature and distribution of fluid inclusions in V1 samples is presented in Figure 3.2 and a photomicrograph of a typical thin-section field of view is shown in Figure 3.3. A summary of the main optical characteristics is presented in Table 3.1.

Figure 3.2

Figure 3.2: Synoptic sketches of fluid inclusion assemblages.

Summary sketches of V1, V2, V3 and V4 veins showing major inclusion types and modes of occurrence. Dotted lines indicate quartz grain boundaries, scale bar is 1mm long in each case. For clarity, inclusions are drawn approximately 10x true size.

A. V1 vein sample:

a) Solitary inclusion of V1 type

b) Cluster of inclusions of V1 type

c) Trail of inclusions of V1 type defining annealed microfracture, crosscut by recrystallised sutured grain boundary (with new small strain-free crystals)

d) Trail of inclusions of V2 type, crosscutting grain boundary

e) Apparently isolated inclusion of V2 type

B. V2 vein sample:

a) Solitary inclusion of V2 type

b) Cluster of inclusions of V2 type

c) Trail of inclusions of V2 type, crosscut by sutured grain boundary

d) Trail of inclusions of V2 type, crosscutting grain boundary

e) Cluster of 3-phase, CO_2-vapour-rich inclusions (V3 type 5) in late, crosscutting fracture

f) Cluster of H_2O-rich inclusions (V3 type 1) in late, crosscutting fracture

g) 2- and/or 3-phase CO_2-vapour-rich inclusions (V3 type 4, 5) intrails crosscutting grain boundaries and late fracture

h) Apparently isolated cluster of CO_2-vapour-rich inclusions (V3 type 4, 5)

C. V3 vein sample:

a) Cluster of V3 type 1 and 2 inclusions

b) Cluster of V3 type 3 and 4 inclusions

c) Trail of V3 type 1 inclusions, crosscutting grain boundary

d) Parallel trails of V3 type 1 and V3 type 2, 4 inclusions, crosscut by sutured grain boundary

e) Solitary V3 type 5 inclusion

f) Trail of V3 type 2, 4 inclusions, crosscutting grain boundaries

g) 3D-array of V3 type 6 inclusions

D. $V4_N$ or $V4_W$ vein sample:

a) Isolated, primary fluid inclusion

b) Cluster of elongate fluid inclusions

c) Curved trail of inclusions, crosscutting grain boundaries

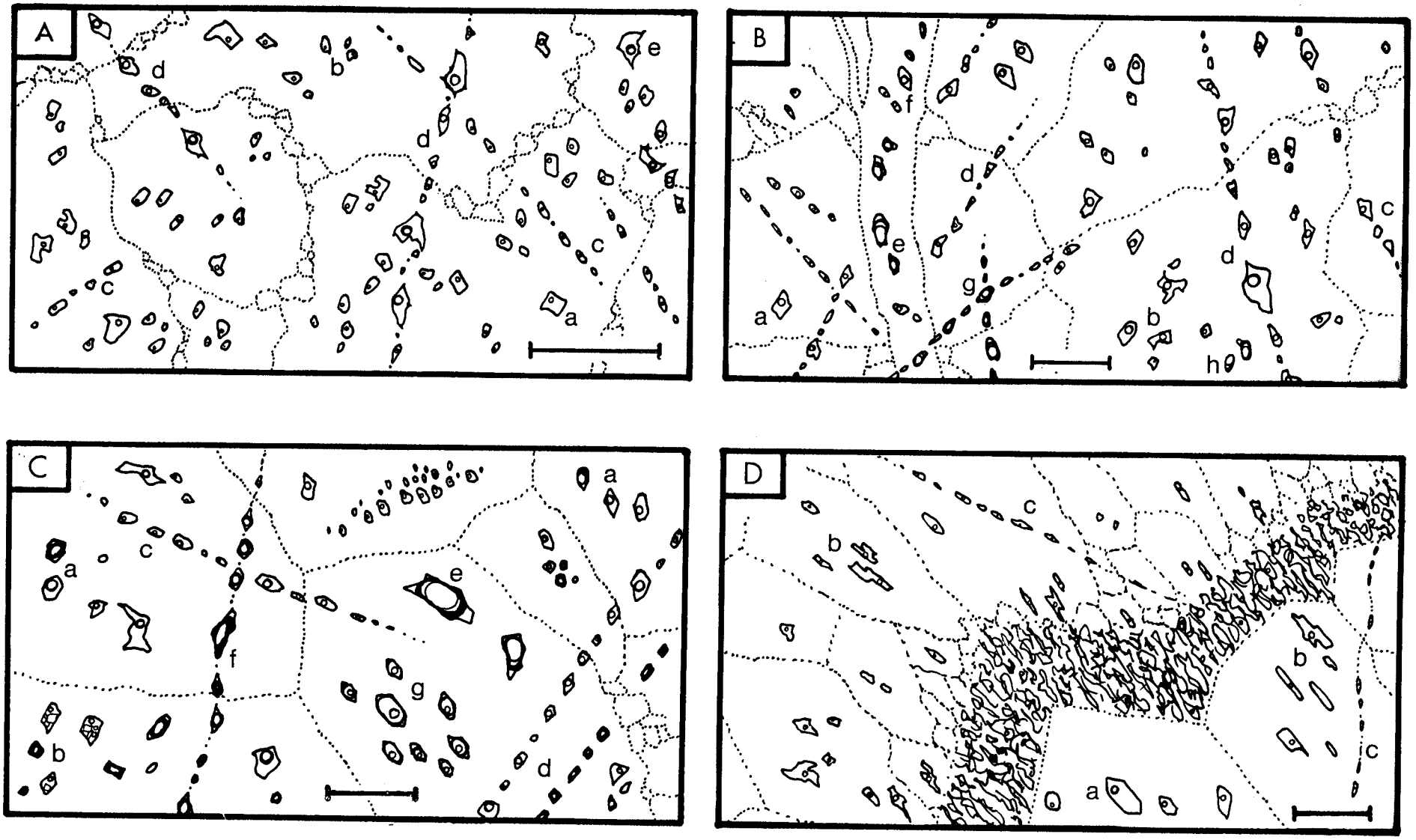
A
d
b
e
d
c
a
B
f
d
e
g
a
b
h
c
d
C
a
c
a
e
f
g
b
d
D
c
b
b
a
c

Figure 3.3

Figure 3.3: Fluid inclusion photomicrographs

The two following plates illustrate a range of fluid inclusion types observed during the course of this study. All of the photomicrographs were taken at the same magnification; the height of each picture is equivalent to approximately 150μm.

First Page:

A. $V1_T$ vein (*J105GW*) with ellipsoidal, rounded and sub-negative crystal fluid inclusions up to 15μm in size. All inclusions are two-phase, aqueous liquid + vapour (V1 type 1).

B. $V2_T$ vein (*J48BR*) with ellipsoidal or sub-negative crystal inclusions up to 15μm in size. All inclusions are two-phase, aqueous liquid + vapour (V2 type 1).

C. $V3_G$ vein (*J64DR*) with two sub-parallel, well-annealed microfractures containing V3 type 1 (upper trail) and V3 type 2/4 inclusions (lower trail). Cogenetic liquid- and vapour-rich inclusions indicate fluid immiscibility.

D. $V3_G$ vein (*J93TP*) with mixed fluid inclusion assemblage. Lower left: large, elongate V3 type 1 inclusion (aqueous liquid + vapour); lower right: large, irregular V3 type 3 inclusion containing halite daughter mineral; middle right: rounded, vapour-rich (V3 type 4) inclusion.

Second Page:

A. $V3_G$ vein (*D4PS1*) with two- and three-phase, CO_2-rich fluid inclusions at 20°C. Note small, faint CO_2 vapour bubble in most of the inclusions, surrounded by CO_2-rich liquid. H_2O-rich liquid is also present at the bottom of the large inclusion to the middle-right.

B. Multitude of rounded to negative crystal fluid inclusions defining annealed microfracture in pegmatitic quartz ($V4_P$ vein). Inclusions all contain H_2O-rich liquid surrounding a low density, CO_2-bearing vapour.

C. Large (≈60μm) $V4_P$ type DV1 inclusion, containing H_2O-rich, moderately saline liquid and low density, CO_2-bearing vapour (*JW008*).

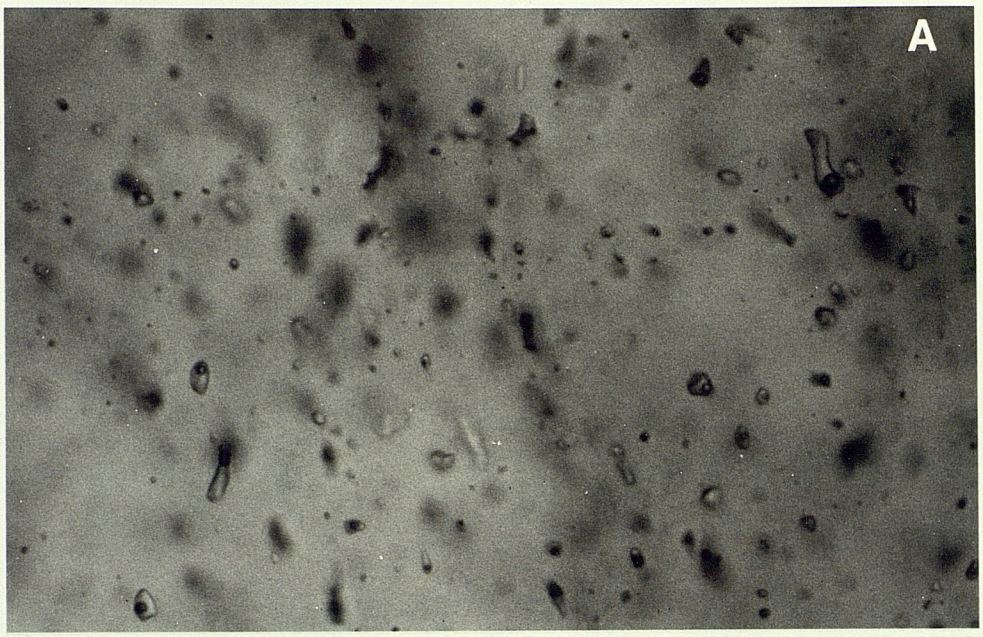
A

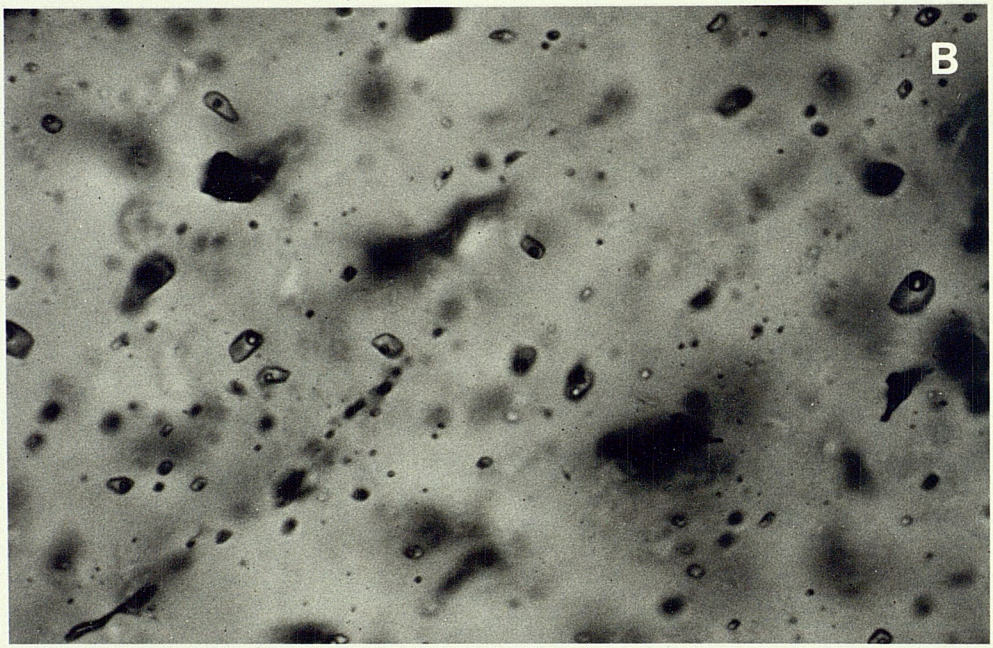
B

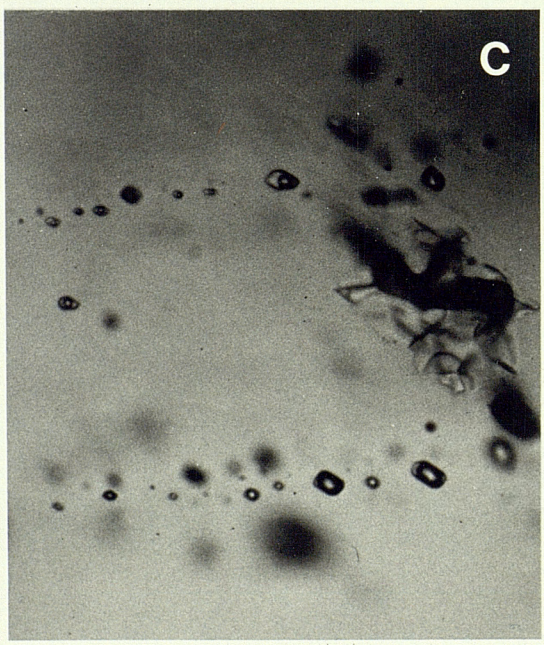
C

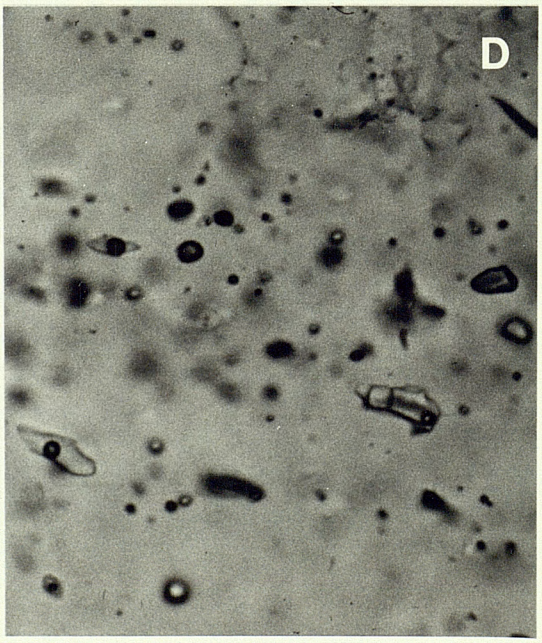
D

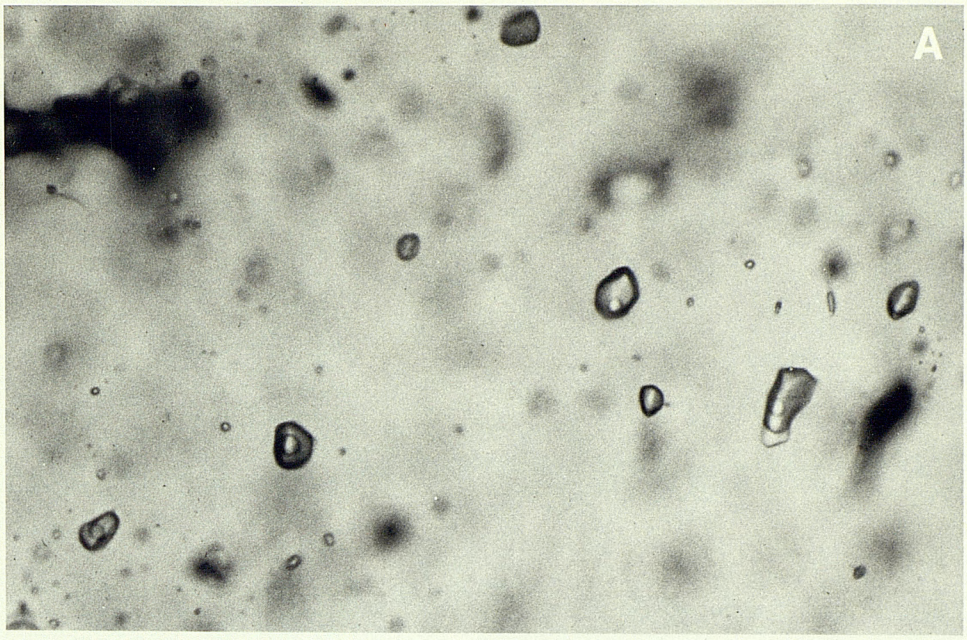
A

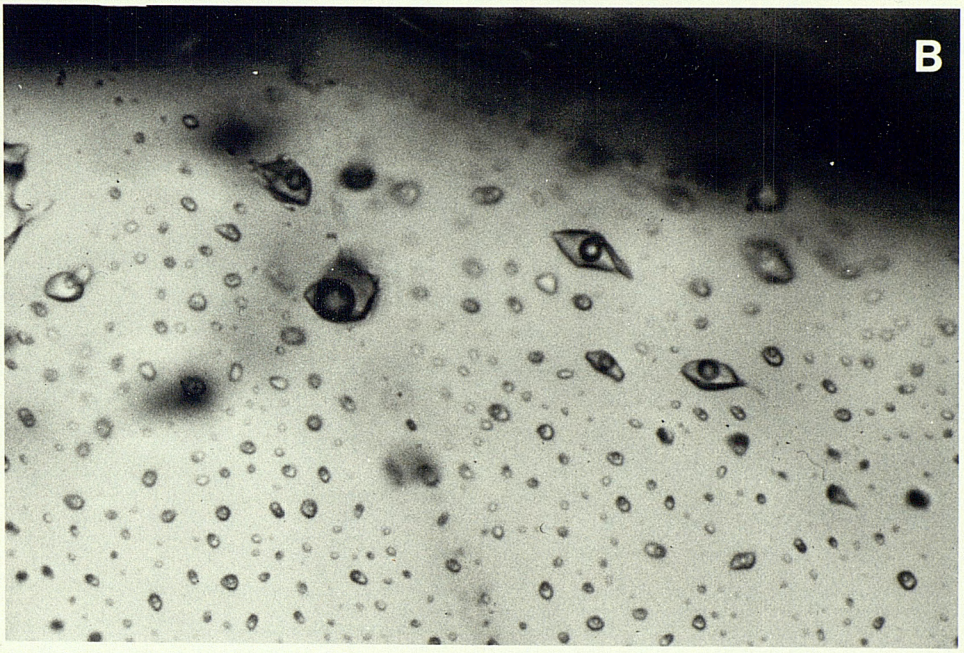
B

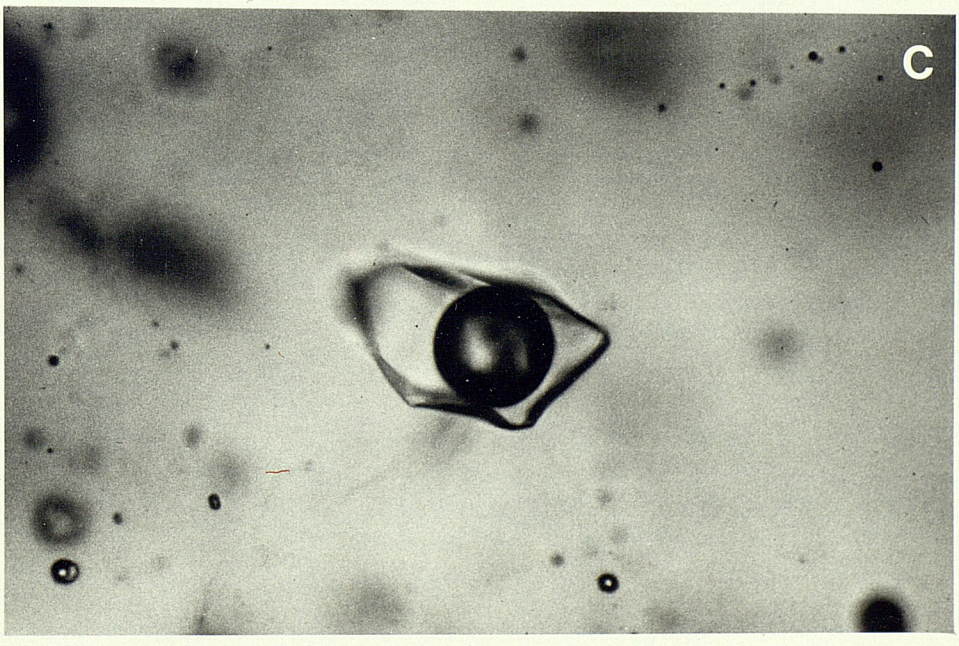
C

Table 3.1 Summary of optical characteristics: V1 fluid inclusions

TYPE	DESCRIPTION	SPATIAL DISTRIBUTION	INTERPRETATION
1	**Size:** <15μm. **Shape:** negative crystal, ellipsoidal or irregular, often flattened. **Phases:** aqueous liquid + vapour (F=0.85-0.95).	Isolated; in clusters; or in annealed microfractures usually crosscut by recrystallised grain boundaries.	Inclusions represent trapping of V1 fluid during and subsequent to vein growth.
2	**Size:** 10-20μm. **Shape:** usually irregular with cuspate margins. **Phases:** aqueous liquid + vapour (F=0.65-0.8).	Rarely isolated; commonly in annealed microfractures crosscutting recrystallised grain boundaries.	Inclusions represent post-D1 fluid event; thermometric data suggest V2 overprint of V1 quartz.

At room temperature, V1 inclusions are two-phase containing an aqueous liquid enclosing a low density vapour bubble. Phase volumes are estimated by visual comparison with standard charts (Shepherd *et al.* 1985, Appendix II). For the dominant (type 1) inclusions (see Table 3.1), the degree of fill *F*, which is defined as the volume fraction of the aqueous phase in the inclusion, ranges from 0.85-0.95 (Fig. 3.4). The small additional population present on the degree of fill frequency histogram is interpreted as a V2 overprint (see 3.2.3).

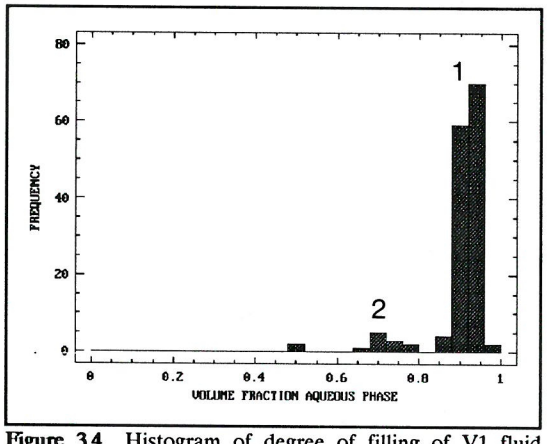

Figure 3.4 Histogram of degree of filling of V1 fluid inclusions.

Thermometric characteristics

Microthermometric data for V1 fluid inclusions are presented in Appendix D2. A summary of this information, in the form of temperature ranges for the phase changes observed, is presented in Table 3.2 below. A summary of the abbreviations used may be found in the relevant section of Appendix E. Important features of the data are discussed in the following section.

Table 3.2 Summary of V1 thermometric data

TYPE	*Th* (°C)	*S* (wt% NaCl eq.)	COMMENTS
1	100-240 (L)	1-4.5	Major population
2	220-300 (L)	4-7.5	Late overprint

Total homogenisation in V1 inclusions occurs by shrinkage and disappearance of the vapour bubble on heating; this is usually referred to as homogenisation to the liquid phase (L), or homogenisation by vapour disappearance. A homogenisation temperature (*Th*) frequency histogram (Fig. 3.5) shows a dominant population which corresponds with type 1 inclusions (see Table 3.1). A small, higher temperature population is also apparent, which may be correlated with the type 2 inclusions described above. Several *Th* values of >300°C are probably the result of measurement of inclusions which have lost liquid, either by necking down or by leakage.

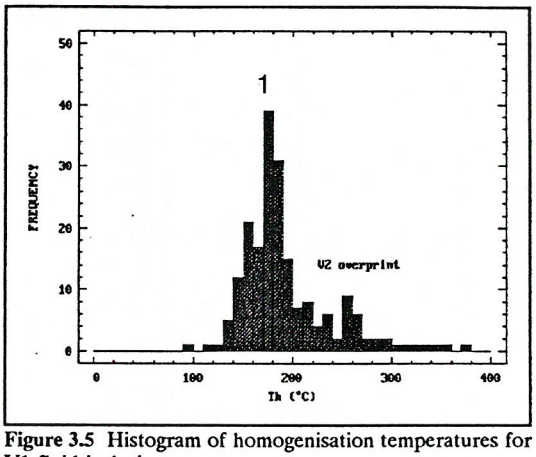

Figure 3.5 Histogram of homogenisation temperatures for V1 fluid inclusions.

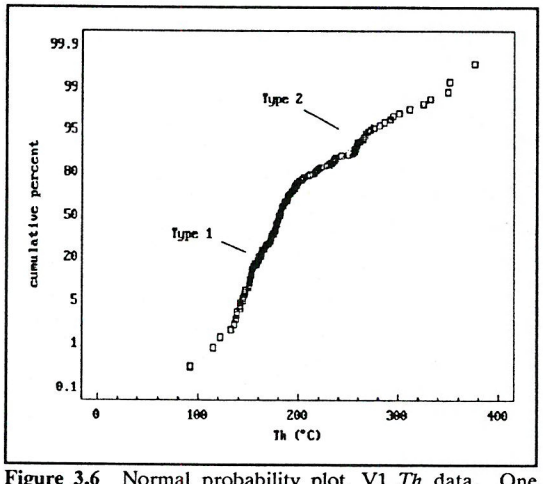

Figure 3.6 Normal probability plot, V1 *Th* data. One inflection separates V1 type 1 and V1 type 2 inclusions.

The two populations are clearly distinguished on a normal probability plot (Fig. 3.6). The vertical axis has been scaled so that the cumulative distribution function of a normal distribution will plot as a straight line. As can be seen, there is one major inflection separating two sets of data which correspond with the type 1 and type 2 inclusions. Fitting of normal distribution curves to the two populations yields a mean *Th* of 173°C and a standard deviation of 18°C for the type 1 population and a mean *Th* of 252°C and standard deviation of 18°C for the type 2 inclusions.

Fluid salinity estimates are usually made by referring the final ice melting temperatures in the inclusions to the NaCl-H_2O system, using the data regression of Potter *et al.* (1978). Such estimates neglect the effect of other solutes. However, several measurements of first melting (eutectic) temperatures in these inclusions of -20 to -30°C indicate that NaCl is the dominant dissolved phase. A salinity frequency histogram (Fig. 3.7) shows that the two inclusion populations may again be distinguished. No liquid or solid volatile phases or gas hydrates were observed on cooling to -196°C, indicating that H_2O is the dominant volatile component of these fluids. This conclusion is supported by bulk volatile data (see 3.4).

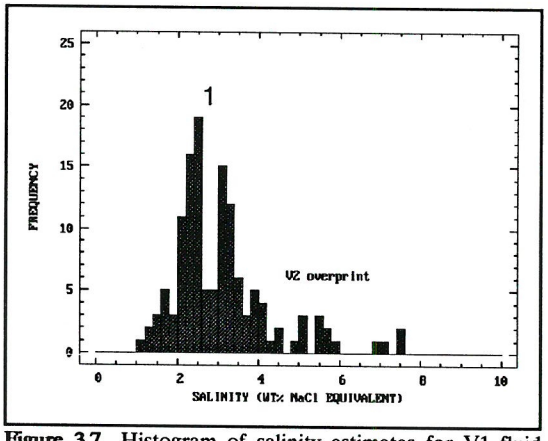

Figure 3.7 Histogram of salinity estimates for V1 fluid inclusions.

The type 1 and type 2 inclusion populations are clearly distinguished on a *Th-S* bivariate plot (Fig. 3.8). Comparison with a similar plot for V2 inclusion data (Fig. 3.11) shows that the type 2 population in V1 samples is compositionally consistent with a V2 fluid overprint. This is in agreement with the optical observations described above.

Despite careful sampling to avoid V1 veins deformed by D2, it would be very unlikely to completely avoid a V2 fluid overprint in V1 samples. This would only occur if there were no significant grain boundary or transient microfracture permeability in the rock system during D2. All the data are consistent with the type 2 inclusion population being of V2 origin (see 3.2.3).

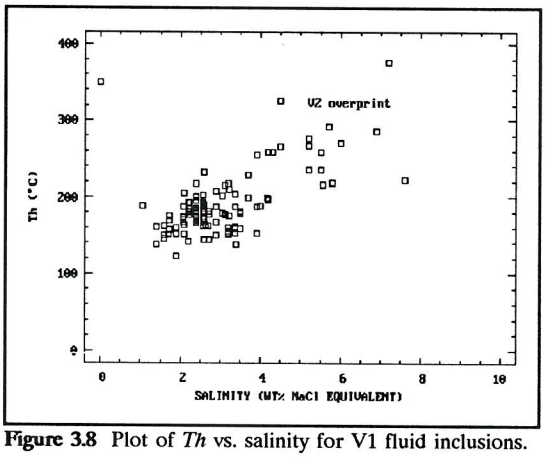

Figure 3.8 Plot of *Th* vs. salinity for V1 fluid inclusions.

3.2.3 V2 fluid inclusions

Optical characteristics

V2 veins are composed of quartz displaying fibrous, granular or irregular grain fabrics (see 2.2.5-7). As with V1 veins, the quartz has an opaque, milky appearance due to the presence of millions of tiny fluid inclusions. The important features of V2 inclusion assemblages are shown in a synoptic sketch (Fig. 3.2) and are summarised in Table 3.3 below. A photomicrograph of a typical field of view in thin section is shown in Figure 3.3.

Table 3.3 Summary of optical characteristics: V2 fluid inclusions

TYPE	DESCRIPTION	SPATIAL DISTRIBUTION	INTERPRETATION
1	**Size:** 5-15μm. **Shape:** sub-negative crystal or ellipsoidal; less commonly irregular. **Phases:** aqueous liquid + vapour (F=0.8-0.95).	Isolated; in clusters; or in annealed microfractures crosscut by, or truncating, grain boundaries.	Inclusions represent trapping of V2 fluid during and subsequent to vein growth.
2	**Size:** 10-20μm. **Shape:** Elongate, sub-negative crystal, ellipsoidal or more irregular. **Phases:** aqueous liquid + vapour (F=0.45-0.8).	Rarely isolated or in clusters; commonly in annealed microfractures crosscutting grain boundaries, or in crosscutting veinlets.	Inclusions may represent post-D2 fluid event; thermometric data suggest possible V3 overprint of V2 quartz.
3	**Size:** 10-20μm. **Shape:** Elongate, ellipsoidal or more irregular. **Phases:** aqueous liquid + CO_2-rich vapour ± CO_2-rich liquid (F=0-0.2).	Rarely isolated or in clusters; commonly in annealed microfractures crosscutting grain boundaries, or in crosscutting veinlets.	Inclusions probably represent post-D2 fluid event; thermometric data suggest possible V3 overprint of V2 quartz. Association with type 2 inclusions suggests immiscible fluids
4	**Size:** <10μm. **Shape:** Tubular, ellipsoidal, commonly flattened. **Phases:** aqueous liquid + vapour (F=0.9-0.98).	Invariably in poorly annealed trails, crosscutting grain boundaries and late veinlets.	Late fluid overprint in one sample (*J125LB*); composition comparable with $V4_N$ fluid inclusions.

Textural evidence for the relative age of the CO_2-rich inclusions is ambiguous. They are clearly accompanied by an assemblage of aqueous liquid-rich inclusions; however, it is not obvious in thin section if they are contemporaneous with the majority of the H_2O-rich inclusions or only cogenetic with a distinct H_2O-rich population. The exclusive occurrence of CO_2 vapour-rich inclusions with H_2O liquid-rich inclusions with lower degrees of fill (F=0.45-0.9) in small crosscutting veinlets and in zones of recrystallised quartz (Fig. 3.2) suggests that this assemblage is likely to be a late overprint.

Thermometric characteristics

Full microthermometric data for V2 fluid inclusions, a summary of which is presented in Table 3.4 below, may be found in Appendix D2. Thermometric data support the distinction of two fluid inclusion assemblages (see below). The thermometric characteristics of type 2 and 3 inclusions are comparable with data for V3 fluids (see 3.2.4) suggesting a genetic relationship.

Table 3.4 Summary of V2 thermometric data

TYPE	*Th* (°C)	*S* (wt% NaCl eq.)	COMMENTS
1	160-300 (L)	0.7-11.0	Major population
2	280-390 (L/C)	0.8-8.5	?V3 overprint
3	370-400 (V)	5.2	?V3 overprint
4	80-150 (L)	1.0-2.2	$V4_N$-type overprint

The dominant inclusion population (type 1) is illustrated by a *Th* frequency histogram (Fig. 3.9). A small, broad, higher temperature population is also evident which reflects the higher *Th* range of the type 2 and 3 inclusions. This group is characterised by homogenisation to liquid (L), to vapour (V) and by critical homogenisation (C), which occurs by fading of the meniscus between the two phases. The association of inclusions with widely varying phase ratios homogenising to the liquid and vapour states over the same temperature range is indicative of trapping of two immiscible fluids. The type 2 and 3 inclusions display a similar *Th* range to that of V3 inclusions (see 3.2.4), supporting the interpretation of type 2 and 3 inclusions as representing a V3 overprint. A small, low temperature peak is also present in the *Th* frequency histogram. This is due to measurement of a group of late, low salinity fluid inclusions in one sample (*J125LB*). These inclusions are thermometrically similar to much later $V4_N$ fluid inclusions (see 3.2.7). Statistical treatment of the *Th* data yields a mean *Th* for type 1 inclusions of 206°C with a standard deviation of 20°C, and a mean *Th* for the high temperature peak of 345±22°C.

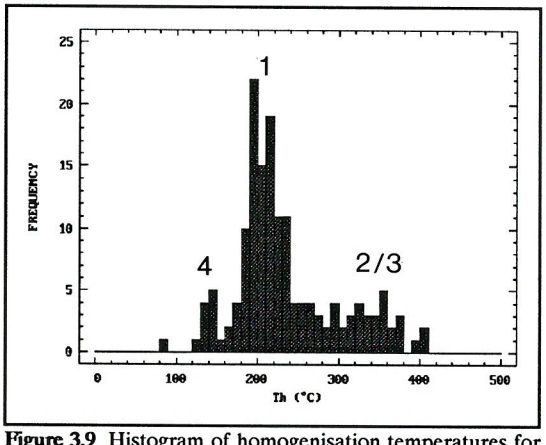

Figure 3.9 Histogram of homogenisation temperatures for V2 fluid inclusions.

A salinity frequency histogram (Fig. 3.10) shows only one broad peak as a result of the superposition of data for all 3 inclusion types. Three fields, corresponding to the type 1, type 2/3 and type 4 fluid inclusion assemblages, may be resolved on a *Th-S* bivariate plot (Fig. 3.11).

The coexistence of type 2 and 3 inclusions with different modes of homogenisation and salinities over the same *Th* range is clearly illustrated. A trend of increasing salinity with slightly increasing *Th* is apparent for the type 1 assemblage. The significance of this is addressed in section 4.3.5.

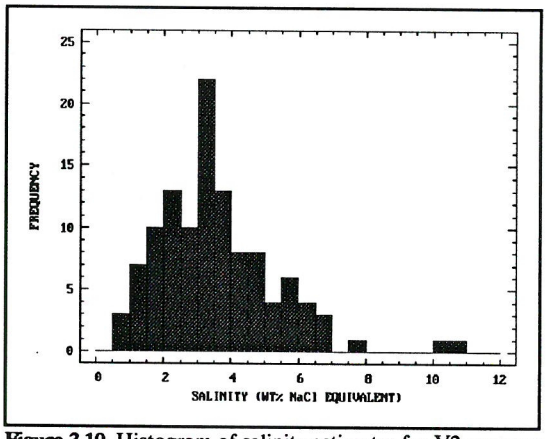

Figure 3.10 Histogram of salinity estimates for V2 aqueous fluid inclusions.

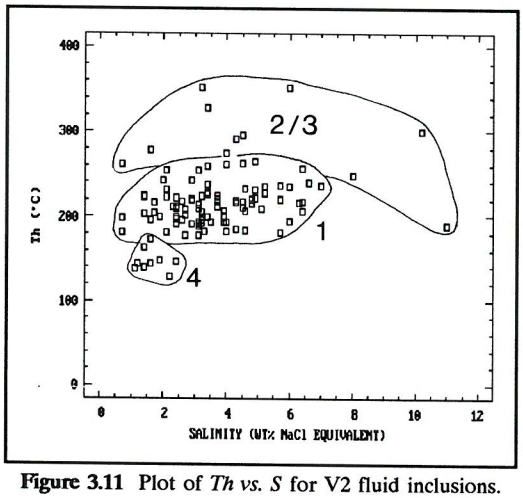

Figure 3.11 Plot of *Th vs. S* for V2 fluid inclusions.

Type 3 vapour-rich inclusions develop solid CO_2 on cooling to -110°C. Several measurements of $TmCO_2$ were obtained on the warming cycle, ranging from -60 to -57.1°C. The depression of the melting of solid CO_2 below the triple point of pure CO_2 (-56.6°C) indicates the presence of other volatiles, predominantly CH_4 and N_2 (see 3.4). Solid CO_2 melting also takes place over a temperature interval of 0.1-0.5°C indicating that melting occurs along a univariant curve in a mixed gas system, rather than at an invariant triple point.

During the cooling procedure, "double freezing" is sometimes observed in type 2 and 3 fluid inclusions. This involves contraction of the vapour bubble at two temperatures; the first, usually at approximately -30°C, results from the formation of a gas hydrate (clathrate) and the second event, which usually occurs around -40°C, is due to freezing of the aqueous phase to form ice. The clathrate is most likely to be the CO_2 hydrate $CO_2.5^3/_4H_2O$, although some substitution by other gases may occur (Van der Waals & Platteeuw 1959).

The formation of clathrate in type 2 inclusions is significant, not only because it indicates the presence of CO_2 (and/or other gases), but also because clathrate locks up water in its structure, thus enriching the residual aqueous phase in dissolved salts. Since clathrate generally melts at a higher temperature than ice, ice melting occurs in the presence of clathrate, with the ice melting temperature reflecting the salinity of the residual aqueous phase. For this reason, the salinity estimates made for this group of inclusions must be treated as maximum values. For inclusions containing an aqueous liquid, liquid CO_2 and CO_2 vapour, the clathrate melting temperature may be used to estimate the salinity of the aqueous phase (Collins 1979). The three-phase type 3 inclusions are suitable for this method, and give salinities of 0.8-1.5 wt% NaCl equivalent for the aqueous phase (see Appendix D2).

Clathrate melting temperatures (*TmC*) range from 5.5-9.8°C, the lower values usually being recorded for type 2 inclusions. There is also distinct variability in *TmC* between samples, although the data are too limited to allow a more detailed analysis.

Homogenisation of the CO_2 phases in type 3 inclusions occurs by expansion of the vapour bubble (homogenisation to vapour) mainly in the range 25.6-28.4°C. This indicates CO_2 densities between 0.26 and 0.30 g cm^{-3}. However, a few inclusions homogenise to vapour as low as -12.3°C indicating that low density CO_2 is likely to be present in most type 3 inclusions.

Estimates of the proportion of CO_2 in the bulk inclusion fluid (see Appendix D2) range from 4.7-8.3 mole percent for inclusions displaying total homogenisation (*Th*) to the liquid, and 10.9-36.4 mole percent for inclusions homogenising to the vapour. One inclusion showing critical homogenisation gave a bulk composition of 11.5 mole percent CO_2. The data are somewhat limited but are consistent with the coexistence of two immiscible fluids at *c.* 350°C (Bowers & Helgeson 1983b) during fracturing and microveining of V2 quartz, probably during D3, in the Parc-an-als/Loe Bar/Blue Rock section (Fig. 1.4; see 4.4).

3.2.4 V3 fluid inclusions

Optical characteristics

V3 vein quartz is typically a translucent grey colour with a distinctive greasy lustre (see 2.2.8-10). It is composed of equant to prismatic quartz crystals, from several millimetres to several centimetres long. The clarity of the quartz, combined with the large grain size and generally weak deformation result in easy observation of large, regular fluid inclusions (Fig. 3.3). Six inclusion types may be distinguished optically at room temperature; these are illustrated in Figure 3.12. A synoptic sketch is presented in Figure 3.2 and the major optical characteristics are summarised in Table 3.5 below.

Type 3 inclusions (Fig. 3.3), which contain up to six solid phases, have been opened and analysed using an S.E.M./E.D.X. technique. This method allows the identification of the solid phases, as well as providing qualitative information on the solutes present by analysis of the residue left behind after evaporation of the inclusion fluids. The presence of halite and sylvite daughter minerals has been confirmed (Fig. 3.23) and Ca and Fe/Mn chlorides have also been identified.

Detailed examination of the relationships between quartz grain boundaries, subgrain boundaries and annealed microfractures containing fluid inclusions (see Fig. 3.2) indicates that inclusions of different types occur in fractures formed at all stages of quartz crystallisation and deformation. Type 1 and 2 inclusions are commonly observed in the same or parallel microfractures (Fig. 3.3) as are type 3 and 4 inclusions. Relationships such as these imply that the majority of inclusions were cogenetic and represent trapping in a complex, continuously varying fluid system (Wilkinson, in press). The fact that inclusions of all types often display criteria indicative of a primary origin (Roedder 1984) indicates that the fluids responsible for vein formation were the same as those flowing through microfractures during subsequent deformation. Not only does this suggest that pervasive microfracturing (on a scale of μm-mm) was an important contributor to bulk permeability at this stage (see 6.1.4), it also implies that vein formation was a relatively rapid process, with primary quartz crystals "freezing-in" a snapshot of an extended fluid flow event.

Table 3.5 Summary of optical characteristics: V3 fluid inclusions

TYPE	DESCRIPTION	SPATIAL DISTRIBUTION	INTERPRETATION
1	**Size:** 5-40μm. **Shape:** negative crystal, rounded;less commonly irregular. **Phases:** aqueous liquid + very low density CO_2-H_2O vapour (F=0.6-0.95).	Isolated, in clusters, in 3D arrays, or in annealed microfractures crosscutting grain boundaries. Often associated with type 2.	Inclusions represent trapping of immiscible, H_2O-rich liquid, during and subsequent to vein growth.
2	**Size:** 10-30μm. **Shape:** negative crystal, rounded or elongate and irregular. **Phases:** low density CO_2-rich vapour + aqueous liquid (F=0.2-0.5).	Isolated, in clusters, in 3D arrays; commonly in annealed microfractures crosscutting grain boundaries. Often associated with type 1 (sometimes in same or parallel microfractures).	Inclusions represent trapping of immiscible, CO_2-bearing vapour, during and subsequent to vein growth.
3	**Size:** 10-40μm. **Shape:** generally flattened, orthogonal or irregular. **Phases:** aqueous liquid + vapour + 1-6 solid phases (F=0.8-0.95).	Rarely isolated, commonly in clusters and in annealed microfractures crosscutting grain boundaries. Often associated with type 4.	Inclusions represent trapping of immiscible brine, during and subsequent to vein growth.
4	**Size:** 5-25μm. **Shape:** negative crystal, rounded or elongate and irregular. **Phases:** low density CO_2-rich vapour ± aqueous liquid (F<0.2).	Isolated, in clusters, often in annealed microfractures crosscutting grain boundaries.	Inclusions represent trapping of immiscible, low density CO_2-rich vapour, during and subsequent to vein growth.
5	**Size:** 5-40μm. **Shape:** sub-negative crystal, rounded or irregular. **Phases:** CO_2-rich vapour, CO_2-rich liquid ± aqueous liquid (F=0.05-0.5).	Commonly isolated or in clusters, also in annealed microfractures crosscutting grain boundaries.	Inclusions represent trapping of immiscible, moderate density CO_2-rich fluid, during and subsequent to vein growth.
6	**Size:** 5-25μm. **Shape:** negative crystal or rounded, rarely irregular. **Phases:** CO_2-rich liquid, CO_2-rich vapour ± aqueous liquid (F=0.05-0.2).	Isolated, commonly in clusters and 3D arrays; rarely in microfractures.	Inclusions represent trapping of condensed CO_2-rich vapour during vein growth.

Thermometric characteristics

Microthermometric data for V3 vein samples are presented in full in Appendix D2. This information for the six different inclusion types is summarised in Table 3.6. These data indicate that the divisions between the six groups are somewhat arbitrary since there are compositional gradations between many of them. These compositional relationships are illustrated schematically in Figure 3.12.

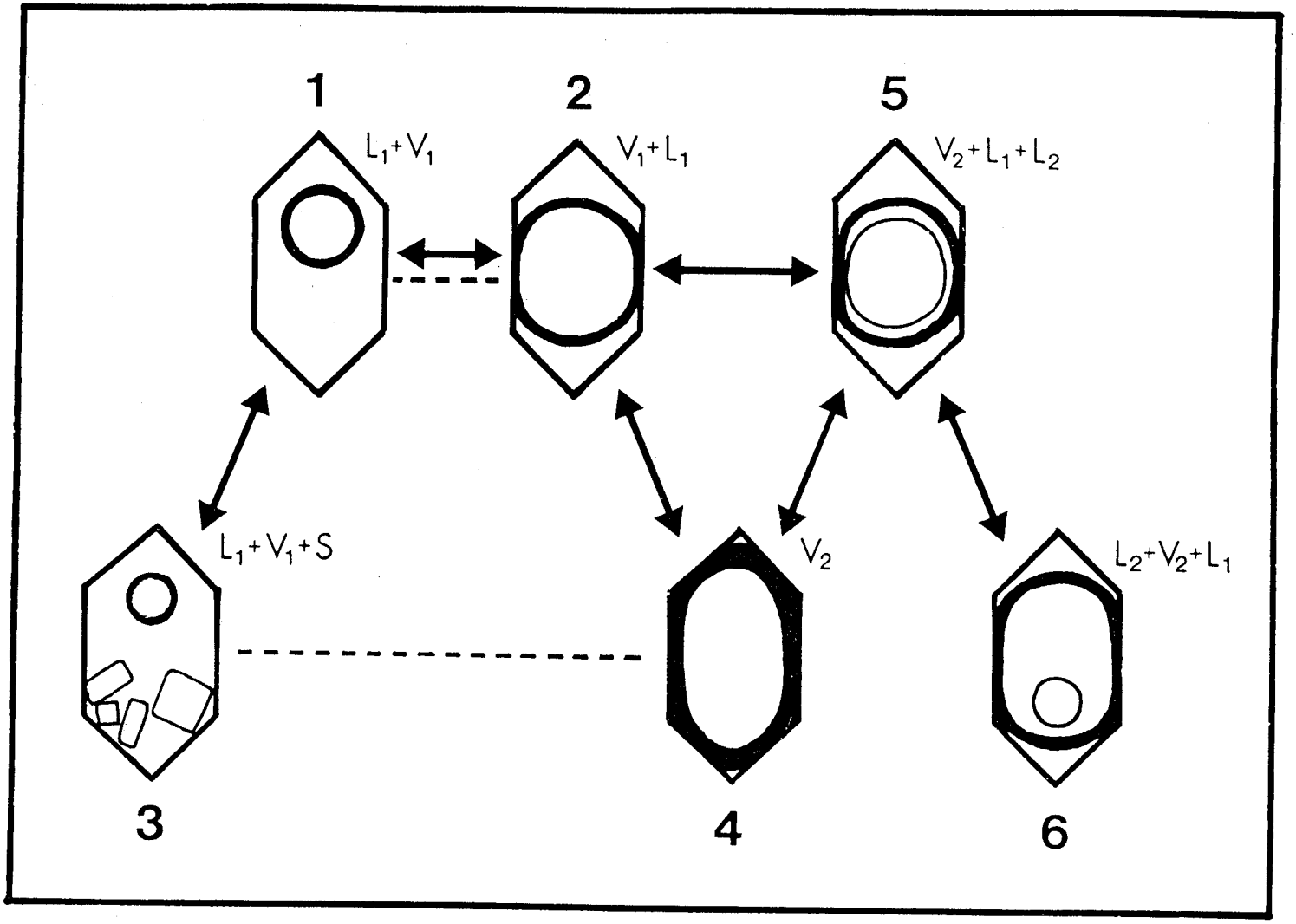

Figure 3.12 V3 fluid inclusion classification scheme. Solid arrows indicate complete gradation between inclusion types; dashed lines indicate coexisting immiscible fluids. $L_1 = H_2O$-rich liquid, $V_1 = H_2O$-rich vapour, $L_2 = CO_2$-rich liquid, $V_2 = CO_2$-rich vapour, S = solid phase(s).

Table 3.6 Summary of V3 thermometric data

TYPE	*Th*	*S*	$TmCO_2$	*TmC*	$ThCO_2$	COMMENTS
1	100-440 (L)	1-20	-60.3 to -57.8	1.6-10.6	-	High temperature liquid
2	260-480 (V)	0-14	-63.9 to -56.7	1.5-13.0	-18.4-20.8 (V)	High temperature vapour
3	200-360 (H)	20-45	-	-	-	Lower T brine
4	200-420 (V)	<4	-61.2 to -56.8	8.5-9.4	-20.2-21.0 (V)	Lower T vapour
5	240-450 (V)	low	-60.0 to -56.6	-	21.0-31.1 (V)	Intermediate density vapour
6	180-420 (V)	0-6	-58.9 to -56.5	4-10	21.2-31.4 (L)	High density condensate

Type 1 inclusions are relatively H_2O-rich (Figs. 3.4, 3.13). The sharp cut-off in the histogram at $F=0.5$ is an artefact arising from the somewhat arbitrary nature of the classification scheme. Type 2 inclusions display a similar distribution, but with $F<0.6$ (Fig. 3.17). Type 1 fluids display moderate salinities (Fig. 3.14), ranging from 8-16 wt% NaCl equivalent. The small, low salinity population present is the result of measurement of a group of late inclusions in one sample. Their textural and thermometric characteristics suggest an origin by $V4_N$ fluid overprinting (see 3.2.7).

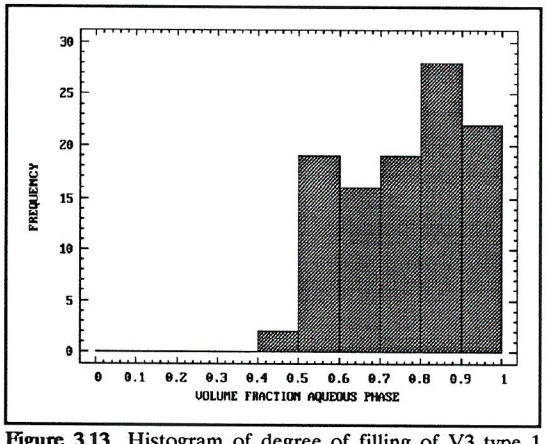

Figure 3.13 Histogram of degree of filling of V3 type 1 fluid inclusions

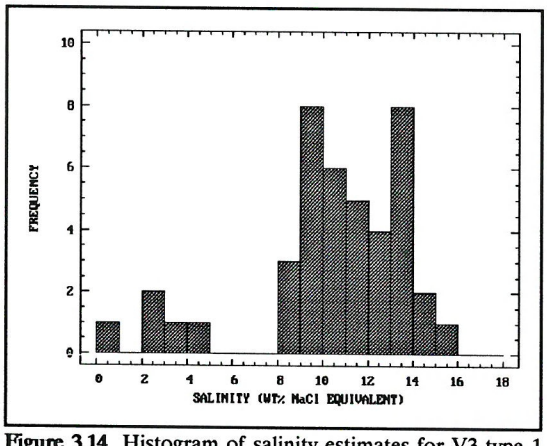

Figure 3.14 Histogram of salinity estimates for V3 type 1 fluid inclusions

Type 1 inclusions generally homogenise to the liquid phase, although a few examples of critical homogenisation in the temperature range 353-418°C have been observed. The *Th* data define two peaks centred on 350°C and 230°C (Fig. 3.16). Reference to a *Th-S* bivariate plot for type 1 inclusions (Fig. 3.16) shows a clear trend of increasing salinity with decreasing *Th*. This trend suggests that a single H_2O-rich fluid was present which gradually changed in composition with time (see 4.4.1).

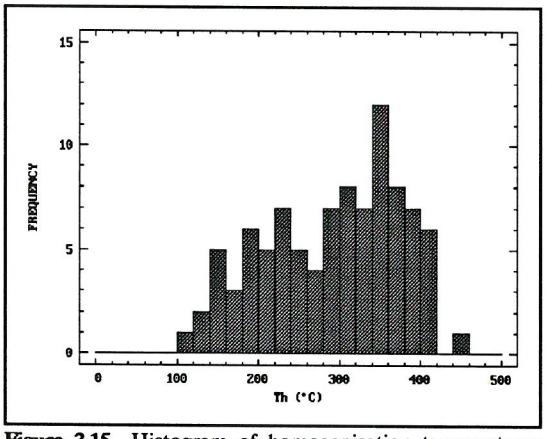

Figure 3.15 Histogram of homogenisation temperatures for V3 type 1 fluid inclusions

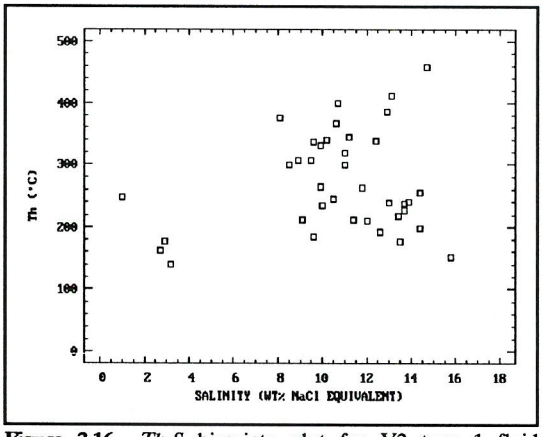

Figure 3.16 *Th-S* bivariate plot for V3 type 1 fluid inclusions

Cooling type 1 inclusions to below -100°C sometimes results in the formation of a small grain of solid CO_2. On warming back to room temperature, this melts between -60.3 and -57.8°C indicating the presence of other gases (primarily CH_4, N_2). First (eutectic) melting usually occurs at around -21°C, suggesting that NaCl is the dominant dissolved phase. Occasionally, first melting as low as -62°C is observed, indicating the presence of other dissolved salts, probably including K, Ca and possibly even Li chlorides (Borisenko 1977).

A hydrated salt phase has been observed in some type 1 inclusions, melting in the range -21.7 to -19.3°C. This is close to the eutectic temperature in the NaCl-H_2O system of -21.2°C (Borisenko 1977), suggesting that the phase is hydrohalite (NaCl.2H_2O). The identification of hydrohalite is supported by the optical properties of the solid (*i.e.* high relief, rounded crystals) and D-ICP data (see 3.3.1) which indicate that Na is the dominant cation in these fluids. The low temperature data discussed above indicate that type 1 inclusion fluids may be approximated by the NaCl-H_2O system.

Clathrate melting has been observed in some type 1 inclusions, confirming the presence of CO_2 and/or other gases. *TmC* values range from 1.6-10.6°C with a mode at 6-7°C. The absence of liquid CO_2 in these inclusions means that the salinity cannot be estimated from *TmC* and experimental data on the NaCl-H_2O-CO_2 system (Collins 1979), since the inclusions do not lie on the H_2O(L)-CO_2(G)-CO_2(L)-ice-clathrate univariant curve, along which clathrate melting occurs.

As concluded above, the low temperature data are generally consistent with the NaCl-H_2O system. Despite the confirmed presence of small quantities of CO_2, this approximation is still believed to be valid, hence the reporting of salinities based on ice melting temperatures. It should be noted that on this basis the reported salinities represent maximum values; the true salinities will be somewhat lower.

Type 2 inclusions are moderately vapour-rich (Fig. 3.3). As with type 1 inclusions, the degree of fill data do not display a normal distribution (Fig. 3.17), with sharp cut-offs at $F=0.1$ and $F=0.6$ due to the nature of the inclusion classification scheme. The continuum in phase proportions between type 1 and 2 inclusions is readily apparent.

Salinity estimates were made from clathrate melting temperatures, since ice melting was not observed. The data are limited, but indicate salinities in the range 0.8-14.1 wt% NaCl equivalent. Although liquid CO_2 is present in some of the inclusions at *TmC* ($TmC<ThCO_2<$ room T), it was

not conclusively identified in all the inclusions for which salinity was determined. As mentioned above, the presence of liquid CO_2 is essential for the determination of salinity by the method of Collins (1979). Salinities for inclusions in which liquid CO_2 was observed at *TmC* range from 1.4-7.6 wt% NaCl equivalent. Comparison between the salinity ranges for the type 1 and type 2 inclusion fluids shows that there is a continuum in salinity. This relationship is clearly illustrated on a *Th-S* bivariate plot for all V3 inclusion types (Fig. 3.38).

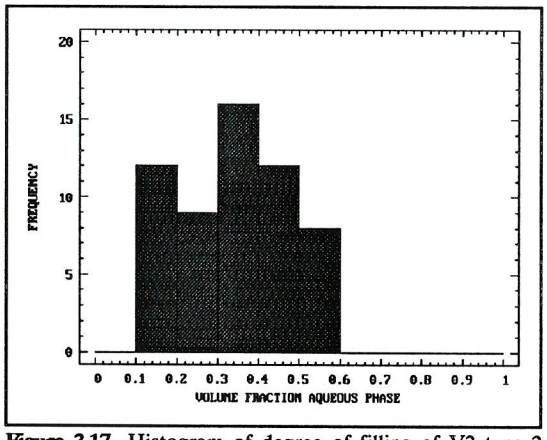

Figure 3.17 Histogram of degree of filling of V3 type 2 fluid inclusions

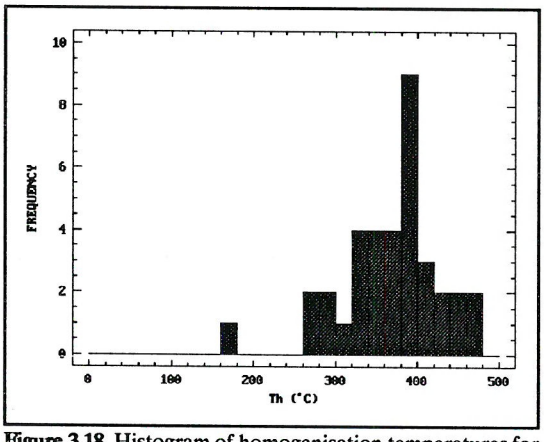

Figure 3.18 Histogram of homogenisation temperatures for V3 type 2 fluid inclusions

Homogenisation of type 2 inclusions occurs to the vapour at 260-470°C (Fig. 3.18). The data display a broad peak centred on 390°C, suggesting that the inclusions represent a single fluid. Normal distribution fitting to the type 2 *Th* data yields a mean *Th* of 375°C with a standard deviation of 50°C. Type 2 homogenisation occurs over the same temperature range as the higher temperature type 1 inclusions. This is important evidence regarding the possible generation of these two fluids by unmixing (see 4.4.1). A *Th-S* plot for V3 data (Fig. 3.38) illustrates the relationships between type 1 and 2 inclusions. Although there is some overlap the groups are distinct, having similar *Th* values but different estimated salinities.

Low temperature data for type 2 inclusions indicate the dominance of CO_2 in the vapour phase. Solid CO_2 melting is observed between -56.9 and -63.7, with a distinct mode at -59 to -60°C (Fig. 3.19). The depression of $TmCO_2$ below the CO_2 triple point (-56.6°C) indicates the presence of additional gases. The amounts of these gases cannot be constrained, partly because there is insufficient experimental data for the H_2O-CO_2-CH_4-NaCl or H_2O-CO_2-N_2-NaCl systems (these being the closest quaternary approximations to the inclusion fluids), and partly as a result of the presence of clathrate at $TmCO_2$. The latter phenomenon has been shown to have an effect on $TmCO_2$ (*e.g.* Ramboz *et al.* 1985; Seitz *et al.* 1987) because of preferential take-up of one gas in the clathrate structure.

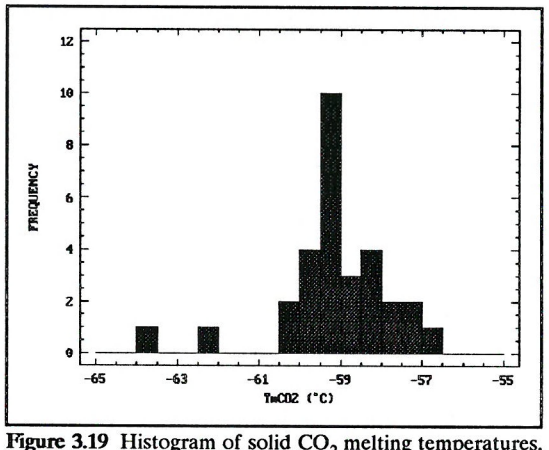

Figure 3.19 Histogram of solid CO_2 melting temperatures, V3 type 2 fluid inclusions

Clathrate melting is often observed in type 2 inclusions. To facilitate measurement of the phase change, a cycling technique, similar to that described by Shepherd *et al.* (1985), was routinely

employed. A *TmC* frequency histogram (Fig. 3.20) illustrates the range over which clathrate melting occurs. The discrete populations present are likely to be an artefact resulting from the small data set, although some inter-sample variability is apparent. A plot of *Th vs. TmC* (Fig. 3.21) shows that the data display a trend of increasing *TmC* with decreasing *Th*. This suggests that a decrease in salinity and/or an increase in the proportion of gases other than CO_2 accompanied decreasing *Th*. Both these alternatives are consistent with an origin for type 2 vapours by unmixing (see 4.4.1).

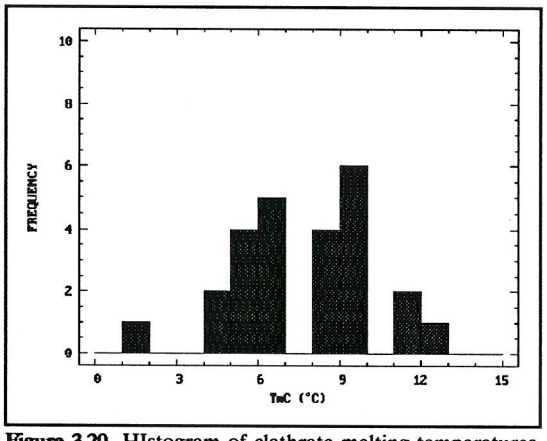

Figure 3.20 HIstogram of clathrate melting temperatures, V3 type 2 fluid inclusions

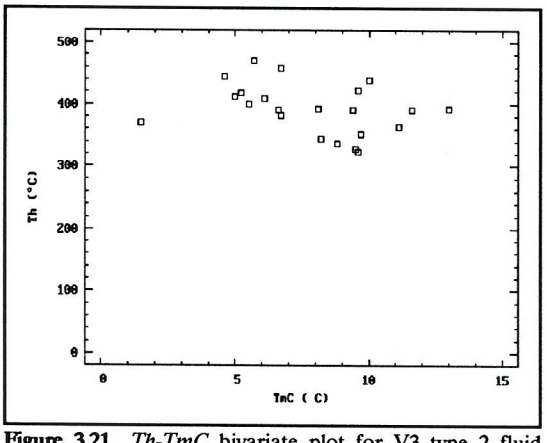

Figure 3.21 *Th-TmC* bivariate plot for V3 type 2 fluid inclusions

Liquid CO_2 is only rarely observed when type 2 inclusions are cooled below ambient temperature. As a result, only a few measurements of $ThCO_2$ have been recorded. These range from -18.4 to +20.8°C, indicating CO_2 densities between 0.04 and 0.20 gcm^{-3}. In cases where $TmCO_2 < TmC$, the measured value of $TmCO_2$ will be dependent on clathrate composition (Ramboz *et al.* 1985). Thus, the $ThCO_2$ values only provide estimates of the density of the CO_2 phase, being dependent on clathrate composition, the amount of clathrate formed and the proportion of other gases apart from CO_2 present. The extension of CO_2 homogenisation to ambient temperature illustrates the continuum between type 2 and type 5 inclusions summarised in Figure 3.12.

Type 3 inclusions are distinctive in terms of their morphology as well as the presence of commonly two, and sometimes as many as six, solid phases (Fig. 3.3). Halite and sylvite daughter minerals have been identified by S.E.M./E.D.X. (Fig. 3.23).

Degrees of fill have been estimated with reference to the size of the vapour bubble and hence reflect the volume fraction of the aqueous liquid plus any solid phases present. The volume fraction of the vapour phase is thus equal to 1-F. The volume fraction of the solid phases is generally in the range 0.1-0.2. Figure 3.22 illustrates the low proportion of vapour in type 3 inclusions, with a prominent mode at $F = 0.9$-0.98.

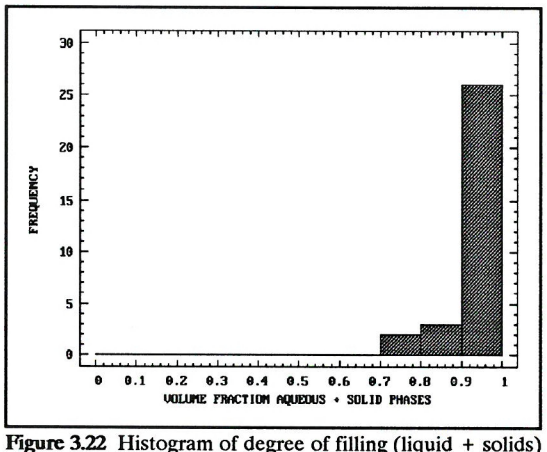

Figure 3.22 Histogram of degree of filling (liquid + solids) of V3 type 3 fluid inclusions.

Estimation of total salinity in type 3 inclusions is problematic since a number of dissolved salts are present. Below it will be shown that

Figure 3.23

SEM photographs of opened fluid inclusions on fractured quartz surfaces

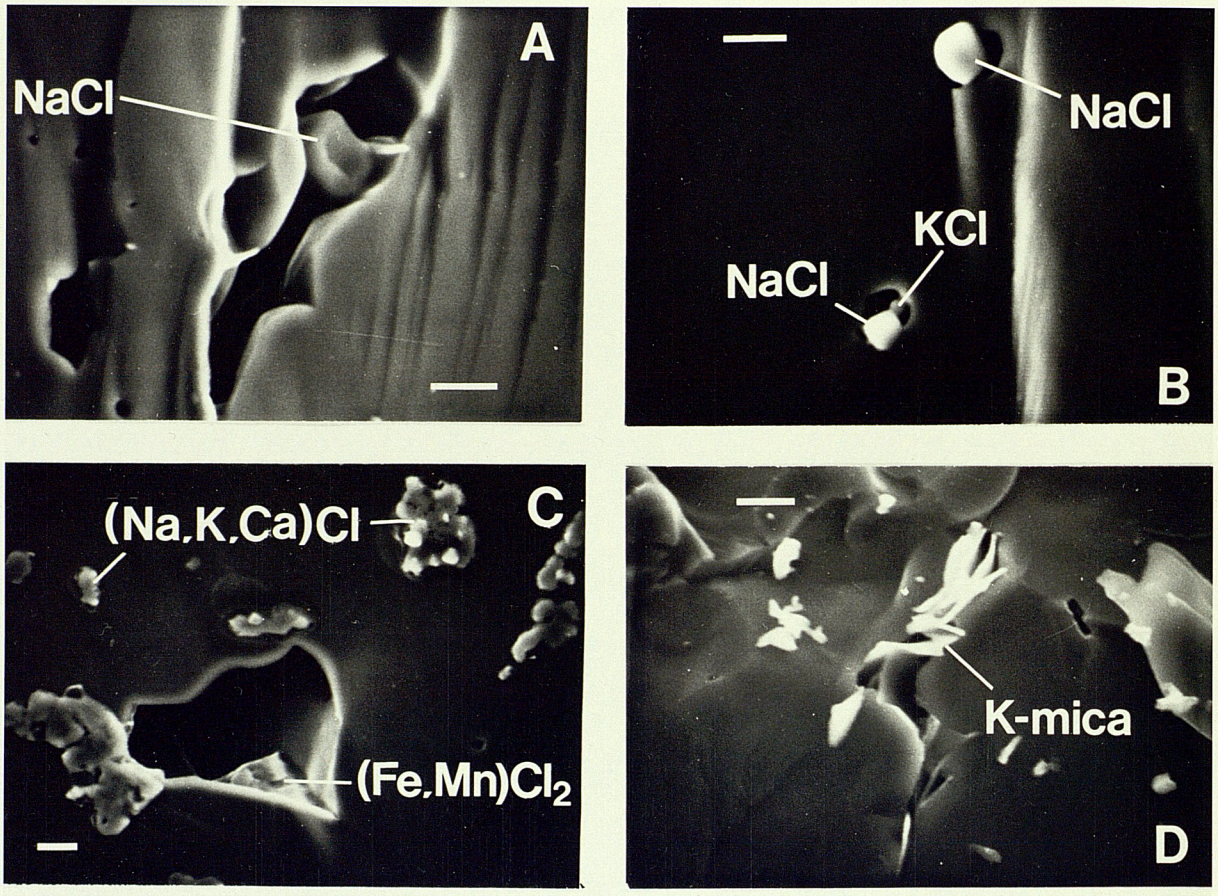

A. Cubic halite daughter crystal in irregular V3 type 3 fluid inclusion (*J93TP*).

B. Halite and sylvite daughter crystals in negative crystal V3 type 3 fluid inclusions (*J93TP*).

C. Na, K and Ca chloride residue formed on evaporation of inclusion fluid. Tabular Iron-manganese chloride daughter mineral (*JW008*).

D. Abundant K-mica flakes in irregular fluid inclusion from growth zone in $V4_W$ quartz vein (*J98PC2D*).

All scale bars are equivalent to 5μm.

most of the fluids may be conveniently modelled by the NaCl-KCl-H_2O system; hence salinities are reported in terms of wt% NaCl and KCl where appropriate thermometric data exist. Total salinity is then the sum of the estimated NaCl and KCl contents. In some instances, salinity has been estimated on the basis of the dissolution temperature of halite, in which case the quoted value is in terms of wt% NaCl equivalent and only approximates the total salinity.

Ice melting temperatures range from -50.3 to -19.5°C, with a prominent mode at -25 to -23°C (Fig. 3.24). This corresponds closely to the NaCl-KCl-H_2O eutectic of -23.5°C reported by Borisenko (1977). This agrees with the optical observations, with those inclusions saturated with respect to halite and sylvite at room temperature displaying final ice melting at the eutectic. These inclusions, which closely approximate to the NaCl-KCl-H_2O system, are dominant in the V3 type 3 classification.

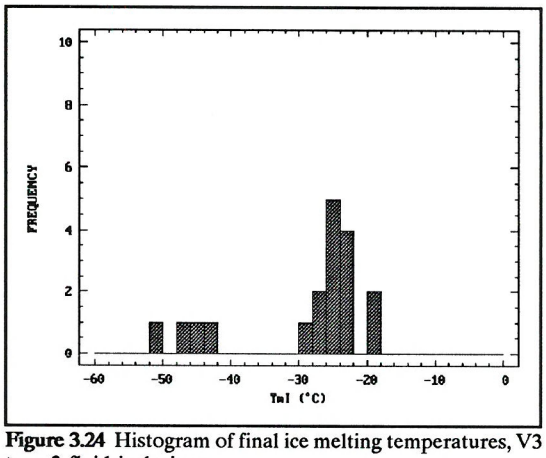

Figure 3.24 Histogram of final ice melting temperatures, V3 type 3 fluid inclusions.

Inclusions with more than two daughter minerals have ice melting temperatures below -26°C. First melting temperatures of -58 to -54°C and *TmI* values as low as -50.3°C in these inclusions indicate the probable presence of $CaCl_2$. Accurate modelling of these fluids is not possible in the absence of data for the NaCl-KCl-$CaCl_2$-H_2O quaternary system. Cation abundances in the order Na>K>Ca, as determined by D-ICP analysis (see 3.3.1) agree with these observations.

The composition of inclusions approximating to the NaCl-KCl-H_2O system may be estimated from experimental data (Sterner *et al.* 1988). For type 3 inclusions, the NaCl and KCl contents are defined by the dissolution temperature of sylvite and the dissolution temperature of halite (TsH) as shown in Figure 3.25. Type 3 inclusions for which appropriate data exist (*i.e. TsH, TsS* and in some cases *TmI* and *Tmh*) are plotted on the ternary diagram shown in Figure 3.25. The data indicate that V3 type 3 fluids contain approximately 16-31 wt% NaCl and 4-22 wt% KCl, with a total salinity of 26-47 wt%. This compares with a total salinity estimate of 28-42 wt%, determined from halite dissolution temperatures alone. The Na/K weight ratios of 1.4-4.9 defined by this data are lower than those obtained from bulk D-ICP analyses (5.75-10.6). The reason for this disparity is probably the fact that the bulk D-ICP analyses reflect the composition of a variety of inclusion types, including type 1 inclusions, which display higher Na/K ratios.

During heating of type 3 inclusions, the fluid phases homogenise first, at 110-250°C. This "partial homogenisation" is to the liquid (L+V+S -> L+S). Total homogenisation occurs by dissolution of halite (*i.e.* L+S -> L) in inclusions containing halite and sylvite. These "total homogenisation" temperatures are in the range 200-350°C (Fig. 3.26). For inclusions containing more than these two daughter minerals, halite is the last phase to dissolve; the other phases do not homogenise below 600°C and total homogenisation *sensu stricto* is not achieved. This may be due to unfavourable dissolution kinetics of the other daughter phases, or the presence of trapped phases in the inclusions, rather than true daughter minerals. Total homogenisation in these inclusions cannot be positively determined.

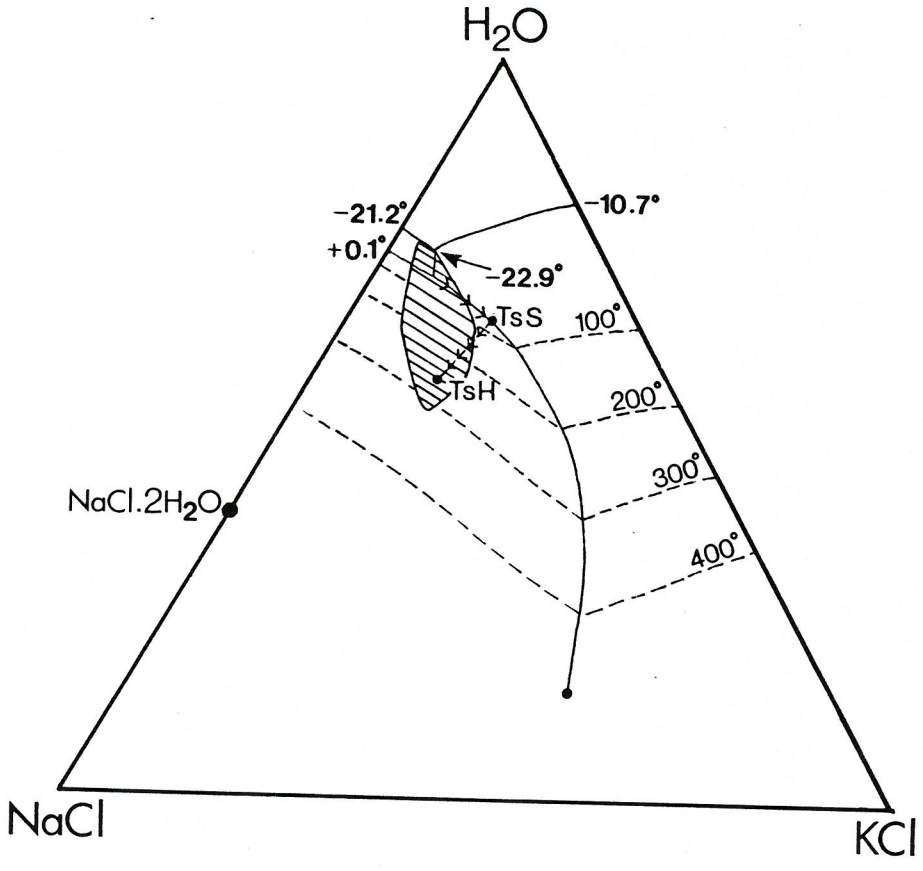

Figure 3.25 NaCl-KCl-H_2O ternary system (from Sterner *et al.* 1988). Data for V3 type 3 fluids (hatched area) are plotted on the basis of sylvite and halite melting temperatures. An example heating path for an inclusion is shown by the arrowed line.

In several instances, inclusions decrepitated prior to total or partial homogenisation. Decrepitation, characterised by sudden fracturing of the inclusion wall and escape of the fluid phases, occurs when the internal pressure in the inclusion exceeds the strength of the quartz. Type 3 inclusions are particularly subject to this phenomenon because they contain high density fluids.

Comparison between thermometric data for type 1 and type 3 inclusions indicates that the two fluids are probably related. Ice melting temperatures display a continuous range from -5.2°C to -29.1°C (see Appendix D2). Type 3 total homogenisation temperatures (Fig. 3.26) overlap with type 1 homogenisation tempreatures. A *Th-S* plot for all V3 inclusion data (Fig. 3.38), with total salinities estimated from clathrate melting, ice melting and halite dissolution temperatures, illustrates the likely continuum between type 1 and type 3 inclusions.

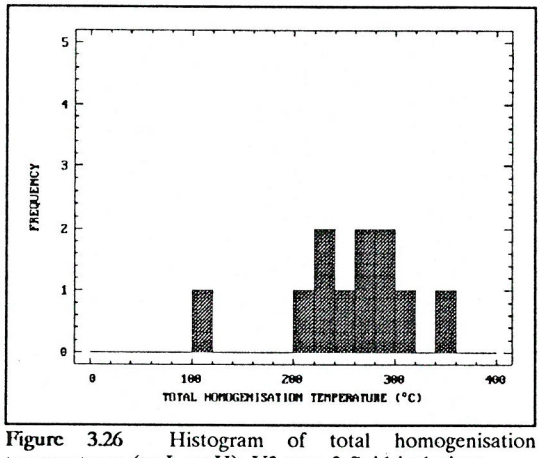

Figure 3.26 Histogram of total homogenisation temperatures (to L or H), V3 type 3 fluid inclusions.

Type 4 inclusions are filled almost entirely by vapour (Fig. 3.3). A liquid phase is present, wetting the inclusion wall, but the volumetric proportion at room temperature is often too low to resolve it under the microscope. It is estimated that the volume fraction of the aqueous phase in these inclusions is between 0 and 0.2. In terms of degree of fill, type 4 inclusions form a continuous range with type 2 inclusions, the division being set at $F=0.2$ (below which an aqueous phase is generally not visible).

There are few salinity estimates for type 4 fluids, since ice melting is not observed and clathrate melting is only rarely apparent. Where clathrate melting is observed, it does not always occur in the presence of liquid CO_2 so that the method described by Collins (1979) for the estimation of salinity may not be used. Thus, there are only two salinity determinations for these inclusions: 2.5 and 3.4 wt% NaCl equivalent. These values are in the expected range for low density vapours, in which NaCl has a relatively low solubility (Takenouchi & Kennedy 1965).

Another result of the low degree of fill of type 4 inclusions is that it is very difficult to measure the homogenisation temperature accurately, with estimated measurement errors of 1-30°C. Homogenisation occurs by expansion of the vapour bubble to fill the inclusion and can usually only be determined in inclusions which have an elongate or cuspate protrusion, within which the liquid/vapour meniscus is more readily observed. The *Th* frequency histogram presented in Figure 3.27 shows one dominant population centred on 260°C, with a possible subordinate grouping, comparable with type 2 inclusions, at 360-420°C. Fitting a normal distribution to the main population gives a mean of 268°C and standard deviation of 36°C. The main population coincides with total homogenisation in type 3 inclusions, supporting a genetic association (see 4.2).

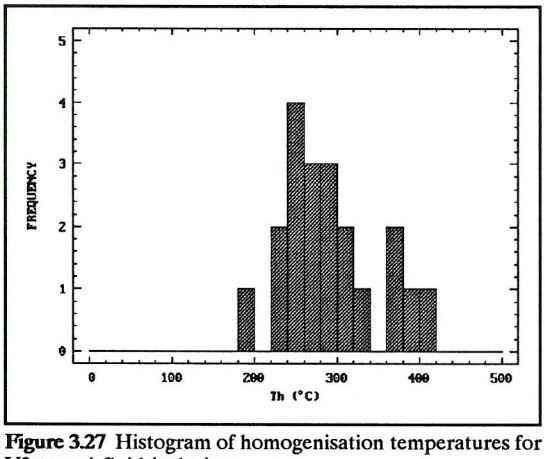

Figure 3.27 Histogram of homogenisation temperatures for V3 type 4 fluid inclusions

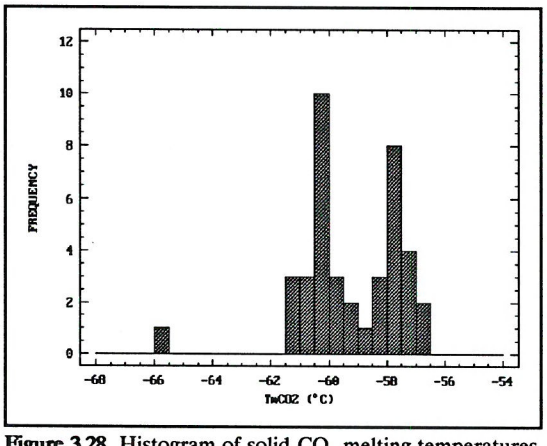

Figure 3.28 Histogram of solid CO_2 melting temperatures, V3 type 4 fluid inclusions

Solid CO_2 forms in most type 4 inclusions on cooling to -110°C. Melting of this phase mainly occurs in the range -61.2 to -56.8°C, although one inclusion had a $TmCO_2$ of -65.5°C (Fig. 3.28). These data indicate that CO_2 is the dominant volatile phase after H_2O, and that variable amounts of other gases are present. The reason for the bimodal distribution in the data is not clear. There is a correlation between these groups and the spatial distribution of the samples, with samples in the north (locality codes TP, GR, DR) dominantly containing the lower $TmCO_2$ population and the samples further south (locality code PS) containing the higher temperature assemblage.

Clathrate melting is rarely observed in type 4 inclusions. The three values obtained for *TmC* of 8.5, 9.0 and 9.4°C, fall in the same range as the major *TmC* population in type 2 inclusions.

Homogenisation of the CO_2 phases occurs below ambient temperature. In many inclusions, $ThCO_2$ is not observed at all, as a result of the extremely low CO_2 densities. Measured $ThCO_2$ values are predominantly between 8 and 21°C, although $ThCO_2$ in the presence of clathrate (which will affect the homogenisation temperature) has been observed as low as -20.2°C. CO_2 density estimates based on these data, assuming that pure CO_2 is present, range from 0.04-0.20 g cm-3. These CO_2 densities are comparable with those estimated for type 2 inclusions (see above), although the bulk fluid densities are lower (Appendix D2).

Type 5 inclusions are compositionally related to type 2, type 4 and type 6 inclusions (Fig. 3.12). Their compositions are intermediate between the range of fluids represented by type 2 and 4 inclusions, and the end-member fluid composition represented by type 6 inclusions. The volumetric proportion of the aqueous phase is similar to type 4 inclusions, dominantly ranging from 0 to 0.3, although rare examples with *F* as high as 0.8 have been observed (Fig. 3.29). These latter inclusions are identical to types 1 or 2, apart from the presence of a small amount of liquid CO_2 at room temperature.

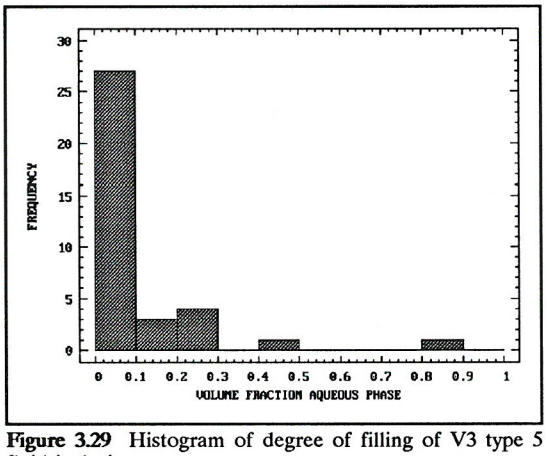

Figure 3.29 Histogram of degree of filling of V3 type 5 fluid inclusions

It has proved impossible to estimate the salinity of type 5 fluids since neither clathrate melting nor ice melting could be observed. As electrolytes are only sparingly soluble in CO_2-rich fluids (Takenouchi & Kennedy 1965), and by analogy with type 2 and 4 inclusions, it is likely that type 5 inclusion fluids contain few dissolved salts.

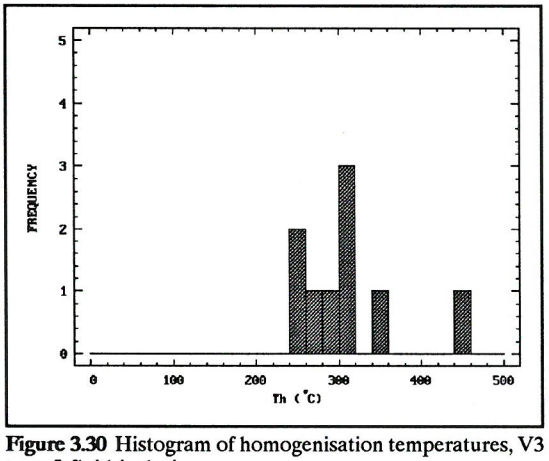

Figure 3.30 Histogram of homogenisation temperatures, V3 type 5 fluid inclusions

Total homogenisation is difficult to observe due to the low degrees of fill, hence the data are limited. Figure 3.30 suggests that only one *Th* population is present. The *Th* range compares closely with that for type 4 inclusions and is lower than the dominant population in both type 1 and type 2 inclusion assemblages.

Low temperature data indicate that CO_2 is the dominant volatile component in the non-aqueous part of the inclusions. CO_2 melting usually occurs between -57.9 and -56.6°C, although $TmCO_2$ has been measured as low as -60°C (Fig. 3.31). The dominant population is comparable with the higher temperature $TmCO_2$ group in type 4 inclusions (Fig. 3.28) and a minor population in the type 2 data (Fig. 3.19).

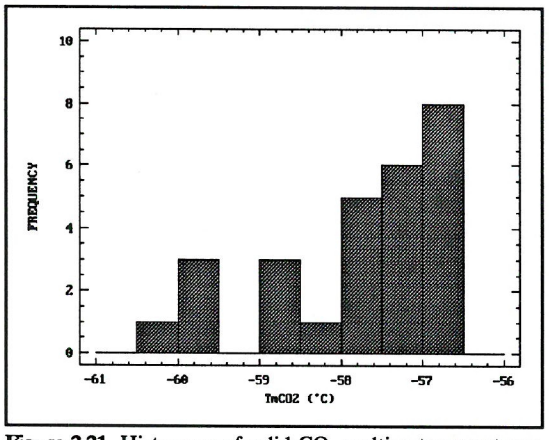

Figure 3.31 Histogram of solid CO_2 melting temperatures, V3 type 5 fluid inclusions

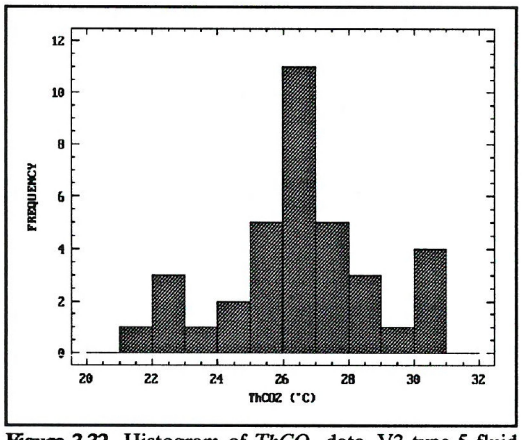

Figure 3.32 Histogram of $ThCO_2$ data, V3 type 5 fluid inclusions

CO_2 homogenisation to vapour is observed anywhere between room temperature and the critical point of pure CO_2 (31.1°C). There is a prominent mode in the $ThCO_2$ data at 26-27°C (Fig. 3.32), corresponding to a CO_2 density of ≈0.27 g cm-3.

Thermometric data for inclusion types 4 and 5 are very similar, suggesting the two fluids are related. The only distinguishing feature, which is reflected by their different appearances at room temperature, is the density of the non-aqueous part of the inclusions. The continuum between the two types indicates trapping of a range of fluids, varying in terms of bulk density and mole fraction CO_2, under a range of P-T conditions.

Type 6 inclusions are very distinct CO_2-rich inclusions, usually containing 3 phases at room temperature (Fig. 3.3). The aqueous portion, which wets the inclusion wall, has a volumetric proportion of 0.05-0.4, with the majority of the data falling between 0 and 0.1. In the cases where an aqueous phase was not observed, the degree of fill was estimated at 0.05.

Salinity for type 6 inclusions has been estimated from clathrate melting temperatures. In many examples, the proportion of aqueous liquid was too low for clathrate melting to be observed; as a result, the data are limited. A frequency histogram (Fig 3.33) shows that *TmC* is mainly in the range 7-10°C, corresponding to salinities of 0.0-5.5 wt% NaCl equivalent. The presence of a low proportion of other volatile phases in these inclusions, confirmed by low temperature data (see below), artificially raises *TmC*. The result of this is that the salinities quoted are probably slight underestimates.

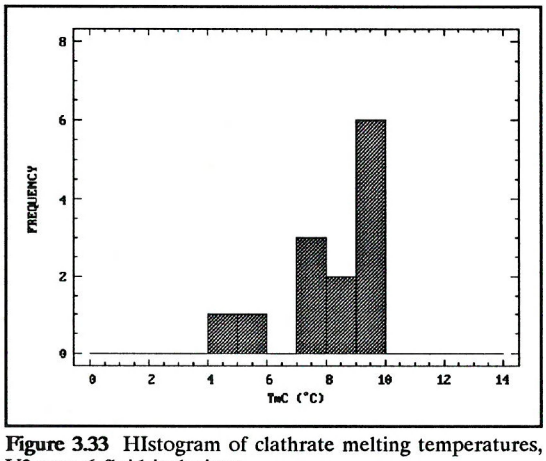

Figure 3.33 HIstogram of clathrate melting temperatures, V3 type 6 fluid inclusions

Homogenisation (to vapour) has only been observed in relatively few inclusions because of the low degrees of fill. Figure 3.34 illustrates one *Th* population with a prominent mode at 300°C. The data approximate to a normal distribution with a mean *Th* of 296°C and standard deviation of 42°C. Comparison with the other V3 inclusion types indicates that type 6 inclusions have a similar *Th* range

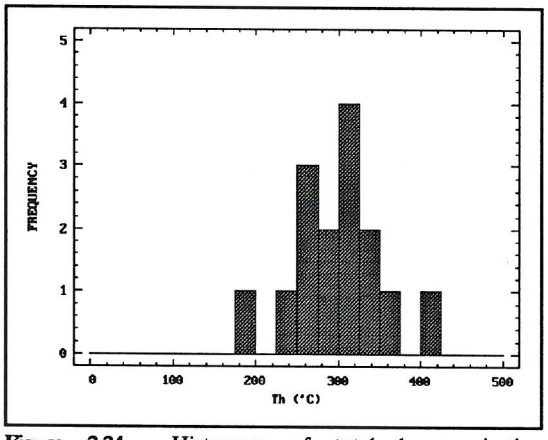

Figure 3.34 Histogram of total homogenisation temperatures for V3 type 6 fluid inclusions

and mean to type 5 inclusions, and are intermediate in *Th* between the type 1-2 association (*c.* 370°C) and the type 3-4 association (*c.* 270°C). In *Th-S* space, the type 6 data define a field below and to the low salinity side of type 1 and 2 inclusions (Fig. 3.38).

CO_2 homogenisation occurs to the liquid in the range 21.2-31.4°C (Fig. 3.35), corresponding to CO_2 densities of 0.77-0.47 gcm^{-3}. $TmCO_2$ data for type 6 inclusions display a bimodal distribution (Fig. 3.36), with peaks centred on -57°C and -57.9°C. The depression of $TmCO_2$ below the triple point of pure CO_2 indicates the presence of other gases, shown by bulk volatile analyses (see 3.4) to be dominated by N_2 and CH_4.

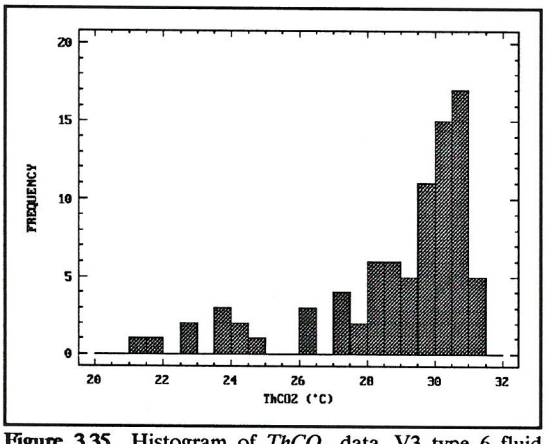

Figure 3.35 Histogram of $ThCO_2$ data, V3 type 6 fluid inclusions

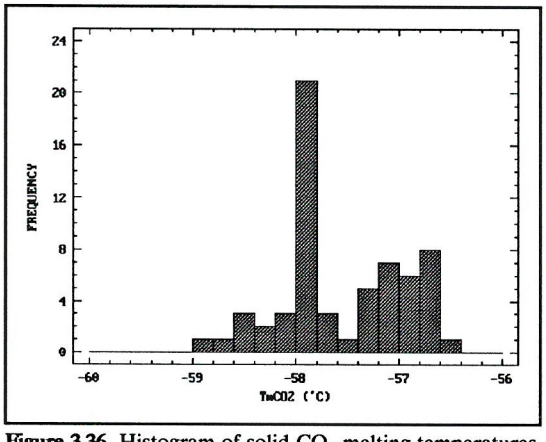

Figure 3.36 Histogram of solid CO_2 melting temperatures, V3 type 6 fluid inclusions

Type 6 data illustrate a correlation between $TmCO_2$ and $ThCO_2$ which is also observed for the other V3 inclusion types (Fig. 3.37). The linear trend in $TmCO_2$-$ThCO_2$ space is probably controlled by equilibria in the H_2O-CO_2-CH_4-N_2 system. Increasing proportions of volatiles other than CO_2 and H_2O in the inclusion fluids would tend to depress both $TmCO_2$ and $ThCO_2$, explaining the direction of the trend. The fact that a linear array is produced rather than a spread of data may be explained by an equilibrium control of CO_2/CH_4 and CO_2/N_2 ratios, such that a change in CO_2 content of the fluid is intrinsically linked to changes in the proportion of CH_4 and/or N_2. These changes may, in turn, be the result of variations in intensive parameters, the most important being T and fO_2. The reason for the presence of two sub-parallel trends, the second having a slightly steeper slope in $TmCO_2$-$ThCO_2$ space, is unclear. It is known that the presence of clathrate has an effect on the melting point of solid CO_2 (Ramboz *et al.* 1985) and it is conceivable that it is a property of the clathrate itself, or the thermodynamics of its formation, which cause the observed depression of $TmCO_2$ in some inclusions.

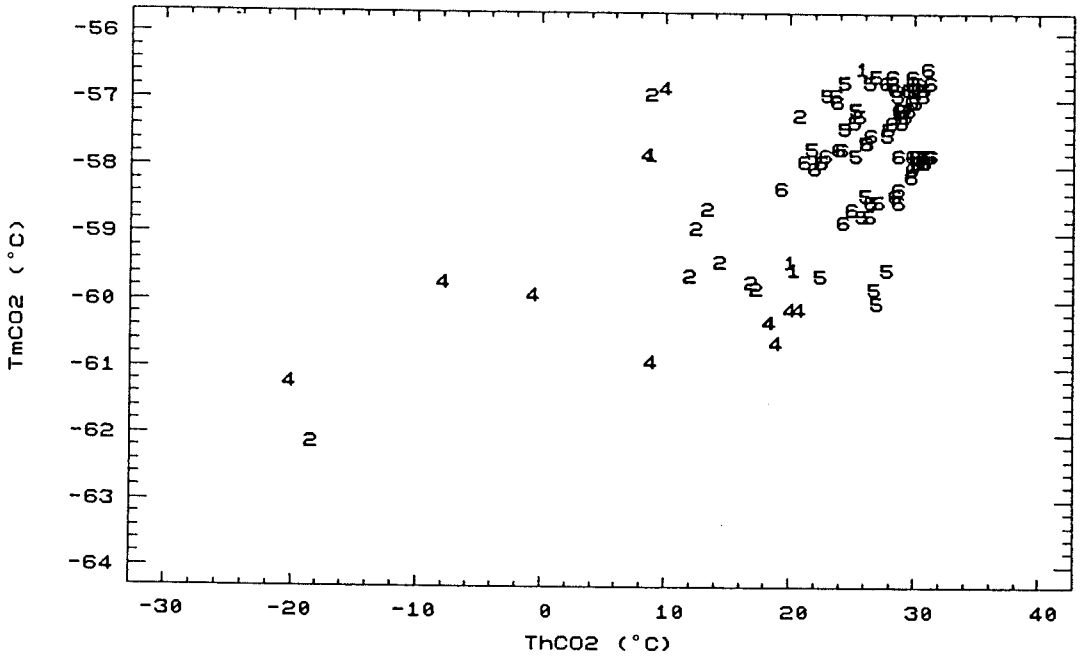

Figure 3.37 $ThCO_2$-$TmCO_2$ plot for V3 fluid inclusions. Numbers refer to each inclusion type.

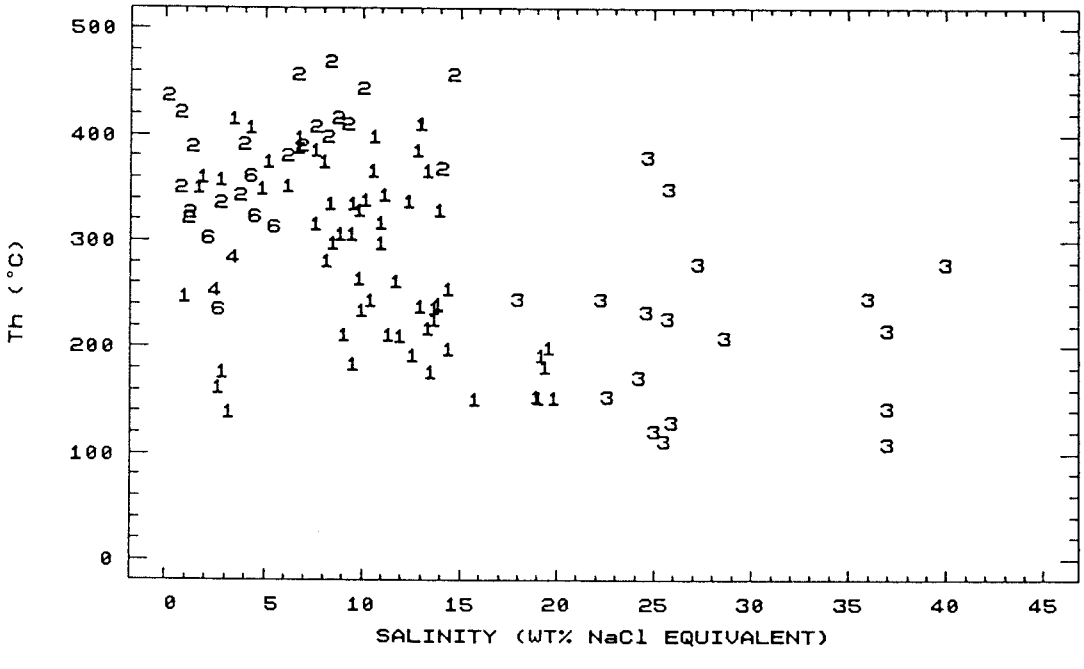

Figure 3.38 *Th-S* plot for V3 inclusions, illustrating compositional relationships between inclusion types. Numbers refer to inclusion types. Salinities estimated from TmI, TmC and TsH.

Summary

The V3 data described above clearly indicate that the divisions between type 1 and 3, type 2 and 4 and type 4, 5 and 6 inclusions based on optical criteria (Fig. 3.12) are somewhat arbitrary, since compositions are gradational between the different groups. This is illustrated by a *Th-S* plot for all V3 inclusions (Fig. 3.38). There is convincing evidence to suggest that inclusion types 1 and 3 represent liquids produced by moderate and extreme unmixing respectively. Inclusion types 2 and 4 represent the vapours produced by moderate and extreme unmixing. The complex compositional variations, including the occurrence of type 5 and 6 fluids may be explained by local fluctuations in P and T during V3 vein growth (see 4.4).

3.2.5 $V4_P$ fluid inclusions

Fluid inclusions in quartz crystals from the Megilligar pegmatite-aplite sill complex (see Fig. 1.4; section 1.3.2) are discussed in this section. They are considered separately because of their unique origin, being intimately related to late magmatic events, and consequent importance in understanding the transition between magmatic and hydrothermal fluid systems. The inclusion populations present in samples from the pegmatite itself, and those present in "distal" pegmatite-related quartz veins (see sections 1.3.2, 2.2.11), are optically and thermometrically distinct and are considered below. Full microthermometric data for these samples are presented in Appendix D2.

Optical characteristics

The Megiliggar pegmatites and "distal" quartz veins contain clear quartz crystals, up to several centimetres in diameter. The large crystal size, optical clarity and lack of deformation allow easy observation of large fluid inclusions (Fig 3.3). Pegmatitic quartz contains three types of fluid inclusions which may be distinguished optically (P1-3 in Table 3.7). The distal quartz veins also contain three inclusion types (DV1-3), which differ markedly in composition and mode of origin to the pegmatite-hosted inclusions. The major optical characteristics of the two inclusion assemblages are summarised in Table 3.7 below. Examples of P1 and DV1 inclusions are shown in Figure 3.3.

Table 3.7 Summary of optical characteristics: $V4_P$ fluid inclusions

TYPE	DESCRIPTION	SPATIAL DISTRIBUTION	INTERPRETATION
P1	**Size:** 10-30μm. **Shape:** negative crystal, ellipsoidal or rounded. **Phases:** aqueous liquid + very low density CO_2-H_2O vapour (F=0.55-0.95).	Isolated, in clusters, in 3D arrays, or in annealed microfractures.	Inclusions represent trapping of H_2O-rich liquid, during and subsequent to crystallisation of pegmatite quartz.
P2	**Size:** 10-30μm. **Shape:** negative crystal, rounded or elongate and irregular. **Phases:** very low density CO_2-rich vapour + aqueous liquid (F<0.3).	Isolated, in clusters, commonly in annealed microfractures crosscutting grain boundaries.	Inclusions may represent overprint of low density vapour which separated from P1 fluid at late stage of pegmatite crystallisation.
P3	**Size:** 5-40μm. **Shape:** sub-negative crystal to flattened and highly irregular. **Phases:** aqueous liquid ± vapour (F=0.9-1.0).	Commonly in clusters and in annealed microfractures crosscutting grain boundaries.	Inclusions represent trapping of $V4_{J1}$-type fluid subsequent to pegmatite crystallisation.
DV1	**Size:** 10-60μm. **Shape:** negative crystal, rounded or slightly irregular. **Phases:** aqueous liquid + low density H_2O-CO_2 vapour (F=0.5-0.9).	Isolated, in clusters, in 3D arrays and in annealed microfractures.	Inclusions represent trapping of immiscible, H_2O-rich fluid during and subsequent to crystallisation of distal quartz.
DV2	**Size:** 10-40μm. **Shape:** negative crystal, rounded or slightly irregular. **Phases:** CO_2-bearing vapour, + aqueous liquid (F<0.4).	Commonly isolated or in clusters, also in 3D arrays and in annealed microfractures.	Inclusions represent trapping of immiscible, low to moderate density CO_2-bearing fluid, during and subsequent to crystallisation of distal quartz.
DV3	**Size:** 5-50μm. **Shape:** sub-negative crystal to flattened, irregular. **Phases:** aqueous liquid + vapour (F=0.9-0.95).	Rarely isolated, commonly in clusters and in well- or poorly-annealed microfractures.	Inclusions represent trapping of $V4_{J1}$-type fluids, subsequent to formation of distal quartz veins.

The textural evidence briefly outlined in the table suggests that three inclusion types are present in both sample types. These optical distinctions are supported by the thermometric data (see below). P1 inclusions (Fig. 3.3) are interpreted as primary inclusions *sensu stricto* whereas P2 and P3 inclusions are comparable with DV2 and $V4_N$ inclusions respectively. DV1 and DV2 inclusions are interpreted as genetically-related primary inclusions postdating P1 inclusions, and DV3 inclusions are comparable with $V4_{J1}$ inclusions (see 3.2.6).

Thermometric characteristics

Thermometric data for $V4_P$ fluid inclusions are summarised in Table 3.8. Undoubtedly, the data only provide a simple picture of what was probably a very complex magmatic-hydrothermal fluid system. Due to the nature of the study and the limited time available, these fluids could not be studied in greater detail.

Table 3.8 Summary of $V4_P$ thermometric data

TYPE	*Th*	*S*	*$TmCO_2$*	*TmC*	*$ThCO_2$*	COMMENTS
P1	200-330 (L)	1-5	-	7.0-9.0	-	H_2O-rich magmatic fluid
P2	300-400 (V)	2-8	-62.4 to -61.6	5.6-10.1	-7.1 (V)	CO_2-bearing vapour (?DV2)
P3	120-180 (L)	<4	-	-	-	Low T dilute fluid (?$V4_N$)
DV1	360-430 (L)	8-10	-64.3 to -60.8	8.3-9.7	-	Immiscible H_2O-rich liquid
DV2	360-480 (V)	0-9	-62.6 to -61.2	5	10 (V)	Immiscible CO_2-rich vapour
DV3	240-320 (V)	7-13	-	-	-	Moderate T, saline fluid

Type P inclusions. A degree of fill frequency histogram for $V4_P$ type P inclusions (Fig. 3.39) allows resolution of liquid-rich type P1 and vapour-rich type P2 inclusions. Liquid-rich type P3 inclusions are obscured by the dominant P1 population. The P1 and P3 populations may be distinguished on a salinity frequency histogram (Fig. 3.40), represented by modes at 1.5 and 4 wt% NaCl equivalent respectively. Salinities for type P2 vapour-rich assemblages could not be determined, due to the low proportion of aqueous liquid and the absence of liquid CO_2.

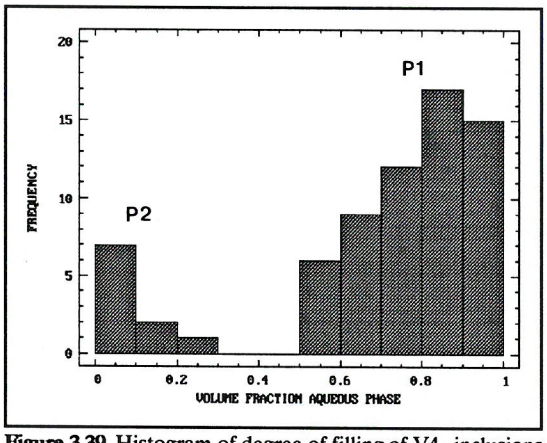

Figure 3.39 Histogram of degree of filling of $V4_P$ inclusions from pegmatitic quartz

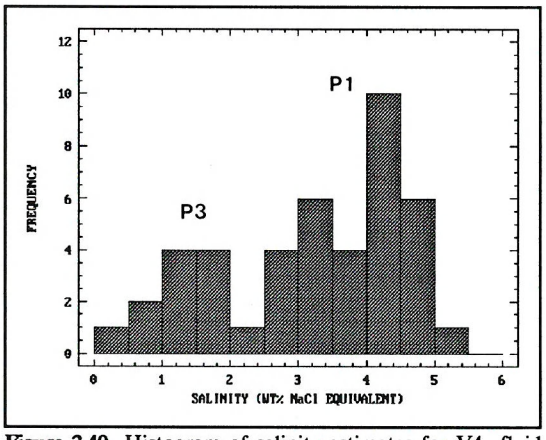

Figure 3.40 Histogram of salinity estimates for $V4_P$ fluid inclusions, pegmatitic quartz

Type P1 inclusions are responsible for the major *Th* population present in a *Th*-frequency histogram (Fig. 3.41). Type P2 inclusions, homogenising to vapour, form the high temperature grouping at 300-400°C. The small low temperature population apparent in the data results from measurement of type P3 inclusions.

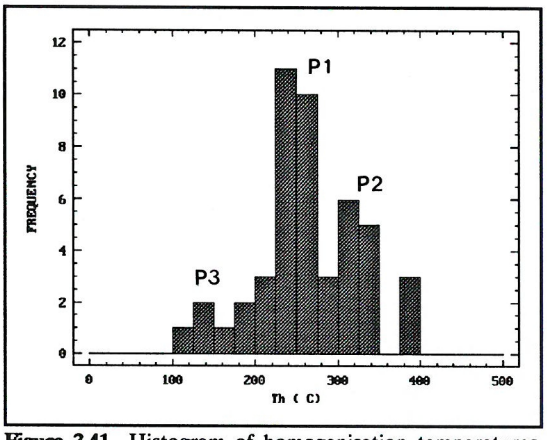

Figure 3.41 Histogram of homogenisation temperatures, $V4_P$ inclusions in pegmatitic quartz

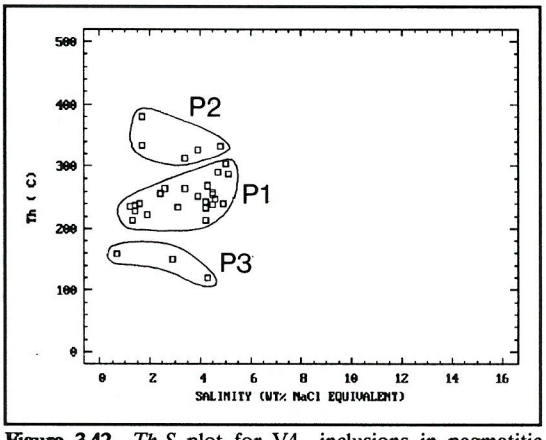

Figure 3.42 *Th-S* plot for $V4_P$ inclusions in pegmatitic quartz, illustrating 3 inclusion types

On cooling to -120°C, solid CO_2 is only seen to form in P2 inclusions. Melting of this phase occurs between -62.4 and -61.6°C, indicating the presence of a significant proportion of volatiles other than CO_2 and H_2O, most likely alternatives being CH_4 and N_2. Clathrate melting in P2 inclusions occurs in the range 5.6-10.1°C indicating low salinities. These data are consistent with that for type DV2 inclusions (see below) suggesting that the P2 inclusions represent an overprint by type DV2 fluids. The presence of low proportions of CO_2 in type P1 inclusions is confirmed by the observation of clathrate melting in these inclusions at 7-9°C. This is an important observation as it indicates that the P1 fluid, interpreted as an H_2O-rich magmatic fluid, contains low proportions of additional volatile phases. A *Th-S* bivariate plot may be used to distinguish the various fluid populations described above (Fig. 3.42).

Type DV inclusions. Three fluid inclusion populations have been distinguished in $V4_P$ distal quartz veins. These are optically and thermometrically distinct from type P1 and type P3 inclusions. Type DV2 vapour-rich inclusions are optically and thermometrically similar to type P2 inclusions and are believed to be related.

Reference to a degree of fill frequency histogram for $V4_P$ distal quartz veins illustrates the wide range of volumetric phase proportions exhibited (Fig. 3.43). A vapour-rich (type DV2) population may be distinguished at low degrees of fill; the broad peak present at higher degrees of fill results from the overlap of DV1 and DV3 populations.

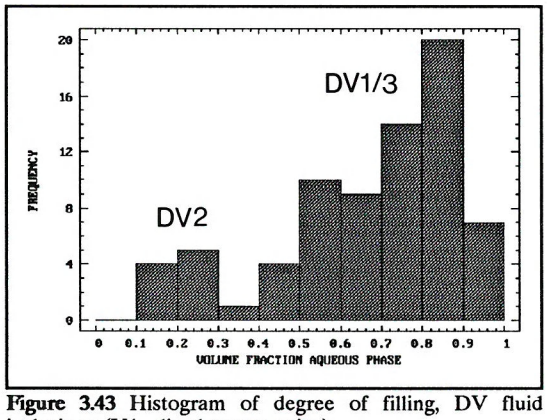

Figure 3.43 Histogram of degree of filling, DV fluid inclusions ($V4_P$ distal quartz veins)

Salinity data are misleading (Fig. 3.44) because they suggest that two distinct populations are present. Reference to Table 3.8 and Figure 3.46 shows that this is an artefact which may be traced to the measurement of a large number of inclusions with very similar thermometric characteristics from one field of view. *Th* data (Fig. 3.45) display a bimodal distribution with a high *Th* mode resulting from the DV1/2 inclusions and a lower *Th* peak representing the DV3 inclusions. The fact that liquid-rich DV1 and vapour-rich DV2 inclusions have similar morphological and textural characteristics and coexist over the same *Th* range is good evidence for fluid immiscibility at this stage.

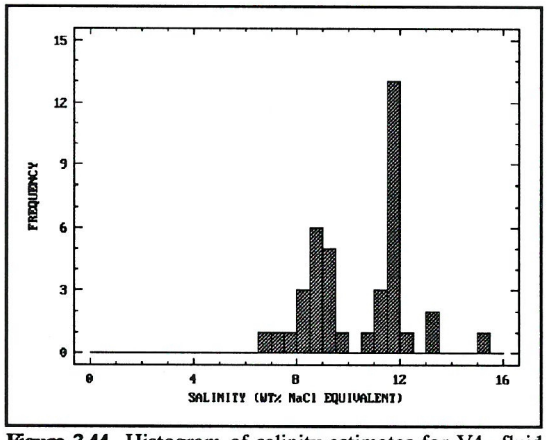

Figure 3.44 Histogram of salinity estimates for $V4_P$ fluid inclusions, distal quartz veins

DV1 and DV3 inclusion data may be divided into two groups on a *Th-S* plot (Fig. 3.46). This plot shows that lower *Th* DV1 inclusions are compositionally similar to DV3 inclusions and there may be a genetic relationship between the two fluid types (see 4.5, 6.2.2).

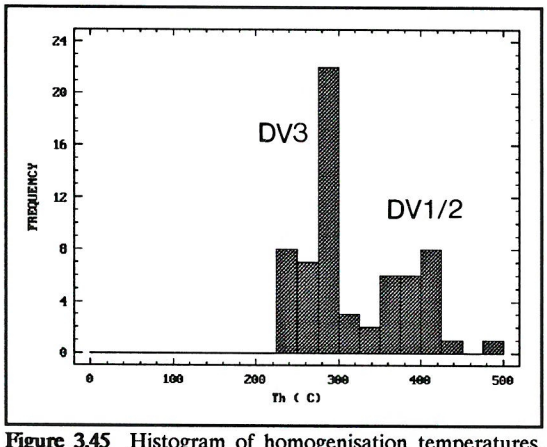

Figure 3.45 Histogram of homogenisation temperatures, $V4_P$ fluid inclusions (distal quartz veins)

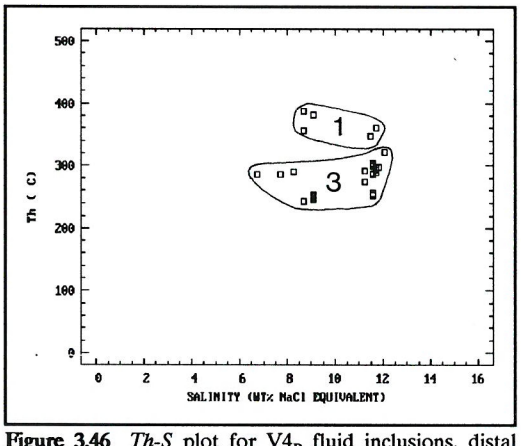

Figure 3.46 *Th-S* plot for $V4_P$ fluid inclusions, distal quartz veins

CO_2 melting has been observed in both DV1 and DV2 inclusions. In both cases, $TmCO_2$ ranged from -64.3 to -60.8°C, similar to the pegmatite vapour-rich inclusions, and well below the triple point of CO_2. This indicates that an important component of other volatile phases are present. *TmC* in the same inclusions has been recorded between 5 and 9.7°C. Two measurements of $ThCO_2$ (+10 and -15°C) in DV2 inclusions confirm the presence of low density CO_2 ($\approx$0.05-0.13 g cm^{-3}).

Summary

Six types of inclusions may be distinguished in pegmatite-related quartz. Two-phase H_2O-rich inclusions (type P1) in pegmatitic quartz are believed to represent the magmatic aqueous fluid which separated from the pegmatite during crystallisation. This fluid may have unmixed during separation from the melt to generate the liquid- and vapour-rich inclusion assemblage observed in the distal quartz veins (types DV1, DV2). These unmixed fluids also appear to have flowed through

microfractures in crystallised pegmatite. Later overprinting by $V4_J$ and $V4_N$-type fluids is also observed (inclusion types P3 and DV3 respectively).

3.2.6 $V4_J$ fluid inclusions

The data are rather limited for inclusions in $V4_J$ quartz veins, hosted by sub-vertical joints in the country rock close to the Tregonning granite. However, the measurements obtained provide some useful constraints on the temperature, composition and evolution of fluids mobilised close to the Tregonning granite stock soon after its emplacement. Microthermometric data for $V4_J$ veins are tabulated in Appendix D2.

Optical characteristics

Three fluid inclusion populations may be distinguished optically at room temperature. These groups are optically and thermometrically similar to the DV inclusions from $V4_P$ quartz described above. The morphological characteristics and distribution of these inclusion types are summarised in Table 3.9 below.

Table 3.9 Summary of optical characteristics: $V4_J$ fluid inclusions

TYPE	DESCRIPTION	SPATIAL DISTRIBUTION	INTERPRETATION
1	**Size:** 5-30μm. **Shape:** negative crystal, ellipsoidal or slightly irregular. **Phases:** aqueous liquid + vapour (F=0.5-0.9).	Isolated or in clusters, less commonly in annealed microfractures.	Inclusions represent trapping of H_2O-rich fluid, primarily during vein growth.
2	**Size:** 5-30μm. **Shape:** negative crystal, rounded or slightly irregular. **Phases:** vapour + aqueous liquid (F<0.4).	Isolated or in clusters, also in annealed microfractures.	Rare inclusions represent trapping of vapour produced by occasional unmixing of type 1 fluid during vein growth.
3	**Size:** 5-30μm. **Shape:** rarely negative crystal, commonly flattened and irregular. **Phases:** liquid + vapour (F=0.8-0.95).	Occasionally isolated, commonly in well- or poorly-annealed microfractures	Inclusions represent fluid flow ($V4_N$-type) subsequent to formation of $V4_J$ veins.

Thermometric characteristics

The important thermometric characteristics of the three inclusion types present in $V4_J$ samples are summarised in Table 3.10 below.

Table 3.10 Summary of $V4_J$ thermometric data

TYPE	*Th*	*S*	*$TmCO_2$*	*TmC*	*$ThCO_2$*	COMMENTS
1	200-400 (L)	9-14	-	6.0	1.5 (L)	H_2O-rich fluid (evolved DV1?)
2	270-350 (V)	low	-62.1	-	-	CO_2-bearing vapour
3	170-320 (L)	<4	-	-	-	Late, dilute fluid (?$V4_N$)

Type 1 and 3 inclusions cannot be distinguished on a degree of fill frequency histogram (Fig. 3.47) because of the overlapping ranges. However, the rare, vapour-rich inclusions (type 2) are represented at low degrees of fill.

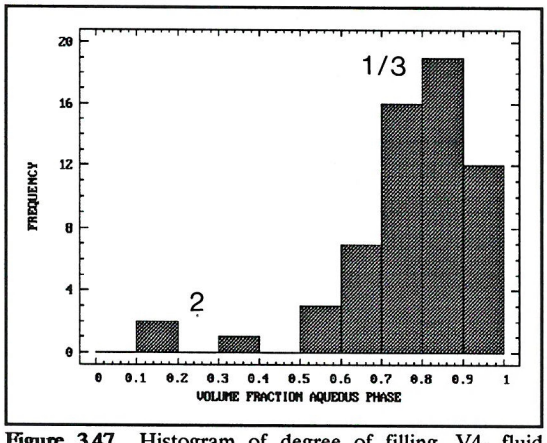

Figure 3.47 Histogram of degree of filling, $V4_J$ fluid inclusions

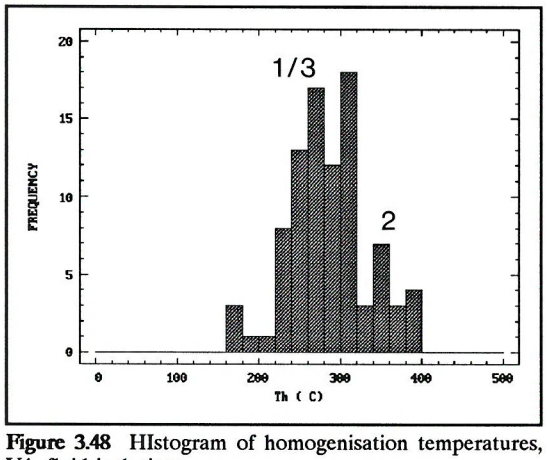

Figure 3.48 HIstogram of homogenisation temperatures, $V4_J$ fluid inclusions

The *Th* frequency histogram shown in Figure 3.48 illustrates that the dominant inclusion population present comprises type 1 inclusions. The low salinity type 3 inclusions have relatively high homogenisation temperatures (for $V4_N$ fluids) and are obscured by the type 1 population.

Salinity estimates have only been obtained for type 1 and type 3 inclusions. Ice melting was not observed in vapour-rich type 2 inclusions. A salinity frequency histogram (Fig. 3.49) clearly illustrates the two H_2O-rich inclusion populations. A *Th-S* plot for $V4_J$ fluid inclusions (Fig. 3.50), also distinguishes the type 1 and type 3 fluids. Comparison of this plot with that for $V4_P$ distal fluid inclusions (Fig. 3.46) shows that the $V4_J$ type 1 inclusions are thermometrically very similar to DV3 inclusions. This supports an interpretation of the DV3 inclusions as representing an overprint of $V4_P$ distal quartz by the fluids subsequently mobilised in joints.

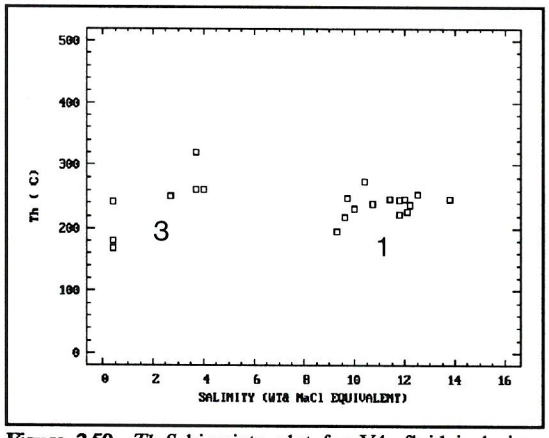

Figure 3.50 *Th-S* bivariate plot for $V4_J$ fluid inclusions illustrating type 1 and type 3 populations

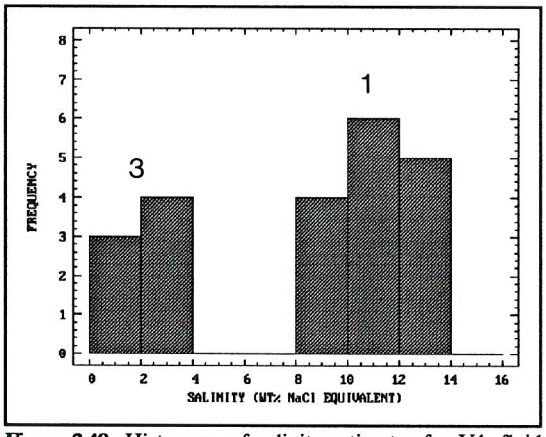

Figure 3.49 Histogram of salinity estimates for $V4_J$ fluid inclusions

One measurement of $TmCO_2$ at -62.1°C confirms the presence of CO_2 in the type 2 vapour-rich inclusions and indicates the presence of other gases. The fact that $ThCO_2$ is not observed in type 2 inclusions indicates very low CO_2 densities (less than 0.05 gcm^{-3}). The presence of clathrate was occasionally detected in type 1 and type 2 inclusions.

Summary

The primary fluids mobilised in early joints are dominantly H_2O-rich with a low proportion of CO_2 (<5 mole %). Occasional unmixing resulted in the generation of low density, CO_2-bearing vapour, containing a significant proportion of other gases. Fluids of this type also flowed through microfractures in earlier pegmatite-related quartz. A low salinity fluid is also observed in these veins, probably representing a later fluid flow event.

3.2.7 $V4_N$ fluid inclusions

Full microthermometric data for $V4_N$ samples are presented in Appendix D2. The important optical characteristics are described below.

Optical characteristics

$V4_N$ quartz veins, associated with post-intrusive normal faults, are typically composed of large, prismatic quartz crystals with distinctive growth zoning (see 2.2.14). A synoptic sketch of a typical field of view is shown in Figure 3.2 and a summary of the optical characteristics of the three inclusion types observed is presented in Table 3.11 below.

Table 3.11 Summary of optical characteristics: $V4_N$ and $V4_W$ fluid inclusions

TYPE	DESCRIPTION	SPATIAL DISTRIBUTION	INTERPRETATION
1	**Size:** 10-40μm. **Shape:** negative crystal, tubular or flattened and irregular, commonly orthogonally indendate. **Phases:** aqueous liquid + vapour (F=0.8-0.95).	Isolated or in clusters, less commonly in annealed microfractures.	Inclusions represent trapping of H_2O-rich fluid, primarily during vein growth.
2	**Size:** 5-30μm. **Shape:** negative crystal, tubular or flattened and irregular. **Phases:** aqueous liquid.	Occasionally isolated, commonly in well- or poorly-annealed microfractures.	Inclusions represent lower T type 1 fluids which have failed to nucleate a vapour bubble.
3	**Size:** 10-30μm. **Shape:** commonly rounded or irregular. **Phases:** vapour ± aqueous liquid (F<0.5).	Generally isolated, occasionally in clusters.	Rare inclusions - probably represent necking of irregular type 1 inclusions.

Type 1 inclusions are by far the most abundant in $V4_N$ samples. Negative crystal type 1 inclusions are relatively rare, but are useful when found as they often display criteria, typically parallelling the crystallographic orientation, indicative of a primary origin. Irregular type 1 inclusions are the most common type, occurring as secondary inclusions *sensu stricto* in fractures clearly cross-cutting crystal boundaries. However, thermometric data indicate that the latter inclusions are compositionally identical to the former. Type 3 inclusions often show evidence of having necked down (Roedder 1984) and these were avoided during thermometric analysis.

Thermometric characteristics

A summary of thermometric data for $V4_N$ inclusion types 1 and 3 is presented in Table 3.12. There are no thermometric data for type 2 inclusions.

Table 3.12 Summary of $V4_N$ thermometric data

TYPE	*Th*	*S*	*TmCO₂*	*TmC*	*ThCO₂*	COMMENTS
1	100-320 (L)	0-11	-	-	-	H_2O-rich meteoric fluid.
2	-	-	-	-	-	Low T type 1, bubble failed to nucleate.
3	>180 (V)	-	-	-	-	Necked type 1 inclusion.

A degree of fill frequency histogram (Fig. 3.51) illustrates the dominance of type 1 liquid-rich inclusions. The few vapour-rich type 3 inclusions recorded, which did not show any evidence of having necked-down or leaked, are nevertheless interpreted as being the result of one of these phenomena.

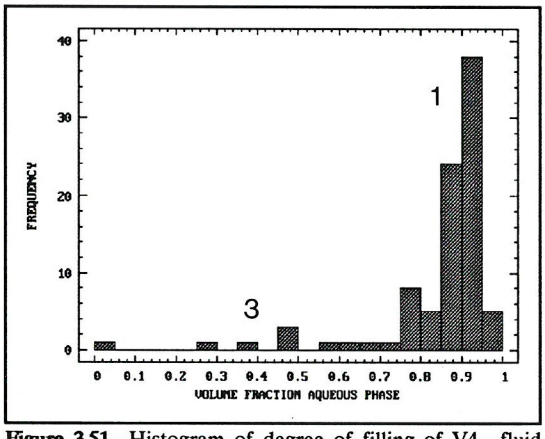

Figure 3.51 Histogram of degree of filling of $V4_N$ fluid inclusions

Final ice melting is easily recognised in type 1 inclusions, occurring in the range -7.5 to 0°C, corresponding to salinities of 0-11.1 wt% NaCl equivalent (Fig. 3.52). The extension of type 1 fluids to moderate salinities has an important genetic significance (see 3.2.8, 4.6.4). Metastable behaviour was sometimes observed in both type 1 and type 2 inclusions, where the bubble collapsed on freezing. Such inclusions exhibit artificially high *TmI* values, with ice existing as high as +3.2°C, at extreme negative pressures, before melting (Roedder 1984). Ice melting in monophase inclusions which originally contained a vapour phase occurred suddenly, upon renucleation of the vapour bubble.

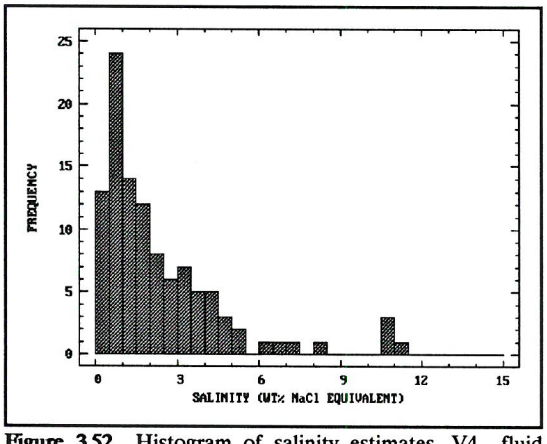

Figure 3.52 Histogram of salinity estimates, $V4_N$ fluid inclusions

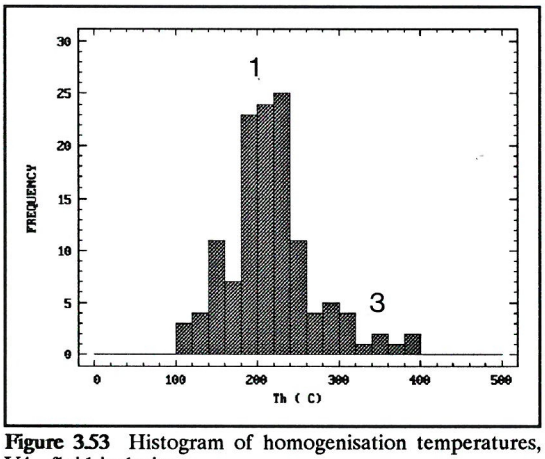

Figure 3.53 Histogram of homogenisation temperatures, $V4_N$ fluid inclusions

Homogenisation temperature data (Fig. 3.53) display a prominent mode at 180-240°C, corresponding to the dominant type 1 population. Normal distribution fitting to this population yielded a mean *Th* of 220°C and standard deviation of 41°C. The extension of *Th* values to temperatures in excess of 300°C is probably due to measurement of type 3 inclusions which have attained artificially high vapour proportions by necking-down or leakage of the aqueous fluid.

Plotting the data on a *Th*-salinity plot (Fig. 3.54) shows a clear trend of increasing salinity with slightly decreasing homogenisation temperature. This relationship is also observed in the data for $V4_W$ fluids (see 3.2.8), hinting at a linked evolutionary process (see 4.6.4).

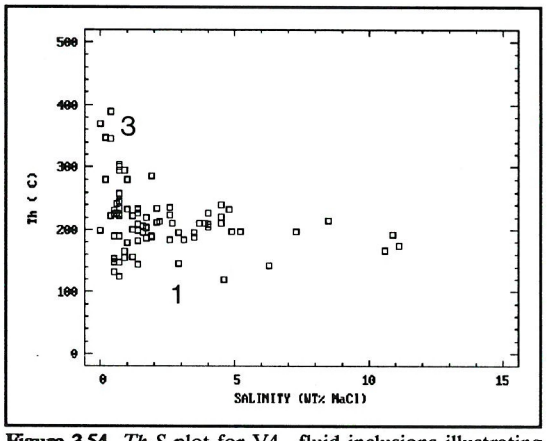

Figure 3.54 *Th-S* plot for $V4_N$ fluid inclusions illustrating trend of increasing salinity at constant *Th*

3.2.8 $V4_W$ fluid inclusions

Full microthermometric data for fluid inclusions in vein quartz associated with wrench faults are presented in Appendix D2. The main optical characteristics are described below.

Optical characteristics

Although $V4_W$ veins contain drusy siderite in addition to quartz (see 2.2.15), only quartz was found to contain fluid inclusions large enough for thermometric analysis. Quartz crystals are transparent and often contain growth zones which appear milky in hand specimen and are defined by thousands of highly irregular fluid inclusions and tiny solid phases (Fig. 2.14), identified by optical microscopy and S.E.M./E.D.X. as muscovite (Fig. 3.23).

The fluid inclusions present in $V4_W$ samples are optically similar to those described above from $V4_N$ veins. The synoptic sketch for $V4_N$ inclusions (Fig. 3.2) also applies to $V4_W$ samples. The main optical features are summarised in Table 3.11.

Thermometric characteristics

Thermometric data for the three types of inclusions which may be distinguished optically at room temperature are summarised in Table 3.13 below.

Table 3.13 Summary of $V4_W$ thermometric data

TYPE	*Th*	*S*	*TmCO₂*	*TmC*	*ThCO₂*	COMMENTS
1	100-320 (L)	0-11	-	-	-	H_2O-rich meteoric fluid.
2	-	-	-	-	-	Low T type 1, bubble failed to nucleate.
3	>180 (V)	-	-	-	-	Necked type 1 inclusion.

The liquid-rich nature of $V4_W$ inclusions is illustrated by the high estimates for the degree of fill (Fig. 3.55). The occasional vapour-rich inclusions measured are almost certainly the result of necking or fluid leakage.

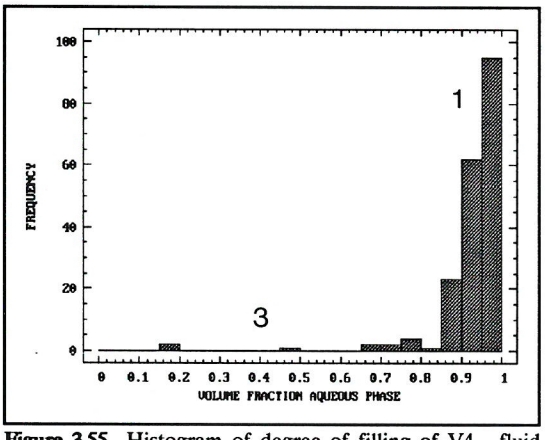

Figure 3.55 Histogram of degree of filling of $V4_W$ fluid inclusions

First (eutectic) melting is relatively easy to observe in type 1 and 2 inclusions. This is due to the way the fine grained, brownish appearance of the frozen inclusions changes to a clear, granular texture on melting. *Tfm* values (Fig. 3.56) display a distinct mode at *c.* -56°C, comparable with the $NaCl-CaCl_2-H_2O$ ternary eutectic reported by Borisenko (1977). A minor, lower temperature grouping at -75°C suggests the presence of LiCl; this has been confirmed by D-ICP studies (see 3.3.1).

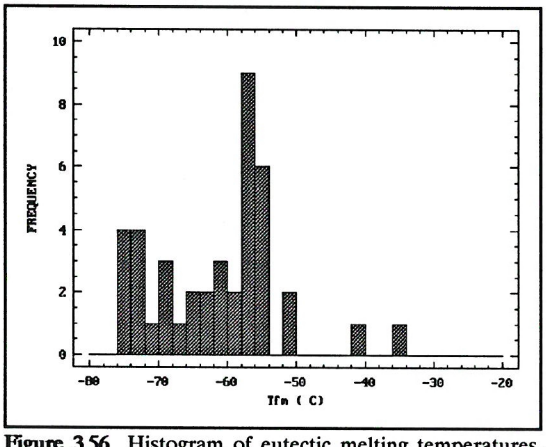

Figure 3.56 Histogram of eutectic melting temperatures, $V4_W$ fluid inclusions

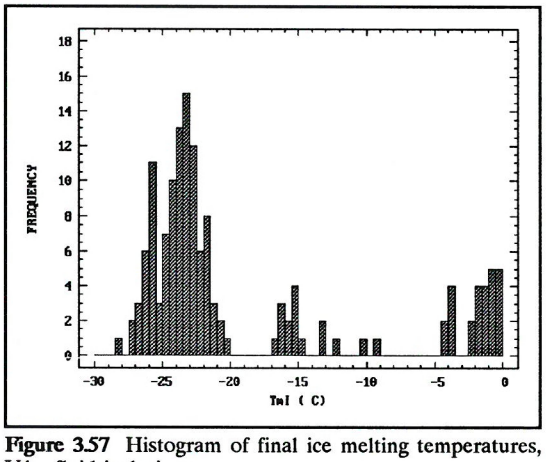

Figure 3.57 Histogram of final ice melting temperatures, $V4_W$ fluid inclusions

Equilibrium ice melting temperatures display a range from -27.3 to -0.5°C (Fig. 3.57). Several values recorded above -0.5°C, including temperatures above 0.0°C, are due to metastable ice melting. A frequency histogram of *TmI* values (Fig. 3.57) shows that three main populations are present. The high *TmI* population at -4.3 to -0.5°C, corresponding to salinities of 0-7 wt% NaCl equivalent, is

indistinguishable from the *TmI* values for $V4_N$ fluids (see 3.2.7). The intermediate population centred on -15.5°C is only observed in one sample (*J19GWa*) and represents an intermediate salinity fluid. The dominant *TmI* population has been modelled as a normal distribution, yielding a mean *TmI* of -23.4°C and standard deviation of 1.4°C. This is statistically indistinguishable from the NaCl-KCl-H_2O eutectic of -23.5°C reported by Borisenko (1977). Final ice melting at such a ternary eutectic implies that another phase should be present which melts at a higher temperature (unless the fluid has the eutectic composition). This additional phase is observed in these inclusions, usually manifest as small, rounded, high relief grains, melting in the range -22.8 to +15.8°C (Fig. 3.58). The optical properties of the solid suggest that it is a salt hydrate, probably hydrohalite, although a mixed NaCl-KCl hydrate cannot be ruled out.

The low temperature data discussed above indicate that the dominant inclusions in $V4_W$ samples (type 1) represent two types of fluid, with some compositional gradation between. The low salinity fluid inclusions are optically and thermometrically indistinguishable from $V4_N$ type 1 inclusions (see 3.2.7). The saline inclusions present may be accurately modelled by the NaCl-$CaCl_2$-KCl-H_2O system and are compositionally similar to modern and ancient basinal brines (see 4.6.3).

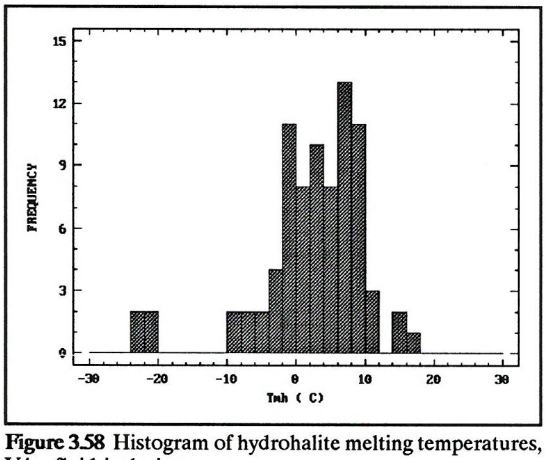

Figure 3.58 Histogram of hydrohalite melting temperatures, $V4_W$ fluid inclusions

The abundance of Na, Ca and K in $V4_W$ saline fluids has been confirmed by D-ICP analysis (see 3.3.1). Unfortunately, there are no low temperature experimental data for the quaternary system, only for the two ternary end-members: NaCl-$CaCl_2$-H_2O and NaCl-KCl-H_2O (Borisenko 1977; Sterner *et al.* 1988). The presence of calcium in the fluid has a greater effect on the topology of the quaternary phase diagram than potassium, hence it is more accurate to model the fluid in the NaCl-$CaCl_2$-H_2O system. Furthermore, D-ICP data show that there is less than 2.5 wt% KCl in $V4_W$ fluids (see 3.3.1). Reference to Figure 3.25 shows that, at these levels of KCl, the NaCl-KCl-H_2O system is closely approximated by NaCl-H_2O.

$V4_W$ fluid inclusions homogenise to the liquid at temperatures between 90 and 220°C (Fig. 3.59). A number of measurements at higher temperatures are probably due to the inadvertent analysis of type 3 inclusions which have necked-down or leaked. Normal distribution fitting to the *Th* mode gives a mean *Th* of 121°C and standard deviation of 14°C. This dominant low *Th* population corresponds to the saline fluid inclusions discussed above. The low salinity type $V4_N$ fluids present in $V4_W$ samples have higher homogenisation temperatures, ranging from 151-217°C.

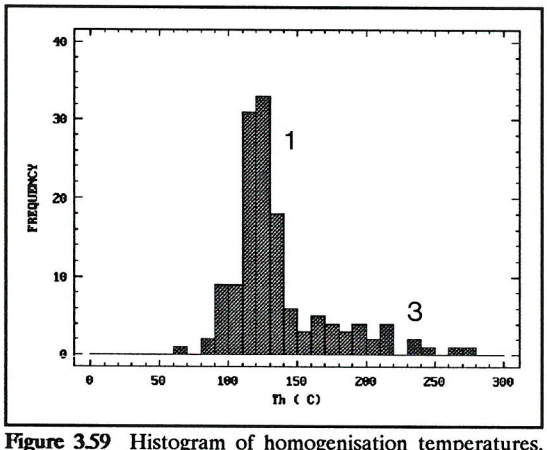

Figure 3.59 Histogram of homogenisation temperatures, $V4_W$ fluid inclusions

A *Th-S* plot (Fig. 3.60) illustrates the relationships between the dilute and saline fluids present in $V4_W$ quartz. The vertical array at high *Th* and high salinity values is probably due to necking or leakage. A more important trend of variable salinity at approximately constant *Th* is also apparent. Comparison with Figure 3.54 shows that this trend is very similar to that observed in $V4_N$ samples. This is interpreted as indicating mixing between dilute (meteoric) fluids and saline (basinal brines) during late stage wrench and normal faulting (see 4.6.4, 6.2.3).

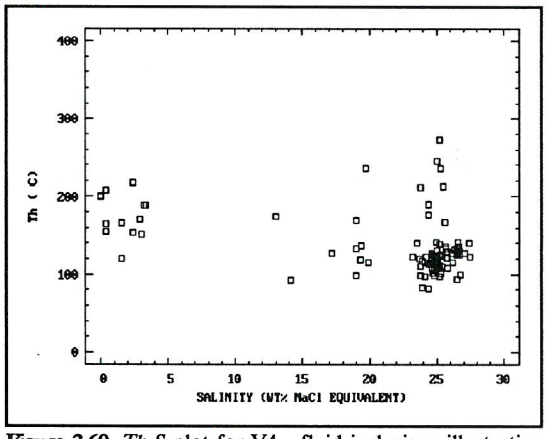

Figure 3.60 *Th-S* plot for $V4_W$ fluid inclusions illustrating trend from low to high salinity fluids.

3.2.9 Summary

In the preceding subsections, the fluid inclusions present in the complete spectrum of veins developed in the study area have been described in detail. Seven main stages of fluid mobilisation have been defined. Thermometric data suggest that most of these fluid flow "events" may be linked in an almost continuous history of fluid evolution, which may be traced from peak regional metamorphism right through to post-orogenic low temperature basinal fluids. This evolutionary scheme is examined in more detail in the following chapters, utilising the thermometric data presented above and the more detailed compositional information discussed in the remainder of this chapter.

3.3 BULK SOLUTE ANALYSIS

As outlined in section 3.1, bulk solute analyses were carried out in order to determine the major dissolved components in the inclusion fluids. The two techniques used both involve the analysis of all inclusions present in a sample. For this reason, samples were carefully selected so as to minimise problems caused by measurement of several fluid generations with contrasting compositions. A minor overprint of comparatively low salinity fluid, observed in some samples, will only introduce small uncertainties into the composition determinations.

The data obtained from these studies, combined with thermometric data for individual fluid inclusions and fluid generations, tightly constrain the composition of H_2O-bearing fluids, and hence the composition of most of the fluids mobilised in the south Cornish crustal segment during the Hercynian orogeny.

3.3.1 Decrepitation-linked I.C.P. analysis (D-ICP)

The majority of methods currently in use for the determination of solutes in fluid inclusions involve the analysis of fluids extracted either by a crush-leach process or by decrepitation (Roedder 1984). In this study, the latter approach was adopted since it avoids a number of problems inherent in the crush-leach method (see Thompson *et al.* 1980 for details). The decrepitation technique introduces its own uncertainties, mainly relating to the possible preferential loss or retention of components in the fluid inclusions as decrepitation occurs. However, recent results suggest that this is only likely to be a problem for inclusions containing daughter minerals (A.H. Rankin, pers. comm. 1989).

In this investigation, inclusion fluids were released from purified, graded quartz chips by thermal decrepitation, directly into the plasma torch of an inductively-coupled plasma atomic emission spectrometer. This instrument is capable of the simultaneous determination of up to 40 elements. Details of the sample preparation technique and equipment calibration methods are documented in Appendices B and C respectively. A summary of the laboratory procedure is outlined below.

Experimental method

The samples analysed consisted of approximately 0.5 g splits of clean quartz chips 0.5-2.0 mm in size (see Appendix B). Each sample was placed in a silica test tube and rapidly heated to 600°C in an electric furnace. Argon gas flowing through the sample tube at a constant rate flushed the volatilised inclusion fluids into a narrow plasma torch. The resulting emission spectrum was integrated over 30 seconds until decrepitation activity ceased. Elements were separated according to the emission wavelength, with peak intensities measured as a current (mA) in the spectrometer. A series of corrections were automatically applied to take spectral interferences into account.

Empty silica tubes were run as blanks every fifth sample to monitor variations in the background emission spectrum. At the end of the run, the background spectrum was subtracted from sample spectra and the data were then calibrated. Calibration was carried out by analysing standard solutions and comparing the peak intensity for each element with that measured for each sample. The resulting values are in terms of "equivalent ppm"; absolute concentrations cannot be determined by this method because the amount of fluid analysed is unknown. An example of the calibration procedure is outlined in Appendix C2.

Results

Standard practice is to ratio the "equivalent ppm" values obtained to sodium, since it is usually the most abundant cation in crustal fluids (Alderton *et al.* 1982). In this study, the Na/element ratio is used to avoid the inconvenience of continuously dealing in fractions.

The data for all runs are presented in Table 3.14. Up to four duplicate splits of each sample were analysed in order to assess within-sample variability. Table 3.15 illustrates errors due to within-sample variability by comparison of major element ratios obtained on four duplicate runs of sample *J48BR*. Standard deviations for the ratios on this admittedly small number of measurements, range from 7.1 to 21.3% of the mean value. Errors for elements present at low concentrations in the inclusion fluids are considerably greater, with duplicate analyses often varying by up to 50% (*e.g.* Ba).

Table 3.14 Bulk fluid inclusion Na/element weight ratios determined by D-ICP analysis

SAMPLE	TYPE	Na/K	Na/Li	Na/Ca	Na/Sr	Na/Ba	Na/Mn	Na/Cu	Na/Mo	Na/Fe	Na/Mg	Na/Zn	Na/B
J53JR	V1F	7.8	185	28.1	1350	732	2160	113	63	226	14	20	19
J53JR	V1F	7.6	212	37.0	920	885		127	87	78	20	147	32
J53JR	V1F				64								
J11PB	V1B	10.3	261	82.0	1700	1770	3510	353	98	317	30	701	42
J11PB	V1B	15.0	315	98.7	2450	2710		405	135	1020	50	278	34
J11PB	V1B	9	218	47	1390	1230	1750			136			47
J138GW	V1B	13.1	181	59.3	406	1330	2540	4320	1220	4670	344	1210	153
J138GW	V1B	14.2	224	83.7	386	1360	2480	277	8310	5130	1300	1320	125
J105GW	V1T	16.0	221	43.8	819	1770		1120	228	518	83	1630	53
J105GW	V1T	17.8	232	105.0	1260	2070	9670	1300	391	489	112	285	51
J105GW	V1T	9.5	184	106									55
J06GW	V1T	21.3	245	93.2	1100	1710			569		895		68
J06GW	V1T	10.1	198	44	640	884	489			26			55
J06GW	V1T				764								
J48BR	V2T	10.9	339	12.9	469	2660	1630	1800	340	401	103	1270	92
J48BR	V2T	12.3	306	15.4	566	1830		915	148	290	68	321	64
J48BR	V2T	13.6	307	16.8	525	3890	3140	2850	600		687	484	50
J48BR	V2T	9.8	287	18.9	597								
D2BR2	V2T	13.2	248	141	434	1180	2360						76
D2BR2	V2T	12.3	278	153	405	1130	2990						74
J99BR	V2T	10.6	211	114	811					362			68
J99BR	V2T	11.4	217	112	821								75
J125LB	V2F	14.7	337	53.7	663	2770	4000	3730	3330		604	950	102
J125LB	V2F	12.5	274	53	593	1390							91
J40LB	V2E				369								
J40LB	V2E				814								
D2bPC	V2E	10.8	282	15.3	199	776	739			76			
D2bPC	V2E	7.9	191	21.9	200	604	567			46			113
D3CZ1	V3C	11.2	524	16.8	159	1040	24			38		59	730
D3CZ1	V3C	7.8	279	13.2	150	593				45			
D3CZ1	V3C	13.4	285	16.1	161	682				46			
J145PS	V3G	7.3	125	11.5	204	1080	1160			287		242	109
J82PS	V3G	5.6	257	16.6	84	3010	868			493	588	642	418
J82PS	V3G	5.8	265	13.7		3110	1770					773	
J82PS	V3G	5.8	243	12.5	74	2290	768			48		531	
J64DR	V3G	7.2	148	15.9	90	1460	842			291		455	399
J64DR	V3G	6	143	22.9	90	1700	3790			576			466
J64DR	V3G	6.9	142	18.1	84	1520	2990			458			443
J93TP	V3G	4.8	102	7.8	325	388	206			138			58
J93TP	V3G	8.8	136	8	356		261			145			85
J98PC2M	V3S	9.3	459	6.6	220	2200	326			70			285
J98PC2M	V3S	8.1	420	5.73	191	1500	1540						
J98PC2M	V3S	8.3	610	5.75	205								
JW005	V4J1	13.3	297	14.4	303	706	89	8780	3690	669	996	274	191
JW005	V4J1	14.6	323	15.4	312	672	162			638		242	
JW005	V4J1	14.7	311	16.6	316	679	182			947		260	
J118TC	V4J2	5.5	168	3.2	143	493	1650	303	787	510	124	288	449
J38LB	V4N	11.2	221	12.2	410								89
J38LB	V4N	12.3	214	12.1	404	1240							97
J78PSa	V4N	13.5	1580	5.5	247								
J78PSa	V4N	12.7	925	6	245								
VL1	V4W	11.6	1440	3.7	198	4030							
VL1	V4W	10.7	736	4.3	180								
VL1	V4W	9.2	950	4.4	177								
J131/6	V4W	7.4	1240	4.1	212	2390				151			
J131/6	V4W	6	914	4.1	212	1720				101			
J98PC2D	V4W	5.8	1140	4.5	238	3530	1830			146	135	5300	1070
J98PC2D	V4W	8.4	818	4.4	215	2290	535			172			
J98PC2D	V4W	8.1		4	210								
J98PC2D	V4W	9.8		3.6	186								

Table 3.15 Estimation of errors due to within-sample variability

RATIO	RUN 1	RUN 2	RUN 3	RUN 4	MEAN	S.D.
Na/K	10.9	12.3	13.6	9.8	11.65	1.42
Na/Li	339	306	307	287	309.54	18.57
Na/Ca	12.9	15.4	16.8	18.9	16.01	2.19
Na/Sr	469	566	525	597	539.18	47.90
Na/Ba	2660	1830	3890		2793.33	846.26
Na/Mn	1630		3140		2385.00	755.00
Na/Cu	1800	915	2850		1855.04	790.87
Na/Mo	340	148	600		362.85	185.25
Na/Fe	401	290			345.41	55.81
Na/Mg	103	68	687		285.95	283.83
Na/Zn	1270	321	484		691.57	414.43
Na/B	92	64	50		68.97	17.60

The errors for the major element ratios are comparable with D-ICP data reported by Rankin & Graham (1988) for fluid inclusions in fluorite from the South Pennine orefield. Eight duplicate runs gave standard deviations of 19.5% of the mean value for Na/K and 6.6% for Na/Li. From the above discussion it is clear that within-sample variability is the major source of uncertainty in the data. Measurement and calibration errors are insignificant in comparison.

Discussion

Na/element ratios determined by the D-ICP method may be used in a variety of ways to constrain fluid composition, to provide evidence of fluid source, and to define evolutionary trends (see Chapter 4).

True concentrations of the major cations in solution may be estimated by combining the Na/element ratios with the NaCl concentration estimated by microthermometry (see section 3.2). The concentration values obtained (Table 3.16) are subject to a degree of uncertainty dependent on the reproducibility of the ratio between duplicate D-ICP runs and the accuracy of the salinity estimate. In general, fluid salinity estimates, in terms of wt% NaCl equivalent, are within 10% of the true NaCl concentration (since NaCl usually makes up >80% by weight of the solute load). The figure of ≈10% error in absolute Na concentration comes from iterative calculations involving the estimated salinity and major element ratios (Na/K, Na/Ca) determined by D-ICP.

Several samples containing fluids with widely varying salinities (V3 veins) are problematic; the salinity estimates are subject to much greater errors, hence the concentration data must be treated very cautiously.

The estimated fluid compositions (Table 3.16) indicate that Na is invariably the dominant cation, followed by K in low or moderate salinity fluids, or Ca in low temperature, high salinity brines ($V4_w$ fluids). These general observations are in agreement with theoretical predictions of the

Table 3.16 Estimated fluid composition (ppm)

SAMPLE	TYPE	WT%	Na	K.	Li	Ca	Sr	Ba	Mn	Fe	Cu	Zn	Ma	B.	Br
J53JR	V1F	2.3	9042.7	1158.2	48.9	322.1	6.7	12.3			79.7	453.0	143.9	466.9	
J53JR	V1F	2.3	9042.7	1197.5	42.6	244.2	9.8	10.2		115.9	71.4	61.4	104.1	278.8	
J53JR	V1F	2.3	9042.7				141.3								
J11PB	V1B	2.8	11008.5	1073.7	42.2	134.3	6.5	6.2		34.7	31.2		112.0	264.9	
J11PB	V1B	2.8	11008.5		34.9	111.6	4.5						81.3	325.3	
J11PB	V1B	2.8	11008.5	1223.2	50.5	234.2	7.9	9.0	6.3	80.9				234.2	
J105GW	V1T	2.6	10222.2	637.8	46.2	233.5	12.5	5.8		19.7				191.3	
J105GW	V1T	2.6	10222.2	574.8	44.1	97.7	8.1	4.9				35.9		199.2	
J105GW	V1T	2.6	10222.2	1076.0	55.6	96.4								185.9	
J06GW	V1T	4	15726.5	738.8	64.1	168.7	14.3	9.2						230.8	71.0
J06GW	V1T	4	15726.5	1557.1	79.4	357.4	24.6	17.8	32.2	614.3				285.9	
J06GW	V1T	4	15726.5				20.6								
J48BR	V2T	5	19658.1	1797.0	58.0	1527.3	41.9	7.4	12.1	49.0				212.7	
J48BR	V2T	5	19658.1	1598.0	64.3	1273.6	34.7	10.7		67.9		61.3	132.6	304.9	
J48BR	V2T	5	19658.1	1449.0	64.1	1166.7	37.5							393.0	78.0
J48BR	V2T	5	19658.1	2272.6	63.0	1985.7	49.8	9.6							
J48BR	V2T	5	19658.1	2005.9	68.5	1040.1	32.9								
J99BR	V2T	3.9	15333.3	1446.5	72.7	134.5	18.9			42.4				225.5	
J99BR	V2T	3.9	15333.3	1345.0	70.7	136.9	18.7							204.4	
J125LB	V2F	2.2	8649.6	586.6	25.6	161.1	13.0	3.1						84.6	
J125LB	V2F	2.2	8649.6	692.0	31.6	163.2	14.6	6.2						95.1	
J125LB	V2F	2.2	8649.6	1218.2	52.7	154.5	11.7	9.7		26.6				135.1	
J40LB	V2E	2.7	10615.4				28.8								20.0
J40LB	V2E	2.7	10615.4				13.0								
D3CZ1	V3C	20	78632.5	7007.6	149.9	4692.8	495.1	75.8	3238.3	2057.5		1321.7			
D3CZ1	V3C	20	78632.5	10081.1	281.8	5957.0	524.2	132.6	1585.3	1747.4		961.3			
D3CZ1	V3C	20	78632.5	5868.0	275.9	4884.0	488.4	115.3	1492.1	1709.4		1262.2			
J145PS	V3G	5	19658.1	2683.1	157.2	1706.8	96.5	18.1	17.0	68.6		81.4		180.7	
J82PS	V3G	13	51111.1	9084.5	198.6	3070.8	607.5	17.0	58.9	103.8		79.6		122.4	360.0
J82PS	V3G	13	51111.1	8888.9	192.9	3730.7		16.4	28.9			66.1			
J82PS	V3G	13	51111.1	8888.9	210.3	4088.9	690.7	22.3	66.6	1064.8		96.3			
J64DR	V3G	10	39316.2	5430.9	265.9	2466.7	435.5	27.0	46.7	135.1		86.4		98.6	
J64DR	V3G	10	39316.2	6552.7	274.9	1716.9	436.8	23.1	10.4	68.3				84.4	
J64DR	V3G	10	39316.2	5698.0	276.9	2172.2	468.1	25.9	13.1	85.8				88.7	
J93TPb	V3G	25	98290.5	20477.2	963.6	12601.3	302.4	253.4	477.1	712.3		472.6		1694.6	
J93TPb	V3G	25	98290.5	11169.3	722.7	12286.3	276.1		376.6	677.9		284.8		1156.4	
J98PC2M	V3S	4.8	18871.8	2029.2	41.1	2859.4	85.8	8.6	57.9	269.6				66.2	120.0
J98PC2M	V3S	4.8	18871.8	2329.9	44.9	3293.5	98.8	12.6	12.3						
J98PC2M	V3S	4.8	18871.8	2273.7	30.9	3282.1	92.1								
JW005	V4J1	11	43247.9	3240.3	145.6	3007.9	142.5	61.2	483.7	64.7	4.9	157.6	11.7	226.4	120.0
JW005	V4J1	11	43247.9	2962.2	133.9	2808.3	138.6	64.4	267.0	67.8		178.7			
JW005	V4J1	11	43247.9	2942.0	139.1	2605.3	136.9	63.7	237.6	45.7		166.3			
J38LB	V4N	3.4	13367.5	1193.5	60.5	1095.7	32.6							150.2	
J38LB	V4N	3.4	13367.5	1086.8	62.5	1104.8	33.1	10.8						137.8	
J78PSa	V4N	0.9	3538.5	262.1	2.2	643.4	14.3								
J78PSa	V4N	0.9	3538.5	278.6	3.8	589.7	14.4								
VL1	V4W	21	82564.1	7122.2	57.2	22053.6	416.7	20.5							
VL1	V4W	21	82564.1	7716.3	112.2	19201.0	458.7								
VL1	V4W	21	82564.1	8974.4	86.9	18764.6	466.5								
J131/6	V4W	20	78632.5	10626.0	63.4	19178.7	370.9	32.9		520.7					
J131/6	V4W	20	78632.5	13105.4	86.0	19178.7	370.9	45.7		778.5					
J98PC2D	V4W	20	78632.5	13497.3	69.1	17604.3	331.0	22.3	42.9	539.1					460.0
J98PC2D	V4W	20	78632.5	9361.0	96.1	17871.0	365.7	34.3	147.0	457.2					
J98PC2D	V4W	20	78632.5	9683.8		19907.0	374.4								
J98PC2D	V4W	20	78632.5	8031.9		22150.0	422.8								

composition of aqueous chloride-rich fluids in equilibrium with common crustal rocks. Such mineral-fluid equilibria calculations indicate the general abundance order Na>K>Ca>Fe>Mg, with variations dependent on mineral assemblage, salinity and temperature (Bischoff *et al.* 1981; Eugster & Gunter 1981; Vidale 1983).

The significance of the aqueous fluid compositions defined in this section in terms of fluid source and fluid evolution processes is discussed fully in Chapter 4.

Alkali geothermometry

The temperature dependence of alkali ratios in geothermal fluids has been used by a number of workers to produce a simple means of estimating fluid reservoir temperatures. These geothermometers are empirical, being derived from a large body of data recorded from a variety of geothermal fields. However, the geothermometers have a sound theoretical basis, since the major mineral phases controlling the alkali composition of aqueous crustal fluids are feldspars and micas which buffer a coexisting fluid to increasingly sodic compositions with decreasing temperature.

An alternative application, emphasised by Giggenbach (1988) is the use of such geothermometers in indicating the degree of equilibration of an aqueous fluid with a given mineral assemblage. In dynamic hydrothermal systems, full fluid-rock equilibrium is rarely attained so that the assumption of equilibrium conditions when estimating fluid temperatures can result in serious errors. Giggenbach (1988) suggested that Na/K ratios in geothermal fluids are relatively slow to adjust to changing P-T conditions on ascent. Thus, a disequilibrium situation arises whereby the Na/K ratio reflects the temperature of the reservoir region rather than the true temperature.

Thus, alkali geothermometry can provide useful constraints, not only with respect to estimation of fluid temperature, but also to assessment of the degree of fluid-rock disequilibrium and temperatures of fluid source regions. For these reasons, five published alkali geothermometers were applied to the bulk D-ICP data presented above. Three of these are based on the Na/K ratios in the fluid (Fournier 1981; Truesdell 1984; Giggenbach 1988) one on the Na/Li ratio (Fouillac & Michard 1981) and one on the Na-K-Ca composition (Fournier & Truesdell 1973). The results for all the samples analysed by D-ICP are presented in Table 3.17. The significance of these fluid temperatures and their use in modelling fluid evolution are considered in Chapter 4.

3.3.2 Neutron activation analysis (NAA)

NAA is a very sensitive technique which is capable of simultaneously determining a wide range of elements present in fluid inclusions (Czamanske *et al.* 1963; Touray 1976; Grappin *et al.* 1979). The technique can be used to analyse bulk samples as well as solutions produced by crushing and leaching of the inclusion fluids. Both methods were used in this study, in order to compare the data obtained and assess the errors involved.

The majority of the samples were prepared in an identical manner to those analysed by D-ICP, as well as those used for bulk volatile and stable isotope analyses (see Appendix B and sections 3.4 and 3.5 respectively). Also analysed were several cleaned doubly-polished wafers, normally used for microthermometry. These were measured to determine whether the method was sensitive enough

Table 3.17 **Fluid equilibration temperatures (°C) obtained from published alkali geothermometers**

SAMPLE	TYPE	T Na-Li	T Na-K (F)	T Na-K (T)	T Na-K-Ca	T Na-K (G)
J53JR	V1	368	239	216	250	253
J53JR	V1	344	242	220	256	256
J11PB	V1	312	215	185	246	230
J11PB	V1	340	226	199	248	241
J105GW	V1	337	180	142	208	197
J105GW	V1	330	172	133	211	190
J105GW	V1	369	221	193	253	236
J06GW	V1	321	160	118	203	178
J06GW	V1	356	216	186	243	232
J48BR	V2	275	209	178	227	225
J48BR	V2	289	200	166	221	216
J48BR	V2	289	192	157	216	209
J48BR	V2	286	230	204	240	244
J48BR	V2	298	219	190	238	234
J125LB	V2	276	186	149	214	203
J125LB	V2	305	199	165	224	215
J125LB	V2	390	248	228	265	261
J99BR	V2	345	212	181	251	228
J99BR	V2	340	206	174	246	222
D3CZ1	V3	224	207	175	244	223
D3CZ1	V3	302	239	216	267	253
D3CZ1	V3	299	193	158	231	210
J145PS	V3	446	245	224	253	258
J82PS	V3	314	272	259	291	283
J82PS	V3	309	270	256	287	281
J82PS	V3	322	270	256	285	281
J64DR	V3	410	246	225	267	259
J64DR	V3	417	265	250	287	277
J64DR	V3	419	251	231	272	264
J93TPb	V3	495	289	283	303	299
J93TPb	V3	428	228	202	255	243
JW005	V4J1	293	193	158	223	210
JW005	V4J1	282	187	150	218	204
JW005	V4J1	287	186	149	219	203
J38LB	V4N	337	207	176	220	223
J38LB	V4N	343	200	166	214	216
J78PSa	V4N	128	193	157	188	209
J78PSa	V4N	169	197	163	192	214
VL1	V4W	135	205	172	225	221
VL1	V4W	190	211	180	232	227
VL1	V4W	167	224	197	243	239
J131/6	V4W	146	244	222	257	258
J131/6	V4W	170	265	250	273	277
J98PC2D	V4W	153	268	254	276	279
J98PC2D	V4W	180	232	207	248	247
J98PC2D	V4W	-	236	211	250	249
J98PC2D	V4W	-	219	190	235	234

T Na-Li from Fouillac & Michard (1981), T Na-K(F) from Fournier (1981), T Na-K(T) from Truesdell (1984), T Na-K-Ca from Fournier & Truesdell (1973) and T Na-K(G) from Giggenbach (1988).

to analyse such small samples. The equipment calibration method is described in Appendix C3 and a summary of the experimental procedure is presented below.

Experimental method

Samples of clean, graded (0.5-2.0mm) quartz chips, ranging from 0.1 to 0.4 g in weight, were accurately weighed into small polythene capsules. Also loaded were a number of cleaned polished wafers, which weighed from 0.04 to 0.1 g. The capsules were then placed in 10 cm tubes, with a small iron disk between each sample, used to measure flux variations in the tube during irradiation. Several universal multi-element standards, in the form of solid powders, and specially prepared standards (Na, Br, Au), produced by evaporation of gravimetrically prepared solutions onto high grade filter paper, were included in the sample tubes.

The tubes were irradiated in a neutron flux of approximately $2x10^{12}cm^{-2}s^{-1}$ for 2 days at the Aldermaston reactor centre, Berkshire. The gamma activity induced in each sample was measured at Southampton for 1-3 hours during the following 2 days, using a shielded gamma detector. Several additional experiments were carried out in which activated inclusion fluids were extracted from quartz chip samples using a conventional crush-leach process (*e.g.* Bottrell *et al.* 1988). The leachates were then analysed in order to compare the data for the leached inclusion fluids with that for the bulk samples.

Elemental concentrations were calculated by comparison of the photopeak areas of the samples with those of the standards, taking into account peak overlaps, flux variations and the decay time between measurement of samples. To facilitate data processing, a FORTRAN 77 computer program was written in collaboration with Dr I.W. Croudace, for automatic determination of elemental abundances. A listing of this program is presented in Appendix C4, together with an example calculation.

Due to the nature of the irradiation and counting procedures, only certain elements could be determined. These elements have activated species with half lives of the same order of magnitude as the period over which the samples were counted, *i.e.* several hours to several days. Activated species with very short half lives (*e.g.* Cl, F) completely decayed before the samples could be measured. Species with much longer half lives produced levels of gamma activity insufficient for accurate determination.

Results

The data obtained for the quartz chip and polished wafer samples are presented in Tables 3.18 and 3.19 respectively. Duplicate splits of four of the quartz chip samples were run in order to assess within-sample variability. From the data it is apparent that Na and Br values are extremely reproducible with most fluctuations falling within the range of analytical error. Furthermore, similar Na/Br ratios are observed in the leachates, implying that these elements are present in the fluid inclusions, as opposed to existing in impurities in the quartz.

In contrast, data for the other elements determined (*e.g.* Au, As, Sb, W) show wide variations between duplicate runs. This evidence, combined with the relatively high levels of elements such as As and Sb and their absence in the leachates, indicates that these components are present as impurities in the quartz rather than in solution in the fluid inclusions.

Table 3.18 Bulk sample compositions (quartz chips) determined by NAA (ppm)

SAMPLE	J06GW	J48BR/1	J48BR/1	J48BR/2	J99BR/1	J40LB/1	J82PS/1	J82PS/1	J82PS/2	J98M/1	J98M/2	JW005	J98D/1	J98D/1	J98D/2
TYPE	V1E	V2T	V2T	V2T	V2T	V2E	V3G	V3G	V3G	V3S	V3S	V4J1	V4W	V4W	V4W
WEIGHT (g)	0.2982	0.2363	0.2363	0.2912	0.3040	0.3283	0.2091	0.2091	0.3118	0.1546	0.2251	0.2611	0.2455	0.2455	0.3491
Na	43(3)	41(4)	33(2)	32(3)	54(3)	95(3)	41(1)	49(4)	40(3)	41(2)	40(3)	61(3)	55(1)	52(4)	57(3)
Cs	0.056(9)	0.30(5)		0.15(4)	0.25(4)	0.25(5)			0.15(5)		0.24(5)	2.6(2)		0.1(1)	0.06(1)
Br	0.22(3)	0.18(4)	0.15(4)	0.13(4)	0.27(3)	0.16(4)	0.25(2)	0.32(3)	0.33(2)	0.24(3)	0.29(3)	0.18(4)	0.29(3)	0.29(4)	0.38(2)
Sc						0.013(8)			0.01(1)			0.01(2)			0.049(3)
Cr							0.61(4)								
Co															0.06(2)
As	0.02(1)	0.049(7)	0.046(7)	0.02(1)	0.03(1)	0.03(1)	0.098(3)	0.12(5)	0.16(3)	3.0(1)	0.52(2)	0.706(2)	0.14(4)	0.15(4)	0.71(2)
Sb	0.23(1)	0.24(2)	0.20(1)	0.21(1)	0.36(1)	0.27(1)	0.13(1)	0.15(2)	0.15(1)	0.42(1)	0.40(1)	0.062(3)	1.8(1)	1.9(1)	2.6(1)
W													0.04(1)		
Au (ppb)	0.36(4)		1.3(4)		0.58(4)	0.39(5)	0.43(4)	0.2(1)	0.07(2)	23(1)	15(1)	0.2(1)	5.2(2)	2.3(3)	0.70(4)
La				0.01(1)											0.014(9)
Yb							0.022(4)	0.029(9)	0.01(1)			0.04(1)			
Sm		0.001(1)		0.01(2)		0.004(4)		0.006(4)	0.002(6)	0.008(1)		0.001(1)			0.002(5)
Tm	0.02(2)	0.03(2)				0.02(2)					0.02(3)				0.04(2)
Gd		0.002(1)		0.018(2)		0.007(4)			0.003(6)			0.002(1)			0.006(5)
Na/Br	190	230	220	250	200	600	160	150	120	170	140	340	190	180	150
WT% NaCl	4.0	5.0	5.0	5.0	3.9	2.7	13	13	13	4.6	4.6	11	20	20	20
Na (ppm)	15700	19700	19700	19700	15300	10600	51100	51100	51100	18100	18100	43200	78600	78600	78600
Br (ppm)	83	86	90	79	77	18	320	340	430	110	130	130	410	440	520
H2O (mg/g)	2.74	2.08	1.68	1.62	3.53	8.96	0.80	0.96	0.78	2.27	2.21	1.41	0.70	0.66	0.73

Figures given in parentheses are analytical errors in last digit (1σ). Figures after slashes in sample numbers refer to aliquot number.

Table 3.19 Bulk sample compositions (polished wafers) determined by NAA (ppm)

SAMPLE	J11PB	J14GW	J47BR	J64DR	J78PS
TYPE	V1B	V2F	?V3S	V3G	V4N
WEIGHT (g)	0.1015	0.0415	0.0429	0.0276	0.0816
Na	72(4)	65(4)	72(4)	30(4)	20(4)
Cs				0.24(5)	0.1(1)
Br	0.21(7)	0.27(6)	0.34(7)	0.17(9)	0.06(1)
Sc					
As		0.098(3)		0.46(5)	2.3(2)
Sb	0.008(4)	0.093(4)	0.27(3)	0.16(4)	1.7(1)
Au (ppb)	1.7(4)	1.1(6)	3.3(4)	5.1(3)	3.6(2)
Yb				0.07(1)	
Sm		0.005(6)			0.003(7)
Tm					
Gd	0.008(8)	0.016(6)	0.01(1)	0.023(7)	0.010(7)
Na/Br	340	240	210	180	340
WT% NaCl	2.8	?	?	10	0.9
Na (ppm)	11000	?	?	39300	3500
Br (ppm)	90	?	?	130	440
H2O (mg/g)	1.82	?	?	2.21	0.66

Figures given in parentheses are analytical errors in last digit (1σ)

Discussion

The actual concentration of Br in solution may be calculated in an identical manner to that applied to the D-ICP data (see section 3.3.1), using the Na/Br weight ratio determined by NAA and the concentration of Na in solution estimated from microthermometry. The amount of Na in each sample is known, so that the total mass of fluid in each sample may also be calculated. These data are presented, along with the Na/Br ratios determined and estimated fluid composition, in Tables 3.18 and 3.19.

An important observation is that the fluid contents of the samples estimated by this method are in close agreement with those determined experimentally (see section 3.4; Table 3.20). Samples *J11PB*, *J48BR* and *J82PS* have experimentally measured H_2O contents 11-37% higher than the NAA/microthermometry estimates, whereas sample *J99BR* is 55% lower. The discrepancies may be explained by errors in the NAA analyses as evidenced by duplicate analyses of the same sample. A single split of *J48BR*, *J82PS* and *J98PC2D* were run twice to provide an indication of reproducibility in the analyses. The data for these runs (*J48BR/1*, *J82PS/1* and *J98D/1* in Table 3.18) indicate that the estimated H_2O content can vary by as much as 20%. Thus, this could account for the at least part of the differences between estimated and measured values. Another contributing factor, which can account for low H_2O estimates from the combined NAA/microthermometry data, is the assumption

that sodium is the sole dissolved cation. Although Na is dominant in the fluids under consideration, the wt% NaCl equivalent estimated from ice melting temperatures may overestimate the Na content by ≈10%. This, in turn, will result in an underestimation of the H_2O content by the same order of magnitude.

As emphasised at the beginning of the chapter, there are unavoidable uncertainties in much of the data obtained by analysing fluid inclusions. However, the internal consistency displayed by the combined NAA and microthermometry data and the experimental H_2O determinations provides a high level of confidence in the results obtained from these techniques, which would not be provided by any one technique in isolation.

3.4 BULK VOLATILE ANALYSIS

A method for the bulk determination of volatile species present in fluid inclusions has been developed by Dr. T.J. Shepherd at the British Geological Survey Isotope Laboratories, London. Using this technique, the proportions of H_2O, CO_2, CH_4 and N_2 present in a sample may be determined. A qualitative indication of the presence of other gas species such as C_2H_6, H_2, Ar and CO may also be obtained.

The samples analysed were splits of the same material used in the D-ICP and NAA solute determinations. Details of the sample preparation technique and experimental calibration procedure are presented in Appendices B and C respectively. The method is summarised below.

Experimental method

The automated procedure involves the release of inclusion fluids (either by crushing or, as in this case, decrepitation) into a high vacuum line and monitoring the evolved gases by mass spectrometry. Partial pressures of H_2O, CO_2 and non-condensible (NC) gases (at -196°C) are measured after cryogenic separation and subsequently recalculated to mole fractions. N_2, CH_4 and minor components such as C_2H_6, H_2, Ar and CO can also be determined from the NC gas mass spectrum.

Results

Data obtained from the analysis of 14 quartz chip samples are presented in Table 3.20. In addition, the molar ratios for the major volatile species have been calculated and are included in Table 3.20. For samples containing essentially one fluid inclusion population, the bulk fluid compositions determined (in terms of mole fractions of H_2O, CO_2 and N_2+CH_4) are comparable with those estimated from microthermometry (see section 3.2). For samples containing a variety of inclusion types (*e.g.* V3 veins; see section 3.2.4), the data are more difficult to interpret, although some general observations may be made.

Analytical errors in the data are small (≈1%) and insignificant compared with both within-sample variability and interpretative problems due to analysis of mixed fluid inclusion populations.

Table 3.20 Bulk fluid inclusion volatile composition (mole fraction)

SAMPLE	TYPE	H2O	CO2	N2	CH4	N.C.	H2O/CO2	H2O/N2	H2O/CH4	CO2/N2	CO2/CH4	N2/CH4	YIELD
J53JR	V1F	0.9876	0.0093	0.0008	0.0012	0.0011	106.2	1234.5	823.0	11.6	7.8	0.7	0.93
J11PB	V1B	0.9862	0.0116	0.0014	0.0004	0.0004	85.0	704.4	2465.5	8.3	29.0	3.5	2.05
J48BR	V2T	0.9815	0.0167	0.0012	0.0003	0.0003	58.8	817.9	3271.7	13.9	55.7	4.0	2.22
D2BR2	V2T	0.9671	0.0301	0.0022	0.0003	0.0004	32.1	439.6	3223.7	13.7	100.3	7.3	1.76
J99BR	V2T	0.9569	0.0400	0.0023	0.0004	0.0005	23.9	416.0	2392.3	17.4	100.0	5.8	1.59
J125LB	V2F	0.9060	0.0877	0.0047	0.0010	0.0004	10.3	192.8	906.0	18.7	87.7	4.7	1.21
D3CZ1	V3C	0.9380	0.0535	0.0035	0.0042	0.0008	17.5	268.0	223.3	15.3	12.7	0.8	0.95
J145PS	V3G	0.7825	0.2041	0.0119	0.0007	0.0007	3.8	65.8	1117.9	17.2	291.6	17.0	0.89
J82PS	V3G	0.7931	0.1982	0.0069	0.0012	0.0006	4.0	114.9	660.9	28.7	165.2	5.8	0.98
J64DR	V3G	0.7217	0.2591	0.0168	0.0013	0.0012	2.8	43.0	555.2	15.4	199.3	12.9	0.56
J118TC	V4J2	0.9978	0.0015	0.0002	0.0000	0.0004	665.2	4989.0	-	7.5	-	-	3.51
J38LB	V4N	0.9876	0.0111	0.0004	0.0003	0.0006	89.0	2469.0	3292.0	27.8	37.0	1.3	2.43
J78PS	V4N	0.9977	0.0023	0.0000	0.0000	0.0000	433.8	-	-	-	-	-	0.73
J131/6	V4W	0.9975	0.0017	0.0000	0.0000	0.0008	586.8	-	-	-	-	-	0.55

N.C. = Non-condensible fraction at -196°C. Yield = H2O released (mg/g sample)

Discussion

The two V1 samples analysed contain essentially only one fluid inclusion population (see section 3.2.2), so that a bulk analysis is representative of the dominant inclusion type present. The data confirm that H_2O is the major volatile component of the fluid with less than 2 mole percent additional volatiles, predominantly CO_2. These levels are such that the minor components would not be detectable by microthermometry.

The V2 data display a wider range in volatile abundances than observed for V1 fluids. H_2O is by far the most abundant component (as indicated by microthermometry), although significant quantities of CO_2 are present (up to 8.77 mole%). The increase in the proportion of CO_2 may be correlated with the occurrence of ?late, low density, CO_2-rich and H_2O- rich CO_2-bearing inclusions (V2 types 3 and 2 respectively; Table 3.3), observed both optically and during thermometric analysis (see section 3.2.3). The fact that these inclusions are only rarely observed in samples *J48BR* and *D2BR2* suggests that the dominant V2 fluid, represented by V2 type 1 inclusions, contains <3mole% CO_2, *i.e.* a slightly higher CO_2 component than the V1 fluids. The remaining important gases (N_2 and CH_4) are both more abundant in the more CO_2-rich samples. This correlation indicates that these components are also enriched in the relatively CO_2-rich fluid inclusions present in the samples.

The V3 volatile data clearly reflect the abundance of CO_2-rich fluid inclusions at this stage. The bulk compositions are not as useful for these samples because a variety of inclusion types are present (see section 3.2.4). However, a number of notable features are still apparent.

Sample *D3CZ1* is distinct in that it contains a much higher proportion of H_2O-rich inclusions and has significantly higher H_2O/CO_2 and H_2O/N_2 ratios than the other V3 samples. However, despite the abundance of H_2O, the H_2O/CH_4 and consequently CO_2/CH_4 and N_2/CH_4 ratios are much lower (Table 3.20). The relative abundance of methane in this sample is likely to be due, at least in part, to the dominance of V3 type 4 (low density vapour) fluid inclusions in the sample, and the probable origin of this fluid by unmixing (see 4.4.1). An alternative control of the $H_2O/CO_2/CH_4(/N_2)$ ratios is the oxygen fugacity (fO_2) of the fluid. This is discussed further in section 4.4.7.

Assuming an unmixing origin for the range of fluid inclusions observed in V3 samples (see 4.4.1), and that there is no preferential trapping of a particular fluid type during vein growth, the bulk volatile analyses should reflect the composition of the parent fluid. Evidence that these assumptions are valid comes indirectly from the consistency of the data from the three $V3_G$ samples, which contain differing proportions of the six V3 inclusion types. Experimental data (Gehrig 1980; Bowers & Helgeson 1983a) support these assertions, since the composition of a fluid unmixing at *c.* 400°C to produce the observed immiscible fluid pairs must lie in the range 10-40 mole% CO_2 at the appropriate P-T conditions (see 4.4.1).

It is interesting to note that although the proportions of CO_2 and N_2 are significantly higher in the $V3_G$ fluids, the CO_2/N_2 ratios are little different to those for the V1 and V2 fluids. The constancy of the CO_2/N_2 ratio in fluids from a particular province is a common phenomenon (*e.g.* Shepherd *et al.* 1985). The ratio is controlled by a linked redox equilibrium between C-O-H species and N_2 in the fluid and carbon-bearing species, Fe oxides and NH_4^+ (mainly contained in micas) in the wallrocks (Ohmoto & Kerrick 1977; Crawford 1981a; Holloway 1981, 1984). Calculations in the C-O-H-S-N system (Ferry & Baumgartner 1987) indicate that the CO_2/N_2 ratio is almost constant over the

temperature range 350-500°C for a fluid at 3.5 kbar in equilibrium with pyrite-pyrrhotite-graphite-biotite-K-feldspar. The data reported above suggest that such a relationship may exist over a wide range of crustal conditions.

$V4_J$, $V4_N$ and $V4_W$ samples are dominated by H_2O, containing ≤1 mole% CO_2. The other volatile species are present in very low quantities or are absent. These data are in agreement with the microthermometric studies which failed to detect the presence of CO_2 (see sections 3.2.6 to 3.2.8). These fluids contain lower proportions of volatiles other than H_2O than any of the other fluids investigated. Only sample *J38LB* provided CO_2/CH_4 and N_2/CH_4 ratios, which are both relatively low (*i.e.* CH_4 is relatively high). This has implications for the fO_2 state of the fluids at this stage.

3.5 STABLE ISOTOPE ANALYSIS

The stable isotopic composition of fluids can provide important evidence regarding fluid source, fluid temperature and evolutionary processes such as fluid-rock interaction and fluid mixing. As these parameters are of particular interest in the present study, and stable isotopic data from southwest England are scarce, this piece of work was considered especially important.

Analyses of purified quartz chip samples were carried out at the Scottish Universities' Research and Reactor Centre (SURRC), East Kilbride, by Dr. A. Fallick and Dr G. Jenkin. The relative abundance of ^{18}O with respect to ^{16}O was determined for quartz and CO_2 released during decrepitation of the fluid inclusions. The data were then recalculated to $\delta^{18}O$ values (in parts per thousand) reflecting the relative enrichment or depletion of the heavier isotope with respect to the international standard SMOW (Standard Mean Ocean Water). $\delta^{18}O$ for the inclusion fluids cannot be determined directly since they have undergone isotopic re-equilibration with the quartz host subsequent to trapping. However, knowing the isotopic composition of the quartz, the appropriate quartz-water fractionation factor (Matsuhisa *et al.* 1979), and the fluid temperature, the $\delta^{18}O$ of the fluid responsible for precipitating the quartz may be estimated (assuming no significant isotopic exchange has occurred in the bulk quartz sample subsequent to vein formation).

The relative abundance of the heavy isotope of hydrogen (^3H or D) was determined for H_2O released by decrepitation. Since hydrogen is only present in very small amounts within the quartz lattice, no significant isotopic exchange will have occurred subsequent to fluid trapping. Thus the δD values determined, which reflect the relative enrichment or depletion of the heavy isotope with respect to SMOW, may be taken to represent the composition of the fluid when trapped.

For samples evolving sufficient CO_2 during decrepitation, the relative abundance of ^{13}C with respect to the abundant isotope ^{12}C was measured and subsequently recalculated to a $\delta^{13}C$ value. This reflects the relative enrichment or depletion of the heavy isotope with respect to the international PDB standard.

Experimental method

The experimental method is summarised below. The samples analysed were duplicate splits of purified quartz chips, as used for the bulk fluid inclusion analytical techniques discussed above (see

Appendix B).

The analytical procedure for the determination of $\delta^{18}O$(quartz) involves the liberation of oxygen from approximately 50 mg samples of clean quartz by reaction with ClF_3 in a nickel bomb at 600°C. This is subsequently converted to CO_2 by reaction with a hot carbon rod. The oxygen isotope abundances in the CO_2 produced are measured by mass spectrometer and the data are then recalculated to $\delta^{18}O$ values. Direct $\delta D(H_2O)$, $\delta^{13}C(CO_2)$ and $\delta^{18}O(CO_2)$ determinations on inclusion fluids are carried out by decrepitating the samples under vacuum at 1000°C and analysing the isotopic compositions of the gases released.

Results

Data for the 18 samples analysed are presented in Table 3.21. The "O YIELD" column indicates the mole percent oxygen released from each quartz sample, relative to the theoretical oxygen content and calculated on the basis of the sample mass. The closer the yield to 100%, the more reliable the $\delta^{18}O$ determination. Where low yields were obtained (<85%), duplicate runs were carried out to provide supporting data.

Fluid $\delta^{18}O$ values are calculated from experimentally determined, temperature-dependent fractionation factors. The data used in the present study is that of Matsuhisa *et al.* (1979). Their equation relates $\delta^{18}O$(quartz) to $\delta^{18}O$(water) by:

$$10^3 \ln\alpha = (3.34 \times 10^6/T^2) - 3.31 \qquad \text{...(3.1)}$$

where α is the fractionation factor, T is in Kelvins and $10^3 \ln\alpha = \delta^{18}O(\text{quartz}) - \delta^{18}O(H_2O)$.

Fluid temperature estimates ("TEMP" column in Table 3.21) are based on a variety of temperature constraints, including mineral assemblages and vitrinite reflectance (V1 fluids), alkali geothermometry (V1, V2, V3, V4 fluids) and fluid inclusion homogenisation temperatures (V1, V2, V3, V4 fluids). Details of the methods of temperature estimation are discussed in sections 3.3.1, 4.2.1, 4.3.1, 4.4.1 and 4.6.1.

Table 3.21 also displays bulk volatile data, calculated from the relative proportions of volatile species released during sample decrepitation. These data may be directly compared with those obtained by bulk volatile analyses carried out on the B.G.S. line (see section 3.4; Table 3.20). The non-condensible fraction determined during stable isotope analyses contains CH_4 and N_2 amongst other gases; these were not determined individually. At first sight, the volatile data determined during the stable isotopic analyses appear to diverge considerably from that obtained on the purpose-built line (compare H_2O and CO_2 mole fractions in Tables 3.20 and 3.21). However, the differences are primarily the result of a larger NC fraction in the stable isotope analyses; the H_2O/CO_2 ratios determined are very similar. The larger NC fraction determined during stable isotope analyses is almost certainly due to the fact that samples were heated to higher temperatures (1000°C rather than 600°C). A duplicate analysis of *J99BR*, which was heated to temperatures in excess of 1000°C for over 1 hour, resulted in a 200% increase in the mole fraction of NC gases present. This indicates that there are unknown, probably solid, impurities in the quartz which break down at high temperatures to evolve NC gases such as N_2, CH_4 and probably higher hydrocarbons as well.

Table 3.21 Stable isotopic and bulk volatile data

SAMPLE	TYPE	QUARTZ d18O	O YIELD %	H2O TEMP	H2O d18O	H2O dD	H2O YIELD µMol	CO2 d13C	CO2 d18O	CO2 YIELD µMol	MOLE FRACTIONS H2O	MOLE FRACTIONS CO2	MOLE FRACTIONS N.C.
J53JR	V1F	18.2	93.9	350	12.9	-18.3	104.2			0.81	0.946	0.007	0.047
J11PB	V1B	17.8	92.0	320	11.6	-10.4	128.3			1.68	0.928	0.012	0.06
J138GW	V1B	17.3	94.1	300	10.4	-10.3	88.99	-14.1	18.9	5.29	0.878	0.052	0.07
J48BR	V2T	17.7	94.4	290	10.5	-15.1	134.6	-7.1	24.5	2.74	0.966	0.02	0.014
D2BR2	V2T	16.9	91.8	290	9.7	-26.2	106.79	-6.4	23.5	3.43	0.925	0.03	0.045
J99BR	V2T	17.2	95.1	300	10.3	-27.6	74.16	-10.5	26.3	3.06	0.915	0.038	0.047
J125LB	V2F	16	98.1	300	9.1	-12.5	71.57			5	0.867	0.061	0.072
D2bPC	V2E	16.4		285	9.0	-24							
D3CZ1	V3C	16.7	88.6	300	9.8	-22.9	42.67			2	0.784	0.037	0.18
J145PS	V3G	16	92.4	320	9.8	-36	50.06						
J82PS	V3G	15.2	100.3	340	9.6	-31.7	39.58			12	0.555	0.168	0.277
J64DR	V3G	14.3		340	8.7	-42		-11.9			0.543	0.251	0.206
J93TP	V3G	15.6	85.3	320	9.4	-43.2	23.54			0.41	0.781	0.014	0.205
J118TC	V4J2	15.2	88.3	250	6.3	-27.9	128.67	-13.9	31	0.97	0.973	0.007	0.02
J38LB	V4N	16.2		200	4.6	-20.6	95.11	-3.9	25.3	2	0.958	0.02	0.022
J78PS	V4N	12.6	87.5	200	1.0	-25.1	42.44				0.913		0.087
VL1	V4W	18	86.3	150	2.6	-54.7	21.55	-19.5	?70.7	0.42	0.849	0.017	0.134
J131/6	V4W	19.8	94.8	150	4.4	-52.1	29.86				0.871		0.129

Oxygen yield as % of theoretical yield from quartz. d18O(H2O) calculated from estimated fluid temperature and quartz-water fractionation factor (Matsuhisa et al., 1979). H2O, CO2 yields as µMol released during decrepitation. N.C.= non-candensible gases at -196°C. All d values are in parts per thousand. See text for further details.

Discussion

The calculated $\delta^{18}O(H_2O)$ values and corresponding measured $\delta D(H_2O)$ values for the fluids studied are plotted on a $\delta^{18}O$-δD diagram (Fig. 3.61). The data for each vein group (*i.e.* V1, V2 etc.) plot in discrete clusters, showing that each of the main fluid types displays distinct compositional characteristics.

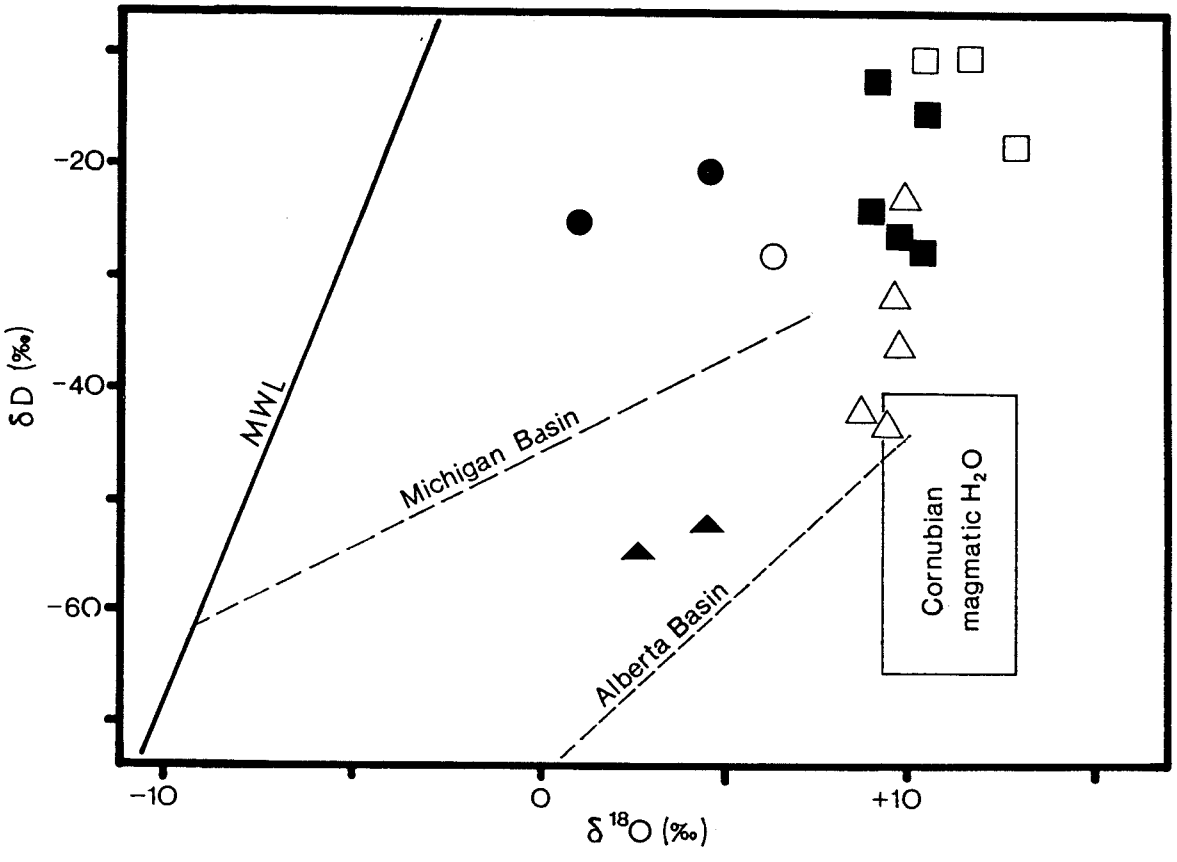

Figure 3.61 Plot of δD *vs.* $\delta^{18}O$ for Hercynian crustal fluids of south Cornwall. Open squares = V1 fluids; filled squares = V2 fluids; open triangles = V3 fluids; open circles = $V4_{J2}$; filled circles = $V4_N$; filled triangles = $V4_W$. MWL = meteoric water line. Trends for modern oilfield brines are also shown.

V1 and V2 fluids are closely related, indicating a possible continuum in fluid isotopic composition, in agreement with the relationship suggested by both solute and volatile data (see sections 3.3, 3.4). V3 fluids range in isotopic composition from fluids comparable with Cornubian magmatic waters (Sheppard 1977; Fig. 3.61) to isotopic compositions indistinguishable from V2 fluids. Possible explanations for this trend of variable δD with constant $\delta^{18}O$ are discussed in section 4.4.3.

The V4 data are dependent on vein type, with the $V4_{J2}$ and $V4_N$ samples displaying decreasing $\delta^{18}O$ at approximately constant δD, consistent with an increasing meteoric water component. This strongly supports the compositional evidence, which indicates that $V4_N$ fluids are very dilute with major solute proportions comparable with published data for meteoric waters (Fig. 4.12). A more detailed discussion is presented in section 4.5.

$V4_W$ fluids are apparently very depleted in deuterium whilst relatively enriched in ^{18}O. The low δD values may be the result of a fractionation effect during measurement of very small samples (G. Jenkin, pers. comm. 1989). A plot of δD vs. H_2O yield (Fig. 3.62) shows that at yields of less

than 35 μMol, δD values become increasingly negative. Both $V4_W$ samples analysed, due to the low abundance of fluid inclusions present, fall in this low H_2O yield range suggesting that the δD values are anomalously negative. However, the hydrogen isotopic compositions are consistent with the origin of the $V4_W$ fluids as basinal brines (see 4.6.2, 4.6.3), which commonly have H_2O compositions depleted in deuterium (Sheppard 1986; Fig. 3.61). In summary, the low δD values for these two samples may not be due to a measurement effect; the correlation between low yields and low δD may be coincidental. Nevertheless, the possible error in these values must be borne in mind when interpreting the data.

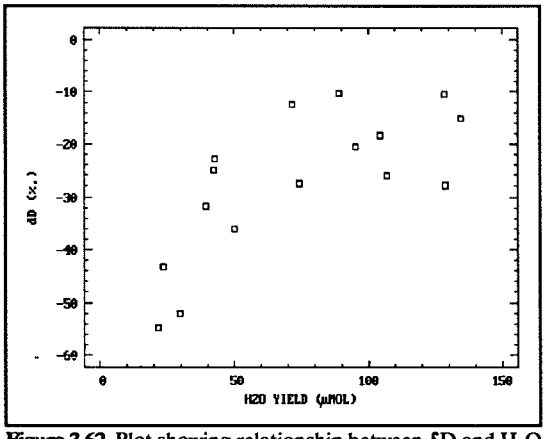

Figure 3.62 Plot showing relationship between δD and H_2O yield, illustating possible fractionation at small sample size.

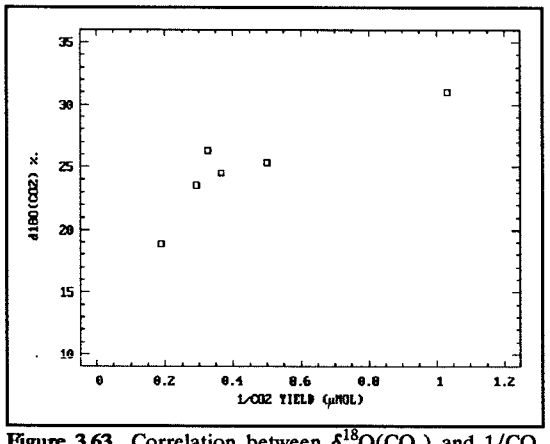

Figure 3.63 Correlation between $\delta^{18}O(CO_2)$ and $1/CO_2$ yield.

Two lines of evidence indicate that at least some of the $\delta^{18}O(CO_2)$ values determined are not realistic. If the $\delta^{18}O(CO_2)$ data is plotted as a function of $1/(CO_2$ yield), a trend of increasing $\delta^{18}O(CO_2)$ with decreasing yield is observed (Fig. 3.63). The linearity suggests that even the lowest $\delta^{18}O(CO_2)$ values may have had their $\delta^{18}O$ increased by mixing with a small amount of gas with an apparent high $\delta^{18}O$. NO_2 could be responsible for such an increase by contributing to the mass 46 peak, which is the peak measured to determine $\delta^{18}O$. However, there is no positive correlation between the N_2 content of the fluid (Table 3.20) and the $\delta^{18}O(CO_2)$ value, so that NO_2 contamination (at least via oxidation of N_2 during high temperature extraction) is unlikely. A kinetic effect during the extraction process, dependent on sample size is an alternative explanation (T. Fallick, pers. comm., 1989). The data for samples yielding more than 2 μMol CO_2 plot in a cluster rather than a linear array suggesting that these values are more likely to be reliable.

The possibility of an artificial increase in the height of the mass 46 peak in the mass spectrum, resulting in anomalously high $\delta^{18}O(CO_2)$ values (at least for *J118TC* and *VL1*), has important implications for the corresponding $\delta^{13}C(CO_2)$ data. These values will be decreased relative to the true value as a result of the overestimated mass 46 peak (G. Jenkin, pers. comm. 1989). However, the effect will be relatively small (at most decreasing $\delta^{13}C$ by 2‰), so that interpretation of the data is not seriously affected. Furthermore, a plot of $\delta^{13}C(CO_2)$ *vs.* $1/(CO_2$ yield) does not display a linear trend (Fig. 3.64), suggesting that the spread in $\delta^{13}C$ is due to a primary variation between samples rather than an artefact resulting from variable (small) sample size.

The $\delta^{13}C(CO_2)$ values for V1 and V2 fluids are relatively depleted in ^{13}C compared with most terrestrial carbon reservoirs. Dissolved carbonate (mostly as HCO_3^-) in the oceans has $\delta^{13}C$ values close to 0‰, with modern and Phanerozoic marine limestones having compositions in equilibrium

with this, ranging from -1 to +2‰ (Veizer *et al.* 1980; Ohmoto 1986). Estimates of the isotopic composition of mantle carbon are predominantly in the range -5±2‰, although values as disparate as -35‰ and -4.7‰ have been determined (Deines & Gold 1973; Deines 1980), suggesting that significant local heterogeneities may exist. Igneous rocks contain carbon which generally has $\delta^{13}C$ values between -5 and -8‰ (Taylor *et al.* 1967; Deines 1970). CO_2 is actually enriched slightly in ^{13}C relative to its source magma, with $\delta^{13}C$ ranging from -9 to +1‰. Only organic carbon has lower $\delta^{13}C$ values than those determined for V1 and V2 fluids, generally ranging from -10 to -30‰. CO_2 produced by thermal decomposition of this organic matter is likely to have a similar isotopic composition to the parent material (Ohmoto & Rye 1979), whereas any CH_4 produced may have very depleted $\delta^{13}C$ compositions, typically -55 to -35‰. This suggests that organic carbon (probably mainly present in kerogens) is a viable source of the CO_2 in both V1 and V2 fluids. Fractionation during decarbonation reactions does not explain the low $\delta^{13}C$ values, since the CO_2 evolved will be enriched in the heavy isotope relative to the rock (Valley 1986).

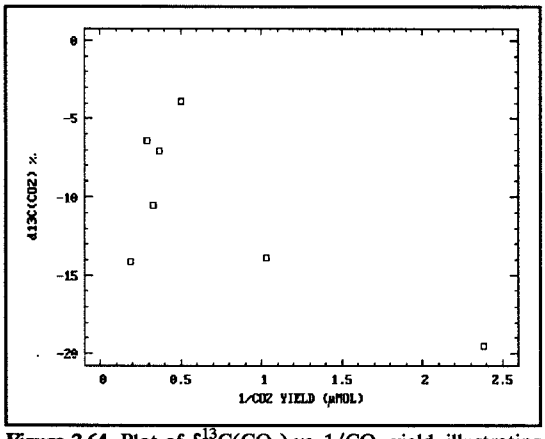

Figure 3.64 Plot of $\delta^{13}C(CO_2)$ *vs.* $1/CO_2$ yield, illustrating lack of correlation.

The single $\delta^{13}C$ value on a V3 sample (*J64DR*) is important as it indicates that the CO_2 present was not solely derived from a magmatic source. Isotopic re-equilibration of magmatic CO_2, either by assimilation of low $\delta^{13}C$ material (*e.g.* organic-rich metasediments) or by re-equilibration of magmatic fluid within the contact aureole can explain the low $\delta^{13}C$ value. Alternatively, the light isotopic composition may be the result of mixing between CO_2 bearing a magmatic signature and CO_2 derived in the contact aureole from oxidation of ^{13}C-depleted organic carbon. These possibilities are discussed in relation to other compositional parameters in section 4.4.3.

3.6 X-RAY DIFFRACTION STUDY

An exploratory XRD study of wallrock alteration was carried out in order to provide additional evidence concerning fluid composition and temperature. The data obtained also allow constraints to be placed on the nature and extent of fluid-rock interaction, as well as on possible fluid evolution paths.

Experimental method

Host rocks were sampled in the field at distances of up to several metres away from "type" quartz veins. Sampling at greater distances was not possible because of the presence of other veins. Square prisms 1 cm^2 in diameter were cut from the samples in the laboratory and slices taken from these at regular intervals to provide a representative transect into the wallrocks. Powders were prepared by crushing using a steel roller and fine grinding in a pestle and mortar.

Bulk rock analyses were carried out by spreading a thin layer of powder onto a glass slide and measuring backscattered X-rays in a conventional automated X-ray diffractometer, at beam incidence angles of 2-60°. Peaks in the resulting spectra were identified using standard reference tables. The majority of the major spectral lines could be related to common minerals, although in some cases mineral identification was only tentative.

The clay fraction (<2μm grain size) was also analysed in six sample profiles to determine the identity and semi-quantitative proportions of the clay minerals present. Clay fractions were separated from the powders by flotation and centrifuging and were then smeared onto glass slides. Duplicate slides were air dried, dried at 375°C (which resulted in conversion of any smectite present to illite) and glycolated (in order to confirm the presence of smectite). Each slide was analysed at beam angles of 2-30° and the major peaks identified. Semi-quantitative determination of the proportions of each phase involved digital measurement of the major peak area for each clay, empirically correcting for intensity variations between phases (*i.e.* divide by 2 for chlorite, 2 for kaolinite, 3 for smectite) and peak overlaps (kaolinite/chlorite), and normalising to 100%. The values obtained are not a true percentage in terms of volumetric or weight proportions; they are relative, reflecting variations in the proportions of each phase in different samples.

Results

The bulk mineralogy and composition of the clay mineral fractions in the wallrock alteration profiles are presented in Tables 3.22 and 3.23 respectively. The bulk mineralogical determinations are purely qualitative and only indicate the presence or absence of the common phases. "Absence" in this context means where the spectral lines for a mineral fall below background; this usually occurs at approximately 5 wt% of the mineral in the bulk sample.

V1, V2, and V3 veins

Syn-orogenic veins (V1, V2, V3) display no significant changes in bulk rock mineralogy in the wallrock profiles, and variations in the proportions of the clays present show no systematic variations. The most useful result of these analyses was confirmation of the bulk rock mineralogy as determined by transmitted light microscopy (see 1.3.4) and identification of the fine-grained phyllosilicate minerals present. The fact that K-feldspar was not detected and albite was only observed in three of the four V1/V2 sample profiles (see Table 3.22) has important implications for fluid-rock equilibria and the use of alkali geothermometry (see 4.2.1, 4.2.2).

The presence of kaolinite and/or smectite in the clay separates (Table 3.23), which are unlikely to be stable during either D1 or D2 (Figs. 4.3, 4.7; see 4.2.2), are interpreted as the result of recent weathering. The possible problem of weathering precludes a detailed discussion of variations in the proportions of the clay minerals in relation to wallrock alteration.

V4 veins

Sample *J118TC* (a $V4_{J2}$ vein) displays clear evidence of extensive fluid-rock interaction in hand specimen, with zones of haematitic and goethitic alteration. Quartz, K-mica and chlorite (ripidolite) are the major minerals occurring throughout the alteration profile. The presence of smectite and kaolinite, displaying systematic variations away from the vein contact, indicates that argillic alteration

Table 3.22 **Minerals identified in wallrock alteration profiles**

PROFILE	TYPE	DISTANCE (mm)	QZ	AB	PAR	KSP	MUSC	RIP	APH	ANK	SID	GN	CPY
J53JR	V1F	0-2	▪	▪			▪	▪			▪		
Grey-blue sideritic greywacke		3-7	▪	▪			▪	▪			▪		
		8-12	▪	▪			▪	▪		▪	▪		
		13-22	▪	▪			▪	▪		▪	▪		
		23-28	▪	▪			▪	▪			▪		
D2BR	V2T	0-5	▪	▪			▪	▪		▪			
Grey-blue ankeritic greywacke		15-20	▪	▪			▪	▪		▪			
		27-32	▪	▪			▪	▪		▪			
		120-125	▪	▪			▪	▪		▪			
D2aPC	V2E	0-2	▪				▪	▪					
Grey-green sandstone		2-5	▪				▪	▪					
		8-11	▪				▪	▪					
		15-20	▪				▪	▪					
		100-105	▪				▪	▪					
D2bPC	V2E	0-5	▪				▪	▪					
Buff sandstone		8-12	▪				▪	▪					
		12-16	▪				▪	▪					
		100-105	▪	▪			▪	▪					
D3CZ	V3C	0-5				▪	▪		▪				
Dark grey slate		15-20				▪	▪		▪				
		30-40				▪	▪		▪				
		100-105				▪	▪		▪				
VG2	V3S	0-3	▪	▪			▪	▪					
Green slate		7-13	▪	▪			▪	▪					
		14-22	▪	▪			▪	▪					
		24-35	▪	▪			▪	▪					
		66-74	▪	▪			▪	▪					
J118TC	V4J2	0-4	▪				▪	▪					
Grey spotted slate		9-11	▪				▪	▪					
		19-22	▪				▪	▪					
		25-30	▪				▪	▪					
		33-37	▪				▪	▪					
		95-100	▪				▪	▪					
J19GWa	V4N	0-2	▪	▪			▪						
Grey-green sandstone		3-7	▪	▪			▪	▪			▪		
		8-12	▪	▪			▪	▪			▪		
		13-22	▪	▪			▪	▪					
		23-28	▪	▪			▪	▪					
J98PC2D	V4W	0-1	▪				▪				▪	▪	▪
Dark grey slate		3-8	▪				▪	▪			▪	▪	
		10-16	▪				▪	▪			▪	▪	
		16-20	▪	▪			▪	▪					
		2000	▪	▪			▪	▪					
PCC	V4W	0-5	▪			▪		▪					
Metabasite		5-10	▪			▪		▪					
		15-20	▪		▪	▪		▪					
		30-35	▪			▪		▪			▪		
		60-65	▪	▪	▪	▪	▪	▪			▪		
		125-130	▪	▪	▪	▪	▪	▪			▪		

Mineral abbreviations: QZ - quartz, AB - albite, PAR - Na mica, KSP - K-feldspar, MUSC - K-mica, RIP - ripidolite, APH - aphrosiderite, ANK - ankerite, SID - siderite, GN - galena, CPY - chalcopyrite.

Table 3.23 **Composition of clay mineral fraction in wallrock alteration profiles (%)**

PROFILE	TYPE	DISTANCE (mm)	ILLITE	CHLORITE	SMECTITE	KAOLINITE	PARAGONITE	TALC
D2BR	V2T	0-5	50	42	8	-	-	-
		15-20	55	37	8	-	-	-
Grey-blue ankeritic		27-32	53	41	6	-	-	-
greywacke		120-125	63	29	8	-	-	-
D2aPC	V2E	0-2	73	22	-	5	-	-
		2-5	61	29	-	10	-	-
Grey-green		8-11	64	25	-	11	-	-
sandstone		15-20	54	29	-	17	-	-
		100-105	43	30	-	27	-	-
D2bPC	V2E	0-5	50	32	1	17	-	-
		8-12	70	18	-	12	-	-
Buff		12-16	80	14	-	6	-	-
sandstone		100-105	48	29	-	23	-	-
D3CZ	V3C	0-5	81	19	-	-	-	-
		15-20	79	21	-	-	-	-
Dark grey		30-40	74	26	-	-	-	-
slate		100-105	77	23	-	-	-	-
J118TC	V4J2	0-4	11	84	5	-	-	-
		9-11	34	18	40	8	-	-
		19-22	31	18	33	18	-	-
Grey		25-30	29	20	19	33	-	-
spotted slate		33-37	32	22	26	19	-	-
		95-100	35	31	23	11	-	-
PCC	V4W	0-5	12	88	-	-	-	-
		5-10	12	83	-	-	5	-
		15-20	7	88	-	-	5	-
Metabasite		30-35	10	71	-	-	8	10
		60-65	8	71	7	-	4	10
		125-130	10	79	11	-	-	-

of slates was dominant during $V4_{J2}$ fluid flow.

Profile *PCC*, adjacent to a greenstone-hosted, $V4_W$ vein, illustrates that quartz, K-feldspar and chlorite (ripidolite) occur in the metabasites in detectable amounts, irrespective of vein proximity (Table 3.22). The presence of four other major minerals only at distances in excess of 15mm from the vein suggests that significant wallrock alteration (and hence initial fluid-rock disequilibrium) occurred in proximity to $V4_W$ veins, at least in greenstone host rock. This is not surprising, considering the acidic nature of $V4_W$ brines (see 4.6.5). However, there is also evidence of preferential weathering at the vein-host rock interface. The rock displays fine pitting in this zone, attributable to supergene removal of carbonate.

3.7 SUMMARY

In this chapter, data have been presented which constrain the P-V-T-X characteristics of fluids mobilised at different stages of the Hercynian orogeny in south Cornwall. The different experimental techniques used to obtain these data have been outlined and the limitations of the information obtained are discussed. In the subsequent chapters, this data is used to model fluid evolution processes, with particular emphasis on the transport and deposition of ore-forming elements.

Seven main stages of fluid mobilisation have been identified which may be distinct both temporally and spatially:

1. V1 fluids - mobilised during peak regional metamorphism, syn-D1, at relatively deep crustal levels;

2. V2 fluids - mobilised during later stages of crustal compression (syn-D2) and at higher crustal levels;

3. V3 fluids - mobilised in the contact aureole, during emplacement of the Cornubian batholith and/or Tregonning granite stock;

4. $V4_P$ fluids - mobilised in the contact zone of the Tregonning granite stock during or soon after emplacement;

5. $V4_J$ fluids - mobilised in joints in the metasedimentary carapace of the Cornubian batholith, syn- and post-emplacement;

6. $V4_N$ fluids - mobilised in normal faults, post-granite emplacement;

7. $V4_W$ fluids - mobilised in wrench faults, post-granite emplacement.

Each group of fluids display distinct solute, volatile and isotopic characteristics, which relate to the fluid source, the intensive controls of fluid composition (P, T, fO_2 *etc.*) and the nature of fluid-rock interaction. These features are considered in detail in Chapter 4.

CHAPTER 4: FLUID EVOLUTION

The purpose of this chapter is to constrain a number of fluid parameters, based on the data reported in Chapter 3, and use these to illustrate changes in the nature of fluids flowing through the crustal slab of south Cornwall during the Hercynian orogeny. The data provide evidence regarding the source of the fluids, controls of fluid P-T-X evolution, and possible implications for metal transport and deposition.

4.1 INTRODUCTION

4.1.1 Fluid source

Two classes of fluid source are considered:

(1) Internal fluids, defined as fluids derived locally, from the rocks in the immediate vicinity of the veins studied;

(2) External fluids, defined as fluids derived from outside the immediate rock system.

Type 1 fluids could include pore waters expelled from sediments due to burial and compaction, fluids released during diagenetic devolatilisation reactions and fluids evolved during prograde metamorphic devolatilisation reactions. The important property common to all these fluid types is that they are internally buffered (Greenwood 1975), *i.e.* they are in equilibrium with their source rocks at the prevailing conditions of temperature and pressure.

Prograde metamorphism results in the obliteration of fluid inclusion evidence of the first two fluid types, through recrystallisation and new mineral growth. However, the P-T-X characteristics of the third fluid type may be constrained by studies of peak metamorphic mineral assemblages and related fluid inclusions. Possible examples of such fluids in the present study (V1, V2, ?V3) are discussed in sections 4.2 to 4.4.

Type 2 fluids could include those derived from a magmatic source, juvenile fluids originating in the mantle, meteoric fluids percolating down from the surface, or connate fluids which have migrated from their source. (The latter were defined by White (1957) as fossil interstitial water of unmetamorphosed sediments and extrusive volcanic rocks, and water that has been driven from these

rocks). All these fluid types are externally buffered, at least initially, *i.e.* their compositions are essentially controlled by mineral-fluid reactions occurring outside the rock system in which their effects are observed. These fluids are likely, although not necessarily, to have been evolved under different P-T conditions to those prevailing in the system into which they are migrating. Fluids interpreted as being of this type were also encountered in the present study (?V3, $V4_J$, $V4_N$, $V4_W$) and are discussed in sections 4.4 to 4.6.

4.1.2 Fluid evolution processes

There are three major processes which result in changes in the four most important fluid parameters: P, T, X and density (D). These processes: fluid-rock reactions, fluid-fluid mixing and fluid unmixing, are controlled by a number of variables and, in turn, result in changes in various groups of fluid parameters. These inter-relationships are summarised in Figure 4.1. Any of the processes may be combined to produce a range of complex fluid evolution paths, each with distinct P-T-X-time trajectories.

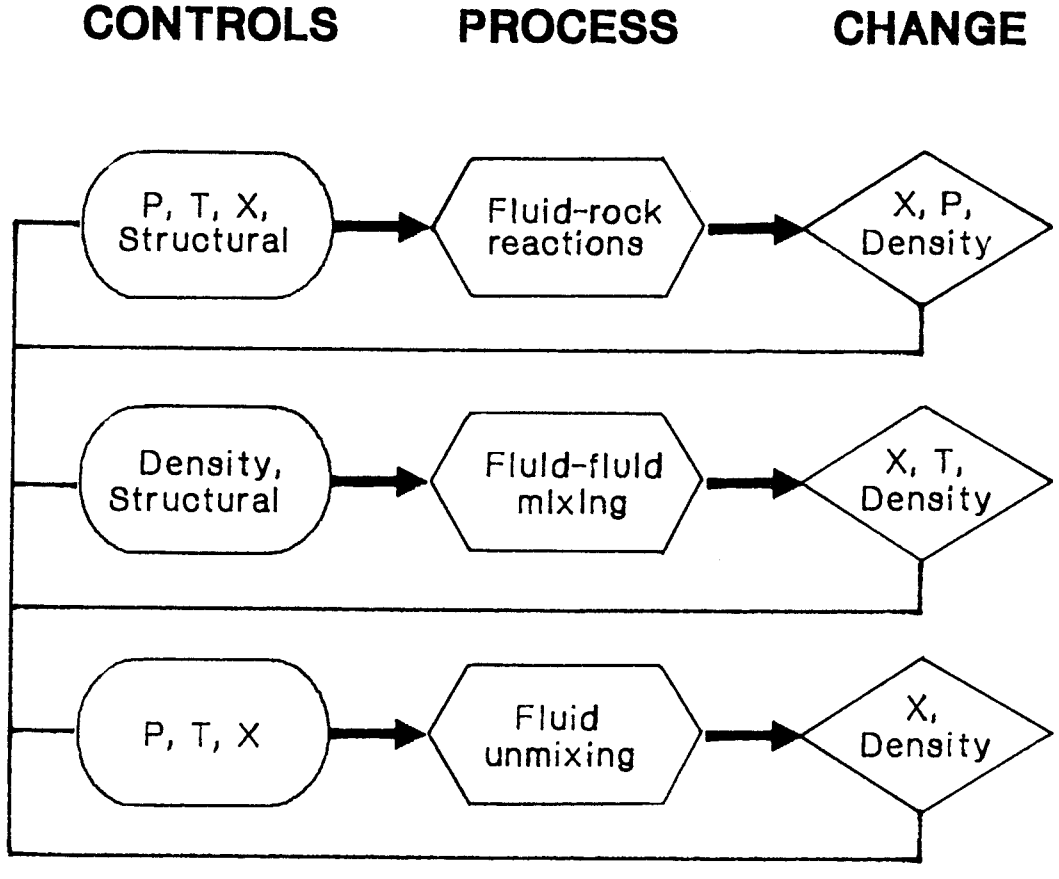

Fig. 4.1 Flow chart illustrating controls and effects of different fluid evolution processes.

4.1.3 Ore deposition

A number of general conditions must be met before an ore deposit can form. The primary condition is that there is a suitable fluid medium for transport of metals to the deposition site. A high concentration of metals in solution is not a necessity, as long as the deposition mechanism is efficient and/or high fluid-rock ratios are attained.

Secondly, there must be a suitable site for ore deposition, the nature of which is dependent on the controls of ore mineral precipitation. If, for instance, reaction with the wallrocks is of fundamental importance, ore deposition will only occur in an appropriate host lithology where the structural setting allows sufficient fluid-rock interaction. Alternatively, if ore deposition is primarily the result of mixing with another fluid, there must be an appropriate conjunction of structural and tectonic conditions for this mixing to occur.

Finally, the externally and/or internally-controlled parameters P, T, fO_2, fH_2S, and in some cases X, must not preclude ore deposition. In some instances, these variables may be the controlling factors. For example, a drastic reduction in metal solubility related to cooling is a common cause of ore formation.

The nature of the fluid source and the type of fluid evolution processes discussed in sections 4.1.1 and 4.1.2, are clearly intimately related to the controls of ore deposition considered above. These relationships are examined in more detail below, in order to constrain the origin of the deposits observed in the field area. The thermodynamics of selected systems are considered in Chapter 5, and a wider appraisal of the role of these processes in the development of the Cornubian metallogenic province forms part of Chapter 6.

4.2 FLUIDS EVOLVED DURING LOW GRADE REGIONAL METAMORPHISM

Relatively few detailed fluid inclusion studies have been carried out in low grade metamorphic terrains (see reviews in Crawford 1981a; Roedder 1984; Crawford & Hollister 1986). Combined data concerning the solute, volatile and stable isotopic compositions of low grade metamorphic fluids are extremely scarce in the literature. A number of workers have touched on this aspect of regional metamorphism in southwest England (*e.g.* Primmer 1985; Pamplin 1988) but there is no relevant information from south Cornwall. As a result, the well-constrained V1 fluid composition outlined in Chapter 3 is important, not only in a local sense, but also in aiding understanding of the evolution and transport of fluids in similar terrains elsewhere.

The combined V1 and V2 fluid inclusion data provide relatively tight constraints on the P-T evolution of the sequence during erosion and uplift of the nappe pile. Such detail could not be achieved by any other method of thermobarometry, particularly in such a low grade terrain.

4.2.1 P-T conditions during peak metamorphism

There have been few detailed studies of the regional metamorphic event which affected south Cornwall during the Early-Middle Carboniferous (see 1.3.4). The presence of low grade metamorphic mineral assemblages was recognised by the early Geological Survey workers (*e.g.* Reid 1907; Flett 1946). However, it was only relatively recently that peak metamorphic P-T conditions could be estimated with the identification of diagnostic pumpellyite-actinolite mineral assemblages (Barnes & Andrews 1981).

V1 fluid inclusion data, discussed in section 3.2.2, and more detailed compositional information (see 3.3, 3.4) may be used to further constrain the P-T conditions developed during regional metamorphism. Several related methods may be used, all of which are dependent on the location in P-T space of the appropriate isochore (line of constant density) for peak metamorphic (V1) fluids. Knowledge of the position of this isochore, in conjunction with an independent temperature or pressure constraint, allows the determination of the peak metamorphic P-T conditions.

A variety of independent temperature constraints are available, including alkali geothermometry (see 3.3.1), vitrinite reflectance data (see 1.3.4), and empirically-derived stability fields for the peak metamorphic assemblage (Hinrichsen & Schurmann 1969; Schiffman & Liou 1980; Liou *et al.* 1985). The latter data also provide limits on the lithostatic pressures attained during the metamorphic event.

Constraining the P-T conditions of regional metamorphism by constructing an isochore for V1 fluids is dependent on the assumptions that the V1 veins studied were formed during peak metamorphism and that the fluid inclusions analysed are representative of the peak metamorphic fluid. The evidence in support of these assumptions is discussed in sections 2.2 and 3.2 respectively. Several other limitations come from the uncertainty in thermometric, compositional, experimental and theoretical data from which the position of the isochore is determined. The production of parallel data in this study from independent techniques (*e.g.* estimation of volatile compositions from microthermometry and bulk analysis; estimation of fluid density from *Th* data and optical estimation of phase proportions + fluid compositional data) provides a high level of confidence in the raw data. The major sources of uncertainty are in the experimental and theoretical arguments upon which the location of the isochore is based (*e.g.* Brown & Lamb 1988), and the independent P or T constraint.

A selection of isochores for V1 fluids are shown in Figure 4.2; the data used in their construction are discussed below. The different isochores are based on a variety of density and compositional approximations and together give an indication of the errors involved in determining trapping P-T conditions using this method.

A mean fluid density of 0.95 ± 0.03 gcm^{-3} was calculated from the optical estimation of phase proportions (mean $F = 0.93 \pm 0.03$) combined with the density of the H_2O - 2.4 ± 0.3 wt% NaCl phase using:

$$\text{Bulk density } (D) = (F \text{ x density of aqueous phase}) + (1\text{-}F) \text{ x (density of vapour phase)} \quad \text{..(4.1)}$$

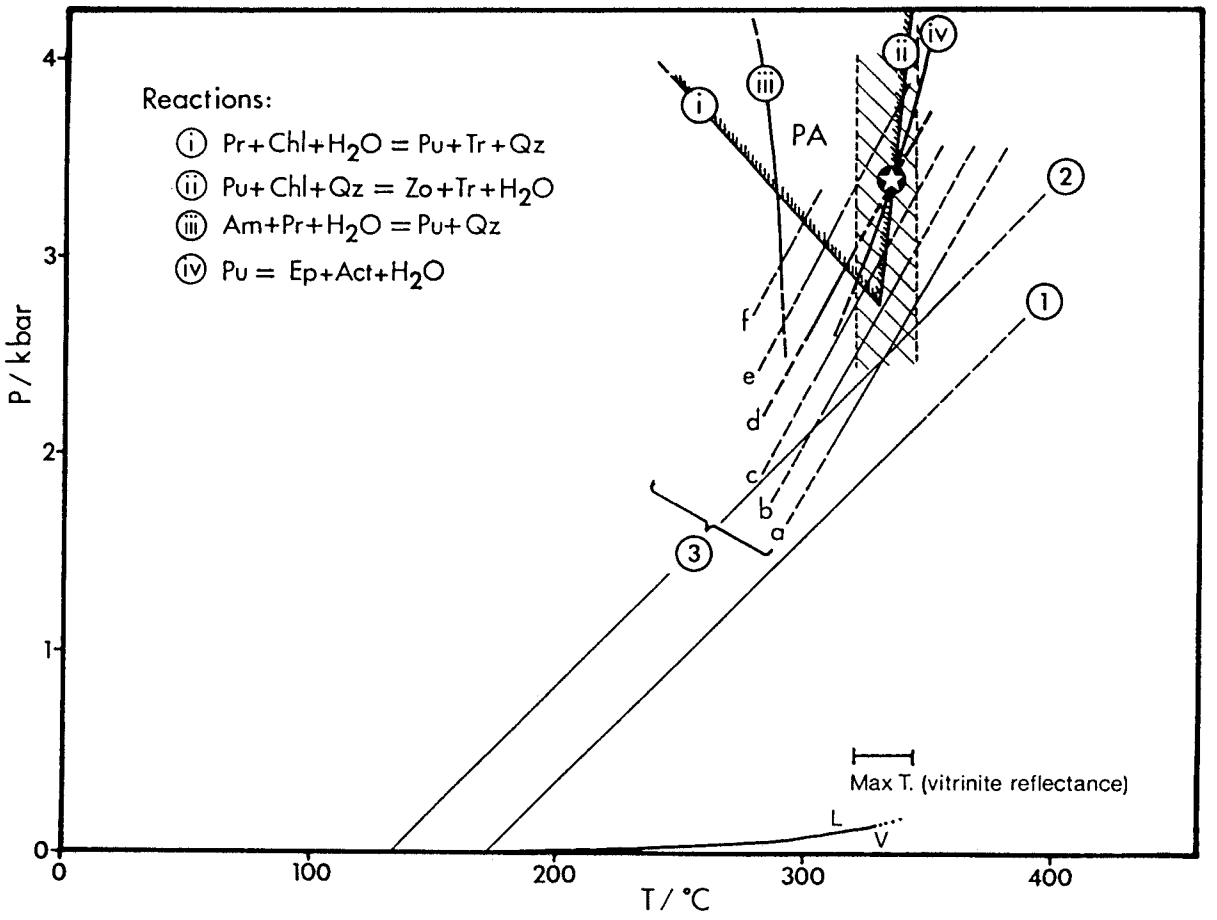

Figure 4.2 P-T diagram showing isochores for V1 fluids. Solid lines with Roman numerals represent univariant mineral equilibria; PA = pumpellyite-actinolite facies field. Lines numbered 1, 2 and 3 represent the isochores discussed in the text (dashed lines indicate uncertain extrapolations). Also shown is the maximum metamorphic temperature range indicated by vitrinite reflectance and the liquid (L) vapour (V) equilibrium curve for an H_2O - 2.4 wt% NaCl solution (from Haas 1976). The star indicates the best estimate of peak metamorphic conditions. Pr = prehnite, Chl = chlorite, Pu = pumpellyite, Tr = tremolite, Qz = quartz, Zo = zoisite, Am = amesite, Ep = epidote, Act = actinolite.

The density of the vapour phase is negligible so that the bulk density is given by:

$$D = (F \text{ x density of aqueous phase}) = 0.93 \text{ x } 1.02 = \underline{0.95 \pm 0.03 \text{ gcm}^{-3}}$$

This method provides an independent check on the fluid density predicted from experimental data on the NaCl-H_2O system (Potter & Brown 1977; Haas 1976) and that estimated theoretically from an equation of state. Predicted fluid densities from both these approaches, consistent with independent P-T constraints (represented by isochores 1 and 3 on Fig. 4.2), are within error of the V1 fluid density estimated above (0.95 ± 0.03 gcm^{-3}).

Isochore 1

The mean *Th* of 173±18°C for V1 fluids (see 3.2.1) is used to locate the point at which the appropriate isochore leaves the L+V univariant curve (Fig. 4.2). The position of this curve is based on data reported in Haas (1976) for the NaCl-H_2O system; the addition of small amounts of CO_2 has little effect. The isochore was plotted using data from Potter and Brown (1977) for a H_2O - 2.4 wt% NaCl solution (*i.e.* using the modal salinity determined by microthermometry and ignoring the effect of CO_2). This approach yields a fluid density of 0.92 gcm^{-3}, just within error of the density estimate of 0.95 ± 0.03 gcm^{-3} made by the visual estimation of phase proportions (see above).

Isochore 2

This isochore is based on the assumption that the density estimated from the relative phase proportions is accurate. This density and P-V-T data for a 2.4 wt% NaCl solution from Potter & Brown (1977) yields a theoretical *Th* of 135°C, outside the 1σ deviation from the mean *Th* value.

Isochores 3a, b, c, d, e, f

These isochores were located using the equation of state of Bowers & Helgeson (1983a). This equation, in common with a number of other published versions of the modified Redlich-Kwong (MRK) equation of state (*e.g.* Holloway 1977; Swanenberg 1980; Kerrick & Jacobs 1981), may be used to predict the P-V-T properties of fluids in the system NaCl-H_2O-CO_2, or its binary sub-systems, under a range of P-T conditions. The ternary approximation is justified in the present case, since the V1 fluids are compositionally very close to the simple ternary system (see 3.2.1). The equation defined by Bowers & Helgeson (1983a) is strictly only valid for temperatures in excess of 300°C and pressures up to 3 kbar. Extrapolations beyond this region of P-T space are unreliable.

The six sub-parallel isochores shown represent a range in fluid density from 0.92-0.97 gcm^{-3}, spanning the error range in estimated fluid density (0.95 ± 0.03 gcm^{-3}). An isochore for a 0.98 gcm^{-3} fluid would fall outside the P-T limits of the equation and is therefore not shown. The set of isochores are for an average V1 fluid, containing 1.045 mole% CO_2 in the volatile component (see 3.4) and 2.4 wt% NaCl dissolved in the aqueous phase. This is equivalent to a bulk composition of 98.22 mol% H_2O, 1.04 mol% CO_2 and 0.74 mol% NaCl.

Discussion

Figure 4.2 shows that the addition of CO_2 shifts V1 isochores to higher values of pressure at a given temperature and to lower values of temperature at a given pressure. Ignoring even the small quantity of CO_2 (1.04 mol%) present in V1 fluids would result in a significant overestimation of the trapping temperature or underestimation of the trapping pressure.

Also shown in Figure 4.2 are independent P-T constraints provided by vitrinite reflectance data and experimentally-determined stability limits of pumpellyite (from Hinrichsen & Schurmann 1969; Nitsch 1971; Schiffman & Liou 1979; Liou *et al.* 1985). The equilibrium curve for coexistence of pumpellyite and actinolite (+ epidote, chlorite, quartz and fluid) provides a useful constraint in the present study, where peak metamorphic assemblages commonly reflect this equilibrium association (Barnes & Andrews 1981).

V1 fluid temperature estimates provided by alkali geothermometry (see 3.3.1) are significantly lower than the V1 fluid temperatures suggested by the other data (apart from Na-Li geothermometry). In many cases, the alkali geothermometers give unreasonable values, below the range of measured *Th*, which represent minimum possible trapping temperatures. This is due to the fact that the system in question does not equate with the natural systems from which the geothermometers are derived; the V1 fluids are either not in complete equilibrium with the appropriate quartz-feldspar-mica assemblages (*e.g.* Giggenbach 1988), or the appropriate buffering assemblage is absent (see 3.3.1 for discussion). In view of the fact that V1 fluids are likely to be in equilibrium with the host rocks (see 4.2.2), the latter explanation is more likely. The absence of K-feldspar from the system (see 3.6) may explain this phenomenon.

Summary

The data discussed above and presented in Figure 4.2 allow relatively tight constraints to be placed on the P-T conditions developed during the low grade regional metamorphic event in south Cornwall. The isochore considered to be most representative of the V1 fluids is that calculated from the equation of state of Bowers & Helgeson (1983a) for the average V1 fluid composition determined by microthermometry and bulk volatile analysis, and estimated bulk density of 0.95 gcm^{-3}. Although extrapolation of this isochore to lower temperatures and pressures is not justified thermodynamically, it is interesting to note that it would intersect the L+V curve for H_2O - 2.4 wt% NaCl (which would be shifted to slightly higher pressures by the addition of CO_2) close to the mean V1 *Th* of 173±18°C.

This isochore intersects the pumpellyite-actinolite-epidote-fluid equilibrium curve within the temperature range determined from vitrinite reflectance data, and within the stability field of pumpellyite. This point, at 330°C and 3.4 kbar, is considered to represent the best estimate of fluid trapping P and T, and hence peak metamorphic conditions. The errors on these values, estimated from uncertainties in the various P-T constraints are ±30°C and ±0.5kbar respectively. It must be emphasised that the pressure determined by the average isochore and independent temperature constraint is a fluid pressure. It is assumed that under regional metamorphic conditions, $P_F \approx P_L$ (Walther & Wood 1986), so that the lithostatic pressure during peak metamorphism is also estimated to be 3.4 kbar.

4.2.2 V1 fluid source and fluid-rock interaction

Volatile components

Fluid inclusion studies in metamorphic rocks from a variety of grades and rock types show that the volatile composition of metamorphic fluids is related to the prevailing P-T conditions (Crawford & Hollister 1986; Crawford 1981b; Touret 1981; Roedder 1984). The variations in fluid composition, particularly regarding phases in the C-O-H system, qualitatively agree with thermodynamic predictions.

Frey *et al.* (1980) and Mullis *et al.* (1983) showed how the volatile composition of crustal fluids evolved during Alpine metamorphism varied as a function of metamorphic grade in the Swiss Alps. The fluids progressively change in composition from ≈1 to >80 mol% higher hydrocarbons (HHC) in unmetamorphosed rocks; ≈1 to >90 mol% CH_4, <1 mol% HHC below the pyrophyllite isograd (lower anchizone); ≈70 to >99 mol% H_2O, <1 mol% CH_4 below the staurolite isograd (higher anchizone, epizone); and ≈10 to >60 mol% CO_2 at higher grades (mesozone). In the granulite facies, fluids are dominantly composed of CO_2 (Touret 1981).

The V1 and V2 fluids encountered in the present study both fall in the "water zone" of Mullis *et al.* (1983). The composition of fluids in this zone and at higher grades is thought to be controlled by equilibria between dispersed carbon, iron-bearing silicate and iron oxide oxygen buffers, and H_2O and CO_2 produced by devolatilisation reactions (Ohmoto & Kerrick 1977; Frost 1979; Holloway 1981, 1984). Organic carbon may play a role in the generation and buffering of V1 fluids (as suggested by stable isotopic data; see 3.5), although iron-bearing silicates (*e.g.* chlorite) and iron oxides are also probably important. Graphite has not been observed, although it is likely to be present at the P-T conditions of peak metamorphism *i.e.* 330°C, 3.4 kbar (Holloway 1984).

The compositions of C-O-H fluids are sensitive to fO_2 as well as temperature, so that fluid inclusion compositions can be used to infer the oxygen fugacity in the metamorphic system. This, in turn, has important consequences for the solubility of metals in such fluids, and hence on the ore-forming potential. This approach has been applied to V1 fluids (see 4.2.7).

Solute components

Assuming that V1 fluids are produced as a result of devolatilisation reactions occurring contemporaneously with peak metamorphism, their composition will be buffered by the local mineral assemblages. The major element composition of the fluid, as determined by D-ICP in this study (see 3.1.1), may be used to test this hypothesis.

There are both empirical and theoretical methods which may be used to test for fluid-rock equilibrium. A variety of empirical alkali geothermometers are available which may be used to determine the temperature of equilibration of an aqueous fluid phase with common quartz-feldspar-mica assemblages. Alternatively, as pointed out by Giggenbach (1988), these geothermometers may be used to test for the degree of equilibration between a fluid and such a mineral assemblage.

A thermodynamic approach may also be used to assess whether the V1 fluids are compositionally in equilibrium with the relevant mineral assemblages. This method was pioneered by Helgeson (1968, 1969) and Holloway (1977) and discussed with different emphasis by various workers (*e.g.* Montoya & Hemley 1975; Eugster & Gunter 1981; Reed 1982). The procedure involves

the calculation of equilibrium constants for relevant mineral-mineral equilibria (in the presence of fluid) at a given temperature and pressure, using one of a number of equations of state. For complex systems, a large number of simultaneous equations have to be solved and a number of computer programs have been designed to carry out these calculations (*e.g.* "SUPCRT" - Helgeson *et al.*, unpublished; "EQ3" - Wolery 1983). An example calculation, to determine the stability limits of phases in the Na-K-SiO_2-HCl-H_2O system, and to estimate the composition of a fluid in equilibrium with these phases is set out below:

Phases of interest: K-feldspar (Ksp), muscovite (Mu), Na-feldspar (Ab), paragonite (Par), kaolinite (Kaol), quartz (Qz)

Equilibria:

(1) $Ksp + Na^+ = Ab + K^+$ $\quad K_1 = \frac{(a.K^+)}{(a.Na^+)}$ ...(4.2)

(2) $1.5Ksp + H^+ = 0.5Mu + K^+ + 3Qz$ $\quad K_2 = \frac{(a.K^+)}{(a.H^+)}$ ...(4.3)

(3) $Mu + H^+ + 1.5H_2O = 1.5Kaol + K^+$ $\quad K_3 = \frac{(a.K^+)}{(a.H^+)}$ ...(4.4)

(4) $Mu + Na^+ = Par + K^+$ $\quad K_4 = \frac{(a.K^+)}{(a.Na^+)}$ ...(4.5)

(5) $1.5Ab + H^+ = 0.5Par + Na^+ + 3Qz$ $\quad K_5 = \frac{(a.Na^+)}{(a.H^+)}$ ...(4.6)

(6) $1.5Ab + H^+ + 0.5K^+ = 0.5Mu + 1.5Na^+ + 3Qz$ $\quad K_6 = \frac{(a.Na^+)^{1.5}}{(a.K^+)^{0.5}(a.H^+)}$ ...(4.7)

(7) $Par + H^+ + 1.5H_2O = 1.5Kaol + Na^+$ $\quad K_7 = \frac{(a.Na^+)}{(a.H^+)}$ ...(4.8)

The change in Gibbs' free energy for each reaction at a given P and T ($\blacktriangle G^{\circ P,T}_r$) can be calculated from:

$$\blacktriangle G^\circ_r = \blacktriangle G^\circ_f(\text{products}) - \blacktriangle G^\circ_f(\text{reactants}) \qquad ...(4.9)$$

as long as the standard Gibbs' free energies of formation ($\blacktriangle G^\circ_f$) of the phases at P and T are known. These data have been derived from empirically determined values, measured at some standard reference state, (P_s, T_s; usually 1 bar, 298K) and extrapolated to P and T using an equation of the form:

$$\blacktriangle G^{\circ P,T}_f = \blacktriangle G^{\circ Ps,Ts}_f + \blacktriangle G^{\circ Ps,Ts \to P,T} \qquad ...(4.10)$$

$$\text{where } \blacktriangle G^{\circ Ps,Ts \to P,T}_f = -S^\circ(T-Ts) + a(T-Ts-T.\ln(T/Ts)) + \frac{(c-bT.Ts^2)(T-Ts)^2}{2T.Ts^2} + V^\circ(P-Ps) \qquad ...(4.11)$$

$S°$ is the standard entropy for the phase at reference state (assumed not to be a function of temperature); *a*, *b* and *c* are the *Maier-Kelley* coefficients of the species, which are empirically determined fit coefficients, constraining variations in heat capacity with temperature (*e.g.* Sverjensky 1987). Tabulations of $\blacktriangle G°_f^{Ps,Ts}$ data and Maier-Kelley coefficients have been published (*e.g.* Helgeson *et al.* 1978; Tanger & Helgeson 1987) and this information is used below.

Equation 4.11 is valid for the calculation of $\blacktriangle G°_f^{P,T}$ for minerals. For gases, the last term may be dropped because $\blacktriangle G°_f^{P,T}$ is independent of pressure. The expression for aqueous species is more complex, with additional terms added to account for variations in solvent parameters (*e.g.* the dielectric constant of water (ϵ)), with P and T (see Sverjensky 1987 for full equation).

Once $\blacktriangle G°_f^{P,T}$ has been calculated for each species using Eq. 4.10, $\blacktriangle G°_r^{P,T}$ may be determined by substituting these values into Eq. 4.9. $LogK^{P,T}$ may then be calculated using:

$$\blacktriangle G°_r{}^{P,T} = -2.303\ R.T.logK^{P,T} \qquad ...(4.12)$$

where R is the gas constant (in appropriate units). K is then substituted into equations 4.2 - 4.8 to yield a variety of activity ratios for some of the major ions in solution.

The procedure outlined above has been carried out for the NaCl-KCl-SiO_2-HCl-H_2O system using the equilibrium reactions represented by Eqns. 4.2 to 4.8 and at the estimated peak metamorphic conditions (330°C, 3.4 kbar). The equilibrium constant data obtained may be depicted graphically in an activity diagram (Fig. 4.3) which illustrates the positions of the stability fields of the different phases in the system.

The V1 fluid temperature estimated in section 4.2.1 is significantly higher than equilibrium fluid temperatures determined using Na-K and Na-K-Ca geothermometers (see 3.3.1). As mentioned above, these geothermometers are based on empirical observation of fluids in equilibrium with complex natural assemblages in geothermal fields. The rocks in the system being studied are dominated by quartz + chlorite + K-mica assemblages, with variable amounts of albite (originally plagioclase). The absence of K-feldspar and low buffering capacity of plagioclase are probably the cause of the apparent disequilibrium between the fluid and the host rocks.

The activity diagram constructed above and shown in Figure 4.3 may be used to explain the discrepancy between the V1 fluid temperature estimated in section 4.2.1, and the alkali geothermometry. Molal Na/K ratios define a series of straight lines on the diagram, parallel to the paragonite-muscovite boundary (Fig. 4.3). The range of Na/K ratios for V1 fluids (see 3.3.1) is shown as a hatched region on the diagram. The location of these lines is based on the assumption that $a.Na^+/a.K^+ \approx$ molal Na/K, a valid approximation for the conditions in question (Helgeson *et al.* 1981). XRD and petrographic studies indicate that albite is in equilibrium with V1 fluids. This observation, combined with the Na/K range of V1 fluids, implies that the V1 fluids plot on the albite-muscovite phase boundary, close to the albite-muscovite-paragonite invariant point (shaded area, Fig. 4.3). The fact that the V1 fluids are demonstrably not in equilibrium with K-feldspar at peak metamorphic conditions explains the low temperature values obtained by conventional Na-K and Na-K-Ca geothermometry (see 3.3.1). These anomalously low temperatures result from the relatively low K content of the fluids; the low K content is due to buffering of the fluid by a relatively Na-rich, albite + muscovite ± paragonite assemblage, rather than the typical albite + K-feldspar +

muscovite assemblage on which the geothermometers are based. Chlorite, although an important constituent of the mineral assemblage, does not play a significant role in the buffering of the alkali content of the fluid.

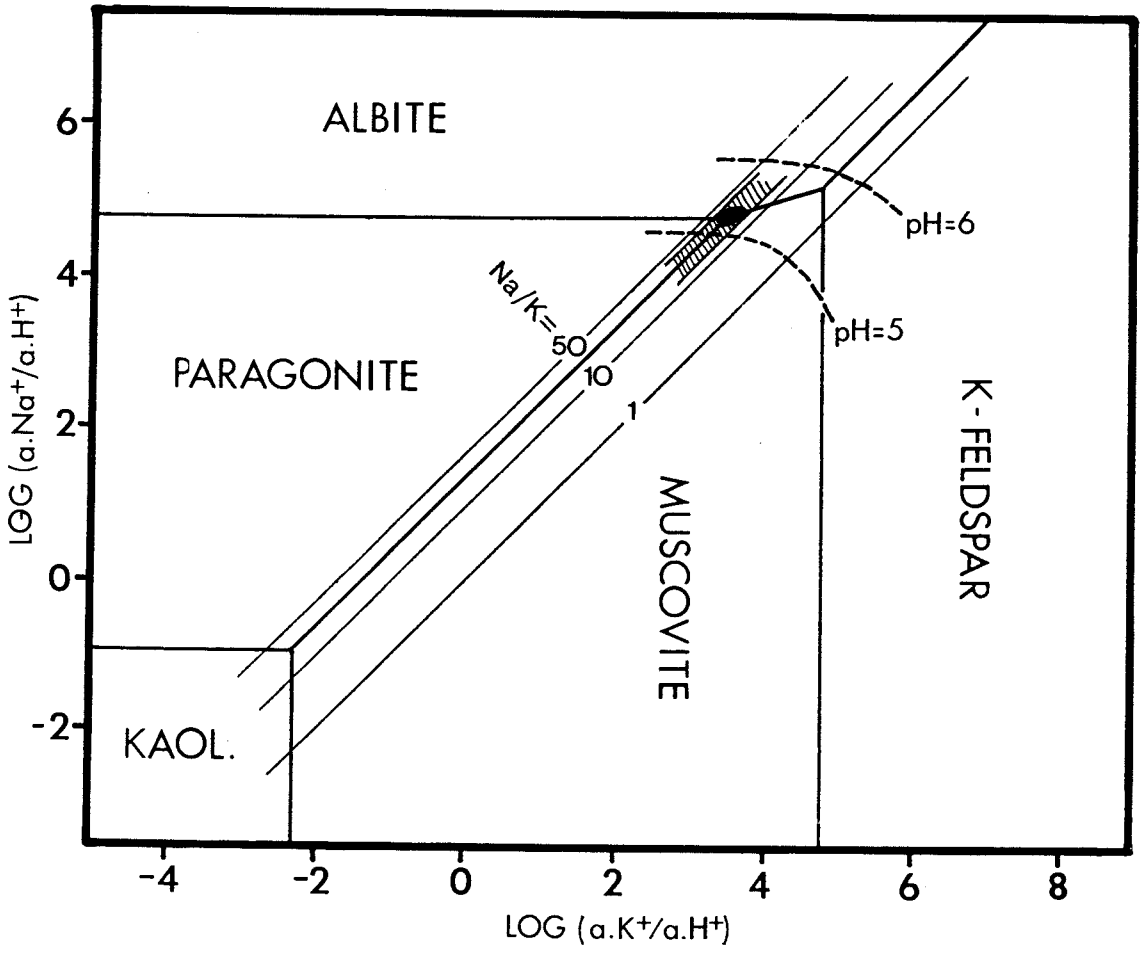

Figure 4.3 Activity diagram for the system NaCl-KCl-HCl-H_2O-SiO_2 constructed for 330°C and 3.4 kbar.

Summary

It is concluded that the V1 fluids analysed individually by microthermometry and in bulk by D-ICP were in equilibrium with a K-mica-albite-quartz(-chlorite ± paragonite) assemblage during peak regional metamorphism. This indicates that the fluid was internally-derived, by devolatilisation reactions, and its solute composition was buffered by the metamorphic mineral assemblage. The volatile composition of the fluid was controlled by the nature of the devolatilisation reactions which, in low grade pelites, are dominated by dehydration, and the oxygen fugacity (see 4.2.7).

4.2.3 Structural controls of V1 fluid composition

Although the data are limited, there is some evidence to support the assertion that V1 fluid composition is independent of the nature of the permeability. The ideal comparison is between data

obtained from V1 veins in different structural settings from the same part of the sequence, thus avoiding bulk rock compositional variations. Such compositional information for V1 fluids only exists for samples *J138GW*, *J105GW* and *J06GW* (see Tables 3.14, 3.16) which represent vein types $V1_B$, $V1_T$ and $V1_T$ respectively, and were all taken from Gunwalloe Fishing Cove Beach (see Fig. 1.4).

A plot of the ranges in major element ratios for fluid inclusions in these samples as a function of structural setting (Fig. 4.4) shows that there are no significant differences between the solute compositions of fluids mobilised in different structures. The volatile compositional data are too limited to allow any evaluation of structurally-related variations in this parameter.

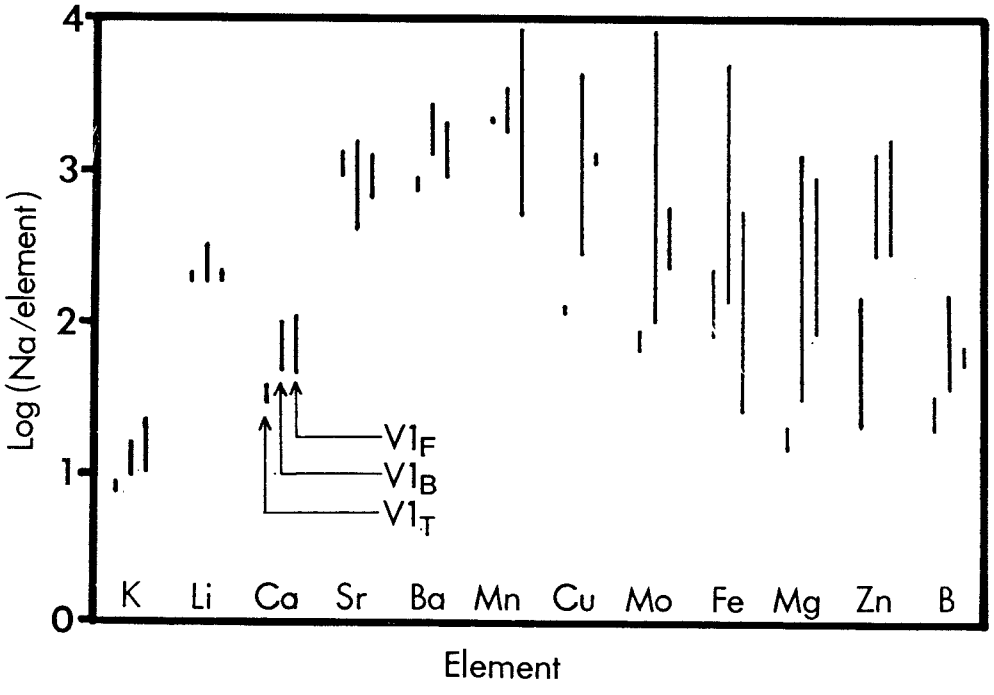

Figure 4.4 Plot of Na/element (weight) ranges for V1 fluids as a function of vein type.

The evidence outlined above suggests that V1 fluid composition was buffered by the host rocks under peak metamorphic conditions. This is true both for fluids which permeated dilatant fractures, as well as for those which migrated along thrust planes. These data attest to the homogeneity of fluids flowing through the currently exposed crustal segment during regional metamorphism in south Cornwall.

4.2.4 Spatial variations in V1 fluid composition

Previous studies of fluid inclusions in metamorphic rocks suggest that the cation composition is controlled by the associated mineral assemblages (see references cited in Crawford 1981b; Crawford & Hollister 1986). This is in agreement with the theoretical arguments presented in section 4.2.2, which indicate that the alkali composition of the V1 equilibrium fluids is controlled by the dominant mineral assemblage. However, where variations in bulk rock mineralogy occur, parallel variations in

fluid composition may be expected.

The limited data set precludes a detailed analysis of any systematic spatial variations in V1 fluid composition. However, the five V1 samples, from three sampling zones, on which fluid compositional information has been obtained (see Tables 3.14, 3.16) do suggest that there were some local controls of fluid composition. Unfortunately, there is no data on V1 variation between the two major, compositionally distinct, rock formations in the study area: the Mylor Slate Formation and the Portscatho Formation (see 1.3.1). This is due to the proximity of the former Formation to the Cornubian batholith, which has resulted in intense deformation and overprinting of V1 (and V2) material.

Alkali metals

The partitioning of alkali cations between rock and fluid during peak metamorphism was considered in section 4.2.2. The alkali compositional data for samples taken from a variety of lithologies within the Portscatho Formation (Tables 3.14, 3.16) indicate that no significant variations exist. This is very likely due to the ubiquitous presence of albite-muscovite(-chlorite ± paragonite) assemblages, buffering the alkali content of the fluid.

Alkali earth metals

Consideration of the Mg, Ca, Sr and Ba composition of V1 fluids reveals several correlations between alkali earth concentration and rock type. V1 samples from Jangye-ryn (*J53JR*; Fig. 1.4), taken from ankerite-rich greywackes, contain fluids enriched in Ca, Ba and Mg relative to other V1 samples. This suggests that the presence of significant quantities of carbonate in the host rock locally buffered the fluid to higher alkali earth concentrations. The common occurrence of carbonate minerals within the veins (see 2.2.1 to 2.2.4) indicates that the fluids were probably close to saturation with respect to carbonate phases and that local fluctuations in fluid P-T-X caused occasional precipitation.

Transition metals

The transition metals, particularly copper, zinc and molybdenum, are relatively abundant in sample *J53JR*, but below the D-ICP detection limit in most of the other V1 (and V2) samples. Despite the measurable quantities of Cu, Zn and Mo in these samples (estimated fluid composition of 31-80 ppm Cu, 36-450 ppm Zn and 81-144 ppm Mo; Table 3.16), the reason for their relative abundance is unclear. However, the fact that elevated levels of transition metals are present in at least some of the V1 fluids has important consequences for the transport of such ore-forming metals in low grade regional metamorphic fluids (see 5.3).

4.2.5 V1 fluid salinity

The salinity of H_2O-rich metamorphic fluids, such as the V1 fluids investigated in the present study, is controlled by the amount of anions in solution which, under most conditions, are dominated by Cl^-. Prediction of the anion composition of such aqueous fluids from mineral-fluid equilibria

calculations (as discussed for cations in section 4.2.2) is not straightforward, because of the presence of Cl^- (and other species such as Br^-) which do not occur in major quantities in the associated mineral phases. As a result, thermodynamic predictions of aqueous fluid compositions are invariably based on the assumption of a particular chloride concentration (*e.g.* Eugster & Gunter 1981; Eugster 1982).

For the reasons outlined above, the estimated fluid salinity of 2.4 wt% NaCl equivalent (≈0.41 molal Cl^-) cannot be modelled thermodynamically. This can be a problem when considering the reasons behind changes in salinity of such fluids, *e.g.* the salinity increase between V1 and V2 fluids (see 4.3.5).

4.2.6 V1 fluid pH

The activity diagram constructed in section 4.2.2 may be used to estimate the pH of V1 fluids. The location in $a.Na^+/a.H^+$ - $a.K^+/a.H^+$ space of the V1 fluid composition, as defined by the Na/K ratio and the equilibrium mineral assemblage, uniquely fixes the pH for a fluid of given salinity. A series of curves of constant pH were plotted on Figure 4.3, assuming a total salinity of 2.4 wt% NaCl equivalent, or 0.41 molal chloride. The location of these curves is based on the assumptions that Na and K are the dominant cations in solution, that Cl^- is the major anion and that the presence of other volatiles (*e.g.* CO_2) does not significantly affect the activity ratios of the ionic species.

Using this approach, a fluid in equilibrium with albite and muscovite at 330°C and 3.4 kbar is constrained to have a pH of between 5 and 6. The values of $a.Na^+/a.H^+$ and $a.K^+/a.H^+$ for the average V1 fluid gave a pH of 5.3, assuming a salinity of 0.41 molal chloride. This is slightly lower than neutral pH for a chloride-rich fluid at 330°C and 3.4 kbar.

4.2.7 Oxygen fugacity

As mentioned in section 4.2.2, the C-O-H phases in fluid inclusions may be used to infer the oxygen fugacity in the system at the time of fluid trapping. Once this has been constrained, it is also possible to estimate the sulphur or H_2S fugacity of the fluid. Both fO_2 and fH_2S are vital parameters controlling metal transport and ore deposition.

The approach used here is that followed by French (1966) and Eugster & Skippen (1967), summarised by Holloway (1987). In the initial calculation, a C-O-H fluid is assumed to be in equilibrium with crystalline graphite at peak metamorphic conditions, *i.e.* 330°C, 3.4 kbar.

The following reactions may be written to define fluid-graphite equilibria:

(1) $C + O_2 = CO_2$ $\quad K_1 = \frac{fCO_2}{(a.C)(fO_2)}$ ...(4.13)

(2) $C + 0.5O_2 = CO$ $\quad K_2 = \frac{fCO}{(a.C)(fO_2)^{0.5}}$ ...(4.14)

(3) $C + 2H_2 = CH_4$ $\quad K_3 = \frac{fCH_4}{(a.C)(fH_2)^2}$ ...(4.15)

(4) $H_2 + 0.5O_2 = H_2O$ $\quad K_4 = \frac{fH_2O}{(fH_2)(fO_2)^{0.5}}$ ...(4.16)

The fugacity coefficient of component *i* at P and T (ϕ_i), defined by Redlich & Kwong (1949), is given by:

$$\phi_i = f_i/(X_i \times P_F) \qquad ...(4.17)$$

where f_i is the fugacity of component *i* in the mixture at P and T. Although a simplification, ignoring the effect of non-ideal mixing, calculations by Poulson & Ohmoto (1989) indicate that the differences are not significant at the P and T of interest. Rearranging equation 4.17 and substituting into 4.16 gives:

$$K_4 = (X_{H2O} \times \phi_{H2O} \times P_F)/(fH_2 \times fO_2^{0.5})$$

$$\text{--> } fO_2 = ((X_{H2O} \times \phi_{H2O} \times P_F)/(K_4 \times fH_2))^2 \qquad ...(4.18)$$

Similarly, starting with equation 4.15 and substituting in the expression for the fugacity coefficient (eq. 4.17):

$$fH_2 = ((X_{CH4} \times \phi_{CH4} \times P_F)/(K_3 \times a.C))^{0.5} \qquad ...(4.19)$$

Finally, equation 4.19 is substituted into 4.18 to yield an expression for fO_2 involving the mole fractions of H_2O and CH_4 (known from bulk volatile analyses), the fugacity coefficients for H_2O and CH_4 (Burnham *et al.* 1969; Ryzhenko & Volkov 1971), the total fluid pressure (3.4 kbar), the activity of carbon (=1 for crystalline graphite) and the equilibrium constants for reactions 3 and 4:

$$fO_2 = (X_{H2O}^2 \times \phi_{H2O}^2 \times P_F \times a.C \times K_3)/(X_{CH4} \times \phi_{CH4} \times K_4^2) \qquad ...(4.20)$$

The latter two quantities are determined from the standard free energies of reaction for reactions 3 and 4 at the pressure and temperature of interest, calculated using equations 4.10 and 4.11 (section 4.2.2).

Using the method outlined above, $\log(fO_2)$ for the peak metamorphic fluids was estimated to be -30.8. Decreasing the activity of carbon decreases the $\log(fO_2)$ by the same order of magnitude, *i.e.* if $a.C=0.1$, $\log(fO_2)= -31.8$. This indicates that the $\log(fO_2)$ estimate is not affected significantly by selecting a carbon activity of less than one (*i.e.* if a disordered form of graphite is present). Work

by Landis (1971) and others indicated that graphite present in pumpellyite-actinolite facies rocks is of intermediate disorder, hence the activity of carbon will be <1. This means that the calculated oxygen fugacity is à maximum and the true value may be one or two log units lower.

Discussion

The fO_2 value calculated above is consistent with graphite stability and with several equilibria of importance in the peak metamorphic mineral assemblage. A log(fO_2) *vs.* T plot (Fig. 4.5) shows how the calculated fO_2 at 330°C, 3.4 kbar is consistent with common silicate equilibria such as paragonite + quartz = albite + andalusite + H_2O and muscovite + quartz = andalusite + K-feldspar + H_2O (Ohmoto & Kerrick 1977). In section 4.2.2, V1 fluids were shown to be in equilibrium with a paragonite + muscovite + albite + quartz assemblage. This suggests that the calculated oxygen fugacity is reasonable, despite the simplifying assumptions involved.

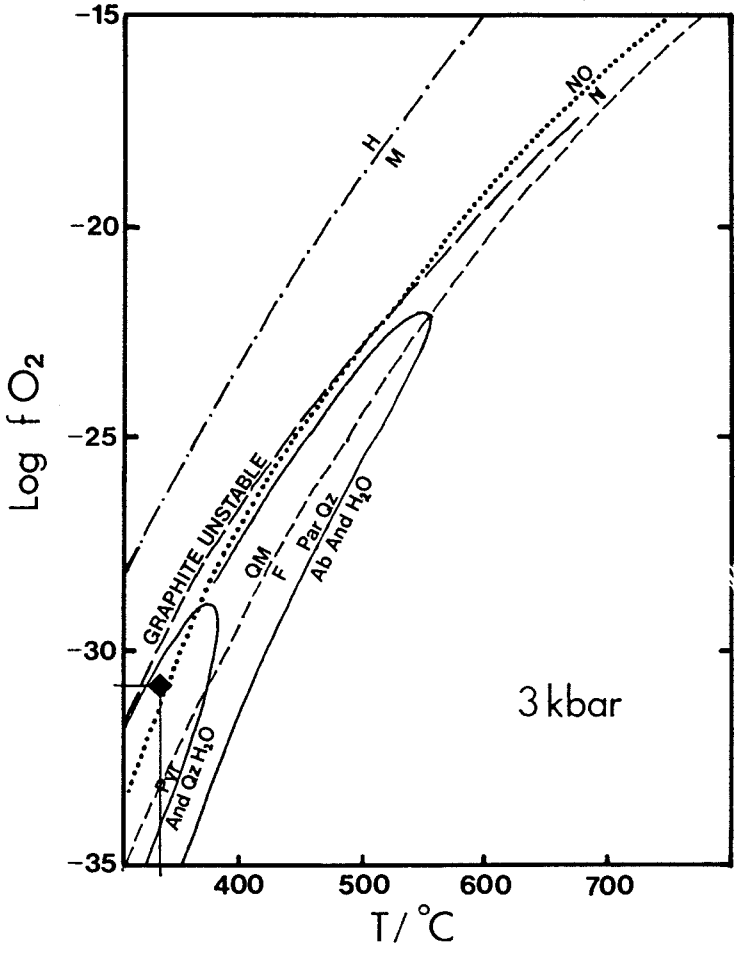

Figure 4.5 fO_2 - temperature diagram at 3 kbar, interpolated from Ohmoto & Kerrick (1977). Common buffering assemblages: H-M = haematite-magnetite, N-NO = nickel-nickel oxide, QM-F = quartz-magnetite-fayalite. Also shown are the graphite stability field and two silicate dehydration equilibria: pyrophyllite = andalusite+quartz+water, and paragonite+quartz = albite+andalusite+water. The estimated fO_2-T conditions for V1 fluids are represented by the solid diamond, close to the NNO buffer.

Assuming that $a.C=1$ (*i.e.* crystalline graphite), the calculated fO_2 is 2 log units above the quartz-fayalite-magnetite (QFM) buffer and 0.5 log units above the nickel-nickel oxide (NNO) buffer. If, as would probably be the case under the relatively low grade conditions, $a.C<1$ then the calculated fO_2 would be closer to NNO and QFM. A carbon activity of 0.01 would be required for a V1 oxygen fugacity equivalent to QFM at 330°C, or 0.3 for fO_2=NNO at 330°C. Wood & Walther (1986) suggest that oxygen fugacity is likely to be close to NNQ during regional metamorphism of pelites. In the absence of additional data, it is impossible to further constrain the controls of fO_2 of the V1 fluids. The relative importance of chlorite and/or other Fe silicates or oxides in controlling fO_2 is unknown.

The carbon isotopic composition of CO_2 in V1 fluids (see 3.5) provides some evidence that organic carbon is involved in the generation of CO_2 during peak metamorphism. This suggests that carbon in some form in the rock (presumably disordered graphite), of organic origin, was in equilibrium with pore fluids evolved during prograde devolatilisation reactions. It is concluded from the preceding discussion that the V1 volatile composition is consistent with an origin via devolatilisation reactions in the presence of a graphite buffer. Comparison with other estimates of fO_2 during regional metamorphism suggests that the oxygen fugacity of V1 fluids was buffered by carbon with $a.C\approx0.3$.

The evidence obtained in this study thus suggests that disordered graphite buffering may be an important control of the composition of peak metamorphic fluids.

4.2.8 Sulphur fugacity

The same procedure to that described in section 4.2.7 may be used to calculate the H_2S and SO_2 fugacities of V1 fluids. Two additional reactions can be written:

(5) $H_2 + 0.5S_2 = H_2S$ $\qquad K_5 = \dfrac{fH_2S}{(fH_2)(fS_2)^{0.5}}$ ...(4.21)

(6) $O_2 + 0.5S_2 = SO_2$ $\qquad K_6 = \dfrac{fSO_2}{(fO_2)(fS_2)^{0.5}}$ ...(4.22)

K_5 and K_6 can be calculated from the $\blacktriangle G°_r$ at P and T as described above. fO_2 is known from the previous calculation and fH_2 can be determined from equation 4.19. The remaining unknown in eqs. 4.21 and 4.22 is fS_2, which must be specified in order to constrain fH_2S and fSO_2.

It is necessary to assume that the sulphur fugacity in the fluid is buffered by sulphur-bearing minerals in the rock. A common approach is to assume buffering of sulphur by a pyrite-pyrrhotite assemblage (*e.g.* Poulson & Ohmoto 1989; Holloway 1987). Although pyrrhotite has not been observed in the present study, it is likely that it would have been produced at an early stage of metamorphism of pyrite-bearing pelites (Poulson & Ohmoto 1989). Such rocks are common in the field area and so the assumption is believed to be justified. Absence of pyrrhotite would imply that fS_2 and hence fH_2S and fSO_2 were in fact greater than the calculated values.

Several expressions for the P-T dependence of fS_2 in equilibrium with pyrite-pyrrhotite have been reported in the literature; the equation used here is that of Poulson & Ohmoto (1989):

$$\log(fS_2) = 0.00468T + 8.899 - (13060/T) + 0.030(P-1)/T \quad \text{...(4.23)}$$

This yields an fS_2 of -9.8 for the V1 fluids. Substitution of this value into equations 4.21 and 4.22 gives a $\log(fH_2S)$ of -0.27 and a $\log(fSO_2)$ of -8.6. The significance of these figures is primarily in the implications for metal transport which is discussed in detail in section 5.3.

4.3 RETROGRESSION DURING UPLIFT AND EROSION

The V2 fluids studied represent a transition from post-peak metamorphic conditions through to the late stages of imbricate thrusting which marked the end of the D2 deformation event. The clear evolution of the basic fluid parameters derived from microthermometric studies (*i.e. Th* and *S*) from D1 to D2 (see 3.2.2, 3.2.3) illustrate that fluid evolution in the crustal slab was essentially continuous during the compressional tectonic event.

4.3.1 P-T evolution during D2

A similar approach to that used to characterise the P-T trapping conditions of V1 fluids was used for V2 fluids. The modal degree of fill for V2 type 1 inclusions is 0.9, giving a bulk *D* of 0.92 gcm^{-3} (eq. 4.1); however, a mean calculated for all inclusions homogenising to liquid gives a value of 0.88 ± 0.12 gcm^{-3}. An average salinity of 3.1 ± 1.3 wt% NaCl equivalent was determined by fitting a normal distribution to the V2 *S* data (Fig. 3.10) and a representative *Th* of 206 ± 20°C was defined by the same method (Fig. 3.9). A CO_2 content of 4 mol% was used for the average V2 fluid composition, based on bulk volatile analyses (see 3.4), taking into account the effect of overprinting by the CO_2-rich fluid inclusion population (see 3.2.3). Three isochores, based on these experimental data, are shown in Figure 4.6.

Isochore 1

Isochore 1 was plotted for V2 fluids, assuming an approximation to the NaCl-H_2O system. The mean *Th* of 206°C located the point on the liquid+vapour curve (data for a 3.1 wt% NaCl fluid interpolated from data in Haas 1976) at which the isochore originates. The slope of the isochore was determined from the data regression of Potter & Brown (1977). This approach yields a fluid density of 0.88 gcm^{-3}, identical to the mean density estimated for V2 H_2O-rich inclusions.

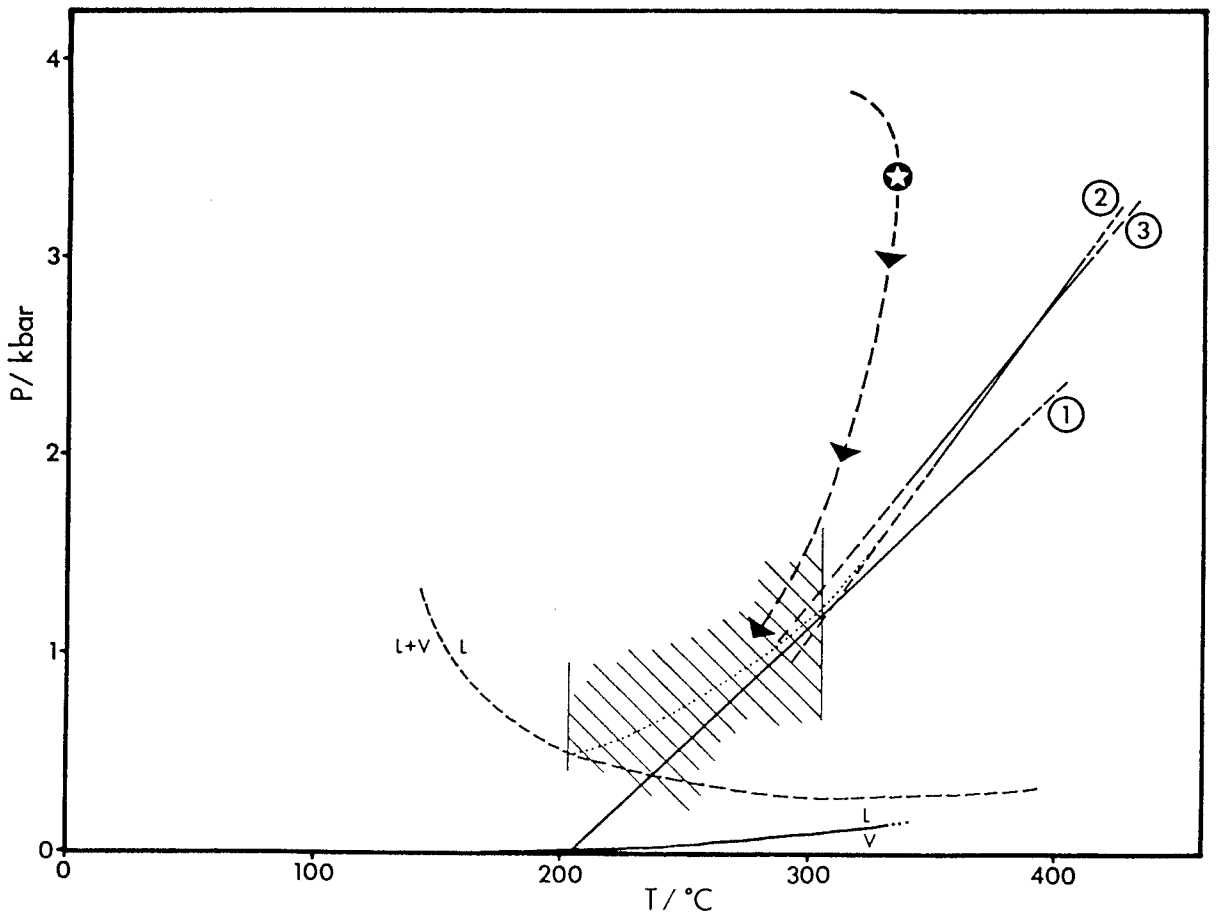

Figure 4.6 P-T diagram showing inferred trapping conditions of V2 fluids (hatched area). Isochores 1, 2 and 3 are described in the text. The dashed arrowed line represents the P-T-time path followed by the rocks in the study area from D1 (star) to D2. Curved dashed line represents limits of the two-phase field in the H_2O - 4 mol% CO_2 - 3.1 wt% NaCl system (from Gehrig *et al.* 1985); solid curved line represents the two-phase curve in the H_2O - 3.1 wt% NaCl system (from Haas, 1976).

Isochore 2

Thermodynamic calculation of the average isochore for a fluid of the composition outlined above is not a simple procedure, since the various published equations of state do not adequately define the behaviour of two-component fluids close to the two-phase region, let alone more complex systems. The only equation of state describing the CO_2-H_2O-NaCl ternary system, that of Bowers & Helgeson (1983a), is not valid below 350°C and 500 bars. However, the position of the isochore (for an H_2O - 4 mol% CO_2 - 3.1 wt% NaCl fluid) was calculated above 300°C to give some idea of its location in P-T space.

Isochore 3

A second isochore, based on the maximum possible CO_2 content of V2 fluids (as determined by bulk volatile analysis) was also determined to constrain the upper limit of the trapping pressure. This isochore, constructed for a bulk CO_2 content of 8.7 mol% and NaCl content of 0.9 mol% (3.1 wt% NaCl with respect to NaCl-H_2O), raises the pressure estimate, relative to isochore 2, by ≈150 bars at 300°C.

Discussion

Neither isochore 2 nor isochore 3 intersect the liquid+vapour curve for a 4 mol% CO_2, 3.1 wt% NaCl fluid (see Fig. 4.6; data from Gehrig *et al.* 1985) within error of the mean *Th* determined by microthermometry (206°C). This is probably due to the inability of the Bowers-Helgeson equation of state to model the behaviour of fluids in the system concerned in the region just above the solvus. If isochores 2 and 3 are projected to the H_2O - 4 mol% CO_2 - 3.1 wt% NaCl liquid+vapour curve at 206°C, then they must flatten significantly in this region. Such flattening of isochores close to the liquid+vapour equilibrium curve is also observed in the H_2O-CO_2 and H_2O-NaCl binary systems (see Shepherd *et al.* 1985, p.138 and Potter & Brown 1977 respectively). Thus, this behaviour may also be expected in the ternary system. Assuming this interpretation of the data is correct, and taking isochore 2 as being most representative of V2 fluids above 300°C, a curved isochore for V2 fluids is defined in the super-solvus region, at temperatures between 206 and 300°C.

By analogy with V1 fluids, alkali geothermometry on V2 fluids will yield values below the true equilibration temperature as a result of the absence of K-feldspar from the buffering assemblage (see 4.2.2). The Na-K-Ca geothermometer (Fournier & Truesdell 1973) yields the highest values for V2 fluids (apart from the Na-Li geothermometer which consistently gives the highest temperatures), with temperatures ranging from 203-243°C (Table 3.17). The lower limit of 203°C thus provides an estimate of the minimum temperature reached during D2.

Na-Li geothermometry on V1 fluids yields temperatures of 285-369°C (Table 3.17) in broad agreement with, or slightly higher than, those estimated by other means. This suggests that the fluid-mineral equilibria controlling the Na/Li ratio during D1 have a comparable effect to those which were implicit in the calibration of the geothermometer. By analogy, the Na-Li geothermometer may be expected to give a reasonable estimate of the temperature of V2 fluids, assuming they were also in equilibrium with the wallrocks. The observation of limited wallrock alteration around some V2 veins (see 3.6) casts doubt on the general validity of this assumption. Nevertheless, Na-Li temperatures of 275-305°C (with the exception of *J99BR* which gives temperatures of 340-345°C and

displays a significant CO_2-rich fluid inclusion overprint), are in the range expected for V2 fluids *i.e.* below peak metamorphic temperatures and above the temperature minimum discussed above. Thus, V2 fluids probably ranged in temperature from *c.*300°C to *c.*200°C during the course of D2.

The combination of the isochores constructed for V2 fluids and the temperature constraints described above limit the fluid pressures developed during D2 to between 0.5 and 1.3 kbar (Fig. 4.6).

Summary

The combination of the isochores and the independent temperature constraints discussed above limit the P-T trapping conditions of V2 fluids to 203-305°C and 0.5-1.3 kbar. A P-T-time path may be plotted between the P-T conditions determined for V1 and V2 fluids (Fig. 4.6). This line represents the P-T evolution of fluids mobilised during thin-skinned thrust tectonics in south Cornwall, from peak regional metamorphism through the subsequent uplift and erosion history of the nappe pile.

4.3.2 V2 fluid source and fluid-rock interaction

Volatile components

The most obvious change in volatile components from V1 to V2 is the increase in the proportion of CO_2. Fluid inclusion evidence indicates that the increases in CO_2 recorded in bulk analyses (section 3.4) are not solely due to an increasing proportion of CO_2 in typical, H_2O-rich V1/V2 inclusions, but also to apparent overprinting by, or possible cogenetic formation of, low density, CO_2 vapour-rich inclusions.

There are two likely explanations for the increased proportions of CO_2 and N_2 in V2 vein samples, as recorded by bulk analyses:

(1) Oxidation of carbonaceous material in the wallrocks;
(2) Overprinting by CO_2- and N_2-rich fluids.

(1) Oxidation of carbon in V2 vein wallrocks would result in an increase of CO_2 in the fluid relative to H_2O. Furthermore, such a process could also result in an increase in the proportion of nitrogen as a result of additional oxidation of NH^{4+} (contained in sheet silicates) in the rock, according to:

$$3O_2 + 4NH_4^+ = 2N_2 + 4H^+ + 6H_2O$$

Such fixing of oxygen in the wallrocks would be expected as a consequence of decreasing fluid fO_2 on cooling. The calculated fO_2 for V2 fluids (see 4.3.7) indicates a significant decrease in oxygen fugacity from V1 to V2, supporting this interpretation. The reaction considered above implies a decrease in pH, which is also supported by V2 fluid data (see 4.3.6).

(2) The second possibility, suggested by the fluid inclusion study, is that the CO_2-rich fluid inclusions present in V2 samples are solely the result of an overprint by later, CO_2-rich (V3-type) fluids. In this case, the high CO_2 contents recorded by bulk analysis are due to the measurement of mixed fluid

inclusion populations.

The qualitative correlation between abundance of low density CO_2-rich inclusions in a sample and bulk CO_2 content suggests that the presence of the CO_2-rich inclusion population is the cause of the bulk CO_2 increase. However, a change in fO_2 causing an increase in X_{CO2} cannot be ruled out as the primary control, since this could cause unmixing of a CO_2-rich vapour, producing the observed inclusion assemblage.

The fluid inclusion data do not support the theory that the CO_2-rich inclusions were produced by unmixing of a typical V2 fluid. The distinctly higher *Th* values for the CO_2-rich inclusions (V2 type 3), and presence of associated moderately liquid-rich (V2 type 2) inclusions (see Figs. 3.9 and 3.11), suggest that they may have been produced by unmixing of a different fluid. This hypothesis of overprinting by an unmixing fluid is preferred in the absence of evidence to the contrary. The similarities between the high *Th* "unmixing" inclusion assemblage in V2 samples and V3 fluid inclusions suggest that trapping of V3 fluids in microfractures in V2 samples is a plausible explanation.

Solute components

An identical approach to that used to evaluate mineral-fluid equilibria during D1 (see discussion of solute components, section 4.2.2) has been used to examine fluid rock interaction during D2. An activity diagram for the NaCl-KCl-SiO_2-H_2O-HCl system at 250°C and 800 bars has been constructed (Fig. 4.7), using the same modified Redlich-Kwong (MRK) equation of state and thermodynamic data referred to in section 4.2.2 (see Sverjensky 1987 for details). A pressure of 800 bars and temperature of 250°C were chosen as representative of the average conditions prevailing during D2.

Plotted on the diagram (shaded region) is the field of V1 fluids defined in section 4.2.2. The V1 fluids lie just in the stability field of muscovite at 250°C and 800 bars. Straight lines of constant Na/K atomic ratios are also shown, with the hatched area representing the range of Na/K ratios determined for V2 fluids by D-ICP (see Table 3.14).

The Na^+/H^+ and K^+/H^+ ratios for V2 fluids are consistent with their origin as V1-type fluids which have flowed down temperature and pressure gradients to be trapped in D2 structures. The fact that V2 fluids are probably not in equilibrium with the wallrocks, as evidenced by alteration of albite to sericite (see 3.6), lends further support to this hypothesis. Figure 4.7 shows that a fluid of V1 composition at 250°C and 800 bars is not in equilibrium with albite, lying in the muscovite stability field. This means that a fluid of this composition flowing through D2 structures will react with albite in the wallrocks to produce K-mica. As this reaction proceeds, the fluid will become gradually enriched in Na, approaching the composition which would be in equilibrium with albite and muscovite at 250°C and 800 bars. The degree of fluid-rock disequilibrium is slight, which explains the limited sericitic alteration observed, even in zones of pervasive fluid-rock interaction (*e.g.* D2 "shear zones"; see 1.3.3). Another consequence of this reaction is the release of silica, which may either be precipitated in association with K-mica or taken into solution depending on pH and local P-T conditions. Sericitic alteration in, and removal of quartz from, S_2 cleavage domains (see 2.2.6, 2.2.7) attests to the local importance of deformation processes in controlling solution chemistry.

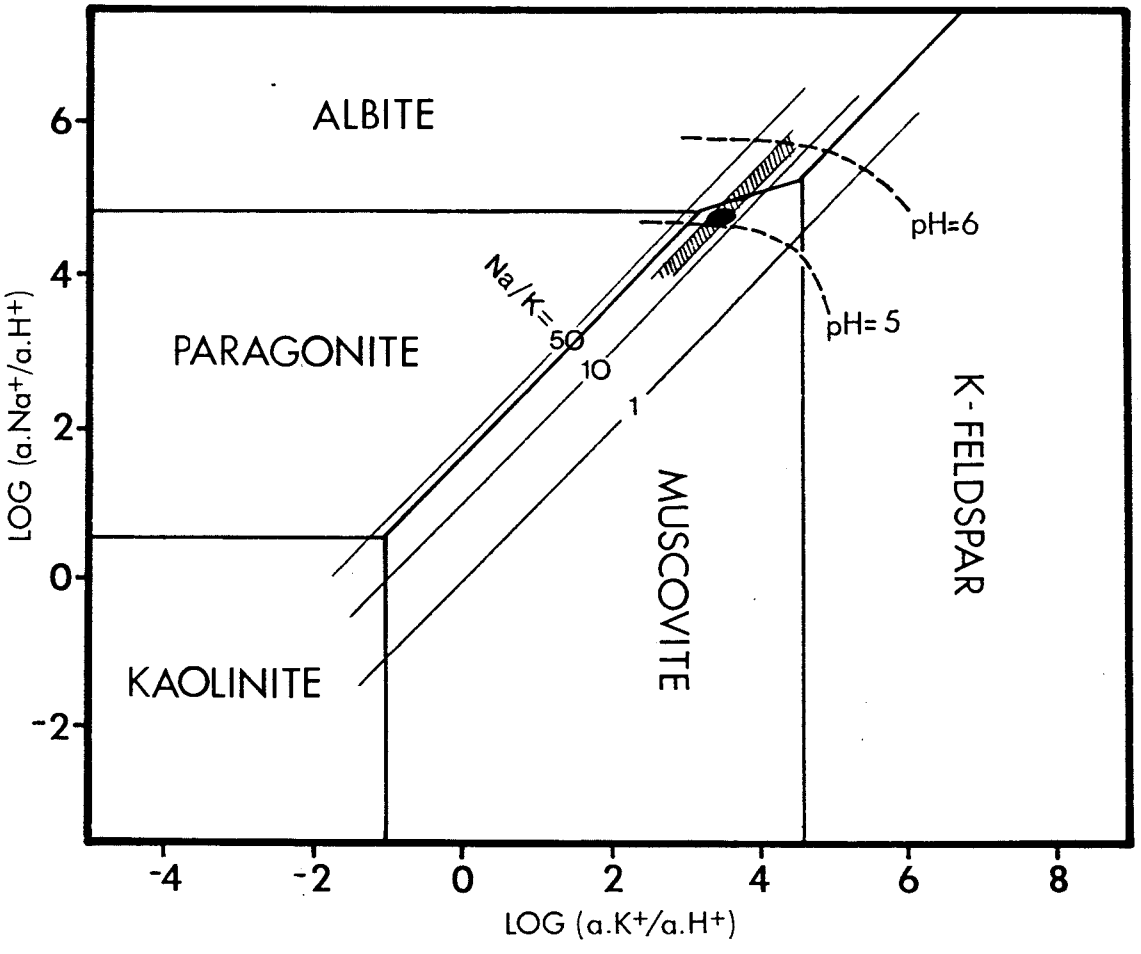

Figure 4.7 Activity diagram for the system NaCl-KCl-HCl-H_2O-SiO_2, constructed for 250°C, 800 bars.

Summary

The evidence discussed above indicates that the V2 fluid was probably sourced at depth and flowed through major structures to higher levels. Slight disequilibrium between the fluid and the lower temperature rocks into which it flowed resulted in limited wallrock alteration, with albite breaking down to K-mica.

4.3.3 Structural controls of V2 fluid composition

Despite the relatively limited data set, it is fairly clear that there are no systematic variations in the major element composition of V2 fluids as a function of the structure through which the fluid was flowing (Table 3.14). This is not surprising if the majority of V2 fluids were sourced at depth and flowed primarily along D2 thrusts, locally entering dilatant structures and S_2 cleavage domains. Similar fluids would be trapped in any of these settings.

The salinity of fluids flowing along D2 thrusts tends to be higher than observed for other D2 structures (Fig. 4.8). This phenomenon, interpreted as being due to increased fluid-rock interaction

and retrogression in these zones of higher strain and higher fluid-rock ratios, is discussed further in section 4.3.5

4.3.4 Spatial variations in V2 fluid composition

Unfortunately, the samples studied do not allow a thorough evaluation of local controls of fluid composition during the D2 event. It was not possible within the time constraints of the study, and with the outcrop available, to select and study a range of samples which would allow isolation of one variable of interest, whilst keeping other factors constant. Despite these problems, several generalisations may be made about variations in V2 fluid composition and controls thereof.

Alkali metals

The alkali content of V2 fluids is extremely consistent and no systematic trends are apparent. The lack of variations in V2 alkali content attests to the homogeneity of the source fluid (the alkali homogeneity of V1 fluids was demonstrated in section 4.2.2), and to the similarity of any subsequent compositional changes. This is probably due to the ubiquitous presence of Na-feldspar/K-mica assemblages controlling the relative alkali content of the fluids. Small fluctuations in Na/K ratios and the observed development of disequilibrium fluid compositions can be explained by the limited buffering capacity of this assemblage. This may be as a result of the restricted occurrence of one or more of the phases of the buffering assemblage in any one place, and/or high fluid-rock ratios (so that equilibrium was not attained).

Alkali earth metals

As with V1 fluids, the alkali earth content of V2 fluids (Table 3.16) shows significant variation (over an order of magnitude for Ca and Mg). In particular, there appears to be no obvious reason why certain samples have distinctly low Na/Ca ratios. Unlike V1 fluids, there is no correlation between these samples and the distribution of ankeritic host rocks. These observations may be explained if, as proposed, the V2 fluids were sourced at depth and did not reached equilibrium with the host rocks at the site of trapping. The alkali earth contents may thus reflect fluid compositional heterogeneity at source, or heterogeneity derived by interaction with differing lithologies during upward flow.

Transition metals

There are relatively low levels of transition metals in V2 samples (Table 3.16) and these bear no obvious relation to host rock composition. As mentioned in section 4.3.3, $V2_T$ samples tend to contain higher levels of these elements, being closer in transition metal composition to the proposed source fluid (V1). This may be due, in part, to the higher salinity of these fluids, resulting in a greater degree of complexing by Cl^-.

4.3.5 V2 fluid salinity

As discussed in section 4.2.5, it is difficult to quantitatively model the salinity of a metamorphic fluid. However, it is possible to propose a variety of processes which may result in changes in fluid salinity. Prograde metamorphic reactions may be expected to reduce the salinity of pore fluids by the preferential release of H_2O with respect to Cl^- (see 4.2.5). Conversely, fluid salinity may be increased during retrogression (hydration) of a peak metamorphic assemblage by preferential incorporation of H_2O in the rock. Evidence for the operation of the latter process has been widely observed, particularly in the retrogression of marbles (*e.g.* Crawford *et al.* 1979).

The increase in salinity between V1 and V2 fluids may be explained by retrogression during D2. The salinity determinations for individual inclusions indicate that this trend is not an artefact which could be produced, for example, by the introduction of late, secondary saline fluids (*e.g.* a V3 type 3 fluid overprint). Figure 4.8 shows how V1 fluids evolve progressively towards V2 compositions in terms of salinity and inferred trapping temperature (determined using the estimated P-T-time path for D1 and D2 shown in Fig. 4.6).

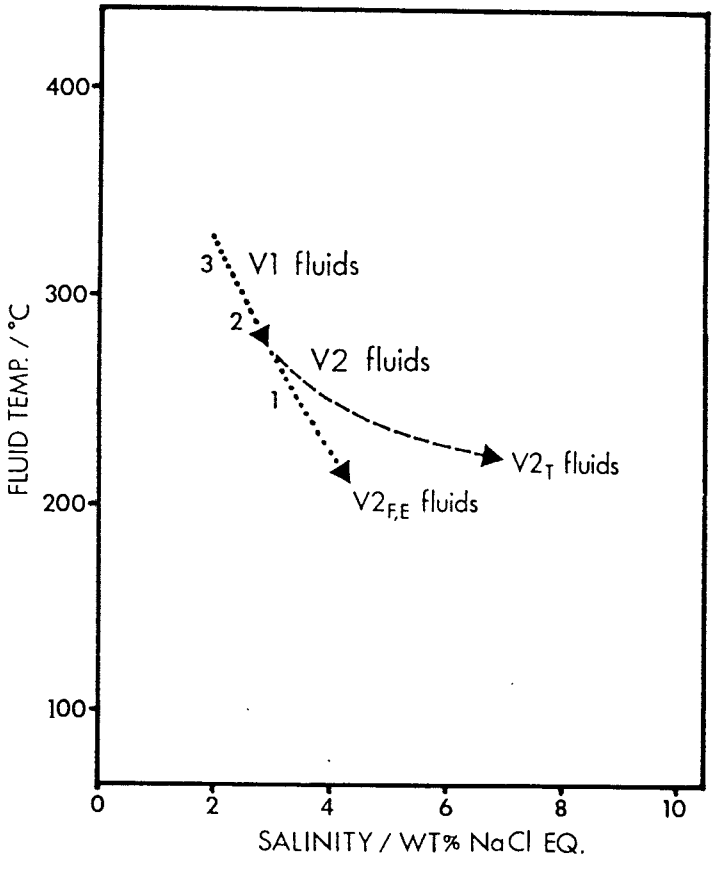

Figure 4.8 Diagram showing the fluid temperature - salinity evolution of V1 and V2 fluids. Note increased salinity of fluids flowing along thrust planes ($V2_T$ veins).

The trend of increasing salinity, which is particularly apparent in $V2_T$ samples, is interpreted as being the result of sericitisation of feldspars and chloritisation (*i.e.* rehydration) during D2. The importance of these processes has already been discussed, particularly regarding the alkali content of V2 fluids (see 4.3.2). The increase in salinity can be regarded as due to the effective removal of H_2O from the fluid during the production of more hydrated assemblages.

Enhanced fluid-rock interaction in D2 thrust zones, characterised by pervasive (microfracture and/or grain boundary flow) and abundant fracture-controlled fluid flow, promotes more extreme retrogression. This can account for the elevated salinities observed in $V2_T$ fluids. Greywacke and slate-hosted disseminated mineralisation in such zones (see 1.3.5) provides evidence for pervasive V2 fluid flow.

It should be emphasised that the development of chloritic alteration is even more effective at increasing retrogressive fluid salinity than sericitic alteration. One formula unit of chlorite (containing 8 atoms of Si+Al) contains 16 OH-groups, compared to 2 OH-groups in muscovite. In addition, petrographic evidence and preliminary XRD studies of wallrock alteration around V2 veins (see 3.6) indicate that chloritic alteration is probably more important than sericitic alteration in this environment.

4.3.6 V2 fluid pH

The activity diagram constructed for V2 fluids at 250°C and 800 bars may be used to estimate fluid pH, as discussed for V1 fluids (see 4.2.6). The modal V2 salinity of 3.1 wt% NaCl equivalent (equivalent to 0.53 molal chloride) was used in the calculations. Isopleths for pH 5 and pH 6 are plotted on the V2 Na/K activity diagram shown in Figure 4.7. Assuming that V2 fluids were sourced from depth and had similar compositions to the V1 fluids (see Fig. 4.7), the estimated pH is 5.1. If V2 fluids were in equilibrium with K-mica and albite (conflicting with petrographic evidence) the pH would have been 5.4. The fact that K-mica is clearly stable in the presence of V2 fluid whereas albite is not implies that a pH of 5.4 for V2 fluids at 250°C is a maximum estimate.

Discussion

The decrease in pH from V1 to V2 is probably primarily controlled by the temperature dependence of the HCl dissociation constant. With decreasing temperature, the dissociation constant for the reaction:

$$HCl^\circ = H^+ + Cl^-$$

increases dramatically (over 1.5 log units for each 100°C decrease in temperature), as solvated ions become increasingly more thermodynamically stable (Fig. 4.9). A pH decrease would therefore be expected as a natural consequence of cooling in many fluid systems (*e.g.* Brimhall & Crerar 1987).

4.3.7 Oxygen fugacity

An identical procedure to that described in section 4.2.6 was used to estimate the oxygen fugacity during D2, at 250°C and 800 bars. Due to the problems with possible V3 overprinting of V2 fluid inclusion assemblages (see 4.3.2), bulk volatile data for samples with no obvious CO_2-rich inclusions were used in the calculations. Using an estimated X_{H2O}=0.9743 and X_{CH4}=0.0004, the calculated log(fO_2) is -36.8. This represents a decrease in fO_2 of 6 log units relative to V1 fluids.

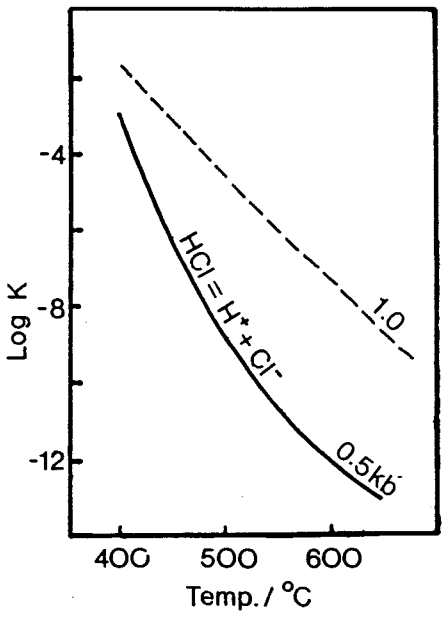

Figure 4.9 Temperature and pressure dependence of the dissociation constant of HCl (from Eugster 1986).

Discussion

The decrease in oxygen fugacity from V1 to V2 is a natural result of the strong temperature control of C-O-H fluid equilibria in graphite-buffered systems. Assuming that high temperature (V1-type) fluids migrate upwards along major zones of permeability into cooler host rocks as discussed in section 4.3.2, they will be out of equilibrium both in terms of their solute content (see 4.3.2) and in terms of their oxygen fugacity. The response of the fluid will be to reduce excess oxygen by oxidation of relatively reduced species in the wallrock, *e.g.* carbon, NH_4^+ and possibly Fe^{2+} (held in chlorite for example). Thus, a V1 infiltration mechanism, which can account for the solute composition of V2 fluids, can also explain the volatile composition, particularly the increases in CO_2 and N_2.

A problem with the interpretation of graphite buffering of C-O-H species in V1 and V2 fluids is the possibility of a temperature-related kinetic control of graphite-fluid equilibration. It has been suggested that such a mechanism may have controlled the fluid volatile composition during a contact metamorphic event in the Massif Central, France (Ramboz *et al.* 1985), with graphite-fluid equilibration blocked below 370°C. Below this temperature, the composition of the C-O-H fluid is controlled by internal equilibration of the component species and reactive species in the wallrocks. Although a real possibility, the data obtained in this study do not provide any evidence of the operation of such a kinetic-blocking process. Both V1 and V2 fluid compositions can be explained in terms of graphite-fluid equilibria.

4.3.8 Sulphur fugacity

The sulphur fugacity and subsequently fH_2S and fSO_2 were calculated for V2 fluids as described for V1 fluids in section 4.2.8. Application of the expression for fS_2 of Poulson & Ohmoto (1989) (Eq. 4.23) yields a log(fS_2) of -13.6. Equations 4.21 and 4.22 give fH_2S = -2.1 and fSO_2 = -11.6 respectively. The significance of these values lies in their importance in controlling metal solubility and ore deposition (see 5.3).

4.3.9 Summary of fluid evolution during Hercynian compression

Fluid inclusion data provide evidence of the continuous nature of fluid evolution during active thrusting in south Cornwall. Internally buffered fluids were evolved during peak regional metamorphism as a result of prograde devolatilisation reactions. These low salinity, H_2O-rich fluids had alkali contents buffered by albite + muscovite ± paragonite assemblages. The rocks of the Portscatho Formation exposed in the study section were at a depth of the order of 13 km when maximum temperatures of 330±20°C were attained at fluid pressures (≈lithostatic pressure) of 3.4±0.5 kbar. This corresponds to a low average geothermal gradient of 26°C km^{-1}, typical of thickened continental crust (see 6.1).

Imbricate thrusts active during D2 acted as important channelways for the upward migration of metamorphic fluids still being generated at depth. These fluids were in slight chemical and possibly thermal disequilibrium with the rocks into which they flowed, resulting in limited sericitic and chloritic alteration.

The transition from V1 to V2 fluids was accompanied by a decrease in pH from 5.4 to 5.1, primarily as a result of the increasing dissociation of acid species with decreasing temperature. Salinity increases were probably the result of retrogressive hydration reactions which occurred in zones of high fluid flux. Oxygen fugacity decreased from $10^{-30.8}$ to $10^{-36.8}$ bars, primarily as a result of the temperature drop. These changes in fluid and rock composition may be represented by a balanced equation of the type:

$$2\ CH_4 + 2\ H_2O + 5\ O_2 + HCl^\circ + 4\ K^+ + 6\ Fe^{2+} + 12\ NaAlSi_3O_8 \text{ --> }$$
$$4\ KAl_3Si_3O_{10}(OH)_2 + 2\ Fe_3O_4 + 24\ SiO_2 + 2\ CO_2 + 12\ Na^+ + 5\ H^+ + Cl^-$$

Although such a reaction is obviously a simplification of the actual processes that occurred, it does adequately describe the major changes in rock mineralogy and fluid composition during retrogression and uplift of the nappe pile. In reality, the iron on the right hand side of the reaction would probably be primarily present in chlorite, since chlorite is known to be produced during syn-D2 rehydration.

4.4 GRANITE INTRUSION AND CONTACT METAMORPHISM

Recent studies of fluid flow and contact metamorphism associated with intrusive activity suggest that high fluid fluxes are common (*e.g.* Ferry 1989). Mathematical modelling of both plutonic and epithermal systems indicate that fluid convection will occur where sufficient permeability is developed (*e.g.* Norton & Knight 1977). There are three common sources for the fluids which become involved in such convective systems: magmatic fluids, metamorphic fluids (produced by contact metamorphic devolatilisation), and meteoric fluids.

Previous studies of the role of convective hydrothermal circulation in southwest England have concentrated on essentially post-magmatic events (Jackson *et al.* 1982; Fehn 1985; see 4.5) involving

magmatic and meteoric waters. Few workers have considered the possible involvement of contact metamorphic fluids in the early (syn-intrusion) history of the Cornubian batholith. A small number of studies have addressed this problem (Jackson *et al.* 1982; Primmer 1985), yet the role of such fluids remains unconstrained.

The V3 fluids of the present study provide the first direct evidence concerning fluids mobilised in the contact metamorphic aureole of the Cornubian batholith during granite emplacement. In this section, the possible source or sources of these fluids are considered, and the evidence for the possible involvement of contact metamorphic fluids in convective circulation is evaluated. In addition, the P-T-X evolution of these fluids is discussed with particular emphasis on the importance of unmixing during the V3 fluid event.

4.4.1 Evidence for immiscibility

A number of criteria must be met by a fluid inclusion assemblage before immiscibility between two inclusion fluid types can be demonstrated. The term "immiscibility" is used here in the general sense, to indicate separation of two phases of contrasting composition and density. This process is often termed "boiling" for H_2O-rich fluids. The characteristic features of a fluid inclusion population resulting from fluid immiscibility, discussed by Ramboz *et al.* (1985), are listed below:

(1) Coexisting fluid inclusions with variable phase proportions

(2) Homogenisation of inclusions to L, V or critical over the same *Th* range

(3) Compositions of coexisting fluids in agreement with experimental data

V3 fluid inclusions, as described in section 3.2.4, meet these three conditions. Optical observations show that fluid inclusions with similar morphologies but with widely varying compositions apparently coexist in V3 vein samples. *Th* data show that CO_2 vapour-rich and H_2O liquid-rich inclusions homogenise to vapour and liquid respectively (occasionally critical) over similar temperature ranges (Fig. 3.38). The extension of vapour homogenisation to higher temperatures indicates that heterogeneous trapping of non-equilibrium compositions is common for low density fluids. This is probably the result of preferential wetting of the growing quartz crystal surface by the H_2O-rich phase, which, coincidentally, will be carrying most of the silica required for crystal growth to the precipitation site. A thin film of H_2O-rich liquid is thus trapped with the CO_2-rich phase, resulting in anomalously high *Th* values.

A plot of *Th versus S* for V3 inclusions (*S* estimated variously from ice melting, clathrate melting or halite dissolution) is shown in Figure 3.38. The vapour-rich inclusions represent trapping of low *D*, low *S* fluids, whereas the liquid-rich inclusions represent trapping of coexisting moderately to highly saline, high density fluids. Such solute partitioning is expected in unmixing fluids as salts are much more soluble in the H_2O-rich liquid phase. A plot of bulk inclusion density against *Th* (Fig. 4.10) also illustrates the unmixing process, showing fluids of contrasting densities coexisting with each other over the same range of *Th*.

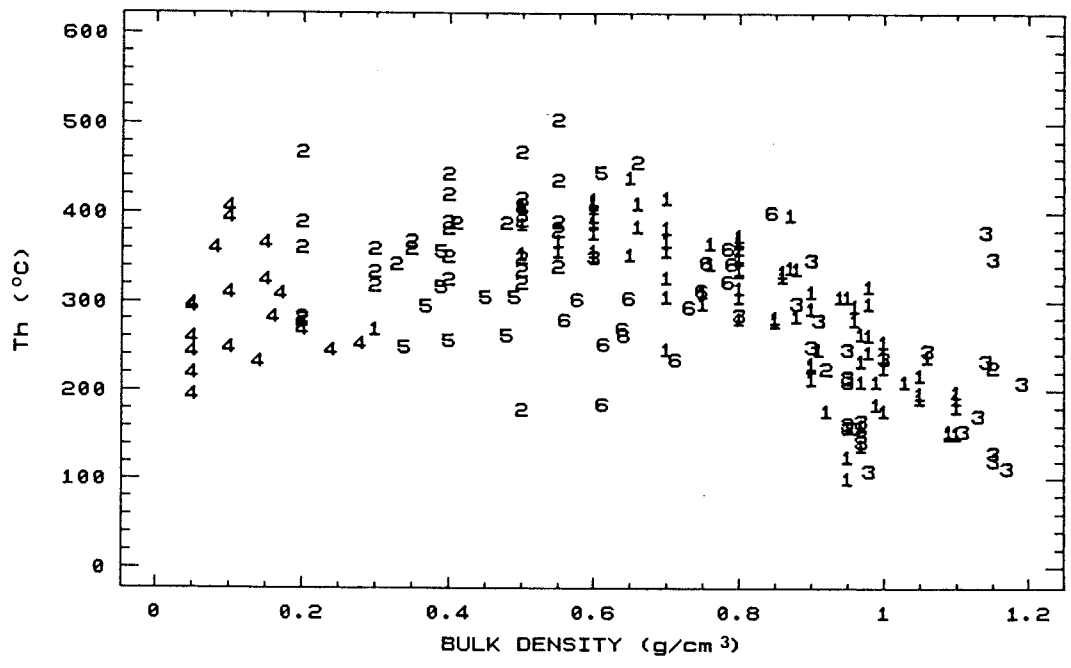

Figure 4.10 Plot of *Th vs.* bulk density for V3 fluid inclusions, illustrating unmixing of two fluids of contrasting composition. Numbers refer to V3 inclusion type.

Calculation of inclusion compositions was carried out using the following formulae:

$$\text{Wt\% } CO_2 \text{ (C)} = \frac{100 \times F_{CO2} \times D_{CO2}}{(F_{CO2} \times D_{CO2}) + (F \times D_{H2O\text{-}NaCl})} \quad \text{...(4.24)}$$

$$X_{CO2} = (C/44)/\left(\frac{C}{44} + \frac{S(100-C)}{5850} + \frac{(100-C)(100-S)}{1800}\right) \quad \text{...(4.25)}$$

These data for the complete range of V3 fluid inclusion compositions are plotted as a function of *Th* (Fig. 4.11). A broad solvus is defined, representing trapping of coexisting fluids over a range of P-T conditions (hence the spread in the data). Also shown on Figure 4.11 are a series of solvi determined experimentally for a range of pressures and fluid salinities (Gehrig 1980; Bowers & Helgeson 1983b). The close correlation between V3 data and the solvi for 500-1000 bars and 6 wt% NaCl supports the conclusion that two immiscible fluids were coexisting at this stage. The fact of immiscibility implies that the fluids were trapped on the solvus, hence *Th* is equivalent to trapping temperature (400-200°C). The close agreement between temperatures estimated by alkali geothermometry (see 3.3.1), temperatures suggested by the (apparently) coexisting mineral assemblages (see 1.3.4, 4.4.2) and *Th* values, also supports the conclusion that fluid trapping temperatures were the same as measured *Th* values. This is further evidence in favour of an unmixing hypothesis for V3 fluids.

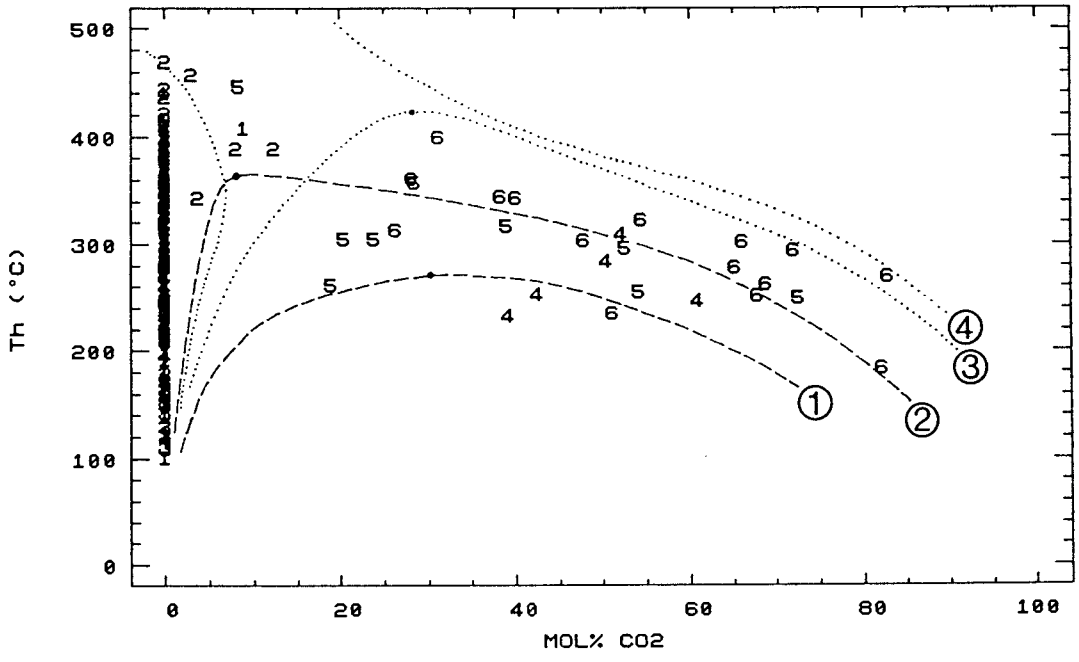

Figure 4.11 Plot showing variation in calculated CO_2 composition with *Th*, V3 fluids. Numbers refer to V3 inclusion type; note large body of data with no visible CO_2. Dashed curves represent solvi in the H_2O-CO_2 system: 1. 1000 bars; 2. 500 bars. Dotted lines are solvi in the system H_2O-CO_2-6wt% NaCl: 3. 1000 bars; 4. 500 bars. Data from Takenouchi & Kennedy (1965) and Gehrig (1980).

4.4.2 P-T conditions during contact metamorphism

A combination of methods may be used to estimate the P-T conditions that prevailed during the contact metamorphic event. As mentioned above, a combination of V3 fluid inclusion data and experimental measurements may be used to estimate the fluid pressure and temperature during unmixing. Alternative sources of information include alkali geothermometry, which has limitations because of the requirement of chemical equilibrium (see 3.3.1 for discussion), and the stabilities of contact metamorphic minerals.

Fluid inclusion constraints

As discussed in section 4.4.1, the conclusion that two immiscible fluids coexisted during or late in D3 implies that *Th* values are equivalent to fluid trapping temperatures. As a result of non-equilibrium trapping of the low density fluid (see 4.4.1), *Th(V)* measurements are often anomalously high. In addition, V3 type 1 fluid inclusions are observed which probably postdate the immiscible fluid stage and did not coexist with a low density fluid (see 3.2.4). For these reasons, the *Th* range (and hence fluid T range) estimated for the unmixing fluids is taken as the range over which both vapour and liquid homogenisation was observed. The upper temperature limit is thus given by the maximum

Th(L) values. This approach yields a temperature range of 400-200°C for the unmixing event.

Pressure may be estimated by comparison of fluid compositions determined by microthermometry with experimental data (see 4.1.1; Fig. 4.11). The T-X_{CO2} relations of V3 fluids are consistent with T-X_{CO2} data for a CO_2 - H_2O - 6 wt% NaCl fluid at 1000-500 bars. The errors involved in the estimation of phase proportions and resulting uncertainty in X_{CO2} estimates mean that trapping pressure cannot be more tightly constrained. Other problems include the uncertainty in the bulk NaCl content and limited information concerning its effect on the H_2O-CO_2 solvus, and the effects of other gases (*e.g.* CH_4, N_2) and solutes on P-V-T properties in quaternary and higher systems. It is assumed in the present study that the effects of additional, minor components are not significant and the fluids may be adequately modelled by the CO_2-H_2O-NaCl system.

Summary

Structural observations (see 2.2.8 to 2.2.10) are consistent with the majority of V3 veins forming late or post-D3, implying that much of the V3 fluid activity in the study section was contemporaneous with the final stages of batholith emplacement and/or intrusion of the Tregonning granite stock. The fluid data discussed above constrains the pressure at this stage to between 1000 and 500 bars; the fluid trapping temperatures between Tregear Point and Porthleven Sands (Fig. 1.4) are estimated at 400-200°C. Peak contact metamorphic temperatures in the same part of the section are estimated at 450-300°C from the presence of the "biotite in" and "hornblende in" isograds in metabasites (Fig. 1.4).

4.4.3 Fluid source

The timing of V3 fluid mobilisation is well constrained to late or post-D3 (except perhaps for $V3_C$ fluids which may be slightly earlier; see 2.2.8) and contemporaneous with stock-related contact metamorphism. However, the source of the V3 fluids is uncertain. Possible sources include magmatic fluids, expelled from granitic melt as it crystallised; contact metamorphic fluid, derived by devolatllisation reactions in the contact aureole; and surface waters, either seawater or meteoric water depending on the palaeogeography at the time.

On the basis of thermometric data and bulk inclusion analyses, the latter sources may be ruled out. Neither the salinity of the fluids nor their chemical composition are consistent with the presence of a significant component of meteoric water or seawater (Fig. 4.12). However, their composition is ambiguous with regard to the other possible sources, namely magmatic fluids and contact metamorphic fluids (Wilkinson, in press).

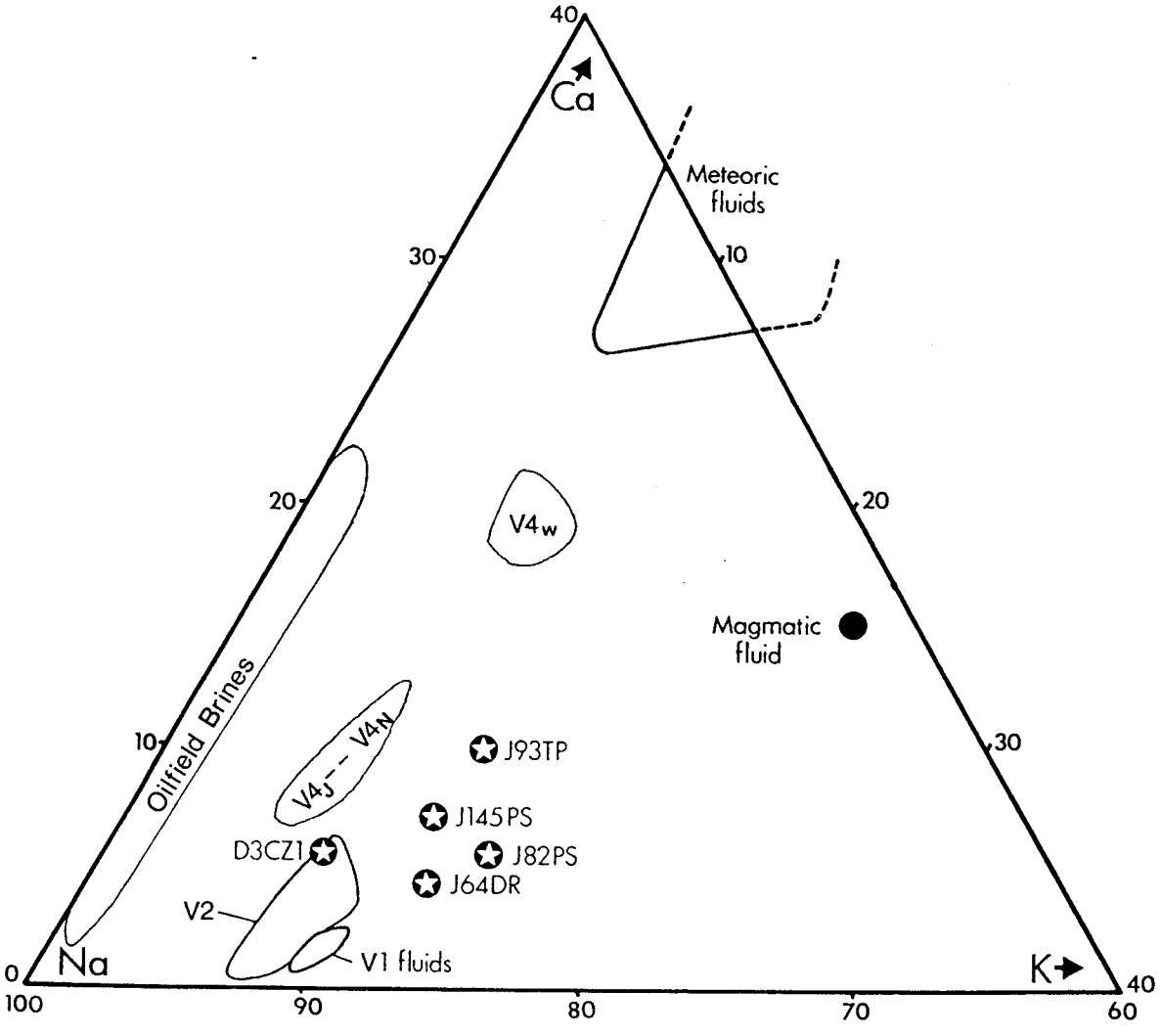

Figure 4.12 Major element composition (by weight) of aqueous fluids from south Cornwall (stars = V3 fluids). Shown for comparison are a number of fields for possible source fluids: meteoric field from data in Rankama & Sahama (1950); magmatic fluid from Bottrell & Yardley (1988); oilfield brines from White (1974).

Volatile components

The amount of water that would be expected to be evolved from a pelite in going from low to high metamorphic grade may be of the order of 2 wt% (*e.g.* Wood & Walther 1986). Thus, significant volumes of water must be evolved in the contact aureole synchronously with granite emplacement. The coincident timing of this fluid release and V3 vein formation indicates that it is extremely likely that H_2O evolved during prograde dehydration was involved in the generation of V3 fluids. However, magmatic fluids will also be H_2O-rich and will be released during granite crystallisation so that they cannot be ruled out as a possible contributor to the V3 fluid budget.

Neither magmatic nor metamorphic fluids are obvious candidates for the relatively CO_2-rich V3 fluids observed. The fluids released from crystallising granitic magmas are thought to contain CO_2, but only in relatively low concentrations (*e.g.* Giggenbach 1988). Fluid inclusions from the Megilligar pegmatites, which formed from late stage, volatile-rich magmas (see 1.3.2) contain <3

mol% CO_2 (see 3.2.5). From this observation, it is unlikely that less evolved Cornubian magmas will contain a significantly higher proportion of CO_2. Even the V3 H_2O-rich fluids (V3 type 1 inclusions) are estimated to contain as much, if not more, CO_2 than this (Appendix D2) so it is unlikely that magmatic fluids are the primary source of the V3 CO_2 component.

The aureole host rocks contain limited carbonate, which would be an obvious source of CO_2 during contact metamorphic devolatilisation. Greywackes of the Gramscatho Group occasionally contain abundant carbonate cement (Fig. 1.4) and the metabasite sills also contain variable amounts of carbonate. The carbonate content of the Mylor slates is unknown, but by analogy with "average" slates (Greensmith 1981), they may have contained up to 10.8 wt% CO_2 and/or up to 11.5 wt% organic carbon prior to metamorphic devolatilisation. Some of this would have been lost during regional metamorphism (see 4.2.2) and it is impossible to estimate the relative proportions of CO_2 and H_2O that would have been generated during contact metamorphism. However, it is possible to conclude that at least some CO_2 must have been evolved in the contact aureole by decarbonation.

An alternative source of CO_2 is from oxidation of organic carbon, contained in kerogens, which are relatively abundant in the Mylor slates. The feasibility of such a mechanism is unknown, although it is perhaps one of the only ways of accounting for the elevated levels of CO_2 observed in the aureole fluids.

The relatively high nitrogen content of V3 fluids (bulk N_2 up to 1.6 mol%; see 3.4) cannot be easily explained solely in terms of a typical magmatic source. However, the relatively high levels of ammonium in slates (contained primarily in micas), documented by Wlotzka (1972) and specifically in southwest England (Hall 1988), indicate that significant quantities of N_2 may be expected in an equilibrium metamorphic fluid, particularly if relatively oxidising conditions prevailed. Organic N-bearing compounds are another possible source of N_2 in the slates which could account for the relatively N_2-rich nature of V3 fluids.

Many workers have argued for the enrichment of "pelitic" components such as CO_2, ^{18}O, NH_4^+ and Sn in the Cornubian granites as a result of assimilation during their ascent. Such a hypothesis, if correct, would mean that fluids driven off the crystallising magmas (*i.e.* Cornubian magmatic fluids) could also be enriched in these components, particularly the volatiles. This argument was used by Miller (1989) to account for the relatively low (-9.8 to -7 ‰) $\delta^{13}C$ values measured for CO_2 of assumed magmatic origin associated with wolframite mineralisation in the Hemerdon tungsten deposit, Dartmoor. The depletion of ^{13}C in this "magmatic" fluid was interpreted as being due to incorporation of low ^{13}C "organic" carbon in the magma, derived from assimilated pelitic material. However, it is possible that the CO_2 was partly sourced in the contact aureole and, if produced by oxidation of organic carbon, would necessarily display ^{13}C depletion. One $\delta^{13}C$ value of -11.9‰, for V3 CO_2 (Table 3.21) supports this hypothesis.

The chicken-and-egg argument discussed above is, at present, unresolved. Further studies will be required to resolve these particular problems.

Solutes

The solute composition of V3 aqueous fluids (Tables 3.14, 3.16) is intermediate between hypothetical "magmatic" and "metamorphic" end-members. Plotting the major element (Na, K, Ca) fluid composition for several V3 samples on a triangular diagram (Fig. 4.12) illustrates a trend of slightly

decreasing Ca with rapidly decreasing K content. Also shown are the composition of fluid inclusions from a quartz-topaz rock from the St. Austell district, Cornwall (Bottrell & Yardley 1988), interpreted as a primary magmatic fluid, and the composition of V1 "equilibrium" fluids (see 4.2.2). The latter fluids, although not involved in contact metamorphism, provide an estimate of what the major element composition of an "equilibrium" contact metamorphic fluid would have been at *c.* 300-350°C).

The V3 fluid trend shown on Figure 4.12 falls between the two end-member fluids discussed above. This may either be interpreted as a magmatic-metamorphic mixing trend or as a magmatic re-equilibration trend. The latter possibility arises because a magmatic fluid flowing outwards into the contact aureole will modify its composition as a result of cooling and reaction with the slates so as to approach an equilibrium (*i.e.* "contact metamorphic") fluid composition. It is extremely difficult to distinguish between these two alternatives, because any compositional parameter which can be measured, including stable isotopic compositions, will display similar values for either process. One approach to solving this problem is by considering the kinetic controls of the magmatic fluid re-equilibration process. Some components of the magmatic fluid would quickly attain equilibrium with the rocks in the contact aureole (*e.g.* K/Mg ratio) whereas others would be relatively slow to adjust (*e.g.* Na/K; Giggenbach 1988). A mixing process, in contrast, would be expected to result in rapid homogenisation of all fluid components. Thus, the Na/K ratio of a magmatic fluid re-equilibrating in the aureole would be lower than would be expected for the appropriate fluid temperature. Although the data are insufficient to provide a convincing argument, the Na/K ratios of V3 fluids are generally higher than would be expected for equilibrium, with conventional Na/K geothermometry yielding anomalously low temperatures (see 3.3.1). On the basis of this evidence, a disequilibrium argument would imply that V3 fluids were derived from a lower temperature reservoir, rather than from a higher temperature source (*i.e.* the granite). Application of the relationships of Lagache & Weisbrod (1977) for a fluid in equilibrium with two alkali feldspars + quartz (*i.e.* granite) yields fluid equilibration temperatures of 300-385°C. These temperatures are comparable with V3 fluid trapping temperatures (see 4.4.2) which suggests that the fluids were not derived from a higher temperature (granite) source, but were derived *in situ* via devolatilisation reactions (Wilkinson, in press).

Salinity

Further evidence in support of a mixing hypothesis comes from the chloride content of the fluids involved. The "magmatic" fluid of Bottrell & Yardley (1988) had an estimated salinity of 3 molal chloride (17.6 wt% NaCl equivalent). Mixing in equal proportions with a "contact metamorphic" fluid of 2 wt% NaCl (comparable with V1 "equilibrium" fluids) would produce a fluid of *c.* 10 wt% NaCl equivalent. This is an appropriate salinity for a V3 parent (pre-unmixing) fluid. Significantly, V3 major element ratios, if interpreted as being purely the result of mixing of magmatic and metamorphic end-member fluids, also suggest mixing of approximately equal proportions of the two fluid types. In addition, estimation of the total amounts of magmatic and contact metamophic water evolved throughout the duration of intrusive activity suggests that similar proportions of the two fluid types may have been generated.

Stable isotopes

Stable isotopic evidence for V3 H_2O-rich fluids (see 3.5) is also ambiguous and can be explained either by fluid-fluid mixing or by isotopic re-equilibration of a magmatic fluid. Sample *J93TP* plots very close to the Cornubian magmatic field defined by Sheppard (1977). The remaining V3 samples display a trend of increasing δD with approximately constant $\delta^{18}O$. Such a trend could be generated by a magmatic fluid flowing into the contact aureole and isotopically re-equilibrating with relatively high δD slates. If the isotopic composition of the slates is taken as $\delta^{18}O = 13.4‰$, $\delta D = -58‰$ (Sheppard 1977), this path may be calculated assuming appropriate fluid-rock fractionation factors. Figure 4.13 shows such a series of paths calculated for 300, 400 and 500°C, and indicates that V3 data are consistent with re-equilibration of a magmatic fluid at low water/rock ratios (0.03-1 by weight).

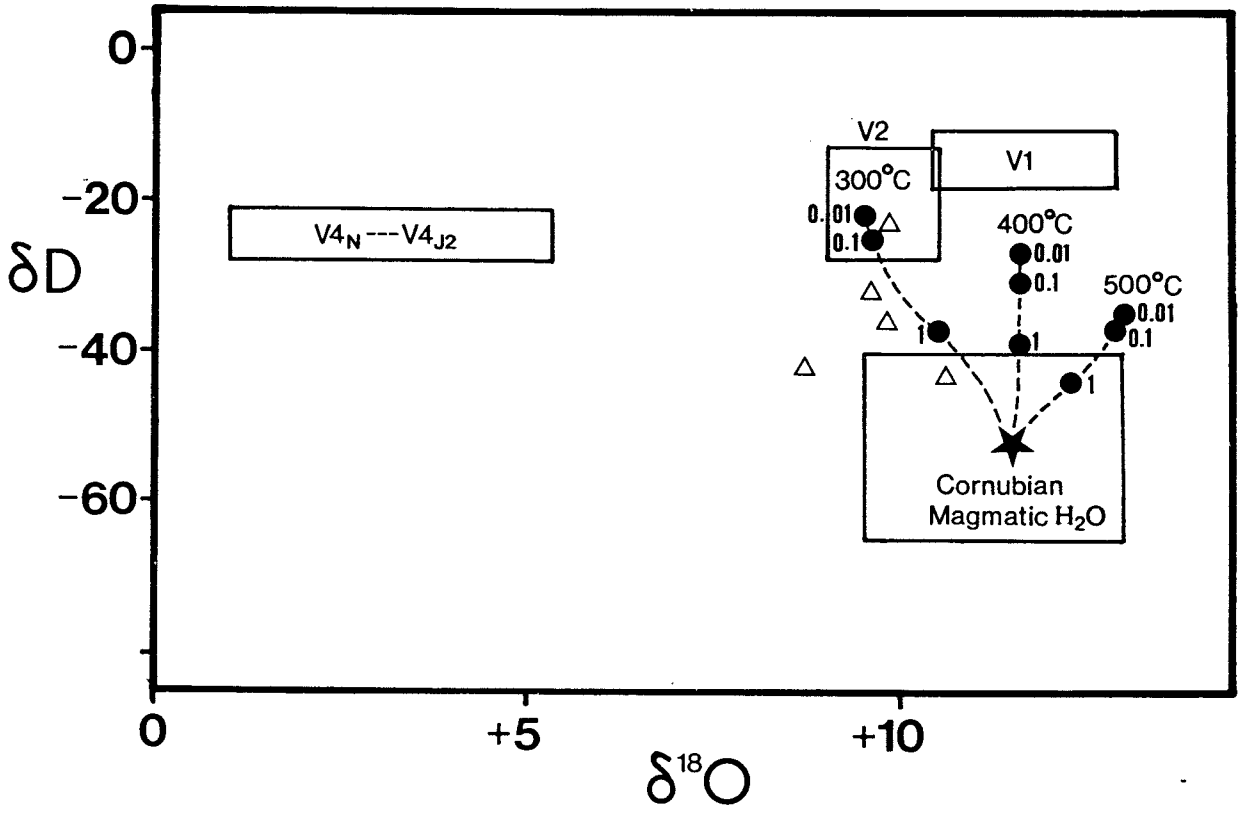

Figure 4.13 Stable isotopic composition of V3 aqueous fluids (triangles) and possible equilibration paths (dashed). Re-equilibration paths were calculated for a magmatic fluid of initial composition $\delta^{18}O = +12$, $\delta D = -52$ (star), flowing into slates with $\delta^{18}O = +13.4$, $\delta D = -58$ (Sheppard 1977) at 300, 400 and 500°C. Numbers on equilibration paths refer to molar ratios of exchangeable oxygen in water to that in the rock (divide by 2 for water/rock weight ratios).

The V3 isotopic data also define a trend between the estimated composition of Cornubian magmatic waters and hypothetical "equilibrium" contact metamorphic water (represented by the V1 field). This indicates that mixing between two such fluids could account for the observed isotopic characteristics. Furthermore, the data suggest mixing of similar proportions of the end-member compositions, in agreement with the evidence from other sources outlined above.

Another significant point is that the fluids which are closest isotopically to Cornubian magmatic fluids (*e.g. J93TP*) are also closest chemically (Fig. 4.12). This is strong evidence that magmatic fluids are, at least partially, responsible for V3 fluid compositions.

The observation made by Giggenbach (1988), that the Na/K ratio of a fluid is slow to re-equilibrate down P, T gradients may be used in conjunction with stable isotopic data as a test to identify whether the V3 aqueous fluids were derived from a high temperature (magmatic) source or whether they were derived effectively *in situ* via devolatilisation reactions. A plot of Na/K ratios for V3 H_2O-rich fluids against the hydrogen isotopic composition of the water (Fig. 4.14) would be expected to yield a straight line for fluid-fluid mixing (since complete chemical and isotopic homogenisation would occur). In contrast, a magmatic fluid that had flowed out into the contact aureole would be expected to equilibrate with respect to hydrogen isotopes much more rapidly than with respect to Na/K, and would result in a curved trend on the diagram, concave towards the Na/K axis. The data for V3 fluids (Fig. 4.14) displays an approximate linear trend suggesting that the former process was operating.

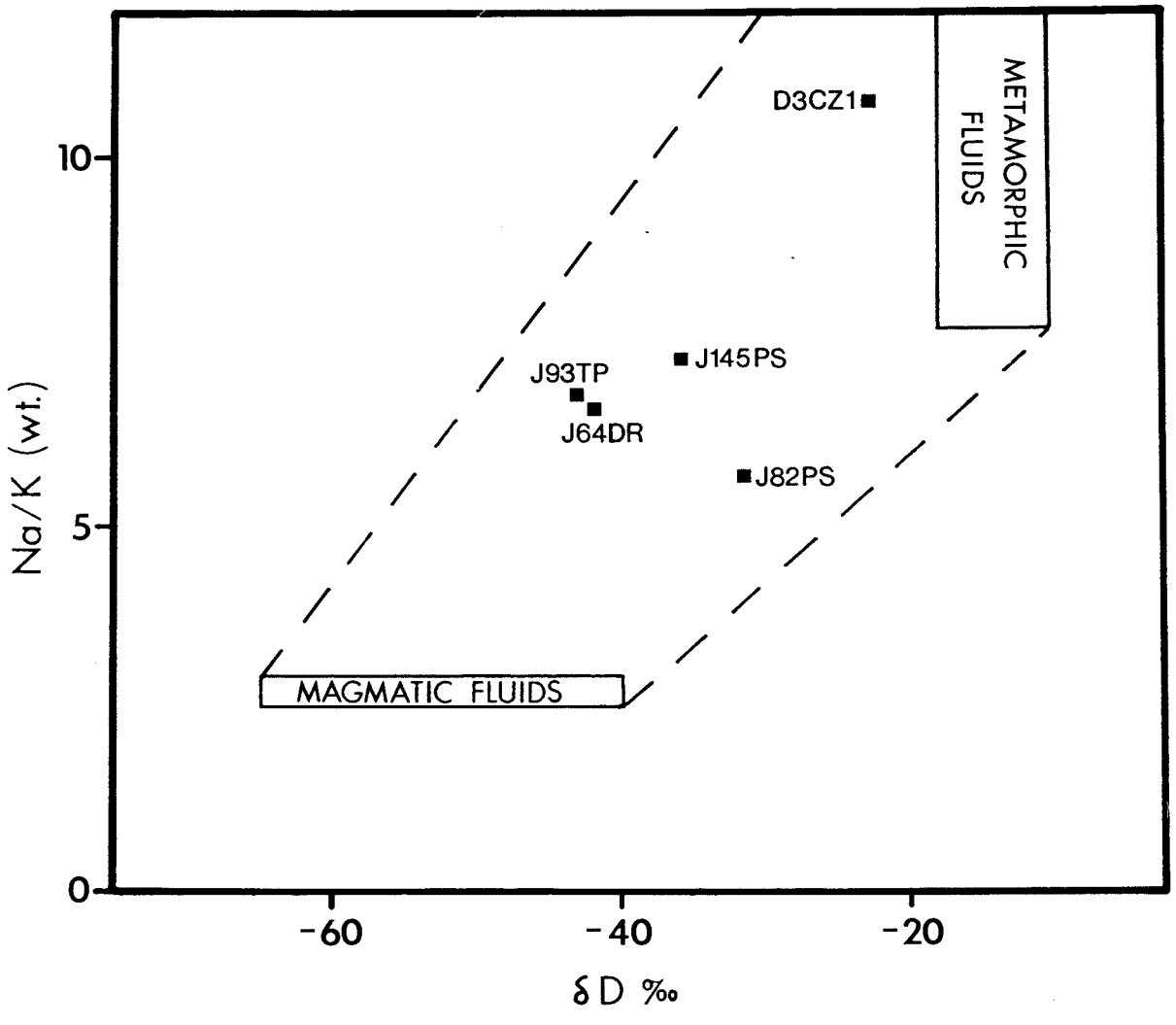

Figure 4.14 Na/K *vs.* δD plot illustrating possible mixing trend for V3 aqueous fluids.

Source of V3 type 6 fluids

Despite the apparent gradation between V3 inclusion types 1-5, type 6 inclusions are more distinct texturally and compositionally. Their estimated CO_2 contents of 28-86 mol% (Appendix D2) and

relatively high bulk density of 0.5-0.8 gcm^{-3} make them difficult to explain by an unmixing process. Such problems, and the common observation of fluid inclusion assemblages dominated by type 6 inclusions, require an alternative explanation.

One possibility is that the inclusions represent a CO_2-rich fluid derived externally by decarbonation of carbonate-rich rocks. The absence of carbonates from the Devonian rocks of south Cornwall (apart from the restricted occurrence of the Veryan limestones within the Gramscatho Group) suggest that this mechanism is unlikely.

A significant observation, which may have implications for the mode of origin of V3 type 6 fluids is the fact that they have only been observed in V3 veins developed at distances >2km from exposed granite. This observation led to the idea that these fluids may represent a condensate of low density, CO_2-rich fluids (V3 type 4 and 5 inclusions), which came into contact with cooler host rocks. Compositionally, they show close affinities with type 5 fluids, lending support to this argument. It is envisaged that vapour, produced by unmixing, separated from its parent fluid and flowed down a temperature gradient to eventually condense to form type 6 fluids. If this occurred contemporaneously with granite emplacement, later stages of intrusion could result in overprinting of veins which were formed by vapour condensates by higher temperature/lower pressure inclusion assemblages (*i.e.* inclusion types 1-5). In the absence of further data it is extremely difficult to demonstrate the validity of this hypothesis.

Summary

There are believed to be two possible sources for the V3 fluids defined in this study: magmatic and contact metamorphic. Although inconclusive, there is some evidence to suggest that the V3 fluids were generated by mixing of similar proportions of the two fluid types. Mixing may have occurred either prior to CO_2-H_2O unmixing, or contemporaneously with phase separation. In the latter case, it is envisaged that moderately saline, H_2O-rich magmatic fluids mixed with contact metamorphic H_2O-CO_2 fluids whilst a low density CO_2-rich phase was unmixing. It is conceivable that the mixing of the magmatic fluid with the metamorphic fluid caused unmixing of CO_2 from the latter fluid by increasing the salinity of the aqueous phase until CO_2 saturation was reached.

It is suggested that the dense, CO_2-rich V3 type 6 fluids represent a condensate of low density, CO_2-rich vapour, produced in cooler, distal parts of the contact aureole.

4.4.4 Spatial variations in V3 fluid composition

As with the previous sample groups discussed, the identification and explanation of spatial variations in V3 fluid composition are hindered by the limited amount of data available. Nevertheless, a number of important points have been brought to light, particularly as a result of microthermometric studies. Compositional variations and variations in fluid inclusion assemblages have been examined, ranging from millimetre-scale variations within one polished wafer, to kilometre-scale variations between different V3 veins.

Vein-scale compositional variations

Detailed fluid inclusion studies of several V3 samples from within a single vein (cm-scale), and from different parts of the same polished wafer (mm-scale) show that significant heterogeneity exists.

Samples *D4PS1* and *D4PS2* came from a 15cm thick $V3_G$ vein, where it cut a greenstone sill and at its termination (1.5 m into slate) respectively. Several fields of view were studied at increasing distances from the vein margin in both samples. The most obvious difference is that *D4PS1* contains a mixture of inclusion types, including V3 type 6, whereas *D4PS2* is dominated by V3 type 4, 5 and 1 inclusions. In addition, type 4 and 5 inclusions display a distinct variation in $TmCO_2$ with distance from the vein margin (Fig. 4.15).

These data indicate that complex variations in fluid P-T-X occurred during and subsequent to vein growth. If the vein growth mechanism is known and the fluid inclusions may be assigned to a primary or secondary origin, then the fluid evolution history can be determined. It is beyond the scope of this study to examine these variations in greater detail. However, the fact that they do exist has important implications regarding the validity of the assumption that one polished wafer is representative of a complete vein, especially where complex fluid evolution is observed.

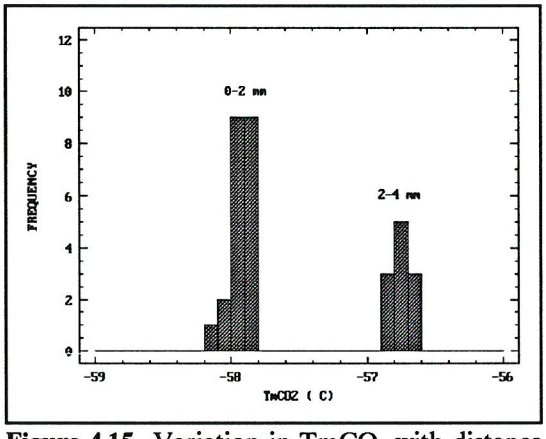

Figure 4.15 Variation in $TmCO_2$ with distance from vein margin (*D4PS1*).

Sample *J93TP* shows evidence of a different type of vein-scale variation in fluid composition. Optical examination of the vein, both in thin section and polished wafer, revealed that V3 type 3 (multi-solid) inclusions are particularly abundant at the vein margins where fibrous actinolite is growing into the vein from the metabasite wallrock. Conversely, quartz in the vein centre is dominated by vapour-rich (V3 type 4) inclusions. This phenomenon is interpreted as being a result of the different physical properties of the two immiscible fluids. The saline liquid would have a much greater viscosity and higher surface tension, preferentially wetting the walls of the propagating fracture. The low density CO_2 vapour phase may tend to be concentrated towards the centre of the fracture. This process could account for the observed spatial separation of the coexisting fluids.

The extent to which the growth of a hydrated phase, such as the actinolite mentioned above, can affect the local composition of a fluid is uncertain. In theory, such a process could increase salinity either by directly decreasing $a.H_2O$ in the fluid, or by increasing X_{CO2} and hence promoting further phase separation.

CO_2-rich fluids in $V3_S$ veins

$V3_S$ veins are developed up to 5 km from exposed granite (Blue Rock zone) and contain several different fluid inclusion associations. Samples proximal to the granite (*e.g. D4GR1, D4GR2*) are dominated by low density CO_2-rich inclusions in association with H_2O-rich inclusions of moderate to high salinity (V3 types 1 & 3). In contrast, $V3_S$ veins >3 km from the granite contain denser CO_2-rich inclusions (types 5 or 6), usually in association with type 1 inclusions. This spatial variation in fluids flowing through contemporaneous structures implies that fluid P-T conditions varied

considerably across the area at this stage. The reasons for these fluctuations were considered briefly in section 4.4.3.

Summary

Complex variations in the V3 fluids trapped in similar structures from different localities, and within single structures through time, indicate that rapid fluctuations in fluid P-T conditions occurred. This is not surprising for the contact metamorphic environment where high P and T gradients can develop. Assuming a depth of 4 km, fluid pressure could fluctuate from ≈1100 bars to ≈400 bars (*cf.* fluid pressures estimated for V3 fluids; see 4.4.2) depending on whether lithostatic or hydrostatic conditions prevailed. In such an environment, P_F could vary between P_L to P_H as fractures sealed or propagated to the near surface. Pressure fluctuations probably played an important role in controlling the umnixing processes discussed in section 4.4.1.

4.4.5 Fluid convection during contact metamorphism

The possibility of convective fluid circulation around plutonic intrusives has been considered by a number of workers (*e.g.* Norton & Knight 1977; Labotka *et al.* 1985; Ferry 1989). Although still a subject of controversy, it seems likely that such circulation, driven by density gradients (largely a function of temperature in H_2O-dominated systems), can occur if sufficient permeability is developed.

There are insufficient data in the present study to confirm syn-intrusive convection during emplacement of the Cornish granites. However, there are several lines of evidence which indicate that transport of fluids over quite large distances did occur and that significant permeability was developed in the slates during granite emplacement. The occurrence of metasomatic mineral growth (*e.g.* tourmaline, ilmenite, arsenopyrite) at distances up to several kilometres from the Tregonning granite (see 1.3.4) suggests that pervasive fluid flow occurred through a large volume of rock during granite emplacement. Such fluid flow was responsible for significant local redistribution of components (*e.g.* Chesher 1971; Jackson *et al.* 1982).

Pervasive fluid flow probably occurred either along the S3 cleavage planes or through microfracture permeability (or both). Numerous secondary microfractures (containing V3 fluid inclusions) are observed in V3 quartz veins, dominantly sub-parallel to the S3 fabric, indicating that such microfracture permeability was developed during the V3 fluid event. The size and frequency of V3 quartz veins is further evidence that significant permeability in the form of macroscopic fractures was also developed during or immediately post-D3 (see 6.1.4).

If a convective system was set up around the batholith during emplacement, and/or around the late stage stocks, there are important consequences for the early stages of granite-related fluid evolution. Not only does such a mechanism provide a convenient means of mixing magmatic fluids expelled from the crystallising granites with contact metamorphic fluids, but it can also explain enrichments of "pelitic" components in the granites by introduction by a fluid phase. Charoy (1986) suggested such a mechanism to account for anomalous geochemical characteristics of late-stage magmas in the St. Austell pluton.

Since fluid convection is driven by density gradients, unmixing to produce low density vapour and dense saline fluid would have a major control on the nature of the convective system. If convection of V3 fluids occurred, the low density vapour would separate from the cogenetic brine and each fluid would follow different flow paths. The vapour would tend to flow upwards and away from the heat source, whereas the dense brines (particularly the V3 type 3 hypersaline fluids) would circulate downwards and towards the granite. As these fluids are capable of transporting significant quantities of metals (see 5.4), this mechanism would be of extreme importance in the genesis of a potential ore-forming solution (Wilkinson, in press).

An interesting observation is that V3 fluids display a number of features which strongly favour fluid convection, assuming sufficient permeability. Their temperature range (200-400°C) is the most favourable for convection of H_2O-rich fluids. This is a result of maxima in heat capacity and ratio of thermal expansivity to compressibility (developing maximum P per unit increase in T) and minima in density and viscosity of H_2O at 300-400°C (Norton 1984; Brimhall & Crerar 1987). In addition, unmixing produces extreme fluid density contrasts, promoting fluid separation and driving convection.

4.4.6 V3 brine pH

The activity diagram calculated for V1 fluids (Fig. 4.3) was used to estimate the pH of V3 brines (V3 type 3 fluids) in a similar manner to that described in section 4.2.6. The use of the diagram for V1 fluids is a valid approximation since the V1 and V3 fluid temperatures are similar, and pressure only has a minor effect on the position of the phase boundaries.

The Na/K activity ratio was determined by estimating the activity coefficients of Na^+ and K^+ from the extended Debye-Hückel equation (see 5.2), and using the average Na/K atomic ratio of 2.9 determined from microthermometric measurements (see 3.2.4). This ratio defines a line on the activity diagram (Fig. 4.3) which passes through the K-feldspar + albite + K-mica invariant point. Assuming equilibrium with these three phases (justified on the basis of alkali geothermometry - see 3.3.1, 4.4.3) and a chloride concentration of 5.75 molal, a pH of 5.7 was calculated for the V3 brines at 330°C.

4.4.7 V3 oxygen fugacity

The oxygen fugacity of V3 brines was estimated by a similar method to that outlined in section 4.2.6, assuming a temperature of 350°C and pressure of 700 bars. Using this approach (*i.e.* assuming equilibrium with graphite), an fO_2 of 1.76×10^{-30} was determined ($\log fO_2 = -29.8$). The additional compositional complexities of the V3 fluids mean that this can at best only be regarded as an order-of-magnitude estimate.

4.4.8 Sulphur fugacity

Assuming fluid-pyrite-pyrrhotite equilibrium (Poulson & Ohmoto 1989), gives $fS_2=7.68x10^{-10}$. The first and second dissociation constants of H_2S may be used to estimate the H_2S fugacity as detailed in section 4.2.8. These yield $fH_2S=0.315$, which is equivalent to a mole fraction of 0.000548. This value assumes a one phase fluid, which is not the case for the V3 system. The concentration of H_2S in the V3 brines, required for mineral solubility calculations (see 5.4), was estimated by consideration of the distribution of H_2S between an aqueous liquid and a coexisting vapour:

$$H_2S_{(aq)} = H_2S_{(g)} \qquad K = \frac{a.H_2S_{(g)}}{a.H_2S_{(aq)}} \approx 25.1 \text{ at } 350°C$$

This gives a value of $a.H_2S$ for the aqueous fluid of $\approx 4.1x10^{-3}$ (equivalent to 140 ppm). This estimate is subject to larger uncertainties than previous determinations and must be treated with caution.

4.5 GRANITE-RELATED FLUID EVOLUTION

4.5.1 Evolution of pegmatite-related fluids

Data obtained in this study are in agreement with previous studies on pegmatite-hosted fluid inclusions both in southwest England (Jackson *et al.* 1982) and elsewhere (Mangas & Arribas 1987), and indicate that pegmatite development is intimately related to the separation of an H_2O-rich fluid from a melt. Such an event is the beginning of a complex fluid evolution history which may involve the development of a mineralising fluid and subsequent generation of an ore deposit.

Typical fluid inclusions from the Megiliggar pegmatite quartz display features indicative of a primary origin (see 3.2.4). These inclusions represent trapping of a moderate density, H_2O-rich homogeneous fluid; here interpreted as a magmatic fluid. In contrast, fluid inclusions from within quartz veins intimately associated with the pegmatite provide clear evidence of the trapping of two immiscible fluids; an H_2O-rich, moderately saline liquid and a low density, H_2O-CO_2 (+N_2, CH_4) vapour. These quartz veins have been interpreted as being formed by the crystallisation of an aqueous fluid which separated from the solidifying pegmatites (Badham 1980). The H_2O-rich fluid inclusions observed are consistent with this hypothesis; the presence of an immiscible vapour phase indicates that P-T-X conditions were such that liquid-fluid immiscibility occurred essentially contemporaneously with melt-fluid separation.

The one-phase fluid observed in the pegmatites and the immiscible fluids present in the "distal" quartz veins are closely related compositionally (see 3.2.5) and in terms of P-T characteristics. The trapping temperature of the pegmatite fluid may be estimated at 500-600°C, based on experimental determination of the granite solidus in B- and F-bearing melts (Manning 1981; Pichavant 1981). The immiscible fluids were trapped on the H_2O-CO_2-NaCl solvus; thus *Th* values of 440-340°C for the high temperature (unmixing) inclusion population (Fig. 3.45) represent fluid

trapping temperatures. Rare critical homogenisation indicates trapping near the solvus crest. Some of the inclusions (type DV1) in the distal veins may have been trapped above the solvus, in which case 600>T>420°C.

A plot of estimated trapping temperature *vs.* salinity for $V4_P$ type P1 and $V4_P$ type DV1/2 fluids (Fig. 4.16) illustrates the possible evolutionary link between them. The data suggest that a moderate density (≈0.7 gcm^{-3}), H_2O-rich fluid separated from the pegmatites during crystallisation and cooling from 600°C. This began to unmix at *c.* 420°C to produce a moderately saline fluid (10-14 wt% NaCl eq.) and a low density (≈0.2 gcm^{-3}), low CO_2 (≈5 mol%) vapour. These fluids display clear similarities with the V3 immiscible fluids discussed earlier. They are probably not directly related, since there are significant compositional differences (V3 vapours have much higher CO_2 contents, for instance). However, as suggested in section 4.4.3, it is quite likely that fluids of this "pegmatite"-type or other "magmatic" fluids were at least partly responsible for the generation of the V3 fluids.

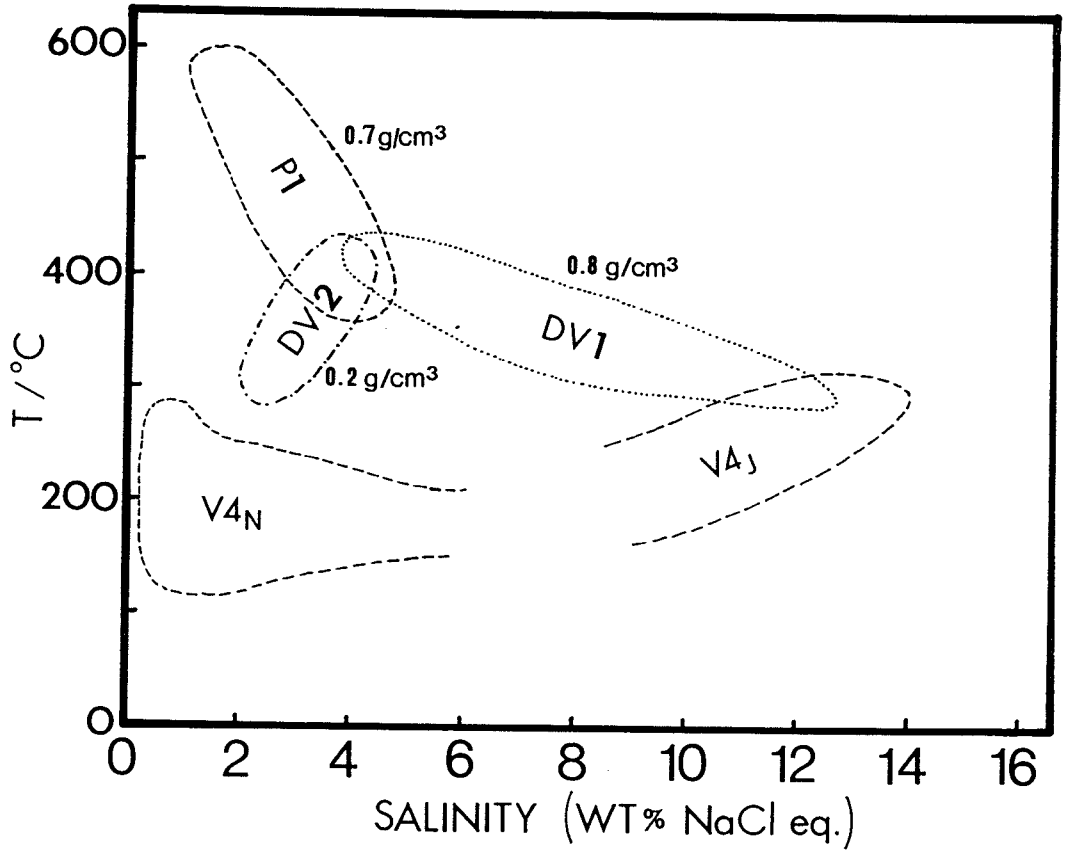

Figure 4.16 Plot of estimated trapping temperature *vs.* salinity for granite-related fluids. P1=Primary inclusions in pegmatitic quartz; DV1=primary, liquid-rich inclusions in distal veins; DV2=primary, vapour-rich inclusions in distal veins. $V4_J$ and $V4_N$ inclusion data are also shown.

4.5.2 The nature of the Cornubian hydrothermal system

The so-called "mainstage" Sn-W-polymetallic sulphide mineralising event in the Cornubian orefield was related to the protracted crystallisation and cooling history of the granite batholith. Early studies defined the most important mineral parageneses and showed a broad spatial zonation of ores around the granite apophyses (Dines 1956). The concept of fluids carrying metals in solution outward from the granites and depositing them as temperature decreased was first discussed in detail by Dines (1956). Since then, major advances have been made, both in terms of characterising the fluids associated with ore deposition (Sheppard 1977; Jackson *et al.* 1982), and in accounting for the complex superposition of ore parageneses in terms of protracted hydrothermal circulation.

It is now widely accepted that granite-driven convective circulation was active in the Cornubian batholith over a long period of time. Many authors have suggested that episodic fluid circulation continued through the Mesozoic, Cainozoic and even to the present day, as evidenced by contemporary hot spring activity (experienced by the author in South Crofty Mine). The life of the Cornubian system is many orders of magnitude longer than has been estimated for a number of natural and hypothetical systems, which are usually of the order of 10^4-10^5 years (Norton & Knight 1977; Ferry 1989). This can be accounted for by the high content of heat producing elements in the Cornubian magma, allowing a thermal anomaly to persist over a long period of time.

The nature and evolution of the fluids involved in the hydrothermal system have been investigated by a number of workers. Fluid inclusions have provided direct evidence concerning the temperature and composition of the mineralising fluids (Sawkins 1966; Jackson *et al.* 1982; Rankin & Alderton 1985; Shepherd *et al.* 1985). Evidence regarding the fluid source has been obtained from the chemical and isotopic signatures of fluid inclusions (Bottrell & Yardley 1988; Jackson *et al.* 1982; Shepherd *et al.* 1985) and from the isotopic compositions of hydrothermal minerals (Sheppard 1977). Most of the evidence suggests that magmatic fluids were involved at an early stage and were rapidly diluted by deeply circulating meteoric fluids as fracture permeability increased with consolidation of the batholith (Jackson *et al.*, in press). The data discussed in the previous section indicates that contact metamorphic fluids were also probably involved at an early stage, prior to the major influx of surface-derived fluids. It is generally regarded that most of the mineralisation occurred as a result of mixing of fluids of dominantly magmatic and meteoric origin, in the granite apophyses and adjacent country rocks (Jackson *et al.* 1982; Jackson *et al.*, in press).

4.5.3 Early joint-hosted fluid flow

The data on fluids flowing through joints ($V4_{J1}$, $V4_{J2}$ veins) and normal faults ($V4_N$ veins) obtained in this study (see 3.2.6, 3.2.7) support the general model outlined above. High temperature fluids which flowed through early joints in hornfelsed slate proximal to the Tregonning granite ($V4_{J1}$) are compositionally similar to "magmatic" fluids produced by melt-fluid separation and liquid-vapour unmixing as observed in the nearby pegmatites and related quartz veins (see 4.5.2).

Trapping temperature-salinity data for $V4_{J1}$ and $V4_N$ fluids are presented in Figure 4.16. Also shown for comparison are fields for the pegmatite-related fluids discussed in section 4.5.1. Fluid temperature is taken as equivalent to *Th* for the unmixing $V4_P$ fluids and for the $V4_J$ and $V4_N$ fluids, which probably only require small corrections due to pressure to convert *Th* to T. Trapping temperatures for the pegmatite fluids are estimated in section 4.5.1. It is evident that in terms of fluid T and salinity, the $V4_J$ and $V4_N$ fluids appear to be closely related, with a possible evolutionary trend between. This trend is best explained by mixing of meteoric ($V4_N$-type) fluids (see below) with H_2O-rich fluids of magmatic departure ($V4_P$ "distal"-type) during the early stages of joint-controlled fluid flow.

Although this model is highly simplified, based on a limited data set, it is in broad agreement with fluid inclusion studies carried out on similar veins elsewhere in the orefield (*e.g.* Charoy 1979; Jackson *et al.* 1982; see 6.2.2). Obviously, more extensive fluid inclusion studies of these veins in the field area would be required to confirm the model and identify local anomalies.

4.5.4 Meteoric-dominated fluids in joints and faults

The influx of dilute meteoric fluids into the convective system is clearly indicated by the decreasing salinity and temperature of fluids trapped in late-stage structures ($V4_{J2}$ and $V4_N$ veins). *Th* and salinity data for these fluids (Fig. 4.16) illustrate a gradual trend of decreasing salinity and temperature from the *c.*12 wt% NaCl eq. fluids at 300-400°C associated with the early magmatic-?metamorphic circulation to the *c.*2 wt% NaCl fluids at 150-300°C typical of the late, meteoric-dominated system (Fig. 4.16).

Convincing evidence in support of a meteoric source for these fluids comes from stable isotopic analyses (see 3.5). $V4_{J2}$ and $V4_N$ fluids are very depleted in ^{18}O relative to other Cornubian waters. The ^{18}O compositions and trend of increasing $\delta^{18}O$ with approximately constant δD (Fig. 3.62) are consistent with a dominantly meteoric origin with some fluid-rock isotopic equilibration with increasing temperature. This type of isotopic trend in the late hydrothermal fluids was first recognised by Sheppard (1977) and confirmed by Jackson *et al.* (1982), on the basis of isotopic analyses of alteration minerals. It is interesting to note that the direct fluid isotopic analyses presented in this study suggest that the Permo-Triassic meteoric fluids had more negative δD values (*c.* -25‰) than previously estimated from the isotopic composition of hydrothermal sericites (Jackson *et al.* 1982). Work by Jenkin (pers. comm. 1989) indicates that the sericite-fluid fractionation factor becomes temperature-invariant below ≈400°C (with $1000\ln\alpha \approx -25$), so that the sericites analysed by Jackson *et al.* (1982) would have been in equilibrium with fluids with δD values of -6 to -20‰. The differences between the measured and estimated δD values may be due to spatial or temporal fluctuations in meteoric water composition, or possibly to uncertainties in the sericite-H_2O fractionation factor at low temperatures. It is known that Cornubian meteoric fluids became progressively depleted in deuterium from the Permian onwards as a result of increasing latitude (Jackson *et al.* 1982, Fig. 10) so that temporal fluctuations can account for the observed compositional differences.

Chemically, the $V4_J$-$V4_N$ fluids are dominated by H_2O with very low proportions of other gases (see 3.4) and few dissolved salts. These features are consistent with a dominantly meteoric origin. Major element compositions (Fig. 4.12) display a trend of decreasing Na/Ca at constant Na/K, which suggests mixing of an early hydrothermal fluid of $V4_{J1}$ type with a meteoric fluid. Significantly, sample *J78PS*, which has the lowest salinity and lowest $\delta^{18}O$ of all the fluids analysed, is also closest chemically to the meteoric fluid field defined on Figure 4.12. This sample thus contains fluid inclusions which are a close approximation to the surface waters which became involved in the Cornubian hydrothermal system.

It is clear that mixing processes played an important role in controlling the chemical composition and evolution of the convecting hydrothermal fluids. Chemical re-equilibration of meteoric fluids would have occurred as they were sucked down into the convective system and heated. However, this is not an observable effect at the crustal level examined, with no difference in the Na/K ratio between the $V4_{J1}$ and $V4_N$ fluids analysed. This is explained by the *Th* data which indicate that both fluid types were trapped at similar temperatures (Fig. 4.16). However, isotopic re-equilibration of heated meteoric fluids did occur (see above).

Consequences for mineralisation

The data discussed above support previous models for the evolution of the Cornubian hydrothermal system. In simple terms, early magmatic-hydrothermal mineralisation occurred contemporaneously with granite emplacement (*e.g.* "Type I metasomatisms" of Jackson *et al.* 1982), with meteoric-dominated fluids controlling mineralisation during and after consolidation. Bottrell & Yardley (1988) suggested that high temperature oxides (*e.g.* cassiterite, haematite) were precipitated as a result of neutralisation of acidic magmatic fluids by reaction with granitic wallrocks (producing greisen alteration). Subsequent mixing with dilute, ?sulphur-bearing meteoric fluids would have resulted in deposition of chalcophile elements, initially enriched in the magmatic fluid (Bottrell & Yardley 1988). The meteoric fluids may have scavenged base metals (*e.g.* Sn, Pb, Cu, Zn, Fe) from the pelites during their descent, thus concentrating additional ore-forming components in the granite apophyses (see 6.2).

In this study, a probable magmatic component has been recognised in fluids responsible for early quartz-tourmaline alteration. By the time the system had cooled to below 300°C, the hydrothermal fluids were dominated by surface-derived, meteoric water. Dominantly meteoric fluids flowed through normal faults on the southern flank of the Cornubian batholith at *c.* 200°C during the latter stages of hydrothermal convection.

4.6 BASE METAL BEARING BRINES

The base metal mineral paragenesis in southwest England has long been recognised as being distinct from the bulk of Cornubian mineralisation phenomena, both in terms of its age and structural setting. The galena-sphalerite-chalcopyrite-pyrite-siderite-quartz paragenesis observed in the field area (see 1.3.5, 2.2.15) is one of a number of low temperature mineral suites common in the

province. Such mineralisation is almost always hosted by sub-vertical N-S or NNW-SSE trending structures ("cross-courses"), with evidence of repeated faulting and open-space filling. Both wrench (commonly dextral) and oblique offsets of the E-W trending mainstage lodes are observed, which has been taken to indicate that this phase of mineralisation was a late event. However, fluid inclusion data reported by Shepherd & Scrivener (1987), suggested that the fluids responsible for base metal mineralisation (see below) penetrated the E-W structures during deposition of late mainstage mineralisation. Thus, there is some evidence to suggest that there are closer temporal links between granite-driven convective circulation and cross-course mineralisation than was originally thought.

Previous workers have suggested that cross-course mineralisation was the result of an external basinal brine interacting with the granite-driven convective circulation (*e.g.* Alderton 1975, 1978; Jackson *et al.*, in press), but there is little evidence to directly support this hypothesis. Data reported in sections 3.2.8 and 3.3 and discussed below shows that, at least within the study area, there is clear evidence of interaction between such fluids. Modelling of this interaction (see 5.5) indicates that it can account for the observed spatial distribution of base metal ore deposits in the Cornubian peninsula.

4.6.1 P-T conditions during base metal mineralisation

The fluid inclusions studied in $V4_W$ veins may be used to constrain the pressure and temperature at which base metal mineralisation occurred in the field area. The nature of the mineralisation, its emplacement in brittle structures, and low homogenisation temperatures, when taken together, suggest that this was a low temperature event. These fluids have been compared with those responsible for Mississippi Valley-type deposits (Alderton 1978) and with those related to base metal mineralisation in the north Pennine orefield (Rankin & Graham 1988). These deposits are believed to have formed in the temperature range 50-200°C.

An average isochore has been constructed for $V4_W$ fluids, in a similar manner to that described in section 4.2.1. As they are brines dominated by NaCl and $CaCl_2$, with a significant component of KCl (see 3.3.1), the method of Zhang & Frantz (1987) was used to estimate the P-V-T properties of the mixed salt system. The isochore shown in Figure 4.17 was determined using the mean *Th* of 121°C (see 3.2.8) and an average solution composition of 3.476 molal NaCl, 0.489 m $CaCl_2$ and 0.251 m KCl (Table 3.16). Assuming the depth of trapping was less than or equal to the maximum depth of emplacement of the top of the Cornubian batholith (*i.e.* ≤5 km; *e.g.* Jackson *et al.*, in press), and $P_F \approx P_H$ (suggested by open-cavity filling textures), a maximum trapping pressure of *c.*500 bars can be estimated. This corresponds to a maximum trapping temperature of 144°C for the modal $V4_W$ fluids (Fig. 4.17).

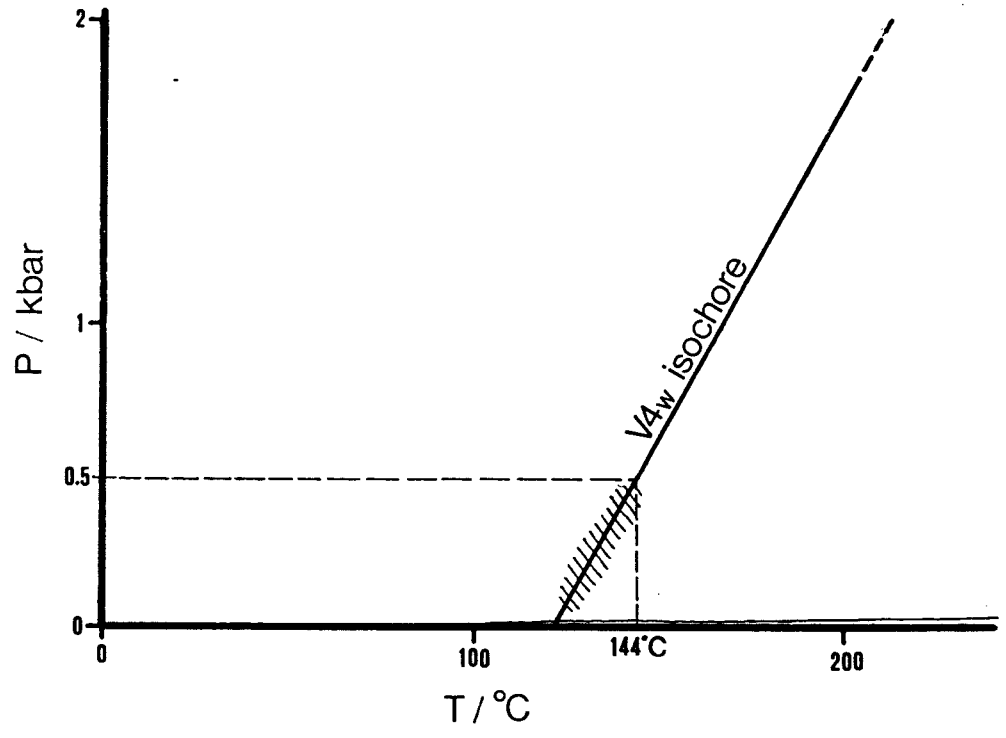

Figure 4.17 Average isochore constructed for $V4_W$ fluids, using the method of Zhang & Frantz (1987). Hatched area represents P-T trapping conditions.

Summary

From the above discussion it can be concluded that most of the cross-course base metal mineralisation observed in the study area formed at temperatures of 120-140°C at fluid pressures of <500 bars. The temperature determinations indicate that the mineralising event significantly post-dated peak contact metamorphism, with a temperature decrease of the order of 200°C between the two events at the same crustal level.

4.6.2 $V4_W$ fluid source

Volatile components

Bulk volatile data reported in section 3.4 indicate that $V4_W$ fluids are extremely H_2O-rich with <0.2 mol CO_2, <0.01 mol% CH_4, <0.01 mol% N_2 and <0.1 mol% non-condensible gases. The volatile components are not a good indicator of fluid source; most of the common "end-member" fluid types are H_2O-rich and so this is not a diagnostic feature.

Solute components

In terms of their solute components, $V4_W$ fluids are very distinctive with high total dissolved solids (generally just below saturation at room temperature) and elevated levels of calcium. On a major element plot (Fig. 4.12), they are clearly distinguished from other Cornubian fluids, plotting closer to

the fields for meteoric fluids and oilfield brines.

Previous workers (*e.g.* Alderton 1978) have noted the similarities in chemical composition between the Cornish base metal mineralising fluids and oilfield brines. The Cornish brines are also very similar to those responsible for post-Hercynian base metal mineralisation in West Germany (Behr & Gerler 1987; see Table 4.1). The data reported in this study support this comparison, in terms of salinity, the major solutes, and minor components such as lithium, boron and bromine (Table 4.1).

Table 4.1 Composition of $V4_W$ fluids and a variety of other oilfield and formation brines (ppm and weight ratios)

	POST-HERCYNIAN BASE METAL BRINES					MODERN OILFIELD BRINES		
	$V4_W$	Harz[2]	Rheinische Schiefer-gebirge[2]	Schwarz-wald[2]	Oberpfalz[2]	Central Mississ-ippi[3]	Seaboard Field, California[1]	Elliott Co., Kentucky[1]
Li	82					34		
Na	79900	47000	52000	53000	57500	58361	14800	40200
K	9790					2275	251	191
Mg	~580					2395	832	3350
Ca	19500	39500	31000	41000	34000	31529	2190	12300
Sr	400					1585		628
Ba	31					52	42	
Fe	570					202		0.52
B	~70						8.3	
Cl	~129000	143000	122000	160500	149000	155666	29000	93900
Br	460	1050	2150	2300	1275	1376	108	817
Na/Li	1030					2373		
Na/K	8.6					58	59	210
Na/Mg	135					27.9	17.8	12.0
Na/Ca	4.1	1.2	1.7	1.3	1.7	2.2	6.8	3.3
Na/Sr	203					43		64
Na/Ba	2790					1866	352	
Na/Fe	143					2043		77300
Na/B	1070						1780	
Na/Br	170	46	24	23	47	50	137	49
Cl/Br	~280	135	56	70	123	132	270	115

[1]From analyses reported by White (1957); [2]From Behr & Gerler (1987); [3]Mean of 81 analyses, Carpenter *et al.* (1974)

Stable isotopes

Interpretation of the stable isotopic compositions of $V4_W$ fluids is somewhat problematic. This is because of the possibility of deuterium fractionation resulting from the low H_2O yields obtained during analysis (see 3.5). However, the apparent correlation between low H_2O yield and low δD may be a coincidence and this has important implications for the source of the $V4_W$ brines.

Assuming the isotopic determinations are valid, the $V4_W$ fluids are isotopically light, being depleted in both ^3H and ^{18}O. On a δD *vs.* $\delta^{18}O$ plot (Fig. 3.62), they plot just on the ^{18}O-rich side of the meteoric water line. Comparison with the isotopic compositions estimated for a variety of natural waters (Fig. 3.62) shows that they are most similar to present day oilfield brines, such as those of the Alberta and Michigan Basins, USA. This is in agreement with the chemical data which also indicate that $V4_W$ fluids are comparable with these formation waters.

Summary

The chemical and isotopic compositions of the brines responsible for late base metal mineralisation in the study area are very similar to those reported for comparable fluids elsewhere in the Cornubian orefield, and from other parts of the Hercynian belt. The detailed compositional data discussed above provide convincing evidence in support of a basinal origin for these fluids. It is envisaged that the brines were expelled from Permo-Triassic sedimentary basins developing to the south of the Cornubian peninsula and migrated in towards the active granite-hydrothermal system (see 6.1.6).

The reasons for differences in composition between $V4_W$ (and comparable fluids) and their assumed precursors (oilfield brines) are considered in the following section. The implications for metal transport and ore deposition are discussed in section 5.5.

4.6.3 The genesis and evolution of formation brines

The remarkable compositional similarities between oilfield brines and ancient ore-forming solutions have been discussed in detail, with particular reference to the genesis of Mississippi Valley-type deposits (e.g. Barnes 1979; Roedder 1967). According to the basinal brine model of ore formation (*e.g.* Ohle 1980), hot saline solutions similar to oilfield brines migrate out of sedimentary basins, along aquifers, and eventually form base metal deposits in sedimentary rocks at distances of the order of 100 km from the source region. The compositional differences between oilfield brines and the final ore-forming solutions are probably the result of water-rock interactions during migration (*e.g.* Sverjensky 1984).

The genesis of sedimentary brines

Stable isotopic data indicate that meteoric water is an important constituent of the North American oilfield brines (Clayton *et al.* 1966; Hitchon & Friedman 1969). The high salinity of the fluids has been explained by evaporation of seawater prior to sediment burial (Carpenter *et al.* 1974), by solution of evaporites by pore fluids, and by clay membrane filtration (Hanshaw & Coplen 1973). It would be inappropriate to discuss these possibilities in detail here; for further information the reader is referred to Barnes (1979). Whatever the mechanism of generation, Na-Ca-Cl brines are invariably observed in deep sedimentary basins and are potential ore-forming solutions.

Oilfield brines as potential ore-forming solutions

Despite the similarities between oilfield brines and ancient ore-forming solutions, there is a relatively limited amount of detailed information concerning their aqueous chemistry. Particularly controversial are the parameters important for ore transport and deposition, including pH, oxidation state, and contents of trace metals and sulphur. If, as seems likely, oilfield brines are commonly responsible for the formation of stratiform, stratabound and vein-hosted base metal deposits, a knowledge of their chemical evolution is vital in defining the controls of metal transport and deposition.

Any model for the evolution of an oilfield brine to a mineralising fluid must account for the observed chemical differences between them. Most striking is the difference in the Na/K ratio,

which is generally higher for oilfield brines (*e.g.* Hanor 1979). A histogram of Na/K ratios for 81 brines from the central Mississippi district, USA (data from Carpenter *et al.* 1974), is shown in Figure 4.18. The apparent bimodal distribution is an artefact; the Na/K ratios can in fact be explained as a continuous evolutionary trend, with typical oilfield brines (high Na/K group) gradually evolving to fluids with lower Na/K ratios (see below). The peak in the histogram at Na/K=5-10 can be accounted for by the attainment of an "equilibrium" fluid composition, beyond which further significant change in Na/K cannot occur.

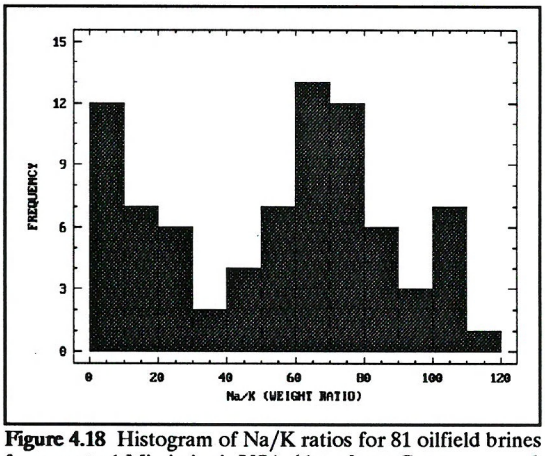

Figure 4.18 Histogram of Na/K ratios for 81 oilfield brines from central Mississippi, USA (data from Carpenter *et al.* 1974).

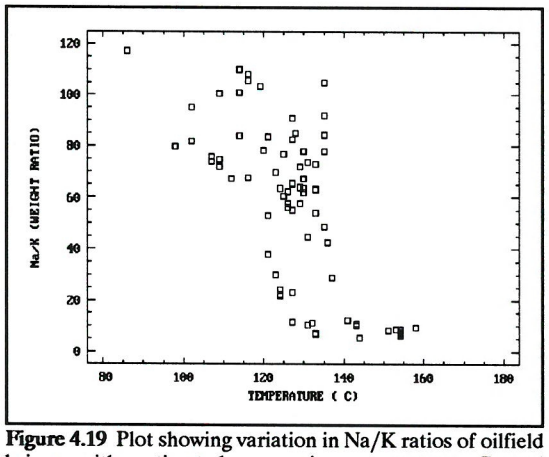

Figure 4.19 Plot showing variation in Na/K ratios of oilfield brines with estimated reservoir temperature, Central Mississippi, USA (data from Carpenter *et al.* 1974).

The clear correlation between estimated fluid reservoir temperature and Na/K ratio for the same group of fluids (Fig. 4.19) illustrates this process. The Na/K ratios decrease rapidly with increasing temperature between 86°C and 140°C, at which point an Na/K "limit" is reached. Further temperature increase results in no observable change in the Na/K ratio. A possible explanation for this phenomenon is that the low temperature brines are initially significantly out of equilibrium with their host rocks and rapid reaction, involving breakdown of K-bearing phases, occurs. The Na/K ratio thus decreases with increasing T until an equilibrium value (probably defined by mica-feldspar-fluid equilibria) is reached. The subsequent decrease in Na/K with increasing temperature will be much smaller for a buffered fluid and would not be observed in the temperature range considered above.

One possible reason for such a mechanism is suggested by the dominant meteoric water source for these fluids, indicated by light stable isotopic data (Hitchon & Friedman 1969). If these brines are the result of downward infiltration of surface waters, then significant changes in fluid composition would be expected with increasing temperature. Trends of isotopic re-equilibration of these fluids are clearly evident on δD-$\delta^{18}O$ plots (*e.g.* Fig. 3.62; see Barnes 1979), thus comparable chemical changes would be inevitable.

Whatever the mechanism, there is evidence to suggest that oilfield brines evolve to more potassic compositions with increasing temperature, attaining those comparable with ancient mineralising fluids (*i.e.* Na/K = 21-36, Sverjensky 1984; 5.8-11.6, this study) at temperatures above 120°C. It is interesting that the $V4_W$ fluids in the present study lie on the Na/K-temperature evolution trend for the Mississippi brines with an estimated temperature of 121-144°C and Na/K ratios in the range 5.8-11.6.

Other components of the fluid which display variations between the oilfield brine precursor and the mineralising fluid are alkali earth elements and transition metals, particularly Fe and Mn. However, these components also vary considerably between different basins and between mineralising fluids in different districts. It seems likely, therefore, that fluctuations in these components are related to the bulk composition of the basinal sediments, with a particular geochemical character being picked up by the fluid during migration. There is an example of this type in the Cornubian orefield, where broadly comparable fluids in south Cornwall (this study) and south Devon (*e.g.* Shepherd & Scrivener 1987) result in relatively Fe-Cl-rich (siderite+quartz) and Ca-F-rich (calcite+fluorite) gangue parageneses respectively. This may reflect a difference in the source basin or, perhaps more likely, a difference in the composition of the rocks through which the brines flowed.

4.6.4 $V4_W$ fluid evolution

Microthermometric data from a range of $V4_W$ samples (see 3.2.8) illustrate two main evolutionary trends. Measurements of ice and hydrohalite melting temperatures have been used to estimate the $NaCl-CaCl_2-H_2O$ composition of fluid inclusions from different parts of growth zoned quartz and from different samples. These data illustrate a trend of changing Na/Ca ratio at approximately constant salinity (Fig. 4.20).

Ice melting temperatures in a number of samples indicate that fluids of both high and low salinity are present, occurring in both apparent primary and secondary inclusions. The combined data for $V4_W$ fluids and $V4_N$ fluids strongly suggest that interaction of the two fluid types occurred. This mixing relationship has been examined in detail by sampling in the vicinity of Wheal Rose (Fig. 1.4), where a N-S trending wrench structure intersects a normal fault.

The constant salinity trend

The compositions of $V4_W$ fluid inclusions in the $NaCl-CaCl_2-H_2O$ system are depicted in Figure 4.20. This diagram shows how the $NaCl/CaCl_2$ ratio for $V4_W$ fluids varies significantly (Na/Ca weight ratio of 0.8-14.5) but at almost constant total salinity. The spread in Na/Ca ratios may be artificially enhanced by slight metastable melting of hydrohalite and the fact that the isotherms in the ice and hydrohalite fields are at a low angle to the ice-hydrohalite phase boundary. However, the trend is still believed to exist.

The controls of salinity and the Na/Ca ratio of these fluids may be in the source region or in the rocks through which the fluid migrated, or both. The salinity of oilfield brines is primarily a function of depth (*e.g.* Dickey 1969), so that tapping of the basinal fluids at a particular level may be expected to result in release of a fluid with constant salinity. Examination of the wallrocks adjacent to $V4_W$ veins by XRD showed no obvious signs of Na/Ca exchange (such as replacement of albite by plagioclase). It is suggested that the Na/Ca ratio was also controlled at source and that the significant decrease in the (presumed) later fluids was due to exhaustion of the Ca supply in the source region.

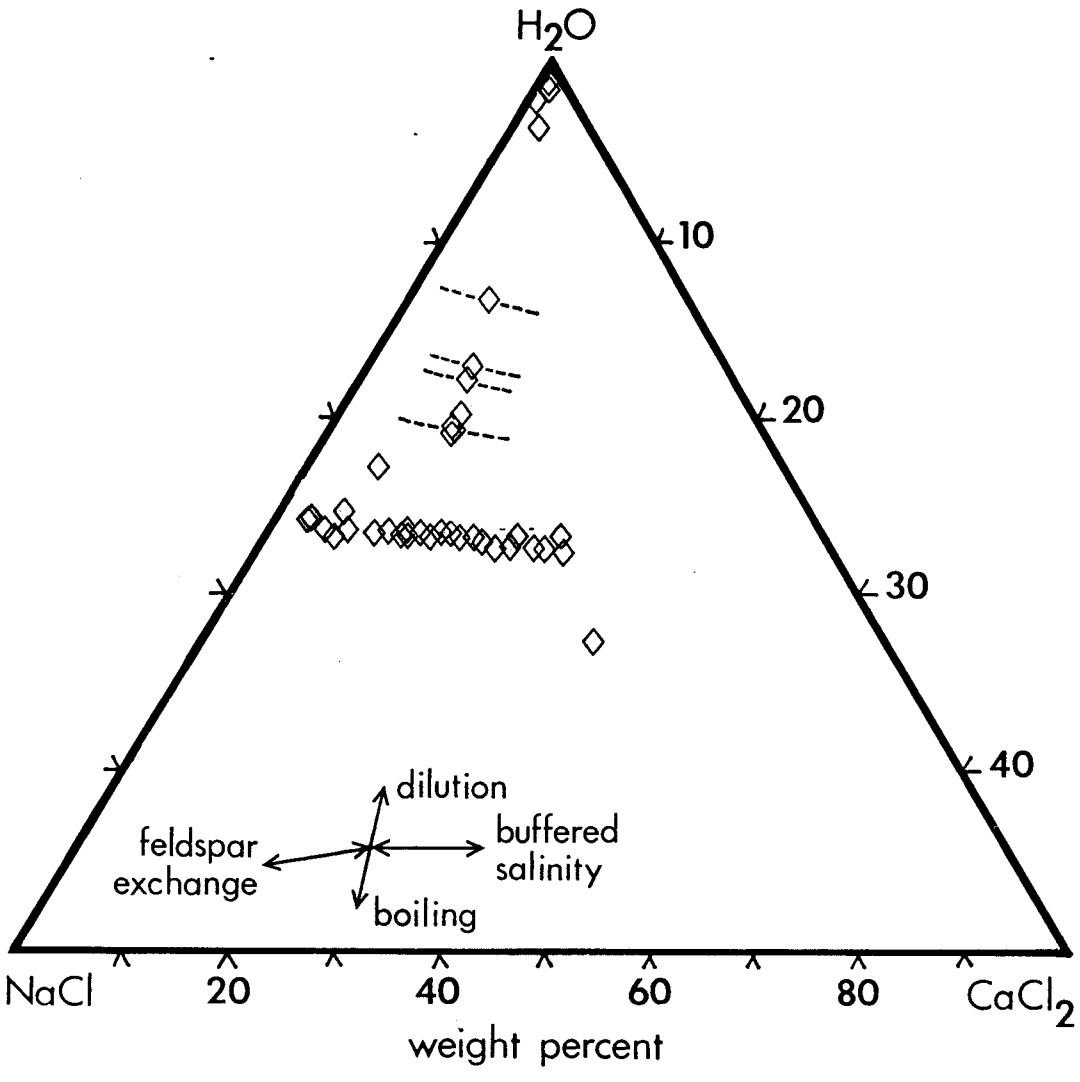

Figure 4.20 Composition of $V4_W$ fluid inclusions in the NaCl-$CaCl_2$-H_2O system (diamonds). Dashed lines represent uncertainty in the Na/Ca ratio due to difficulties in accurately determining *Tmh*. Isotherms for the liquidus surface were taken from Borisenko (1977).

In comparison, brines responsible for base metal-fluorite deposits in the Tamar Valley (Shepherd & Scrivener 1987), are relatively Ca-rich (comparable to the most calcic fluids on Figure 4.20). They do not display a fluctuation in the Na/Ca composition of the brine but do appear to evolve subsequently by mixing with a dilute fluid, as observed in the $V4_W$ data.

The mixing trend

Microthermometric data indicate that dilute "meteoric-type" fluid inclusions are present in $V4_W$ veins, demonstrating that these fluids did flow through $V4_W$ structures at some stage. The presence of fluids of intermediate salinity in these veins (Fig. 3.60) and also in $V4_N$ veins (Fig. 3.54), suggests that a mixing relationship may exist, *i.e.* the two fluids were, at least occasionaly, able to penetrate the same structures at the same time. A plot of the combined *Th-S* data for both vein types (see 6.1.5; Fig. 6.8) supports this interpretation. The two end-member fluids are dominant in the two vein

types, with an increasing salinity trend in the $V4_N$ fluids and a decreasing salinity trend in the $V4_W$ fluids. The data suggest that limited mixing occurred between meteoric-dominated granite-hydrothermal fluids at ≈200°C and basinal brines at ≈140°C. Samples which contain the mixed fluid come from $V4_W$ veins where a structural link between $V4_W$ and $V4_N$ may be demonstrated. This has allowed a more detailed consideration of the role of tectonic processes in controlling the mixing process (see 6.1.6).

4.6.5 $V4_W$ fluid pH

Two alternative methods have been used to estimate the pH of the $V4_W$ fluids. The first method involves the assumption of equilibrium between siderite, H_2O and CO_2. The presence of siderite is ubiquitous in $V4_W$ veins in the study area so it is reasonable to assume that the fluid was close to saturation with respect to this phase at the prevailing fCO_2 conditions. The following reaction describes the relevant equilibrium:

$$FeCO_3 + 2H^+ = Fe^{2+} + H_2O + CO_2 \qquad K = \frac{(a.Fe^{2+})(fH_2O)(fCO_2)}{(a.FeCO_3)(a.H^+)^2} \qquad ...(4.26)$$

$\blacktriangle G^\circ_r$ for the reaction was calculated in an identical manner to that described in section 4.2.2. This was then used to determine a value of 4.63 for logK using eq. 4.12. As a result of the high salinity of these fluids, the approximation used previously, that the concentration of a species in solution is equivalent to the activity, is invalid. The activity of Fe^{2+} required in equation 4.26 was calculated by using the estimated total Fe in solution (0.01025m) and an activity coefficient of 0.17 extracted from a calculation given by Sverjensky (1984) for a similar fluid. The activity of Fe^{2+} is then given by:

$$a.Fe^{2+} = 0.17 \times 0.01025 = 1.743 \times 10^{-3}$$

The fugacities of H_2O and CO_2 were determined assuming ideal mixing using eq. 4.17. The mole fractions of the two components were taken from Table 3.20, their fugacity coefficients from Burnham *et al.* (1969) and Ryzhenko & Volkov (1971) and the fluid pressure was taken as 400 bars. Assuming $a.FeCO_3 = 1$ means that $a.H^+$ can be calculated from eq. 4.26. This procedure gives a pH of 3.5 for the $V4_W$ fluids.

An alternative approach was also used, based on the assumption of buffering of the fluid pH by silicate phases in the wallrock, as applied to V1 and V2 fluids (sections 4.2.6, 4.3.6). An Na-K activity diagram, given by Sverjensky (1984), for 125°C, 2.3 bars, $a.H_2O = 0.95$ and quartz saturation (Fig. 4.21) was used as a good approximation to the $V4_W$ fluid system. Plotted on the diagram are two straight lines representing the range of Na/K activities displayed by $V4_W$ fluids. As mentioned above, there is a significant deviation from ideality in concentrated brines, so that ion activities have to be used. The activity coefficients for Na and K (0.66 and 0.55 respectively) were extracted from data given by Sverjensky (1984). Also shown on the diagram are a series of pH isopleths calculated in the same manner as that described in section 4.2.6.

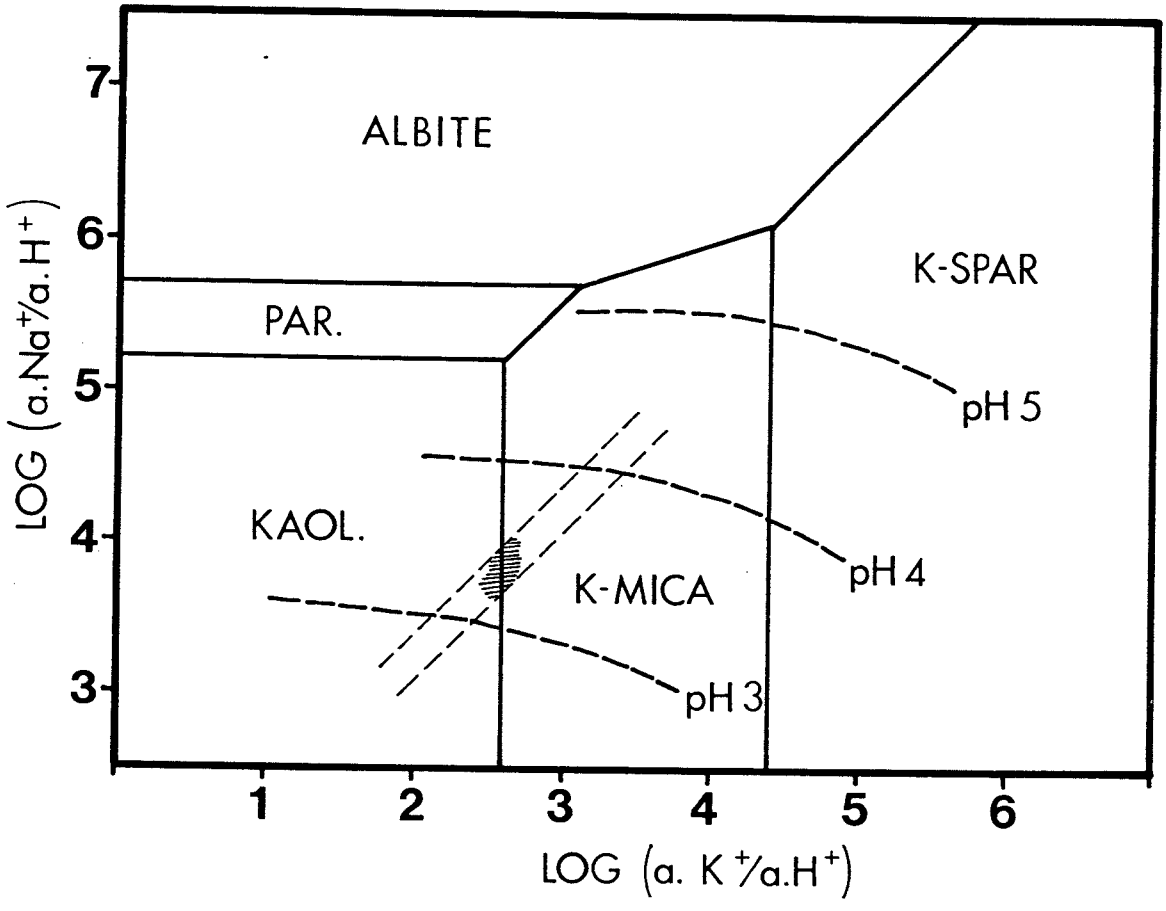

Figure 4.21 Activity diagram for the system NaCl-KCl-HCl-H_2O-SiO_2 at 125°C, 2.3 bars (after Sverjensky 1984). Hatched area represents composition of $V4_W$ fluid in equilibrium with kaolinite and muscovite.

Studies of common reservoir rocks (*e.g.* Kharaka *et al.* 1980; Carpenter *et al.* 1974) indicate that brines of $V4_W$ type are probably close to equilibrium with kaolinite and muscovite and well out of equilibrium with respect to K-feldspar and albite. Assuming that $V4_W$ fluids are close to equilibrium with kaolinite and muscovite, the pH is constrained to approximately 3.3. This is in good agreement with the value of 3.5 estimated from the siderite-CO_2 equilibrium.

A pH in the region of 3.4 for the $V4_W$ fluids is 0.8 log units lower than was estimated for an oilfield brine by Kharaka *et al.* 1980 and is consistent with the maximum pH of 5.7 estimated by Sverjensky (1984). The low pH may be correlated with the relatively high K and Fe contents of the fluid (see Table 4.1) The fact that the $V4_W$ fluids have such a low pH, more than 2 log units below neutral at 140°C (Sverjensky 1984), is extremely important for base metal transport. As outlined by Sverjensky (1984), a low pH, high salinity fluid is capable of transporting significant quantities of Pb and Zn, in addition to reduced sulphur. The low pH means that the fluid can transport enough reduced sulphur for galena and sphalerite to be close to saturation so that an alternative source of sulphur is not required for mineralisation. Any mechanism whereby the pH is suddenly increased, or the fluid diluted, will result in ore deposition. A more detailed discussion of metal transport in $V4_W$ fluids is presented in section 5.5.

4.6.6 $V4_w$ oxygen fugacity

An estimate of the oxygen fugacity of the $V4_w$ brines was made assuming equilibrium between siderite and haematite:

$$Fe_2O_3 + 2CO_2 = 2FeCO_3 + 0.5O_2 \qquad K = \frac{(fO_2)^{0.5}(a.FeCO_3)^2}{(fCO_2)^2(a.Fe_2O_3)} \qquad ...(4.27)$$

Although haematite is commonly observed in $V4_w$ structures (*e.g.* Hosking 1964) it is often interpreted as forming through oxidation of siderite. If this is the case, the oxygen fugacity calculated by this method will be a maximum. Log K was calculated using eqs. 4.9-4.12. Rearranging eq. 4.27 then gives an expression for the oxygen fugacity:

$$fO_2 = K^2 \times (fCO_2)^4 \qquad ...(4.28)$$

The CO_2 fugacity can be calculated from eq. 4.17 since X_{CO2} and P_F are known, and with ϕ_{CO2} taken from Ryzhenko & Volkov (1971). As before, this procedure assumes ideal mixing between the components in the fluid.

The method outlined above gives a maximum $\log fO_2$ of -52.2 for the $V4_w$ fluids. This is 1.8 log units lower than that given by Sverjensky (1984) for a "typical potential ore-forming solution".

4.6.7 Sulphur fugacity

A similar procedure to that used to estimate the sulphur fugacity of V1 and V2 fluids has been applied to the $V4_w$ basinal brines. The fact that the pH and fO_2 of the fluids are known means that fH_2S can be calculated just by specifying equilibrium with one sulphur-bearing phase. Pyrite was selected because it is a common component of the pelites and is ubiquitous in the $V4_w$ ore paragenesis. A reaction linking the H_2S fugacity to the oxygen fugacity and pH may be written:

$$FeS_2 + H_2O + 2H^+ = 2H_2S + Fe^{2+} + 0.5O_2 \qquad K = \frac{(a.H_2S)^2(a.O_2)^{0.5}(a.Fe^{2+})}{(a.H_2O)(a.FeS_2)(a.H^+)^2} \qquad ...(4.30)$$

Equations 4.9-4.12 were used to determine a value for logK of -28.19. Substituting this, and the appropriate values for the other parameters into eq. 4.30 gave an H_2S fugacity of 6.92×10^{-3} (log fH_2S = -2.2). The fugacity coefficient for H_2S was determined for the appropriate P and T using the expression of Ryzhenko & Volkov (1971) and substituted into eq. 4.17 to yield the mole fraction H_2S present in the fluid. This gave $X_{H2S} = 2.5 \times 10^{-5}$, which is equivalent to 54 ppm H_2S in solution (assuming $X_{H2O} = 0.998$, $X_{CO2} = 0.002$). This compares with measured H_2S concentrations in oilfield brines of 0.5-2.0 ppm (Kharaka *et al.* 1980) and total reduced sulphide of 3-500 ppm (Carpenter *et al.* 1974). Barrett & Anderson (1982) calculated that a 3m NaCl solution with a pH of 4.3 at 100°C could contain 2.5 ppm Zn and 1.5 ppm H_2S or 1.8 ppm Pb and 0.3 ppm H_2S. At higher pH and

higher temperature it would be expected that the amounts of dissolved H_2S and base metals would increase significantly.

4.7 SUMMARY

In this chapter, the evolution of fluids in the crustal slab of south Cornwall during Hercynian compression and post-orogenic extension has been examined in detail. The fluid data presented in Chapter 3 has been used to constrain the tectonothermal evolution of the area and the major fluid evolution processes.

V1 fluid data indicate that peak regional metamorphism occurred at 300±30°C and 3.4±0.5 kbar. V1 fluids were derived by devolatilisation of pelites undergoing prograde metamorphism. The alkali content of these fluids was buffered by albite + muscovite ± paragonite assemblages in greywackes of the Portscatho Formation. The pH of V1 equilibrium fluids, with an average salinity of 0.41 molal chloride is estimated to be 5.3.

The volatile composition of V1 fluids is consistent with buffering by carbon in the wallrocks, with carbon activities of <1. The oxygen fugacity defined by graphite buffering is close to the NNO buffer, with $\log(fO_2) = -30.8$ at peak metamorphic conditions. Sulphur fugacity, assuming pyrite-pyrrhotite buffering, is -9.8, corresponding to an H_2S fugacity of -0.27.

The P-V-T-X properties of V2 fluids indicate that relatively high temperatures (250°C) were maintained at a late stage of thrusting, when pressures had decreased to ≈800 bars.

V2 fluids are compositionally consistent with an origin as V1-type fluids which flowed to higher levels in the crust. Slight fluid-rock disequilibrium explains the limited occurrence of sericitic and chloritic alteration. Slight salinity increases may be explained by rehydration of the rock and resulting decrease in $a.H_2O$ in the fluid phase. pH also increased in the V2 fluids, predominantly as a result of the temperature decrease.

A decrease in fO_2 of six log units as the fluids evolved from V1 to V2, primarily as a result of cooling, led to an increase in the proportion of CO_2 and N_2 by oxidation of carbon and ammonium in the wallrocks. A corresponding decrease in fH_2S has important implications for metal transport and deposition during regional metamorphism (see 5.3).

Compositionally varied V3 fluids were mobilised in the contact aureole of the Cornubian granites at 420-200°C and 1000-500 bars. Moderate and extreme fluid immiscibility occurred, resulting in the generation of saline aqueous liquids and CO_2-rich, low density vapours. Vapour condensation may have occurred in the outer regions of the contact aureole, resulting in the formation of dense, very CO_2-rich fluids.

The source of the V3 fluids is ambiguous but the evidence favours an origin via mixing of magmatic and contact metamorphic fluids. The $\log(fO_2)$ of V3 fluids is estimated at -29.8, assuming graphite buffering. The corresponding fH_2S is 0.315, estimated to be equivalent to 140 ppm in the aqueous phase.

Granite-related fluids display complex evolutionary trends, evolving from an early magmatic-dominated system at 600-400°C to one dominated by dilute meteoric fluids below 300°C. There is evidence for mixing of basinal brines with dilute meteoric fluids in the outer margins of the granite hydrothermal system at 140-200°C and <500 bars.

The fluid evolution processes proposed and fluid parameters estimated in this chapter are used in Chapter 5 to model the transport of metals in the solutions and to identify possible deposition mechanisms for the observed mineralisation phenomena. The data are also used to suggest possible structural and geochemical settings in which the non-mineralising fluids in the study area may have resulted in the formation of an ore deposit. These ideas are developed further in Chapter 6 to produce several new exploration models for the area.

CHAPTER 5: METAL TRANSPORT AND ORE DEPOSITION

The stability of many ore and gangue minerals in aqueous solutions can be conveniently related to the acidity and oxidation state of the fluid. As a result, knowledge of parameters such as pH, Eh and fO_2 are vital in understanding metal transport and ore deposition processes. These parameters have been defined for a number of the fluids investigated in this study (see Chapter 4), thus allowing thermodynamic calculation of ore metal solubilities in these solutions.

5.1 INTRODUCTION

5.1.1 Metal complexing in hydrothermal solutions

Thermodynamic calculation of the concentration of simple metal ions (*e.g.* Pb^{2+}) in aqueous solutions commonly yields values many orders of magnitude lower than experimentally determined solubilities. This is because metals rarely exist as simple ions in solution, forming instead a variety of complexes with neutral or negatively charged species (ligands). Associations of this type may be described by the general equation:

$$M^{z+} + n\,L^{y-} = (ML_n)^{z-ny} \qquad ...(5.1)$$

where M represents a metal cation with charge z and L represents a ligand with charge y.

Any metal in solution will form a variety of complexes with available ligands, the proportions of each being determined by their relative thermodynamic stabilities and reaction kinetics. If equilibrium is assumed between the various complexes, a thermodynamic approach may be used to identify the complexes responsible for metal transport in a given fluid, as well as to estimate ore mineral solubilities.

Despite numerous experimental studies, the solubilities of most rock- and ore-forming minerals as functions of P, T and fluid composition (X) under geological conditions are poorly known (*e.g.* Eugster & Baumgartner 1987). The general approach adopted in a variety of studies involves the extrapolation of thermodynamic properties measured at 298K and 1 bar to the P and T of interest using an equation of state and a series of correlation algorithms (see 4.2.2) in conjunction with relevant experimental data, measured over the P-T range of interest (see Sverjensky 1987; Henley *et al.* 1984 for details). This method is outlined in section 5.2 below.

5.2 DETERMINATION OF METAL SPECIATION AND ORE MINERAL SOLUBILITY

5.2.1 Thermodynamic method

Rigorous calculation of metal speciation and solubility of a wide range of ore-forming minerals in aqueous electrolyte solutions is now possible to 1000°C and 5 kbar with recent advances in aqueous solution chemistry (Shock & Helgeson 1987; Sverjensky 1987; Tanger & Helgeson 1987). The method, outlined by Sverjensky (1987), allows estimation of the thermodynamic properties of many complexes of interest over a wide range of P-T conditions. This data may then be used to calculate formation constants for these complexes which are essential for speciation and solubility calculations.

Due to the complex nature of the procedure and the presence of a number of errors in the text of the only published version of the calculation (Sverjensky 1987), a simplified approach was used in the present study. It follows that described by Henley *et al.* (1984) and has the advantage that it relies more heavily on experimental data. While this means that the method is restricted to species which have been studied experimentally, uncertainties in many of the parameters involved are significantly reduced. Thus, one can have a higher level of confidence in the results obtained.

For the sake of clarity, the method is outlined below using the example of lead complexing in chloride-rich aqueous fluids. This example is appropriate in the present study where most of the fluids studied are dominated by chloride ions.

The total concentration of lead in solution is the sum of the concentrations of each of its complexes:

$$\Sigma Pb = mPb^{2+} + mPbCl^{+} + mPbCl_2^{\circ} + mPbCl_3^{-} + mPbCl_4^{2-} \qquad ...(5.2)$$

This assumes that the contribution of other Pb complexes (such as sulphide- or thio-complexes) is minimal.

The cumulative formation constants (β_n) for each of the complexes considered above are given by:

$$Pb^{2+} + Cl^{-} = PbCl^{+} \qquad \beta_1 = \frac{a.PbCl^{+}}{(a.Pb^{2+})(a.Cl^{-})} \qquad ...(5.3)$$

$$Pb^{2+} + 2Cl^{-} = PbCl_2^{\circ} \qquad \beta_2 = \frac{a.PbCl_2^{\circ}}{(a.Pb^{2+})(a.Cl^{-})^2} \qquad ...(5.4)$$

$$Pb^{2+} + 3Cl^{-} = PbCl_3^{-} \qquad \beta_3 = \frac{a.PbCl_3^{-}}{(a.Pb^{2+})(a.Cl^{-})^3} \qquad ...(5.5)$$

$$Pb^{2+} + 4Cl^{-} = PbCl_4^{2-} \qquad \beta_4 = \frac{a.PbCl_4^{2-}}{(a.Pb^{2+})(a.Cl^{-})^4} \qquad ...(5.6)$$

Substituting activity coefficients (ϕ_i) and molalities (m_i) of the species in equations 5.3-5.6 ($a_i = \phi_i m_i$) and rearranging yields a series of expressions for the concentration of each complex in solution of the form:

$$m\mathrm{PbCl}_n^{2-n} = (\beta_n \,.\, \phi\mathrm{Pb}^{2+} \,.\, m\mathrm{Pb}^{2+} \,.\, (\phi\mathrm{Cl}^- \,.\, m\mathrm{Cl}^-)^n)/\phi\mathrm{PbCl}_n^{2-n} \qquad \text{...(5.7)}$$

These may be substituted into eq. 5.2 to yield:

$$\Sigma\mathrm{Pb} = m\mathrm{Pb}^{2+}\Big(1 + \frac{\beta_1.\phi\mathrm{Pb}^{2+}.\phi\mathrm{Cl}^-.m\mathrm{Cl}^-}{\phi\mathrm{PbCl}^+} + \frac{\beta_2.\phi\mathrm{Pb}^{2+}.(\phi\mathrm{Cl}^-.m\mathrm{Cl}^-)^2}{\phi\mathrm{PbCl}_2^\circ} + \frac{\beta_3.\phi\mathrm{Pb}^{2+}.(\phi\mathrm{Cl}^-.m\mathrm{Cl}^-)^3}{\phi\mathrm{PbCl}_3^-} + \frac{\beta_4.\phi\mathrm{Pb}^{2+}.(\phi\mathrm{Cl}^-.m\mathrm{Cl}^-)^4}{\phi\mathrm{PbCl}_4^{2-}}\Big) \qquad \text{...(5.8)}$$

Some of the cumulative formation constants used in the present study have been experimentally determined by a variety of authors (Pb - Seward 1984; Zn - Ruaya & Seward 1986; Ag - Seward 1976; Sn - Jackson & Helgeson 1985). Other formation constants used are those calculated theoretically by Helgeson (1969). The concentration of Cl^- is taken as equivalent to the total dissolved chloride (estimated by microthermometry) and the activity coefficients of the various species may be calculated from the extended Debye-Hückel equation (see Helgeson *et al.* 1981 for details). The only remaining unknown is the concentration of Pb^{2+} in solution which may be determined from the hydrolysis constant of galena:

$$\mathrm{PbS} + 2\mathrm{H}^+ = \mathrm{Pb}^{2+} + \mathrm{H_2S} \qquad K_{PbS} = \frac{(a.\mathrm{Pb}^{2+})(a.\mathrm{H_2S})}{(a.\mathrm{H}^+)^2} \qquad \text{...(5.9)}$$

The value of K_{PbS} has been experimentally determined for a variety of temperatures. For other metal sulphides (MS), K_{MS} may be estimated from the reaction:

$$\mathrm{MS}_n = \mathrm{M}^{2n+} + n\mathrm{S}^{2-} \qquad K = (a.\mathrm{M}^{2n+})(a.\mathrm{S}^{2-})^n \qquad \text{...(5.10)}$$

in combination with the first and second dissociation constants of H_2S (Helgeson 1969):

$$\mathrm{H_2S} = \mathrm{H}^+ + \mathrm{HS}^- \qquad K_1 = \frac{(a.\mathrm{H}^+)(a.\mathrm{HS}^-)}{a.\mathrm{H_2S}} \qquad \text{...(5.11)}$$

$$\mathrm{HS}^- = \mathrm{H}^+ + \mathrm{S}^{2-} \qquad K_2 = \frac{(a.\mathrm{H}^+)(a.\mathrm{S}^{2-})}{a.\mathrm{HS}^-} \qquad \text{...(5.12)}$$

The value of $a.HS^-$ may be estimated from eq. 5.11 since both $a.H^+$ and $a.H_2S$ are known (assuming $\phi H_2S = 1$). This can then be substituted into eq. 5.12 to yield $a.S^{2-}$. Equation 5.10 then gives $a.M^{2n+}$ and hence mM^{2n+}. Substituting activity coefficients and molalities and rearranging eq. 5.9 yields:

$$m\mathrm{Pb}^{2+} = \frac{K_{PbS} \,.\, (a.\mathrm{H}^+)^2}{\phi\mathrm{H_2S} \,.\, m\mathrm{H_2S} \,.\, \phi\mathrm{Pb}^{2+}} \qquad \text{...(5.13)}$$

Finally, this result is substituted into eq. 5.8 to yield the total concentration of Pb in solution and the relative contributions of each of the complexes (each term in the brackets in eq. 5.8 represents the relative molal proportion of each complex in solution).

A complication arises where a metal can exist in a number of oxidation states. Consideration of the equilibrium constants for redox reactions between species such as:

$$Cu^{2+} + 0.5\ H_2O = Cu^{+} + 0.25\ O_2 + H^{+}$$

shows that the reduced species (in this case Cu^{+}) is always dominant in the fluids investigated in this study. As a result, the solubilities of ore minerals containing the reduced species were calculated rather than their oxidised equivalents.

5.2.2 Results

The method described above has been applied to V1, V2 and $V4_W$ fluids, for which the intensive parameters P, T, pH and fO_2 are relatively well-constrained. An approximate calculation for V3 type 3 fluids was also carried out, to assess their potential for metal transport. The results of the calculations are presented in Table 5.1.

5.2.3 Discussion

The solubilities calculated above assume saturation with respect to the ore mineral. This means that the calculated values should only reflect solution composition if the ore mineral is in equilibrium with the fluid. Thus, a fluid from which an ore mineral was precipitating should be saturated with respect to that phase, and measured metal concentrations and calculated solubilities should be comparable. For fluids where metal concentrations have been determined directly (*e.g.* by D-ICP), it is possible to compare the saturation and estimated true metal concentrations. This indicates whether the fluid was well below or close to saturation with respect to the ore mineral. In addition, the calculated mineral solubilities give an indication of the metal carrying potential of the different fluids. A high solubility does not mean that the fluid was transporting large quantities of metal; however, it does indicate that the fluid could transport significant quantities of metal under favourable circumstances.

The calculations presented above only provide a general picture of the metal transport potential and metal speciation in a variety of chloride-rich crustal fluids. Due to errors inherent in the thermodynamic data, in experimentally and thermodynamically estimated complex formation constants, and in the intensive parameters defined in this study, the values quoted in Table 5.1 can only be treated as order-of-magnitude estimates. However, the trends in mineral solubility and speciation are valid and a number of important conclusions can be drawn (see 5.3).

Table 5.1 Calculated solubilities of ore minerals (ppm metal), metal-chloride and tin-hydroxide speciation (molal %) in crustal fluids, south Cornwall.

		Solubility	M^{z+}	MCl^{z-1}	MCl_2^{z-2}	MCl_3^{z-3}	MCl_4^{z-4}	$Sn(OH)^+$	$Sn(OH)_2^\circ$	$Sn(OH)_3^-$
	SnO_2	0.15	0.00002	0.003	0.02	0.06		0.15	99.8	0.0002
	PbS	0.5	0.02	2.6	43.9	53.5				
	ZnS	38	0.0001	6.4	4.3		89.3			
V1	Cu_2S	680	0.00001		6.8	93.2				
	Cu_5FeS_4	36	0.00001		6.8	93.2				
	Ag°	2.1	0.02	3.7	96.3					
	Ag_2S	0.8	0.02	3.7	96.3					
	Hg°	$2x10^{-8}$	$4x10^{-8}$	0.002	3.2	96.8				
	HgS	$2x10^{-7}$	$4x10^{-8}$	0.002	3.2	96.8				
	SnO_2	0.0056	0.0009	0.03	0.1	0.4		0.3	92.9	6.3
	PbS	0.1	0.2	7.8	58.9	33.2				
	ZnS	1.6	0.007	39.3	14.6	0.1	45.9			
V2	Cu_2S	35	0.00006		10.1	89.9				
	Cu_5FeS_4	3.4	0.00006		10.1	89.9				
	Ag°	0.4	0.01	1.4	98.6					
	Ag_2S	0.4	0.01	1.4	98.6					
	Hg°	$3x10^{-9}$	$1x10^{-8}$	0.0002	0.8	99.2				
	HgS	$4x10^{-9}$	$1x10^{-8}$	0.0002	0.8	99.2				
	SnO_2	28	0.000004	0.01	1.9	91.5		0.008	6.2	0.3
V3	PbS	1800	0.00003	0.009	1.4	98.6				
brine	ZnS	560	0.00005	23.7	76.3					
	Ag°	7780	0.0002	0.1	99.9					
	Ag_2S	760	0.0002	0.1	99.9					
	SnO_2	0.00014	0.01	0.4	7.5	92.5		0.005	0.01	$6x10^{-6}$
	PbS	73	0.007	0.3	8.5	12.9	78.3			
	ZnS	1080	0.001	0.4	0.9	0.3	98.4			
	Cu_2S	90	0.000002		2.0	98.0				
$V4_w$	Cu_5FeS_4	15	0.000002		2.0	98.0				
	Ag°	0.7	0.0001	0.3	22.1	77.6				
	Ag_2S	1.1	0.0001	0.3	22.1	77.6				
	Hg°	$4x10^{-8}$	$1x10^{-11}$	0.000002	0.5	99.5				
	HgS	$4x10^{-8}$	$1x10^{-11}$	0.000002	0.5	99.5				

Cumulative formation constants for complexes used to calculate solubility and aqueous speciation were taken from Jackson & Helgeson 1985 (Sn), Seward 1984 (Pb), Ruaya & Seward 1986 (Zn), Seward 1976 (Ag) and Helgeson 1969 (Cu, Hg). Equilibrium constants for hydrolysis, redox and dissociation reactions were taken from Helgeson (1969) and Henley *et al.* (1984).

5.3 METAL TRANSPORT IN REGIONAL METAMORPHIC FLUIDS

A number of bulk rock studies of the composition of pelites have shown that there is a depletion in many trace metals with increasing metamorphic grade (*e.g.* Haack *et al.* 1984). This has led to the suggestion that many metals are mobilised during metamorphic processes and, indeed, many ore deposits are believed to have been formed as a result of such processes (Barnes 1979). The solubility and fluid compositional data presented in section 5.2 suggest that metals were mobilised by regional metamorphic fluids in south Cornwall. This has important consequences for the development of the metallogenic province.

5.3.1 Metal solubility

The data presented in Table 5.1 show that metals complexed by chloride (primarily the base metals Pb, Zn, Cu) can achieve significant concentrations, even in relatively dilute solutions (0.41m Cl^-). The calculated solubility of sphalerite in V1 fluids (38 ppm Zn) is close to the two estimates of total zinc (61.4, 35.9 ppm) from D-ICP data (Table 3.3). This suggests that the peak regional metamorphic fluids were close to equilibrium with sphalerite (*i.e.* saturated with Zn). The D-ICP estimates of copper in solution (31.2-79.7 ppm) are comparable with the calculated solubility of bornite in V1 fluids. This indicates that the V1 fluids were probably close to saturation with respect to bornite at 300°C and 3 kbar. However, V1 fluids were significantly undersaturated with respect to chalcocite and, if they had encountered a chalcocite-bearing assemblage, could have dissolved up to *c.*700 ppm Cu.

The calculated solubilities of native silver and argentite (Ag_2S) suggest that important (ppm) quantities of silver could have been transported in V1 fluids as chloride complexes. In contrast, the data for mercury indicate that Hg^{2+}-chloride complexing was virtually non-existent under conditions of low-grade regional metamorphism.

The mobility of tin in regional metamorphic fluids in Cornubia is particularly interesting because of the development of a major tin province in the region. The solubility calculations indicate that the peak metamorphic fluids mobilised in the study area could have carried up to 0.15 ppm Sn. This has important implications for the redistribution of tin during regional metamorphism (see 5.3.3).

Comparison between V1 and V2 solubility data indicates that V2 fluids were much less effective at transporting base metals, tin, silver and mercury. In general, calculated solubilities are an order of magnitude lower, despite the 30% increase in salinity. If V2 fluids were essentially V1 fluids that flowed to higher crustal levels as suggested in section 4.3.2, the significant decrease in solubilities would have had important consequences. Phases initially close to saturation in V1 fluids would precipitate during fluid ascent. This phenomenon is discussed further in section 5.3.4.

5.3.2 Metal complexing

The speciation calculations presented in section 5.2 show that free metal ions are only present in tiny amounts in a variety of crustal fluids (see 5.1.1). The solubilities of many ore minerals in such fluids can only be accounted for by the formation of a variety of associated species, which, in chloride-rich fluids, will tend to be dominated by chloro-complexes (at least for the base metals). Although complexing of base metals by sulphido- and hydrosulphido- ligands probably occurs, it is unlikely to be an important process under the relatively low sulphur fugacities developed in most crustal fluids (*e.g.* Henley *et al.* 1984). The correlation between total zinc in solution and estimated sphalerite solubility in V1 fluids suggests that chloride complexing alone can account for zinc solubility.

The calculations of base metal-chloride speciation in V1 fluids show that the higher coordination numbers are favoured, with zinc dominantly transported as $ZnCl_4^{2-}$, copper as $CuCl_3^{2-}$ and lead as $PbCl_2^{\circ}$ and $PbCl_3^-$. This is in agreement with observations made by Helgeson (1969) that

high temperatures and high chloride concentrations favour the more associated species. The V2 data reinforce this point, with the less associated species $ZnCl_2^\circ$, $PbCl^+$, $PbCl_2^\circ$ and $CuCl_2^-$ becoming increasingly important with decreasing temperature.

According to the calculations, the speciation of silver and mercury is much less temperature- and chloride-dependent. Both species show an opposite relationship to the base metals, with the more associated complexes being slightly favoured at lower temperatures. Although the predicted silver solubilities are easily high enough to account for silver transport via chloride complexing, the mercury solubilities are not. This suggests that an alternative ligand, possibly HS^-, is more likely to be responsible for mercury transport in regional metamorphic fluids. Although the calculations have not been carried out, a similar argument would apply to the transport of gold in solutions of this type.

The speciation of tin in V1 and V2 fluids is in complete contrast to the chloride-dominated complexing of base metals. The calculations suggest that in V1 fluids, tin is almost solely transported by the neutral $Sn(OH)_2^\circ$ complex, with minor contributions from other hydroxy- and chloro-complexes. This behaviour is comparable to that displayed by the preceding Group IV element silicon, which also forms hydroxy- complexes in aqueous solution (Cotton & Wilkinson 1980). With decreasing temperature and increasing salinity, the $Sn(OH)_3^-$ complex is increasingly favoured, although the neutral hydroxy- complex is still dominant. The increase in chloride concentration in V2 fluids is reflected by slight increases in the proportion of chloro- complexes, with the trichloride as the most important.

5.3.3 Ore deposition

The hypothetical deposition of ore minerals from V1 and V2 fluids can be considered qualitatively with reference to hydrolysis, redox and complex formation equilibria. These considerations allow prediction of environments and conditions under which an ore deposit could form from the passage of such fluids.

Cassiterite

As discussed in section 5.2, tin is primarily complexed by hydroxide in the regional metamorphic fluids. Reference to the cassiterite hydrolysis equilibrium:

$$SnO_2 + 2H^+ = Sn^{2+} + 0.5O_2 + H_2O$$

shows that cassiterite precipitation is favoured by increases in $a.Sn^{2+}$, fO_2 or $a.H_2O$. The effect of increasing pH, which at first glance would appear to decrease cassiterite solubility, is counterbalanced by the increased hydroxy-complexing of Sn^{2+}. The decrease in fO_2 from V1 to V2 would be expected to enhance cassiterite solubility. However, the decrease in temperature is more important, hence the reduced solubility of cassiterite in V2 fluids (Table 5.1). This means that a V1 fluid saturated with respect to cassiterite would necessarily precipitate cassiterite upon evolution to a V2 composition (see 5.3.4). An independent increase in fO_2, perhaps as a result of the fluid migrating into a more

oxidised environment (such as a red bed sequence), could result in deposition of cassiterite. Boiling, or fluid neutralisation by wallrock hydrogen metasomatism would not favour cassiterite precipitation because of the pH-dependence of the tin hydroxy-complexes.

Base metal sulphides

Consideration of the relevant equilibria for base metal sulphides shows that ore deposition will be favoured by:

1) an increase in sulphur fugacity;
2) a decrease in temperature;
3) a decrease in $a.Cl^-$;
4) an increase in pH.

Process 1 could occur if the fluid flowed into a lithology which could buffer it to higher sulphur fugacities, *e.g.* an assemblage containing pyrite instead of pyrite-pyrrhotite or pyrite-bornite instead of chalcopyrite (*e.g.* Barton & Skinner 1979).

A simple temperature decrease would result in precipitation of minerals initially close to saturation levels in the fluid (*e.g.* sphalerite). However, low temperature gradients would mean that significant concentrations of ore minerals would not occur. Minor mineralisation associated with some of the more important thrust faults in the area (*e.g.* the Blue Rock Thrust; see 1.3.5) could be accounted for by cooling of fluids which were rapidly pumped to higher structural levels during fault movement.

Mixing of the V1 or V2 fluids with dilute, possibly surface-derived, fluids could cause deposition of ore minerals by decreasing $a.Cl^-$ and hence destabilising chloro-complexes. Penetration of surface waters into thrust faults could conceivably occur in association with sub-aerial emergent thrusting. Such a process has been documented by Kerrich (1986). However, the fluid inclusion data presented in Chapter 3 indicate that such a process did not occur in the study area.

A pH increase via hydrogen metasomatism of wallrocks could also promote mineral deposition. A pH increase by boiling, for which there is some ambiguous evidence in V2 fluids (see 3.2.3), would be offset by a decrease in $a.H_2S$ and increase in $a.Cl^-$, both of which would increase sulphide solubility.

5.3.4 Metal concentration during regional metamorphism

Although ore deposits of conclusively metamorphic origin are not observed in the province (see 1.3.5), the fluid compositions and solubility data discussed above may be used to infer possible mechanisms whereby disseminated or concentrated ore accumulations could form.

Upward metal fluxing

The solubility and fluid compositional data for V1 and V2 fluids suggest that significant quantities of base metals, silver, mercury and other metals complexed by either chloride or sulphur-bearing ligands

may be deposited as fluids, released by devolatilisation reactions, flowed upward into overlying rocks. Field and petrographic data indicate that permeability during D1 was probably dominantly pervasive (microfracture-, grain boundary-, or cleavage-controlled), with locally developed macroscopic fracture systems (see 6.1.2). Later stage, or higher level (D2) permeability was characterised by much more abundant macroscopic fracturing and only locally-developed pervasive fluid flow along cleavage domains. These features imply that fluids flowing down P, T gradients, upward through the crust, would form a root-like distribution (Fig. 5.1).

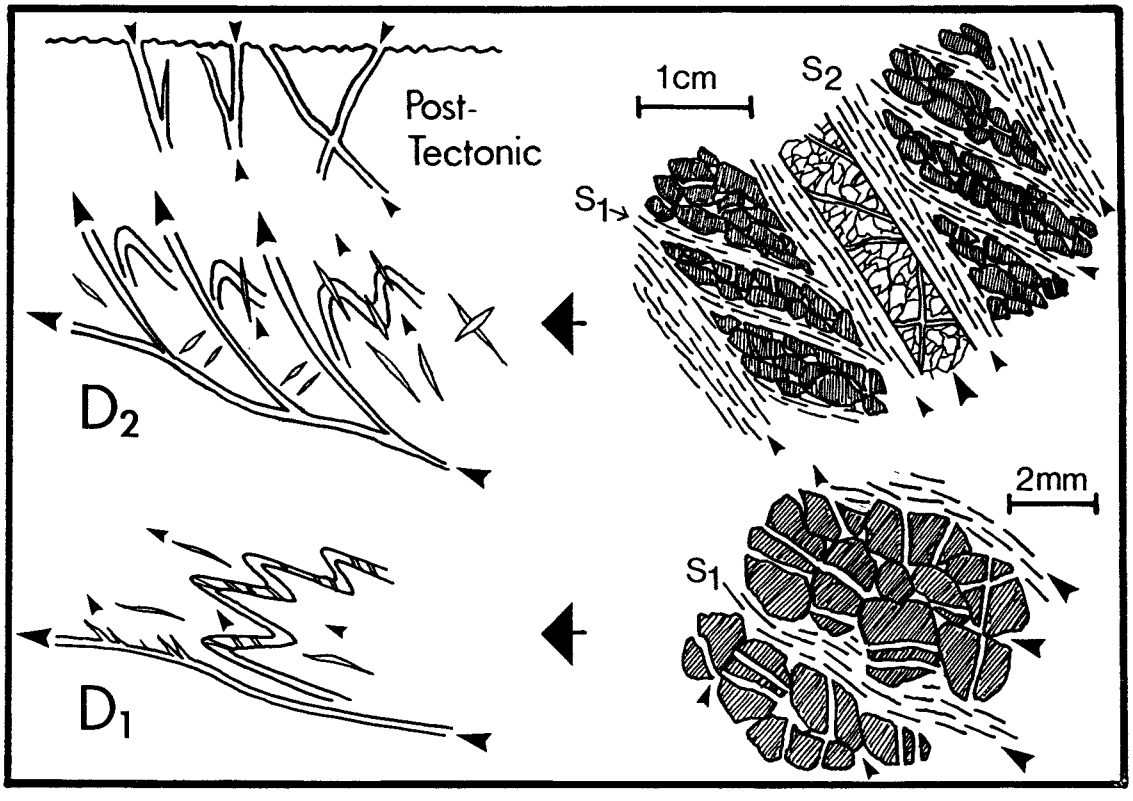

Figure 5.1 Schematic representation of macroscopic and microscopic permeability developed during D1 and D2. Tail-less arrows indicate fluid pathways.

On the basis of this type of model, metals carried in relatively high quantities in the high temperature fluids would tend to deposit ore minerals at higher crustal levels and in increasingly fewer structural sites. The lowermost zones of the crust would be characterised by metal depletion, the central zones by no net loss or gain and the upper regions by metal enrichment (Fig. 5.2). The absence of major (10-100 km scale) fracture permeability in the field area as well as generally in south Cornwall mean that any metal concentration which occurred at low metamorphic grades would have been relatively disseminated.

If this was a viable mechanism, it could account for pre-enrichments of a variety of ore-forming components at high levels in the crust prior to granite emplacement and the development of Sn-W-polymetallic sulphide mineralisation. Thus, regional metamorphic fluid flow could be an important intermediate stage in the development of a metallogenic province.

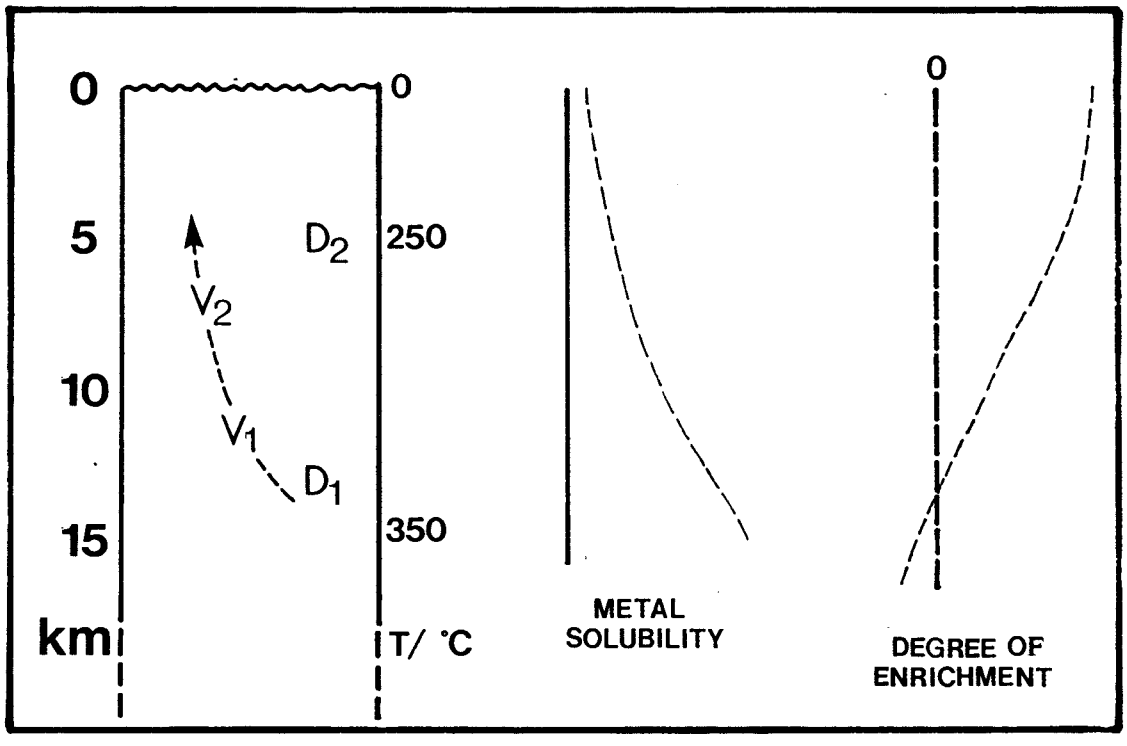

Figure 5.2 Schematic representation of V1 and V2 fluid flow and resultant metal enrichment in the upper crust during Hercynian tectonism and regional metamorphism in south Cornwall.

Metamorphic ore deposits

Although ore deposits of unequivocal metamorphic origin are not observed in the Cornubian province, the solubilities of some of the major ore-forming minerals in the V1 fluids indicate that the metamorphic fluids were potential ore-forming solutions. Whether undiscovered deposits of this type exist or not is an open question. However, it is important to note that mineral exploration in southwest England has always been directed towards granite-related phenomena. It is possible that deposits spatially and temporally unrelated to the Cornubian batholith have been overlooked.

For an ore deposit to form as a result of metamorphic fluid flow, a number of conditions must be met (see 4.1.3). In the present case, the development of a major (up to crustal scale) structure would be extremely important in channelling large volumes of fluid through a relatively small volume of rock. Although simple cooling and associated changes in fO_2, fS_2 and pH is a viable mechanism for precipitation of some ore minerals (see 5.3.1), more drastic changes in these parameters would be required for rapid dumping of metal within a restricted volume of rock. Such changes could be caused by boiling, fluid mixing, or interaction with a chemically contrasting lithology (*e.g.* a metabasite, a sulphidic/graphitic lithology, or a carbonate). There is no conclusive evidence in the present study of the operation of either of the first two processes. However, it is possible that the conjunction of a major fluid channelway and a lithology contrast could have resulted in ore deposition. This idea is developed as an exploration model in section 6.3.1.

5.4 METAL TRANSPORT IN V3 BRINES

This study has demonstrated the existence of highly saline fluids (up to 42 wt% NaCl equivalent), which were mobilised in the contact aureole of the Cornubian batholith during granite emplacement. Fluid inclusions of similar composition have been observed in granite quartz in the province (Shepherd *et al.* 1985), but their origin is uncertain because of repeated episodes of hydrothermal activity and quartz recrystallisation. They have been interpreted as trapped saline magmatic fluids (Rankin & Alderton 1985); however, the present study indicates that they could have a totally different origin.

5.4.1 Potential metal sources

The significance of the V3 brines in the metallogenic development of the Cornubian orefield lies in their high potential for leaching and transporting metals, particularly those commonly complexed by Cl^- (*e.g.* Pb, Zn, Cu, Fe, Sn). Many of these components are known to be enriched in the granites and in the immediate country rocks (Edwards 1976; Beer & Ball 1986). However, the source of these metals and the enrichment mechanism have long been subjects of controversy (see discussion of V3 fluid source, section 4.4.3).

The two often cited sources for these and other ore-forming metals involved in Cornubian metallogenesis are:

(1) Elevated levels in the source material for the Cornubian magmas;

(2) Elevated levels in the pelites into which granites were intruded;
    [a] incorporated into magma and thence magmatic fluid via assimilation;
    [b] incorporated into magmatic-hydrothermal system via leaching of pelites (by descending meteoric fluids or V3 fluids?).

Many studies have considered these possibilities, but the question remains unanswered. This is primarily a consequence of the ambiguous nature of much of the evidence we see today which is the end-product of a complex and long-lived hydrothermal system. The present study does not provide an answer to these questions; it does, however, shed some light on the processes which occurred in the contact aureole at an early stage of the mineralising history of the area. These processes are likely to have played an important role in the early development of slate-hosted mineralisation ("Type I metasomatisms" of Jackson *et al.* 1982) and possibly in the chemical evolution of a primary ore fluid.

5.4.2 Metal solubility

Direct analyses indicate that metal concentrations in V3 brines are considerable. Samples *D3CZ1* and *J93TP* have liquid-rich inclusion assemblages dominated by V3 type 3 inclusions which will supply the majority of the solutes in bulk D-ICP analyses. These give estimated concentrations of 680-2060 ppm Fe, 285-1320 ppm Zn and 380-3240 ppm Mn (Table 3.16). The identification of Fe-chloride and Fe/Mn carbonate daughter minerals in these inclusions by SEM/EDX attest to the high concentration of these metals, which are saturated with respect to chloride and/or carbonate at room temperature.

The Na/element weight ratios determined by bulk analysis of samples *D3CZ1* and *J93TP* suggest that these metal enrichments are not solely due to solute concentration in the residual aqueous phase during unmixing and vapour loss. For example, Na/Fe and Na/Mn ratios are considerably lower in these two V3 samples than for the others analysed. This is not just a function of temperature since these two samples have quite different estimated fluid trapping temperatures. The equilibrium relationships demonstrated between V3 saline fluids and contact metamorphic mineral assemblages (*e.g. J93TP*) suggest that these enrichments are the result of fluid-rock equilibration with an increasingly saline fluid coexisting with a vapour. Textural observations of this type are supported by the work of Bowers & Helgeson (1983b), who showed that a mineral assemblage can coexist in equilibrium with two immiscible fluids, where conditions are such that unmixing occurs.

The solubility calculations carried out in section 5.2 provide an approximate guide to the potential of V3 brines for metal transport. The calculated sphalerite solubility of 560 ppm Zn is comparable to the total dissolved zinc determined by D-ICP (285-473 ppm for *J93TP*). Considering the fact that total zinc was determined by bulk analysis (albeit for a sample dominated by V3 type 3 inclusions), the comparison is rather remarkable, and suggests that the V3 brines were saturated with respect to sphalerite. The estimated solubility of galena is also high (1800 ppm). It is unlikely that the V3 brines were saturated with respect to galena, because such high lead concentrations would have resulted in Pb determinations above background during D-ICP analysis. A similar argument also applies to silver.

Perhaps the most interesting solubility figure determined in this study is that of cassiterite in the V3 brines. The calculations suggest that these fluids could carry up to 28 ppm tin in solution (Table 5.1), an order of magnitude higher than that determined for peak regional metamorphic fluids. Average figures quoted for the concentration of tin in unaltered pelitic rocks from southwest England range from 3 ppm (Beer & Ball 1986) to 22 ppm (Henley 1974). This compares with a world average of 6 ppm estimated by Turekian & Wedepohl (1961). On the basis of these figures, it is reasonable to assume that V3 brines could easily have reached saturation with respect to cassiterite. In conclusion, the V3 brines are likely to have been very efficient at leaching tin from the aureole rocks and concentrating it in the fluid phase, forming a potential tin-mineralising fluid.

Summary

There is considerable evidence to suggest that V3 saline fluids carried significant quantities of ore metals in solution. It appears likely that metal concentration in these fluids was not solely a result of unmixing and preferential vapour loss, but also due to fluid-rock equilibration with an increasingly saline fluid. Although highly soluble in V3 brines, the concentration in solution of metals complexed by chloride would have been limited by available metal within the rock. Nevertheless, the solubility estimates indicate that these fluids were capable of leaching significant quantities of metal from the contact aureole and thus may have played an important role in the mineralisation history.

The combination of solubility and concentration data indicates that the fluids were probably saturated with respect to sphalerite, and undersaturated with respect to the other base metals and silver.

The flow direction of this fluid and its role in mineralising processes is uncertain. However, if syn-intrusion convection did occur (see 4.4.5) it is likely that this fluid did become involved in the evolution of the early, high temperature mineralising fluids.

5.4.3 Metal complexing

The speciation calculations for V3 brines presented in section 5.2 indicate that free ions are virtually non-existent. The data suggest that lead is predominantly transported as the $PbCl_3^-$ complex, with the neutral complex being much less important than was the case for lead transport in regional metamorphic fluids. In contrast, zinc and silver are mainly present as the MCl_2^{z-2o} complex, with a lesser contribution from MCl^{z-1}.

The speciation of tin in V3 brines is particularly interesting, with chloro-complexes being responsible for much of the tin transport. Hydroxy complexes, which were responsible for over 99.95% of tin transport in V1 fluids, account for less than 7% in V3 type 3 fluids. The dominant species is $SnCl_3^-$, making up 91.5% of the total. The reason for the extreme contrast in speciation between V1 and V3 type 3 fluids is the difference in salinity (the fluid temperatures being similar). The calculations show that an order of magnitude increase in the chloride molality results in a dramatic switch in tin speciation from almost wholly hydroxy-complexing to dominantly chloro-complexing.

5.4.4 Ore deposition

A variety of changes in intensive parameters could result in precipitation of metals from V3 brines. Ore minerals particularly sensitive to changes in fluid chemistry are those initially close to saturation in the fluid. From the discussion of ore mineral solubilities (section 5.4.2) it is likely that both sphalerite and cassiterite could precipitate as a result of relatively small shifts in different parameters.

Cassiterite

Cassiterite would be precipitated from a V3 brine by:

1) an increase in oxygen fugacity;
2) a decrease in temperature;
3) a decrease in $a.Cl^-$ (most likely by dilution);
4) an increase in pH.

The first and second possibilities will tend to counteract each other since decreasing temperature also implies decreasing fO_2 in a buffered system. An increase in pH could be caused by phase separation, which was an important process in the evolution of V3 fluids. However, the increase in pH which could promote cassiterite precipitation would be counterbalanced by a parallel increase in chloride concentration, tending to enhance cassiterite solubility. Thus, cassiterite mineralisation could occur as a result of either a T decrease or phase separation, but only where disequilibrium conditions prevailed. Either an independent increase in fO_2 or decrease in $a.Cl^-$ could also cause cassiterite deposition from V3 brines.

The preceding discussion is entirely hypothetical. There is no evidence at present to suggest that any of these processes occurred during the evolution of the Cornubian orefield. However, the points are useful when it comes to planning an exploration strategy (see 6.3).

Base metal sulphides

Sphalerite could be precipitated from a V3 brine by:

1) an increase in sulphur fugacity;
2) a decrease in temperature;
3) a decrease in $a.Cl^-$;
4) an increase in pH.

Boiling could cause sphalerite deposition by increasing pH; however a parallel decrease in the sulphur fugacity, caused by preferential H_2S loss to the vapour phase, would tend to increase sphalerite solubility. Unlike cassiterite, a simple temperature decrease is likely to cause sphalerite deposition because the sulphur fugacity is less sensitive to temperature than fO_2.

Although the other base and transition metals which form sulphide ore minerals were probably below saturation in V3 brines, similar, although more extreme, changes in intensive parameters could have led to ore deposition.

5.5 METAL TRANSPORT IN BASINAL BRINES

The thorough characterisation of the fluids responsible for base metal mineralisation in the study area (see 4.6) has allowed the formulation of a detailed model of ore genesis. This model encompasses the mechanisms of base metal enrichment and transport, as well as the processes ultimately responsible for ore deposition. The model highlights the important role played by granite-driven hydrothermal fluids in the genesis of the base metal deposits in the study area. This has implications for the genesis of cross-course mineralisation throughout the Cornubian province.

5.5.1 Metal solubility

The ore mineral solubilities calculated in section 5.2 indicate that significant quantities of base metals could have been transported as chloride complexes in $V4_W$ brines. The calculated solubility of sphalerite (1080 ppm) appears to be at odds with fluid compositional data and field observations. The presence of sphalerite in some of the $V4_W$ veins (*e.g.* Wheal Rose) suggests that the fluids should be close to saturation with respect to sphalerite. However, Zn was below the detection limit in D-ICP analyses, *i.e.* below a Na/Zn weight ratio of approximately 1000, suggesting that the total zinc concentration was below *c.*80 ppm. This implies that zinc was well below saturation in the fluids analysed, assuming the thermodynamic calculations are correct.

The major sources of error in the calculations of sphalerite solubility probably come from the estimation of the intensive parameters fS_2 and fO_2. The estimation of fS_2 (see 4.6.7) was based on equilibrium with pyrite at the fO_2 conditions defined by siderite-haematite equilibrium. This may overestimate fO_2, resulting in an underestimation of $a.H_2S$ and thus an overestimation of sulphide solubilities. For example, an order of magnitude overestimation of fO_2 would result in a 44% overestimation of sphalerite solubility. Despite this uncertainty, high base metal sulphide solubilities are likely in $V4_W$ fluids, according to the thermodynamic data.

One explanation for the apparent contradiction discussed above is that the $V4_W$ fluids analysed represent brines that have already deposited sphalerite. Vein petrography has revealed that this is in fact the case (see 2.2.15), with sphalerite occurring early in the paragenesis, prior to quartz growth (Fig. 2.16). Thus, the fluids analysed represent brines that were no longer saturated with respect to sphalerite (as indicated above). In contrast, galena occurs throughout the veins, albeit at distinct stages, suggesting that the $V4_W$ fluids analysed were likely to be closer to saturation with respect to galena. On the basis of this argument, the galena solubility of 73 ppm Pb predicted by the thermodynamic calculations is likely to be a good estimate of the total lead in solution.

Copper was not detected above background by D-ICP analysis, which implies that there was $\leq$60 ppm in solution. The solubility of copper(I) minerals in the basinal brines are just at this level, which means that the fluids could have been saturated with respect to chalcocite or bornite. Petrographic studies indicate that, at least during the early stages of vein growth, the fluids were saturated with respect to chalcopyrite (Fig. 2.16).

According to the calculations, the solubility of mercury as chloride complexes is negligible in $V4_W$ fluids. This is perhaps surprising as mercury is often precipitated from low temperature fluids.

This could be explained by mercury being predominantly complexed by sulphide-bearing ligands rather than by chloride.

The ppm-levels of silver that the $V4_w$ fluids could carry accords with the observation that galena from cross-courses in southwest England is usually argentiferous (Hosking 1964). The co-precipitation of galena and silver would be expected if silver was transported primarily as chloro-complexes which would be destabilised by the same processes which would lead to galena precipitation.

Cassiterite is relatively insoluble in $V4_w$ fluids and they are thus considered to be unsuitable for tin transport.

5.5.2 Metal complexing

Apart from mercury, as mentioned above, it is highly likely that all the base metals are transported as chloro-complexes in low temperature, chloride-rich fluids. The low temperatures and high chloride molality mean that both lead and zinc are predominantly transported by the MCl_4^{z-4} complex, rather than by MCl_3^{z-3} which occurs at higher temperatures, or by MCl_2^{z-2} which tends to occur at lower chloride concentrations. Copper is primarily present as $CuCl_3^{2-}$, which appears to be the most stable copper chloro-complex in a wide range of fluid compositions.

The salinity is high enough for tin to also be dominantly transported by chloro-complexes, rather than by hydroxy-complexes, as was also the case for the V3 brines.

5.5.3 Ore deposition

Deposition mechanisms

In theory, there are four different shifts in intensive parameters which could result in base metal sulphide deposition:

1) an increase in sulphur fugacity;
2) a decrease in temperature;
3) a decrease in $a.Cl^-$;
4) an increase in pH.

In practice, these possibilities can be considered in conjunction with field and laboratory observations in order to model the ore deposition process.

The most significant observations made in this study, relating particularly to galena deposition, are:

a) there is no discernible change in temperature associated with sulphide deposition (Fig. 5.3);

b) galena is usually precipitated on quartz immediately after a growth zone (Figs. 2.14, 5.3);

c) there is clear fluid inclusion evidence for interaction of $V4_W$ brines with dilute, meteoric fluids.

Fluid inclusion data suggest that there were no significant changes of temperature accompanying ore deposition (Fig. 5.3). This rules out a simple temperature decrease as the cause of sulphide precipitation. Fluid-rock interaction could play a role in sulphide deposition in zones of intense brecciation and silicification, by neutralisation of the acidic fluids (hydrogen metasomatism) during feldspar breakdown reactions. However, this process cannot account for galena precipitation in symmetrical syntaxial lodes (Figs. 2.14, 2.16) where the late fluids responsible for sulphide precipitation are isolated from the wallrocks by inert quartz. In this, the most important environment of base metal mineralisation in the area, the most likely cause of sulphide deposition is mixing with low salinity fluids.

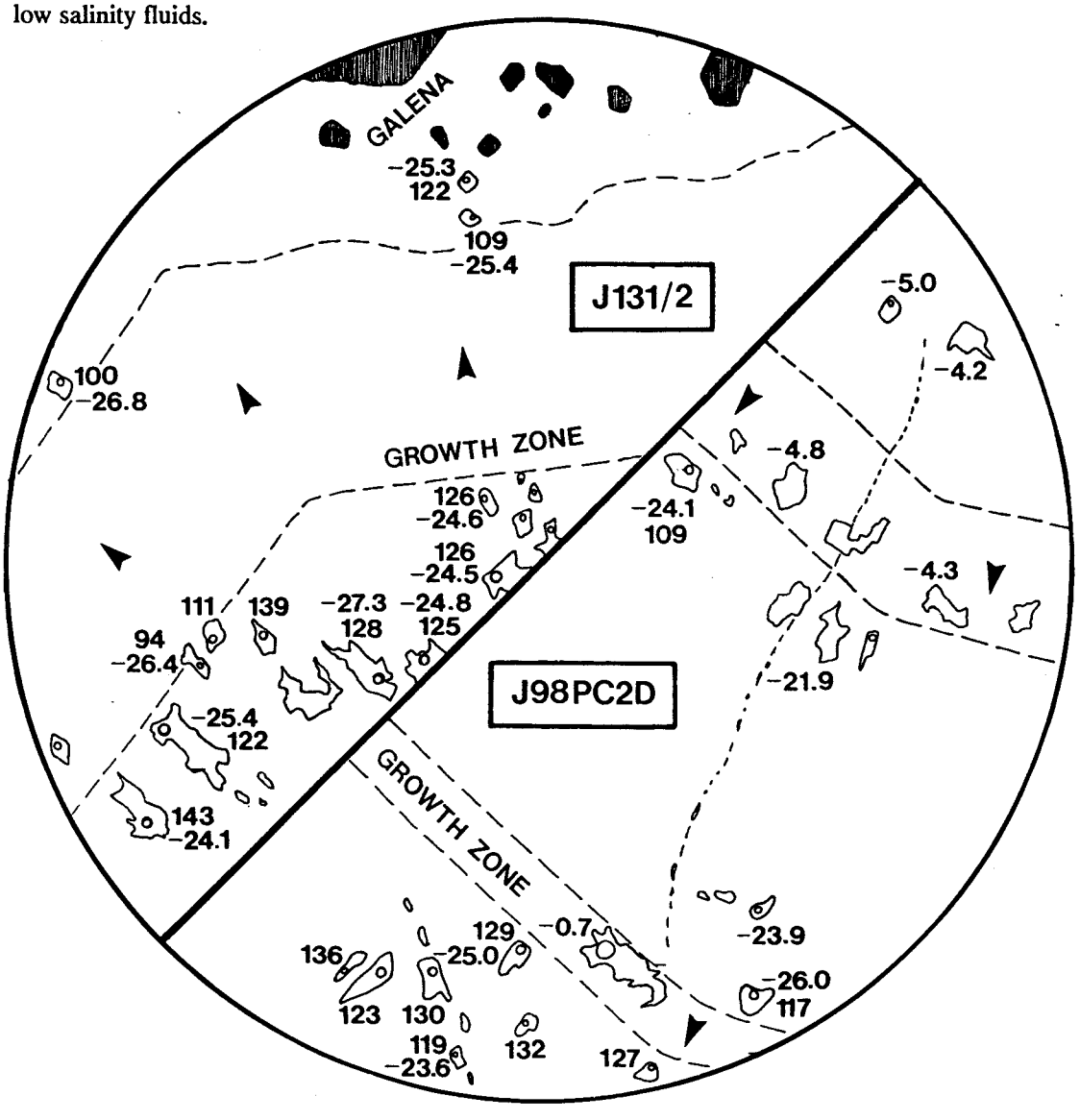

Figure 5.3 Fields of view from two $V4_W$ samples from Wheal Rose, illustrating inclusion morphology, *TmI* and *Th* data and relationships with growth zones and galena crystals.

Basinal brine - meteoric mixing

Th-S data for $V4_N$ and $V4_W$ fluids (Fig. 6.8) suggest that on a broad scale, mixing between the two fluids occurred. The relationship between growth zones in quartz and galena crystals (Fig. 5.3) suggests that each growth zone could represent a mixing event, some of which led to galena precipitation. This hypothesis is supported by the presence of abundant fine mica flakes in the growth zones, occurring as solid inclusions in quartz and as trapped crystals in fluid inclusions (Fig. 3.23). According to K-mica hydrolysis:

$$KAl_3Si_3O_{10}(OH)_2 + 10H^+ = K^+ + 3Al^{3+} + 3Si(OH)_4$$

$$K = \frac{(a.K^+)(a.Al^{3+})^3(a.Si(OH)_4)^3}{(a.H^+)^{10}} \qquad ...(5.14)$$

K-mica precipitation from a fluid is extremely sensitive to changes in $a.H^+$, being strongly favoured by an increase in pH (*i.e.* a decrease in $a.H^+$). Mixing with a dilute fluid of $V4_N$ type, although resulting in a reduction in the activities of the species in the numerator of eq. 5.14, would have a much greater effect on the denominator, resulting in K-mica precipitation. Consideration of the four mechanisms for sulphide precipitation outllned above indicates that mixing can cause sulphide precipitation by simultaneously increasing pH and decreasing the chloride concentration.

Controls of base metal mineralisation

The data discussed above indicate that the vein-hosted base metal deposits in the field area were probably formed as a result of mixing between convecting, meteoric-dominated fluids and basinal brines migrating northwards along wrench faults and associated extensional structures. Such mixing occurred at structurally-controlled sites where N-S or NNW-SSE trending wrench faults intersected ENE-WSW trending normal faults. This model can account for the observed distribution of base metal deposits in the Cornubian province, being most abundant on the southern flanks of the batholith (*e.g.* Willis-Richards & Jackson, in press) with the most important deposits associated with the larger wrench faults (see 6.1.5).

5.6 SUMMARY

In this chapter, thermodynamic data have been used to estimate ore mineral solubilities and metal speciation in the most important fluid systems considered in this study. In combination with the intensive parameters estimated in Chapter 4, this data has allowed detailed modelling of the transport and deposition mechanisms of metals in a variety of compositionally distinct crustal fluids.

The calculations indicate that low grade regional metamorphic fluids could transport significant quantities of base metals as chloro-complexes with coordination numbers greater than 2. Sub-ppm quantities of tin could also have been transported predominantly as the neutral $Sn(OH)_2^\circ$

complex. Metal solubilities decrease by over an order of magnitude between V1 and V2 fluid types, suggesting that regional metamorphic fluid flow acts as a differentiation mechanism, resulting in metal enrichment in the upper levels of the crust.

The solubility of metals complexed by chloride is considerable in the hypersaline brines generated in the contact aureole of the Cornubian batholith by fluid unmixing. Metal enrichments in these fluids appear to be the result of equilibration of the saline fluid generated by unmixing with the vein wallrocks. Cassiterite solubility in the V3 brines was estimated at 28 ppm Sn, indicating that significant mobilisation of tin in the contact aureole was likely during granite emplacement.

According to thermodynamic predictions, the saline, acidic basinal brines, which migrated into the Cornubian peninsula contemporaneously with granite-hydrothermal convection, could have transported up to 73 ppm lead, 1080 ppm zinc, 90 ppm copper and 1.1 ppm silver as chloro-complexes. Complex coordination numbers of 3 or 4 are favoured at low temperatures and high chloride concentrations. Dilution by mixing with meteoric fluids provides an efficient mechanism for deposition of base metal sulphides.

The implications of these models of metal transport and ore deposition for the development of the Cornubian metallogenic province are considered in Chapter 6.

CHAPTER 6: THE CORNUBIAN METALLOGENIC PROVINCE

Wherever universal geological processes are in operation - weathering, sedimentation, metamorphism, deposition by underground waters and vulcanism - there mineral deposits may be forming as they have done during the long ages of the earth's history. Over larger or smaller areas the conditions may at a given time be favorable for the deposition of useful minerals. Such areas are called minerogenetic or metallogenetic provinces.

Waldemar Lindgren, 1919

The purpose of this chapter is to present a model summarising the evolution of the Cornubian metallogenic province, incorporating data from the preceding chapters, in addition to that from previous studies. The model encompasses the roles played by tectonic, metamorphic and magmatic processes, with emphasis on the importance of the fluid phase in metallogenesis. The thermobarometric and compositional fluid evolution trends defined in the present study are incorporated into the existing framework of Cornubian fluid evolution. On the basis of the model, a number of exploration models are proposed which apply to the Cornubian orefield as well as to similar terrains in other parts of the world.

6.1 TECTONOTHERMAL AND METALLOGENIC EVOLUTION OF SOUTH CORNWALL

In the following sections, a series of qualitative and quantitative observations are brought together into a model describing processes important in the evolution of the Cornubian metallogenic province. These features are summarised in a tectonothermal-metallogenic diagram (Fig. 6.1).

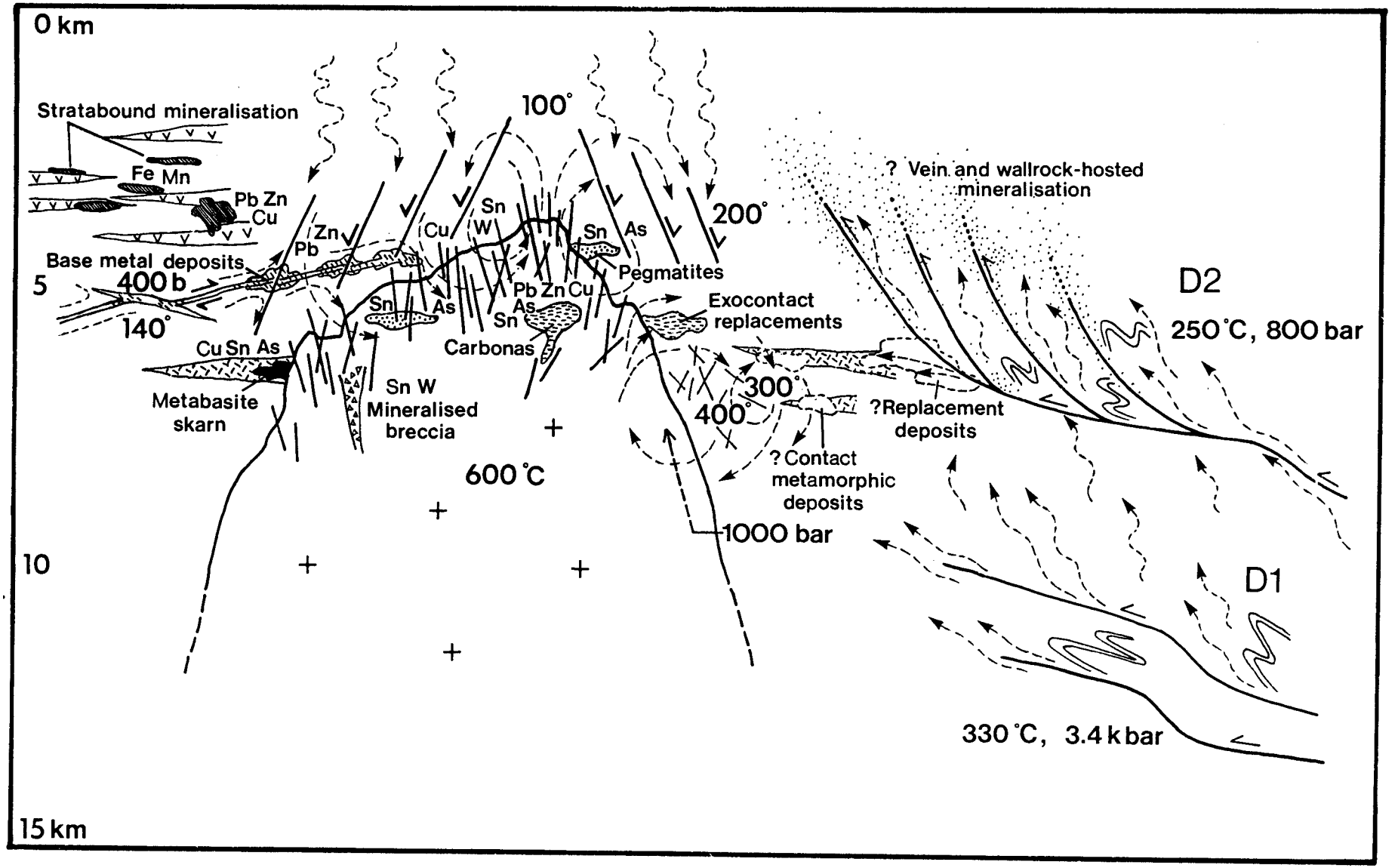

Figure 6.1 Synoptic diagram illustrating the metallogenic evolution of the Cornubian province. Compiled from data obtained in this study, Jackson *et al.* (in press) and Jackson *et al.* 1982. Dashed arrows denote fluid movement, with estimated fluid temperatures and pressures; thick solid lines represent faults/fractures. Symbols used are as follows: v = volcanics; crosses = granite; cross-hatch = metabasite; dots = pegmatite; triangles = breccia; short dashes = replacement deposits; solid = skarn; diagonal hatch = stratabound deposits.

6.1.1 Tectonothermal evolution during crustal compression

Geothermal gradient

Microthermometric and other data were used to estimate peak regional metamorphic conditions in south Cornwall of 330±30°C and 3.4±0.5 kbar (see 4.2.1). A lithostatic pressure of 3.4 kbar implies that the rocks currently exposed were at a depth of the order of 13 km during pumpellyite-actinolite grade metamorphism (syn-D1). These data give an "average" geothermal gradient of 26°C km^{-1}. Note that this does not represent the true geothermal gradient which existed at any one time.

Nappe pile thickness

If a simple model for crustal compression is considered, such as that described by Holder & Leveridge (1986), the data discussed above may be used to constrain the thickness of the overthrust sequence.

Assuming that the continental crust had an average thickness of 30 km prior to thrusting, the approximate thickness of the shortened crust when the currently exposed rocks reached the metamorphic peak would have been 43 km. This means that a series of nappes of ≈13 km total thickness were thrust over the Gramscatho Group sediments during Hercynian compression. Gramscatho Group rocks in the study area are currently overlain by approximately 1 km stratigraphic thickness of sediments (the Carne Formation) which are, in turn, overlain by the Lizard Complex (Fig. 1.4). The Lizard Complex is known to comprise a 1-2 km thick wedge of mafic and ultramafic rocks (Al-Rawi 1980) so that of the order of 10 km of overburden must have been removed by erosion between the Hercynian and the present day. This overburden may be represented by the "Normanian Nappe" in the model of Holder & Leveridge (1986).

Uplift rate

The estimated P-T conditions for the late stages of D2 (*i.e.* 250°C, 800 bars fluid pressure; see 4.3.1) may be used to estimate an average uplift rate during crustal shortening. If P_F (800 bars) was equal to lithostatic pressure towards the end of D2, a pressure of 800 bars would represent an overburden of 3 km. This would mean that ≈10 km of cover had been eroded from the crustal segment during compression. Alternatively, if P_F was equivalent to hydrostatic pressure during D2, 800 bars would represent ≈8 km of cover. This suggests a 5 km thickness of rock was removed.

The discovery of Late Famennian palynomorphs in slates from south of Loe Bar (Wilkinson & Knight 1989) indicates that sedimentation occurred at least to the end of the Devonian. Thus, significant compression is unlikely to have occurred before the Lower Carboniferous. The initiation of thrusting is, therefore, limited to no earlier than 360 Ma (Harland *et al.* 1982). The emplacement of the Cornubian batholith at ≈290 Ma (see 1.3.2) gives a maximum time interval for thrust stacking of 70 My. Combining this with the maximum and minimum estimates of the thickness of crust eroded yields a minimum average uplift rate of 0.07-0.14 mm yr^{-1}. Reducing the duration of thrusting to a perhaps more reasonable estimate of 35 My gives an average uplift rate of 0.14-0.29 mm yr^{-1}. On the basis of these figures, an average uplift rate of the order of 0.2 mm yr^{-1} seems likely. This is close to the average uplift rate of 0.3-0.4 mm yr^{-1} estimated for Alpine schists in New Zealand, subsequent to Jurassic regional metamorphism (Adams 1981).

6.1.2 Fluid flow during regional metamorphism

Controls of fluid flow

Estimates of the amount of fluid released by average pelites during metamorphism are of the order of 2 moles per kg of rock, equivalent to 130 cm^3 per litre of rock (Walther & Orville 1982). The rate of fluid release through devolatilisation reactions is likely to be at maximum during peak low-grade metamorphism (Wood & Walther 1986). Therefore, it follows that a significant proportion of the total fluid released will be evolved at this stage. However, in the study area, peak metamorphic (V1) quartz veins are relatively scarce, suggesting that macroscopic fractures only account for a small fraction of the bulk rock permeability.

V1 quartz veins contain abundant microfractures with fluid inclusions that have P-V-T-X properties consistent with a peak metamorphic origin. These observations support the concept that significant microfracture permeability developed during D1. It is thus concluded that fluid flow during D1 was dominantly pervasive, via microfracture and possibly also grain boundary permeability (Fig. 5.1).

Fluid-rock ratios

Using the estimate of 2 moles of fluid evolved per kg of rock during regional metamorphism (see above), a minimum "time-integrated" water/rock weight ratio (Wood & Walther 1986) of 0.04 may be determined. This calculation assumes that the fluid generated internally by each unit of rock only equilibrates with that unit of rock. This is clearly a limiting case. Any externally-derived fluid flowing through that unit of rock would result in a higher fluid/rock ratio than that calculated above.

Fluid volume

During the more brittle conditions typical of D2, fracture permeability was far more important than during D1. Petrographic observations suggest that significant pervasive fluid flow was limited to high strain zones where S2 was well-developed (see 1.3.3; Fig. 2.4). Thermodynamic treatment of fluid inclusion compositional data (see 4.3.2) and wallrock alteration studies (see 3.6) suggest that this fluid originated as a V1-type fluid, pumped to higher levels during thrust propagation.

An estimate of the total volume of fluid which flowed through unit area of the crustal slab under study may be made by calculating the amount of fluid required to deposit the total volume of vein quartz observed.

Using an estimate of the average fracture width and spacing as 1 cm and 1 m^{-1} respectively, the volume of vein quartz per m^3 of rock is 0.01m^3 (26 kg). Cooling of a V1-type fluid at 330°C to a V2-type fluid at 250°C would result in a decrease in silica solubility from 738 to 471 ppm (Fournier & Potter 1982). The other parameters which change between V1 and V2 (pH, $f\,O_2$ *etc.*) do not significantly affect silica solubility (Krauskopf 1979). Neglecting kinetic considerations (*i.e.* assuming that all the excess 267 ppm silica is deposited), the total mass of fluid which flowed through each m^3 of rock is 9.7 x 10^4kg. This gives a total water/rock weight ratio of 35 (108 by volume) for the entire D1-D2 stage. This estimate is probably a minimum as it is unlikely that the fluid will remain in complete equilibrium with respect to silica during cooling, attaining a small degree of supersaturation. Thus, not all of the 267 ppm excess silica will be deposited.

The water/rock ratio calculated above is high compared to the estimates of water/rock volume ratios for regional metamorphism of less than 10 given by Wood & Walther (1986). If the calculated fluid volume is correct, there is a significant potential for the transportation, and possibly deposition of economic quantities of metal (see 6.1.3).

Fluid flux

A model used to calculate the fluid flux which flowed through the crustal slab during Hercynian compression is schematically illustrated in Figure 6.2. A 1 cm thick vein per m^3 rock is considered to open by a crack-seal mechanism. Each microfracture opens to a width of 100μm (Ramsay & Huber 1983) so that the vein forms in 100 cracking events. Each microfracture is assumed to form instantaneously and remain open with fluid flowing through it until sealed by quartz precipitation. Both the "true" fluid flux during each cracking event and a "time-integrated" fluid flux over the entire duration of D1-D2 fluid flow may be calculated.

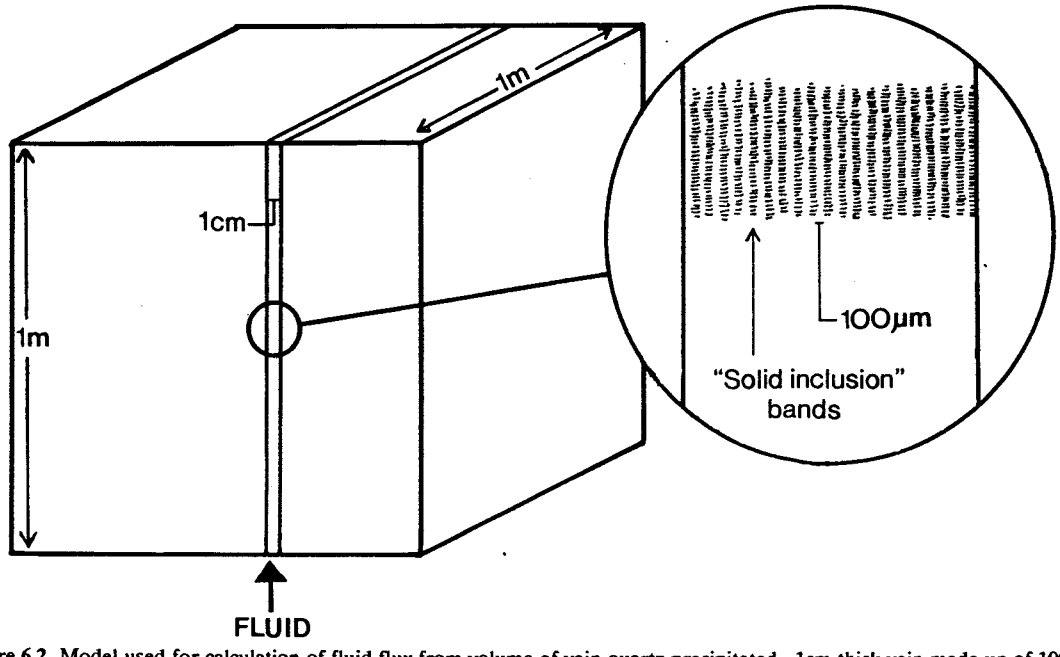

Figure 6.2 Model used for calculation of fluid flux from volume of vein quartz precipitated. 1cm thick vein made up of 100 crack-seal increments of 100μm in $1m^3$ of rock.

A simple equation for calculating the fluid flux is given below:

$$\text{Fluid flux (m s}^{-1}) = \frac{\text{Fluid volume}}{\text{duration of flow x permeability}} \quad \ldots(6.1)$$

where the "permeability" is the area (per unit area) through which the fluid flows during each cracking event. For a microfracture of initial width 100μm and final width 0μm, filled at a constant rate, the time-integrated "permeability" is $5 \times 10^{-5} m^2$ per unit area. Using an experimentally-determined value for the rate of quartz precipitation of 10^{-7} cm s^{-1} parallel to the c-axis (Baronnet 1984) yields a sealing time for each 100μm fracture of 10^5s (1.2 days). In this time, one hundredth of the total volume of fluid per m^3 (*i.e.* 1.1 m^3) must flow through an average cross-sectional area of $5 \times 10^{-5} m^2$. Substituting these values into eq. 6.1 gives a "true" fluid flux of 0.22 m s^{-1}. This value represents an estimate of the velocity at which fluid flowed through each microfracture.

A time-integrated fluid flux may be determined by considering that the above events occurred over the entire duration of Hercynian thrusting. The total time taken for a 1cm vein to form is given by 100 x 10^5 = 10^7s. The total duration of the thrust stacking event is estimated at 35 My (see 6.1.1) which is equivalent to 1.1 x 10^{15}s. Thus, a time-integrated fluid flux is given by:

$$(10^7/1.1 \times 10^{15}) \times 0.22 = 2 \times 10^{-9} \text{m s}^{-1}.$$

This is comparable with time-integrated fluid fluxes of 3-8 x 10^{-10}m s^{-1} estimated by Ferry (1989) for hornfelses in a contact metamorphic environment. His fluxes were calculated by a "reaction progress" method (Ferry 1986) whereby fluid/rock ratios are calculated assuming that decarbonation reactions were driven by a pervasive infiltration of reactive aqueous fluids. Considering that the two methods of calculation are completely different, as well as the contrasting time periods involved (35 My as opposed to 10^5 years), the calculated average fluid fluxes are remarkably similar.

Average permeability

The fluid flux calculated above may be used in conjunction with Darcy's Law to estimate the average permeability of the crustal slab during regional metamorphism. Darcy's Law relates fluid flux (q) to permeability (k) by:

$$q = -(k/\mu)(dP_F/dz) \qquad \text{...(6.2)}$$

where μ is fluid viscosity and (dP_F/dz) is the fluid pressure gradient (Brace 1980). A fluid pressure gradient between V1 and V2 "end-member" fluids, assuming close to hydrostatic conditions for late D2 (see 6.1.1), is given by the fluid pressure difference (3400-800=2600 bars) divided by the thickness of crust between levels experiencing peak metamorphism and D2 retrogression (≈8km). This yields a value for (dP_F/dz) of 0.33 bar m^{-1}, comparable with the value of 0.28 bar m^{-1} quoted by Wood & Walther (1986). The value of q calculated above, and a fluid viscosity of 10^{-9} bar s (Walther & Orville 1982) may be substituted into eq. 6.2 to yield an average permeability of 6.1 x 10^{-18} m^2 (6.1 x 10^{-6} darcy). This "average permeability" is the same order of magnitude as values of ≤2-53 x 10^{-6} darcy estimated by Ferry (1989) for a variety of lithologies during contact metamorphism. Ferry's estimates were the first of in situ permeability during metamorphism and, along with the permeability estimate made in the present study, fall within the range of laboratory measurements of the permeability of metamorphic rocks (0.05-100 x 10^{-6} darcy; Brace 1980). The calculated value is ≈60 times greater than estimates of the minimum in situ permeability of 10^{-19} m^2 necessary to allow fluid to escape from a layer undergoing metamorphism (Yardley 1986).

6.1.3 Metal enrichments during D2

The solubilities of ore-forming minerals calculated in section 5.2, combined with the fluid fluxes for regional metamorphism estimated above, may be used to estimate expected enrichments of metals in the upper crust during D2. The ore mineral solubilities calculated for V1 fluids represent maximum

values for the metal concentrations in solution; the enrichments determined below, therefore, are maximum values.

The difference in solubility of an ore mineral between V1 and V2 fluids provides a maximum estimate of the amount of metal which will precipitate as a V1 fluid flows upwards and cools. These values are shown in Table 6.1. Assuming a water/rock weight ratio of 35 (see 6.1.2), the maximum enrichments of metal, averaged over the entire D1-D2 thickness, may be determined. These calculated enrichments, given in ppm (with respect to the rock) are also given in Table 6.1.

Table 6.1 Summary of data used to calculate maximum metamorphic metal enrichments

	Sn	Pb	Zn	Cu	Ag	Hg
ppm metal in V1 fluid	0.15	0.5	38	36	0.8	$2x10^{-7}$
ppm metal in V2 fluid	0.0056	0.1	1.6	3.4	0.4	$4x10^{-9}$
ppm metal precipitated	0.144	0.4	36.4	32.6	0.4	$1.96x10^{-7}$
ppm enrichment in rock	5	14	1270	1140	14	$7x10^{-6}$
measured ppm in sediments	3-18	5-360	120-800	12-200	-	-

Data from Henley (1974), Edwards (1976) and Beer & Ball (1986).

The enrichments in tin and lead are feasible, with pre-granite concentrations in Cornish pelites ranging from 3-18 ppm and 5-360 ppm respectively (Edwards 1976; Beer & Ball 1986). The zinc, copper and silver enrichments are unreasonable, suggesting that either these components were not at saturation in V1 fluids (quite likely for Cu and Ag) or that the calculated solubilities are too high. D-ICP data suggests that the zinc concentration in V1 fluids was several tens of ppm. Such concentrations imply that either the model is invalid (with the bulk of the metal in fact being precipitated in concentrated zones, rather than "disseminated"), that the V2 solubilities are underestimated, or that the fluid flux is overestimated. Although the errors on all these parameters are not insignificant, it is clear that large quantities of metal will be transported to higher levels in the crust as a result of low grade regional metamorphism. Even if the fluid flux is reduced by an order of magnitude to the level of water/rock ratios quoted by Walther & Wood (1986), zinc enrichment is still of the order of hundreds of ppm, if dispersed. Thus, the potential for forming an ore deposit if precipitation is concentrated in one place is readily apparent.

Summary

A number of general conclusions may be drawn from the discussions presented in the preceding sections. Firstly, the south Cornish nappe and thrust terrain is fairly typical of foreland thrust zones with thin-skinned compressional tectonics resulting in moderate crustal thickening and low-grade metamorphism of supracrustal rocks. Fluid flow was controlled by pervasive permeability at depth with macroscopic fractures becoming increasingly important at shallower levels. An estimate of average in situ permeability of 6.1×10^{-18} m^2 provides a useful parameter for fluid flow modelling in similar low grade metamorphic terrains. Fluid volumes were significant, with time-integrated water-rock weight ratios of 35. Such a high fluid flux has important implications for metal enrichment at high levels in the crust. Regional metamorphism can thus provide an effective means of bulk metal concentration, which is particularly important in the development of a metallogenic province.

6.1.4 Fluid flow during contact metamorphism

Permeability

It has been demonstrated in this study that macroscopic fracturing and vein formation occurred contemporaneously with contact metamorphism during emplacement of the Cornubian granites (see 2.2.8 to 2.2.10). Abundant microfracturing observed in vein material, wholesale enrichments of granite-derived components (*e.g.* boron) in the contact aureole of the Tregonning granite (Chesher 1971) and mimetic (S3-parallel) growth of contact metamorphic porphyroblasts (see 4.4) suggest that pervasive permeability (on a centimetre-scale) was also important. The dominant orientation of microfractures in vein material indicates that pervasive fluid flow was parallel to the S3 fabric.

Fluid-rock ratios

Stable isotopic data for V3 aqueous fluids reported in section 3.5 may be used to estimate fluid/rock ratios for the contact metamorphic event. There is evidence to suggest that the H_2O-rich V3 fluids may be partly of magmatic origin (see 4.4.3). If a magmatic source is assumed, the stable isotopic compositions of these fluids will be a function of the original magmatic signature and the degree of isotopic re-equilibration in the contact aureole. Using a simple open-system model (*e.g.* Taylor 1977), the water/rock ratio may be calculated from:

$$\delta^{f}_{w} = \frac{\delta^{i}_{r} - \blacktriangle_{r\text{-}w} + \delta^{i}_{w}(W/R)}{1 + (W/R)} \qquad \text{...(6.3)}$$

where $\blacktriangle_{r\text{-}w}$ is the fractionation factor between rock and H_2O-rich fluid, W/R is the ratio of exchangeable atoms of oxygen in the water to those in the rock (a water/rock weight ratio of 1 is equivalent to a W/R of 1.9), and the superscripts i and f represent the initial and final states respectively. Using this approach, the isotopic re-equilibration paths for a Cornubian magmatic fluid flowing into the contact aureole at 500, 400 and 300°C were calculated. These paths are shown on Fig. 4.13 which shows that the measured isotopic compositions of V3 aqueous fluids are consistent with isotopic equilibration at *c.*300°C with water/rock weight ratios of 0.03-1 (volumetric ratios of 0.1-3.4). Similar volumetric water/rock ratios of 1-6.7 have been estimated for contact metamorphic fluid flow in hornfelses associated with the Sierra Nevada batholith (Ferry 1989). The geologically reasonable water/rock ratios determined by this method provide indirect support for the validity of the initial assumption that the V3 aqueous fluids were of magmatic origin.

6.1.5 Granite-related fluid flow

Granite-hosted fluid flow

Fluid flow in the granite plutons subsequent to their emplacement was focussed predominantly along joints and faults with orientations controlled by the regional stress field (*e.g.* Moore 1975). However, the presence of multiple populations of secondary fluid inclusions in granite quartz (Rankin &

Alderton 1985) attests to the additional importance of microfracturing and pervasive fluid flow. Rankin & Alderton (1983) showed how an abundance of these fluid inclusions could be correlated with areas of known mineralisation, probably reflecting high pervasive fluid fluxes in those zones.

6.1.6 Normal faults, wrench faults, meteoric fluids and basinal brines

Hydrothermal convection

The data reported in the present study indicate that normal faults were the dominant conduits for fluid flow at the outer margins of the granite convective system (see 3.2.7, 4.5.4). Inconclusive fluid inclusion evidence (see 3.2.8) suggests that the most distal structure which may have channelled granite-hydrothermal (meteoric) fluids is 5.8 km SSE of exposed granite (*J19GW*). However, there are no structures further than 3.2 km SSE of the Tregonning granite (*J98PC*) which show clear evidence (in the form of dilute, low *Th* fluid inclusions) of having channelled meteoric-dominated convecting hydrothermal fluids (see 3.2.7). This observation provides an estimate of the maximum width of the convection cells, perpendicular to the batholith axis. Lateral limits of convection of this order are smaller by ≈50% than predicted by mathematical models of hydrothermal circulation around cooling plutons (*e.g.* Norton & Knight 1977). Such models indicate convective cells extending out to 2-4 km from small plutons (3 km width) and up to 10 km away from a "batholith" with a width of 54 km (approximately twice the width of the Cornubian batholith). Downflow zones at distances of the order of 5-6 km would be expected for the Cornubian batholith. However, these models assume constant, "pervasive" permeability in the host rocks, which is clearly not the case for most systems of this type. Only a few normal faults, concentrated relatively close to the granite, controlled most of the fluid flow on the flank of the batholith in the study area. Thus it is not surprising that convection was limited to a relatively narrow zone, at least in the south Cornish region (Fig. 6.3).

Fluid-rock ratios

Stable isotopic data for $V4_N$ and $V4_{J2}$ fluids reported in section 3.5 may be used to estimate the effective water-rock ratio for hydrothermal circulation in the country rocks. Assuming a rock with an initial isotopic composition of $\delta^{18}O = 13.4‰$ and $\delta D = -58‰$ (Sheppard 1977) is infiltrated by meteoric water with $\delta^{18}O = -6‰$, $\delta D = -25‰$, at 300°C, the fluid path shown on Figure 6.4 was calculated using eq. 6.3. This shows that 1 mass unit of the most primitive meteoric water (*J78PS*) could have attained its isotopic signature by isotopic equilibration with 1 mass unit of rock. Fluid/rock weight ratios of the order of 0.1 are suggested by the other two samples, according to the simple model outlined above. In reality, the situation would probably have been far more complex, especially if complete recirculation of fluids occurred. Sheppard (1977) suggested that effective water-rock ratios in the Cornish granites were probably low, but did not quote values. Jackson *et al.* (1982) concurred, quoting values of <0.5 by weight. The isotopic data obtained in the present study support fluid/rock ratios of this order of magnitude. The channelling of convecting fluids in the outer margins of the hydrothermal system into relatively few fault zones may explain the higher fluid-rock ratios observed in these areas. Alternatively, samples such as *J78PS* may represent relatively "young" meteoric fluids which have not interacted with large volumes of rock.

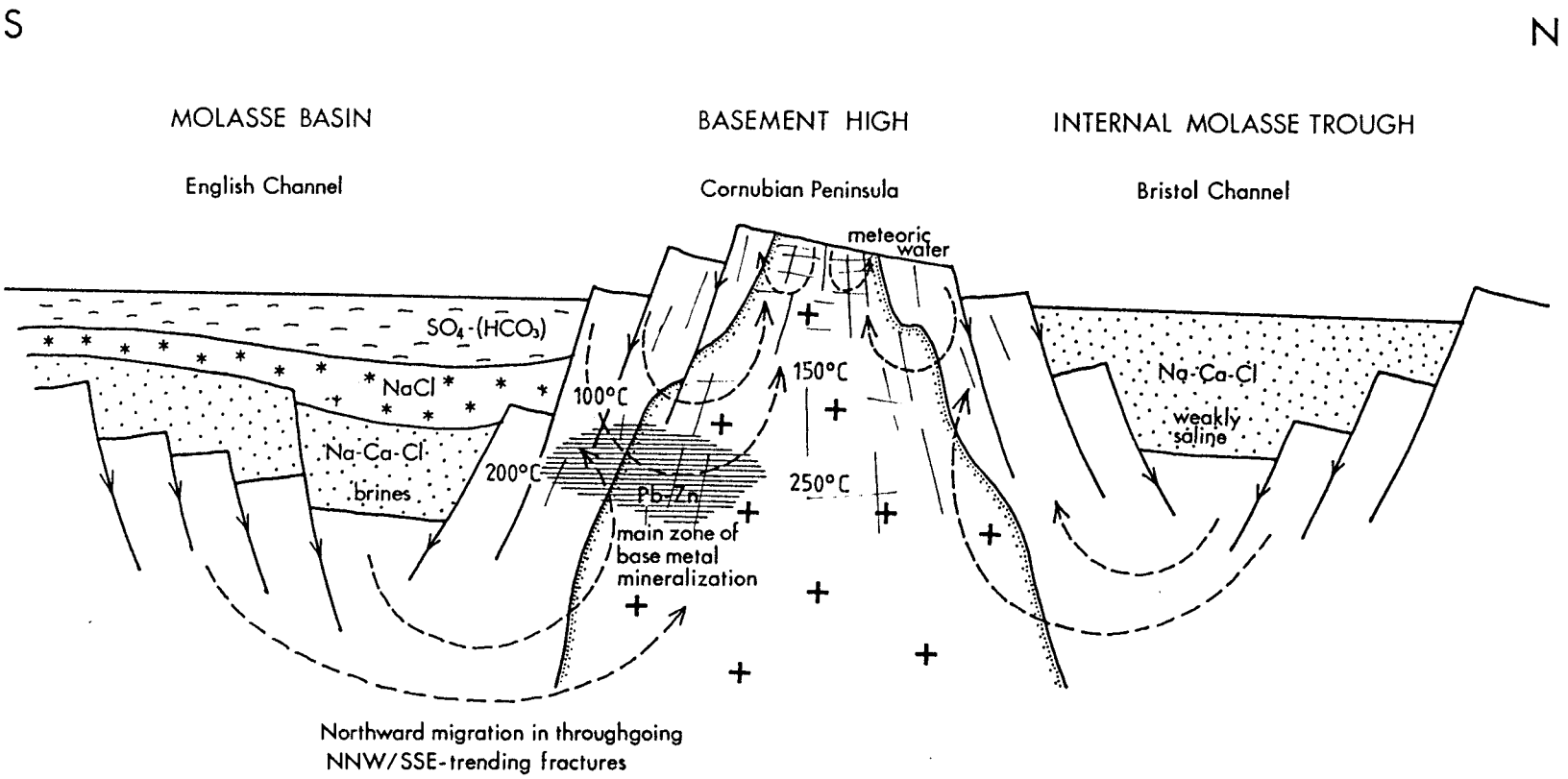

Figure 6.3 Schematic cross-section through the Cornubian peninsula, illustrating post-Hercynian interaction between convecting meteoric fluids and basinal brines.

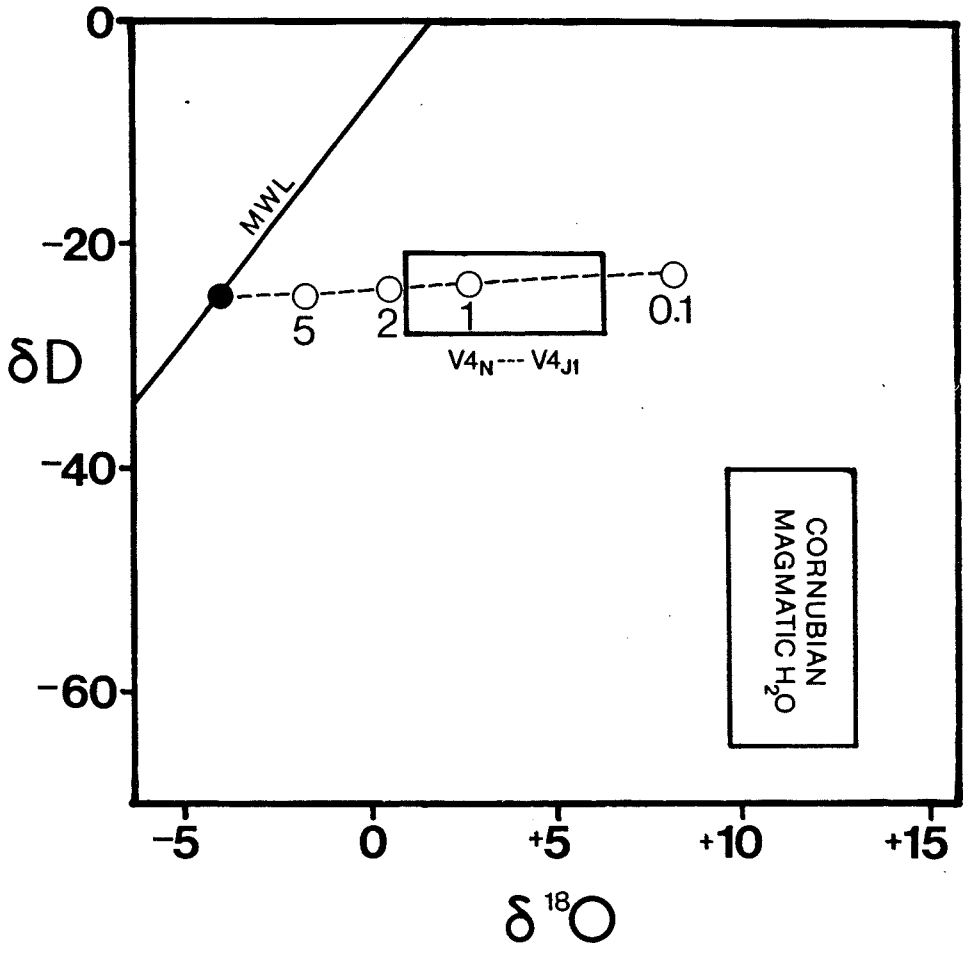

Figure 6.4 Calculated isotopic equilibration trend for a meteoric fluid of initial $\delta^{18}O = -6\%$, $\delta D = -25\%$ interacting with slates with $\delta^{18}O = +13.4\%$, $\delta D = -58\%$, at 300°C. Numbers refer to ratio of exchangeable atoms of oxygen in water to those in rock (divide by 2 for W/R weight ratios). Fields for $V4_N$-$V4_{J2}$ and Cornubian magmatic waters (Sheppard 1977) are shown.

Wrench faults and brine migration

Data reported in section 3.2.8 and discussed in section 4.6 indicate that fluids similar to modern basinal brines flowed through NNW-SSE trending dextral wrench faults and associated extensional fractures which were active during post-Hercynian extension. The wrench faults often reactivate earlier structures and probably acted as transfer faults during the development of Permo-Triassic basins to the north (Bristol Channel) and south (English Channel) of the Cornubian peninsula (Fig. 6.3).

Brine migration was probably controlled by tectonic activity, but may have been greatly aided by the development of an interconnected fracture system. Such a fractue network would have allowed the granite-driven convecting fluids to draw the cool brines into the convective system (Fig. 6.3).

Mixing between meteoric fluids flowing down ENE-WSW trending normal faults, and basinal brines flowing laterally towards the granite thermal and topographic "high", occurred at structural intersections, resulting in base metal precipitation.

A similar scenario has been envisaged for post-Hercynian fluid flow in West Germany (Behr & Gerler 1987), with saline and weakly saline brines flowing out of molasse basins and internal

molasse troughs respectively, into a thermally anomalous culmination zone. Quartz, barite, fluorite and carbonate veins, often containing base metal sulphides, formed in these regions. Remobilisation and secondary mineralisation of older Cu, Pb, Zn, U, Au, W and Fe deposits also occurred.

Summary

It is clear from the above discussion that post-granite tectonic and fluid evolution were intimately related during a phase of crustal extension. The conjunction of particular structural and thermal features allowed interaction of fluids derived from different sources. Evidence from elsewhere in the Hercynian belt suggests that not only were such processes common but that the fluids involved were also of similar composition. Thus, the generation and migration of such fluids appears to be an integral part of the Hercynian continental compression-extension cycle.

6.2 FLUID EVOLUTION IN SOUTH-WEST ENGLAND

The purpose of this section is to relate the proposed model of fluid evolution in the study area to previous work on the subject in southwest England. The extensive literature on the subject precludes an exhaustive review of previous studies of granite-related fluid evolution. However, the most important studies are considered and the fluid and metallogenic models presented are reconsidered in the light of the new data reported in this work. For further details the reader is referred to Jackson *et al.* (in press) and the bibliography of Halls *et al.* (1985).

6.2.1 Regional metamorphic fluids

The fluid P-T-X data and fluid evolutionary model presented in Chapters 3 and 4 respectively form the first detailed study of regional metamorphic fluid flow in southwest England. The work also represents one of very few studies to consider the genesis and evolution of low-grade metamorphic fluids. As a result, there is little published data with which to compare the results obtained.

Pamplin (1988) reported the results of a preliminary fluid inclusion study on fluids mobilised during Hercynian regional metamorphism in north Cornwall. Figure 6.5 illustrates fields for his pre- and syn-D2 fluids in *Th-S* space, with the fields for V1 and V2 fluids defined in this study shown for comparison. The veins described by Pamplin (1988) as being pre-D2 are equally likely to have formed syn-D2 and this is supported by the close correspondence between thermometric data for the "pre-" and "syn-D2" fluid inclusions.

The similarities between the data for south and north Cornwall are readily apparent (Fig. 6.5). This is somewhat surprising considering the differences between the nature of the D2 event in north Cornwall, compared with south Cornwall. The former deformation event was characterised by moderate to intense ductile shear and greenschist facies regional metamorphism. In contrast, D2 in south Cornwall region was typified by high-level brittle imbrication and retrogression. The tectonic evolution of the two areas are clearly distinct, yet the fluids mobilised are compositionally similar.

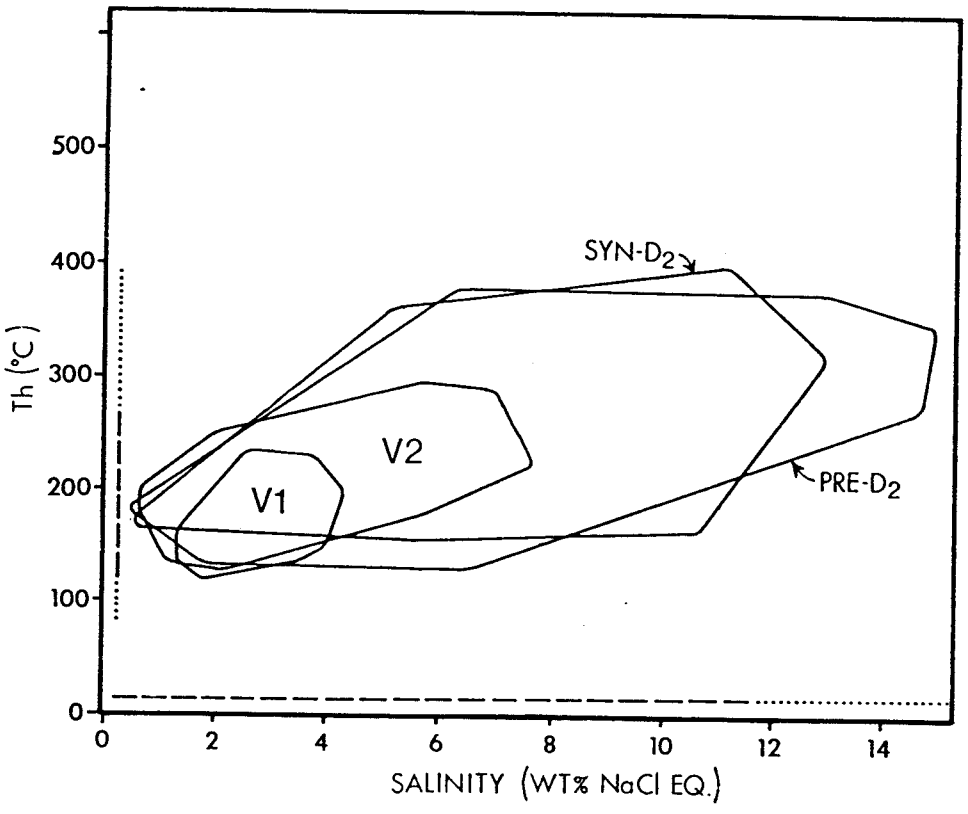

Figure 6.5 *Th vs. S* plot for syn-tectonic fluid inclusions from north Cornwall (Pamplin 1988) and south Cornwall (this study). The dashed lines at the edges of the plot represent ranges in *Th* and *S* reported by Behr *et al.* (1987) from West Germany.

The scarcity of published data on Hercynian fluid inclusions from elsewhere in the orogenic belt precludes a detailed comparison. Data from one study in West Germany (Behr *et al.* 1987) are shown on Figure 6.5, in terms of dominant *Th* and *S* ranges. Again, the data are very similar to the V1 and V2 data reported in this study.

Summary

Although limited, fluid inclusion data from Hercynian syn-tectonic veins suggest that fluids mobilised during low grade metamorphism were similar across the whole orogenic belt. This is perhaps not surprising when one considers the general uniformity in lithofacies and tectonothermal evolution along the orogen (*e.g.* Zwart 1967).

6.2.2 Granite-related fluids

Prior to this study, no work had been carried out on the fluids mobilised in the contact aureole of the Cornubian batholith during granite emplacement. Fluid inclusion data suggest that these fluids contained components ultimately derived from a magmatic source, as well as components derived from the contact aureole (see 4.4.3). Comparison between thermometric data for V3 H_2O-rich fluid inclusions and for H_2O-rich fluid inclusions in mineralised sheeted vein swarms and lodes from

previous studies (Fig. 6.6) illustrates the similarities between the V3 type 1 and type 3 fluids with those responsible for high temperature mineralisation. The field for $V4_P$ "distal" fluid inclusions also shows that many of the mineralising fluids are thermometrically similar to fluids with clear magmatic affinities.

The limited fluid inclusion data obtained on tourmaline greisen and other high temperature veins ($V4_{J1}$) in the present study are also shown on Figure 6.6. The data display some overlap with low *Th* V3 type 1 inclusions, as well as $V4_P$ "distal" inclusions, and are comparable with data from sheeted vein systems at Hemerdon (Dartmoor), Kit Hill (Dartmoor-Bodmin Moor), and Cligga Head (Shepherd *et al.* 1985; Charoy 1979).

Model for granite-related fluid evolution in southwest England

It is envisaged that the mineralising fluids (represented by the various fields in Fig. 6.6) developed from low salinity "parent fluids" at temperatures in excess of 400°C. These fluids were initially of dominantly magmatic origin within the granites and of mixed magmatic-metamorphic origin in the contact aureole. The fluids then followed trends of increasing salinity with cooling, either as a result of unmixing (particularly true in the contact aureole where CO_2 contents were higher and temperatures lower), boiling (in high level granite apices where sheeted vein systems developed) or early greisening (rock hydration). The magnitude of the increase in salinity was dependent on the process responsible and on intensive parameters such as P and T. Local variations in these controls generated a series of evolutionary trends (*e.g.* see Fig. 6.6).

Stable isotopic data on V3 and V4 aqueous fluids, in agreement with previous studies (*e.g.* Jackson *et al.* 1982) suggest that meteoric fluids did not penetrate the exposed levels of the granite or contact aureole until the system had cooled to below 400°C. The distribution of *Th-S* data for a variety of localities and vein types (Fig. 6.6) is interpreted as reflecting a major influx of meteoric water at around 300°C, with subsequent dilution to meteoric-dominated waters at *c.*200°C. It is suggested, therefore, that meteoric fluids entered the system at maximum temperatures of 300-400°C, which is the same temperature range over which most of the cassiterite mineralisation occurred in the Cornubian orefield, as well as in other tin provinces around the world (Jackson *et al.* 1982; Haapala & Kinnunen 1982). Dilution of moderately saline fluids by meteoric fluids would be an effective mechanism for precipitation of cassiterite and base metal sulphides by destabilisation of chloro-complexes (see 5.3.3).

A schematic representation of these events, including elements of the models presented by Shepherd *et al.* (1985) and Jackson *et al.* (in press), is presented in Figure 6.7.

6.2.3 Late-stage fluids

Analysis of fluid inclusions in vein quartz hosted by normal faults distal to the Cornubian batholith has identified the presence of extremely dilute (predominantly 0.4-1.4 wt% NaCl eq.) fluids. Stable isotopic data indicate that these fluids are of meteoric origin which have undergone slight isotopic exchange with the country rocks (Fig. 6.4). The chemical and isotopic characteristics of these fluids (*e.g.* sample *J78PS*) provide the closest determination yet obtained of the composition of Cornubian

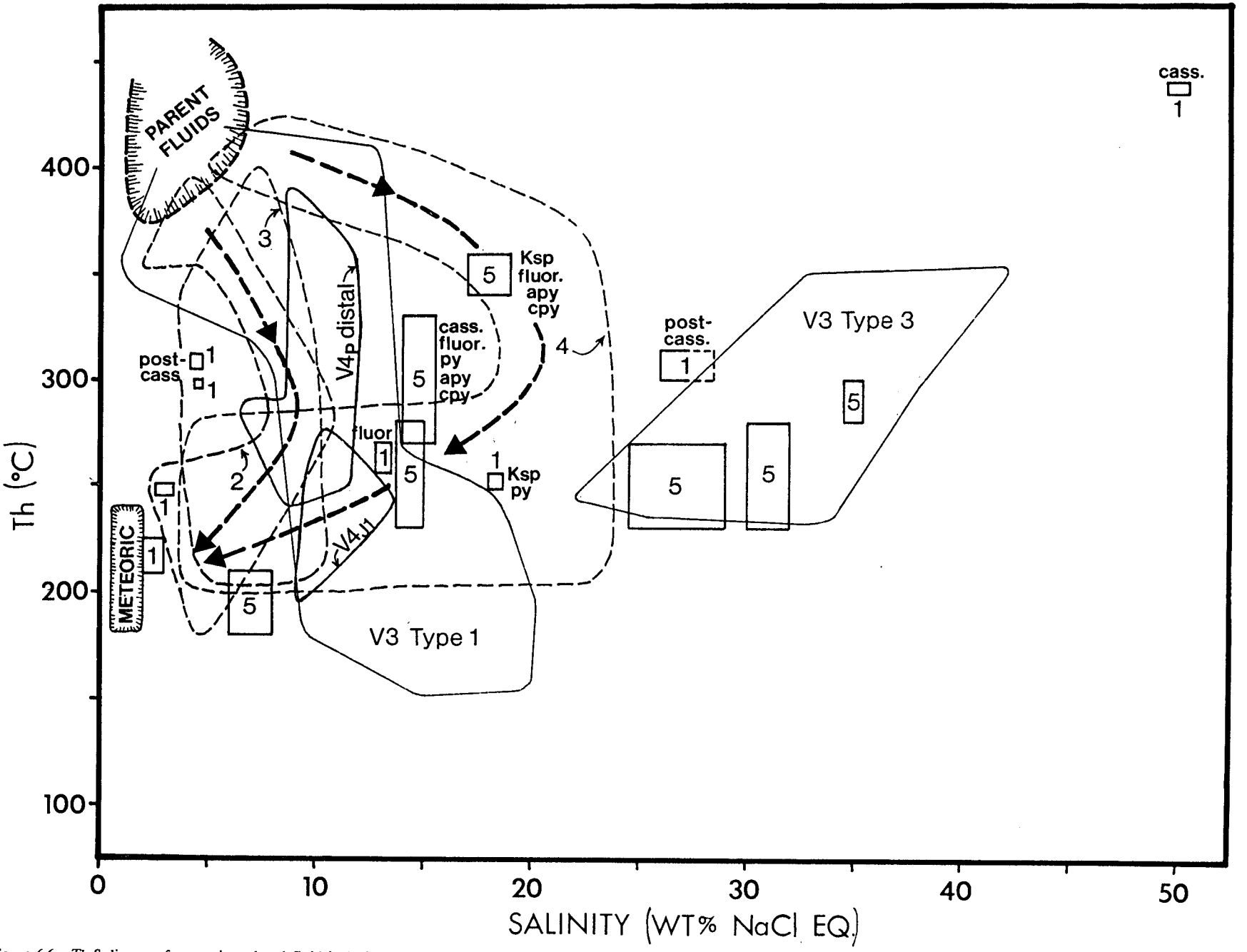

Figure 6.6 *Th-S* diagram for granite-related fluid inclusions. Rectangular boxes and dashed fields represent data from previous studies: 1. Various localities, Sawkins (1966); 2. Cligga Head, Charoy (1979); 3. Kit Hill, Shepherd *et al.* (1985); 4. Hemerdon, Shepherd *et al.* (1985); 5. St. Just, Jackson *et al.* (1982); V3 and V4 fluid inclusions (this study). Also shown are fields for meteoric fluids (this study) and "parental" ore fluids (see text).

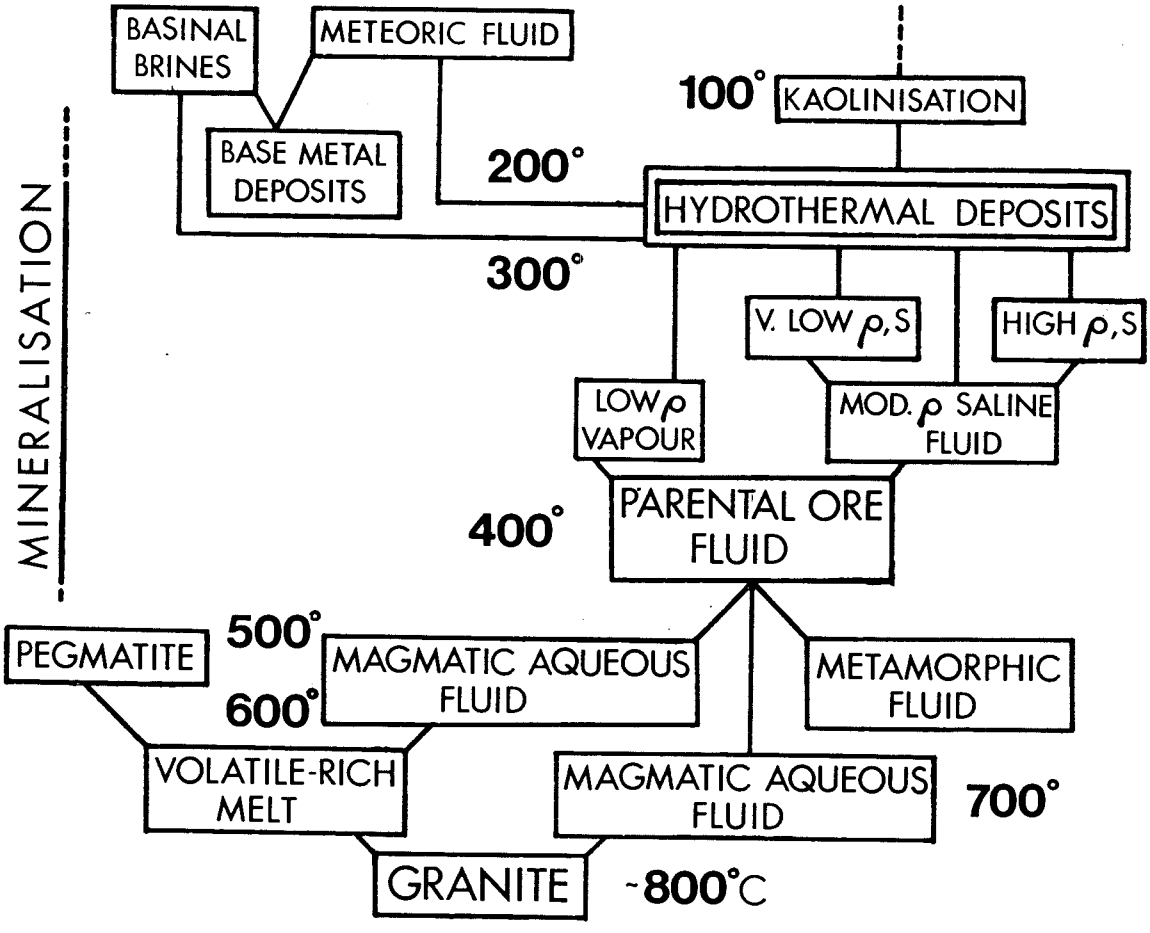

Figure 6.7 Schematic representation of evolution of mineralising fluids in southwest England. Elements taken from Shepherd *et al.* (1985) and Jackson *et al.* (in press).

meteoric waters. As such, the data provide a useful end-member composition for modelling of fluid evolution in the Cornubian orefield.

The Cornubian meteoric fluids did not initially carry significant quantities of metals or sulphur. Evidence outlined in this study suggests that their primary importance in the evolution of the orefield was in promoting efficient ore deposition from metal-rich magmatic-metamorphic fluids. It is likely, however, that the more evolved meteoric fluids were also involved in primary, and undoubtedly in secondary, mineralisation phenomena.

Thermometric data for $V4_W$ fluid inclusions are comparable with previous fluid inclusion studies of cross-course mineralisation in southwest England (Fig. 6.8). The diagram shows *Th-S* data reported by Alderton (1978) and Shepherd & Scrivener (1987) for fluid inclusions in quartz and fluorite. Also shown are fields for $V4_N$ fluid inclusions, and inclusions in E-W trending "mainstage" lodes from the Kit Hill-Gunnislake district between Dartmoor and Bodmin Moor, including those specifically associated with quartz-sulphide assemblages. Two basinal brine-granite hydrothermal fluid mixing trends are suggested by the data. Trend 1 (this study) indicates that mixing between brines and moderate to low temperature meteoric fluids occurred in normal faults developed on the southern flanks of the Cornubian peninsula. Trend 2 (Shepherd & Scrivener 1987) indicates that

brines penetrated E-W trending lode structures during the quartz-chlorite-polymetallic sulphide stage of ore deposition (see 1.3.5).

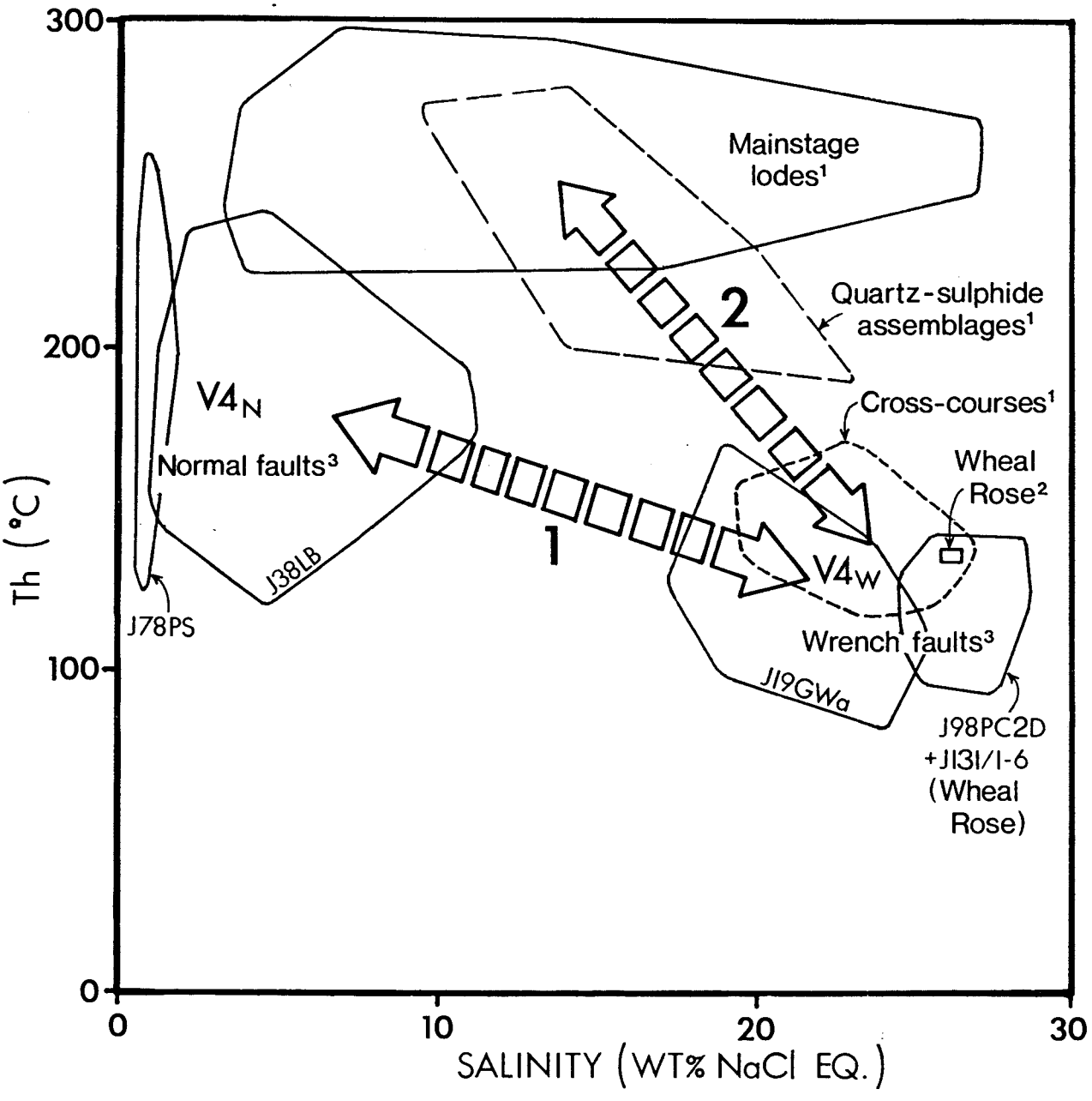

Figure 6.8 *Th*-salinity diagram for fluid inclusions in Cornish cross-courses. [1]Shepherd & Scrivener (1987); [2]Alderton (1978); [3]this study.

The fluid inclusion data discussed above show that the migration of basinal brines into the Cornubian province began relatively early in the mineralising history and continued at least until the convecting fluids on the flanks of the batholith had cooled to below 150°C. The fluids thus played an important role in the development of the Cornubian metallogenic province.

6.3 EXPLORATION MODELS

Based on the data and fluid evolution models presented here, three simple genetic exploration models are proposed which not only apply to the Cornubian metallogenic province, but may also be applicable in similar terrains elsewhere. These models illustrate that modelling fluid flow and fluid-rock interaction may be of use in delineating favourable areas for the location of "blind" ore deposits.

6.3.1 Structurally and lithologically controlled D1/D2 mineralisation

A favourable site for the formation of an ore deposit from fluids carrying relatively low levels of metals (such as regional metamorphic fluids) will be where large fluid-rock ratios are attained in conjunction with an efficient precipitation mechanism. It is highly likely that the most important channelways for V1- and V2-type fluids during Hercynian compression in southwest England were the major thrust faults. The Carrick Thrust, and/or equivalent major detachments (Wilkinson & Knight 1989) is an example of such a structure, interpreted as transporting the allochthonous Gramscatho Group rocks of south Cornwall northward over the parautochthonous Mylor Slate Formation in the foreland (see 1.3.3).

The second requirement for formation of an ore deposit, that of an efficient precipitation mechanism, may be met where a relatively rapid change in intensive parameters (P, T, fO_2, fS_2 *etc.*) occurs, resulting in destabilisation of metal complexes. In the case of the Carrick Thrust, such a situation may have occurred at the frontal ramp where fluids migrating up the fault zone would have first encountered Mylor Slate lithofacies rocks (Fig. 6.9). These rocks would have been relatively reducing in comparison with the Gramscatho Group turbiditic sandstone-shale sequences with which V1 fluids would have initially been in equilibrium. Reduction of V1 fluids entering the contrasting chemical environment could have resulted in precipitation of certain metals.

As discussed in section 5.3.3, cassiterite precipitation would be favoured by an increase in fO_2. The above scenario would result in a reduction of fO_2 in the fluid, so that cassiterite precipitation would be unlikely to occur (unless a significant T decrease also occurred). In contrast, base metal sulphides are likely to precipitate in such an environment (see 5.3.3). Downward percolation of surface waters into an emergent thrust, as has been documented by Kerrich (1986), would also favour base metal deposition by decreasing $a.Cl^-$ (see 5.3.3).

Of more economic interest than a base metal sulphide orebody, would be a gold deposit. Although the levels of gold in solution will be much lower than the base metals, the relatively high H_2S content of V1 fluids means that they could transport significant quantities of gold as thio-complexes. Deposition of gold from the neutral $AuHS^\circ$ complex, which is likely to be the major gold complex at relatively low pH (Seward, in press), can be described by the simple redox reaction:

$$AuHS^\circ + e^- = Au^\circ + HS^-$$

Gold deposition will be favoured if the fluid enters a more reducing environment, such as that described above. Thus, quartz veins, particularly antitaxial veins sub-parallel to the penetrative

cleavage, and altered slate at the frontal ramp of the Carrick Thrust where it cuts Mylor Slate lithofacies rocks, could be a site of gold mineralisation (Fig. 6.9).

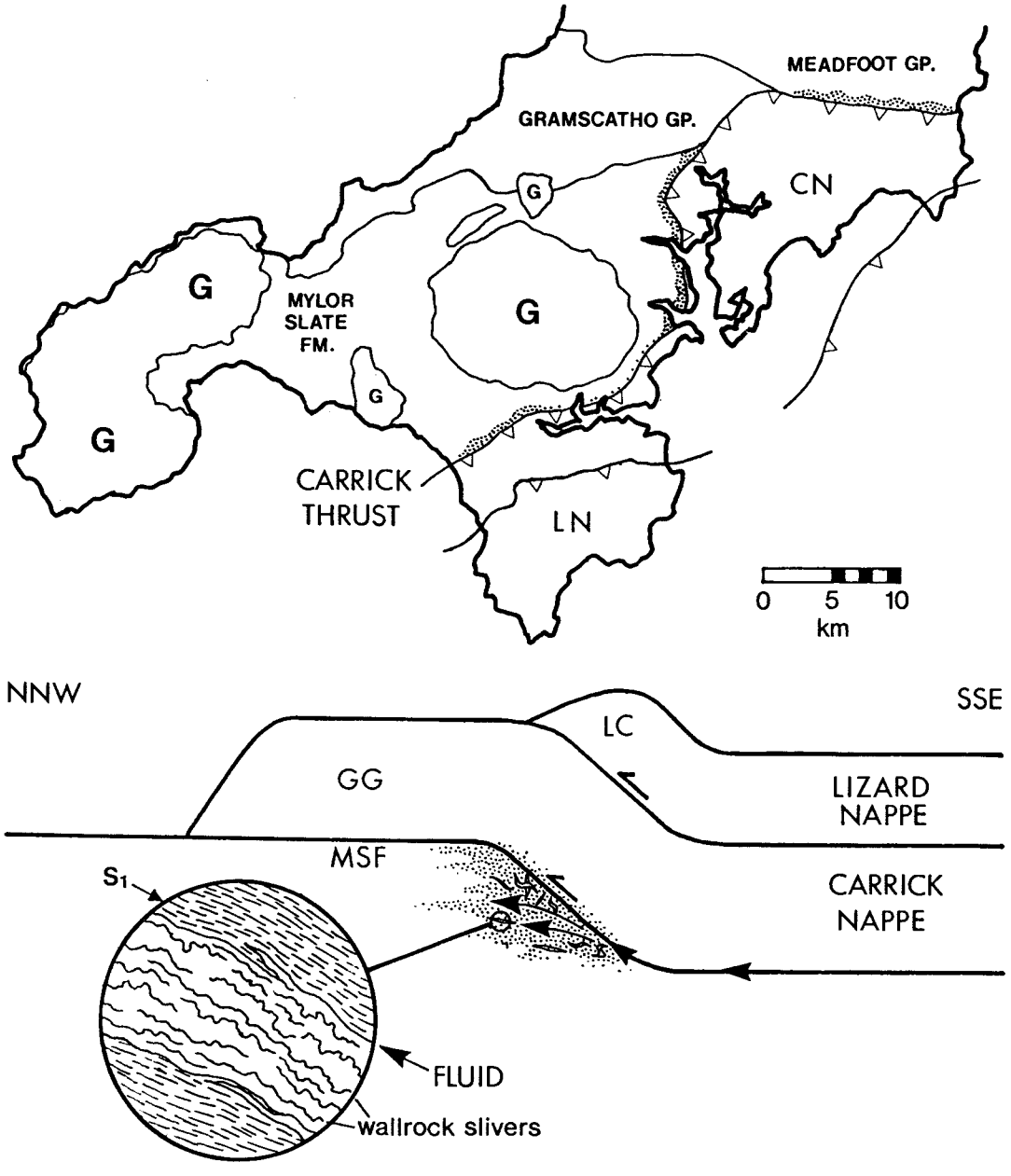

Figure 6.9 Map and cross-section illustrating potential location of a base metal and/or gold orebody in south Cornwall (dotted region). G=granite, CN=Carrick Nappe, LN=Lizard Nappe. Arrows denote fluid flow. Inset: antitaxial vein formed sub-parallel to the penetrative cleavage, with extensive fluid-rock interaction.

An alternative site for gold deposition would be in basic, iron-rich lithologies, where fluid sulphur fugacities are reduced by pyritisation of wallrocks, resulting in destabilisation of gold-thio complexes. In Cornwall, the greenstones form a suitable lithology. However, they are of limited extent and are not cut by the Carrick Thrust, so that exposed mineralisation of this type may be ruled out. This does not preclude the possibility of greenstone-hosted gold mineralisation occurring at depth.

The high temperatures and pervasive fluid flow which characterised the contact metamorphic event in the province, in addition to the high estimated H_2S fugacities, are likely to have resulted in remobilisation of gold in the contact aureole (see below). This means that a deposit of this type of purely regional metamorphic origin would probably only have survived if it formed more than 3-4 km from where the granites were subsequently intruded.

6.3.2 Mineralisation during contact metamorphism

Low grade skarn-type tin orebodies have been described from the Cornubian orefield and are probably formed as a result of infiltration of rocks in the contact aureole by reactive fluids of magmatic±metamorphic origin. Mineralisation of this type is hosted by metabasites or impure calcareous metasediments, with tin being contained in a variety of silicate minerals (Jackson *et al.*, in press). Orebodies of this type may be considered to form as a result of fluid flow contemporaneous with contact metamorphism. The source of the fluids is uncertain, although data reported in this study suggest that both magmatic and metamorphic components were involved.

Fluid evolution in the contact aureole was complex (see 4.4) and thus it is difficult to predict favourable sites for mineralisation. The metabasic lithologies clearly provided chemically reactive horizons which may also have been relatively permeable as a result of volume loss during dehydration and decarbonation reactions. Replacement and/or disseminated Sn-As-Cu-Pb-Zn-Fe mineralisation may be expected in these rocks (*e.g.* Tregear Point greenstone; see 1.3.5; Fig. 6.1).

The high levels of H_2S estimated for V3 fluids implies that gold could have been mobilised by these fluids in the contact aureole. Deposition could occur either as a result of pyritisation of Fe-rich wallrocks (*e.g.* metabasites) or by reduction through interaction with carbon-bearing slates and/or cooling. The combination of low gold contents of sediments and granitic rocks (1.5-8.1 ppb; Crocket, in press) and relatively low fluid-rock ratios developed in the contact aureole mean that concentration of economic quantities of gold is unlikely. Neutron activation analyses of V3 vein quartz (see 3.3.2) show that gold concentration in veins did occur, with up to 25 ppb recorded. The wallrocks are likely to show greater enrichment if fluid-rock interaction was the mechanism for gold deposition. Probably the best prospect for finding gold of this type would be associated with $V3_S$ veins, which formed antitaxially, allowing greater degrees of fluid-rock interaction (Fig. 6.9).

6.3.3 Base metal mineralisation

The structural controls of late base metal mineralisation have already been noted (see 6.1.5). As with the previous models, large fluid-rock ratios favour the formation of an economic ore deposit. The major wrench fault structures are those which are most likely to fulfil this condition and would therefore be the preferred sites for exploration (Fig. 6.10). Maps of the distribution of base metal production in the Cornubian province (Willis-Richards & Jackson, in press) reveal that zinc, silver and lead have been mined predominantly in the major wrench fault zones, particularly in a N-S trending region which divides the orefield into its western and eastern compartments.

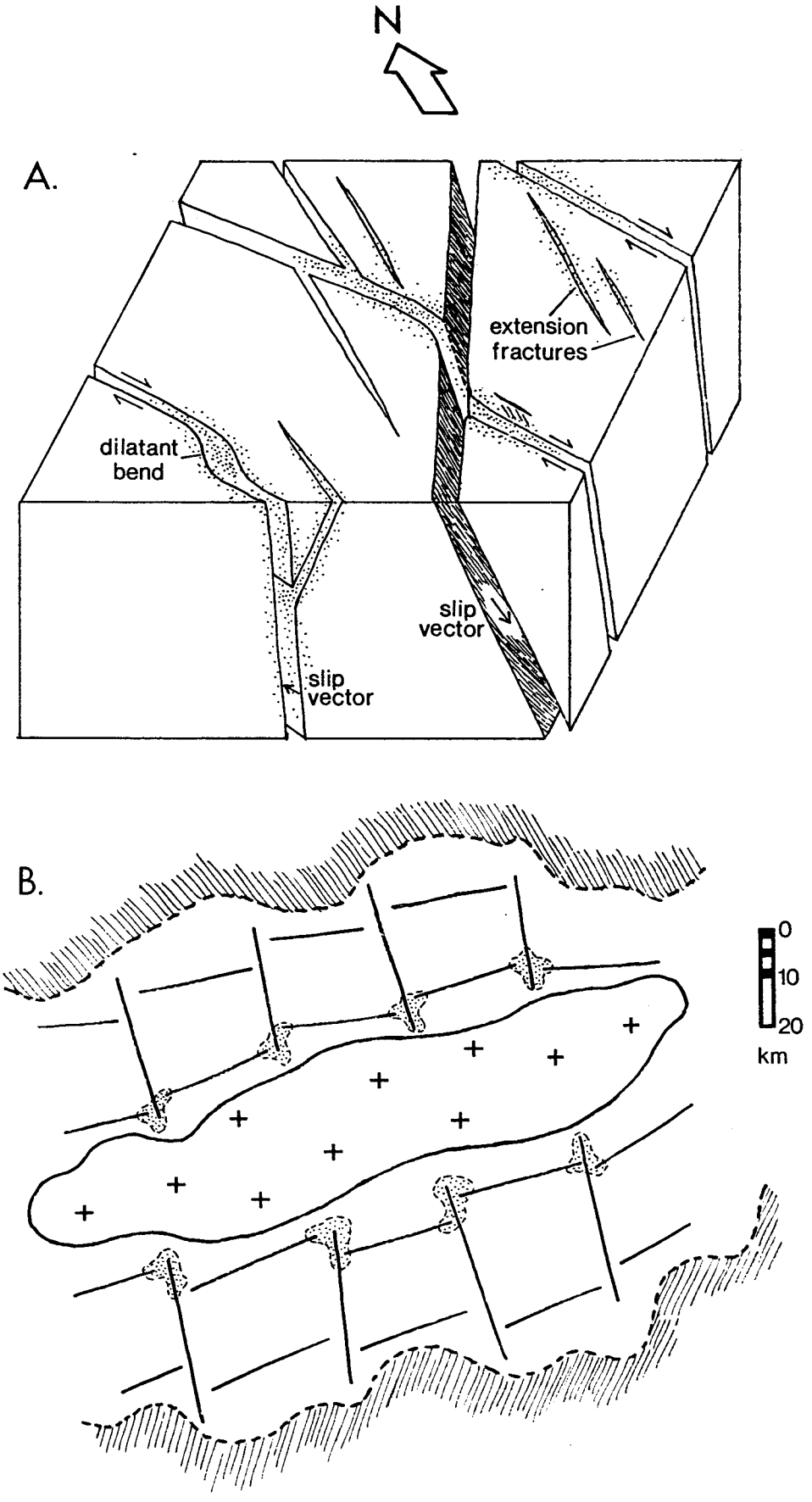

Figure 6.10 Schematic representation of potential sites for post-tectonic base metal mineralisation (dotted areas) associated with a high-heat-producing granitic batholith. **A.** Block diagram illustrating local structural controls of mineralisation; favorable sites at fault intersections, in extensional veins and dilatant bends; **B.** Map illustrating regional structural controls of mineralisation; favourable sites at transfer/normal fault intersections on flanks of batholith. Shaded area represents unconformable sediments associated with post-orogenic extensional phase.

The probable role of meteoric water-brine mixing in the genesis of the deposits limits the major precipitation zones to the external parts of the granite-hydrothermal system (Fig. 6.3). An interconnected fracture system is envisaged whereby the bulk of base metal deposition occurred in the marginal down-flow zones (Fig. 6.10). Large brine fluxes in some cross-courses could mean that significant dilution did not occur in the marginal zones, allowing mineralisation to occur closer to or within the granites themselves. If temporary hiatuses in granite convection occurred, brines could again penetrate further before precipitating their dissolved metal load by an alternative mechanism (*e.g.* neutralisation by granitic wallrocks).

This model would be applicable in other terrains where post-orogenic basins developed in proximity to high heat producing granites which could maintain prolonged hydrothermal convection.

6.4 SUMMARY

This chapter provides a summary of the tectonic, thermal and metallogenic evolution of the Cornubian province. Pervasive and fracture permeability channelled large volumes of fluid during low grade regional metamorphism, with important implications for mass transport upward through the crust and pre-granite concentration of ore metals. Total fluid/rock weight ratios of 35 have been calculated for D1-D2 fluid flow and time-integrated fluid fluxes and permeabilities of 2×10^{-9} ms^{-1} and 6.1×10^{-18} m^2 respectively have been estimated for the same stage.

Complex patterns of pervasive and fracture-controlled fluid flow in the contact aureole of the Cornubian batholith formed an integral part of early granite-related evolutionary processes. Relatively low fluid/rock weight ratios of 0.03-1 have been estimated for contact metamorphic fluid flow from stable isotopic data.

Parent ore fluids of magmatic-metamorphic origin were probably responsible for early mineralisation phenomena, with the bulk of the polymetallic deposits forming in response to an influx of meteoric fluids. Low temperature hydrothermal convection on the southern flank of the batholith was probably limited to distances of less than 3.2 km laterally from the batholith roof, and was controlled by normal faults. Fluid/rock weight ratios of 0.1-1 have been estimated for this stage of fluid evolution.

Basinal brines infiltrated the system contemporaneously with mainstage mineralisation, resulting in simple Pb-Zn dominated deposits in the marginal zones, these having formed as a result of mixing with convecting meteoric fluids.

Three genetic exploration models, incorporating structural, lithological, geochemical and thermodynamic considerations are proposed. These illustrate the potential of detailed fluid studies in understanding the chemical and physical controls of ore genesis, and in delineating likely sites for mineralisation.

CHAPTER 7: CONCLUSIONS

The major conclusions reached in this study are summarised briefly below. In addition, suggestions for further research are proposed.

7.1 MAIN CONCLUSIONS

1. Veins generated during four tectonic stages have been classified according to their lithological and structural settings. In all, 14 vein types are distinguished, each of which represent fluid flow through different structures and at different stages of the Hercynian orogeny in south Cornwall.

2. Fluid inclusion data, in combination with pumpellyite-actinolite mineral assemblages in metabasites and vitrinite reflectance data, indicate that regional metamorphism in south Cornwall occurred at 3.4±0.5 kbar and 330±30°C.

3. Low salinity (1-4.5 wt% NaCl equivalent), H_2O-rich fluids were evolved via prograde devolatilisation reactions during regional metamorphism. These fluids were in equilibrium with albite-quartz-K-mica-chlorite±paragonite assemblages in slate and greywacke host rocks. Decrepitation-linked ICP analyses indicate that the order of abundance of the major solutes in these fluids was Na>K>Ca, with Na/K weight ratios of 7.6-21.3 and Na/Ca weight ratios of 28.1-105. Na/Li ratios of 181-261, Na/B ratios of 19-68 and Na/Br ratios of 190 are distinctive, and may be useful parameters for fingerprinting low grade metamorphic fluids. Bulk analyses show that proportions of volatiles apart from H_2O were low, with X_{CO2}=0.0093-0.0116, X_{N2}=0.0008-0.0014 and X_{CH4}=0.0004-0.0012).

4. South Cornish peak metamorphic fluids may have transported significant quantities of lead, zinc, copper, tin and silver, amongst other metals. Thermodynamic calculations suggest that such fluids could have carried up to 0.15 ppm Sn, 0.5 ppm Pb, 38 ppm Zn, 680 ppm Cu and 2.1 ppm Ag.

5. The crust was thickened to approximately 40 km during compression. Pressure and temperature decreased, concomitant with uplift and erosion of the nappe pile, with fluid pressures of 800 bars and temperatures of 250°C prevailing at the presently exposed crustal level towards the end of Hercynian thrusting. A time-integrated fluid flux of 2×10^{-9} ms^{-1} and average permeability of $6.1 \times 10^{-18} m^2$ are estimated for the upper crust of south Cornwall during Hercynian tectonism and metamorphism.

6. Slight retrogression (sericitisation/chloritisation) of peak mineral assemblages occurred as a result of high temperature fluids migrating up thrusts to higher structural levels. These fluids were characterised by Na/K and Na/Ca ratios of 7.9-14.7 and 12.9-153 respectively, similar to the peak metamorphic fluids. However, fluid salinity (up to 8 wt% NaCl equivalent), Na/Li ratios of 191-339, Na/B ratios of 50-113 and Na/Br weight ratios of 200-250 were generally higher, reflecting the lower temperatures and retrogression associated with D2.

7. The decreases in solubility estimated for a variety of ore-forming metals, as a result of upward flow of metamorphic fluids through the crust, would result in ore precipitation at higher crustal levels. Thus, regional metamorphism could have provided an effective mechanism for metal enrichment in the upper crust.

8. CO_2-bearing fluids of mixed magmatic-contact metamorphic origin were mobilised in the contact aureole of the Cornubian granite, up to 5 km laterally from the roof zone, during granite emplacement. These fluids unmixed to produce low density, CO_2-rich vapour and moderately to highly saline aqueous fluids, of up to 42 wt% NaCl equivalent. High density CO_2-rich fluids were produced in distal parts of the contact aureole, possibly as a result of condensation of low density vapours. Estimated fluid-rock weight ratios of 0.03-1 were attained during contact metamorphism.

9. Significant quantities of tin (up to 28 ppm) could have been transported by the saline fluids generated in the contact aureole. Thus, the generation of saline, contact metamorphic fluids provides an effective mechanism for the extraction of tin from the pelitic rocks hosting the Cornubian granites.

10. Low salinity (1-5 wt% NaCl equivalent), H_2O-rich fluids separated from the Megilliggar pegmatites during crystallisation. This fluid unmixed at *c.*400°C to produce a low density CO_2-bearing vapour and moderately saline (8-10 wt% NaCl equivalent) H_2O-rich liquid. Magmatic ± metamorphic fluids of this type were responsible for early, high temperature mineralisation phenomena.

11. An influx of dilute meteoric fluids into the system at *c.*300°C resulted in formation of the bulk of the Cornubian ore deposits. Estimated fluid-rock weight ratios of 0.1-1 were developed in the slates on the southern flank of the Cornubian batholith at this stage. Convective circulation of meteoric fluids occurred in normal faults on the southern flank of the Cornubian batholith in south Cornwall at distances of up to 3.2 km laterally from the granite.

12. Basinal brines flowed into the Cornubian region contemporaneously with granite-driven convection of meteoric fluids. The Na-Ca-K brines were responsible for late base metal (cross-course) mineralisation. Mixing of brines and meteoric fluids at structural intersections caused base metal sulphide deposition by increasing pH and reducing fluid salinity.

7.2 FURTHER WORK

There are a large number of avenues of research which could have proved useful in the present study but which, as a result of the time constraints imposed, could not be pursued. These areas of possible further work are listed below. Such additional studies, in combination with the fluid evolution models outlined in this thesis, could provide an extremely detailed picture of the controls and effects of fluid movement in the crust.

1) Electron microprobe studies of regional metamorphic mineral assemblages, in order to assess the importance of solid solution effects in the major mineral phases in controlling fluid composition;

2) Electron microprobe studies of wallrock mineralogy to identify variations in trace components of mineral phases and relate these to fluid compositions;

3) Electron microprobe studies of chlorite compositions, on chlorites developed at all stages, to provide additional constraints on oxygen fugacity and Fe-Mg compositions of fluids;

4) Crush-leach + ICP-atomic emission spectrometry and/or atomic absorption analysis of fluid inclusions to compare with D-ICP data;

5) Crush-leach + ICP-mass spectrometry studies of fluid inclusion compositions to provide data on trace element compositions of crustal fluids, with particular reference to trace metals;

6) Laser-Raman microprobe studies of individual fluid inclusions, particularly on V3 syn-granite fluids, to provide more detailed volatile compositions;

7) Bulk volatile analysis of H_2S content of inclusion fluids for comparison with thermodynamic predictions;

8) Additional oxygen and hydrogen isotope work on fluid inclusions, as well as on vein and wallrock mineral phases and bulk rocks, to confirm and amplify the evolutionary trends identified to date;

9) Sulphur isotope studies of inclusion fluids and mineral phases to constrain sulphur source and to constrain the conditions of sulphide precipitation;

10) Additional microthermometric analysis to further constrain spatial variations in fluid compositions, both from vein to vein as well as within individual veins;

11) Additional microthermometric analysis of the complex magmatic-hydrothermal transition stage observed in the Megilliggar pegmatite-aplite complex;

12) More advanced thermodynamic modelling of metal transport, deposition mechanisms, and fluid-rock interaction in the fluid systems studied, utilising existing computer programs and developing further relevant software☺

REFERENCE LIST

ADAMS, C.J. 1981. Uplift rates and thermal structure in the Alpine Fault Zone and Alpine Schists, Southern Alps, New Zealand. *In:* McCLAY, K.R. & PRICE, N.J. (eds) *Thrust and nappe tectonics*. Special publication of the Geological Society, London, No.9, 211-22.

ALDERTON, D.H.M. 1975. Fluid inclusion studies in S.W. England. *Proc. Ussher Soc.,* **3,** 214-7.

------ 1978. Fluid inclusion data for lead-zinc ores from S.W. England. *Trans. Inst. Min. Metall.,* **87,** B132-5.

------ & RANKIN, A.H. 1982. Fluid inclusion studies in the St. Austell granite. *J. Geol. Soc. London,* **140,** 297-310.

------, THOMPSON, M., RANKIN, A.H. & CHRYSSOULIS, S.L. 1982. Developments of the ICP-linked decrepitation technique for the analysis of fluid inclusions in quartz. *Chem. Geol.,* **37,** 203-13.

AL-RAWI, F.R.J. 1980. A geophysical study of deep structure in southwest Britain. *Ph.D. Thesis, University of Wales.*

ANGUS, S., ARMSTRONG, B., deREUCK, K.M., ALTUNIN, V.V., GADETSKII, O.G., CHAPELA, G.A. &ROWLINSON, J.S. 1976. *International Thermodynamic Tables of the Fluid State*, Vol.3, *Carbon Dioxide,* Pergamon Press, Oxford, 385 p.

BADHAM, J.P.N. 1980. Late magmatic phenomena in the Cornish batholith, useful guides for tin mineralisation. *Proc. Ussher Soc.,* **5,** 44-53.

BARNES, H.L. (ed) 1979. *Geochemistry of hydrothermal ore deposits.* 2nd Edition, John Wiley & Sons, London, 798 p.

BARNES, R.P. 1982. The geology of south Cornish melanges. *Ph.D. thesis, University of Southampton.*

------ & ANDREWS, J.R. 1981. Pumpellyite-actinolite grade regional metamorphism in south Cornwall. *Proc. Ussher Soc.,* **5,** 139-46.

BARONNET, A. 1984. Growth kinetics of the silicates. A review of basic concepts. *Fortschr. Mineral.,* **62,** 187-232.

BARRETT, T.J. & ANDERSON, G.M. 1982. The solubility of sphalerite and galena in NaCl brines. *Econ. Geol.,* **77,** 1923-33.

BARTON, P.B. Jr. & SKINNER, B.J. 1979. Sulphide mineral stabilities. *In:* BARNES, H.L. (ed) *Geochemistry of hydrothermal ore deposits,* 2nd Edition, John Wiley & Sons, London, 278-403.

BATEMAN, R. 1985. Aureole deformation by flattening around a diapir during in situ ballooning: the Cannibal Creek Granite. *J. Geol.,* **93,** 293-310.

BEACH, A. 1977. Vein arrays, hydraulic fractures and pressure solution structures in a deformed flysch sequence, S.W. England. *Tectonophysics,* **40,** 201-25.

------ 1979. Pressure solution as a metamorphic process in deformed terrigenous sedimentary rocks. *Lithos,* **12,** 51-8.

BEER, K. & BALL, T.K. 1986. Tin and tungsten in pelitic rocks from S.W. England and their behaviour in contact zones of granites and in mineralised areas. *Proc. Ussher Soc.,* **6,** 330-7.

BEHR, H.J. & GERLER, J. 1987. Inclusions of sedimentary brines in post-Variscan mineralizations in the Federal Republic of Germany - A study by neutron activation analysis. *Chem. Geol.,* **61,** 65-77.

------, HORN, E.E., FRENTZEL-BEYME, K. & REUTEL, Chr. 1987. Fluid inclusion characteristics of the Variscan and post-Variscan mineralizing fluids in the Federal Republic of Germany. *Chem. Geol.,* **61,** 273-85.

BISCHOFF, J.L., RADTKE, A.S. & ROSENBAUER, R.J. 1981. Hydrothermal alteration of graywacke by brine and seawater: role of alteration and chloride complexing on metal solubilization at 200°C and 350°C. *Econ. Geol.,* **76,** 659-76.

BORISENKO, A.S. 1977. Study of the salt composition of solutions in gas-liquid inclusions in minerals by the cryometric method. *Soviet Geol. & Geophys.,* **18,** 11-19.

BOTTRELL, S.H. & Yardley, B.W.D. 1988. The composition of a primary granite-derived ore fluid from S.W. England, determined by fluid inclusion analysis. *Geochim. Cosmochim. Acta,* **52**, 585-8.

------, ------ & BUCKLEY, F. 1988. A modified crush-leach method for the analysis of fluid inclusion electrolytes. *Bull. Mineral.,* **111**, 279-90.

BOWERS, T.S. & HELGESON, H.C. 1983a. Calculation of the thermodynamic and geochemical consequences of non-ideal mixing in the system H_2O-CO_2-NaCl on phase relations in geologic systems: equation of state for H_2O-CO_2-NaCl fluids at high pressures and temperatures. *Geochim. Cosmochim. Acta,* **47**, 1247-75.

------ & ------ 1983b. Calculation of the thermodynamic and geochemical consequences of non-ideal mixing in the system H_2O-CO_2-NaCl on phase relations in geologic systems: Metamorphic equilibria at high pressures and temperatures. *Am. Mineral.,* **68**, 1059-75.

BRACE, W.F. 1980. The permeability of crystalline and argillaceous rocks. *Int. J. Rock Mech. Min. Sci.,* **17**, 241-51.

BRIMHALL, G.H. & CRERAR, D.A. 1987. Ore fluids: Magmatic to supergene. *In:* CARMICHAEL, I.S.E. & EUGSTER, H.P. (eds) *Thermodynamic Modelling of Geological Materials: Minerals, Fluids and Melts.* Reviews in Mineralogy, **17**, Mineralogical Society of America, 235-321.

BROMLEY, A.V. & HOLL, J. 1987. Tin mineralisation in S.W. England. *Proc. NATO Mineral Processing Conference, Falmouth,* 195-262.

BROWN, P.E. & LAMB, W.M. 1988. P-V-T properties of fluids in the system $H_2O \pm CO_2 \pm$NaCl: New graphical presentations and implications for fluid inclusion studies. *Geochim. Cosmochim. Acta,* **53**, 1209-21.

BURNHAM, W., HOLLOWAY, J.R. & DAVIS, N.F. 1969. Thermodynamic properties of water to 1000°C and 10,000 bars. *Geol. Soc. Amer. Special paper,* **132**.

BUTLER, R.W.H. 1982. The terminology of structures in thrust belts. *J. Struct. Geol.,* **4**, 239-45.

CAREW, R.C. 1602. *Survey of Cornwall.* Printed by T. Bensley, London for J. Faulder, London and Rees Curtis, Plymouth. 459 p.

CARNE, J. 1822. On the relative ages of the veins of Cornwall. *Trans. Royal Geol. Soc. Cornwall,* **2**, 49-128.

CARPENTER, A.B., TROUT, M.L. & PICKETT, E.E. 1974. Preliminary report on the origin and chemical evolution of lead- and zinc-rich oilfield brines in Central Mississippi. *Econ. Geol.,* **69**, 1191-1206.

CARTER, A.H.C. 1990. Transport and deposition of gold in a major Archaean shear zone, Dalny Mine, Zimbabwe. *Ph.D. Thesis, University of Southampton.*

CHAROY, B. 1979. Definition et importance des phenomenes deuteriques et des fluides associes dans les granites. Consequences metallogeniques. *Mem. Sci. de la Terre, Nancy,* **37**, 364 p.

------ 1986. The genesis of the Cornubian batholith, S.W. England: the example of the Carnmenellis pluton. *J. Petrol.,* **27**, 571-604.

CHESHER, S.E. 1971. The metasomatic effects of the intrusion of the Tregonning Godolphin Granite into the Mylor Slates, South Cornwall. *Ph.D. Thesis, University of Exeter.*

CLAYTON, R.N., FRIEDMAN, I., GRAF, D.L., MAYEDA, T.K., MEENTS, W.F. & SHIMP, N.F. 1966. The origin of saline formation waters. I. Isotopic composition. *J. Geophys. Res.,* **71**, 3869-82.

COLLINS, P.L.F. 1979. Gas hydrates in CO_2-bearing fluid inclusions and the use of freezing data for estimation of salinity. *Econ. Geol.,* **74**, 1435-44.

COOK, A.C., MURCHISON, D.G. & SCOTT,E. 1972. A British meta-anthracite coal of Devonian age. *Geol. Jour.,* **8**, 83-94.

COOMBS, D.S., NAKAMURA, Y. & VUAGNAT, M. 1976. Pumpellyite-actinolite facies schists of the Taveyanne Formation near Loeche, Valais, Switzerland. *J. Petrol.,* **17**, 440-71.

COTTON, F.A. & WILKINSON, G. 1980. *Advanced Inorganic Chemistry.* Fourth Edition, Wiley Interscience, New York, 1396 p.

COX, S.F. 1987. Antitaxial crack-seal vein microstructures and their relationship to displacement paths. *J. Struct. Geol.,* **9,** 779-87.

------ & ETHERIDGE, M.A. 1981. The development of deformation micro-fabrics in low grade metavolcanics and associated rocks, Mount Lyell area, Tasmania. *Geol. Soc. Australia, Abstr.,* **4,** 24.

------ & ------ 1983. Crack-seal fibre growth mechanisms and their significance in the development of oriented layer silicate microstructures. *Tectonophysics,* **92,** 147-70.

CRAWFORD, M.L. 1981a. Phase equilibria in aqueous fluid inclusions. *In:* HOLLISTER, L.S. & CRAWFORD, M.L. (eds) *A short course in fluid inclusions.* Mineralogical Association of Canada Short Course Handbook, **6,** 75-100.

------ 1981b. Fluid inclusions in metamorphic rocks - low and medium grade. *In:* HOLLISTER, L.S. & CRAWFORD, M.L. (eds) *A short course in fluid inclusions.* Mineralogical Association of Canada Short Course Handbook, **6,** 75-100.

------, FILER, J. & WOOD, C. 1979. Saline fluid inclusions associated with retrograde metamorphism. *Bull. Mineral.,* **102,** 562-8.

------ & HOLLISTER, L.S. 1986. Metamorphic fluids: the evidence from fluid inclusions. *In:* WALTHER, J.V. & WOOD, B.J. (eds.) *Fluid-rock interactions during metamorphism.* Advances in Physical Geochemistry, Vol. 5, Springer-Verlag, New York, 1-35.

CROCKET, J.H. (in press). Distribution of gold in the Earth's crust. *In:* FOSTER, R.P. (ed) *Gold Metallogeny and Exploration.* Blackie & Son Ltd., Glasgow.

CZAMANSKE, G.K., ROEDDER, E. & BURNS, F.C. 1963. Neutron activation analysis of fluid inclusions for Cu, Mn and Zn. *Science,* **140,** 401-3.

DANGERFIELD, J. & HAWKES, J.R. 1969. Unroofing of the Dartmoor granite and possible consequences with regard to mineralisation. *Proc. Ussher Soc.,* **2,** 122-31.

DARBYSHIRE, D.P.F. & SHEPHERD, T.J. 1985. Chronology of granite magmatism and associated mineralisation, S.W. England. *J. Geol. Soc. London,* **142,** 1159-77.

------ & ------ 1987. Chronology of magmatism in S.W. England: the minor intrusions. *Proc. Ussher Soc.,* **6,** 431-8.

DAY, G.A. 1985. The Hercynian evolution of the south west British continental margin. *In:* BARAZANGI, M. & BROWN, L. (eds) *International symposium on deep structure of the continental crust: results from reflection seismic.* Geodynamic, **14.**

DEARMAN, W.R. 1963. Wrench faulting in Cornwall and south Devon. *Proc. Geol. Assoc. London,* **74,** 265-87.

------ 1969. Tergiversate folds from south-west England. *Proc. Ussher Soc.,* **2,** 112-5.

------, LEVERIDGE, B.E., RATTEY, P.R. & SANDERSON, D.J. 1980. Superposed folding at Rosemullion Head, S. Cornwall. *Proc. Ussher Soc.,* **5,** 33-8.

DEINES, P. 1970. The carbon and oxygen isotopic composition of carbonatites from the Oka carbonatite complex, Quebec, Canada. *Geochim. Cosmochim. Acta,* **34,** 1199-1225.

------ 1980a. The carbon isotopic composition of diamonds: Relationship to diamond shape, colour, occurrence and vapour composition. *Geochim. Cosmochim. Acta,* **44,** 943-61.

------ 1980b. The isotopic composition of reduced organic carbon. *In:* FRITZ, P. & FONTES, J.C. (eds) *Handbook of Environmental Isotope Geology,* Vol.1, Springer-Verlag, Berlin, 329-406.

------ & GOLD, D.P. 1973. The isotopic composition of carbonatite and kimberlite carbonates and their bearing on the isotopic composition of deep-seated carbon. *Geochim. Cosmochim. Acta,* **37,** 1709.

DICKEY, P.A. 1969. Increasing concentration of subsurface brines with depth. *Chem Geol.,* **4,** 361-70.

DINES, H.G. 1956. The metalliferous mining region of southwest England. *Mem. Geol. Survey, U.K.,* H.M.S.O, London, 2 vols., 795 p.

DIXON, J.M. 1975. Finite strain and progressive deformation in models of diapiric structures. *Tectonophysics,* **28,** 89-124.

DUNHAM, K., BEER, K.E., ELLIS, R.A., GALLAGHER, M.J., NUTT, M.J.C. & WEBB, B.C. 1978. Mineral Deposits of Europe: United Kingdom. *In:* BOWIE, S.H.U. *et al.* (eds) *Mineral Deposits of Europe, Vol.1,* Institute of Mining and Metallurgy and the Mineralogical Society, 263-317.

DURNEY, D.A. & RAMSAY, J.G. 1973. Incremental strains as measured by syntectonic crystal growth. *In:* DeJONG, K.A. & SCHOLTEN, R. (eds): *Gravity and Tectonics*, Wiley Interscience, London, 67-96.

DURRANCE, E.M., BROMLEY, A.V., BRISTOW, C.M., HEATH, M.J. & PENMAN, J.M. 1983. Hydrothermal circulation and post-magmatic changes in the granites of S.W. England. *Proc. Ussher Soc.,* **5,** 304-20.

DODSON, M.H. & REX, D.C. 1971. Potassium-argon ages of slates and phyllites from south-west England. *Q. J. Geol. Soc. London,* **126,** 465-99.

EDWARDS, R.P. 1976. Aspects of trace metal and ore distribution in Cornwall. *Trans. Inst. Min. Metall.,* **85,** B83-90.

ETHERIDGE, M.A., WALL, V.J. & VERNON, R.H. 1983. The role of the fluid phase during regional metamorphism and deformation. *J. Met. Geol.,* **1,** 205-26.

EUGSTER, H.P. 1982. Rock-fluid equilibrium systems. *In:* SCHREYER, W. (ed) *High pressure researches in Geoscience*, Section VI: Thermodynamics and equilibria, 501-18.

------ 1986. Minerals in hot water. *Am. Mineral.,* **71,** 655-73.

------ & BAUMGARTNER, L. 1987. Mineral solubilities and speciation in metamorphic fluids. *In:* CARMICHAEL, I.S.E. & EUGSTER, H.P. (eds) *Thermodynamic Modelling of Geological Materials: Minerals, Fluids and Melts.* Reviews in Mineralogy, **17,** Mineralogical Society of America, 367-403.

------ & GUNTER, W.D. 1981. The composition of supercritical metamorphic solutions. *Bull. Soc. Franc. Mineral. Cristall.,* **104,** 817-26.

------ & SKIPPEN, G.B. 1967. Igneous and metamorphic equilibria involving gas equilibria. *In:* ABELSON, P.H. (ed) *Researches in Geochemistry,* Vol.2, John Wiley & Sons, New York.

EXLEY, C.S. & STONE, M. 1964. The granitic rocks of southwest England. *In:* HOSKING, K.F.G. & SHRIMPTON, G.J. (eds) *Present views of some aspects of the geology of Cornwall and Devon,* 150th Anniversary Volume, Royal Geological Society of Cornwall, 131-84.

------, ------ & FLOYD, P.A. 1983. Composition and petrogenesis of the Cornubian batholith and post-orogenic rocks in S.W. England. *In:* HANCOCK, P.L. (ed) *The Variscan fold belt in the British Isles,* Adam Hilger Ltd., Bristol, 153-77.

FARMER C. 1988. Paragenetic and structural relationships of tin mineralisation at South Crofty Mine, Cornwall. *Abstracts Volume, Mineral Deposits Studies Group A.G.M.*, Royal Holloway & Bedford New College, Dec. 1988.

FEHN, U. 1985. Post-magmatic convection related to high heat production in granites of S.W. England: a theoretical study. In *High Heat Production (HHP) Granites, Hydrothermal Circulation and Ore Genesis.* Inst. Min. Metall., 99-112.

FERRY, J.M. 1978. Fluid interaction between granite and sediment during metamorphism, South Central Maine. *Am. J. Sci.,* **278,** 1025-56.

------ 1979. A case study of the amount and distribution of heat and fluid during metamorphism. *Contrib. Min. Petrol.,* **71,** 373-85.

------ 1986. Reaction progress: A monitor of fluid-rock interaction during metamorphic and hydrothermal events. *In:* WALTHER, J.V. & WOOD, B.J. (eds.) *Fluid-rock interactions during metamorphism.* Advances in Physical Geochemistry, Vol. 5, Springer-Verlag, New York, 60-88.

------ 1989. Contact metamorphism of roof pendants at Hope Valley, Alpine County, California, USA. *Contrib. Mineral. Petrol.,* **101,** 402-17.

FLETT, J.S. 1933. The geology of the Meneage. *Mem. Geol. Survey Gt. Britain,* **2,** 1-14.

------ 1946. The geology of the Lizard and Meneage. *Mem. Geol. Survey, Gt. Britain.*

FLINN, D. 1962. On folding during three dimensional progressive deformation. *Q. J. Geol. Soc. London,* **118,** 385-428.

FLOYD, P.A. 1972. Geochemistry, origin and tectonic setting of the basic and acidic rocks of Cornubia, England. *Proc. Geol. Assoc. London,* **83,** 385-404.

------ & LEVERIDGE, B.E. 1987. Tectonic environment of the Devonian Gramscatho Basin, south Cornwall, framework mode and geochemical evidence for turbiditic sandstones. *J. Geol. Soc. London,* **144,** 531-42.

FOURNIER, R.O. 1981. Application of water geochemistry to geothermal exploration and reservoir engineering. *In:* RYBACH, L. & MUFFLER, L.J.P. (eds) *Geothermal systems: principles and case histories,* Wiley, Chichester, 109-43.

------ & POTTER, R.W. 1982. A revised and expanded silica (quartz) geothermometer. *Geotherm. Research Council Bull.,* **11,** 3-9.

------ & TRUESDELL, A.H. 1973. An empirical Na-Ca-K geothermometer for natural waters. *Geochim. Cosmochim. Acta,* **37,** 1255-75.

FRENCH, B.M. 1966. Some geological implications of equilibrium between graphite and a C-H-O gas phase at high temperatures and pressures. *Rev. Geophys.,* **4,** 223-53.

FREY, M., BUCHER, K., FRANK, E. & MULLIS, J. 1980. Alpine metamorphism along the Geotraverse Basel-Chiasso - a review. *Eclogae. Geol. Helv.,* **73,** 527-46.

FRY, N. 1979. Random point distributions and strain measurement in rocks. *Tectonophysics,* **60,** 89-105.

FROST, B.R. 1979. Mineral equilibria involving mixed volatiles in a C-O-H fluid phase: the stabiliteies of graphite and siderite. *Am. J. Sci.,* **279,** 1033-59.

FYFE, W.S. & KERRICH, R. 1985. Fluids and thrusting. *Chem. Geol.,* **49,** 353-62.

------, PRICE, N.J. & THOMPSON, A.B. 1978. *Fluids in the Earth's Crust.* Elsevier, Amsterdam, 383 p.

GARNETT, R.H.T. 1961. Structural control of mineralisation in southwest England. *Mining Mag.,* **105,** 329-37.

GEHRIG, M. 1980. Phasengleichgewichte und PVT-Daten ternarer Mischungen aus Wasser, Kohlendioxide, und Natriumchlorid bis 3 kbar und 550 C. *Doctoral dissertation, University of Karlsruhe, Hochschulverlag, Freiburg.*

------, LENTZ, H. & FRANCK, E.U. 1979. Thermodynamic properties of water-carbon dioxide-sodium chloride mixtures at high temperatures and pressures. *In:* TIMMERHAUS, K.D. & BARBER, M.S. (eds) *High pressure science and technology, 1: Physical properties and material synthesis,* 539-42.

GIGGENBACH, W.F. 1981. Geothermal mineral equilibria. *Geochim. Cosmochim. Acta,* **45,** 393-410.

------ 1988. Geothermal solute equilibria. Derivation of Na-K-Mg-Ca geoindicators. *Geochim. Cosmochim. Acta,* **52,** 2749-65.

GRAPPIN, C., SALIOT, P., SABOURAUD, C. & TOURAY, J-C. 1979. Les variations des rapports Cl/Br, Na/Br et K/Br dans les inclusions fluides des quartz de la cicatrice évaporitique de Bramans-Termignan (Vanoise, Alpes Francais). *Chem. Geol.,* **25,** 41-52.

GREENSMITH, J.T. 1981. *Petrology of the Sedimentary Rocks,* 6th Edition, George Allen & Unwin, London, 241 p.

GREENWOOD, H.J. 1975. Buffering of pore fluids by metamorphic reactions. *Am. J. Sci.,* **275,** 573-93.

HAACK, U., HEINRICHS, H., BONEß, M. & SCHNEIDER, A. 1984. Loss of metals from pelites during regional metamorphism. *Contrib. Min. Petrol.,* **85,** 116-32.

HAAPALA, I. & KINNUNEN, K. 1982. Fluid inclusion evidence on the genesis of tin deposits. *In:* EVANS, A.M. (ed) *Metallization associated with acid magmatism,* Vol. 6, John Wiley & Sons, London, 101-9.

HAAS, J.L. 1976. Physical properties of the coexisting phases and thermochemical properties of the H_2O component in boiling NaCl solutions. (Preliminary steam tables for NaCl solutions). *U.S. Geol. Surv. Bull.,* **1421-A.**

HALL, A. 1988. The distribution of ammonium in granites from S.W. England. *J. Geol. Soc. London,* **145**, 37-41.

HALL, S. 1930. The geology of the Godolphin granite. A study of the coastal geology between Perranuthoe and Loe Pool. *Proc. Geol. Assoc. London,* **41**, 117-47.

HALLIDAY, A.N. 1980. The timing of early and mainstage ore mineralisation in southwest Cornwall. *Econ. Geol.,* **75**, 752-9.

HALLS, C. 1987. A mechanistic approach to the paragenetic interpretation of mineral lodes in Cornwall. *Proc. Ussher Soc.,* **6**, 548-54.

------, C., EXLEY, C.S. & BRUNTON, E.V. 1985. Bibliography of magmatism and mineralisation in southwest England. Special Publication, Institute of Mining and Metallurgy, 46 p.

HANOR, J.S. 1979. The sedimentary genesis of hydrothermal fluids. *In:* BARNES, H.L. (ed) *Geochemistry of hydrothermal ore deposits,* 2nd Edition, John Wiley & Sons, London, 137-72.

HANSHAW, B.B. & COPLEN, T.B. 1973. Ultrafiltration by a compacted clay membrane - II. Sodium ion exclusion at various ionic strengths. *Geochim. Cosmochim Acta,* **37**, 2311-27.

HARLAND, W.B., COX, A.B., LLEWELLYN, P.G., PICKTON, C.A.G., SMITH, A.G. & WALTERS, R. 1982. *A Geologic Time Scale.* Cambridge University Press, 131 p.

HAWKES, J.R. 1974. Volcanism and metallogenesis: the tin province of S.W. England. *Bull. Vulcanol.,* **38**, 1125-46.

------ & DANGERFIELD,J. 1978. The Variscan granites of S.W. England: a progress report. *Proc. Ussher Soc.,* **4**, 158-71.

HELGESON, H.C. 1964. *Complexing and hydrothermal ore deposits.* Pergamon Press, New York, 128 p.

------ 1968. Evaluation of irreversible reactions in geochemical processes involving minerals and aqueous solutions. I. Thermodynamic relations. *Geochim. Cosmochim. Acta,* **32**, 853-77.

------ 1969. Thermodynamics of hydrothermal systems at elevated temperatures and pressures. *Am. J. Sci.,* **267**, 729-804.

------, DELANEY, J.M., NESBITT, H.W. & BIRD, D.K. 1978. Summary and critique of the thermodynamic properties of rock-forming minerals. *Am. J. Sci.,* **278-A**, 1-229.

------, KIRKHAM, D.H. & FLOWERS, G.C. 1981. Theoretical prediction of the thermodynamic properties of aqueous electrolytes at high temperatures and pressures. IV. Calculation of activity coefficients, osmotic coefficients, and apparent molal and standard and relative partial molal properties to 5 kb and 600°C. *Am. J. Sci.,* **281**, 1241-1516.

HEMLEY, J.J. & JONES, W.R. 1964. Chemical aspects of hydrothermal alteration with emphasis on hydrogen metasomatism. *Econ. Geol.,* **59**, 538-69.

HENDEL, E.M. & HOLLISTER, L.S. (1981). An empirical solvus for CO_2-H_2O-2.6 wt% salt. *Geochim. Cosmochim. Acta,* **45**, 225-8.

HENDRIKS, E.M.L. 1937. Rock succession and structure in south Cornwall, a revision. With notes on the central Eurpean facies and Variscan folding there present. *Q. J. Geol. Soc. London,* **93**, 322-60.

------, HOUSE, M.R. & RHODES, F.H.T. 1971. Evidence bearing on the stratigraphical successions in south Cornwall. *Proc. Ussher Soc.,* **2**, 270-5.

HENLEY, R.W., TRUESDELL, A.H. & BARTON, P.B. Jr. 1984. *Fluid-mineral equilibria in hydrothermal systems.* Reviews in Economic Geology, Vol.1, Society of Economic Geologists.

HENLEY, S. 1974. Geochemistry of Devonian sediments in the Perranporth area, Cornwall. *Proc. Ussher Soc.,* **3**, 128-36.

HENWOOD, W.J. 1843. On the metalliferous deposits of Cornwall and Devon. *Trans. Royal Geol. Soc. Cornwall,* **5**, 1-386.

HEY, M.H. 1954. A new review of the chlorites. *Min. Mag.,* **30**, 277.

HILL, J.B. & MacALLISTER, D.A. 1906. The geology of Falmouth and Truro, and of the mining district of Camborne and Redruth. *Mem. Geol. Surv., Gt. Britain.*

HINRICHSEN, T. & SCHÜRMANN, K. 1969. Untersuchungen zur Stabilität von Pumpellyit. *Neues Jb. Miner. Mh.,* **10,** 441-5.

HITCHON, B. & FRIEDMAN, I. 1969. Geochemistry and origin of formation waters in the western Canada sedimentary basin - I. Stable isotopes of hydrogen and oxygen. *Geochim. Cosmochim. Acta,* **33,** 1321-49.

HOBBS, B.E., MEANS, W.D. & WILLIAMS, P.F. 1976. *An outline of structural geology.* John Wiley & Sons, New York, 571 p.

HOLDER, M.T. & LEVERIDGE, B.E. 1986. A model for the tectonic evolution of south Cornwall. *J. Geol. Soc. London,* **143,** 125-34.

HOLLISTER, L.S., BURRUSS, R.C., HENRY, D.L. & HENDEL, E.M. 1979. Physical conditions during uplift of metamorphic terrains, as recorded by fluid inclusions. *Bull. Mineral.,* **102,** 555-61.

------ & CRAWFORD, M.L. (eds) 1981. *A short course in fluid inclusions.* Mineralogical Association of Canada Short Course Handbook, **Vol.6,** 304 p.

HOLLOWAY, J.R. 1977. Fugacity and activity of molecular species in supercritical fluids. *In:* FRASER, D.G. (ed) *Thermodynamics in Geology,* D. Reidel, Dordrecht, Holland, 161-81.

------ 1981. Compositions and volumes of supercritical fluids in the earth's crust. *In:* HOLLISTER, L.S. & CRAWFORD, M.L. (eds) *A short course in fluid inclusions.* Mineralogical Association of Canada Short Course Handbook, **6,** 75-100.

------ 1984. Graphite-CH_4-H_2O-CO_2 equilibria at low-grade metamorphic conditions. *Geology,* **12,** 455-8.

------ 1987. Igneous fluids. *In:* CARMICHAEL, I.S.E. & EUGSTER, H.P. (eds) *Thermodynamic Modelling of Geological Materials: Minerals, Fluids and Melts.* Reviews in Mineralogy, **17,** Mineralogical Society of America, 211-33.

HOLLOWAY, S. & CHADWICK, R.A. 1986. The Sticklepath-Lustleigh fault zone: Tertiary sinistral reactivation of a Variscan dextral strike-slip fault. *J. Geol. Soc. London,* **143,** 447-52.

HOSKING, K.F.G. 1964. Permo-Carboniferous and later primary mineralisation of Cornwall and S.W. Devon. *In:* HOSKING, K.F.G. & SHRIMPTON, G.J. (eds) *Present views of some aspects of the geology of Cornwall and Devon,* 150th Anniversary Volume, Royal Geological Society of Cornwall, 201-45.

HOUSE, M.R. 1968. *Continental drift and the Devonian system.* Inaugural lecture, University of Hull, 1-24.

HUTTON, D.H.W & SANDERSON, D.J. (eds) 1984. *Variscan tectonics of the north Atlantic region.* Special Publication of the Geological Society, London, **14.**

JACKSON, J.A. & McKENZIE, D.P. 1983. The geometric evolution of normal fault systems. *J. Struct. Geol.,* **5,** 471-82.

JACKSON, K.J. & HELGESON, H.C. 1985. Chemical and thermodynamic constraints on the hydrothermal transport and deposition of tin: I. Calculation of the solubility of cassiterite at high pressures and temperatures. *Geochim. Cosmochim. Acta,* **49,** 1-22.

JACKSON, N.J. 1977. The geology and mineralisation of the St. Just mining district, west Cornwall. *Ph.D thesis, University of London.*

------, HALLIDAY, A.N., SHEPPARD, S.M.F. & MITCHELL, J.G. 1982. Hydrothermal activity in the St. Just mining district, Cornwall. *In:* EVANS, A.M. (ed) *Metallization associated with acid magmatism,* Vol. 6, John Wiley & Sons, London, 137-79.

------ & RANKIN, A.H. 1976. Fluid inclusion studies at St. Michael's Mount. *Proc. Ussher Soc.,* **3,** 430-4.

------, WILLIS-RICHARDS, J., MANNING, D.A.C. & SAMS, M. (in press). Evolution of the Cornubian orefield, S.W. England. Part II: Mineral deposits and ore-forming processes. *Econ. Geol.* Special publication.

KERRICH, R. 1986. Fluid infiltration into fault zones: chemical, isotopic and mechanical effects. *Pageoph.*, **124,** 225-68.

KERRICK, D.M. & JACOBS, G.K. 1981. A modified Redlich-Kwong equation for H_2O, CO_2 and H_2O-CO_2 mixtures at elevated temperatures and pressures. *Am. J. Sci.,* **281,** 735-67.

KHARAKA, Y.K., LICO, M.S., WRIGHT, V.A. & CAROTHERS, W.W. 1980. Geochemistry of formation waters from Pleasant Bayou No.2 well and adjacent areas in coastal Texas. *Geopressured-Geothermal Energy Conf., 4th, Austin, Texas, 1980,* Proceedings, 46-84.

KRAUSKOPF, K.B. 1979. *Introduction to Geochemistry.* 2nd Edition, McGraw-Hill, New York, 617p.

LABOTKA, T.C., WHITE, C.E. & PAPIKE, J.J. 1985. The evolution of water in the contact-metamorphic aureole of the Duluth Complex, northeastern Minnesota. *Geol. Soc. Am. Bull.,* **95,** 788-804.

LAGACHE, M. & WEISBROD, A. 1977. The system two alkali feldspars KCl-NaCl-H_2O at moderate to high temperatures and low pressures. *Contrib. Mineral. Petrol.,* **62,** 77-101.

LANDIS, C.A. 1971. Graphitization of dispersed carbonaceous material in metamorphic rocks. *Contrib. Mineral. Petrol.,* **30,** 30-45.

LE GALL, B., LE HERISSE, A. & DEUNFF, J. 1985. New palynological data from the Gramscatho Group at the Lizard front (Cornwall): palaeogeographical and geodynamical implications. *Proc. Geol. Assoc. London,* **96,** 237-53.

LEVERIDGE, B.E. & HOLDER, M.T. 1985. Olistostromic breccias at the Mylor/Gramscatho boundary, south Cornwall. *Proc. Ussher Soc.,* **6,** 147-54.

------, HOLDER, M.T. & DAY, G.A. 1984. Thrust nappe tectonics in the Devonian of south Cornwall and the western English Channel. *In:* HUTTON, D.H.W & SANDERSON, D.J. (eds) 1984. *Variscan tectonics of the north Atlantic region.* Special Publication of the Geological Society, London, **14.**

LUCKSCHEITER, B. & PAREKH, P.P. 1979. A new method for the determination of dissolved elements in fluid inclusions. *N. Jb. Mineral. Mitt.,* 135-44.

LIOU, J.G., MARUYAMA, S. & CHO, M. 1985. Phase equilibria and mineral parageneses of metabasites in low-grade metamorphism. *Min. Mag.,* **49,** 321-33.

MACDONALD, A.J. & SPOONER, E.T.C. 1981. Calibration of a Linkam TH600 programmable heating-cooling stage for microthermometric examination of fluid inclusions. *Econ. Geol.,* **74,** 1248-58.

McKENZIE, D.A. 1978. Active tectonics of the Alpine-Himalayan Belt: the Aegean Sea and surrounding regions. *Geophys. J. Royal Astr. Soc.,* **55,** 217-54.

MANGAS, J. & ARRIBAS, A. 1987. Fluid inclusion study in different types of tin deposits associated with the Hercynian granites of western Spain. *Chem. Geol.,* **61,** 193-208.

MANNING, D.A.C. 1979. An experimental study of the effect of flourine, in addition to water, on crystallisation in the system Qz-Ab-Or and its application to Cornish granite rocks rich in fluorine. *Proc. Ussher Soc.,* **4,** 380-9.

------ 1981. The effect of fluorine on liquidus relationships in the system Qz-Ab-Or with excess water at 1kb. *Contrib. Min. Petrol.,* **76,** 206-15.

------ 1985. Comparison of the the influence of magmatic water on the formation of granite-hosted Sn-W deposits and associated tourmalinisation from Thailand and S.W. England. *In: High heat production (HHP) granites, hydrothermal circulation and ore genesis.* Inst. Min. Metall. Special Publication, 203-212.

MATSUHISA, Y., GOLDSMITH, J.R. & CLAYTON, R.N. 1979. Oxygen isotopic fractionation in the system quartz-albite-anorthite-water. *Geochim. Cosmochim. Acta,* **43,** 1131-40.

MILLER, J.A. & MOHR, P.A. 1964. Potassium-argon measurements of the granites and some associated rocks from south-west England. *Geol. J.,* **4,** 105-26.

MILLER, M.F., SHEPHERD, T.J., YUCHENG, L. & HALLS, C. 1989. The source and significance of carbon isotopes in fluid inclusions from mineralised areas of S.W. England and S. China. (Abstract) *ECROFI X, Imperial College, London.*

MONTOYA, J.W. & HEMLEY, J.J. 1975. Activity relations and stabilities in alkali feldspar and mica alteration reactions. *Econ. Geol.,* **70,** 577-94.

MOORE, J. McM. 1975. A mechanical interpretation of the vein and dyke systems of the S.W. England orefield. *Mineral. Deposita,* **10,** 374-88.

MORTON, W.H. & BLACK, R. 1975. Crustal attenuation in Afar. *In:* PILGER, A. & ROSLER, A. (eds) *Afar Depression of Ethiopia, Inter-Union Commission on Geodynamics.* Scientific Report, No.**14**, E. Schweizerbart'sche Verlagsbuchhandlung, Stuttgart, 55-65.

MULLIS, J. 1979. The system methane-water as a geologic thermometer and barometer from the external part of the Central Alps. *Bull. Mineral.,* **102,** 526-36.

------, J., DUBESSY, J., KOSZTOLANYI, C. & POTY, B. 1983. Fluid evolution in Alpine fissures during prograde and retrograde metamorphism along the geotraverse: Lucerne-Bellinzona (Swiss Alps). *European Current Research on Fluid Inclusions, April 1983.* Soc. Franc. Mineral. et Cristall., Orleans, p. 46.

NITSCH, K.H. 1971. Stabilitätsbuziehungen von prehnite - und pumpellyithaltigen paragenesen. *Contrib. Mineral. Petrol.,* **30,** 240-60.

NORTON, D.L. 1984. Theory of hydrothermal systems. *Ann. Rev. Earth Planet. Sci. Lett.,* **12,** 155-77.

------ & KNIGHT, J. 1977. Transport phenomena in hydrothermal systems: cooling plutons. *Am. J. Sci.,* **277,** 937-81.

OHLE, E.L. 1980. Some considerations in determining the origin of ore deposits of the Mississippi Valley type. Part II. *Econ. Geol.,* **74,** 1255-85.

OHMOTO, H. 1986. Stable isotope geochemistry of ore deposits. *In:* VALLEY, J.W., TAYLOR, H.P. Jr. & O'NEIL, J.R. (eds) *Stable Isotopes in High Temperature Geological Processes.* Reviews in Mineralogy, Vol.16, Mineralogical Society of America, 491-559.

------ & KERRICK, D. 1977. Devolatilisation equilibria in graphitic systems. *Am. J. Sci.,* **277,** 1013-44.

------ & RYE, R.O. 1979. Isotopes of sulphur and carbon. *In:* BARNES, H.L. (ed) *Geochemistry of hydrothermal ore deposits,* 2nd Edition, John Wiley & Sons, London, 509-67.

PAMPLIN, C.F. 1988. A re-examination of the Tintagel high strain zone and the Padstow facing confrontation, Cornwall. *Ph.D. Thesis, University of Southampton.*

PARRISH, W.R. & PRAUSNITZ, J.M. 1972. Dissociation pressures of gas hydrates formed by gas mixtures. *Ind. Eng. Chem. Process. Des. develop.,* **11,** 26-35.

PHILLIPS, W.J. 1974. The development of vein and rock textures by tensile strain crystallisation. *J. Geol. Soc. London,* **130,** 441-8.

PICHAVANT, M. 1981. An experimental study of the effect of B on a water-saturated haplogranite at 1kb, 500-800°C. Problems of mineralisation associated with acid magmatism, Conference Report, *J. Geol. Soc. London,* **138,** 211-6.

POTTER, R.W. II & BROWN, D.L. 1977. The volumetric properties of aqueous sodium chloride solutions from 0° to 500°C at pressures up to 2000 bars based on a regression of available data in the literature. *U.S. Geol. Surv. Bull.,* **1421-C.**

------, CLYNNE, M.A. & BROWN, D.L. 1978. Freezing point depression of aqueous sodium chloride solutions. *Econ. Geol.,* **73,** 284-5.

POULSON, S.R. & OHMOTO, H. 1989. Devolatilisation equilibria in graphite-pyrite-pyrrhotite bearing pelites with application to magma-pelite interaction. *Contrib. Mineral. Petrol.,* **101,** 418-25.

PRIMMER, T.J. 1985. Discussion of the possible contribution of metamorphic water to the mineralizing fluid of south-west England: preliminary stable isotope evidence. *Proc. Ussher Soc.,* **6,** 224-8.

PRYCE, W. 1778. *Mineralogica Cornubiensis,* Bradford Barton Ltd., Truro, 331 p.

PUCHNER, H.F. & HOLLAND, H.D. 1966. Studies in the Providencia area, Mexico, III. Neutron activation analysis of fluid inclusions from Noche Buena. *Econ. Geol.,* **61,** 1390-8.

RAMBOZ, C., PICHAVANT, M. & WEISBROD, A. 1982. Fluid immiscibility in natural processes: use and misuse of fluid inclusion data. *Chem. Geol.,* **37,** 1-48.

------, SCHNAPPER, D. & DUBESSY, J. 1985. The P-V-T-X-*f* O_2 evolution of H_2O-CO_2-CH_4-bearing fluid in a wolframite vein: reconstruction from fluid inclusion studies. *Geochim. Cosmochim. Acta,* **49,** 205-19.

RAMSAY, J.G. 1974. Development of chevron folds. *Geol. Soc. Amer. Bull.,* **85,** 1741-54.

------ 1980. The crack-seal mechanism of rock deformation. *Nature,* **284,** 135-9.

------ & HUBER, M.I. 1983. *The techniques of modern structural geology*, Volume 1: *Strain analysis*. Academic Press Inc., London.

RAMSAY, J.G. & HUBER, M.I. 1987. *The techniques of modern structural geology*, Volume 2: *Folds and fractures*. Academic Press Inc., London.

RANKAMA, K. & SAHAMA, T.G. 1950. *Geochemistry.* University of Chicago Press, Chicago.

RANKIN, A.H. & ALDERTON, D.H.M. 1983. Fluid inclusion petrography of S.W. England granites and its possibilities in mineral exploration. *Mineral. Deposita,* **18,** 335-47.

------ & ------ 1985. Fluids in granites from S.W. England. *In: High heat production (HHP) granites, hydrothermal circulation and ore genesis.* Inst. Min. Metall. Special Publication, 287-99.

------ & GRAHAM, M.J. 1988. Na, K and Li contents of mineralizing fluids in the Northern Pennine Orefield, England, and their genetic significance. *Trans. Inst. Min. Metall.,* **97,** B99-107.

RATTEY, P.R. 1979. The relationship between deformation and intrusion of the Cornubian batholith in S.W. Cornwall. *J. Camborne School of Mines,* **79,** 60-3.

------ 1980*a*. Structural studies in S.W. Cornwall. *Ph.D. Thesis, Queens' University, Belfast.*

------ 1980*b*. Deformation in S.W. Cornwall. *Proc. Ussher Soc.,* **5,** 39-43.

------ & SANDERSON, D.J. 1982. Patterns of folding in nappes and thrust sheets: examples from the Variscan fold belt of S.W. England. *Tectonophysics,* **88,** 247-67.

------ & ------ 1984. The structure of S.W. Cornwall and its bearing on the emplacement of the Lizard Complex. *J. Geol. Soc. London,* **141,** 87-95.

REDLICH, O. & KWONG, J.N.S. 1949. On the thermodynamics of solutions. *Chem. Rev.,* **44,** 233-44.

REED, M.H. 1982. Calculation of multicomponent chemical equilibria and reaction processes in systems involving minerals, gases and an aqueous phase. *Geochim. Cosmochim. Acta,* **46,** 513-28.

REID, C. 1907. The geology of the country around Mevagissey. *Mem. Geol. Survey, U.K.*, 353 & 354.

RIEDEL, W. 1929. Zur Mechanik geologischer Brucherscheinungen. *Zent. Min. Geol. Pal.,* **1929,** 354-68.

ROEDDER, E. 1958. Technique for the extraction and partial chemical analysis of fluid filled inclusions from minerals. *Econ. Geol.,* **53,** 235-69.

------ 1962. Ancient fluids in crystals. *Scientific American,* **207,** 38-47.

------ 1967. Environment of deposition of stratiform (Mississippi Valley type) ore deposits, from studies of fluid inclusions. *Soc. Econ. Geol. Monograph,* **3,** 349-62.

------ 1976. Fluid inclusion evidence on the genesis of ores in sedimentary and volcanic rocks. *In:* ROLF, K.H. (ed) *Handbook of stratabound and stratiform ore deposits,* Vol.2., Elsevier, Amsterdam, 67-110.

------ 1979. Fluid inclusions as samples of ore fluids. *In:* BARNES, H.L. (ed) *Geochemistry of hydrothermal ore deposits,* 2nd Edition, John Wiley & Sons, London, 684-737.

------ 1984. *Fluid inclusions.* Reviews in Mineralogy, **12,** Mineralogical Society of America, 644 p.

RUAYA, J.R. & SEWARD, T.M. 1986. The stability of chlorozinc (II) complexes in hydrothermal solutions up to 350°C. *Geochim. Cosmochim. Acta,* **50,** 651-61.

RYZHENKO, B.N. & VOLKOV, V.P. 1971. Fugacity coefficients of some gases in a broad range of temperatures and pressures. *Geochem. Internat.,* 468-81.

SADLER, P.M. 1973. An interpretation of new stratigraphic evidence from south Cornwall. *Proc. Ussher Soc.,* **2,** 535-50.

SANDERSON, D.J. 1973. The development of fold axes oblique to the regional trend. *Tectonophysics,* **16,** 55-70.

------ & DEARMAN, W.R. 1973. Structural zones of the Variscan fold belt in S.W. England, their location and development. *J. Geol. Soc. London,* **129,** 527-36.

SAWKINS, F.J. 1966. Preliminary fluid inclusion studies of the mineralisation associated with the Hercynian granites of southwest England. *Trans. Inst. Min. Metall.*, **75**, B109-12.

SCHIFFMAN, P. & LIOU, J.G. 1980. Synthesis and stability relations of Mg-Al pumpellyite, $Ca_4Al_5MgSi_6O_{21}(OH)_7$. *J. Petrol.*, **21**, 441-74.

SEITZ, J.C., PASTERIS, J.D. & WOPENKA, B. 1987. Characterization of CO_2-CH_4-H_2O fluid inclusions by microthermometry and laser Raman microprobe spectroscopy: Inferences for clathrate and fluid equilibria. *Geochim. Cosmochim. Acta,* **51**, 1651-64.

SEWARD, T.M. 1976. The stability of chloride complexes of silver in hydrothermal solutions up to 350°C. *Geochim. Cosmochim. Acta,* **40**, 1329-41.

------ 1984. The formation of lead (II) chloride complexes to 300°C: A spectrophotometric study. *Geochim. Cosmochim. Acta,* **48**, 121-34.

------, (in press). The hydrothermal chemistry of gold. *In:* FOSTER, R.P. (ed) *Gold Metallogeny and Exploration*, Blackie & Son Ltd., Glasgow.

SHEPHERD, T.J., MILLER, M.F., SCRIVENER, R.C. & DARBYSHIRE, D.P.F. 1985. Hydrothermal fluid evolution in relation to mineralisation in S.W. England with special reference to the Dartmoor-Bodmin area. *In: High heat production (HHP) granites, hydrothermal circulation and ore genesis.* Inst. Min. Metall. Special Publication, 345-64.

------, RANKIN, A.H. & ALDERTON, D.H.M. 1985. *A practical guide to fluid inclusion studies.* Blackie, London, 239 p.

------ & SCRIVENER, R.C. 1987. The role of basinal brines in the genesis of polymetallic vein deposits. Kit Hill-Gunnislake district, S.W. England. *Proc. Ussher Soc.,* **6**, 491-7.

SHEPPARD, S.M.F. 1977. The Cornubian batholith, S.W. England: D/H and $^{18}O/^{16}O$ studies of kaolinite and other alteration minerals. *J. Geol. Soc. London,* **133**, 573-91.

------ & CHAREF, A. 1986. Eau organique: caracterisation isotopique et evidence de son role dans le gisement Pb-Zn de Fedj-el-Adoum, Tunisie. *C. R. Acad. Sci Paris,* **302**, Serie II, No.19, 1189-92.

SHOCK, E.L. & HELGESON, H.C. 1987. Calculation of the thermodynamic and transport properties of aqueous species at high temperatures and pressures: Correlation algorithms for ionic species and equation of state predictions to 5 kbar and 1000°C. *Geochim. Cosmochim. Acta,* **52**, 2009-36.

SIBSON, R.H., MOORE, J. McM. & RANKIN, A.H. 1975. Seismic pumping - a hydrothermal fluid transport mechanism. *J. Geol. Soc. London,* **131**, 653-59.

SIMPSON, S. 1951. Some solved and unsolved problems of the stratigraphy of the marine Devonian of Great Britain. *Abh. Senkenb. naturforsch. Ges.,* **485**, 53-66.

SMITH, M.A.P. 1965. Repeated folding between Hayle and Portreath, Cornwall. *Proc. Ussher Soc.,* **1**, 170-1.

SORBY, H.C. 1858. On the microscopical structure of crystals, indicating the origin of minerals and rocks. *Q. J. Geol. Soc. London,* **14**, 453-500.

SOURIRAJAN, S. & KENNEDY, G.C. 1962. The system H_2O-NaCl at elevated temperatures and pressures. *Am. J. Sci.,* **260**, 115-41.

SPRY, A. 1969. *Metamorphic textures.* Pergamon Press, Oxford, 350 p.

STERNER, S.M., HALL, D.L. & BODNAR, R.J. 1988. Synthetic fluid inclusions. V. Solubility relations in the system NaCl-KCl-H_2O under vapour-saturated conditions. *Geochim. Cosmochim. Acta,* **52**, 989-1005.

STONE, M. 1966. Fold structures in the Mylor Beds near Porthleven. *Geol. Mag.,* **103**, 440-60.

------ 1969. Nature and origin of banding in the granitic sheets, Tremearne, Porthleven, Cornwall. *Geol. Mag.,* **106**, 142-58.

------ 1975. Structure and petrology of the Tregonning-Godolphin Granite, Cornwall. *Proc. Geol. Assoc.,* **86**, 155-70.

SVERJENSKY, D.A. 1984. Oil field brines as ore-forming solutions. *Econ. Geol.,* **79**, 23-37.

------ 1987. Calculation of the thermodynamic properties of aqueous species and the solubilities of minerals in supercritical electrolyte solutions. *In:* CARMICHAEL, I.S.E. & EUGSTER, H.P. (eds) *Thermodynamic Modelling of Geological Materials: Minerals, Fluids and Melts.* Reviews in Mineralogy, **17,** Mineralogical Society of America, 177-209.

SWANENBERG, H.E.C. 1980. Fluid inclusions in high grade metamorphic rocks from S.W. Norway. *Geologia Ultralectina (Utrecht),* **25.**

TAKENOUCHI, S. & KENNEDY, G.C. 1965. The solubility of carbon dioxide in NaCl solutions at high temperatures and pressures. *Am. J. Sci.,* **263,** 445-54.

TANGER, J.C. & HELGESON, H.C. 1987. Calculation of the thermodynamic and transport properties of aqueous species at high temperatures and pressures: Revised equation of state for the standard partial molal properties of ions and electrolytes. *Am. J. Sci.,* **288,** 19-98.

TAYLOR, H.P., Jr. 1974. The application of oxygen and hydrogen isotope studies to problems of hydrothermal alteration and ore deposition. *Econ. Geol.,* **69,** 843-83.

------ 1977. Water/rock interaction and the origin of H_2O in granitic batholiths. *J. Geol. Soc. London,* **133,** 509-58.

------, FRECHEN, J. & DEGENS, E.T. 1967. Oxygen and carbon isotope studies of carbonatites from the Laacher See District, West Germany, and the Alno District, Sweden. *Geochim. Cosmochim. Acta,* **31,** 407-30.

THOMPSON, M., RANKIN, A.H., WALTON, S.J., HALLS, C. & FOO, B.N. 1980. The analysis of fluid inclusion decrepitate by inductively-coupled plasma atomic emission spectroscopy: an exploratory study. *Chem. Geol.* **30,** 121-33.

TOURAY, J.C. 1976. Activation analysis for liquid inclusion studies: a brief review. *Bull. Soc. Fr. Mineral. Cristall.,* **99,** 162-4.

TOURET, J. 1981. Fluid inclusions in high grade metamorphic rocks. *In:* HOLLISTER, L.S. & CRAWFORD, M.L. (eds) *A short course in fluid inclusions.* Mineralogical Association of Canada Short Course Handbook, **6,** 182-208.

TRUESDELL, A.H. 1984. Chemical geothermometers for geothermal exploration. *In:* HENLEY, R.W., TRUESDELL, A.H. & BARTON, P.B. (eds) *Reviews in Economic Geology,* Vol.1, 31-44.

TUREKIAN, K.K. & WEDEPOHL K.H. 1961. Distribution of the elements in some major units of the earth's crust. *Bull. Geol. Soc. Am.,* **72,** 175-91.

TURNER, R.E., TAYLOR, R.G., GOODE, A.J.J. & OWENS, B. 1979. Palynological evidence for the age of the Mylor Slates, Mount Wellington, Cornwall. *Proc. Ussher Soc.,* **4,** 274-83.

TURNER, R.G. 1969. The influence of granite emplacement on structure in southwest England. *Ph.D. thesis, University of Newcastle-upon-Tyne.*

VALLEY, J.W. 1986. Fluid-absent metamorphism in the Adirondacks. *In:* ASHWAL, L.D. (ed) *Early Crustal Genesis.* Lunar and Planetary Inst. Tech. Rep., **86-04,** 107-11.

VAN DER WAALS, J.H. & PLATTEEUW, J.C. 1959. Clathrate solutions. *In:* PRIGOGINE, I. (ed) *Advances in Chemical Physics,* Wiley Interscience, New York, 1-57.

VEIZER, J., HOLSER, W.T. & WILGUS, C.K. 1980. Correlation of $^{13}C/^{12}C$ and $^{34}S/^{32}S$ secular variation. *Geochim. Cosmochim. Acta,* **44,** 579-87.

VIDALE, R. 1983. Pore solution compositions in a pelitic system at high temperatures, pressures, and salinities. *Am. J. Sci.,* **283-A,** 298-313.

WALKER 1978. Deep water sandstone facies and ancient submarine fans: models for exploration for stratigraphic traps. *Bull. American Assoc. Petrol. Geol.,* **62,** 932-66.

WALTHER, J.V. & ORVILLE, P.M. 1982. Rates of metamorphism and volatile production and transport in regional metamorphism. *Contrib. Mineral. Petrol.,* **79,** 252-7.

------ & WOOD, B.J. (eds.) 1986. *Fluid-rock interactions during metamorphism.* Advances in Physical Geochemistry, Vol. 5, Springer-Verlag, New York, 218 p.

WHITE, D.E. 1957. Magmatic, connate and metamorphic waters. *Geol. Soc. Am. Bull.,* **68,** 1659-82.

------ 1974. Diverse origins of hydrothermal ore fluids. *Econ. Geol.,* **69,** 954-73.

WHITE, S.H. 1977. Geological significance of recovery and recrystallisation. *Tectonophysics,* **739,** 143-70.

------ 1988. Crystal plastic processes: deformation mechanisms, microstructures and textures. *Abstr., Geol. Soc. Review Seminar on deformation mechanisms, University of Leeds, November 1988.*

WILKINSON, J.J. (in press). The role of metamorphic fluids in the evolution of the Cornubian orefield: Fluid inclusion evidence from south Cornwall.

WILKINSON, J.J. & KNIGHT, R.W. 1989. Palynological evidence from the Porthleven area, south Cornwall: implications for Devonian stratigraphy and Hercynian tectonic evolution. *J. Geol. Soc. London,* **146,** 739-742.

WILLIS-RICHARDS, J. & JACKSON, N.J. (in press). Evolution of the Cornubian orefield, S.W. England. Part I: Batholith modelling and ore distribution. *Econ. Geol.* Special publication.

WILSON, A.C. & TAYLOR, R.T. 1976. Stratigraphy and sedimentation in W. Cornwall. *Trans. Royal Geol. Soc. Cornwall,* **10,** 246-59.

WINTSCH, R.P. 1985. The possible effects of deformation on chemical processes in metamorphic fault zones. *In:* THOMPSON, A.B. & RUBIE, D.C. (ed) *Metamorphic Reactions: Kinetics, Textures and Deformation,* Advances in Physical Geochemistry, Vol.4, Springer-Verlag, New York, 250-68.

WLOTZKA, F. 1972. Nitrogen. *In:* WEDEPOHL, K.H., (ed) *Handbook of Geochemistry*, Vol.II, Springer-Verlag, Berlin, Chap. 7B-O.

WOLERY, T.J. 1983. EQ3NR: A computer program for geochemical aqueous speciation-solubility calculations, user's guide and documentation. UCRL-53414. Lawrence Livermore Lab., Univ. of California, 12 p.

WOOD, B.J. & WALTHER, J.V. 1986. Fluid flow during metamorphism and its implications for fluid-rock ratios. *In:* WALTHER, J.V. & WOOD, B.J. (eds.) *Fluid-rock interactions during metamorphism*. Advances in Physical Geochemistry, Vol. 5, Springer-Verlag, New York, 89-108.

WOODCOCK, N.H. & UNDERHILL, J.R. 1987. Emplacement-related fault patterns around the Northern Granite, Arran, Scotland. *Geol. Soc. Amer. Bull.,* **98,** 515-27.

YARDLEY, B.W.D. 1986. Fluid migration and veining in the Connemara Schists, Ireland. *In:* WALTHER, J.V. & WOOD, B.J. (eds.) *Fluid-rock interactions during metamorphism.* Advances in Physical Geochemistry, Vol. 5, Springer-Verlag, New York, 109-131.

YARDLEY, B.W.D., BANKS, D.A. & CAMPBELL, L.S. 1989. Chemical evolution of ore fluids from Cornwall, U.K. (Abstract) *ECROFI X, Imperial College, London.*

ZHANG, Y-G. & FRANTZ, J.D. 1987. Determination of the homogenisation temperatures and densities of supercritical fluids in the system NaCl-KCl-$CaCl_2$-H_2O using synthetic fluid inclusions. *Chem Geol.,* **64,** 335-50.

ZWART, H.J. 1967. The duality of orogenic belts. *Geol. Mijnb.,* **46,** 283-98.

APPENDICES

APPENDIX A

SAMPLE NUMBERING AND APPLICATIONS

A1: SAMPLE NUMBERING SCHEME

The simple sample numbering scheme used in this study allows immediate identification of the part of the study section from which a sample was taken. Where sample numbers are referred to in the text, they are always italicised. A full list of the vein samples taken and the techniques which have been applied to them is presented in Appendix A2.

The sample numbering scheme is best ilustrated by an example:

e.g. J93TP

J - personal sample identity letter;
93 - sample locality number, refers to locality description in notebook;
TP - sample zone code (in this example, Tregear Point).

The sampling zones and their corresponding code letters are shown in Figure 1.4. To distinguish samples taken from the same locality, a lower or upper case subscript letter was added to the sample number.

The first ten samples collected (23-24/9/86) were numbered according to a different scheme: *JW001-JW010* inclusive. Samples *JW001-3* came from the *JR* sample zone, *JW004-8* from the *TC* sample zone and *JW009-010* from the *PS* zone. Several samples taken specifically for XRD wallrock alteration studies are prefixed by *D2, D3* or *D4*.

The maps shown on the following three pages are reproductions of Figure 1.4 showing the localities from where the main samples used for detailed fluid inclusion studies in this work were taken.

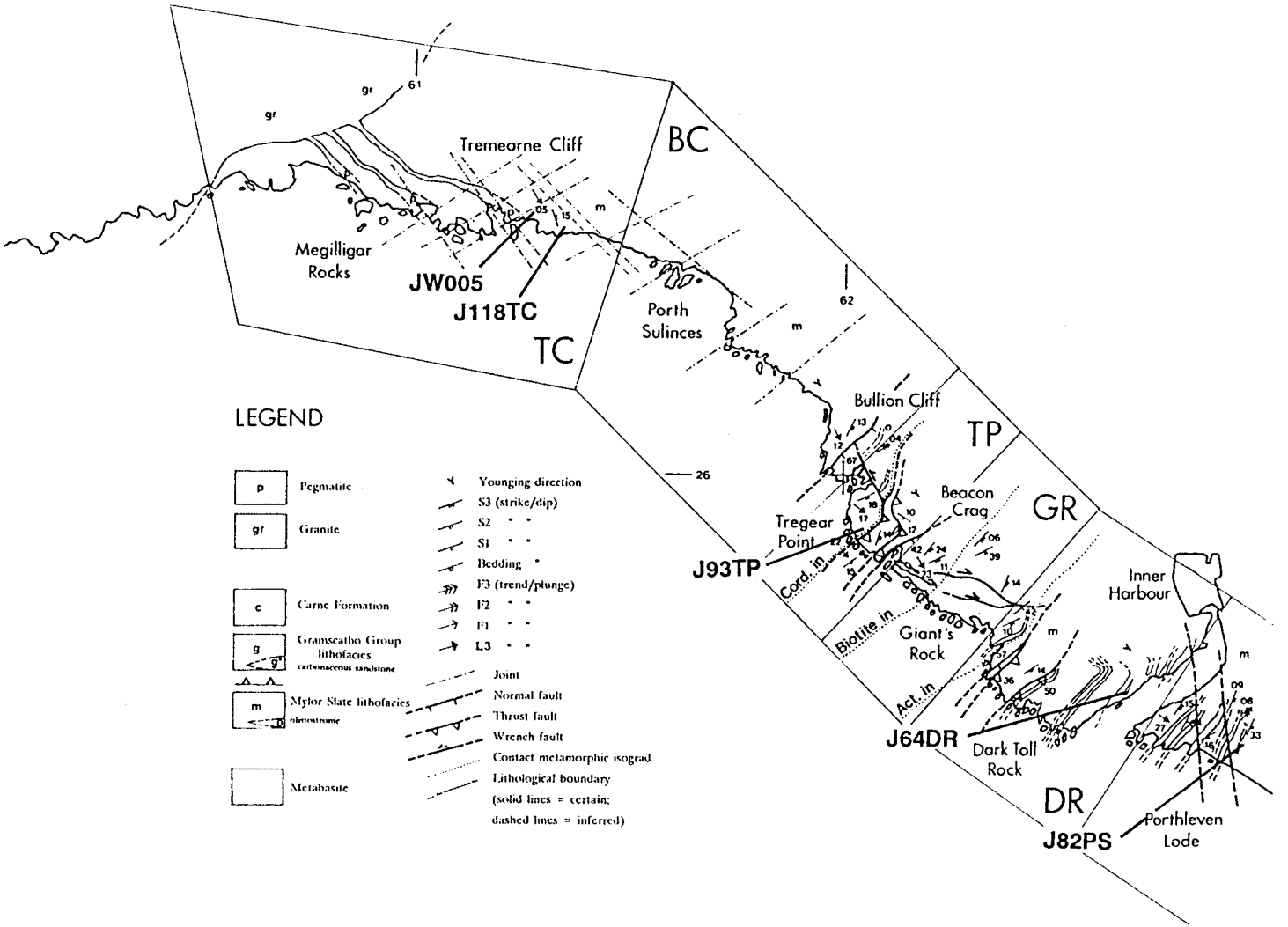
Tremearne Cliff
Megilligor Rocks
JW005
J118TC
TC
BC
Porth Sulinces
Bullion Cliff
TP
Beacon Crag
GR
Tregear Point
J93TP
Cord. in
Biotite in
Act. in
Giant's Rock
Inner Harbour
J64DR
Dark Toll Rock
DR
J82PS
Porthleven Lode
LEGEND
Pegmatite
Granite
Younging direction
S3 (strike/dip)
S2
S1
Bedding
F3 (trend/plunge)
F2
F1
L3
Carne Formation
Gramscatho Group lithofacies
carbonaceous sandstone
Mylor Slate lithofacies
Joint
Normal fault
Thrust fault
Wrench fault
Contact metamorphic isograd
Lithological boundary
(solid lines = certain;
dashed lines = inferred)
Metabasite

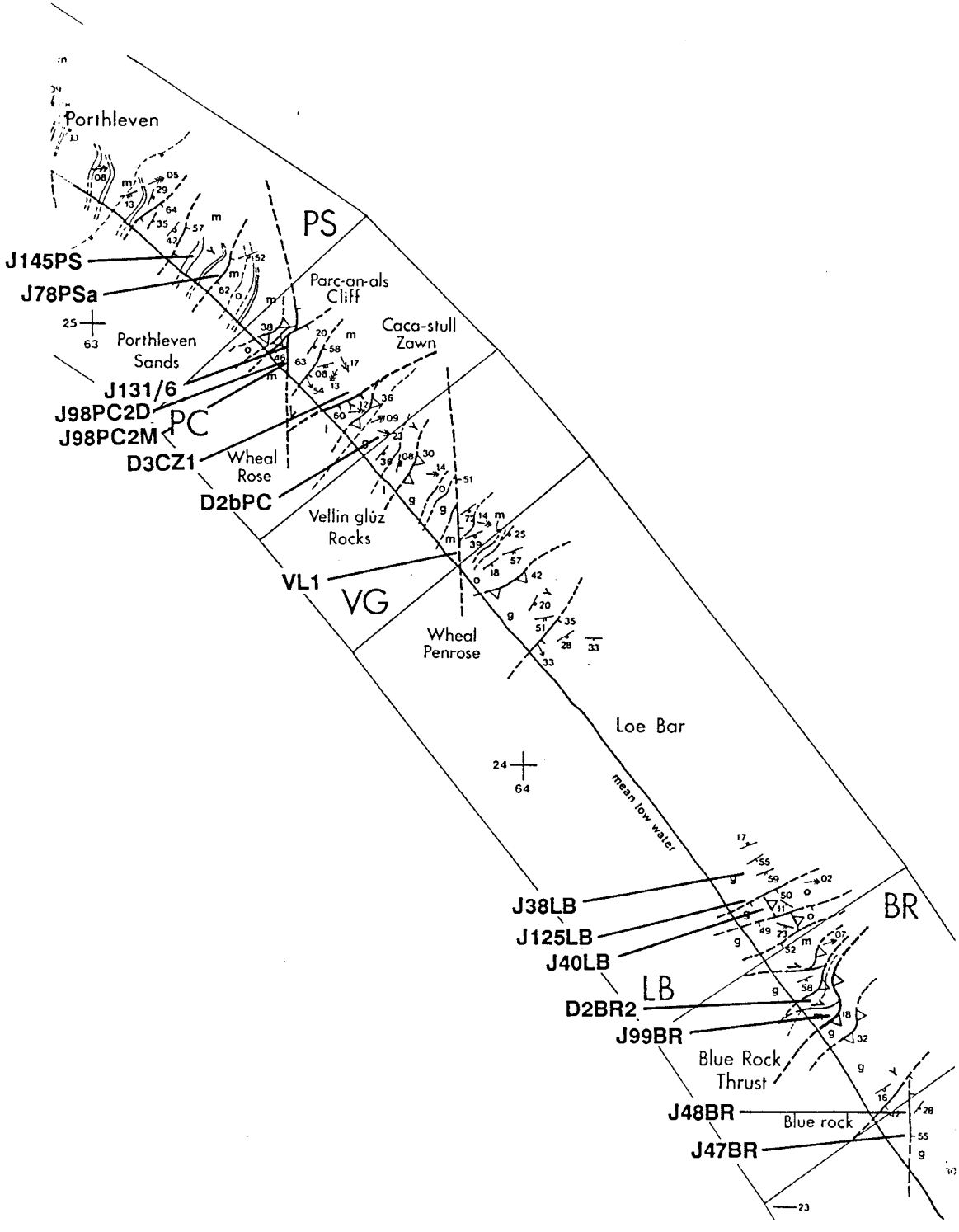
Porthleven
PS
J145PS
J78PSa
Parc-an-als Cliff
Caca-stull Zawn
Porthleven Sands
J131/6
J98PC2D
PC
J98PC2M
D3CZ1
Wheal Rose
D2bPC
Vellin glûz Rocks
VL1
VG
Wheal Penrose
Loe Bar
mean low water
J38LB
J125LB
J40LB
LB
D2BR2
J99BR
BR
Blue Rock Thrust
J48BR
Blue rock
J47BR

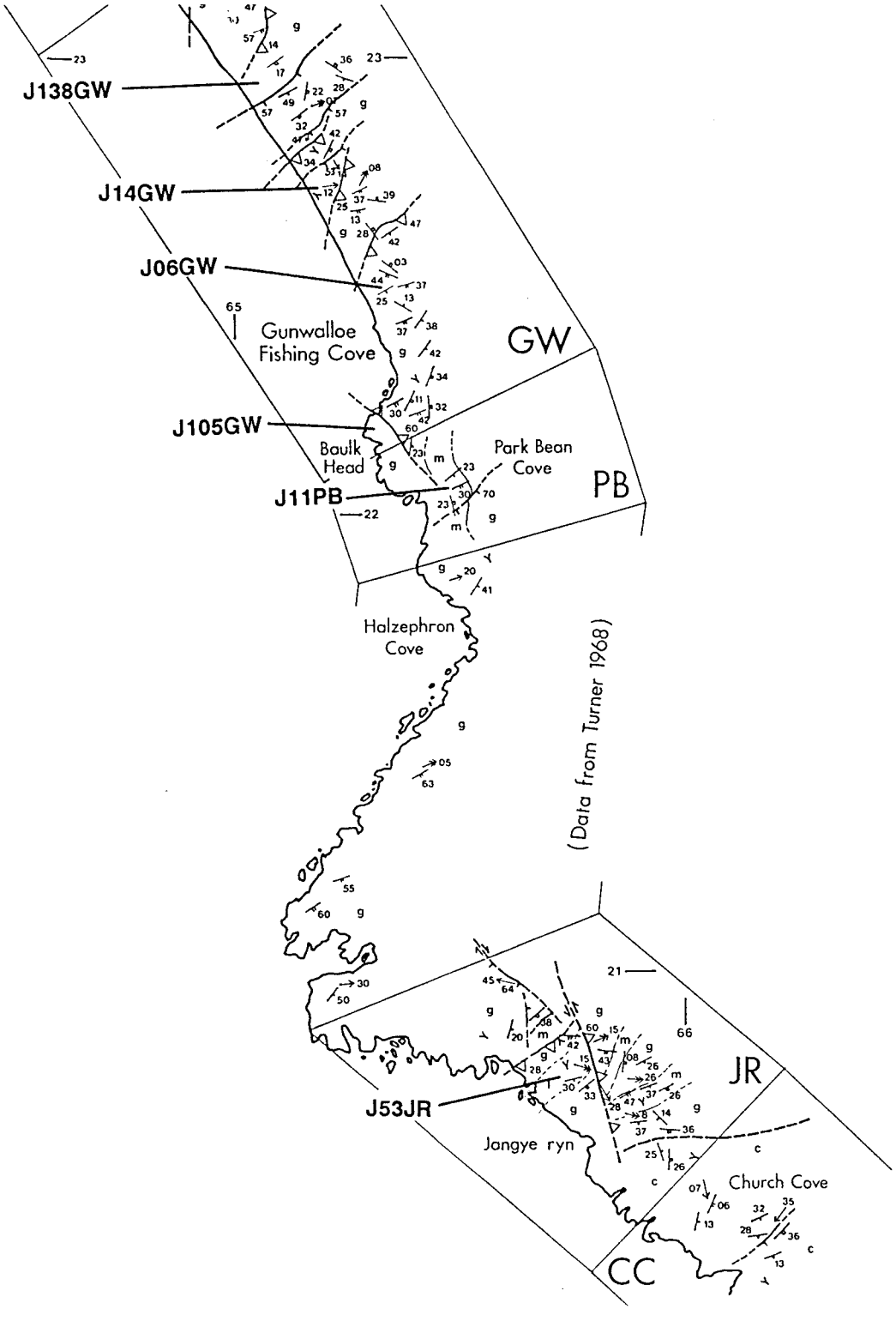
J138GW
J14GW
J06GW
J105GW
J11PB
J53JR
Gunwalloe
Fishing Cove
Baulk
Head
Park Bean
Cove
Halzephron
Cove
Jangye ryn
Church Cove
GW
PB
JR
CC
(Data from Turner 1968)

A2: VEIN SAMPLE LIST AND TECHNIQUES APPLIED

SAMPLE	TYPE	F.I.	D-ICP	NAA	V.A.	S.I.	XRD	PET.
J25CC	?							*
JW001	V1F							*
JW002	V1F							*
JW003	V1F							*
J27JR	?							*
J27JRa	V1G							*
J28JR	V1G							*
J30JR	V2F							*
J33JRa	-							*
J33JRb	V4N							*
J34JR	V2T							*
J35JR	V2F							*
J53JR	V1F	*	*		*	*		*
J11PB	V1B	*	*	*	*	*		*
J11PBa	?							*
J12PBa	-							*
J12PBb	-							*
J139PB	-							*
J01GW	-							*
J02GW	V1G							*
J04GW	V1G							*
J05GW	?							*
J06GW	V1G	*	*	*				*
J08GW	V2T							*
J14GW	-							*
J16GW	-							*
J16GWa	V1T							*
J16GWb	V2F							*
J17GW	V2F							*
J18GW	-							*
J19GW	-							*
J19GWa	V4N	*						*
J21GW	V4N							*
J23GW	V2E							*
J24GW	V2F							*
J105GW	V1T	*	*	*		*		*
J133GW	V2T							*
J135GW	V2T							*
J136GW	?							*
J137GW	V2E							*
J138GW	V1B					*		*
J44BR	-							*
J47BR	V3S(1)			*				*
J48BR	V2T	*	*	*	*	*		*
J50BR	V2T	*						*
J99BR	V2T	*	*	*	*	*		*
D2BR	V2T	*	*	*	*	*	*	*

SAMPLE	TYPE	F.I.	D-ICP	NAA	V.A.	S.I.	XRD	PET.
J36LB	?							*
J38LB	V4N	*	*		*	*	*	*
J38LBa	V2E	*						*
J40LB	V2E	*	*	*				*
J41LB	V4N							*
J41LBa	-							*
J41LBb	-							*
J42LB	V1T							*
J42LBa	V4N							*
J125LB	V2F	*	*	*	*	*		*
J157LB	V3S(1)	*						*
J75VG	V3S(1)							*
J153VG	V4W						*	*
VL1	V4W	*	*	*		*		*
J68PC	?							*
J70PC	V3S(1)	*						*
J72PC	?							*
J72PCa	V2E							*
J73PC	-							*
J74PC	V4N							*
J98PC	V2T/V4N							*
J98PC2M	V3S(1)	*	*	*			*	*
J98PC2D	V4W	*	*	*				*
J131/1	V4W	*						*
J131/2	V4W	*						*
J131/3	V4W							*
J131/4	V4W	*						*
J131/5	V4W							*
J131/6	V4W	*	*	*	*	*		*
D2aPC	V2E						*	*
D2bPC	V2E	*	*	*		*	*	*
D3CZ1	V3C	*	*	*	*	*	*	*
JW009	V3G(1)							*
J57PS	-							*
J58PS	-	*						*
J58PSa	V3S(1)							*
J58PSb	V4W							*
J60PS	V3G(1)	*						*
J61PS	-							*
J61PSa	-							*
J63PS	-	*						*
J78PS	V4N							*
J78PSa	V4N	*	*	*	*	*		*
J81PS	V3G(2)							*
J82PS	V3G(1)	*	*	*	*	*		*
J121PS	V3G(1)							*
J122PS	V3G(2)							*
J142PS	V4W							*
J142PSa	V4W							*
J142PSb	V4W	*					*	*
J143PS	V3G(1)							*
J145PS	V3G(2)	*			*	*		*
D4PS1	V3G(1)	*						*
D4PS2	V3G(1)	*					*	*

SAMPLE	TYPE	F.I.	D-ICP	NAA	V.A.	S.I.	XRD	PET.
J64DR	V3G(1)	*	*	*	*	*		*
J65DR	V3S(1)							*
J90GR	V3S(1)							*
J126GRa	V3G(1)							*
J126GRb	V3S(1)							*
J127GR	V3C							*
D4GR1	V3S(2)	*						*
D4GR2	V3S(2)	*					*	*
J93TP	V3G(1)	*	*		*	*	*	*
JW004	V3S	*						*
JW005	V4J1	*	*	*				*
JW006	V4P	*						*
JW007	V4P/V4J2							*
JW008	V4P	*						*
J118TC	V4J2	*			*		*	*

Column heading abbreviations have the following meanings:

F.I. - Fluid inclusion study
D-ICP - Decrepitation-linked ICP analysis
NAA - Neutron activation analysis
V.A. - Bulk volatile analysis
S.I. - Stable isotope analysis
XRD - X-Ray diffraction study
PET. - Petrographic study (transmitted/reflected light)

Symbols used in the "TYPE" column have the following meanings:

? vein type uncertain
- some constraint on relative vein age, absolute age uncertain
/ more than one vein type in sample
(n) V3 vein set type (see 2.2.9-10)

APPENDIX B

SAMPLE PREPARATION TECHNIQUES

B1: PREPARATION OF QUARTZ CHIP SAMPLES

Scrupulously clean, graded quartz chip samples were prepared for bulk analytical techniques. The preparation method used is summarised below:

1. Approximately 30 g of vein quartz was crushed in a fly-press to a grain size of <5mm;

2. Crushed sample was sieved in brass mesh sieves to obtain 0.5-2.0 mm size fraction;

3. Several grammes of chips were hand-picked under a binocular microscope to remove microcrystalline grains and contaminant phases;

4. Quartz chips obtained were boiled under reflux in 10% (vol.) nitric acid for 24 hours, changing acid twice, to remove surface contamination (10% HCl was used for volatile analysis samples to remove carbonate and avoid nitrogen contamination);

5. Clean chips were boiled for 1 hour in deionised, 5x distilled water, changing water twice, to remove acid contamination;

6. Scrupulously clean chips were rinsed 5 times in deionised, 5x distilled water and air dried in an oven at 98°C.

6. Samples were stored in inert polyethylene vials prior to analysis.

7. 0.25 gramme aliquots for volatile and stable isotope analyses were hand-picked from clean samples under a binocular microscope to select single, unfractured, grains without carbonate dissolution pits.

B2: PREPARATION OF DOUBLY-POLISHED WAFERS FOR THERMOMETRIC ANALYSIS

The procedure used to prepare doubly-polished quartz wafers for thermometric analysis is similar to that described by Shepherd *et al.* (1985), section 2.5, pp.26-33. The procedure is briefly described below:

1. A slice of approximate dimensions 15x15x3 mm is cut from a vein quartz sample using a standard rock saw;

2. One surface of slice is hand ground on a glass plate using silicon carbide grit, down to 800 grade (F scale);

3. Sample is mounted in a cylindrical resin block (as used for reflected light microscopy), ground side down;

4. Ground surface of sample is polished on an automatic rotary lapping machine, using a napped polishing cloth and α-Al_2O_3 polishing powder;

5. Excess material is trimmed off using a fine diamond saw and unpolished side is lapped down to desired wafer thickness (100-200μm in the present study);

6. Second surface of wafer is polished as in step 4;

7. Wafer is removed from remaining resin and cleaned by soaking in petroleum spirit and wiping gently with a cotton bud.

APPENDIX C

CALIBRATION METHODS

C1: CALIBRATION OF THE LINKAM TH600 AND THM600 HEATING-FREEZING STAGES

Microthermometric analysis of fluid inclusions was carried out using the Linkam TH600 and THM600 heating-freezing stages. Cross-sections of the internal arrangement of the TH600 stage is shown in Fig. C1.1. The sample is heated by a resistance heater mounted in the silver block. Cooling is carried out by passing oxygen-free nitrogen gas through a coil immersed in liquid nitrogen and then through the silver block. A range of heating rates may be obtained via the electronic control unit which, at sub-ambient temperatures, balances the power supplied to the heater against the cooling effect of the gas.

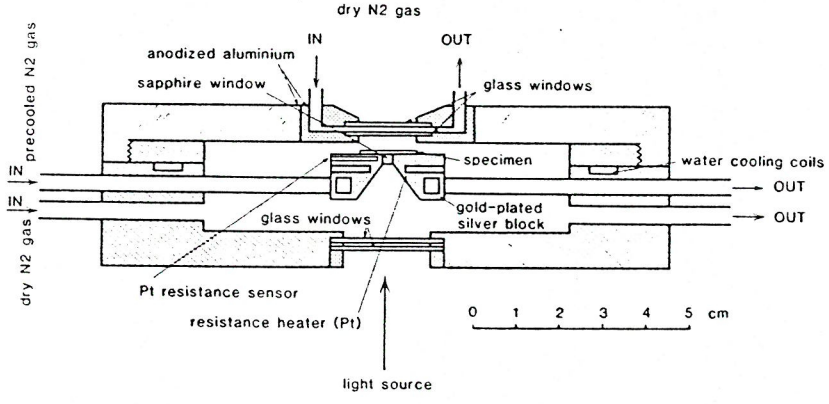

Figure C1.1 Cross-section of TH600 heating-freezing stage (from Shepherd *et al.* 1985).

Temperatures are measured by a platinum resistance sensor mounted in the thermal block below the sample. As a result, there is a temperature difference between the sensor and the inclusion being measured (Fig. C1.1). Furthermore, this temperature difference increases with departure from ambient temperature and also with gradual aging of the temperature sensor. Thus, for accurate measurement of temperatures at which phase changes occur in an inclusion, the stage has to be calibrated to correct for the temperature difference described above.

Calibration is carried out by running a series of high purity chemicals with well-defined melting points in such a configuration so as to approach, as closely as possible, the thermal conditions present in a doubly-polished fluid inclusion wafer. The standards define a true temperature curve to which all subsequent measurements on inclusions are referred.

There are two other sources of error in temperature measurements made on inclusions in a sample which is obviously of finite size and thickness. Firstly, temperature gradients exist across the sapphire window on which the sample sits; thus there will be lateral variations in measured temperatures across the sample. Secondly, thermal gradients exist through the thickness of the sample with the base of the wafer always at a temperature further from ambient than the top.

In the first case, careful calibration at different points on the sapphire window indicate that such errors are small, approaching 4°C across the width of the window at 400°C (Linkam TH600; Shepherd *et al.* 1985), and may be discounted during thermometric analysis. In the second case, measurements on the same inclusion at two different vertical positions (carried out by measuring a phase change in an inclusion, turning the wafer over and re-measuring the same inclusion) indicate that such thermal gradients are negligible at all temperatures and no corrections are required.

Two methods of calibration commonly employed, involving placing minute standard samples (solids or liquids) either between glass cover slips or in glass microcapillary (melting point) tubes. In an exploratory study of these methods it was found that the circular section of the fine-bore tubing resulted in poor thermal contact with the heating block and significantly different melting temperatures were obtained using this method, compared with samples sandwiched between glass cover slips. The latter method was used in the calibration procedure since it more closely approaches the configuration for a sample and its inclusions.

For crystalline solids, a small sample of the material was crushed to a fine powder in a clean agate mortar and a tiny amount placed between two glass cover slips which had been cleaned with alcohol. For organic liquids, a minute drop was placed between cover slips using a 20μl pipette tip (the amount of liquid used would be much less than this). The standard was then placed centrally over the sapphire window (TH600) or in the sample holder (THM600) and the melting point of the substance was recorded, using heating rates not exceeding 0.5°C min^{-1} close to the melting temperature. Replicate measurements were made, each time on a fresh sample, and the average melting temperature and sigma error were determined. These values were plotted on a T/▲T diagram, where ▲T represents the difference between the true melting point of the standard substance and the temperature recorded by the visual display on the control unit.

During the course of the study, three different calibrations were used; two for the "old" TH600 heating-freezing stage and one for the "new" THM600 stage, acquired by the Department of Geology in December, 1988. The three calibration curves are shown in Figure C1.2 below. Further details of calibration techniques may be found in Shepherd *et al.* (1985), Roedder (1984) and MacDonald & Spooner (1981).

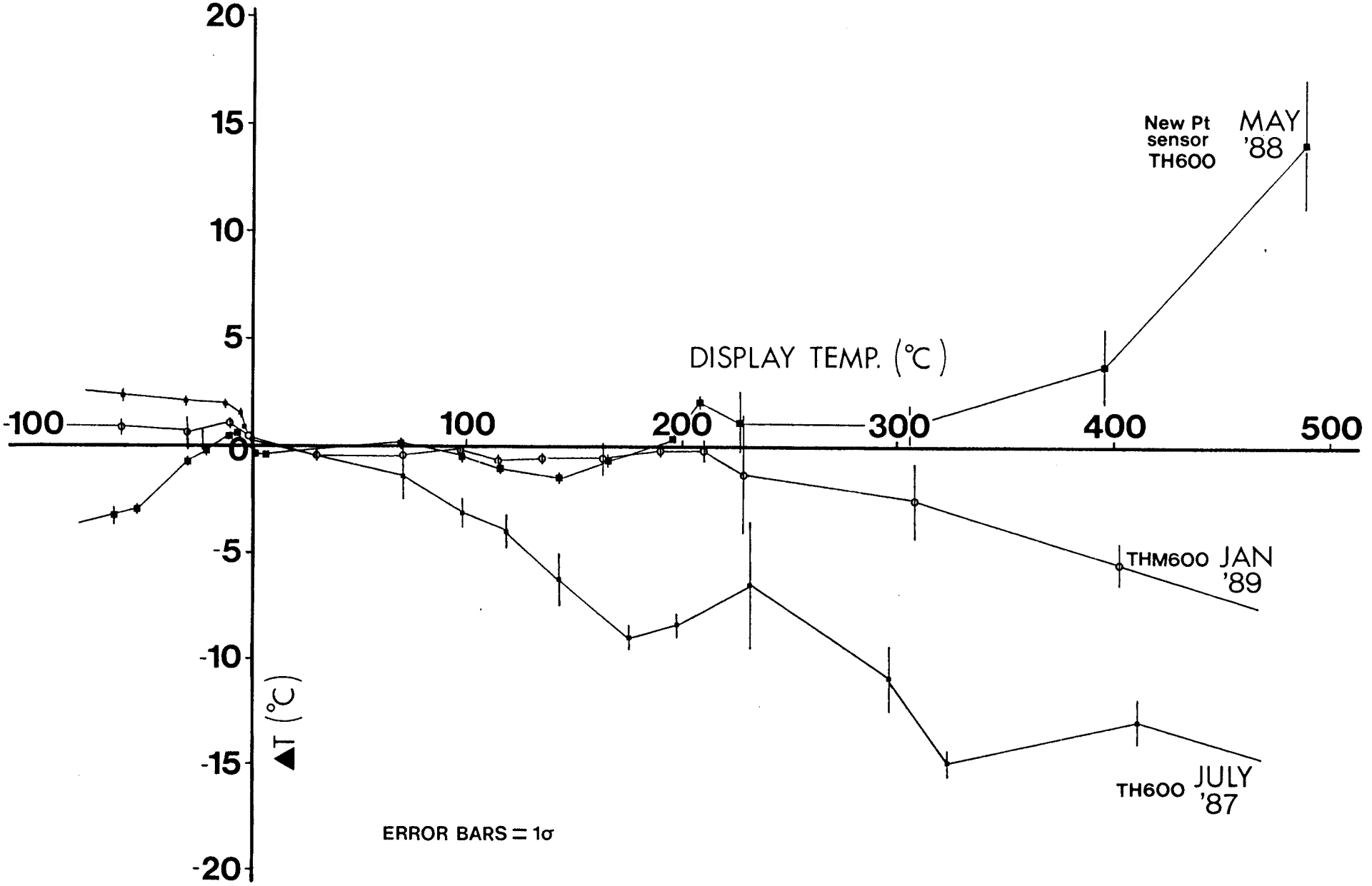

Figure C1.2 Calibration curves used in the present study for Linkam TH600 and THM600 heating-freezing stages. $\blacktriangle T = T_{true} - T_{obs}$.

C2: D-ICP ANALYSIS: CALIBRATION METHOD

Raw data obtained from the ICP spectrometer is in the form of a current (mA) for each spectral line, automatically corrected for peak interferences (see 3.1.1). Calibration of the data is normally carried out by computer to produce "equivalent ppm" values which may be directly ratioed to sodium to give the Na/cation weight ratios reported in this study (Table 3.14). Below, an example calibration is set out to illustrate the procedure.

1. Subtract spectrometer current for element from background. In Table C.1 below, the background for each element is taken as the average of the blank measured before and after the sample in question. In the automatic procedure, the entire series of blank data are fitted to a straight line with which each sample current is compared.

2. Subtract aqueous blank from aqueous standard (AQUA2) for each element. The average of the two "AQUA BLK" measurements is used.

3. Divide current for aqueous standard by concentration of element in standard solution (*e.g.* 100 ppm for Na and Ca) to give 1 "equivalent ppm" for each element in terms of mA.

4. Divide background-corrected currents for samples by spectrometer current equivalent to 1 ppm for each element to yield "equivalent ppm" values for each element.

5. Divide "equivalent ppm" values for Na by "equivalent ppm" values for other elements to yield Na/element weight ratios in decrepitate.

Table C.1 Spectrometer currents and example calibration of D-ICP data

	Na	Na-b.g.	Na "ppm"	Ca	Ca-b.g.	Ca "ppm"	Na/Ca(wt)
BLANK1	49.78			4.580			
BLANK2	49.62			4.610			
BLANK3	46.89			4.480			
BLANK4	45.87			4.430			
BLANK5	45.47			4.410			
J82PS	934.8	889.4	160.1	15.97	11.55	11.70	13.7
J82PS	767.6	722.2	130.0	14.70	10.28	10.42	12.5
J98PC2D	396.8	351.4	63.25	20.22	15.80	16.00	3.95
J98PC2D	421.5	376.1	67.69	23.25	18.83	19.08	3.55
JW005	1042	996.6	179.4	15.94	11.52	11.67	15.4
JW005	1228	1183	212.9	17.10	12.68	12.85	16.6
BLANK6	45.39			4.44			
J40LB	57.85	14.55	2.62	4.42*	0.11	0.111	23.6#
J40LB	55.90	12.60	2.27	4.35*	0.04	0.041	55.4#
J06GW	107.3	64.00	11.52	4.44*	0.13	0.132	87.3#
J06GW	95.46	52.16	9.39	4.35*	770.04	0.041	229.0#
J98PC2M	255.1	211.8	38.12	10.85	6.54	6.63	5.75
J98PC2M	177.6	134.3	24.17	8.42	4.11	4.16	5.81
BLANK7	41.21			4.19			
J48BR	165.9	124.8	22.46	6.43	2.24	2.27	9.89
J48BR	167.7	126.6	22.79	5.38	1.19	1.21	18.8
BLANK8	41.01			4.19			
AV+2σ	52.24			4.73			
AQUA BLK	3.437			0.003			
AQUA2	559.1	555.6		98.68	98.70		
AQUA BLK	3.527			-0.033			
		1 "ppm"= 5.556mA			1 "ppm"= 0.987mA		

Spectrometer currents in mA; AQUA BLK=distilled water blank; AQUA2=standard solution (100ppm Na, 100ppm Ca); **b.g.**=background for element (defined by blank measurements); AV+2σ=detection limit for element (defined by blank measurements); *element current below detection limit; #ratio invalid due to low spectrometer current for Ca.

C3: NEUTRON ACTIVATION ANALYSIS: CALIBRATION METHOD

The gamma activity of an irradiated sample is measured using a shielded gamma detector. The raw data are output to a Canberra APOGEE system which produces a datafile containing a list of the energies of spectral peaks and the integrated number of counts for each. The energy of each spectral line is unique to a particular gamma emitter, thus the "activated species" of an element responsible for each line may be determined. The activated species usually corresponds with the unexcited species of the same element; however, some activated species formed during neutron bombardment are the result of elemental transitions. In such cases, the number of counts (peak area) for a spectral line for an element does not correspond with the amount of that element in the sample, it relates to the amount of the parent species in the sample.

Once the spectral peaks have been assigned to elements present in the sample, the step from "peak area" or "counts" to a concentration value may be made. Different activated species have different emission intensities so that the simplest method of calibration is by comparing the peak area of an element in the sample with that of the same element in a standard of known composition. In theory, it is possible to calculate the concentration directly, because the emission properties of most elements are known. However, the former, comparative method is routinely employed because of its superior accuracy. As a result of this approach, a number of corrections have to be made to take into account differences between the conditions experienced by the samples and the standards during and subsequent to irradiation. These differences include:

1. Differences between sample weights and standards;

2. Flux variations in the sample tubes during irradiation;

3. Different decay times between irradiation and counting of each sample;

The differences between sample weights and standard weights are corrected for by normalising peak areas to unit sample weight (usually one gramme). Flux variations in the sample tube are monitored during irradiation by small iron foil discs placed between the polyethylene sample capsules (Fig. C3.1). The activated iron discs are counted prior to sample counting and a neutron flux profile through the sample tube is constructed from the iron foils (Fig. C3.1). The activity induced in a sample is directly proportional to the flux experienced (over the irradiation times involved) so that flux variations may be removed by normalising all samples and standards to a reference flux level (see Fig. C3.1).

Decay times are corrected for by recalculating all peak intensities (for samples and standards) back to the time of counting of the first sample. This is done using the exponential decay equation:

$$N = N^{\circ} e^{-\lambda t} \qquad \text{...(C3.1)}$$

where N is the peak area (number of counts) for each element at the time of counting of the sample, N° is the corrected peak area at the reference time (when the first sample was counted), λ is the

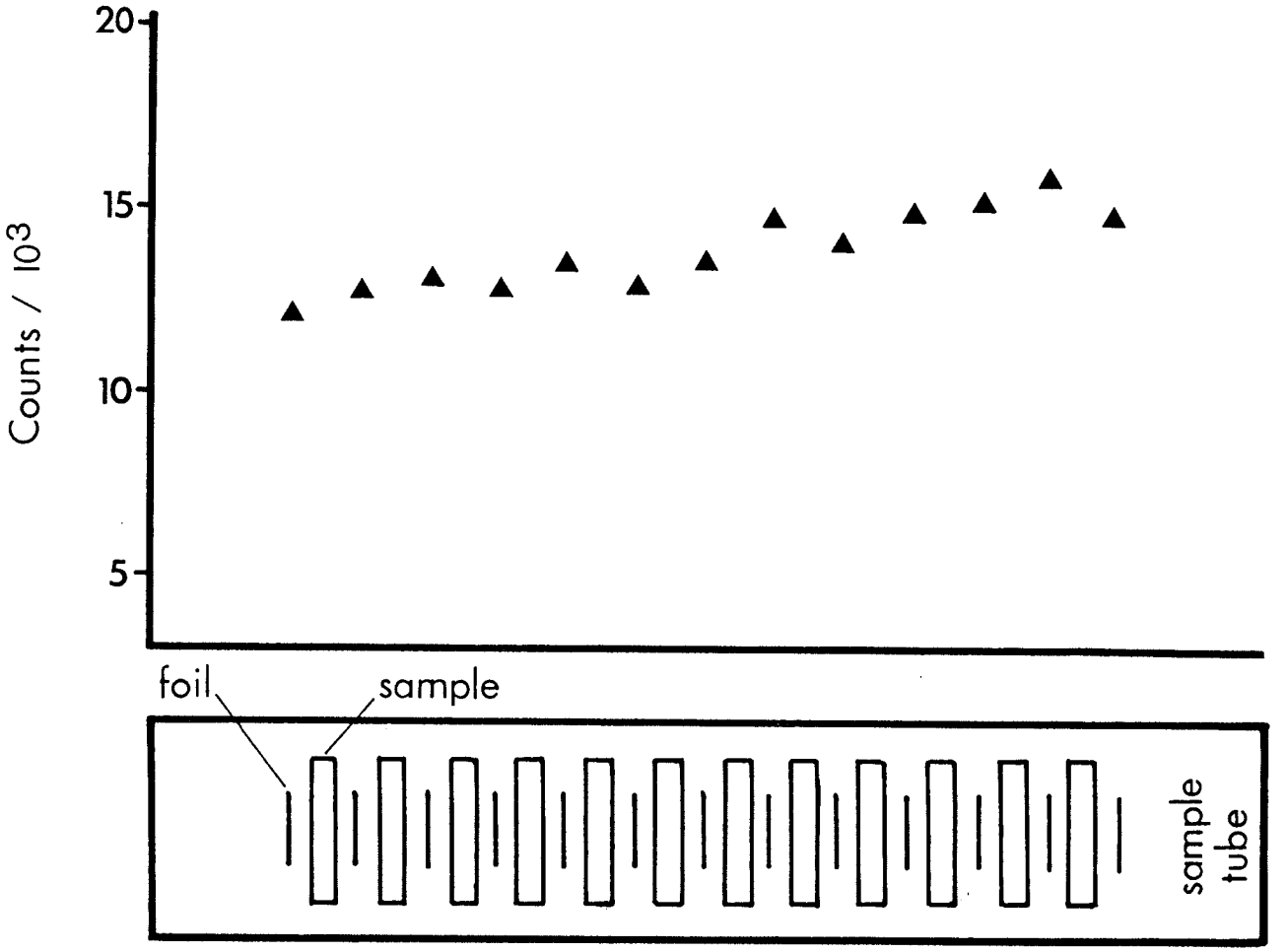

Figure C3.1 Diagram illustrating arrangement of sample capsules and iron foils in tube and flux variation measured for one analysis (Feb 1988).

decay constant of the activated species (in s^{-1}) and t is the time (in seconds) elapsed between the reference time and the count time.

The procedures outlined above are time-consuming if performed manually. In order to speed-up data processing, a FORTRAN 77 computer program was written in collaboration with Dr Ian Croudace of the Department of Geology, University of Southampton. This program, which is listed in Appendix C4, automatically applies the corrections described above to the sample batch files created by the Canberra APOGEE system. This program allows rapid generation of elemental concentration data down to the fractions of parts-per-billion level.

C4: NEUTRON ACTIVATION ANALYSIS: CALIBRATION SOFTWARE

```
      PROGRAM NAASUB
C.....
C
C
C A Program written by Jamie Wilkinson and Ian Croudace of Southampton
C University for Neutron Activation Analysis. The program selects gamma
C energies from batches of files created by Canberra's APOGEE package and
C compares them with those in a user-created library. Successful matches
C are stored in arrays until the complete spectrum has been considered.
C The next file (sample spectrum) is then processed and so on until the
C end of the batch has been reached.
C Standards are highlighted and used as references in order to calculate
C element concentrations in all samples represented by the batch of files.
C Corrections for sample weight, neutron flux variations, counting time, decay
C (half-life) are carried out. The program was written in FORTRAN 77 and
C currently runs on a DIGITAL PDP11/73 mini-computer operating under
C micro-RSX.
C
C
C.....
C
CFE-array contains iron counts for each foil
CFW-array contains foil weights
CS-array holds sample data: S(s,p,1)=counts
C                          S(s,p,2)=energy
C                          S(s,p,3)=isotope number in library
C                                   assigned to peak p
CFLAG-array: FLAG(s,1)=number of peaks in sample s
C            FLAG(s,2)=FLXVAR or 0 (0 if flux variation<5.0%)
C
  BYTE NAM(16,6),NAMSTD,ZI,XX,AI,YI,AB,QUERY,DCY,DATS
      BYTE FILER(12),LIBY,KEY,KEYS,DASH,ABC,ABCD,XI,DETER(8)
  INTEGER C,CL,D,P,FILST,FILEND,YR,ERROR,FLAG,ISTDS(5,2)
  INTEGER DAY,MONTH,YEAR,DY,MON,YE,IDAT(8)
      REAL*4 REC(198),LAMBDA,CONC(16,42),INTER,LIFE,CORFAC(16)
      CHARACTER*10 NAMFIL,NAMFOL
  DIMENSION FE(16),DATLIB(40,4,1),YR(4),MO(4),INTER(6,3)
  DIMENSION LIBY(6,32),NAMSTD(6,9),FLAG(16,2),IPOSN(16)
      DIMENSION STD(32,9),S(16,42,4),DASH(16,11),ERROR(16,42)
      REAL*8 A(336),B(168)
      EQUIVALENCE (B,ERROR)
      EQUIVALENCE (A,CONC)
      DATA NAMFIL/'SP0000.DAT'/,NAMFOL /'SP0000.REP'/
      DATA DETER /' ','L','o','w','H','i','g','h'/
  DATA YI/'Y'/
      DATA FILER/4*' ',4*'-',4*' '/
      DATA KEYS/'-'/,IDAT/6,7,8,9,10,11,12,13/
  DATA ZI/'*'/,ABC/'N'/
  DATA YR/88,92,96,00/
  DATA MO/4,6,9,11/
      DATA DASH/176*'-'/
      DATA ETOLER/0.7/
      DATA IOUT/6/
C
```

```
 555   FORMAT(A1)
       WRITE(5,3115)
3115   FORMAT(1X,'Terminal output (VDU) Y/N ? (Ret=No) ',$)
       READ(5,555)XI
       IF(XI.EQ.YI)IOUT=5
       WRITE(5,2113)
2113   FORMAT(1X,'Is this the 1st. count after irradn.? (Ret=No) ',$)
       READ(5,555)ABCD
       IF(ABCD.EQ.YI) DECTIM=5.0
       IF(ABCD.NE.YI) DECTIM=30.0
C
C     This question determines whether concn. data are output for elements
C     having short half-lives on the second count spectra
C
       OPEN(UNIT=1,NAME='DATRES.DAT',TYPE='OLD')
  READ(1,1301)LIMIT
       DO 1308 I=1,LIMIT
       READ(1,1307)(LIBY(J,I),J=1,6),DATLIB(I,1,1),DATLIB(I,2,1),
     X  DATLIB(I,3,1),DATLIB(I,4,1)
1301   FORMAT(I2)
1307   FORMAT(1X,6A1,F9.2,3X,3(F8.2,1X))
1308   CONTINUE
       CALL CLOSE(1)
       OPEN(UNIT=1,NAME='STDDAT.DAT',TYPE='OLD')
  READ(1,1302)NSTD
       READ(1,1304)((NAMSTD(I,J),I=1,6),J=1,NSTD)
1302   FORMAT(I1)
1304   FORMAT(/,8X,9(6A1,2X))
       DO 1305 I=1,LIMIT
       READ(1,1306)(STD(I,J),J=1,NSTD)
1306   FORMAT(6X,9(F7.2,1X))
1305   CONTINUE
       CALL CLOSE(1)
C
8888   WRITE(5,1216)
1216   FORMAT(1X,'Change energy tolerance ? Y/N (Ret=No) ',$)
       READ(5,555)AB
       IF(AB.NE.YI)GO TO 1217
       WRITE(5,1218)
1218   FORMAT(1X,'Input new energy tolerance !',$)
       READ(5,1219)ETOLER
1219   FORMAT(F5.3)
1217   WRITE(5,1212)
1212   FORMAT(1X,'Input starting file no. (I4 format)',$)
       READ(5,1213)FILST
       WRITE(5,1214)
1214   FORMAT(1X,'Input finishing file no. (I4 format)',$)
       READ(5,1213)FILEND
       NSAMPS=FILEND-FILST+1
C
C    !!!!!  Remember to link with the option MAXBUF=1024 !!!!!!
C
C.....
C
C
C      This allows a user to recycle thro' the program without
C      repeating flux data.
C
       DO 11 C=1,NSAMPS
  IF(QUERY.EQ.YI) GOTO 6664
       IF(C.GT.1) GO TO 6664
  FMAX=0.0
105        FORMAT(F5.0)
```

```
10        CONTINUE
773       DO 101 N=1,NSAMPS
C         .....Enter Fe monitor data in F format
C         .....and correct for flux weight.
C         ..... or input XRF data to normalise data.
C
      IF(N.GT.1) GO TO 117
  WRITE(5,8300)
8300    FORMAT(X,
     #   ' What do you wish to normalise to    Fe  flux mons (1) ?',/
     #   '  ..... XRF  Th       (2) ?',/
     #  ,'  ..... XRF  Fe       (3) ?',/
     #  ,'  ..... XRF  Rb       (4) ?',/
     #  ,'  ..... XRF  Na       (5) ?'/
     #  ,'                          Ret=  Option 1 ',//
     #  ,'   Select  a  number **********                ',$)
  READ(5,8301)IASPNO
8301    FORMAT(I1)
  IF(IASPNO.EQ.' '.OR.IASPNO.EQ.0)IASPNO=1
      WRITE(5,116)
116     FORMAT(1X,'Input flux counts only assuming that flux
     X  monitor weights are constant.',/,'  N.B. Flux at
     X  sample position',//,'OR XRF/NAA factors',
     X  ' Type a [Ret] for uniform flux corrections')
117     IF (FE(1).EQ.1.0.AND.IASPNO.EQ.1) GO TO 1101
      WRITE(5,115)N
115     FORMAT(1X,'Sample ',I2)
  READ(5,105)FE(N)
C         ..... This finds max. Fe counts
1101    IF (FE(N).EQ.0.0.AND.IASPNO.EQ.1) FE(N)=1.0
      IF (FE(N).GT.FMAX.AND.IASPNO.EQ.1) FMAX=FE(N)
101       CONTINUE
  WRITE(5,441)
  WRITE(5,441)
  WRITE(5,1008)
1008      FORMAT(6X,'Please wait, calculations in progress!')
6664    CONTINUE
9981    IF(FILST.LT.100)GO TO 9972
      IF(FILST.LT.1000)GO TO 9971
      WRITE(NAMFIL(3:6),'(I4)')FILST
      WRITE(NAMFOL(3:6),'(I4)')FILST
      GO TO 9970
9971    WRITE(NAMFIL(4:6),'(I3)')FILST
      WRITE(NAMFOL(4:6),'(I3)')FILST
      GO TO 9970
9972    WRITE(NAMFIL(5:6),'(I2)')FILST
      WRITE(NAMFOL(5:6),'(I2)')FILST
9970    CONTINUE
1213    FORMAT(I4)
      FILST=FILST+1
      OPEN(UNIT=2,ACCESS='DIRECT',TYPE='OLD',
     X  INITIALSIZE=36,FILE=NAMFIL,ERR=9990)
      OPEN(UNIT=3,ACCESS='SEQUENTIAL',TYPE='OLD',
     X  FILE=NAMFOL,ERR=999)
      GO TO 9980
9990    WRITE(5,9982)FILST-1
9982    FORMAT(1X,' SP',I4,'.DAT missing ... program continuing')
  GO TO 9981
9980    CONTINUE
      READ(2'1,ERR=999)REC
      DETCR=REC(2)
      IF(C.GT.1)GOTO 1992
      DETERR=DETCR
```

```
1991    FORMAT(1X,'Error in det. no. - check SP',I4,'DAT file!!')
1992    IF (DETCR.NE.DETERR)WRITE(5,1991)FILST-1
        IF (DETCR.NE.DETERR)GOTO 899
        IF (C.GT.1) GO TO 1990
        IF(DETCR.EQ.2.OR.DETCR.EQ.5)GO TO 2114
        OPEN(UNIT=1,NAME='OVERHE.DAT',TYPE='OLD')
  GO TO 2115
2114    OPEN(UNIT=1,NAME='OVERLE.DAT',TYPE='OLD')
2115    DO 1390 I=1,6
        READ(1,1391)(INTER(I,J),J=1,3)
C        WRITE(5,1391)(INTER(I,J),J=1,3)
1391    FORMAT(6X,3(F10.4,1X))
1390    CONTINUE
        CALL CLOSE(1)
1990    SW=REC(198)
        CT=REC(25)
        IDTIM=((REC(24)-REC(25))/REC(24))*100.0
        FLAG(C,2)=IDTIM
        IF(C.EQ.1)STIM=CT
  NOEN=3
  NOIS=LIMIT
C .....
C
C.....
        INC=0
        READ(3,1000)(NAM(C,I),I=1,6)
        READ(3,1004)
        DO 1003 JJ=1,200
        READ(3,1001,END=991,ERR=999)KEY,ENERG,AREA,SIGMA
        IF(KEY.EQ.KEYS.OR.ENERG.EQ.0.0) NPKS=JJ-1
  IF(KEY.EQ.KEYS.OR.ENERG.EQ.0.0) GO TO 991
C
C  ***************************** SEEKER *******************************
C
C   This seeks to match energies in a spectrum with those in a library.
C
  NOFIT=0
  DO 220 M=1,NOIS
        LIFE=10.0*DATLIB(M,1,1)
        IF(LIFE.LT.DECTIM) GO TO 220
  DO 210 L=2,1+NOEN
  IF(DATLIB(M,L,1).EQ.0.0) GO TO 210
  ENDIF=ABS(ENERG-DATLIB(M,L,1))
  IF(ENDIF.GT.ETOLER) GO TO 210
        IF(ABCD.EQ.YI.AND.DATLIB(M,1,1).GT.46) GOTO 210
  NOFIT=1
        INC=INC+1
        INCA=1
C
C       This coding stores positions of Th, Fe, Rb or Na
C       for use as normalising factors.
C
  GO TO (1444,1440,1441,1442,1443),IASPNO
1440        IF(M.EQ.11.AND.L.EQ.4)IPOSN(C)=INC
  IM=11
  GO TO 1444
1441        IF(M.EQ.22.AND.L.EQ.2.AND.DETCR.EQ.2)IPOSN(C)=INC
  IF(M.EQ.22.AND.L.EQ.2.AND.DETCR.EO.5)IPOSN(C)=INC
  IF(M.EQ.22.AND.L.EQ.4.AND.DETCR.EQ.1)IPOSN(C)=INC
  IM=22
  GO TO 1444
1442        IF(M.EQ.25)IPOSN(C)=INC
  IM=25
```

```
  GO TO 1444
1443    IF(M.EQ.LIMIT)IPOSN(C)=INC
  IM=LIMIT
C
1444    S(C,INC,4)=SIGMA
  S(C,INC,3)=M
        S(C,INC,2)=DATLIB(M,L,1)
        S(C,INC,1)=AREA
210         CONTINUE
220         CONTINUE
C
  IF(NOFIT.EQ.1) GO TO 230
C
230         CONTINUE
CSEARCH FINISHED
C
        INCA=INCA+1
        IF(INC.LT.1.OR.INCA.GT.2) GO TO 1003
1003    CONTINUE
991     CONTINUE
        FLAG(C,1)=INC
        IF(INC.GT.42)WRITE(IOUT,1909)INC
1909    FORMAT(1X,' Warning - too many peaks matched for array
     #  size ',I2)
        IF (INC.GT.42) GO TO 995
C         WRITE(5,1005)NPKS,NAMFOL,INC,(NAM(C,IL),IL=1,6)
C
C   .....END OF SEEKER.....
        CALL CLOSE(2)
        CALL CLOSE(3)
C*****************************************************************
C*****************************************************************
C     INTERFERENCE CORRECTION AND SEARCH ROUTINE
C
        DO 2103 LP=1,6
        IPOS1=0
        IPOS2=0
        IF (INTER(LP,1).EQ.0.0) GO TO 2103
  DO 2100 LA=1,INC
        IF(IPOS1.GT.0) GO TO 2101
  ENDIF1=ABS(INTER(LP,1)-S(C,LA,2))
  IF(ENDIF1.GT.ETOLER) GO TO 2101
        IPOS1=LA
C         WRITE(5,2107)S(C,LA,2)
        GO TO 2100
2101        ENDIF2=ABS(INTER(LP,2)-S(C,LA,2))
  IF(ENDIF2.GT.ETOLER) GO TO 2100
        IPOS2=LA
C         WRITE(5,2107)S(C,LA,2)
C2107    FORMAT(1X,F10.2,' Matched')
        IF(IPOS1.EQ.0.OR.IPOS2.EQ.0)GO TO 2100
2102    S(C,IPOS1,1)=S(C,IPOS1,1)-INTER(LP,3)*S(C,IPOS2,1)
C         WRITE(5,2105)S(C,IPOS1,1),INTER(LP,3),S(C,IPOS2,1),INC
C2105    FORMAT(1X,F15.1,1X,F7.4,F15.1,1X,I2)
        GO TO 2111
2100    CONTINUE
2103    CONTINUE
2111    CONTINUE
C
C*****************************************************************
C*****************************************************************
C   .....
1000    FORMAT(////////////,28X,6A1,///)
```

```
1001    FORMAT(5X,A1,39X,F7.2,7X,F9.1,3X,F4.1)
1002    FORMAT(1X,I3,'..',F10.1,'..',F10.1,'-',F4.1,F4.0,I2)
1004    FORMAT(/////)
1005    FORMAT(2X,I3,' Pks. read fom -',A10,
     X  3X,I3,'- Peaks matched to library',1X,6A1)
1006    FORMAT(1X,8X,6A1,8X,20A1)
1007    FORMAT(1X,A1,A1,F8.2,2X,F9.1)
C
C
C .....
C
C .     CALCULATE DECAY TIME IN DAYS
C .....
        IF(C.GT.1) GOTO 1801
        WRITE(5,1800)
1800    FORMAT(1X,' Will Decay time be taken from REC(5)? (Ret= No) ',$)
        READ(5,555)DCY
  IF(DCY.EQ.YI)GO TO 3101
  WRITE(5,832)
832     FORMAT(1X,'Will date be taken from REC 6-9 ?      (Ret= Yes) ',$)
  READ(5,555)DATS
  IF(DATS.NE.YI) IJ=1
  IF(DATS.NE.YI) GO TO 1801
        IJ=5
1801    IF(DCY.EQ.YI)GOTO 3101
        IF(C.GT.1)GO TO 1456
        FRACT=REC(IDAT(IJ))
  FRACT=FRACT*0.0000116
        DY=REC(IDAT(IJ+1))
        MON=REC(IDAT(IJ+2))
        YE=REC(IDAT(IJ+3))
1456    IF(C.EQ.1) GO TO 2999
        PART=REC(IDAT(IJ))
  PART=PART*0.0000116
        DAY=REC(IDAT(IJ+1))
        MONTH=REC(IDAT(IJ+2))
        YEAR=REC(IDAT(IJ+3))
C
2999        IF(C.EQ.1) TIME=0.0
  IF(C.EQ.1) GO TO 6665
C
  MTH=MON
  TOT=0.0
  IF(MTH.EQ.MONTH) GOTO 3100
3000        DO 3001 K=1,4
  IF(MO(K).EQ.MTH) GO TO 3030
3001        CONTINUE
  IF(MTH.EQ.2) GO TO 3035
  LEN=31
  GO TO 3045
3030        LEN=30
  GO TO 3045
3035        DO 3002 JJ=1,4
  IF(YR(JJ).EQ.YE) GO TO 3040
3002        CONTINUE
  LEN=28
  GO TO 3045
3040        LEN=29
3045        TOT=TOT+LEN
  MTH=MTH+1
  IF(MTH.EQ.MONTH) GO TO 3100
  IF(MTH.EQ.13) GO TO 3050
  GO TO 3000
```

```
3050      MTH=1
  YE=YE+1
  GO TO 3000
3100      TIME=TOT-DY+DAY-FRACT+PART
      GOTO 6665
3101    TIME=REC(5)
C*0.0006944
C
C .....
C
6665    HOUR=REC(6)*0.00027777
  MIN=(HOUR-AINT(HOUR))*60.0
  IYR=REC(9)-1900
  IF(C.GT.1)GO TO 703
      WRITE(5,4495)
4495    FORMAT(//,'  Total',2X,' # Pks',6X,'Dead',4X,
     #  'Decay time',4X,'Mass',5X,' Date & Time',4X,'Sample',
     #  /,' # peaks ',' matched ','   time ',5X,'(days)',5X,'(grams)'
     #  ,/,80('-'))
703     WRITE(5,9902)NPKS,INC,FLAG(C,2),TIME,REC(198),
     #  IFIX(REC(7)),IFIX(REC(8)),IYR,INT(HOUR),MIN,
     #  (NAM(C,JK),JK=1,6)
9902    FORMAT(1H ,X,I4,4X,I4,6X,I4,'%'4X,F6.2,7X,F7.4,X,
     #  3X,I2,'/',I2,'/',I2,2X,I2,':',I2,3X,6A1)
C
C
CCORRECT PEAK AREAS FOR SAMPLE WEIGHTS
CCORRECT PEAK AREAS FOR FLUX VARIATION
CHALF-LIFE CORRECTIONS
C
      LAMBDA=(0.6931*TIME)
      IF(IASPNO.EQ.1)GO TO 7766
      SINT=STIM/(SW*CT)
      FLXCOR=1.0
      GO TO 7767
7766    FLXCOR=FMAX/FE(C)
      SINT=(STIM*FLXCOR)/(SW*CT)
7767      IF(C.GT.1) GOTO 4446
  WRITE(IOUT,441)
      WRITE(IOUT,4445)(LIBY(P,IM),P=1,2)
4445    FORMAT(2X,'Flx/XRF Fac.',('(',2A1,')',3X,'Deadtime',2X,'Decay',
     #  ' time',3X,'Mass',2X,'Corr. Factor',2X,'Sample',7X,' Date')
      WRITE(IOUT,4443)
4446      IF(IASPNO.NE.1) GO TO 1906
4443    FORMAT(1X,90('-'))
      WRITE(IOUT,1902)FE(C),FLAG(C,2),TIME,REC(198),SINT,
     #  (NAM(C,JK),JK=1,6),IFIX(REC(7)),IFIX(REC(8)),IYR,
     #  INT(HOUR),MIN
      GO TO 1907
1902    FORMAT(1H ,3X,F8.4,13X,I2,'%'7X,F5.2,5X,F6.4,3X,F7.4,5X,6A1,
     #  3X,I2,'/',I2,'/',I2,2X,I2,':',I2)
1906    WRITE(IOUT,1905)FE(C),FLAG(C,2),TIME,REC(198),SINT,
     #  (NAM(C,JK),JK=1,6),IFIX(REC(7)),IFIX(REC(8)),IYR,
     #  IINT(HOUR),MIN
1905    FORMAT(1H ,2X,F7.2,13X,I2,'%'7X,F5.2,5X,F6.4,3X,F8.4,5X,6A1,
     #  3X,I2,'/',I2,'/',I2,2X,I2,':',I2)
1907    DO 40 N=1,FLAG(C,1)
  S(C,N,1)=(S(C,N,1)*SINT)
  S(C,N,1)=S(C,N,1)*EXP(LAMBDA/DATLIB(S(C,N,3),1,1))
40        CONTINUE
C
11        CONTINUE
404     CONTINUE
```

```
C***END OF SAMPLE LOOP***
C
CCOMPARE STANDARDS
C
C       OPEN(UNIT=1,ACCESS='SEQUENTIAL',TYPE='NEW',
C     X  FILE=NAMFAL,CARRIAGECONTROL='FORTRAN',ERR=999)
C
C
      IF(DETERR.EQ.1)MQ=5
      IF(DETERR.EQ.2.OR.DETERR.EQ.5)MQ=1
  WRITE(IOUT,442)(DETER(IX),IX=MQ,MQ+3)
441       FORMAT(X)
442       FORMAT(/,' R-E-S-U-L-T-S',3X,4A1,
     #  ' Energy Detector',/,40('-'),/)
C
C     Select a Standard for concentration calculations
C
  IGG=0
      IG=0
  DO 423 C=1,NSAMPS
1903    FORMAT(1X,'  No standards matched - check names')
1904    FORMAT(1X,'  No standards found in spectra sets- check *')
  IF(NAM(C,1).NE.ZI) IG=IG+1
  IF(NAM(C,1).NE.ZI.AND.IG.EQ.NSAMPS) WRITE(IOUT,1904)
  IF(NAM(C,1).NE.ZI) GO TO 423
      IF(C.GT.1.AND.ISTD.NE.0) GO TO 4213
C     ************************************
      ISTD=0
      DO 4212 CL=1,NSAMPS
      IF(NAM(CL,1).NE.ZI) GO TO 4212
  DO 4221 I=1,9
  DO 4211 J=1,6
  IF(NAMSTD(J,I).NE.NAM(CL,J)) GO TO 4221
      IF(J.EQ.6) ISTD=ISTD+1
  IF(J.EQ.6) ISTDS(ISTD,1)=I
  IF(J.EQ.6) ISTDS(ISTD,2)=CL
4211      CONTINUE
C
  WRITE(5,4411)
  WRITE(5,9071)(NAMSTD(J,I),J=1,6),ISTD,CL
9071      FORMAT(1X,'Standard: ',6A1,X,I1,'at posn ',I2)
4221    CONTINUE
4212    CONTINUE
C     ************************************************
4213      DO 422 I=1,9
  DO 421 J=1,6
      IF(NAMSTD(J,I).NE.NAM(C,J))IGG=IGG+1
  IF(NAMSTD(J,I).NE.NAM(C,J)) GO TO 422
421       CONTINUE
C
  WRITE(IOUT,4411)
  WRITE(IOUT,907)(NAMSTD(J,I),J=1,6)
  WRITE(IOUT,908)
907       FORMAT(1X,'Standard: ',6A1)
908       FORMAT(1X,'----------')
C
C  This initialises array CONC and ERROR using EQUIVALENCE and
C  DOUBLE PRECISION
C
      DO 4233 IIJ=1,336
4233    A(IIJ)=0.0D0
      DO 4234 IIJ=1,168
4234    B(IIJ)=0.0D0
```

```
C
  DO 415 D=1,NSAMPS
  IF(D.EQ.C) GO TO 415
  DO 427 II=1,9
  DO 428 J=1,6
  IF(NAMSTD(J,II).NE.NAM(D,J)) GO TO 427
428         CONTINUE
       GO TO 426
427     CONTINUE
426         CONTINUE
C
  DO 420 N=1,FLAG(D,1)
  CSTD=STD(S(D,N,3),I)
C
C .... FLAG(C,1) CONTAINS NO. OF PEAKS IN THE CURRENT STANDARD.
C
       DO 444 M=1,FLAG(C,1)
C        WRITE(5,840)D,(S(D,N,3)),(S(C,M,3)),S(D,N,1),S(C,M,1),
C     #  (LIBY(P,S(C,M,3)),P=1,2)
C  This code copies the standard data to CONC
  DO 814 IK=1,ISTD
  IF(S(C,M,3).NE.S(D,N,3))GO TO 814
       IF(C.EQ.ISTDS(IK,2))GO TO 814
       CONC(NSAMPS+IK,M)=STD(S(C,M,3),ISTDS(IK,1))
840         FORMAT(X,I2,'  POS 1= ',F3.0,'POS 2 =',F3.0,X,2(F8.0,X),2A1)
814     CONTINUE
  EDIF=ABS(S(C,M,2)-S(D,N,2))
  IF(EDIF.GT.ETOLER.OR.S(C,M,3).NE.S(D,N,3)) GO TO 444
  IF(S(C,M,1).EQ.0.0)GO TO 444
  CONC(D,M)=S(D,N,1)*CSTD/S(C,M,1)
       ERROR(D,M)=NINT(SQRT(S(C,M,4)**2+S(D,N,4)**2)+0.5)
444     CONTINUE
C
420         CONTINUE
  IF(IASPNO.EQ.1) GO TO 415
  IF(IPOSN(D).LE.0) GO TO 415
C
C  ********* THIS IS WHERE RECALCULATIONS OCCUR TO CONC ********
C                        FOR XRF COMPONENTS
C     Note CONC(x,x) size is controlled by the current standard C
C     which has M nuclides
C
C       IPOSN(C)..... position of element in list of flag(C,x)
C       ensure that VALUE does not cause overflow !!!!!!
C
       VALUE=CONC(D,IPOSN(C))
       IF(VALUE.LE.0.0)VALUE=FE(D)
       DO 171 M=1,FLAG(C,1)
C       WRITE(5,7779)D,M,IPOSN(C),CONC(D,IPOSN(C)),CONC(2,22)
  CONC(D,M)=CONC(D,M)*FE(D)/VALUE
       CORFAC(D)=FE(D)/VALUE
171     CONTINUE
172     CONTINUE
7779    FORMAT(1X,3I3,X,2F6.1)
C
C  ************************************************************
C
415         CONTINUE
416         IPRI=8
  IF((NSAMPS+ISTD-2).LE.9)IPRI=9
  IF(IPRI.NE.9)IPRI=NSAMPS-ISTD
  IF(IPRI.GT.9)IPRI=9
C
```

```
C
6666      Q=NSAMPS/IPRI
  LI=IFIX(Q)
      DO 77 LL=0,LI
      KL=LL*IPRI+1
      KM=KL+IPRI-1
C
C   C holds the current position of the standard
C
     IF(NSAMPS.EQ.IPRI.OR.NSAMPS.EQ.IPRI+1.AND.LL.EQ.1)GOTO 77
     IF(NSAMPS.EQ.2*IPRI.OR.NSAMPS.EQ.2*IPRI+1.AND.LL.EQ.2)GOTO 77
     IF(C.LE.IPRI.AND.LL.EQ.0)KM=KM+1
     IF(C.LE.IPRI.AND.LL.GT.0)KL=KL+1
     IF(C.LE.IPRI.AND.LL.GT.0)KM=KM+1
     IF(C.LE.2*IPRI.AND.C.GT.IPRI.AND.LL.GE.1)KM=KM+1
     IF(C.LE.2*IPRI.AND.LL.GT.1)KL=KL+1
     IF(C.LE.NSAMPS.AND.LL.GE.2)KM=KM+1
     IF(KM.GT.NSAMPS) KM=NSAMPS
     WRITE(5,9871)KL,KM,LL,LI,IC,ISTD,IPRI
9871   FORMAT(1X,' KL= ',I2,' KM= ',I2,' LL= ',I2,' LI= ',I2,
    # ' IC= ' ,I2,' ISTD  = ',I2,' IPRI= ',I2)
C
      DO 76 KK=1,FLAG(C,1)
  IF(KK.NE.1) GOTO 73
  WRITE(IOUT,4411)
  WRITE(IOUT,4411)
         WRITE(IOUT,95)
95       FORMAT(1H+,'Isotope  Energy  ',$)
  IC=LL*8
  DO 81 D=KL,KM
      IF(D.EQ.C) GOTO 81
  GOTO 821
820       DO 811 NID=1,ISTD
      IF(C.EQ.ISTDS(NID,2)) GO TO 811
      WRITE(IOUT,129)(NAM(ISTDS(NID,2),J),J=2,6),
    #  (NAM(ISTDS(NID,2),J),J=2,6)
811       CONTINUE
  GO TO 850
821    IF(NAM(D,1).EQ.'*')GO TO 819
      WRITE(IOUT,96)(NAM(D,J),J=1,6)
  IC=IC+1
  IF(D.EQ.KM.AND.LL.EQ.LI)GO TO 820
819       IF(IC.GE.(KM-ISTD).AND.LL.EQ.LI) GO TO 820
81        CONTINUE
850       CONTINUE
  WRITE(IOUT,441)
      WRITE(IOUT,83)
      IC=LL*8
  DO 82 D=KL,KM
      IF(D.EQ.C) GOTO 82
  GO TO 823
824       DO 812 NID=1,ISTD
      IF(C.EQ.ISTDS(NID,2)) GO TO 812
      WRITE(IOUT,816)(DASH(D,J),J=1,11),(DASH(D,J),J=1,11)
812       CONTINUE
      GO TO 851
823    IF(NAM(D,1).EQ.'*')GO TO 835
      WRITE(IOUT,94)(DASH(D,J),J=1,11)
  IC=IC+1
  IF(D.EQ.KM.AND.LL.EQ.LI)GO TO 824
835       IF(IC.GE.(KM-ISTD).AND.LL.EQ.LI) GO TO 824
82        CONTINUE
851       CONTINUE
```

```
C
 WRITE(IOUT,4411)
 73    WRITE(IOUT,441)
       WRITE(IOUT,74)(LIBY(P,S(C,KK,3)),P=1,6),S(C,KK,2)
  IC=LL*8
       DO 78 D=KL,KM
       IF(D.EQ.C) GOTO 78
  GO TO 825
826         DO 813 NID=1,ISTD
       IF(C.EQ.ISTDS(NID,2)) GO TO 813
  IF(CONC(ISTDS(NID,2),KK).GT.0.0) GO TO 815
       IF(CONC(ISTDS(NID,2),KK).LE.0.0)
     #  WRITE(IOUT,817)(FILER(IL),IL=1,12),CONC(KM+NID,KK)
       GO TO 813
815    WRITE(IOUT,818)CONC(ISTDS(NID,2),KK),
     #  ERROR(ISTDS(NID,2),KK),CONC(KM+NID,KK)
C       WRITE(5,828)CONC(ISTDS(NID,2),KK),ISTDS(NID,2),KK
828         FORMAT(1X,F8.2,X,I2,X,'EL NO. ',I2)
813         CONTINUE
       GO TO 852
825    IF(NAM(D,1).EQ.'*')GO TO 853
       IF (CONC(D,KK).GT.0.0) GO TO 87
       WRITE(IOUT,55)(FILER(IL),IL=1,12)
  IC=IC+1
  GOTO 830
87          WRITE(IOUT,98)CONC(D,KK),ERROR(D,KK)
  IC=IC+1
830         IF(D.EQ.KM.AND.LL.EQ.LI)GO TO 826
853         IF(IC.GE.(KM-ISTD).AND.LL.EQ.LI) GO TO 826
78     CONTINUE
852         CONTINUE
C
76          CONTINUE
  WRITE(IOUT,4411)
77     CONTINUE
C
816    FORMAT(1H+,22A1,$)
94     FORMAT(1H+,11A1,$)
83     FORMAT(1H+,23(H-),$)
449    FORMAT(20(H-))
96          FORMAT(1H+,6A1,'      ',$)
129    FORMAT(1H+,5A1,' (M)  ',5A1,' (R)  ',$)
74     FORMAT(1H+,1X,6A1,'-',F6.1,$)
4411   FORMAT(1H )
98          FORMAT(1H+,F8.2,1H(,I2,1H),$)
817         FORMAT(1H+,12A1,F8.2,$)
818         FORMAT(1H+,F8.2,1H(,I2,1H),F8.2,$)
55     FORMAT(1H+,12A1,$)
  WRITE(IOUT,4411)
422         CONTINUE
  IF(IG.EQ.NSAMPS.AND.IGG.GT.0)WRITE(IOUT,1903)
423         CONTINUE
CWRITE(IOUT,5029)((NAM(PZ,JK),JK=1,6),PZ=1,NSAMPS)
CWRITE(IOUT,5028)
C       WRITE(IOUT,5030)(CORFAC(IZ),IZ=1,NSAMPS)
5028   FORMAT(1X,120('-'))
5029   FORMAT(1X,' Sample',18X,16(6A1,2X))
5030   FORMAT(1X,'Flux Corr. factors = ',16(F8.3))
       CALL CLOSE(1)
C
C
C       WRITE(5,7774)
7774   FORMAT(1X,'Do you want to analyse complementary spectra
```

```
    #  using the same flux data ?',$)
C        READ(5,555)QUERY
C        IF (QUERY.EQ.YI) GO TO 8888
  GO TO 899
C
999     WRITE(5,998)FILST-1
998     FORMAT(1X,'READ FAILURE ON SP',I4,'.REP')
        GO TO 995
997     WRITE(5,996)FILST-1
996     FORMAT(1X,'READ FAILURE ON SP',I4,'.DAT')
  GO TO 993
995     WRITE(5,994)FILST-1
994     FORMAT(1X,' Too many peaks matched in SP',I4,'.REP')
993     CALL CLOSE(3)
        CALL CLOSE(2)
C
899         CALL EXIT
        END
C .....
```

APPENDIX D

MICROTHERMOMETRIC DATA

D1: PHASE CHANGES RECORDED DURING THERMOMETRIC ANALYSIS

Summarised below is a list of all the simple phase changes observed in this study during thermometric analysis and the temperature ranges over which they occur. The number of phase changes observed in any one inclusion is a function of inclusion composition and optical resolution.

	PHASE CHANGE	NOTATION	TEMPERATURE RANGE
1.	$CO_2(S)$ -> $CO_2(L)$	*$TmCO_2$*	-65 to -56.6°C
2.	S -> $H_2O(L)$ + solvated ions	*Tfm*	-75 to -20.8°C
3.	$H_2O(S)$ -> $H_2O(L)$	*TmI*	-50 to 0.0°C
4.	Hydrohalite -> $H_2O(L)$ + Na^+ + Cl^- ± NaCl(S)	*Tmh*	-50 to +20°C
5.	$CO_2.5.75H_2O(S)$ -> $CO_2(L)+CO_2(V)+H_2O(L)$	*TmC*	-2 to +13°C
6.	$CO_2(L)+CO_2(V)$ -> CO_2(L and/or V or supercritical fluid)	*$ThCO_2$*	-20 to +31.1°C
7.	Sylvite -> K^+ + Cl^-	*TsS*	+50 to +100°C
8.	Halite -> Na^+ + Cl^-	*TsH*	+100 to +400°C
9.	L + V -> L or V	*Th*	+90 to +500°C

D2: TABLES OF THERMOMETRIC DATA

The following tables contain all the thermometric data obtained in this study. The tables are subdivided according to vein group (V1, V2, V3, $V4_P$, $V4_J$, $V4_N$, $V4_W$). The final table contains data for veins which were ambiguous with respect to their age. Within each table, the samples corresponding with each set of data are identified, and for V3 samples the inclusion type is also specified.

The phase transitions studied, for which thermometric data are presented, are summarised in Appendix D1. The notation used in the tables to represent these phase changes is presented in Appendix E (under section for Chapter 3).

V1 FLUID INCLUSION DATA

SAMPLE	F	Tfm	Tmh	Tml	S	TsH	Th	to	D
J06GW	-	-	-	-	-	-	257	L	-
"	-	-	-	-	-	-	155	L	-
"	-	-	-	-	-	-	132	L	-
"	-	-	-	-	-	-	147	L	-
"	-	-	-	-	-	-	295	L	-
"	-	-	-	-	-	-	173	L	-
"	-	-	-	-	-	-	147	L	-
"	-	-	-	-	-	-	259	L	-
"	-	-	-	-	-	-	163	L	-
"	-	-	-	-	-	-	156	L	-
"	-	-	-	-	-	-	166	L	-
"	-	-	-	-	-	-	177	L	-
"	-	-	-	-	-	-	190	L	-
"	-	-	-	-	-	-	163	L	-
"	-	-	-	-	-	-	250	L	-
"	-	-	-	-	-	-	265	L	-
"	-	-	-	-	-	-	163	L	-
"	-	-	-	-	-	-	137	L	-
"	-	-	-	-	-	-	243	L	-
"	-	-	-	-	-	-	272	L	-
"	-	-	-	-	-	-	192	L	-
"	-	-	-	-	-	-	262	L	-
"	-	-	-	-	-	-	259	L	-
"	-	-	-	-	-	-	257	L	-
"	-	-	-	-	-	-	254	L	-
"	-	-	-	-	-	-	267	L	-
"	-	-	-	-	-	-	220	L	-
"	-	-	-	-	-	-	151	L	-
"	-	-	-	-	-	-	185	L	-
"	-	-	-	-	-	-	181	L	-
"	0.9	-	-	-2.5	4.2	-	198	L	0.930
"	0.95	-	-	-1.9	3.2	-	153	L	0.974
"	0.9	-	-	-1.9	3.2	-	160	L	0.923
"	0.92	-	-	-2.1	3.5	-	182	L	0.945
"	0.9	-	-	-2.3	3.9	-	188	L	0.928
"	0.85	-	-	-1.5	2.6	-	182	L	0.867
"	0.9	-	-	-1.7	2.9	-	150	L	0.920
"	0.75	-	-	-4.8	7.6	-	-		0.795
"	0.5	-	-	-3	4.9	-	-		0.519
"	0.9	-	-	-	-	-	171	L	0.9
"	0.95	-	-	-2.2	3.7	-	-		0.978
"	0.9	-	-	-1.5	2.6	-	190	L	0.918
"	0.95	-	-	-1.9	3.2	-	151	L	0.974
"	0.92	-	-	-1.6	2.7	-	162	L	0.939
"	0.95	-	-	-2.1	3.5	-	179	L	0.976
"	0.9	-	-	-2.1	3.5	-	-		0.925
"	0.9	-	-	-1.5	2.6	-	167	L	0.918
"	0.9	-	-	-1.2	2.1	-	205	L	0.915
"	0.88	-	-	-2.7	4.5	-	325	L	0.911
"	0.9	-	-	-1.3	2.2	-	194	L	0.915
"	0.95	-	-	-1.9	3.2	-	217	L	0.974
"	0.94	-	-	-1.5	2.6	-	172	L	0.959
"	0.9	-	-	-2.1	3.5	-	-		0.925
"	0.92	-	-	-2	3.4	-	-		0.945

V1 FLUID INCLUSION DATA

SAMPLE	F	Tfm	Tmh	Tml	S	TsH	Th	to	D
J06GW	0.9	-	-	-1.3	2.2	-	182	L	0.915
"	0.92	-	-	-1.5	2.6	-	185	L	0.939
"	0.96	-	-	-1.8	3.1	-	-		0.983
"	0.9	-	-	-2.3	3.9	-	255	L	0.928
"	0.95	-	-	-1.8	3.1	-	177	L	0.973
"	0.7	-	-	-	-	-	301	L	0.7
"	0.88	-	-	-2.4	4	-	-		0.908
"	0.7	-	-	-2.6	4.3	-	258	L	0.724
"	0.95	-	-	-2.4	4	-	189	L	0.980
"	0.9	-	-	-2.1	3.5	-	182	L	0.925
"	0.95	-	-	-1.7	2.9	-	167	L	0.972
"	0.95	-	-	-1.7	2.9	-	150	L	0.972
"	0.95	-	-	-1.5	2.6	-	182	L	0.969
"	0.9	-	-	-1.9	3.2	-	-		0.923
"	0.9	-	-	-1.8	3.1	-	-		0.922
"	0.9	-	-	-1.8	3.1	-	-		0.922
"	0.65	-	-	-4.5	7.2	-	376	L	0.687
"	0.5	-	-	0	0	-	349	L	0.5
"	0.9	-	-	-3.2	5.2	-	235	L	0.937
"	0.8	-	-	-3.5	5.7	-	292	L	0.836
"	0.92	-	-	-3.4	5.5	-	236	L	0.960
"	0.96	-	-	-3.6	5.8	-	219	L	1.004
"	0.9	-	-	-3.4	5.5	-	258	L	0.939
"	0.94	-	-	-2.1	3.5	-	159	L	0.966
"	0.95	-	-	-1.5	2.6	-	144	L	0.969
"	0.9	-	-	-1.4	2.4	-	201	L	0.917
"	0.95	-	-	-1.8	3.1	-	215	L	0.973
"	0.75	-	-	-4.3	6.9	-	286	L	0.791
"	0.78	-	-	-2.7	4.5	-	265	L	0.808
"	0.7	-	-	-2.5	4.2	-	258	L	0.723
"	0.85	-	-	-1.8	3.1	-	178	L	0.871
"	0.95	-	-	-1.4	2.4	-	168	L	0.968
"	0.95	-	-	-	-	-	153	L	0.95
"	0.95	-	-	-	-	-	142	L	0.95
"	0.7	-	-	-3.7	6	-	270	L	0.733
"	0.9	-	-	-4.8	7.6	-	222	L	0.954
"	0.7	-	-	-3.2	5.2	-	267	L	0.729
"	0.75	-	-	-3.2	5.2	-	276	L	0.781
J105GW	0.9	-	-	-2	3.4	-	-		0.924
"	0.94	-	-	-1	1.7	-	158	L	0.952
"	0.92	-	-	-1	1.7	-	175	L	0.932
"	0.9	-	-	-0.6	1.0	-	189	L	0.907
"	0.95	-	-	-2.5	4.2	-	200	L	0.981
"	0.94	-	-	-1.4	2.4	-	186	L	0.958
"	0.93	-	-	-1.2	2.1	-	167	L	0.945
"	0.9	-	-	-2	3.4	-	204	L	0.924
"	0.9	-	-	-3.4	5.5	-	216	L	0.939
"	0.93	-	-	-1.5	2.6	-	162	L	0.949
"	0.95	-	-	-1.1	1.9	-	151	L	0.964
"	0.92	-	-	-1.2	2.1	-	173	L	0.935
"	0.95	-	-	-1.1	1.9	-	160	L	0.964
"	0.9	-	-	-1.4	2.4	-	171	L	0.917
"	0.93	-	-	-1.3	2.2	-	177	L	0.946
"	0.9	-	-	-1.5	2.6	-	193	L	0.918

V1 FLUID INCLUSION DATA

SAMPLE	F	Tfm	Tmh	Tml	S	TsH	Th	to	D
J105GW	0.95	-	-	-	-	-	183	L	0.95
"	0.95	-	-	-1.5	2.6	-	172	L	0.969
"	0.94	-	-	-1.9	3.2	-	210	L	0.964
"	0.94	-	-	-1.3	2.2	-	193	L	0.956
"	0.92	-	-	-1.2	2.1	-	188	L	0.935
"	0.9	-	-	-	-	-	213	L	0.9
"	0.95	-	-	-1.4	2.4	-	174	L	0.968
"	0.95	-	-	-1.5	2.6	-	180	L	0.969
"	0.94	-	-	-1.4	2.4	-	218	L	0.958
"	0.93	-	-	-1.5	2.6	-	192	L	0.949
"	0.94	-	-	-1.4	2.4	-	185	L	0.958
"	0.92	-	-	-1.4	2.4	-	180	L	0.937
"	0.94	-	-	-1.7	2.9	-	208	L	0.961
"	0.9	-	-	-1.45	2.5	-	-		0.917
"	0.92	-	-	-1.3	2.2	-	185	L	0.936
"	0.9	-	-	-1.4	2.4	-	196	L	0.917
"	0.93	-	-	-2.2	3.7	-	228	L	0.957
J11PB	0.9	-	-	-1.4	2.4	-	175	L	0.917
"	0.92	-	-	-1.6	2.7	-	178	L	0.940
"	0.9	-	-	-1	1.7	-	169	L	0.912
"	0.9	-	-	-	-	-	173	L	0.9
"	0.9	-	-	-1.2	2.1	-	174	L	0.914
"	0.95	-	-	-2.2	3.7	-	200	L	0.978
"	0.95	-	-	-2	3.4	-	159	L	0.975
"	0.95	-	-	-1.6	2.7	-	144	L	0.970
"	0.95	-	-	-	-	-	183	L	0.95
"	0.95	-	-	-2	3.4	-	188	L	0.975
"	0.9	-	-	-1.9	3.2	-	175	L	0.923
"	0.95	-	-	-	-	-	172	L	0.95
"	0.9	-	-	-1.5	2.6	-	180	L	0.918
"	0.9	-	-	-1.2	2.1	-	171	L	0.914
"	0.94	-30	-	-1.6	2.7	-	181	L	0.960
"	0.95	-	-	-	-	-	180	L	0.95
"	0.95	-	-	-	-	-	176	L	0.95
"	0.95	-	-	-	-	-	175	L	0.95
"	0.95	-	-	-1.85	3.1	-	177	L	0.973
"	0.92	-	-	-	-	-	180	L	0.92
"	0.92	-	-	-2	3.4	-	161	L	0.944
"	0.9	-	-	-1.8	3.1	-	179	L	0.921
"	0.95	-	-	-2	3.4	-	153	L	0.975
"	0.95	-	-	-1.8	3.1	-	202	L	0.973
"	0.9	-	-	-1.9	3.2	-	-		0.923
"	0.92	-	-	-1.3	2.2	-	180	L	0.936
"	0.9	-	-	-1.5	2.6	-	203	L	0.918
"	0.95	-	-	-1.7	2.9	-	188	L	0.971
"	0.95	-	-	-1.5	2.6	-	187	L	0.969
"	0.95	-	-	-1.5	2.6	-	180	L	0.969
"	0.93	-	-	-2	3.4	-	-		0.955
"	0.95	-	-	-	-	-	173	L	0.95
"	0.95	-	-	-1.5	2.6	-	182	L	0.969
"	0.96	-	-	-1.4	2.4	-	166	L	0.978
"	0.92	-	-	-1.55	2.6	-	163	L	0.939
"	-	-	-	-	-	-	186	L	-

V1 FLUID INCLUSION DATA

SAMPLE	F	Tfm	Tmh	Tml	S	TsH	Th	to	D
J11PB	-	-	-	-	-	-	211	L	-
"	-	-	-	-	-	-	92	L	-
"	-	-	-	-	-	-	196	L	-
"	-	-	-	-	-	-	180	L	-
"	-	-	-	-	-	-	154	L	-
"	-	-	-	-	-	-	234	L	-
"	-	-	-	-	-	-	178	L	-
"	-	-	-	-	-	-	235	L	-
"	-	-	-	-	-	-	194	L	-
"	-	-	-	-	-	-	188	L	-
"	-	-	-	-	-	-	142	L	-
"	-	-	-	-	-	-	230	L	-
"	-	-	-	-	-	-	237	L	-
"	-	-	-	-	-	-	332	L	-
"	-	-	-	-	-	-	172	L	-
"	-	-	-	-	-	-	115	L	-
"	-	-	-	-	-	-	196	L	-
"	-	-	-	-	-	-	198	L	-
"	-	-	-	-	-	-	182	L	-
"	-	-	-	-	-	-	230	L	-
"	-	-	-	-	-	-	153	L	-
"	-	-	-	-	-	-	158	L	-
"	-	-	-	-	-	-	311	L	-
"	-	-	-	-	-	-	177	L	-
"	-	-	-	-	-	-	177	L	-
"	-	-	-	-	-	-	177	L	-
"	-	-	-	-	-	-	281	L	-
"	-	-	-	-	-	-	176	L	-
"	-	-	-	-	-	-	181	L	-
"	-	-	-	-	-	-	195	L	-
"	-	-	-	-	-	-	351	L	-
"	-	-	-	-	-	-	189	L	-
"	-	-	-	-	-	-	181	L	-
"	-	-	-	-	-	-	146	L	-
J53JR	0.92	-20	-	-0.8	1.4	-	161	L	0.930
"	0.95	-	-	-0.9	1.6	-	145	L	0.962
"	0.92	-	-	-1	1.7	-	152	L	0.932
"	0.95	-	-	-1.1	1.9	-	122	L	0.964
"	0.98	-	-	-1.4	2.4	-	183	L	0.998
"	0.9	-	-	-1.5	2.6	-	232	L	0.918
"	0.93	-	-	-2.3	3.9	-	153	L	0.959
"	0.96	-	-	-0.8	1.4	-	138	L	0.970
"	0.98	-	-	-0.9	1.6	-	162	L	0.992
"	0.94	-	-	-0.9	1.6	-	150	L	0.952
"	0.95	-	-	-1.25	2.1	-	163	L	0.965
"	0.95	-	-	-2.5	4.2	-	197	L	0.981
"	0.96	-	-	-	-	-	136	L	0.96
"	0.95	-	-	-1.9	3.2	-	155	L	0.974
"	0.93	-	-	-1.2	2.1	-	152	L	0.945
"	0.95	-	-	-1	1.7	-	152	L	0.962
"	0.92	-	-	-1.3	2.2	-	142	L	0.93
"	0.96	-	-	-2	3.4	-	138	L	0.98

V2 FLUID INCLUSION DATA

F	Tfm	Tmh	Tml	S	TsH	Th	to	FCO2	TmCO2	TmC	Sclath	ThCO2	to	D CO2	D	MOL%CO2
J125LB																
0.96	-	-	-1.4	2.4	-	191	L	-	-	-	-	-		-	0.98	0.0
0.95	-	-	-	-	-	135	L	-	-	-	-	-		-	0.95	0.0
0.7	-	-	-2	3.4	-	258	L	0.3	-	5.8	-	-		-	0.72	0.0
0.6	-	-	-0.8	1.4	-	222	L	-	-	-	-	-		-	0.61	0.0
0.9	-	-	-1	1.7	-	-		-	-	-	-	-		-	0.91	0.0
0.8	-	-	-1.2	2.1	-	253	L	-	-	-	-	-		-	0.81	0.0
0.95	-	-	-	-	-	136	L	-	-	-	-	-		-	0.95	0.0
0.95	-	-	-0.65	1.1	-	138	L	-	-	-	-	-		-	0.96	0.0
0.95	-	-	-	-	-	86	L	-	-	-	-	-		-	0.95	0.0
0.9	-	-	-0.9	1.6	-	196	L	-	-	-	-	-		-	0.91	0.0
0.92	-	-	-1.1	1.9	-	148	L	-	-	-	-	-		-	0.93	0.0
0.95	-	-	-	-	-	153	L	-	-	-	-	-		-	0.95	0.0
0.8	-	-	-1.8	3.1	-	214	L	-	-	-	-	-		-	0.82	0.0
0.8	-	-	-	-	-	332	L	-	-	-	-	-		-	0.80	0.0
0.75	-	-	-1.9	3.2	-	352	L	-	-	-	-	-		-	0.77	0.0
0.8	-	-	-	-	-	326	L	-	-	-	-	-		-	0.80	0.0
0.05	-	-	-	-	-	409	L	0.95	-58.6	5.5	10	-		-	0.05	0.0
0.95	-	-	-1.6	2.7	-	178	L	-	-	-	-	-		-	0.97	0.0
0.95	-	-	-0.8	1.4	-	139	L	-	-	-	-	-		-	0.96	0.0
0.95	-	-	-0.9	1.6	-	144	L	-	-	-	-	-		-	0.96	0.0
0.7	-	-	-	-	-	308	L	0.3	-	9.2	1.7	-		-	0.70	0.0
0.9	-	-	-1.4	2.4	-	211	L	-	-	-	-	-		-	0.92	0.0
0.92	-	-	-1.2	2.1	-	222	L	-	-	-	-	-		-	0.94	0.0
0.9	-	-	-1.4	2.4	-	221	L	-	-	-	-	-		-	0.92	0.0
0.9	-	-	-1.7	2.9	-	220	L	-	-	-	-	-		-	0.92	0.0
0.85	-	-	-1.7	2.9	-	219	L	0.15	-	9.7	1	-		-	0.87	0.0
0.8	-	-	-1	1.7	-	216	L	-	-	-	-	-		-	0.81	0.0
0.8	-	-	-1.25	2.1	-	231	L	-	-	-	-	-		-	0.81	0.0
0.6	-	-	-1.15	2	-	241	L	-	-	-	-	-		-	0.61	0.0
0.96	-	-	-1.3	2.2	-	128	L	-	-	-	-	-		-	0.98	0.0
0.6	-	-	-	-	-	286	L	0.4	-58.4	9.5	1.2	-		-	0.60	0.0
0.5	-	-	-	-	-	281	L	-	-	-	-	-		-	0.50	0.0
0.55	-	-	-	-	-	327	L	0.45	-	9.8	0.8	26.9	V	0.27	0.67	8.3
0.45	-	-	-	-	-	350	M	0.55	-58.5	9.4	1.4	26.7	V	0.26	0.59	11.5
0.6	-	-	-	-	-	315	L	0.4	-58.6	-	-	-		-	0.60	0.0
0.7	-	-	-	-	-	324	L	0.3	-58.5	9.3	1.5	-		-	0.70	0.0
0.9	-	-	-1.5	2.6	-	196	L	-	-	-	-	-		-	0.92	0.0
0.5	-	-	-	-	-	350	L/M	0.5	-58.6	-	-	-		-	0.50	0.0
J38LBa																
0.85	-	-	-4	6.4	-	256	L	-	-	-	-	-		-	0.89	0.0
0.9	-	-	-	-	-	291	L	-	-	-	-	-		-	0.90	0.0
0.95	-	-	-	-	-	197	L	-	-	-	-	-		-	0.95	0.0
0.5	-	-	-	-	-	-		0.5	-57.5	-	-	7.2	V	0.12	0.56	4.7
0.95	-	-	-2.2	3.7	-	211	L	-	-	-	-	-		-	0.98	0.0
0.9	-	-	-2.3	3.9	-	-		-	-	-	-	-		-	0.93	0.0
0.8	-	-	-3	4.9	-	264	L	-	-	-	-	-		-	0.83	0.0
0.9	-	-	-1.1	1.9	-	199	L	-	-	-	-	-		-	0.91	0.0
0.92	-	-	-5.1	8	-	248	L	-	-	-	-	-		-	0.98	0.0
0.9	-	-	-6.75	10.2	-	300	L	-	-	-	-	-		-	0.97	0.0
0.97	-	-0.9	-7.4	11	-	190	L	-	-	-	-	-		-	1.06	0.0
0.85	-	-	-	-	-	354	L	-	-	-	-	-		-	0.85	0.0
0.55	-	-	-	-	-	373	V	0.55	-	7.4	5.2	-		-	0.55	0.0
0.8	-	-	-3.7	6	-	352	L	-	-	-	-	-		-	0.84	0.0
0.5	-	-	-	-	-	380	L/M	0.5	-	5.7	8.4	-		-	0.50	0.0
0.95	-	-	-3.2	5.2	-	227	L	-	-	-	-	-		-	0.99	0.0
0.6	-	-	-	-	-	357	L	0.6	-	6.4	6.9	-		-	0.60	0.0
0.75	-	-	-	-	-	354	L	0.75	-	6.1	7.6	-		-	0.75	0.0
0.8	-	-	-	-	-	-		0.8	-	7.4	5.2	-		-	0.80	0.0
0.85	-	-	-4.4	7	-	-		-	-	-	-	-		-	0.90	0.0
0.65	-	-	-	-	-	392	M	0.65	-	5.8	8.1	-		-	0.65	0.0
0.8	-	-	-1.8	3.1	-	254	L	-	-	-	-	-		-	0.82	0.0
0.75	-	-	-	-	-	334	L	-	-	-	-	-		-	0.75	0.0
0.65	-	-	-	-	-	341	L	0.65	-	7	5.6	-		-	0.65	0.0
0.97	-	-	-1.95	3.3	-	183	L	-	-	-	-	-		-	1.00	0.0
0.6	-	-	-2	3.4	-	328	L	-	-	-	-	-		-	0.62	0.0
0.9	-	-	-1.8	3.1	-	209	L	-	-	-	-	-		-	0.92	0.0
0.9	-	-	-	-	-	222	L	-	-	-	-	-		-	0.90	0.0
0.9	-	-	-1.6	2.7	-	208	L	-	-	-	-	-		-	0.92	0.0
0.6	-	-	-	-	-	363	L	0.6	-	8.3	3.3	-		-	0.60	0.0
0.9	-	-	-2	3.4	-	237	L	-	-	-	-	-		-	0.92	0.0
J40LB																
0.85	-	-	-2.4	4	-	274	L	-	-	-	-	-		-	0.88	0.0
0.92	-	-	-2.3	3.9	-	201	L	-	-	-	-	-		-	0.95	0.0
0.95	-	-	-1.7	2.9	-	191	L	-	-	-	-	-		-	0.97	0.0
0.95	-	-	-	-	-	213	L	-	-	-	-	-		-	0.95	0.0
0.88	-	-	-2	3.4	-	226	L	-	-	-	-	-		-	0.90	0.0
0.95	-	-	-1.9	3.2	-	206	L	-	-	-	-	-		-	0.97	0.0
0.9	-	-	-1.6	2.7	-	202	L	-	-	-	-	-		-	0.92	0.0
0.9	-	-	-1.8	3.1	-	193	L	-	-	-	-	-		-	0.92	0.0
0.95	-	-	-0.4	0.7	-	182	L	-	-	-	-	-		-	0.96	0.0
0.9	-	-	-1.7	2.9	-	241	L	-	-	-	-	-		-	0.92	0.0
0.05	-	-	-	-	-	-		0.95	-60	-	-	-12.3	V	0.06	0.11	31.8
0.95	-	-	-1.7	2.9	-	191	L	-	-	-	-	-		-	0.97	0.0
0.95	-	-	-0.4	0.7	-	198	L	-	-	-	-	-		-	0.96	0.0
0.9	-	-	-1.35	2.3	-	212	L	-	-	-	-	-		-	0.92	0.0
0.95	-	-	-1.4	2.4	-	209	L	-	-	-	-	-		-	0.97	0.0
0.92	-	-	-1.5	2.6	-	218	L	-	-	-	-	-		-	0.94	0.0
J48BR																
0.9	-	-	-2.8	4.6	-	232	L	-	-	-	-	-		-	0.93	0.0
0.92	-24	-	-	-	-	198	L	-	-	-	-	-		-	0.92	0.0
0.9	-	-	-	-	-	237	L	-	-	-	-	-		-	0.90	0.0
0.8	-	-	-	-	-	242	L	-	-	-	-	-		-	0.80	0.0
0.8	-	-	-	-	-	272	L	-	-	-	-	-		-	0.80	0.0

V2 FLUID INCLUSION DATA

F	Tfm	Tmh	Tml	S	TsH	Th	to	FCO2	TmCO2	TmC	Sclath	ThCO2	to	D CO2	D	MOL%CO2
0.95	-	-	-	-	-	185	L	-	-	-	-	-		-	0.95	0.0
0.8	-	-	-3.7	6	-	195	L	-	-	-	-	-		-	0.84	0.0
0.8	-	-	-3.1	5.1	-	209	L	-	-	-	-	-		-	0.83	0.0
0.82	-	-	-4.1	6.6	-	239	L	-	-	-	-	-		-	0.86	0.0
0.9	-	-	-3	4.9	-	221	L	-	-	-	-	-		-	0.94	0.0
0.8	-	-	-3.2	5.2	-	234	L	-	-	-	-	-		-	0.83	0.0
0.94	-	-	-1.9	3.2	-	192	L	-	-	-	-	-		-	0.96	0.0
0.85	-	-	-2.7	4.5	-	262	L	-	-	-	-	-		-	0.88	0.0
0.8	-	-	-2.6	4.3	-	219	L	-	-	-	-	-		-	0.83	0.0
0.9	-	-	-3.5	5.7	-	181	L	-	-	-	-	-		-	0.94	0.0
0.8	-	-	-3.5	5.7	-	235	L	-	-	-	-	-		-	0.84	0.0
0.9	-	-	-2.7	4.5	-	218	L	-	-	-	-	-		-	0.93	0.0
0.95	-	-	-0.7	1.2	-	144	L	-	-	-	-	-		-	0.96	0.0
0.9	-	-	-3.9	6.3	-	216	L	-	-	-	-	-		-	0.95	0.0
0.95	-	-	-0.8	1.4	-	164	L	-	-	-	-	-		-	0.96	0.0
0.9	-	-	-1.9	3.2	-	199	L	-	-	-	-	-		-	0.92	0.0
0.9	-	-	-1.8	3.1	-	189	L	-	-	-	-	-		-	0.92	0.0
0.85	-	-	-1.8	3.1	-	191	L	-	-	-	-	-		-	0.87	0.0
0.8	-	-	-3.7	6	-	234	L	-	-	-	-	-		-	0.84	0.0
0.9	-	-	-2.2	3.7	-	218	L	-	-	-	-	-		-	0.93	0.0
0.9	-	-	-4	6.4	-	217	L	-	-	-	-	-		-	0.95	0.0
0.95	-	-	-2.8	4.6	-	184	L	-	-	-	-	-		-	0.98	0.0
0.82	-	-	-2.9	4.8	-	220	L	-	-	-	-	-		-	0.85	0.0
0.95	-	-	-	-	-	-		-	-	-	-	-		-	0.95	0.0
0.9	-	-	-4.4	7	-	236	L	-	-	-	-	-		-	0.95	0.0
0.95	-	-	-2	3.4	-	227	L	-	-	-	-	-		-	0.98	0.0
0.94	-	-	-3	4.9	-	231	L	-	-	-	-	-		-	0.98	0.0
0.8	-	-	-	-	-	240	L	-	-	-	-	-		-	0.80	0.0
0.8	-	-	-4	6.4	-	207	L	-	-	-	-	-		-	0.84	0.0
0.9	-	-	-2.9	4.8	-	215	L	-	-	-	-	-		-	0.93	0.0
0.85	-	-	-1.9	3.2	-	196	L	-	-	-	-	-		-	0.87	0.0
0.9	-	-	-	-	-	180	L	-	-	-	-	-		-	0.90	0.0
0.9	-	-	-2.7	4.5	-	210	L	-	-	-	-	-		-	0.93	0.0
0.95	-	-	-1.9	3.2	-	224	L	-	-	-	-	-		-	0.97	0.0
0.9	-	-	-3.5	5.7	-	220	L	-	-	-	-	-		-	0.94	0.0
0.85	-	-	-3.3	5.4	-	-		-	-	-	-	-		-	0.89	0.0
0.9	-	-	-1.4	2.4	-	199	L	-	-	-	-	-		-	0.92	0.0
0.96	-	-	-2	3.4	-	200	L	-	-	-	-	-		-	0.99	0.0
0.95	-	-	-1.9	3.2	-	-		-	-	-	-	-		-	0.97	0.0
0.95	-	-	-0.9	1.6	-	173	L	-	-	-	-	-		-	0.96	0.0
0.9	-	-	-1.2	2.1	-	182	L	-	-	-	-	-		-	0.92	0.0
J50BR																
0.9	-	-	-1.4	2.4	-	197	L	-	-	-	-	-		-	0.92	0.0
0.88	-	-	-0.9	1.6	-	278	L	-	-	-	-	-		-	0.89	0.0
0.95	-	-	-	-	-	209	L	-	-	-	-	-		-	0.95	0.0
0.9	-	-	-2.3	3.9	-	200	L	-	-	-	-	-		-	0.93	0.0
0.88	-	-	-2.4	4	-	194	L	-	-	-	-	-		-	0.91	0.0
0.93	-	-	-0.8	1.4	-	203	L	-	-	-	-	-		-	0.94	0.0
0.94	-	-	-2.3	3.9	-	193	L	-	-	-	-	-		-	0.97	0.0
0.95	-	-	-2.3	3.9	-	207	L	-	-	-	-	-		-	0.98	0.0
0.9	-	-	-0.8	1.4	-	223	L	-	-	-	-	-		-	0.91	0.0
0.9	-	-	-0.4	0.7	-	261	L	-	-	-	-	-		-	0.91	0.0
0.85	-	-	-2.6	4.3	-	291	L	-	-	-	-	-		-	0.88	0.0
J99BR																
0.2	-	-	-	-	-	310	V	0.4	-57.1	-	-	27.4	V	0.29	0.32	19.2
0.5	-	-	-	-	-	315	V	0.6	-57.1	-	-	25.6	V	0.25	0.65	10.9
0.1	-	-	-	-	-	-		0.2	-57.2	-	-	28.4	V	0.3	0.16	19.7
0.1	-	-	-	-	-	-		0.1	-57.2	-	-	-		-	0.10	0.0
0.1	-	-	-	-	-	-		0.5	-57.3	-	-	27.2	V	0.28	0.24	36.4
0.15	-	-	-	-	-	-		0.5	-57.3	-	-	28.3	V	0.3	0.30	29.0
0.8	-	-	-	-	-	145	L	-	-	-	-	-		-	0.80	0.0
0.9	-	-	-2.8	4.6	-	207	L	-	-	-	-	-		-	0.93	0.0
0.96	-	-	-2.6	4.3	-	185	L	-	-	-	-	-		-	0.99	0.0
0.8	-	-	-1.8	3.1	-	178	L	-	-	-	-	-		-	0.82	0.0
0.9	-	-	-	-	-	166	L	-	-	-	-	-		-	0.90	0.0
0.95	-	-	-1.4	2.4	-	146	L	-	-	-	-	-		-	0.97	0.0
0.9	-	-	-2.1	3.5	-	193	L	-	-	-	-	-		-	0.93	0.0
0.9	-	-	-	-	-	204	L	-	-	-	-	-		-	0.90	0.0
0.85	-	-	-1	1.7	-	204	L	-	-	-	-	-		-	0.86	0.0
0.9	-	-	-2.2	3.7	-	224	L	-	-	-	-	-		-	0.93	0.0
0.6	-	-	-	-	-	366	L	0.65	-	4.4	9.7	-		-	0.60	0.0
0.3	-	-	-	-	-	376	V	-	-	-	-	-		-	0.30	0.0
0.6	-	-	-	-	-	401	V	-	-	-	-	-		-	0.60	0.0
0.15	-	-	-	-	-	-		0.5	-57.4	6.7	6	-		-	0.15	0.0
0.95	-	-	-2.2	3.7	-	220	L	-	-	-	-	-		-	0.98	0.0
0.9	-	-	-2.7	4.5	-	296	L	-	-	-	-	-		-	0.93	0.0
0.95	-	-	-	-	-	311	L	-	-	-	-	-		-	0.95	0.0
0.95	-	-	-2.6	4.3	-	216	L	-	-	-	-	-		-	0.98	0.0
0.95	-	-	-2.4	4	-	183	L	-	-	-	-	-		-	0.98	0.0
0.7	-	-	-	-	-	340	L	-	-	-	-	-		-	0.70	0.0
0.95	-	-	-2.4	4	-	261	L	-	-	-	-	-		-	0.98	0.0

V3 FLUID INCLUSION DATA

Type	F	Tfm	Tmh	Tml	S	TsH	S hal	TsS	Th	to	FCO2	TmCO2	TmC	Sclath	ThCO2	to	D CO2	D	MOL%CO2
D3CZ1																			
1	0.9	-	-21.7	-8.1	11.8	-	-	-	263	L	0.1	-	-	-	-		-	0.98	0.0
1	0.55	-	-	-	-	-	-	-	358	L	-	-	8.1	-	-		-	0.55	0.0
1	0.8	-	-	-	-	-	-	-	317	L	0.2	-	6.1	7.6	-		-	0.8	0.0
1	0.9	-	-	-	-	-	-	-	231	L	-	-	-	-	-		-	0.9	0.0
1	0.6	-	-	-	-	-	-	-	352	L	-	-58.5	9.3	-	-		-	0.6	0.0
1	0.75	-	-	-	-	-	-	-	313	L	-	-	9.9	-	-		-	0.75	0.0
1	0.8	-	-	-	-	-	-	-	336	L	0.2	-	5.6	8.4	-		-	0.8	0.0
1	0.7	-	-	-	-	-	-	-	328	L	-	-	9	-	-		-	0.7	0.0
1	0.9	-21	-	-10.4	14.4	-	-	-	256	L	-	-	-	-	-		-	1	0.0
1	0.65	-	-	-	-	-	-	-	354	L	-	-	8	-	-		-	0.65	0.0
1	0.7	-	-	-	-	-	-	-	307	L	-	-	9	-	-		-	0.7	0.0
1	0.8	-	-	-8.6	12.4	-	-	-	338	L	-	-	-	-	-		-	0.88	0.0
1	0.6	-	-	-	-	-	-	-	414	L	-	-58.6	-	-	-		-	0.6	0.0
1	0.95	-	-	-1.9	3.2	-	-	-	140	L	-	-	-	-	-		-	0.97	0.0
1	0.5	-	-	-	-	-	-	-	355	L	-	-	8.2	-	-		-	0.5	0.0
1	0.8	-	-	-	-	-	-	-	307	L	-	-	-	-	-		-	0.8	0.0
2	0.4	-	-	-	-	-	-	-	409	V	0.6	-59.4	6.1	7.6	14.4	V	0.16	0.5	8.9
2	0.4	-	-	-	-	-	-	-	-		0.6	-59	-	-	-		-	0.4	0.0
2	0.55	-	-	-	-	-	-	-	341	V	0.2	-59.2	-	-	-		-	0.55	0.0
2	0.3	-	-	-	-	-	-	-	271	V	-	-	-	-	-		-	0.3	0.0
2	0.35	-	-	-	-	-	-	-	370	V	0.65	-59.1	1.5	14.1	-		-	0.35	0.0
2	0.4	-	-	-	-	-	-	-	385	V	0.6	-	-	-	-		-	0.4	0.0
2	0.4	-	-	-	-	-	-	-	-		0.6	-59.3	-	-	-		-	0.4	0.0
2	0.2	-	-	-	-	-	-	-	-		0.8	-59.8	-	-	17.4	V	0.18	0.34	23.1
2	0.2	-	-	-	-	-	-	-	-		0.8	-59	-	-	-		-	0.2	0.0
2	0.4	-	-	-	-	-	-	-	-		0.6	-57.9	6.2	-	-		-	0.4	0.0
3	0.95	-	-	-24.5	25.7	-	-	-	228	L	-	-	-	-	-		-	1.15	0.0
3	0.9	-58	-	-19.5	22.3	-	-	-	246	L	0.1	-	-2	18	-		-	1.06	0.0
3	0.95	-	-	-	-	-	-	-	216	L	-	-	-	-	-		-	0.95	0.0
3	0.95	-	-	-22.8	24.6	302	38	70	234	L	-	-	-	-	-		-	1.14	0.0
3	0.92	-	-	-	-	-	-	-	226	L	-	-	-	-	-		-	0.92	0.0
3	0.95	-	-	-	-	-	-	-	212	L	-	-	-	-	-		-	0.95	0.0
3	0.9	-	-	-	-	-	-	-	250	L	-	-	-	-	-		-	0.9	0.0
4	0.1	-	-	-	-	-	-	-	-		0.9	-59.2	-	-	-		-	0.1	0.0
6	0.7	-	-	-	-	-	-	-	370	L	0.3	-59.5	-	-	20.4	L	0.77	0.7	16.8
6	0.55	-	-	-	-	-	-	-	370	L	0.45	-59.4	-	-	20.1	L	0.78	0.55	41.9
D4GR1																			
1	0.9	-	-	-1.7	2.9	-	-	-	178	L	-	-	-	-	-		-	0.92	0.0
1	0.7	-	-	-	-	-	-	-	358	L	-	-	-	-	-		-	0.7	0.0
1	0.6	-	-	-	-	-	-	-	416	d	0.4	-60.3	8.4	3.5	-		-	0.6	0.0
1	0.6	-	-	-	-	-	-	-	408	M	0.4	-	7.9	4.3	-		-	0.6	0.0
1	0.8	-	-	-7.2	10.7	-	-	-	399	L	-	-	-	-	-		-	0.87	0.0
1	0.5	-	-	-	-	-	-	-	389	L	0.5	-	6.6	6.8	-		-	0.5	0.0
1	0.6	-	-	-9	12.9	-	-	-	386	M	0.4	-	6.1	7.6	-		-	0.66	0.0
1	0.7	-	-	-7.6	11.2	-	-	-	344	L	-	-	-	-	-		-	0.76	0.0
1	0.95	-	-	-16	19.6	-	-	-	200	L	-	-	-	-	-		-	1.1	0.0
1	0.6	-	-	-	-	-	-	-	379	L	-	-	-	-	-		-	0.6	0.0
1	0.97	-59	-	-11.8	15.8	-	-	-	152	L	-	-	-	-	-		-	1.09	0.0
1	0.7	-	-	-	-	-	-	-	384	L	-	-	-	-	-		-	0.7	0.0
1	0.8	-	-	-	-	-	-	-	371	L	-	-	-	-	-		-	0.8	0.0
1	0.8	-	-	-6.8	10.2	-	-	-	340	L	-	-	-	-	-		-	0.87	0.0
1	0.95	-	-	-	-	-	-	-	102	L	-	-	-	-	-		-	0.95	0.0
1	0.75	-	-	-5.2	8.1	-	-	-	375	L	0.25	-	7.5	5.2	-		-	0.8	0.0
1	0.7	-	-	-	-	-	-	-	418	L/M	-	-	-	-	-		-	0.7	0.0
1	0.8	-	-	-	-	-	-	-	368	L	-	-	-	-	-		-	0.8	0.0
1	0.95	-	-	-15.2	19	-	-	-	155	L	-	-	-	-	-		-	1.09	0.0
1	0.8	-	-	-6.5	9.9	-	-	-	330	L	0.2	-	1.6	14	-		-	0.86	0.0
1	0.6	-	-	-	-	-	-	-	392	L	-	-	-	-	-		-	0.6	0.0
1	0.6	-	-	-2.9	4.8	-	-	-	-		-	-	-	-	-		-	0.62	0.0
1	0.95	-	-	-15.5	19.2	-	-	-	193	L	-	-	-	-	-		-	1.1	0.0
1	0.8	-	-	-	-	-	-	-	338	L	-	-	-	-	-		-	0.8	0.0
1	0.6	-	-	-	-	-	-	-	390	L	-	-	-	-	-		-	0.6	0.0
1	0.6	-	-	-	-	-	-	-	412	M	-	-	-	-	-		-	0.6	0.0
1	0.95	-62	-21.6	-15.4	19.1	-	-	-	154	L	-	-	-	-	-		-	1.1	0.0
1	0.8	-	-	-	-	-	-	-	350	L	-	-	-	-	-		-	0.8	0.0
1	0.95	-	-	-15.7	19.4	-	-	-	182	L	-	-	-	-	-		-	1.1	0.0
1	0.95	-	-	-16.3	19.9	-	-	-	153	L	-	-	-	-	-		-	1.1	0.0
1	0.6	-	-	-	-	-	-	-	398	L	0.4	-59.7	6.6	6.8	-		-	0.6	0.0
1	0.8	-	-	-6.3	9.6	-	-	-	336	L	-	-	-	-	-		-	0.86	0.0
1	0.7	-	-	-7.1	10.6	-	-	-	367	L	0.2	-	2.1	13.4	-		-	0.76	0.0
1	0.6	-	-	-9.2	13.1	-	-	-	412	L	0.4	-	2.4	13	-		-	0.66	0.0
2	0.2	-	-	-	-	-	-	-	-		0.8	-63.7	-	-	-		-	0.2	0.0
2	0.5	-	-	-	-	-	-	-	411	V	0.5	-	5	9.3	-		-	0.5	0.0
2	0.5	-	-	-	-	-	-	-	418	V	0.5	-	5.2	8.8	-		-	0.5	0.0
2	0.5	-	-	-	-	-	-	-	400	V	0.5	-	5.5	8.3	-		-	0.5	0.0
2	0.5	-	-	-	-	-	-	-	470	V	0.5	-	5.7	8.4	-		-	0.5	0.0
2	0.4	-	-	-	-	-	-	-	445	V	0.6	-	4.6	10.1	-		-	0.4	0.0
2	0.4	-	-	-	-	-	-	-	352	V	0.6	-	9.7	0.8	-		-	0.4	0.0
2	0.55	-	-	-	-	-	-	-	392	V/M	0.4	-	8.1	4	-		-	0.55	0.0
2	0.3	-	-	-	-	-	-	-	361	V	-	-	-	-	-		-	0.3	0.0
2	0.2	-	-	-	-	-	-	-	470	V	-	-	-	-	-		-	0.2	0.0
2	0.5	-	-	-	-	-	-	-	337	V	0.5	-	8.8	2.8	-		-	0.5	0.0
2	0.4	-	-	-	-	-	-	-	327	V	0.6	-	9.5	1.3	-		-	0.4	0.0

V3 FLUID INCLUSION DATA

Type	F	Tfm	Tmh	Tml	S	TsH	S hal	TsS	Th	to	FCO2	TmCO2	TmC	Sclath	ThCO2	to	D CO2	D	MOL%CO2
2	0.55	-	-	-	-	-	-	-	505	V	0.4	-	5.1	9.1	-		-	0.55	0.0
2	0.55	-	-	-10.7	14.7	-	-	-	458	V	0.35	-	6.7	6.7	6.3	V	0.12	0.66	3.0
2	0.5	-	-	-	-	-	-	-	393	V	-	-	-	-	-		-	0.5	0.0
2	0.3	-	-	-	-	-	-	-	344	V	0.7	-62.1	8.2	3.8	-18.4	V	0.04	0.33	3.7
2	0.5	-	-	-	-	-	-	-	323	V	0.5	-	9.6	1.2	-		-	0.5	0.0
3	0.95	-	-9	-24.4	25.6	-	-	-	-		-	-	-	-	-		-	1.14	0.0
3	0.94	-	-	-19.9	22.6	-	-	-	155	L	-	-	-	-	-		-	1.11	0.0
3	0.95	-	-	-24.9	25.9	-	-	-	131	L	-	-	-	-	-		-	1.15	0.0
3	0.97	-	-23	-43.3	-	234	33	70	151	L	-	-	-	-	-		-	0.97	0.0
3	0.96	-	-	-	-	-	-	-	159	L	-	-	-	-	-		-	0.96	0.0
3	0.96	-	-	-23.4	25	-	-	-	122	L	-	-	-	-	-		-	1.15	0.0
3	0.95	-55	-18	-22.3	24.2	-	-	-	173	L	-	-	-	-	-		-	1.13	0.0
3	0.97	-74	0.2	-24.3	25.5	-	-	-	113	L	-	-	-	-	-		-	1.17	0.0
4	0.05	-	-	-	-	-	-	-	-		0.95	-61	-	-	-		-	0.05	0.0
4	0.08	-	-	-	-	-	-	-	363	V	-	-	-	-	-		-	0.08	0.0
4	0.05	-	-	-	-	-	-	-	-		0.95	-61.2	-	-	-20.2	V	0.04	0.09	23.0
4	0.05	-	-	-	-	-	-	-	-		0.95	-	-	-	-17	V	0.05	0.1	27.0
5	0.05	-	-	-	-	-	-	-	-		0.95	-59.6	-	-	22.5	V	0.22	0.26	62.6
D4GR2																			
2	0.2	-	-	-	-	-	-	-	-		0.8	-59.1	-	-	-		-	0.2	0.0
2	0.2	-	-	-	-	-	-	-	282	V	-	-	-	-	-		-	0.2	0.0
2	0.35	-	-	-	-	-	-	-	361	V	-	-	-	-	-		-	0.35	0.0
2	0.3	-	-	-	-	-	-	-	-		0.7	-58.9	-	-	12.5	M	-	0.3	0.0
2	0.2	-	-	-	-	-	-	-	-		0.8	-59.1	-	-	-		-	0.2	0.0
3	0.98	-	-	-	-	284	37	-	110	L	-	-	-	-	-		-	0.98	0.0
3	0.97	-	-	-47.4	-	237	34	82	167	L	-	-	-	-	-		-	0.97	0.0
3	0.97	-	-	-	-	296	37	-	144	L	-	-	-	-	-		-	0.97	0.0
3	0.95	-	-	-50.3	-	278	36	-	247	d	-	-	-	-	-		-	0.95	0.0
3	0.95	-	-	-45	-	-	-	-	164	L	-	-	-	-	-		-	0.95	0.0
3	0.95	-	-20.8	-	-	110	28	54	160	L	-	-	-	-	-		-	0.95	0.0
3	0.98	-	-	-	-	353	42	-	-		-	-	-	-	-		-	0.98	0.0
4	0.05	-	-	-	-	-	-	-	-		0.95	-60.3	-	-	-		-	0.05	0.0
4	0.1	-	-	-	-	-	-	-	409	V	-	-	-	-	-		-	0.1	0.0
4	0.1	-	-	-	-	-	-	-	398	V	-	-	-	-	-		-	0.1	0.0
4	0.1	-	-	-	-	-	-	-	251	V	-	-	-	-	-		-	0.1	0.0
4	0.15	-	-	-	-	-	-	-	368	V	-	-	-	-	-		-	0.15	0.0
4	0.05	-	-	-	-	-	-	-	-		0.95	-58.8	-	-	-		-	0.05	0.0
4	0.15	-	-	-	-	-	-	-	327	V	-	-	-	-	-		-	0.15	0.0
4	0.05	-	-	-	-	-	-	-	285	V	0.95	-60.9	8.5	3.4	8.9	V	0.12	0.16	50.3
4	0.1	-	-	-	-	-	-	-	-		0.9	-60.4	-	-	-		-	0.1	0.0
4	0.05	-	-	-	-	-	-	-	-		0.95	-57.8	-	-	-		-	0.05	0.0
5	0.05	-	-	-	-	-	-	-	-		0.95	-58.7	-	-	25.8	V	0.26	0.3	65.6
5	0.05	-	-	-	-	-	-	-	-		0.95	-58.7	-	-	26.4	V	0.26	0.3	65.6
5	0.05	-	-	-	-	-	-	-	-		0.95	-58.5	-	-	27.1	V	0.27	0.31	66.2
D4PS1																			
-	-	-	-	-	-	-	-	-	-		-	-56.8	-	-	-		-	0	ERR
-	-	-	-	-	-	-	-	-	-		-	-58	-	-	-		-	0	ERR
1	0.6	-	-	-	-	-	-	-	-		0.4	-57.8	10.6	0	8.9	L	-	0.6	0.0
1	0.7	-	-	-	-	-	-	-	-		0.3	-	-	-	9.1	L	-	0.7	0.0
1	0.7	-	-	-	-	-	-	-	-		0.3	-	8.9	2.7	-		-	0.7	0.0
1	0.7	-	-	-	-	-	-	-	-		0.3	-	6.1	7.8	-		-	0.7	0.0
1	0.85	-	-	-	-	-	-	-	279	L	-	-	-	-	-		-	0.85	0.0
1	0.65	-	-	-	-	-	-	-	-		0.35	-	-	-	11.2	L	-	0.65	0.0
2	0.5	-	-	-	-	-	-	-	180	V	0.5	-	-	-	-		-	0.5	0.0
2	0.2	-	-	-	-	-	-	-	274	V	0.8	-	-	-	-		-	0.2	0.0
2	0.2	-	-	-	-	-	-	-	285	V	0.8	-	-	-	-		-	0.2	0.0
5	0.1	-	-	-	-	-	-	-	-		0.9	-	-	-	26.7	V	0.27	0.34	50.6
5	0.1	-	-	-	-	-	-	-	297	V	0.9	-	-	-	28.5	V	0.3	0.37	52.5
5	0.15	-	-	-	-	-	-	-	318	V	0.85	-	-	-	27.3	V	0.28	0.39	39.0
6	0.05	-	-	-	-	-	-	-	-		0.95	-56.6	-	-	-		-	0.05	0.0
6	0.05	-	-	-	-	-	-	-	-		0.95	-57.8	9.8	0.4	28.8	L	0.63	0.6485	83.0
6	0.05	-	-	-	-	-	-	-	-		0.95	-57.9	-	-	30.7	L	0.54	0.563	80.8
6	0.05	-	-	-	-	-	-	-	-		0.95	-57.8	9.7	0.8	30.3	L	0.56	0.582	81.3
6	0.05	-	-	-	-	-	-	-	-		0.95	-	-	-	30.9	L	0.51	0.5345	79.9
6	0.05	-	-	-	-	-	-	-	-		0.95	-	-	-	30.6	L/M	0.55	0.5725	81.0
6	0.05	-	-	-	-	-	-	-	-		0.95	-	-	-	30.7	L	0.54	0.563	80.8
6	0.05	-	-	-	-	-	-	-	-		0.95	-57.9	-	-	30.9	L	0.51	0.5345	79.9
6	0.05	-	-	-	-	-	-	-	-		0.95	-	-	-	30.4	L	0.56	0.582	81.3
6	0.05	-	-	-	-	-	-	-	-		0.95	-57.9	9.2	2	30.8	L	0.53	0.5535	80.5
6	0.05	-	-	-	-	-	-	-	-		0.95	-	-	-	29.9	L	0.58	0.601	81.8
6	0.05	-	-	-	-	-	-	-	-		0.95	-56.7	-	-	29.9	L	0.58	0.601	81.8
6	0.05	-	-	-	-	-	-	-	-		0.95	-56.6	-	-	28.3	L	0.65	0.6675	83.5
6	0.05	-	-	-	-	-	-	-	-		0.95	-	-	-	27.2	L	0.68	0.696	84.1
6	0.05	-	-	-	-	-	-	-	-		0.95	-	-	-	30	L	0.58	0.601	81.8
6	0.05	-	-	-	-	-	-	-	-		0.95	-56.7	-	-	27.7	L	0.67	0.6865	83.9
6	0.05	-	-	-	-	-	-	-	-		0.95	-58	-	-	29.9	L	0.58	0.601	81.8
6	0.05	-	-	-	-	-	-	-	-		0.95	-	-	-	30.1	L	0.57	0.5915	81.6
6	0.2	-	-	-	-	-	-	-	236	V	0.8	-56.8	8.9	2.7	28.5	L	0.64	0.712	51.2
6	0.05	-	-	-	-	-	-	-	-		0.95	-56.7	-	-	31.3	L/M	0.47	0.4965	78.5
6	0.05	-	-	-	-	-	-	-	-		0.95	-57.8	-	-	30.2	L	0.57	0.5915	81.6
6	0.2	-	-	-	-	-	-	-	305	V	0.8	-57.9	-	-	30.4	L	0.56	0.648	47.8
6	0.05	-	-	-	-	-	-	-	-		0.95	-57.9	-	-	30.3	L	0.56	0.582	81.3
6	0.05	-	-	-	-	-	-	-	-		0.95	-57.8	-	-	30.8	L	0.53	0.5535	80.5
6	0.1	-	-	-	-	-	-	-	303	V	0.9	-	9.1	2.2	30.8	L	0.53	0.577	66.1

V3 FLUID INCLUSION DATA

Type	F	Tfm	Tmh	Tml	S	TsH	S hal	TsS	Th	to	FCO2	TmCO2	TmC	Sclath	ThCO2	to	D CO2	D	MOL%CO2
6	0.05	-	-	-	-	-	-	-	-		0.95	-	-	-	30.9	L	0.51	0.5345	79.9
6	0.05	-	-	-	-	-	-	-	-		0.95	-	-	-	27.4	L	0.68	0.696	84.1
6	0.05	-	-	-	-	-	-	-	-		0.95	-57.8	-	-	31.3	L	0.47	0.4965	78.5
6	0.05	-	-	-	-	-	-	-	-		0.95	-	-	-	27.8	L	0.67	0.6865	83.9
6	0.05	-	-	-	-	-	-	-	-		0.95	-57.9	-	-	30.3	L	0.56	0.582	81.3
6	0.05	-	-	-	-	-	-	-	-		0.95	-56.8	-	-	30	L	0.58	0.601	81.8
6	0.05	-	-	-	-	-	-	-	-		0.95	-	-	-	30.3	L	0.56	0.582	81.3
6	0.05	-	-	-	-	-	-	-	-		0.95	-56.7	-	-	28.3	L	0.65	0.6675	83.5
6	0.05	-	-	-	-	-	-	-	-		0.95	-	-	-	29.2	L	0.62	0.639	82.8
6	0.05	-	-	-	-	-	-	-	-		0.95	-58.1	-	-	29.8	L	0.59	0.6105	82.1
6	0.05	-	-	-	-	-	-	-	-		0.95	-	-	-	29.2	L	0.62	0.639	82.8
6	0.05	-	-	-	-	-	-	-	-		0.95	-57.8	-	-	30.8	L	0.53	0.5535	80.5
6	0.05	-	-	-	-	-	-	-	-		0.95	-	-	-	30.4	L	0.56	0.582	81.3
6	0.05	-	-	-	-	-	-	-	-		0.95	-	-	-	31	L	0.49	0.5155	79.2
6	0.05	-	-	-	-	-	-	-	-		0.95	-	-	-	27.2	L	0.68	0.696	84.1
6	0.05	-	-	-	-	-	-	-	-		0.95	-	-	-	29.8	L	0.59	0.6105	82.1
6	0.05	-	-	-	-	-	-	-	-		0.95	-57.9	10	0	30.7	L	0.54	0.563	80.8
6	0.1	-	-	-	-	-	-	-	280	V	0.9	-57.9	-	-	30.9	L	0.51	0.559	65.3
6	0.05	-	-	-	-	-	-	-	-		0.95	-56.6	-	-	29.9	L	0.58	0.601	81.8
6	0.05	-	-	-	-	-	-	-	-		0.95	-57.9	9.9	0.2	30.9	L	0.51	0.5345	79.9
6	0.05	-	-	-	-	-	-	-	-		0.95	-57.8	-	-	31.1	L	0.47	0.4965	78.5
6	0.05	-	-	-	-	-	-	-	-		0.95	-57.8	-	-	31.4	L	0.47	0.4965	78.5
6	0.05	-	-	-	-	-	-	-	-		0.95	-	-	-	30.5	L	0.55	0.5725	81.0
6	0.05	-	-	-	-	-	-	-	-		0.95	-	-	-	30.3	L	0.56	0.582	81.3
6	0.05	-	-	-	-	-	-	-	-		0.95	-56.7	-	-	30.3	L	0.56	0.582	81.3
D4PS2																			
1	0.85	-	-	-	-	-	-	-	283	L	-	-	-	-	-		-	0.85	0.0
1	0.9	-	-	-	-	-	-	-	215	L	-	-	-	-	-		-	0.9	0.0
1	0.92	-52	-	-6.3	9.6	-	-	-	185	L	-	-	-	-	-		-	0.99	0.0
1	0.9	-	-19.3	-7	10.5	-	-	-	245	L	-	-	-	-	-		-	0.98	0.0
1	0.9	-	-20.4	-5.9	9.1	-	-	-	212	L	-	-	-	-	-		-	0.97	0.0
1	0.9	-	-	-6.2	9.5	-	-	-			-	-	-	-	-		-	0.97	0.0
1	0.9	-	-	-6.5	9.9	-	-	-	265	L	-	-	-	-	-		-	0.97	0.0
1	0.9	-58	-20.1	-6.6	10	-	-	-	235	L	-	-	-	-	-		-	0.97	0.0
1	0.95	-33	-	-	-	-	-	-	126	L	-	-	-	-	-		-	0.95	0.0
1	0.88	-	-	-5.8	8.9	-	-	-	307	L	-	-	-	-	-		-	0.94	0.0
2	0.3	-	-	-	-	-	-	-	-		0.7	-59.6	-	-	-		-	0.3	0.0
2	0.4	-	-	-	-	-	-	-	-		0.6	-59.2	-	-	-		-	0.4	0.0
2	0.3	-	-	-	-	-	-	-	-		0.7	-60.2	-	-	-		-	0.3	0.0
4	0.1	-	-	-	-	-	-	-			0.9	-60.4	-	-	-		-	0.1	0.0
4	0.05	-	-	-	-	-	-	-	-		0.95	-61	-	-	-		-	0.05	0.0
4	0.1	-	-	-	-	-	-	-	254	V	0.9	-60.1	9	2.5	20.8	V	0.2	0.28	42.4
4	0.05	-	-	-	-	-	-	-	-		0.95	-60.1	-	-	-		-	0.05	0.0
4	0.05	-	-	-	-	-	-	-	-		0.95	-60	-	-	-		-	0.05	0.0
4	0.05	-	-	-	-	-	-	-	-		0.95	-60.6	-	-	-		-	0.05	0.0
4	0.05	-	-	-	-	-	-	-	-		0.95	-60.6	-	-	19	V	0.19	0.23	59.9
4	0.05	-	-	-	-	-	-	-	-		0.95	-60.3	-	-	18.4	V	0.18	0.22	58.8
4	0.05	-	-	-	-	-	-	-	248	V	0.95	-60.1	-	-	20.1	V	0.2	0.24	60.9
4	0.05	-	-	-	-	-	-	-	-		0.95	-59.8	-	-	-		-	0.05	0.0
4	0.1	-	-	-	-	-	-	-	-		0.9	-57.6	9.4	1.5	-		-	0.1	0.0
4	0.05	-	-	-	-	-	-	-	-		0.95	-59	-	-	-		-	0.05	0.0
4	0.05	-	-	-	-	-	-	-	-		0.95	-60.3	-	-	18.5	V	0.19	0.23	59.9
4	0.05	-	-	-	-	-	-	-	-		0.95	-57.5	-	-	-		-	0.05	0.0
4	0.05	-	-	-	-	-	-	-	-		0.95	-60.4	-	-	-		-	0.05	0.0
5	0.05	-	-	-	-	-	-	-	-		0.95	-59.5	-	-	27.8	V	0.29	0.33	67.4
5	0.05	-	-	-	-	-	-	-	-		0.95	-60	-	-	27	V	0.27	0.31	66.2
5	0.05	-	-	-	-	-	-	-	-		0.95	-57.4	-	-	27.9	V	0.29	0.33	67.4
5	0.05	-	-	-	-	-	-	-	-		0.95	-59.8	-	-	26.8	V	0.27	0.31	66.2
J145PS																			
1	0.8	-	-	-	-	-	-	-	-		0.2	-56.5	-	-	25.8	V	0.26	0.85	2.6
1	0.9	-	-	-0.6	1	-	-	-	248	L	-	-	-	-	-		-	0.91	0.0
1	0.95	-	-	-1.6	2.7	-	-	-	163	L	-	-	-	-	-		-	0.97	0.0
2	0.5	-	-	-	-	-	-	-	-		0.5	-57.2	-	-	20.8	V	0.2	0.6	7.6
5	0.5	-	-	-	-	-	-	-	447	V/d	0.5	-56.9	-	-	23	V	0.22	0.61	8.3
5	0.2	-	-	-	-	-	-	-	-		0.8	-	-	-	26.3	V	0.26	0.41	29.6
5	0.1	-	-	-	-	-	-	-	-		0.9	-56.6	-	-	26.9	V	0.27	0.34	50.6
5	0.25	-	-	-	-	-	-	-	306	V	0.75	-56.7	-	-	26.4	V	0.26	0.45	23.8
5	0.2	-	-	-	-	-	-	-	359	V	0.8	-56.7	-	-	24.4	V	0.24	0.39	28.4
6	0.1	-	-	-	-	-	-	-	-		0.9	-57	-	-	23.8	L	0.74	0.766	73.2
6	0.4	-	-	-	-	-	-	-	401	V/d	0.6	-56.9	-	-	23.7	L	0.74	0.844	31.2
J64DR								-	-										
-	-	-	-	-	-	-	-	-	-		-	-57.2	-	-	-		-	0	ERR
-	-	-	-	-	-	-	-	-	-		-	-57.3	-	-	-		-	0	ERR
-	-	-	-	-	-	-	-	-	-		-	-57.8	-	-	-		-	0	ERR
-	-	-	-	-	-	-	-	-	-		-	-58.7	-	-	-		-	0	ERR
1	0.88	-	-	-6.2	9.5	-	-	-	307	L	-	-	-	-	-		-	0.95	0.0
1	0.9	-	-	-	-	-	-	-	294	L	0.1	-	-	-	-		-	0.9	0.0
1	0.9	-	-	-7.4	11	-	-	-	318	L	-	-	-	-	-		-	0.98	0.0
1	0.92	-	-	-7.5	11.1	-	-	-	-		-	-	-	-	-		-	1	0.0
1	0.96	-	-	-	-	-	-	-	297	L	-	-	-	-	-		-	0.96	0.0
1	0.6	-	-	-	-	-	-	-	-		0.4	-58.6	-	-	-		-	0.6	0.0
2	0.3	-	-	-	-	-	-	-	336	V	0.7	-58.4	-	-	-		-	0.3	0.0
2	0.55	-	-	-	-	-	-	-	381	V	0.3	-58.3	6.7	6.2	-		-	0.55	0.0
2	0.3	-	-	-	-	-	-	-	320	V	0.7	-	-	-	-		-	0.3	0.0

V3 FLUID INCLUSION DATA

Type	F	Tfm	Tmh	Tml	S	TsH	S hal	TsS	Th	to	FCO2	TmCO2	TmC	Sclath	ThCO2	to	D CO2	D	MOL%CO2
2	0.5	-	-	-	-	-	-	-	351	V	0.5	-58.7	-	-	-		-	0.5	0.0
2	0.5	-	-	-	-	-	-	-	-		0.5	-57.5	-	-	-		-	0.5	0.0
2	0.4	-	-	-	-	-	-	-	-		0.6	-58.6	-	-	13.4	L	-	0.4	0.0
4	0.1	-	-	-	-	-	-	-	-		0.9	-58.4	-	-	-		-	0.1	0.0
4	0.05	-	-	-	-	-	-	-	-		0.95	-59.7	-	-	-7.9	V	0.07	0.12	33.7
4	0.05	-	-	-	-	-	-	-	234	V	0.95	-59.9	-	-	-0.6	M	0.09	0.14	39.1
4	0.05	-	-	-	-	-	-	-	-		-	-58	-	-	-		-	0.05	0.0
4	0.05	-	-	-	-	-	-	-	297	V	0.95	-	-	-	-		-	0.05	0.0
4	0.05	-	-	-	-	-	-	-	-		0.95	-57.8	-	-	8.6	V	0.12	0.16	50.3
5	0.9	-42	-24.8	-8.1	11.8	-	-	-	-		0.1	-	-	-	23.7	V	0.23	1	1.0
5	0.3	-	-	-	-	-	-	-	306	V	0.7	-	-	-	26.6	V/M	0.27	0.49	20.4
5	0.3	-	-	-	-	-	-	-	-		0.7	-58.4	6.3	6.9	26.1	V	0.26	0.3	38.7
6	0.05	-	-	-	-	-	-	-	-		0.95	-57.1	-	-	28.8	L/M	0.63	0.6485	83.0
6	0.4	-	-	-	-	-	-	-	-		0.6	-58.3	4.4	9.3	28.8	L	0.63	0.778	27.9
6	0.1	-	-	-	-	-	-	-	-		0.9	-57	-	-	30.1	L	0.57	0.613	67.7
6	0.1	-	-	-	-	-	-	-	264	V	0.9	-57.1	-	-	29.6	L	0.6	0.64	68.8
6	0.3	-	-	-	-	-	-	-	346	V	0.7	-57.3	-	-	28.3	M	0.65	0.755	38.3
6	0.3	-	-	-	-	-	-	-	344	V	0.7	-57.6	-	-	26.2	L	0.7	0.79	40.1
6	0.4	-	-	-	-	-	-	-	314	V	0.6	-57.8	7.2	5.5	29.9	L	0.58	0.748	26.2
6	0.1	-	-	-	-	-	-	-	-		0.9	-58.3	-	-	19.4	L	0.79	0.811	74.4
6	0.4	-	-	-	-	-	-	-	-		0.6	-58.6	5.3	8.6	25	L	0.72	0.832	30.6
6	0.2	-	-	-	-	-	-	-	324	V	0.8	-58.8	7.6	4.5	24.3	L	0.73	0.784	54.4
6	0.1	-	-	-	-	-	-	-	253	V	0.9	-57	-	-	30.1	L	0.57	0.613	67.7
6	0.4	-	-	-	-	-	-	-	362	V	0.6	-58.4	7.7	4.3	28.5	L	0.64	0.784	28.2
6	0.05	-	-	-	-	-	-	-	271	V	0.95	-57.1	-	-	29.1	L	0.62	0.639	82.8
6	0.2	-	-	-	-	-	-	-	-		0.8	-58.5	8.3	3.3	28.8	L	0.63	0.704	50.8
6	0.2	-	-	-	-	-	-	-	-		0.8	-	-	-	30.4	L	0.56	0.648	47.8
6	0.2	-	-	-	-	-	-	-	-		0.8	-58.5	-	-	26.5	L	0.7	0.76	53.4
J82PS																			
1	0.9	-	-	-9.7	13.7	-	-	-	237	L	-	-	-	-	-		-	1	0.0
1	0.94	-	-	-7.8	11.4	-	-	-	212	L	-	-	-	-	-		-	1.03	0.0
1	0.94	-	-	-10.4	14.4	-	-	-	199	L	-	-	-	-	-		-	1.05	0.0
1	0.7	-	-	-5.5	8.5	-	-	-	299	L	-	-	-	-	-		-	0.75	0.0
1	0.96	-	-	-9.1	13	-	-	-	239	L	-	-	-	-	-		-	1.06	0.0
1	0.9	-	-	-	-	-	-	-	349	L	-	-	-	-	-		-	0.9	0.0
1	0.95	-	-	-8.8	12.6	-	-	-	193	L	-	-	-	-	-		-	1.05	0.0
1	0.9	-	-	-9.9	13.9	-	-	-	240	L	-	-	-	-	-		-	1	0.0
1	0.9	-	-	-8.2	12	-	-	-	211	L	-	-	-	-	-		-	0.99	0.0
1	0.95	-	-	-9.5	13.4	-	-	-	218	L	-	-	-	-	-		-	1.05	0.0
1	0.9	-	-	-9.9	13.9	-	-	-	241	L	-	-	-	-	-		-	1	0.0
1	0.9	-	-	-9.7	13.7	-	-	-	227	L	-	-	-	-	-		-	1	0.0
1	0.9	-	-	-9.6	13.5	-	-	-	178	L	-	-	-	-	-		-	1	0.0
1	0.95	-	-	-	-	-	-	-	159	L	-	-	-	-	-		-	0.95	0.0
1	0.7	-	-	-	-	-	-	-	248	L	-	-	-	-	-		-	0.7	0.0
1	0.9	-25	-	-7.4	11	-	-	-	299	L	-	-	-	-	-		-	0.98	0.0
1	0.9	-	-	-	-	-	-	-	229	L	-	-	-	-	-		-	0.9	0.0
1	0.96	-	-	-9.7	13.6	-	-	-	-		-	-	-	-	-		-	1.06	0.0
2	0.6	-	-	-	-	-	-	-	-		0.4	-57.1	-	-	-		-	0.6	0.0
2	0.2	-	-	-	-	-	-	-	-		0.3	-56.9	-	-	8.9	V	0.12	0.24	6.7
2	0.4	-	-	-	-	-	-	-	391	V	0.6	-58.2	6.6	6.9	-		-	0.4	0.0
2	0.6	-	-	-	-	-	-	-	-		0.4	-58.2	-	-	-		-	0.6	0.0
3	0.95	-	-	-	-	279	37	-	217	L	-	-	-	-	-		-	0.95	0.0
3	0.95	-	-	-	-	251	35	-	-		-	-	-	-	-		-	0.95	0.0
4	0.05	-	-	-	-	-	-	-	-		0.95	-57.1	-	-	-		-	0.05	0.0
4	0.05	-	-	-	-	-	-	-	-		0.95	-57.7	-	-	-		-	0.05	0.0
4	0.05	-	-	-	-	-	-	-	311	V	0.95	-56.8	-	-	10	V	0.13	0.17	52.1
4	0.1	-	-	-	-	-	-	-	-		0.9	-56.8	-	-	-		-	0.1	0.0
4	0.2	-	-	-	-	-	-	-	270	V	0.8	-	-	-	-		-	0.2	0.0
4	0.05	-	-	-	-	-	-	-	-		0.95	-57.5	-	-	-		-	0.05	0.0
4	0.2	-	-	-	-	-	-	-	278	V	0.8	-57.1	-	-	-		-	0.2	0.0
4	0.05	-	-	-	-	-	-	-	299	V	0.95	-	-	-	-		-	0.05	0.0
4	0.05	-	-	-	-	-	-	-	262	V	0.95	-	-	-	-		-	0.05	0.0
4	0.1	-	-	-	-	-	-	-	-		0.9	-57.6	-	-	-		-	0.1	0.0
4	0.1	-	-	-	-	-	-	-	-		0.9	-57.2	-	-	-		-	0.1	0.0
4	0.05	-	-	-	-	-	-	-	197	V	0.95	-57.1	-	-	-		-	0.05	0.0
4	0.1	-	-	-	-	-	-	-	313	V	0.9	-57.5	-	-	-		-	0.1	0.0
4	0.05	-	-	-	-	-	-	-	221	V	0.95	-58.4	-	-	-		-	0.05	0.0
5	0.05	-	-	-	-	-	-	-	-		0.95	-	-	-	26.8	V	0.27	0.31	66.2
5	0.3	-	-	-	-	-	-	-	263	V	0.7	-57.1	-	-	25.3	V	0.25	0.48	19.0
5	0.05	-	-	-	-	-	-	-	-		0.95	-57.8	-	-	25.3	V	0.25	0.29	64.9
5	0.1	-	-	-	-	-	-	-	-		0.9	-	-	-	30.1	V	0.35	0.42	55.1
5	0.05	-	-	-	-	-	-	-	-		0.95	-57.3	-	-	25.2	V	0.25	0.29	64.9
5	0.05	-	-	-	-	-	-	-	251	V	0.95	-57.1	-	-	29	V	0.31	0.34	72.6
5	0.05	-	-	-	-	-	-	-	-		0.95	-57.6	-	-	26.1	V	0.26	0.3	65.6
5	0.05	-	-	-	-	-	-	-	-		0.95	-57.2	-	-	25.6	V	0.25	0.29	64.9
5	0.05	-	-	-	-	-	-	-	-		0.95	-56.9	-	-	28.7	V	0.3	0.34	67.9
5	0.05	-	-	-	-	-	-	-	-		0.95	-57.9	-	-	22.5	V/M	0.22	0.26	62.6
5	0.05	-	-	-	-	-	-	-	-		0.95	-56.8	-	-	30.8	V	0.41	0.44	75.9
5	0.05	-	-	-	-	-	-	-	-		0.95	-57.4	-	-	24.4	V	0.24	0.28	64.2
5	0.1	-	-	-	-	-	-	-	257	V	0.9	-56.8	-	-	29.6	V	0.33	0.4	54.1
5	0.1	-	-	-	-	-	-	-	-		0.9	-57.7	-	-	21.8	V	0.21	0.29	43.4
5	0.05	-	-	-	-	-	-	-	-		0.95	-56.8	-	-	30.6	V	0.39	0.42	75.4
5	0.05	-	-	-	-	-	-	-	-		0.95	-	-	-	30.6	M/V	0.39	0.42	75.4
5	0.05	-	-	-	-	-	-	-	-		0.95	-57.5	-	-	27.8	V	0.29	0.33	67.4

V3 FLUID INCLUSION DATA

Type	F	Tfm	Tmh	Tml	S	TsH	S hal	TsS	Th	to	FCO2	TmCO2	TmC	Sclath	ThCO2	to	D CO2	D	MOL%CO2
6	0.05	-	-	-	-	-	-	-	-		0.95	-57.9	-	-	21.2	L	0.77	0.7815	85.7
6	0.05	-	-	-	-	-	-	-	-		0.95	-	-	-	30.6	M/L	0.55	0.5725	81.0
6	0.05	-	-	-	-	-	-	-	185	V	0.95	-57	-	-	29.8	L	0.59	0.6105	82.1
6	0.05	-	-	-	-	-	-	-	-		0.95	-57.9	-	-	22.6	L	0.75	0.7625	85.4
6	0.05	-	-	-	-	-	-	-	-		0.95	-57.3	-	-	29	L	0.63	0.6485	83.0
6	0.05	-	-	-	-	-	-	-	-		0.95	-57.3	-	-	28.3	L	0.65	0.6675	83.5
6	0.2	-	-	-	-	-	-	-	-		0.8	-57.8	-	-	22.9	L	0.75	0.8	55.1
6	0.05	-	-	-	-	-	-	-	-		0.95	-57.7	-	-	23.9	L	0.74	0.753	85.2
6	0.05	-	-	-	-	-	-	-	-		0.95	-56.5	-	-	31.1	L/M	0.47	0.4965	78.5
6	0.1	-	-	-	-	-	-	-	295	V	0.9	-57.5	-	-	26.5	L	0.7	0.73	72.0
6	0.05	-	-	-	-	-	-	-	-		0.95	-57.7	-	-	24.2	L	0.73	0.7435	85.0
6	0.05	-	-	-	-	-	-	-	-		0.95	-57.2	-	-	29.3	L	0.61	0.6295	82.6
6	0.05	-	-	-	-	-	-	-	-		0.95	-56.9	-	-	30.7	L	0.54	0.563	80.8
6	0.2	-	-	-	-	-	-	-	-		0.8	-57.2	-	-	29	L	0.63	0.704	50.8
6	0.05	-	-	-	-	-	-	-	-		0.95	-56.8	-	-	30.7	L	0.54	0.563	80.8
6	0.05	-	-	-	-	-	-	-	-		0.95	-56.8	-	-	29.5	L	0.6	0.62	82.3
6	0.05	-	-	-	-	-	-	-	-		0.95	-58	-	-	22	M/L	0.76	0.772	85.5
6	0.05	-	-	-	-	-	-	-	-		0.95	-	-	-	27.3	L	0.68	0.696	84.1
J93TP																			
1	0.9	-	-	-	-	-	-	-	312	L	-	-	-	-	-		-	0.9	0.0
1	0.8	-	-	-	-	-	-	-	282	L	0.2	-	5.8	8.2	-		-	0.8	0.0
1	0.8	-	-	-	-	-	-	-	353	L/M	0.2	-	7.1	6.2	-		-	0.8	0.0
1	0.6	-	-	-	-	-	-	-	-		0.4	-	9.2	1.8	-		-	0.6	0.0
1	0.8	-	-	-	-	-	-	-	361	L	0.2	-59.5	9.1	1.9	-		-	0.8	0.0
1	0.65	-	-	-	-	-	-	-	441	L	-	-	-	-	-		-	0.65	0.0
1	0.96	-	-	-	-	322	40	-	280	d	-	-	-	-	-		-	0.96	0.0
1	0.6	-	-	-	-	-	-	-	359	L	0.4	-	8.7	2.8	-		-	0.6	0.0
1	0.8	-	-	-	-	-	-	-	350	L	0.2	-	7.7	4.9	-		-	0.8	0.0
1	0.88	-	-	-	-	-	-	-	285	L	-	-	-	-	-		-	0.88	0.0
1	0.6	-	-	-	-	-	-	-	351	C	0.4	-	9.3	1.7	-		-	0.6	0.0
2	0.4	-	-	-	-	-	-	-	422	V	0.6	-59.4	9.6	0.8	-		-	0.4	0.0
2	0.4	-	-	-	-	-	-	-	390	V	0.6	-59.6	9.4	1.4	12	V	0.14	0.48	8.0
2	0.2	-	-	-	-	-	-	-	392	d/V	0.8	-	13	-	-		-	0.2	0.0
2	0.2	-	-	-	-	-	-	-	363	V	0.8	-	11.1	-	-		-	0.2	0.0
2	0.55	-	-	-	-	-	-	-	438	d/V	0.45	-	10	0.2	-		-	0.55	0.0
2	0.3	-	-	-	-	-	-	-	390	V	0.7	-	11.6	-	13	V	0.15	0.41	12.3
2	0.5	-	-	-	-	-	-	-	-		0.5	-59.7	8.7	3.1	17	V	0.17	0.59	6.4
2	0.4	-	-	-	-	-	-	-	-		0.6	-60.1	-	-	-		-	0.4	0.0
3	0.75	-	-	-27	27.3	-	-	-	280	d	-	-	-	-	-		-	0.91	0.0
3	0.96	-	-	-27.3	27.5	-	-	-	-		-	-	-	-	-		-	1.17	0.0
3	0.97	-	-	-29.1	28.6	-	-	-	210	d	-	-	-	-	-		-	1.19	0.0
3	0.95	-	1.4	-23	24.7	-	-	-	380	d	-	-	-	-	-		-	1.14	0.0
3	0.8	-	-6.1	-	-	-	-	-	287	L	-	-	-	-	-		-	0.8	0.0
3	0.88	-42	-5.9	-	-	-	-	-	299	L	-	-	-	-	-		-	0.88	0.0
3	0.95	-54	1.5	-24.7	25.8	213	33	-	350	d	-	-	-	-	-		-	1.15	0.0
4	0.05	-	-	-	-	-	-	-	246	V	0.95	-65.5	-	-	-		-	0.05	0.0

V4P FLUID INCLUSION DATA

F	Tfm	Tmh	Tml	S	TsH	Th	to	FCO2	TmCO2	TmC	Sclath	ThCO2	to
JW006													
0.95	-	-	-2.5	4.2	-	-		-	-	-	-	-	
0.8	-	-	-1.5	2.6	-	-		-	-	-	-	-	
0.8	-	-	-2.9	4.8	-	-		-	-	-	-	-	
0.75	-58	-	-2.7	4.5	-	-		-	-	-	-	-	
1	-	-5.5	-2	3.4	-	-		-	-	-	-	-	
0.93	-23	-	0.5	-	-	-		-	-	-	-	-	
1	-	-	-0.4	0.7	-	-		-	-	-	-	-	
0.9	-	5.9	-	-	-	-		-	-	-	-	-	
0.92	-	-	-0.8	1.4	-	238	L	-	-	-	-	-	
0.65	-	-	-1.8	3.1	-	234	L	-	-	-	-	-	
0.85	-	-	-0.7	1.2	-	236	L	-	-	-	-	-	
0.8	-	-	-0.75	1.3	-	214	L	-	-	-	-	-	
0.88	-	-	-0.8	1.4	-	229	L	-	-	-	-	-	
0.85	-	-	-	-	-	226	L	-	-	-	-	-	
0.7	-	-	-	-	-	316	L	-	-	-	-	-	
0.6	-	-	-	-	-	316	L	-	-	-	-	-	
0.7	-	-	-2	3.4	-	312	L	-	-	-	-	-	
0.8	-	-	-	-	-	313	L	-	-	-	-	-	
0.6	-	-	-0.9	1.6	-	241	L	-	-	-	-	-	
0.7	-	-	-1	1.7	-	334	L	-	-	-	-	-	
0.7	-	-	-1.5	2.6	-	265	L	-	-	-	-	-	
0.88	-	-	-1.4	2.4	-	257	L	-	-	-	-	-	
0.7	-	-	-2	3.4	-	265	L	-	-	-	-	-	
0.9	-	-	-	-	-	149	L	-	-	-	-	-	
0.87	-	-	0.2	-	-	181	L	-	-	-	-	-	
0.9	-	-	-2.4	4	-	-		-	-	-	-	-	
0.96	-	-	-2	3.4	-	-		-	-	-	-	-	
0.93	-	-	-0.4	0.7	-	159	L	-	-	-	-	-	
0.7	-	-	-2.9	4.8	-	332	L	-	-	-	-	-	
0.9	-	-	-0.2	0.4	-	-		-	-	-	-	-	
0.8	-	-	-	-	-	265	L	-	-	-	-	-	
0.85	-	-	-3.1	5.1	-	287	L	-	-	-	-	-	
0.05	-	-	-	-	-	-		0.95	-62.1	-	-	-	
0.55	-	-	-	-	-	380	L	0.45	-	7.4	5.6	-	
0.85	-	-	-2.7	4.5	-	255	L	-	-	-	-	-	
0.9	-	-	-2.6	4.3	-	269	L	0.1	-	9	2.3	-	
0.8	-	-	-2.85	4.7	-	290	L	-	-	-	-	-	
0.7	-	-	-2.8	4.6	-	248	L	-	-	-	-	-	
0.1	-	-	-	-	-	-		0.9	-62.3	-	-	-	
0.05	-	-	-	-	-	-		0.95	-62.1	10.1	0	-7.1	V
0.05	-	-	-	-	-	-		0.95	-62.4	10.1	0	-	
0.7	-	-	-2.3	3.9	-	326	L	-	-	-	-	-	
0.8	-	-	-3.05	5	-	303	L	-	-	-	-	-	
0.8	-	-	-	-	-	311	L	-	-	-	-	-	
0.3	-	-	-	-	-	350	V	0.7	-	5.6	8.2	-	
0.2	-	-	-	-	-	-		0.8	-61.6	-	-	-	
1	-	-	-1.6	2.7	-	-		-	-	-	-	-	
1	-	-	-2	3.4	-	-		-	-	-	-	-	
0.93	-	-	-2.6	4.3	-	121	L	-	-	-	-	-	
1	-	-	-2.3	3.9	-	-		-	-	-	-	-	
0.8	-	-	-2.7	4.5	-	258	L	-	-	-	-	-	
0.92	-	-	-2.7	4.5	-	239	L	-	-	-	-	-	

V4P FLUID INCLUSION DATA

F	Tfm	Tmh	Tml	S	TsH	Th	to	FCO2	TmCO2	TmC	Sclath	ThCO2	to
0.05	-	-	-	-	-	299	V	0.95	-62.4	9.2	1.9	-	
0.05	-	-	-	-	-	-		0.95	-61.9	-	-	-	
0.92	-	-	-	-	-	198	L	-	-	-	-	-	
0.8	-	-	-1.1	1.9	-	222	L	-	-	-	-	-	
0.84	-	-	-3	4.9	-	240	L	0.16	-	7.2	5.8	-	
0.8	-	-	-	-	-	264	L	-	-	-	-	-	
0.9	-	-	-2.5	4.2	-	244	L	-	-	-	-	-	
0.9	-	-22.3	-2.3	3.9	-	253	L	0.1	-	7.6	5.1	-	
0.92	-	-	-2.5	4.2	-	214	L	-	-	-	-	-	
0.6	-	-	-	-	-	-		0.4	-	7	6.3	-	
0.9	-	-	-2.5	4.2	-	233	L	-	-	-	-	-	
0.6	-	-	-1	1.7	-	380	L	-	-	-	-	-	
0.93	-	-	-1.7	2.9	-	150	L	-	-	-	-	-	
0.6	-	-	-	-	-	393	C	0.4	-	7.6	5.1	-	
0.05	-	-23.5	-	-	-	-		-	-	-	-	-	
0.88	-	-	-	-	-	252	L	-	-	-	-	-	
0.2	-	-	-	-	-	334	V	0.8	-	8.1	4	-	
JW008													
0.95	-	-	-	-	-	246	L	-	-	-	-	-	
0.5	-	-	-	-	-	363	M	0.5	-60.8	-	-	-	
-	-	-	-5.9	9.1	-	249	L	-	-	-	-	-	
-	-	-	-5.9	9.1	-	247	L	-	-	-	-	-	
0.95	-	-	-	-	-	246	L	-	-	-	-	-	
0.96	-	-	-	-	-	242	L	-	-	-	-	-	
0.8	-	-	-5.9	9.1	-	252	L	-	-	-	-	-	
0.9	-	-	-	-	-	249	L	-	-	-	-	-	
0.8	-	-	-5.9	9.1	-	250	L	-	-	-	-	-	
0.15	-	-	-	-	-	-		0.85	-	-	-	10	V
0.55	-	-	-8	11.7	-	360	V	0.45	-61.2	8.3	3.3	-	
0.8	-	-	-	-	399	287	L	-	-	-	-	-	
0.7	-	-	-7.9	11.6	-	299	L	-	-	-	-	-	
0.8	-	-	-8.1	11.8	-	298	L	-	-	-	-	-	
0.8	-	-	-8	11.7	-	296	L	-	-	-	-	-	
0.9	-	-	-7.6	11.2	-	273	L	-	-	-	-	-	
0.7	-	-	-7.9	11.6	-	256	L	-	-	-	-	-	
0.9	-	-	-7.9	11.6	-	252	L	-	-	-	-	-	
0.8	-	-	-5.4	8.4	-	-		-	-	-	-	-	
0.96	-	-	-9.5	13.4	-	-		-	-	-	-	-	
0.8	-	-	-7.9	11.6	-	304	L	-	-	-	-	-	
0.2	-	-	-11.2	15.2	-	-		-	-	-	-	-	
-	-	-	-7.2	10.7	-	-		-	-	-	-	-	
0.9	-	-	-8	11.7	-	293	L	-	-	-	-	-	
0.95	-	-	-8	11.7	-	288	L	-	-	-	-	-	
0.3	-	-	-5.6	8.7	-	388	V	-	-	-	-	-	
0.95	-	-	-5.6	8.7	-	244	L	-	-	-	-	-	
0.9	-	-	-7.9	11.6	-	286	L	-	-	-	-	-	
0.8	-	-	-7.9	11.6	-	287	L	-	-	-	-	-	
0.6	-	-	-5.5	8.5	-	-		-	-	-	-	-	
0.9	-	-	-7.9	11.6	-	301	L	-	-	-	-	-	
0.85	-	-	-8	11.7	-	297	L	-	-	-	-	-	
0.8	-	-	-7.8	11.5	-	347	L	-	-	-	-	-	
0.9	-	-	-7.6	11.2	-	291	L	-	-	-	-	-	
0.6	-	-	-4.5	7.2	-	-		-	-	-	-	-	

V4P FLUID INCLUSION DATA

F	Tfm	Tmh	Tml	S	TsH	Th	to	FCO2	TmCO2	TmC	Sclath	ThCO2	to
0.8	-	-	-4.2	6.7	-	286	L	-	-	-	-	-	
0.9	-	-	-4.9	7.7	-	286	L	-	-	-	-	-	
0.8	-	-	-5.3	8.3	-	290	L	-	-	-	-	-	
0.6	-	-	-5.9	9.1	-	381	L	-	-	-	-	-	
0.3	-	-	-5.5	8.5	-	-		-	-	-	-	-	
0.3	-	-	-5.8	8.9	-	-		-	-	-	-	-	
0.6	-	-	-8.3	12.1	-	322	L	-	-	-	-	-	
0.7	-	-	-5.3	8.3	-	-		-	-	-	-	-	
0.5	-	-	-5.6	8.7	-	356	V	-	-	-	-	-	
0.8	-	-	-	-	-	282	L	-	-	-	-	-	
0.9	-	-	-	-	-	261	L	-	-	-	-	-	
0.8	-	-	-	-	-	280	L	-	-	-	-	-	
0.9	-	-	-	-	-	276	L	-	-	-	-	-	
0.9	-	-	-	-	-	280	L	-	-	-	-	-	
0.3	-	-	-	-	-	260	L	-	-	-	-	-	
0.85	-	-	-	-	-	283	L	-	-	-	-	-	
0.3	-	-	-	-	-	386	V	-	-	-	-	-	
0.2	-	-	-	-	-	480	V	-	-	-	-	-	
0.94	-	-	-	-	-	288	L	-	-	-	-	-	
0.9	-	-	-	-	-	286	L	-	-	-	-	-	
0.85	-	-	-	-	-	297	L	-	-	-	-	-	
0.9	-	-	-	-	-	270	L	-	-	-	-	-	
0.7	-	-	-	-	-	395	L	-	-	-	-	-	
0.7	-	-	-	-	-	404	C	-	-	-	-	-	
0.6	-	-	-	-	-	430	L	-	-	-	-	-	
0.6	-	-	-	-	-	391	L	-	-	-	-	-	
0.55	-	-	-	-	-	372	V	-	-	-	-	-	
0.75	-	-	-	-	-	367	L	-	-	-	-	-	
0.65	-	-	-	-	-	409	V	-	-	-	-	-	
0.5	-	-	-	-	-	408	V	-	-	-	-	-	
0.7	-	-	-	-	-	405	L	-	-	-	-	-	
-	-	-	-	-	-	401	L	-	-	-	-	-	
0.7	-	-	-	-	-	393	L	-	-	-	-	-	
0.9	-	-	-	-	-	343	L	-	-	-	-	-	
0.9	-	-	-	-	-	292	L	-	-	-	-	-	
0.7	-	-	-	-	-	406	C	-	-	-	-	-	
0.6	-	-	-	-	-	407	V	-	-	-	-	-	
0.9	-	-	-	-	-	362	L	-	-	-	-	-	
0.4	-	-	-	-	-	420	L	-	-	-	-	-	
0.6	-72	-	-6.4	9.7	-	-		0.4	-	5	9.3	-	
0.2	-	-	-	-	-	-		0.8	-62.6	-	-	-	
0.5	-	-	-	-	-	-		0.5	-64.3	9.7	0.5	-	
0.85	-	-	-9.3	13.2	-	-		0.15	-	-	-	-15	V

V4J1 FLUID INCLUSION DATA

F	Tfm	Tmh	Tml	S	TsH	Th	to	FCO2	TmCO2	TmC	Sclath	ThCO2	to
JW005													
-	-	-	-	-	-	288	L	-	-	-	-	-	
-	-	-	-	-	-	278	L	-	-	-	-	-	
-	-	-	-	-	-	280	L	-	-	-	-	-	
-	-	-	-	-	-	177	L	-	-	-	-	-	
-	-	-	-	-	-	254	L	-	-	-	-	-	
-	-	-	-	-	-	229	L	-	-	-	-	-	
-	-	-	-	-	-	275	L	-	-	-	-	-	
-	-	-	-	-	-	300	L	-	-	-	-	-	
-	-	-	-	-	-	267	L	-	-	-	-	-	
-	-	-	-	-	-	274	L	-	-	-	-	-	
-	-	-	-	-	-	286	L	-	-	-	-	-	
-	-	-	-	-	-	256	L	-	-	-	-	-	
-	-	-	-	-	-	286	L	-	-	-	-	-	
-	-	-	-	-	-	316	L	-	-	-	-	-	
-	-	-	-	-	-	284	L	-	-	-	-	-	
-	-	-	-	-	-	273	L	-	-	-	-	-	
-	-	-	-	-	-	264	L	-	-	-	-	-	
-	-	-	-	-	-	302	L	-	-	-	-	-	
-	-	-	-	-	-	276	L	-	-	-	-	-	
-	-	-	-	-	-	301	L	-	-	-	-	-	
-	-	-	-	-	-	305	L	-	-	-	-	-	
-	-	-	-	-	-	273	L	-	-	-	-	-	
-	-	-	-	-	-	263	L	-	-	-	-	-	
-	-	-	-	-	-	378	L	-	-	-	-	-	
-	-	-	-	-	-	350	L	-	-	-	-	-	
-	-	-	-	-	-	338	L	-	-	-	-	-	
-	-	-	-	-	-	306	L	-	-	-	-	-	
-	-	-	-	-	-	400	L	-	-	-	-	-	
-	-	-	-	-	-	358	L	-	-	-	-	-	
-	-	-	-	-	-	398	L	-	-	-	-	-	
-	-	-	-	-	-	317	L	-	-	-	-	-	
-	-	-	-	-	-	303	L	-	-	-	-	-	
-	-	-	-	-	-	295	L	-	-	-	-	-	
0.8	-	-	-	-	-	295	L	-	-	-	-	-	
0.8	-	-	-	-	-	261	L	-	-	-	-	-	
0.8	-	-	-	-	-	334	L	-	-	-	-	-	
0.9	-	-	-	-	-	279	L	-	-	-	-	-	
0.6	-	-	-	-	-	361	L	-	-	-	-	-	
0.8	-	-	-	-	-	265	L	-	-	-	-	-	
0.9	-	-	-	-	-	288	L	-	-	-	-	-	
0.6	-	-	-	-	-	303	L	-	-	-	-	-	
0.7	-	-	-	-	-	382	L	-	-	-	-	-	
0.7	-	-	-	-	-	303	L	-	-	-	-	-	
0.9	-	-	-	-	-	329	L	-	-	-	-	-	
0.7	-	-	-	-	-	301	L	-	-	-	-	-	
0.8	-	-	-	-	-	385	L	-	-	-	-	-	
0.7	-	-	-	-	-	347	L	-	-	-	-	-	
0.4	-	-	-	-	-	359	L	-	-	-	-	-	
0.9	-	-	-9.8	13.8	-	246	L	-	-	-	-	-	
0.9	-	-	-	-	-	227	L	-	-	-	-	-	
0.82	-	-	-	-	-	304	L	-	-	-	-	-	
0.8	-	-	-	-	-	351	L/C	-	-	-	-	-	
0.7	-	-	-	-	-	309	L	-	-	-	-	-	
0.8	-	-	-	-	-	287	L	-	-	-	-	-	
0.95	-	-	-	-	229	240	L	-	-	-	-	-	
0.2	-	-	-	-	-	272	V	-	-	-	-	-	
0.75	-	-	-	-	-	309	L	-	-	-	-	-	
0.8	-	-	-	-	289	297	L	-	-	-	-	-	
0.8	-	-	-6.9	10.4	-	273	L	-	-	-	-	-	
0.8	-	-	-	-	236	-		-	-	-	-	-	
0.6	-	-	-	-	-	361	L	-	-	-	-	-	
0.8	-	-	-2.4	4	-	261	L	-	-	-	-	-	
0.88	-	-	-2.2	3.7	-	320	L	-	-	-	-	-	

V4J1 FLUID INCLUSION DATA

F	Tfm	Tmh	Tml	S	TsH	Th	to	FCO2	TmCO2	TmC	Sclath	ThCO2	to
0.2	-	-	-	-	-	303	V	0.8	-62.1	1.6	14	-	
0.92	-	-	-6.6	10	-	231	L	-	-	-	-	-	
0.95	-	-	-9.4	13.3	-	-		-	-	-	-	-	
0.9	-	-	-6.3	9.6	-	218	L	-	-	-	-	-	
0.9	-	-	-6.1	9.3	-	195	L	-	-	-	-	-	
0.9	-	-	-6.4	9.7	-	248	L	-	-	-	-	-	
0.9	-	-	-2.2	3.7	-	261	L	-	-	-	-	-	
0.9	-	-	-7.2	10.7	-	239	L	-	-	-	-	-	
0.8	-	-6.6	-	-	-	318	L	-	-	-	-	-	
0.68	-	-	-	-	-	284	L	0.32	-	-	-	1.5	L
0.85	-	-5.3	-	-	-	315	L	-	-	-	-	-	
0.75	-	-5.8	-	-	-	347	L	-	-	-	-	-	
0.92	-	-	-7.7	11.4	-	247	L	-	-	-	-	-	
0.9	-	-	-8.2	12	-	247	L	-	-	-	-	-	
0.9	-	-	-8.1	11.8	-	245	L	-	-	-	-	-	
0.7	-	-	-	-	-	-		0.3	-	6	7.9	-	
0.9	-	-	-	-	-	248	L	-	-	-	-	-	
0.9	-	-	-	-	-	254	L	-	-	-	-	-	
0.95	-39	-	-8.7	12.5	-	254	L	-	-	-	-	-	
0.93	-	-	-8.3	12.1	-	227	L	-	-	-	-	-	
0.9	-	-	-8.1	11.8	-	222	L	-	-	-	-	-	
0.92	-	-	-	-	-	250	L	-	-	-	-	-	
0.9	-	-	-1.6	2.7	-	251	L	-	-	-	-	-	
0.95	-37	-	-8.4	12.2	-	237	L	-	-	-	-	-	
0.8	-	-4.7	-	-	-	315	L	-	-	-	-	-	
0.95	-	-	-	-	-	293	L	-	-	-	-	-	
0.95	-	-	-0.2	0.4	-	242	L	-	-	-	-	-	
0.97	-	-	-0.2	0.4	-	180	L	-	-	-	-	-	
0.92	-	-	-0.2	0.4	167	169	L	-	-	-	-	-	
0.75	-	-5.8	-	-	-	347	L	-	-	-	-	-	

V4N FLUID INCLUSION DATA

SAMPLE	F	Tfm	Tmh	Tml	S	TsH	Th	To	D
J38LB	-	-	-	-5.5	8.5	-	215	L	-
"	-	-	-	-2.1	3.5	-	-		-
"	-	-	-	-4.2	6.7	-	-		-
"	-	-	-	-	-	-	146	L	-
"	-	-	-	-1.8	3.1	-	184	L	-
"	-	-	-	-1.7	2.9	-	195	L	-
"	-	-	-	-1.5	2.6	-	183	L	-
"	-	-	-	-3	4.9	-	197	L	-
"	-	-	-	-2.3	3.9	-	211	L	-
"	-	-	-	-0.5	0.9	-	-		-
"	-	-	-	-1.2	2.1	-	212	L	-
"	-	-	-	-1.2	2.1	-	-		-
"	-	-	-	-2	3.4	-	-		-
"	-	-	-	-	-	-	259	L	-
"	-	-	-	-1.1	1.9	-	285	L	-
"	-	-	-	-	-	-	316	L	-
"	-	-	-	-	-	-	224	L	-
"	-	-	-	-2.1	3.5	-	188	L	-
"	-	-	-	-	-	-	211	L	-
"	-	-	-	-2.4	4	-	209	L	-
"	-	-	-	-	-	-	314	L	-
"	-	-	-	-	-	-	275	L	-
"	-	-	-	-	-	-	249	L	-
"	-	-	-	-	-	-	308	L	-
"	-	-	-	-	-	-	203	L	-
"	-	-	-	-	-	-	251	L	-
"	-	-	-	-	-	-	226	L	-
"	-	-	-	-0.1	0.2	-	347	L	-
"	-	-	-	-	-	-	231	L	-
"	-	-	-	-	-	-	208	L	-
"	-	-	-	-	-	-	182	L	-
"	-	-	-	-	-	-	181	V	-
"	-	-	-	-	-	-	282	L	-
"	-	-	-	-	-	-	212	L	-
"	-	-	-	-	-	-	269	L	-
"	-	-	-	-1.8	3.1	-	-		-
"	-	-	-	-2	3.4	-	-		-
"	-	-	-	-0.9	1.6	-	206	L	-
"	-	-	-	-	-	-	203	L	-
"	-	-	-	-	-	-	161	L	-
"	-	-	-	-	-	-	247	L	-
"	-	-	-	-	-	-	207	L	-
"	-	-	-	-	-	-	209	L	-
"	-	-	-	-	-	-	253	L	-
"	0.96	-	-	-	-	-	240	L	-
"	-	-	-	-0.8	1.4	-	144	L	-
"	0.92	-	-	-2.8	4.6	-	120	L	0.95
"	-	-	-	-1.3	2.2	-	-		-
"	-	-	-	-	-	-	218	L	-
"	-	-	-	-2.6	4.3	-	-		-
"	-	-	-	-	-	-	120	L	-
"	0.95	-	-	-0.5	0.9	-	-		0.96
"	-	-	-	-	-	-	129	L	-
"	0.4	-	-	-	-	-	110	L	-
"	-	-	-	-2.7	4.5	-	-		-
"	0.9	-	-	-3.9	6.3	-	142	L	0.95
"	-	-	-	-3.2	5.2	-	-		-
"	-	-	-	-1.7	2.9	-	146	L	-
"	-	-	-	-1.2	2.1	-	-		-
"	-	-	-	-2.7	4.5	-	241	L	-

V4N FLUID INCLUSION DATA

SAMPLE	F	Tfm	Tmh	Tml	S	TsH	Th	To	D
J38LB	-	-	-	-2.9	4.8	-	233	L	-
"	-	-	-	-2.1	3.5	-	195	L	-
"	0.95	-	-	-	-	-	209	L	-
"	0.92	-	-	-2.2	3.7	-	210	L	0.95
"	0.95	-	-	-0.6	1	-	179	L	0.96
"	0.9	-	-	-0.8	1.4	-	182	L	0.91
"	0.7	-	-	-0.5	0.9	-	155	L	0.71
"	-	-	-	-1.5	2.6	-	224	L	-
"	0.8	-	-	-0.8	1.4	-	234	L	0.81
"	0.95	-	-	-1.6	2.7	-	210	L	0.97
"	0.75	-	-	-7.1	10.6	-	167	L	0.81
"	-	-	-	-7.2	10.7	-	-		-
"	0.92	-	-	-7.5	11.1	-	174	L	1.00
"	0.8	-	-	-	-	-	190	L	-
"	0.3	-	-	-7.3	10.9	-	192	L	0.33
"	0.9	-	-	-1	1.7	-	-		0.91
"	0.9	-	-	-1.1	1.9	-	190	L	0.91
"	0.9	-	-	-1	1.7	-	186	L	0.91
"	0.9	-	-	-1.1	1.9	-	188	L	0.91
"	0.92	-	-	-1	1.7	-	186	L	0.93
"	0.8	-	-	-1.2	2.1	-	235	L	0.81
"	0.95	-	-	-0.8	1.4	-	209	L	0.96
"	0.9	-	-	-1	1.7	-	203	L	0.91
"	0.9	-	-	-1	1.7	-	204	L	0.91
"	-	-	-	-	-	-	208	L	-
"	0.9	-	-	-0.7	1.2	-	200	L	0.91
"	0.85	-	-	-1	1.7	-	220	L	0.86
"	0.9	-	-	-0.8	1.4	-	198	L	0.91
"	0.76	-	-	-1.3	2.2	-	214	L	0.77
"	0.8	-	-	-1.25	2.1	-	235	L	0.81
"	0.9	-	-	-2.7	4.5	-	221	L	0.93
"	0.9	-	-	-1.5	2.6	-	236	L	0.92
"	0.9	-	-	-2.4	4	-	205	L	0.93
"	0.9	-	-	-2.7	4.5	-	211	L	0.93
"	0.95	-	-	-1	1.7	-	-		0.96
"	-	-	-	-0.7	1.2	-	-		-
"	0.92	-	-	-2.4	4	-	227	L	0.95
"	0.9	-	-	-3.2	5.2	-	197	L	0.94
"	0.85	-	-	-4.6	7.3	-	197	L	0.90
J78PS	0.95	-	-	-0.8	1.4	-	-		0.96
"	0.8	-	-	-0.6	1	-	279	L	0.81
"	0.5	-	-	-0.8	1.4	-	-		0.51
"	0.93	-32	-	-0.4	0.7	-	147	L	0.94
"	0.95	-	-	-0.5	0.9	-	166	L	0.96
"	0.05	-	-	-	-	-	324	L	-
"	1	-	-	0	0	-	-		1.00
"	0.8	-	-	-0.9	1.6	-	195	L	0.81
"	0.94	-	-	-	-	-	245	L	-
"	0.85	-	-	-0.8	1.4	-	227	L	0.86
"	0.93	-	-	-0.2	0.4	-	-		0.93
"	0.8	-	-	-0.8	1.4	-	234	L	0.81
"	0.9	-	-	-0.6	1	-	233	L	0.91
"	0.9	-	-	-0.8	1.4	-	233	L	0.91
"	0.92	-	-	-0.7	1.2	-	222	L	0.93
"	0.95	-	-	-0.7	1.2	-	156	L	0.96
"	1	-	-	-	-	280	-		-
"	0.95	-	-	-	-	-	153	L	-
"	0.93	-11	-	-0.35	0.6	-	242	L	0.93
"	0.91	-	-	-0.3	0.5	-	190	L	0.91
"	0.95	-	-	-0.4	0.7	-	222	L	0.96

V4N FLUID INCLUSION DATA

SAMPLE	F	Tfm	Tmh	Tml	S	TsH	Th	To	D
J78PS	0.92	-	-	-0.4	0.7	-	247	L	0.93
"	0.94	-	-	-0.3	0.5	-	232	L	0.94
"	0.94	-	-	-	-	-	178	L	-
"	0.9	-	-	-0.35	0.6	-	227	L	0.90
"	0.94	-	-	-0.3	0.5	-	153	L	0.94
"	0.85	-	-	-0.6	1	-	233	L	0.86
"	0.95	-	-	-0.3	0.5	-	147	L	0.95
"	0.95	-	-	-0.4	0.7	-	258	L	0.96
"	0.95	-	-	-	-	-	163	L	-
"	0.85	-	-	-0.2	0.4	-	345	L	0.85
"	0.94	-	-	-	-	-	139	L	-
"	0.92	-	-	-0.4	0.7	-	225	L	0.93
"	0.94	-	-	-0.4	0.7	-	235	L	0.95
"	0.93	-	-	-0.4	0.7	-	300	L	0.94
"	0.96	-	-	-0.5	0.9	-	-		0.97
"	0.95	-	-	-0.3	0.5	-	225	L	0.95
"	0.95	-	-	-0.4	0.7	-	245	L	0.96
"	0.5	-	-	-	-	-	390	L	-
"	0.9	-	-	-0.5	0.9	-	295	L	0.91
"	0.9	-	-	-0.2	0.4	-	223	L	0.90
"	0.5	-	-	-0.2	0.4	-	389	L	0.50
"	0.6	-	-	0	0	-	370	L	0.60
"	0.95	-	-	-0.4	0.7	-	189	L	0.96
"	0.98	-	-	-0.4	0.7	-	124	L	0.99
"	0.86	-	-	-0.1	0.2	-	279	L	0.86
"	0.65	-	-	-0.4	0.7	-	294	L	0.65
"	0.95	-	-	-0.3	0.5	-	132	L	0.95
"	0.92	-	-	-0.3	0.5	-	148	L	0.92
"	0.88	-	-	-0.4	0.7	-	304	L	0.88

V4W FLUID INCLUSION DATA

SAMPLE	F	Tfm	Tmh	Tml	S	TsH	Th	To	D
J131/1	0.95	-74	-7.6	-25.8	26.5	-	129	L	1.15
"	0.97	-	-	-25.9	26.6	-	125	L	1.18
"	0.96	-	-	-25.9	26.6	-	142	L	1.16
"	0.95	-72	-	-26.1	26.7	-	125	L	1.15
"	0.97	-75	-9.6	-25.8	26.5	-	127	L	1.18
"	0.95	-	-	-25.5	26.3	-	132	L	1.15
"	0.98	-	-	-26.1	26.7	-	127	L	1.19
"	0.97	-67	-	-27.3	27.5	-	122	L	1.18
"	0.96	-	-8	-25.9	26.6	-	130	L	1.16
"	0.97	-	-	-25.8	26.5	-	133	L	1.18
"	0.95	-	-	-	-	-	141	L	-
"	0.97	-	-	-26	26.6	-	136	L	1.18
"	0.96	-70	-	-27.2	27.4	-	141	L	1.17
"	0.98	-	-0.7	-	-	-	-		-
"	0.98	-	-0.4	-	-	-	-		-
"	0.96	-	-0.1	-25.1	26.1	-	-		1.16
"	0.95	-	2.9	-26	26.6	-	136	L	1.15
"	0.9	-	3	-26.1	26.7	-	131	L	1.09
"	0.97	-	-	-25.8	26.5	-	125	L	1.18
"	0.96	-	-	-24.3	25.5	-	-		1.16
"	0.92	-69	0.9	-25.2	26.1	-	127	L	1.11
"	0.97	-	-3.4	-23.8	25.2	-	140	L	1.17
"	0.95	-74	3.6	-25.8	26.5	-	126	L	1.15
"	0.9	-	-	-	-	-	268	L	-
"	0.2	-	-	-	-	-	211	V	-
"	1	-	-	-26.8	27.1	-	-		1.22
"	1	-	-	-26.5	27.0	-	-		1.22
"	1	-	-	-28	27.9	-	-		1.22
J131/2	0.95	-	-	-26.2	26.8	-	100	L	1.15
"	0.98	-	-	-24.7	25.8	-	108	L	1.18
"	0.95	-	7.3	-24.6	25.7	-	121	L	1.15
"	0.95	-	-	-24	25.4	-	101	L	1.14
"	0.98	-59	1.2	-23.4	25.0	-	142	L	1.18
"	0.98	-	6.2	-24.7	25.8	-	121	L	1.18
"	0.98	-	2.4	-25.8	26.5	-	94	L	1.19
"	0.97	-	-	-	-	-	110	L	-
"	0.94	-	2.9	-	-	-	138	L	-
"	0.98	-	2.1	-26.7	27.1	-	127	L	1.19
"	0.98	-	-	-24.5	25.7	-	134	L	1.18
"	0.96	-	-	-23.9	25.3	-	125	L	1.15
"	0.97	-	5.1	-23.8	25.2	-	125	L	1.17
"	0.98	-69	3.7	-24.1	25.4	-	124	L	1.18
J131/4	0.96	-	-	-24.3	25.5	-	-		1.16
"	0.98	-	-	-	-	-	133	L	-
"	0.97	-	4.3	-23.9	25.3	-	126	L	1.17
"	0.98	-	-	-	-	-	134	L	-
"	0.97	-69	2.9	-24.5	25.7	-	136	L	1.17
"	0.97	-	6.7	-24.4	25.6	-	167	L	1.17
"	0.96	-62	6.3	-24.7	25.8	-	130	L	1.16
"	0.96	-	-	-23.8	25.2	-	139	L	1.15
J131/5	0.92	-	-	-1.4	2.4	-	154	L	0.94
"	0.95	-	-	-	-	-	-		-
"	0.9	-	-	-	-	-	199	L	-

V4W FLUID INCLUSION DATA

SAMPLE	F	Tfm	Tmh	Tml	S	TsH	Th	To	D
J131/5	0.95	-	-	-1.7	2.9	-	171	L	0.97
"	0.97	-	-	-1.8	3.1	-	151	L	0.99
"	0.9	-	-	-1.4	2.4	-	217	L	0.92
"	0.95	-	-	-	-	-	144	L	-
"	0.95	-	-	-	-	-	116	L	-
"	0.9	-	-	-0.9	1.6	-	120	L	0.91
"	0.95	-	-	-	-	-	161	L	-
"	0.92	-	-	-2	3.4	-	189	L	0.94
"	0.92	-	-	-1.9	3.2	-	189	L	0.94
J131/6	1	-	-	-4.3	6.9	-	-		1.05
"	1	-	-	-3.6	5.8	-	-		1.05
"	1	-	-	-4.1	6.6	-	-		1.05
"	1	-	-	-3.7	6.0	-	-		1.05
"	0.97	-	7.4	-23.4	25.0	-	108	L	1.16
"	1	-72	-2.1	-21.2	23.5	-	-		1.19
"	0.95	-	-1.4	-23.2	24.8	-	-		1.14
"	0.97	-	4.9	-25.3	26.2	-	116	L	1.17
"	0.9	-35	-	-0.3	0.5	-	-		0.90
"	0.95	-73	8.6	-24.3	25.5	-	-		1.14
"	0.95	-	6.6	-	-	-	131	L	-
"	0.97	-	-	-	-	-	126	L	-
"	0.95	-	7.4	-	-	-	129	L	-
"	0.95	-	-	-22.9	24.6	-	118	L	1.14
"	0.95	-	9.8	-	-	-	135	L	-
"	0.96	-	-	-	-	-	122	L	-
J142PS	1	-	-	-	-	-	-		-
"	1	-	-	-3.7	6.0	-	-		1.05
"	0.9	-	-22.8	-2	3.4	-	-		0.92
"	0.9	-	-	-	-	-	-		-
"	0.8	-	-	-3.6	5.8	-	-		0.84
"	0.9	-	-	-0.9	1.6	-	166	L	0.91
"	1	-	-	-0.5	0.9	-	-		1.01
"	1	-	-	-	-	-	-		-
"	1	-	-	-0.7	1.2	-	-		1.01
"	0.95	-	-	-1	1.7	-	-		0.96
"	1	-	-	-1.5	2.6	-	-		1.02
"	1	-	-	-0.9	1.6	-	-		1.01
J19GWa	0.96	-	-	-15.3	19	-	99	L	1.11
"	0.96	-	-	-15.7	19.4	-	137	L	1.11
"	0.95	-	-	-15.3	19	-	133	L	1.09
"	0.95	-40	-	-15.3	19	-	170	L	1.09
"	0.97	-	-1.7	-13.2	17.2	-	127	L	1.10
"	0.97	-	-	-10.1	14.1	-	93	L	1.08
"	0.96	-	1.4	-	-	201	195	L	-
"	0.9	-75	-	-23	24.7	-	102	L	1.08
"	0.9	-	-	-	-	-	114	L	-
"	-	-	0.9	-24.1	25.4	-	-		0.00
"	0.95	-	-	-21.5	23.7	-	-		1.13
"	0.97	-	-1	-21.6	23.8	-	211	L	1.15
"	0.9	-	-0.7	-23.9	25.3	-	235	L	1.08
"	-	-	-	-15	18.8	-	-		0.00
"	0.8	-	-	-16.3	19.9	-	-		0.93
"	0.9	-	-1.6	-12.2	16.2	-	-		1.02

V4W FLUID INCLUSION DATA

SAMPLE	F	Tfm	Tmh	Tml	S	TsH	Th	To	D
J19GWa	0.75	-50	5.1	-24.2	25.5	-	213	L	0.90
"	0.9	-	-	-16.1	19.7	-	235	L	1.04
"	0.96	-60	7.8	-22.6	24.4	-	177	L	1.15
"	-	-60	-	-24.5	25.7	-	-		0.00
"	0.9	-	-	-20.7	23.2	-	-		1.07
"	0.8	-	-	-23.8	25.2	-	273	L	0.96
"	0.9	-60	0.4	-23.5	25	-	245	L	1.08
"	-	-	0.9	-22.8	24.6	-	-		0.00
"	0.95	-50	-	-20.8	23.2	-	123	L	1.13
"	0.95	-55	-	-22.8	24.6	-	119	L	1.14
"	0.9	-	6.1	-22.1	24.1	-	116	L	1.07
"	0.95	-55	-	-22.5	24.4	-	113	L	1.14
"	0.85	-	-	-23.2	24.8	-	121	L	1.02
"	0.95	-56	-	-22.4	24.3	-	115	L	1.13
"	0.98	-	-	-22.9	24.6	-	122	L	1.17
"	0.95	-	6.1	-22.4	24.3	-	-		1.13
"	0.95	-	-	-24.1	25.4	-	111	L	1.14
"	0.94	-	6.1	-22.3	24.2	-	-		1.12
"	0.2	-	9.1	-	-	-	-		-
"	1	-	-	-16.6	20.1	-	-		1.16
"	0.8	-	-	-21.3	23.6	-	-		0.95
"	0.9	-	-	-24.2	25.5	-	-		1.08
"	0.75	-	-	-32.5	30.9	140	-		0.94
"	0.9	-56	18	-21.7	23.8	-	-		1.07
"	0.95	-	-	-	-	-	-		-
"	0.95	-	-	-16.4	19.9	-	116	L	1.10
"	0.7	-	-2	-22.5	24.4	-	-		0.84
"	0.5	-	-	-	-	90	-		-
"	0.9	-	-	-9.1	13	-	174	L	0.99
"	0.95	-	-	-13.3	17.3	-	-		1.08
"	0.96	-64	-21.7	-21.7	23.8	-	98	L	1.14
"	0.88	-55.5	-21	-1.45	2.5	-	-		0.90
"	0.95	-	-	-20.4	22.9	-	-		1.12
"	0.9	-	-	-15.6	19.3	-	119	L	1.04
"	0.95	-56	1.2	-21.8	23.9	-	83	L	1.13
"	0.92	-54	-6	-21.7	23.8	-	111	L	1.10
"	0.7	-	-22.5	-14.9	18.7	-	-		0.80
"	0.95	-63	0.6	-22.3	24.2	-	123	L	1.13
"	0.96	-	15.6	-	-	-	-		-
"	0.97	-	3.4	-22.7	24.5	-	113	L	1.16
"	0.95	-	-0.8	-21.5	23.7	-	120	L	1.13
"	0.97	-	-	-	-	-	107	L	-
"	0.95	-54	-3	-21.2	23.5	-	141	L	1.13
"	0.9	-		0.7	0	-	199	L	0.90
"	0.97	-	7.5	-21.75	23.9	-	118	L	1.16
"	0.95	-	4.8	-22.1	24.1	-	97	L	1.13
"	1	-	9	-	-	-	-		-
"	0.95	-73	-0.2	-23.7	25.2	-	112	L	1.14
"	0.97	-	5.2	-	-	-	92	L	-
"	0.95	-	-	-23.2	24.8	-	98	L	1.14
J98PC2D	0.97	-64	-	-	-	-	-		-
"	0.96	-	4.9	-25.8	26.5	-	-		1.16
"	0.98	-56	-	-22.5	24.4	-	82	L	1.17

V4W FLUID INCLUSION DATA

SAMPLE	F	Tfm	Tmh	Tml	S	TsH	Th	To	D
J98PC2D	0.97	-	-4.1	-	-	-	-		-
"	0.95	-	-	-	-	-	129	L	-
"	0.95	-58	10.4	-	-	-	117	L	-
"	0.95	-	5.5	-22.8	24.6	-	108	L	1.14
"	0.97	-	-	-	-	-	122	L	-
"	0.96	-	-	-	-	-	131	L	-
"	0.97	-	-	-	-	-	103	L	-
"	0.96	-	-	-	-	-	175	L	-
"	0.96	-	-	-	-	-	130	L	-
"	0.94	-	-	0	0	-	201	L	0.94
"	0.95	-	-	-0.2	0.4	-	165	L	0.95
"	0.95	-	-	-0.2	0.4	-	208	L	0.95
"	0.96	-	-	-0.2	0.4	-	155	L	0.96
"	0.95	-	-	-	-	-	194	L	-
"	0.92	-	15.8	-22.6	24.4	-	190	L	1.10
"	0.97	-56	8.5	-22.9	24.6	-	127	L	1.16
"	0.96	-55	-1.3	-23	24.7	-	125	L	1.15
"	0.94	-	11.6	-23.4	25	-	114	L	1.13
"	0.95	-	-	-	-	-	118	L	-
"	0.97	-	-	-23	24.7	-	-		1.16
"	0.99	-	-	-	-	-	62	L	-
"	0.97	-	-	-	-	-	118	L	-
"	0.98	-57	-5.8	-23.3	24.9	-	124	L	1.18
"	0.96	-	-	-	-	-	120	L	-
"	0.98	-	9.4	-23.4	25	-	115	L	1.18
"	0.97	-	-	-23.1	24.8	-	107	L	1.16
"	0.98	-	-	-	-	-	118	L	-
"	0.97	-	3.9	-23.6	25.1	-	116	L	1.16
"	0.95	-	-	-	-	-	115	L	-
"	0.96	-56	9.1	-	-	-	117	L	-
"	0.98	-57	8.6	-23.3	24.9	-	115	L	1.18
"	0.96	-	9.3	-23.2	24.8	-	114	L	1.15
"	0.92	-56	9.7	-23.4	25	-	131	L	1.10
"	0.94	-	11.8	-	-	-	114	L	-
"	0.95	-	-	-23.6	25.1	-	111	L	1.14
"	0.96	-	6.7	-23.7	25.2	-	97	L	1.15
"	0.97	-	9.8	-23.5	25	-	123	L	1.16

ADDITIONAL FLUID INCLUSION DATA

F	Tfm	Tmh	Tml	S	TsH	Th	to	FCO2	TmCO2	TmC	Sclath	ThCO2	to	D CO2	D	MOL%CO2
J58PS																
0.5	-	-	-	-	-	472	V	0.5	-60.2	7.1	6.2	17.6	V	0.18	0.59	6.9
0.3	-	-	-	-	-	494	V	0.7	-60	3.7	11.6	19.9	V	0.2	0.44	16.0
0.05	-	-	-	-	-	-		0.95	-	-	-	19.5	L	0.79	0.80	86.0
0.05	-	-	-	-	-	-		0.95	-	-	-	19.5	L	0.79	0.80	86.0
0.05	-	-	-	-	-	-		0.95	-59.5	-	-	-		-	0.05	0.0
0.7	-36	-21.7	-	-	-	-		0.3	-60	-	-	-		-	0.70	0.0
0.6	-	-	-	-	-	384	V	0.4	-59.3	-	-	24	L	0.73	0.89	16.6
0.9	-	-	-2	3.4	-	211	L	-	-	-	-	-		-	0.92	0.0
0.9	-	-	-2.3	3.9	-	188	L	-	-	-	-	-		-	0.93	0.0
0.9	-	-	-8.3	12.1	-	-		-	-	-	-	-		-	0.99	0.0
0.95	-	-	-1.5	2.6	-	227	L	-	-	-	-	-		-	0.97	0.0
0.96	-	-	-2	3.4	-	226	L	-	-	-	-	-		-	0.99	0.0
0.95	-	-	-1.5	2.6	-	-		-	-	-	-	-		-	0.97	0.0
0.95	-	-	-1.7	2.9	-	215	L	-	-	-	-	-		-	0.97	0.0
0.96	-	-	-1.5	2.6	-	149	L	-	-	-	-	-		-	0.98	0.0
0.94	-	-	-5	7.9	-	201	L	-	-	-	-	-		-	1.00	0.0
0.9	-	-	-1.3	2.2	-	-		-	-	-	-	-		-	0.92	0.0
0.95	-	-	-2	3.4	-	217	L	-	-	-	-	-		-	0.98	0.0
0.95	-	-	-2.6	4.3	-	-		-	-	-	-	-		-	0.98	0.0
0.85	-	-	-1.7	2.9	-	206	L	-	-	-	-	-		-	0.87	0.0
0.92	-	-	-	-	-	214	L	-	-	-	-	-		-	0.92	0.0
0.96	-	-	-2.1	3.5	-	223	L	-	-	-	-	-		-	0.99	0.0
0.92	-	-	-2	3.4	-	225	L	-	-	-	-	-		-	0.95	0.0
0.9	-	-	-1.9	3.2	-	218	L	-	-	-	-	-		-	0.92	0.0
0.92	-	-	-1.9	3.2	-	229	L	-	-	-	-	-		-	0.94	0.0
0.94	-	-	-1.9	3.2	-	213	L	-	-	-	-	-		-	0.96	0.0
0.9	-	-	-1.8	3.1	-	217	L	-	-	-	-	-		-	0.92	0.0
0.93	-	-	-1.9	3.2	-	-		-	-	-	-	-		-	0.95	0.0
0.9	-	-	-	-	-	284	L	-	-	-	-	-		-	0.90	0.0
0.9	-	-	-	-	-	-		-	-	-	-	-		-	0.90	0.0
0.3	-	-	-	-	-	-		0.7	-59.8	-	-	-		-	0.30	0.0
0.1	-	-	-	-	-	-		0.9	-60.2	-	-	-	V	0.27	0.34	49.9
0.6	-	-	-	-	-	345	L	0.4	-	-	-	-	V	0.26	0.70	6.6
0.7	-	-	-	-	-	355	M/V	0.3	-60.2	9.1	1.9	-		-	0.70	0.0
0.5	-	-	-	-	-	372	V/M	0.5	-60.1	7.4	5.1	-		-	0.50	0.0
0.9	-	-	-5.9	9.1	-	318	L	-	-	-	-	-		-	0.97	0.0
0.95	-	-	-4.8	7.6	-	284	L	-	-	-	-	-		-	1.01	0.0
0.92	-	-	-4.7	7.4	-	299	L	-	-	-	-	-		-	0.97	0.0
0.9	-	-	-1.4	2.4	-	232	L	-	-	-	-	-		-	0.92	0.0
0.9	-	-	-4.8	7.6	-	256	L	-	-	-	-	-		-	0.95	0.0
0.95	-	-	-2.7	4.5	-	247	L	-	-	-	-	-		-	0.98	0.0
0.9	-	-	-5.8	8.9	-	270	L	0.1	-	-	-	-	V	0.12	0.98	0.5
0.8	-	-	-4.7	7.4	-	-		-	-	-	-	-		-	0.85	0.0
0.87	-	-	-4.3	6.9	-	263	L	-	-	-	-	-		-	0.92	0.0
0.88	-	-	-4.3	6.9	-	265	L	-	-	-	-	-		-	0.93	0.0
0.9	-	-	-4.5	7.2	-	259	L	-	-	-	-	-		-	0.95	0.0
0.86	-	-	-4.6	7.3	-	267	L	-	-	-	-	-		-	0.91	0.0
0.95	-	-	-	-	-	217	L	-	-	-	-	-		-	0.95	0.0
0.88	-	-	-4.2	6.7	-	238	L	-	-	-	-	-		-	0.93	0.0
0.95	-	-	-4.8	7.6	-	263	L	-	-	-	-	-		-	1.01	0.0
J63PS																
0.9	-37	-	-3.4	5.5	-	232	L	-	-	-	-	-	-	-	0.94	0.0
0.9	-	-	-	-	-	244	L	-	-	-	-	-	-	-	0.90	0.0
0.9	-	-	-3.8	6.1	-	259	L	-	-	-	-	-	-	-	0.94	0.0
0.88	-	-	-3.6	5.8	-	272	L	-	-	-	-	-	-	-	0.92	0.0
0.92	-	-	-3.8	6.1	-	-		-	-	-	-	-	-	-	0.96	0.0
0.88	-	-	-3.8	6.1	-	234	L	-	-	-	-	-	-	-	0.92	0.0
0.9	-	-	-3.7	6	-	-		-	-	-	-	-	-	-	0.94	0.0
J70PC																
0.05	-	-	-	-	-	-		0.95	-59.7	-	-	16.1	V	0.17	0.21	56.9
0.9	-	-20.8	-18	21.1	-	327	L	0.1	-	1.7	13.7	-		-	1.05	0.0
0.95	-	-	-7.7	11.4	-	177	L	-	-	-	-	-		-	1.04	0.0
0.95	-	-	-	-	-	183	L	-	-	-	-	-		-	0.95	0.0
0.4	-	-	-	-	-	399	V	0.6	-	8.9	2.5	-		-	0.40	0.0
0.3	-	-	-	-	-	-		0.7	-59.5	7.1	6.3	18.1	V	0.19	0.43	15.4
0.05	-	-	-	-	-	-		0.95	-59.4	-	-	16.9	V	0.17	0.21	56.9
0.3	-	-	-	-	-	373	V	0.7	-59.7	5.4	8.9	17.3	V	0.18	0.43	14.7
0.6	-	-	-	-	-	331	L	-	-	-	-	-		-	0.60	0.0
0.75	-	-	-	-	-	368	L	0.25	-	1.1	14.2	-		-	0.75	0.0
0.8	-	-	-	-	-	391	L	0.2	-	-0.4	16	-	-	-	0.80	0.0
0.85	-	-	-0.7	1.2	-	379	L	-	-	-	-	-		-	0.86	0.0
0.84	-	-	-	-	-	275	L	0.16	-	2.3	12.8	-		-	0.84	0.0
0.55	-	-	-	-	-	406	L	0.45	-	-0.1	15.6	-		-	0.55	0.0
0.05	-	-	-	-	-	-		0.95	-60.4	-	-	16.7	V	0.17	0.21	56.9
0.05	-	-	-	-	-	-		0.95	-62.6	-	-	17.6	V	0.18	0.22	58.3
J98PC2M																
0.95	-	-	-4.2	6.7	-	283	L	-	-	-	-	-		-	1.00	0.0
0.2	-	-	-	-	-	-		0.8	-58.7	-	-	22.3	L	0.77	0.82	55.8
0.1	-	-	-	-	-	382	V	0.9	-	-	-	-		-	0.10	0.0
0.2	-	-	-	-	-	-		0.8	-58.8	-	-	-		-	0.20	0.0
0.05	-	-	-	-	-	-		0.95	-58.6	-	-	-14	V	0.06	0.11	31.8
0.2	-	-	-	-	-	-		0.8	-58.4	-	-	-		-	0.20	0.0
-	-	-	-0.6	1.1	-	-		-	-	-	-	-		-	-	-
0.95	-	-	-3	4.9	-	-		-	-	-	-	-		-	0.99	0.0
0.95	-	-	-2.9	4.8	-	233	L	-	-	-	-	-		-	0.99	0.0
0.95	-	-	-	-	-	229	L	-	-	-	-	-		-	0.95	0.0
0.05	-	-	-	-	-	-		0.95	-58.8	-	-	-				
0.5	-	-	-	-	-	476	V	0.5	-58.5	8.1	4	-		-	0.50	0.0
0.9	-	-	-	-	-	304	L	-	-	-	-	-		-	0.90	0.0
-	-	-	-	-	-	302	L	-	-	-	-	-		-	-	-
0.7	-	-	-	-	-	300	L	-	-	-	-	-		-	0.70	0.0
-	-	-	-	-	-	298	L	-	-	-	-	-		-	-	-
0.95	-	-	-	-	-	144	L	-	-	-	-	-		-	0.95	0.0
0.8	-	-	-2.9	4.8	-	291	L	-	-	-	-	-		-	0.83	0.0
0.8	-	-	-2.7	4.5	-	298	L	-	-	-	-	-		-	0.83	0.0
0.96	-	-	-2.4	4	-	183	L	-	-	-	-	-		-	0.99	0.0

ADDITIONAL FLUID INCLUSION DATA

F	Tfm	Tmh	Tml	S	TsH	Th	to	FCO2	TmCO2	TmC	Sclath	ThCO2	to	D CO2	D	MOL%CO2
0.05	-	-	-	-	-	-	L	0.95	-58.3	-	-	16.3	V	0.16	0.20	55.4
0.05	-	-	-	-	-	-	L	0.95	-58.2	-	-	22.7	V	0.21	0.25	62.0
0.05	-	-	-	-	-	-	L	0.95	-58.6	-	-	17.8	V	0.19	0.23	59.6
0.1	-	-	-	-	-	297	V	0.9	-58.1	-	-	18.4	V	0.19	0.27	41.2
JW004																
-	-	-	-	-	-	398	L	-	-	-	-	-		-	-	-
-	-	-	-	-	-	423	L	-	-	-	-	-		-	-	-
-	-	-	-	-	-	407	V	-	-	-	-	-		-	-	-
0.6	-	-	-	-	-	391	V	-	-	-	-	-		-	0.60	0.0
0.95	-	-	-	-	-	250	L	-	-	-	-	-		-	0.95	0.0
0.9	-	-	-	-	-	301	L	-	-	-	-	-		-	0.90	0.0
-	-	-	-	-	-	382	L	-	-	-	-	-		-	-	-
-	-	-	-	-	-	377	L	-	-	-	-	-		-	-	-
0.7	-	-	-	-	-	392	L	-	-	-	-	-		-	0.70	0.0
0.8	-	-	-	-	-	431	L	-	-	-	-	-		-	0.80	0.0
-	-	-	-	-	-	286	L	-	-	-	-	-		-	-	-
0.6	-	-	-	-	-	424	L	-	-	-	-	-		-	0.60	0.0
0.5	-	-	-	-	-	434	V	-	-	-	-	-		-	0.50	0.0
-	-	-	-	-	-	407	V	-	-	-	-	-		-	-	-
-	-	-	-	-	-	433	L	-	-	-	-	-		-	-	-
-	-	-	-	-	-	289	L	-	-	-	-	-		-	-	-
0.96	-	-	-	-	-	301	L	-	-	-	-	-		-	0.96	0.0
-	-	-	-	-	-	245	L	-	-	-	-	-		-	-	-
0.95	-	-	-	-	-	227	L	-	-	-	-	-		-	0.95	0.0
0.95	-	-	-	-	-	221	L	-	-	-	-	-		-	0.95	0.0
-	-	-	-	-	-	204	L	-	-	-	-	-		-	-	-
-	-	-	-	-	-	253	L	-	-	-	-	-		-	-	-
-	-	-	-	-	-	255	L	-	-	-	-	-		-	-	-
-	-	-	-	-	-	231	L	-	-	-	-	-		-	-	-
0.9	-	-	-	-	-	252	L	-	-	-	-	-		-	0.90	0.0
-	-	-	-	-	-	245	L	-	-	-	-	-		-	-	-
0.3	-	-	-	-	-	397	V	-	-	-	-	-		-	0.30	0.0
0.9	-	-	-	-	-	262	L	-	-	-	-	-		-	0.90	0.0
0.6	-	-	-	-	280	-	L	-	-	-	-	-		-	0.60	0.0
0.9	-	-	-	-	-	238	L	-	-	-	-	-		-	0.90	0.0
-	-	-	-	-	-	272	L	-	-	-	-	-		-	-	-
-	-	-	-	-	-	455	V	-	-	-	-	-		-	-	-
-	-	-	-	-	-	368	L	-	-	-	-	-		-	-	-
-	-	-	-	-	-	453	V	-	-	-	-	-		-	-	-
0.7	-	-	-9.1	13.5	-	-	L	-	-	-	-	-		-	0.78	0.0
0.5	-	-2.4	-5.5	8	-	-	L	-	-	-	-	-		-	0.53	0.0

APPENDIX E

SYMBOLS AND ABBREVIATIONS

E1: LIST OF SYMBOLS AND ABBREVIATIONS

The following list contains a summary of all the symbols and abbreviations used in the thesis, subdivided according to the chapter in which they appear.

CHAPTER 1:

Deformation:

D1	First regional deformation phase
D2	Second regional deformation phase
D3	Third regional deformation phase
F1	First phase folds
F2	Second phase folds
F3	Third phase folds
S0	Bedding
S1	Penetrative, slaty cleavage, axial planar to F1
S2	Crenulation/pressure solution cleavage, axial planar to F2
S3	Crenulation cleavage, axial planar to F3
L1	Mineral lineation on S1 surfaces
L2	Mineral lineation on S2 surfaces
L3	Mineral lineation on S3 surfaces

Fluids in the crust:

P_F	Fluid pressure
P_L	Lithostatic pressure
P_H	Hydrostatic pressure

CHAPTER 2:

Vein chronology:

Vn_X	Vein formed during Dn, associated with structure/lithology X. (Classification summarised in Table 2.1)

CHAPTER 3:

Microthermometry:

L	Liquid
G	Gas
S	Solid
F	Degree of fill; volumetric proportion aqueous liquid in inclusion
Tfm	Temperature of first (eutectic) melting of hydrated phase (°C)
Tmh	Hydrohalite melting temperature (°C)
TmI	Ice melting temperature (°C)
S	Salinity determined from ice melting temperature (Potter *et al.* 1978), in weight percent NaCl equivalent
TsS	Sylvite dissolution temperature (°C)
TsH	Halite dissolution temperature (°C)
Shal	Salinity determined from halite dissolution temperature (Sourirajan & Kennedy 1962)

Th	Total homogenisation temperature (°C)
L, (L)	Homogenisation to the liquid phase
V, (V)	Homogenisation to the vapour phase
C, (C)	Critical homogenisation (fading of meniscus)
M, (M)	Critical homogenisation (fading of meniscus)
H, (H)	Total homgenisation by halite dissolution
d, (d)	Decrepitation temperature (°C)
D	Bulk density (g cm^{-3})
F CO_2	Volumetric proportion CO_2 in inclusion (1-*F*)
TmCO_2	Melting temperature of solid CO_2 (°C)
TmC	Clathrate melting temperature (°C)
Sclath	Salinity determined from clathrate melting temperature (Collins 1979), in weight percent NaCl equivalent
ThCO_2	Homogenisation temperature of CO_2 phases (°C)
D CO_2	Density of CO_2 phase (g cm^{-3}), from Angus *et al.* 1976

Fluids (general):

P	Pressure
V	Volume
T	Temperature
X	Composition (general); mole fraction (specific), usually with subscript or bracketed phase following
NC	Non-condensible phase(s) at -196°C
ppm	Parts per million (equivalent to mg kg^{-1})
ppb	Parts per billion (equivalent to μg kg^{-1})

Experimental techniques:

D-ICP	Decrepitation-linked inductively-coupled plasma atomic emission spectrometry
NAA	Neutron activation analysis
XRD	X-Ray diffraction
SEM	Scanning electron microscopy
EDX	Energy dispersive spectrometer (with SEM)

Stable isotopes:

$\delta^{18}O$	$1000((^{18}O/^{16}O_{sample})/(^{18}O/^{16}O_{SMOW})-1)$ ‰ (per mil or parts per thousand)
δD	$1000((^{3}H/^{1}H_{sample})/(^{3}H/^{1}H_{SMOW})-1)$ ‰ (per mil or parts per thousand)
$\delta^{13}C$	$1000((^{13}C/^{12}C_{sample})/(^{13}C/^{12}C_{PDB})-1)$ ‰ (per mil or parts per thousand)
α_{A-B}	fractionation factor = $(^{18}O/^{16}O_A)/(^{18}O/^{16}O_B)$

CHAPTER 4:

Thermodynamics:

K, K_n	Equilibrium constant (as defined)
$f O_2$	Oxygen fugacity (bars)
$f H_2S$	Hydrogen sulphide fugacity (bars)
$f S_2$	Sulphur fugacity (bars)
$f SO_2$	Sulphur dioxide fugacity (bars)
G	Gibbs' free energy
G°	Standard Gibbs' free energy
$\blacktriangle G°_r$	Standard Gibbs' free energy of reaction
$\blacktriangle G°_f$	Standard Gibbs' free energy of formation
P_s	Standard state for pressure (1 bar)
T_s	Standard state for temperature (298 K)
S	Entropy

$S°$	Entropy (standard state)
C_p	Heat capacity
a, b, c	Maier-Kelley coefficients (for temperature dependence of C_p)
R	Gas constant
a.i	Activity of component/phase i
ϕ(i)	Fugacity coefficient or activity coefficient of component/phase i

CHAPTER 5:

Solubility calculations:

m., *m*	Molality
ΣX	Total moles of X
M	Metal ion
L	Anionic/neutral ligand
X	Halide ligand
$ß_n$	Cumulative formation constant for complex ML_n

CHAPTER 6:

Fluid flow:

q	Fluid flux
k	permeability
μ	fluid viscosity
dP/dz	Pressure gradient
W/R	Ratio of exchangeable atoms of oxygen in water to atoms in rock
δ^i_{water}	δ composition of water prior to isotopic equilibration
δ^i_{rock}	δ composition of rock prior to isotoic equilibration
δ^f_{water}	δ composition of water after equilibration
δ^f_{rock}	δ composition of rock after equilibration
$\blacktriangle_{rock\text{-}water}$	δ_{rock}-δ_{water}